Late Quaternary incision dynamics and valley bottom geometry within the Seine River catchment

Diana Chourio-Camacho

PSL UNIVERSITÉ PARIS

THÈSE DE DOCTORAT
DE L'UNIVERSITÉ PSL

Préparée à Mines Paris-PSL

Late Quaternary incision dynamics and valley bottom geometry within the Seine River catchment

Dynamique d'incision du Quaternaire supérieur et géométrie des fonds des vallées dans le bassin versant de la Seine

Soutenue par

Diana Nathaly CHOURIO-CAMACHO

Le 27 Mars 2024

Ecole doctorale n° 398

Géosciences, Ressources Naturelles et Environnement

Spécialité

Géosciences et géo-ingénierie

Composition du jury :

Christian, GORINI Professeur, Sorbonne Université	*Président du jury*
Pierre, ANTOINE Directeur de recherche, LGP CNRS	*Rapporteur*
Gilles, RIXHON Professeur, Université de Strasbourg	*Rapporteur*
Damase, MOURALIS Professeur, Université de Rouen Normandie	*Examinateur*
Paul, BESSIN Maître de conférences, Le Mans Université	*Examinateur*
Mark, NOBLE Maître de Recherche, Mines Paris-PSL	*Examinateur*
Hélène, TISSOUX Chercheure, BRGM	*Examinateur*
Jean-Louis, GRIMAUD Chargé d'Enseignement Recherche, Mines Paris-PSL	*Directeur de thèse*

MINES PARIS | PSL

Remerciements

Premièrement, je tiens à remercier sincèrement et chaleureusement les membres du jury ***M. Christian Gorini, M. Pierre Antoine, M. Gilles Rixhon, et M. Damase Mouralis,*** pour avoir pris le temps de lire et commenter avec passion mon manuscrit de thèse et avec qui j'ai pris du plaisir à discuter pendant la soutenance.

Je souhaite exprimer ici ma profonde reconnaissance à ma super équipe d'encadrement pour leur soutien, leur implication, leur disponibilité et les discussions passionnantes de notre projet de thèse :

- Un grand merci à mon directeur de thèse professeur ***Jean-Louis Grimaud*** pour ce sujet de thèse très passionnant, pour la confiance, pour sa disponibilité pendant ces trois années de thèse et surtout pour la richesse des discussions scientifiques que nous avons pu avoir.
- Un grand merci à mes encadrants de thèse ***Hélène Tissoux, Paul Bessin, Mark Noble et Pierre Voinchet*** pour leur soutien, pour m'avoir fait partager leur grande connaissance de la vallée de la Seine, pour m'avoir guidée sur le terrain, sur les datations, sur la géophysique, ainsi que pour les bons conseils, je vous adore !!!

L'aboutissement de ce travail de thèse a pu être réalisées grâce au financement RGF du Bureau de Recherches Géologiques et Miniers (BRGM). A ce titre, je remercie plus particulièrement ***Pascal Audigane, Florence Quesnel***, ainsi que à tout ***l'équipe qui fait partie de la BSS***. Un grand merci pour toute l'aide.

Je remercie à **l'*Agence de l'Eau Seine Normandie et le Port de Rouen*** pour le partage de données géophysiques avec nous.

Je remercie à ***Jean-Jacques Bahain, Christophe Falgueres, Vincent Lebreton, Olivier Tombre et Camille Daujeard*** pour leur chaleureuse accueil au Muséum d'Histoire Naturelle de Paris (MNHNP).

Je remercie chaleureusement toutes les responsables d'exploitation des carrières ainsi que tout le personnel qui font partie des diverses entreprises pour nous avoir permis de faire les relèvements des coupes de terrain et les échantillonnages pour la datation le long du Bassin de la Seine : à Val-de-Reuil, Manoir Brésil et Bouafles (Cemex) ***Mme. Sabine Binninger*** **et** ***M. Fabrice Coté***, à Saint-Martin-la-Garenne et Sandrancourt (Lafarge) ***M. Alexandre Payet***, à Vimpelles (Lafarge) ***M. Matthieu Ballansat et Mme. Emilie De Oliveira***, à Dordives (Lafarge) ***M. Gaetan Caron, M. Erwan et M. Tony***, à Achère et Carrières-sous-Poissy (GSM) ***M. Jérôme Grumel***, à Citry-Luzancy (GSM) ***M. Matthieu Ballansat***, à Bazoches-les-Bray et Varennes-sur-Seine (GSM) ***M. Olivier Gabens***, à Noyen-Port Montain (A2C) ***M. Thomas Weinbreck***.

Je tiens à exprimer ma reconnaissance à tous ceux qui ont permis que cette étude voie le jour :

- A l'équipe de l'INRAP **Mme.** ***Céline Coussot***, ***Mme. Sofie Clément*** et ***M. Frédéric Blaser*** pour le partage et les bonnes discussions.
- A ***M. Pascal Bertrand*** pour leur aide à l'interprétation de structures post-glacières.
- A ***M. Emmanuel Vartanian*** pour les datations OSL et les discussions.

- Je tiens à remercier chaleureusement l'équipe de géologie et du centre de géosciences de l'Ecole de Mines de Paris que j'ai eu l'opportunité de partager pendant ces trois ans. ***Christine, Caroline, Didier, Fabien, Nicolas Desassis, Irina, Bruno,*** pour les bons moments vécus.
- Je tiens également à remercier à ***MIS QUERIDOS : Damien, Dylan, Loïc, Alexandre, Gabrielito, Léo, Antoine, Nicolas, Léo de Souza, Victor, Louison et Nour***, pour les bons moments partagés.
- Je tiens également à remercier ***Sylvie Boj***. Sylvie, sans toi cette équipe ne fonctionnerait pas, merci beaucoup pour tout ton aide concernant l'administratif, pour les conseils et les bons discussions le matin, je t'adore profondément.
- Un grand merci à ***Mme. Pascale Nalon et toute l'équipe de la bibliothèque de Fontainebleau***, pour m'avoir aidé énormément pendant ces trois années en trouvant des thèses et articles si difficiles.
- Un grand merci à ***Mme. Sandrine Motte et M. Xavier Caillard pour*** tout leur aide et leur soutien pour mes démarches administratives concernant le titre de séjour et la demande de naturalisation, merci du fond de mon cœur.
- Je remercie également les personnes de l'école doctorale GRNE avec qui j'ai pu échanger, ***M. Laurent de Windt, Alexandrine Gesret et Véronique Lachasse*** pour tout l'aide au cours de ces trois ans et surtout pour toutes les démarches administratives à la fin de la thèse.

Je souhaite remercier du fond de mon cœur à une personne qui a cru en moi pour m'avoir motivée à candidater à la bourse d'excellence académique de l'Université Paris Saclay ***Véronique Durand*** grâce à toi j'ai eu l'opportunité d'accomplir l'un de mes plus grands rêves : venir au pays de mes rêves, **la France**. Merci pour ton soutien depuis mon arrivée en 2018 et surtout pour être là pendant mes trois ans de thèse. Je t'adore !!!

Un grand merci aux professeurs du master STePe, et tout particulièrement les professeurs ***Antonio Benedicto, Thomas Blaise, Guillaume Delpech, Jocelyn Barbarand*** pour les bons conseils.

A mes amis quaternaristes ***Iale, Jean-Baptiste et Kim***, avec lesquels j'ai eu le privilège de m'épanouir autour du petit grain de quartz et de faire énormément des hypothèses pour améliorer nos mesures avec beaucoup beaucoup non d'la ! non d'la ! eux me fatiguent de la part de ***M. Pierre***. Merci beaucoup pour votre bonne humeur et vos conseils, Je vous aime !!!

Merci à mes amis du master ***Louise Lenoir et Archange Mbangilwa*** pour être là depuis 2018, je vous adore !!!

Un grand merci à la famille ***Bussière***, notamment ***Odette, Paul, Véra, Marianne, Pierre et Éric*** pour m'avoir accueilli depuis mon arrivée et pour me considérer part de la famille, je vous aime !!!

A mes piliers fondamentaux, pour être mon soutien à la distance ***ma maman chérie Omi et mon frère bien aimé Xavier*** sans vous rien n'est possible, c'est une réussite de nous trois Los amo con todo mi corazón !!!

A ma famille au Venezuela, mes oncles : ***Rafa, Beto, Hugo, Pedro, Toño, Chicho*** ; mes tantes, ***Francy, Mary, Zory, Marilu*** ; mes cousins et cousines : ***Fucho, Franklin, Marco, Guelvis, Caro, Dani, Mariangel, Sofi, Dino…*** Gracias por su amor, los amo !!!

A mes amis, los de siempre, por estar: ***Franklin Urquiola, Frank Eduardo Rivas, Rub Gonzalez, Dayribeth Rivas, Matthias Bachmann, Gerardo Zambrano, Endrina Ángel, Jose Luis Martinez, Jairo Omaña, Katherine Ortega, Gabriel Calderon, Laura Nieto et Crisly Castro.***

A mes professeurs du français pour m'avoir donné l'amour pour la culture et langue française : ***Hubert Tyrode, Domingo Villegas et Urquia Saavedra***.

A mes amis français pour les rigolades et les bons moments, je vous aime : ***Yannick, Rohan, Marc, Hugues, Manu, Jacqui, Ingrid, Théo, Florie et Matthieu***.

A ma troupe d'anges gardiens pour être avec moi tous les jours : ***à mi Cuchita Eva, mi cuchito Antonio, mon Père Nelson et el Panita de la familia Don Elisaul Urdaneta.***

A tous ceux qui font partie de ma vie MERCI BEACOUP, je vous aime !!!

Le rêve est à notre portée mais nous devons lutter avec toute notre force pour cela en le mettant du cœur et surtout en pensant que Todo Saldrá Bien !!!

Diana Nathaly

Contents

List of Figures

List of Tables

Introduction

Introduction

Within the sediment routing system, river valleys are part of the transfer zone that export sediments coming from landscape erosion to their final deposition area in sedimentary basins. There, alluvium storage can buffer sediment flux signals to the sea. Thus, constraining the alluvial infill storage and controls on valley bottom geometry would allow to better quantify the response time of the transfer zone in source-to-sink systems.

Many recent studies highlighted some of the factors that control valley bottom widening such as tectonic deformation or climate variations (e.g., through base level or water discharge variations). Other modulating factors -impacting for instance valley width- such as bedrock lithologies, valley bottom aggradation or valley height were recently investigated. Overall, much remains to be done on the characterization of the geomorphic evolution and processes in valley bottoms, particularly in tectonically quiescent areas where the impacts of climate and bedrock lithology may be relatively stronger.

During valley formation, repeated alternations of vertical incision and lateral erosion lead to the creation of strath terraces, which are abandoned along valley slopes. These terraces are used to infer incision rates. Incision/aggradation alternations can be caused by variations in discharge or sediment supply and are associated with the glacial-interglacial transition during the Quaternary. Climate and tectonics can affect sediment production rates and/or modify the base level to which rivers are graded, causing disequilibrium along the river profiles. In response, an erosional perturbation in the form of a knickpoints can retreat. The analysis of knickpoint distribution -although debated- may thus allow retrieving information about incision dynamics. Most studies however focus on topographic data, which corresponds to the top of alluvium, when a substantial part of information may be buried at the transition between the bedrock and the alluvium.

The Paris basin and the Seine catchment are situated in a non-orogenic area, although they may be influenced by -for instance- far-field alpine deformation to the South-East and by glacio-isostasy to the North. It is known that in the last million years, the alluvial sequences were controlled by climatic variations. Compared to the Somme River, the Seiner River dynamics is still poorly known during the Quaternary. Nevertheless, strath terraces preserving at the edge of valley bottom could be used to constrain incisions. Along the Seine River, slope variations were locally observed, in particular at the alluvium-bedrock interface and interpreted in terms of regressive erosion. No study exists yet that would integrate regionally the distribution of these inferred slope changes. Thus, the Seine River is a good laboratory to further investigate how external and internal factors influence valley evolution. Some of the questions that arise

are: (i) how old are the sediments stored in the valley bottom, (ii) what is the geometry at the bedrock-alluvium interface, (iii) what are the factors controlling valley bottom geometries, and (iv) how much sediment is stored.

This dissertation therefore focuses on the large-scale geometry and geochronology of the major valleys of the Seine catchment. After a literature review (chapter 1), it is divided into two parts: one that focuses on field analysis and the geochronology of terraces and valley bottom using ESR and OSL methods (i.e., chapters 2, 3 and 4) and one that focuses on the restitution of the valley bottom geometry (chapters 5, 6 and 7). A synthesis is presented in Chapter 8.

- Chapter 1 summarizes the current knowledge on geometry and sediment transfer along the fluvial corridors as well as the geological context of the Paris Basin.
- Chapter 2 presents the field description of alluvial deposits that were sampled within the Seine catchment for ESR/OSL geochronology.
- Chapter 3 presents the general principles of the ESR and OSL dating methods as well as the main results obtained for valley bottom and strath terraces of the Seine catchment.
- Chapter 4 focuses on the geometry and geochronology of Manoir Brésil, an alluvial terrace located downstream of Rouen where Late Quternary vertical movements can be discussed.
- Chapter 5 focuses on the construction of a database of the bedrock-alluvium interface within the Seine catchment, as well as the valley bottom delimitation.
- Chapter 6 introduces a morphometric analysis of river length, sub-catchment delimitation and valley width as a function of drainage area and bedrock lithologies.
- Chapter 7 introduces the estimation of the alluvial infill geometries using a kriging method based on Stochastic Partial Differential Equations (SPDE).

Chapter 1: Literature review on fluvial corridors with focus on the Paris Basin during the Late Quaternary

Ce chapitre présente une étude bibliographique sur la géométrie et le transfert sédimentaire à travers les corridors fluviatiles, la compréhension des fonds de vallée en lien avec la formation des terrasses alluviales, ainsi que le contexte géologique et la paléogéographie pendant le Pléistocène moyen et l'Holocène dans le Bassin de Paris.

Chapter 1

1 Geometry and sediment transfer dynamics along fluvial corridors

Fluvial corridors may record phases of aggradation and incision related to changes in sediment supply or water discharge due to tectonics and or climate (Armitage et al., 2011; Tofelde *et al.* 2017; Savi et al., 2020). Within corridors, fluvial deposits are sometimes preserved as alluvial terraces which represent the remnants of abandoned valley bottoms. Morphological and sedimentological features (geometry, architecture, lithology, etc.) of theses terraces are frequently used to track and disentangle tectonic and climatic conditions that influences watershed landscapes and their evolution (Schumm, 1977). The following section provides a general overview of fluvial corridors considering their geometry, they role in sediment transfer and about co-evolutions of river, landscape, climate and tectonic.

1.1 Sediment routing system (SRS)

Sediment routing system (SRS) refers to the transport pathways of sediments from a source area where erosion is active, through a transfer zone where subsidence is almost null, to a sink area where sediments are final deposited (Figure 1.1, Castelltort and Van Den Driessche, 2003; Allen, 2008, 2017; Tofelde et al., 2021).

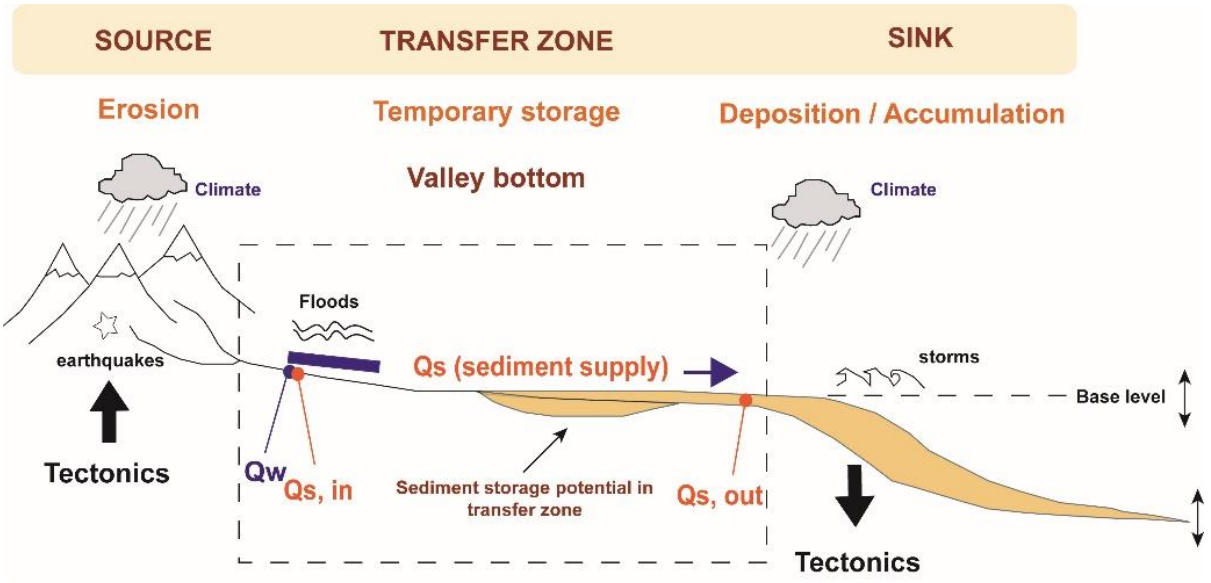

Figure 1.1. Schematic 2-D profile of sediment routing system SRS emphasizing erosion, transfer, and accumulation zones and important controls of tectonics, climate, base level (Qw: Water flow; modified after Romans et al., 2016).

1.1.1 Transfer zone dynamics

The transfer zone is the area where fluvial corridors transport and possibly temporarily store sediments in their valley bottoms. It ensure the connection between the source zone where erosion prevails, and the sink zone where deposition predominates (sedimentary basin; Figure 1.1, Métivier and Gaudemer, 1999; Castelltort and Van Den Driessche, 2003; Jerolmack and Paola, 2010; Blöthe and korup, 2013; Romans et al., 2016). The transfer zone is essentially subject i) to variations in water and sediment supply provided by the source zone at its upstream boundary and, ii) to variations in base level at its downstream limit with the sink area. These variations can trigger complete or buffered responses of the transfer zone through erosion, sediment transport and sediment deposition (Castelltort and Van Den Driessche, 2003; Allen, 2008, 2017; Romans et al., 2016; Tofelde et al., 2021; Castelltort et al., 2023). Thus, the transfer zone remains important to understand how changes in climatic, tectonic or anthropogenic conditions impacts the recorded signal (e.g., sediment volume stored in the valley bottom, temporal and spatial distribution of sediments).

1.1.2 Fluvial systems

Fluvial systems are characterized by one or several active channels with the capacity to laterally migrate within the alluvial plain or the valley bottom. Four main fluvial styles depending on the characteristics of channels and sediment supply are described and characterized (Figure 1.2., Leopold and Wolman, 1957; Friend and Sinha, 1993; Church, 2006):

- ***Straight*** systems consist of single channels (low flow or low flood) with low sinuosity (<1.5). these systems tend to develop deeper and shallower sections. These are called pools and riffles respectively. The spacing development from one pool to the next is about five times the channel width (Figure 1.2, Huggett and Shuttleworth, 2022).
- ***Braided*** systems are characterized by high width/depth ratio (>50). They tend to form where stream energy is high; the channel gradient is steep; bank material is erodible, allowing the channel to shift sideways with relative ease; and where the sediment supply is high (Figure 1.2; Miall, 1981; Huggett,and Shuttleworth, 2022)
- ***Anastomosed*** systems are characterized by low width/depth ratio (<10), low slopes, fine-grained sediments and several straight or meandering stable channels separated by perennial stretches of the valley bottom, which are not reworking during floods. Meandering channels are usually deep and narrow with abrupt bank (Figure 1.2; Miall, 1996).

- ***Meandering*** systems are characterized by low width/depth ratio (<40), single active channels with high sinuosity, low slope, inner bank deposition (point bars) and outer bank erosion (Figure 1.2; Allen, 1965; Miall, 1996).

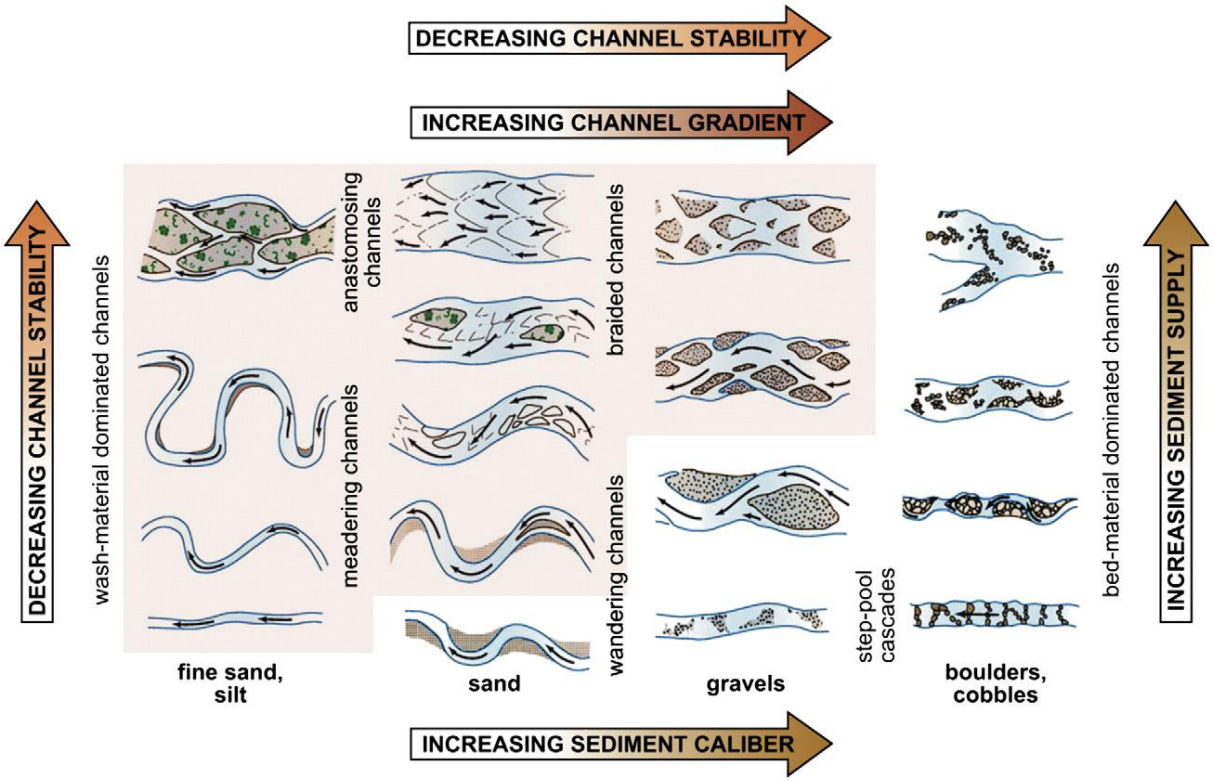

Figure 1.2. Fluvial dynamics type as a function of sediment size and supply, and channel gradient and stability (Church, 2006).

1.1.3 Sediment transport system

In the source zone, rivers exhibit a convergent (tributary, aggregative) pattern, transitioning to a single flow in the transfer zone, and ultimately adopting a divergent (distributary, dispersive) pattern within the sink area (Castelltort et al., 2023). From upstream to downstream, rivers erode soil, bedrock, older sediment, and transport the product of the weathering and erosion processes in four different forms (Figure 1.3):

- The ***dissolved load*** represents the material that are transported by the stream flow while in solution and are not considered as part of the sediment load.
- The ***suspended load*** corresponds to very fine particles (0.01mm < size < 0.1mm, clays, silts) kept in suspension in the water column by low and turbulent movements of the flow stream.

The ***wash load*** is a subset of the suspended load which corresponds to very fine particles (size<0.02 mm) that will never settle to the bottom but will remain in permanent suspension.

- The ***bed load*** describes particles that are too large to be carried as suspended load. Medium-sized particles (0.1mm < size < 100mm: sand, gravels, pebbles) move quickly by saltation than by rolling and sliding. The composition of the bed load depends on the flow stream velocity and the available sediment, it usually consists of sand, gravel, and pebbles (Figure 1.3).

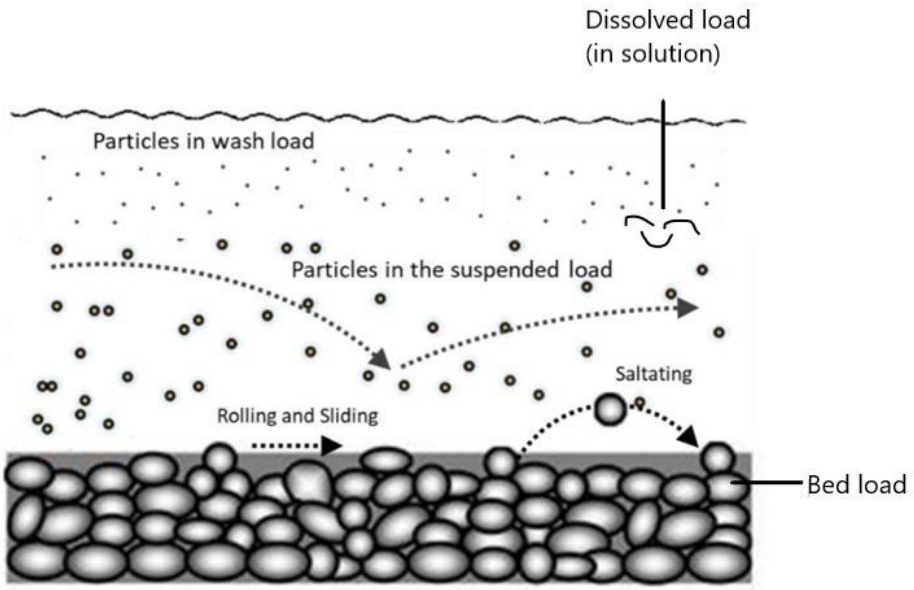

Figure 1.3. Various modes of sediment transport in a river system (Matos et al., 2020).

The relation between sediment behavior in the channel with regards to particle size and flow velocity, is illustrated by the Hjulström diagram (Figure 1.4, Hjulström, 1935). This graph shows the tendency of a particle to be eroded, transported or deposited for different flow velocities and grain size. This diagram is applied only to erosion, transport, and deposition in alluvial channels. The upper curve is a band showing the critical velocities at which grains of a given size start to erode. The curve is a band rather than a single line because the critical velocity depends partly on the position of the grains and the way that they lie on the bed. Notice that medium sand (0.25–0.5 mm) is eroded at the lowest velocities. Clay and silt particles, even though they are smaller than sand particles, require a higher velocity for erosion to occur because they lie within the bottom zone of laminar flow and, in the case of clay particles, because of the cohesive forces holding them together. The lower curve in the Hjulstrøm diagram shows the velocity at which particles already in motion cannot be transported further and fall to the channel bed. This is called the fall velocity. It depends not just on grain size but on density and shape, too, as well as on the viscosity and density of the water. As the flow velocity reduces,

so the coarser grains start to fall out, while the finer grains remain in motion. Clay and silt particles stay in suspension at velocities of 1–2 cm/s, which explains why suspended load deposits are not dumped on streambeds. The region between the lower curve and the upper band defines the velocities at which particles of different sizes are transported. As a rule of thumb, the flow velocity at which erosion starts for grains larger than 0.5 mm is roughly proportional to the square root of the grain size. Thus, to put it another way, the maximum grain size eroded is proportional to the square of the flow velocity (Huggett and Shuttleworth, 2022).

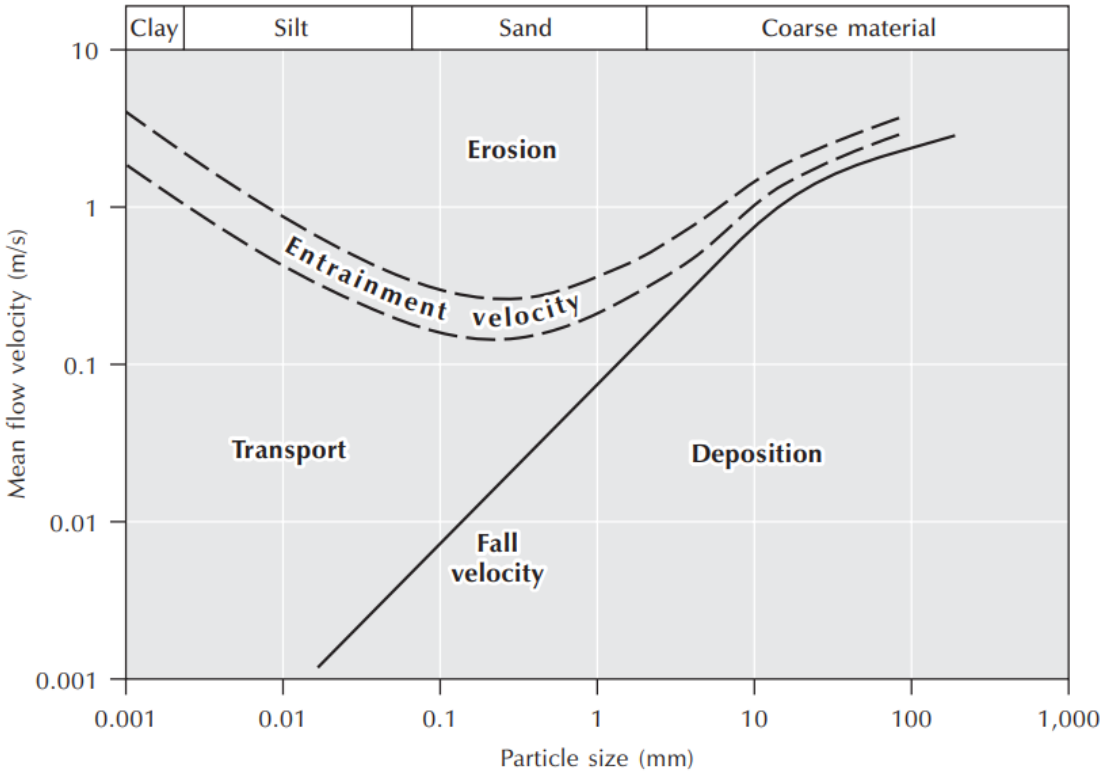

Figure 1.4. Erosion, transport, or deposit sediment diagram (modified after Hjulström, 1935 in Huggett and Shuttleworth, 2022).

The sediment transport is typically conceptualized using the Lane's balance (Lane, 1955), which describes how changes in sediment supply, sediment size, slope and water discharge determine incision or aggradation and sediment flux in the fluvial system. A decrease in water discharge could result in aggradation (Figure 1.5-a). River systems are considered in equilibrium when there is a balance between the amount of sediment load and the water discharge (Figure 1.5-b). In contrast, incision may result from an increase in water discharge or river slope (Figure 1.5-c). The alluvial rivers adjustments to such variations can be recorded

through (i) fill-terrace formation or valley bottom in the transfer zone, (ii) changes in sediment export to sink (i.e. sedimentary basin) (Tofelde et al., 2017, 2019) and iii) longitudinal profile characteristics (Tucker and Slingerland, 1997, Davy and Lague, 2009). In the following section, the main factors that control the evolution of the longitudinal profile is presented.

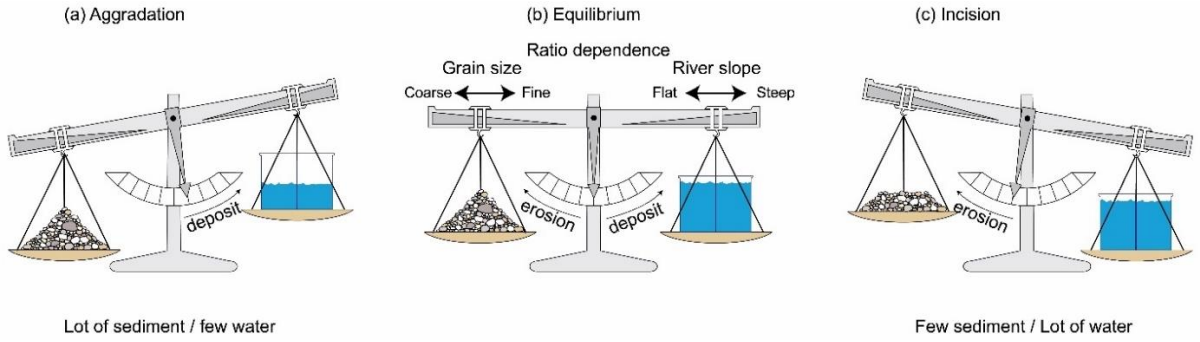

Figure 1.5. Lane's balance describing the (a) aggradation deposit sediment (b) equilibrium in fluvial system, and (c) incision erode through river bed.

1.1.4 Time response and sediment storage in the transfer zone

Rivers adjust their slope (S) and width with respect to the local base level such that, in a graded (steady) state, the incoming water discharge (Qw) can transport the incoming sediment supply (Qs, in) downstream (Figure 1.1). These adjustments follow the next equation 1.1 (Tofelde, et al., 2019).

$$S = f\left(\frac{Qs,in}{Qw}\right) \qquad \text{Equation 1.1}$$

In simplified way, these adjustments cause aggradation or incision until a new graded profile is reached. Incision can be generated when Qw increases while aggradation occurs when Qs exceeds the transport capacity of the river. The necessary time of a river profile to reach steady state or equilibrium determining (Teq) is determined using the following equation 1.2 (Castelltort and Van Den Driessche, 2003):

$$Teq = \left(\frac{L^2}{K}\right) \qquad \text{Equation 1.2}$$

where L (m) is the basin length and K ($\frac{m^2}{s}$) is its coefficient of diffusivity. For short steep river, systems range between 5-10 ka while it exceeds 100 ka for large river systems.

Castelltort and Van Den Driessche (2003), using the database from Hovius (1998), calculated a *Teq* of 41 ka for the Seine River, taking into account the suspended and dissolved loads sediments.

Sediment can be temporarily stored within the valley bottom and reworked/incised when transfer zone boundary conditions (discharge (Qw), sediment supply (Qs,in), sediment export (Qs,out) and base-level) and geometry changes changes (Tofelde et al., 2019). Incision occurs when the incoming water discharge (Qw) and transport capacity (Qc) exceeds the sediment supply (Qs,in), conversely, when sediment supply exceeds the transport capacity, sedimentation occurs (Qs,out < Qs,in) (Merrits et al., 1994; Tofelde et al., 2019). Additionally, in some catchments, valley bottom can adjust to upstream denudation, buffering the transfer zone response and approximately balancing sediment loads over different timescales. In such case, when upstream denudation is reduced, the river might incise its valley bottom to keep the sediment load at the outlet constant. Conversely, if upstream denudation rises, the river is likely to use that increased sediment load to recharge its previously excavated valley bottom (Métivier and Gaudemer, 1999; Phillips, 2003; Phillips and Slattery, 2006; Covault et al., 2013; Romans et al., 2016).

1.2 Dynamic incision

1.2.1 Stream power

The stream power represents an indicator of the erosive capacity or sediment transport capacity and is proportional to the amount of water it carries (Hack, 1957; Whipple and Tucker, 1999; Tomkin et al., 2003). It is defined by the stream power law in equation 1.3:

$$\varepsilon \sim K A^m S^n \qquad \text{Equation 1.3}$$

where ε is the stream power, K is a proportionality constant of erodibility, A is the drainage area, S is the local river slope and m/n exponents are dimensionless constants that are a function of basin hydrology (Howard, 1994; Sklar and Dietrich, 1998; Stock and Montgomery, 1999; Whipple and Tucker, 1999; Kirby and Whipple, 2012).

1.2.1.1 Qualitative description of longitudinal profiles

The longitudinal profile provides the change in elevation of a channel from its headwaters to its outlet, tending towards a form which best facilitate transport of the sediment load and erosion of the bed. Each longitudinal profile is naturally graded to a base level (lowest elevation of the profile) and its shape reflects the dynamics equilibrium between rivers conditions. A longitudinal profile is in steady state or equilibrium when the channel profile has fully adjusted to climatic, lithologic and tectonic conditions imposed upon it. These factors need to be invariant over sufficiently long time to allow the river to adjust its longitudinal profile to the prevailing conditions (Snyder et al., 2002; Whipple et al., 2013). Perturbations that are short compared to the response time (Teq) of the river profile can influence short-term incision rates, but do not persist long enough to much affect the river profile (Whipple, 2001). Thus, steady state is used to refer to a long-term condition where average incision rate balances the average rock uplift rate relative to base level, such that the longitudinal profile varies only slightly through time (Sklar and Dietrich, 1998). Thus, longitudinal profiles can provide valuable information about controlling factors of the overall relief of landscapes evolution. (Whipple and Tucker, 1999; Crosby and Whipple, 2004; Fryirs and Brierley, 2013).

1.2.1.2 Knickpoints

When the base level changes, the longitudinal profile adjusts its slopes, tending to reach a new equilibrium. In response to variations in boundary conditions (e.g. base level drop, uplift rate increase; Bishop et al., 2005; Loget and Van Den Drissche, 2009; Grimaud et al., 2016), the slope increases, and erosion becomes more significant (cf. Lane's model). The point where the river slope increases is called a Knickpoint and mark a disequilibrium in the longitudinal profile (Figure 1.6).When a channel is undergoing a transient response to a change in climatic or tectonic conditions, knickpoints form and migrate slowly upstream at a rate controlled by the water discharge and the erodibility of rocks constituting the stream bed (e.g. knickpoints can be marked at abrupt lithological variations; Stock and Montgomery, 1999). The migration of the knickpoint through a river can modify multiple features including grading, width, erosion processes, bed morphology and bed load characteristics (e.g. grain size; Sklar and Dietrich, 2006; Turowski et al., 2007) and constitute a first approximation of the rate for network to return to equilibrium after a base level drop or a tectonic event (Gardner, 1983; Bonnet and Crave, 2003; Loget and Van Den Drissche, 2009; Grimaud et al., 2016; Allen, 2017).

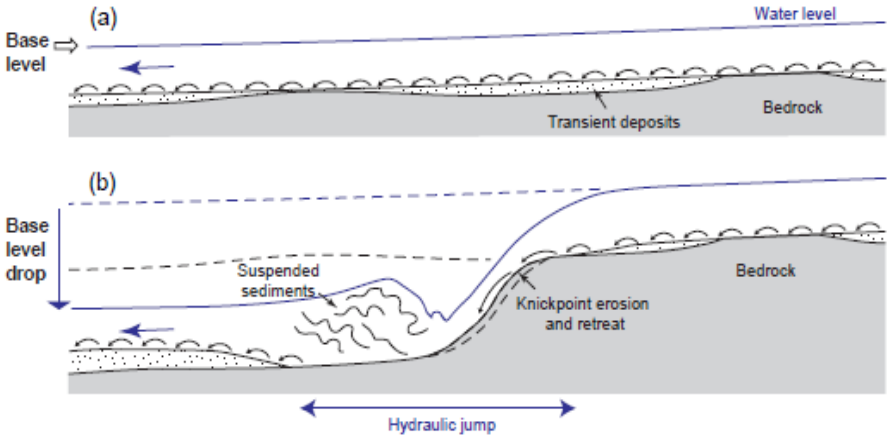

Figure 1.6. Longitudinal section of a river bed before (a) and during (b) the propagation of a knickpoint triggered by relative base-level fall, Grimaud et al., 2016.

Finally, when river reaches a new equilibrium, previously active alluvial can be incised and abandoned, forming alluvial terraces in the transfer zone. These alluvial terraces record the past river dynamics and geometries and can therefore be used to quantify spatial and/or temporal changes in rates of vertical incision and lateral erosion of the river (Malatesta et al., 2017).

1.3 Valley bottom as a part of the transfer zone

Valley bottom corresponds to area where the stream or river channel(s) flows and to the associated low-lying contemporary active floodplain, constituting one of the most important fluvial landforms as a part of the transfer zone (Fryirs et al., 2015; Wheaton et al., 2015; Gilbert et al., 2016). Valley bottoms can be bounded by bedrock hillslopes or by other landforms such as alluvial fans or fluvial terraces (Fryirs et al., 2015). The shape and size of the valley bottom varies depending on the bedrock lithology, the water discharge, the drainage area, the stream channel width, etc. (Fryirs and Brierley, 2010). Thus, Precise delineation of valley bottoms remains important to better understand the mains mechanism that control its morphology. In this study, we delineated the valley bottom of the Seine catchment considering the terraces that are partly 10 m above and partly 10 m below the river elevation based on the harmonization of the 1:50000 French geological maps (more details in chapter 5).

When rivers reach a quasi-equilibrium state characterized by minimal vertical incision or deposition, lateral bank erosion and lateral deposition sediments predominates, involving the repeated reworking of the same sediments and the widening of the valley bottom. Several morphological units can be distinguished as parts of the valley bottom, the space occupied by

a river varies according to the hydrological conditions (Figure 1.7, Umeuduji, 2017; Deleplancque, 2016):

- The ***minor bed*** is the part of channel in which the river flows continuously and sets the maximum flow discharge.
- The ***major bed*** represents the maximum width of the channel in which the valley bottom is include. This area generally tends to be productive by specific vegetation, the riparian zone, forming important seasonal habitats for species.
- The ***floodplain*** is the area that is flooded during overflow floods.
- The ***active valley*** is the area swept by the course of the river during changes in its course, which erodes the old deposits and builds new sedimentary structures reflecting its dynamics.

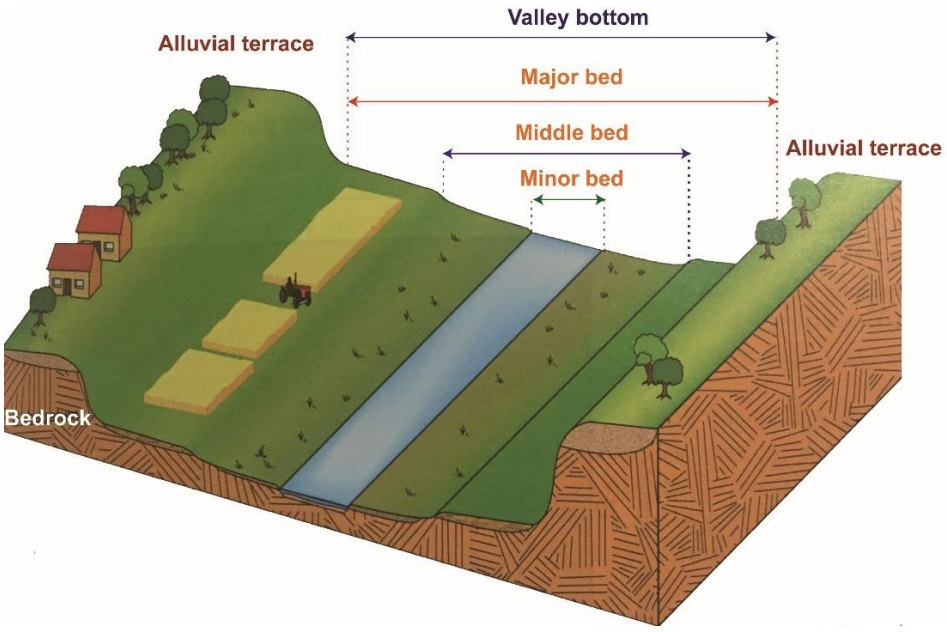

Figure 1.7. Schematic illustration of morphological units of a watercourse, Despriée et al., 2017.

1.3.1 Parameters controlling the valley bottom

1.3.1.1 External factors

River valleys evolve within the valley bottom but knowledge on parameters that controlling the valley bottom is still poorly understood (May et al., 2013). Climate influence river discharge and sediment supply, either cause or hinder valley widening (Clubb et al., 2022). Studies shows that the valley bottom could be influenced by bedrock lithology with valley bottoms widening in soft lithologies or narrowing in hard lithologies (Brocard and Van Der Beek, 2006; Langston

and Temme, 2019; Limaye, 2020; Tofelde et al., 2022). Numerical modeling shows that the widening of the valley bottom requires the erosion of valley walls, representing an important parameter in setting lateral migration rates of the channel. After collapsing, wall materiel needs to be fully removed by the river to widen the valley bottom (Figure 1.8) (Bufe et al., 2019; Tofelde et al., 2019; 2022). When valley walls are high, the large talus piles encroach on the valley bottom and can modify the river hydraulic geometry as well as the valley bottom width (Malatesta et al., 2017).

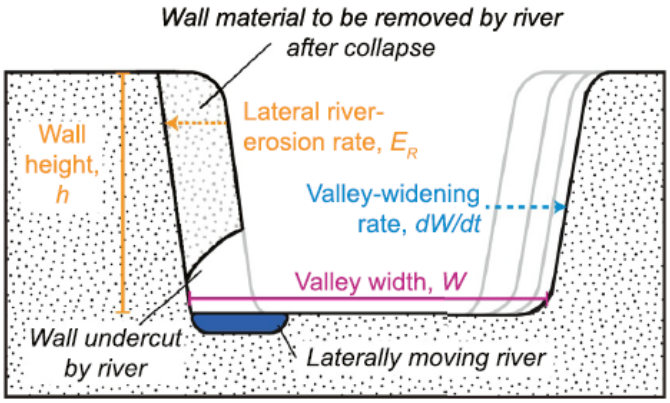

Figure 1.8. Cross-sectional view of valley bottom width. Rivers widen valleys by undercutting the adjacent wall, which triggers wall collapse and the formation of a sediment pile at the wall toe that protects the wall from further lateral erosion until the sediment pile is removed by the river (Tofelde et al., 2022).

To explore valley widening, Club et al. (2023) considers the ratio between the sediment supply (Qs) and the transport capacity (Qc), indicating when the ratio Qs/Qc is low, little sediment will be depositing in the valley bottom, resulting in bedrock incision, on the contrary, when the ration Qs/Qc is higher, thick sediment will deposit in the valley bottom resulting in subsequent valley widening (Figure 1.9). Tectonics controls uplift rates, Finnegan et al., (2005), demonstrated that non-uniform patterns of uplift can influence channel slope. Suggesting that faster flow in steeper channel results in channel occupying a smaller cross section. This implies that channel slope and therefore uplift should be a key control on valley bottom width.

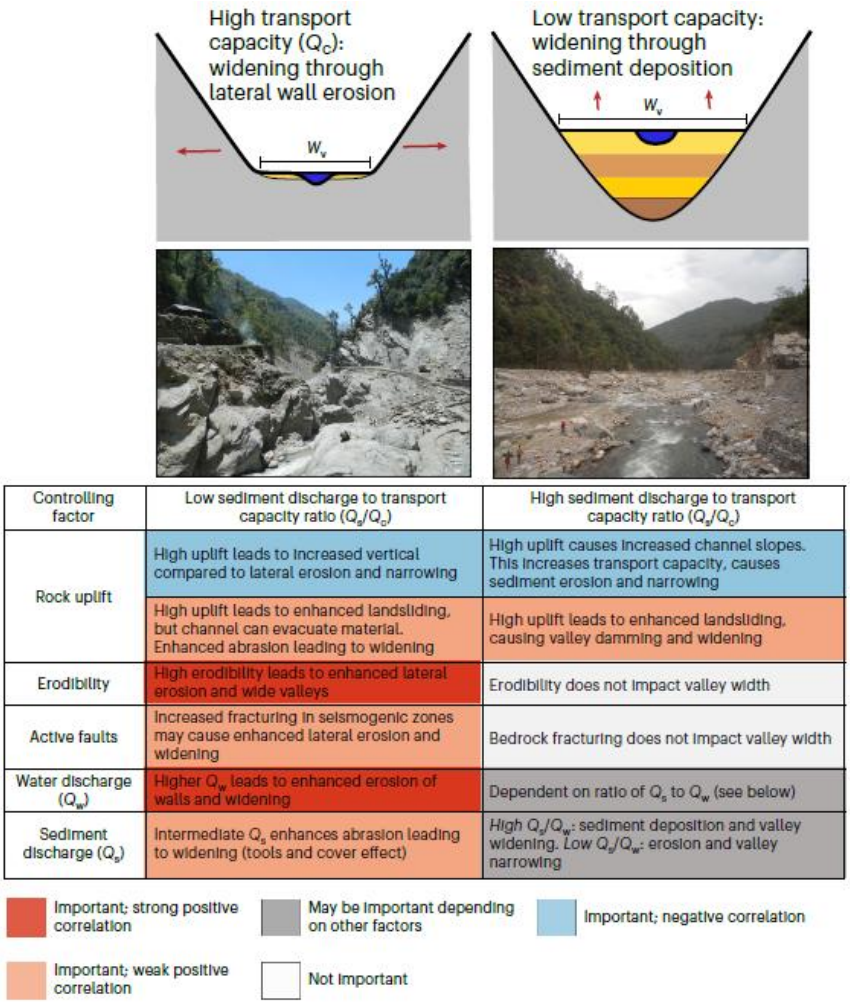

Controlling factor	Low sediment discharge to transport capacity ratio (Q_s/Q_c)	High sediment discharge to transport capacity ratio (Q_s/Q_c)
Rock uplift	High uplift leads to increased vertical compared to lateral erosion and narrowing	High uplift causes increased channel slopes. This increases transport capacity, causes sediment erosion and narrowing
	High uplift leads to enhanced landsliding, but channel can evacuate material. Enhanced abrasion leading to widening	High uplift leads to enhanced landsliding, causing valley damming and widening
Erodibility	High erodibility leads to enhanced lateral erosion and wide valleys	Erodibility does not impact valley width
Active faults	Increased fracturing in seismogenic zones may cause enhanced lateral erosion and widening	Bedrock fracturing does not impact valley width
Water discharge (Q_w)	Higher Q_w leads to enhanced erosion of walls and widening	Dependent on ratio of Q_s to Q_w (see below)
Sediment discharge (Q_s)	Intermediate Q_s enhances abrasion leading to widening (tools and cover effect)	*High* Q_s/Q_w: sediment deposition and valley widening. *Low* Q_s/Q_w: erosion and valley narrowing

Important; strong positive correlation
May be important depending on other factors
Important; negative correlation
Important; weak positive correlation
Not important

Figure 1.9. Conceptual model identifying the widening mechanism and the different factors that control valley width. Wv represents valley bottom width, Wc indicates transport capacity, Qw indicates water discharge and Qs represent the sediment supply (Clubb et al., 2023).

1.3.1.2 Internal factors

Recent studies have demonstrated that internal dynamics during phases of incision can lead to autogenic strath and fill-cut terrace abandonment (Malatesta et al., 2017). Alluvial river incision is frequently considered to be one-dimensional (Schumm, 1973; Leopold and Bull, 1979; Parker, 2015; Malatesta et al., 2017) and consequently, the effect of changes in valley width and lateral river migration are often ignored (Malatesta et al., 2017). Autogenic processes can modulate simple topography. For example, river terraces can be formed autogenically when meander bends self-intersect, forming meander cut-offs (Figure 1.10, Sheingross et al., 2020).

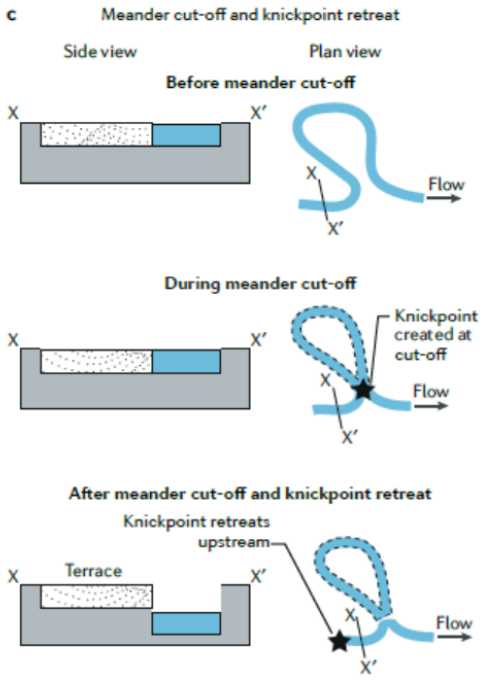

Figure 1.10. Cross-section and plan views demonstrate how meander cut-off results in autogenic knickpoint and terrace formation (Sheingross et al., 2020).

1.4 Fluvial terraces morphologies

When river continues to incise their valley bottom, alluvial deposits or bedrock channel bottoms can be abandoned above the river, forming a fluvial terrace which records the past river dynamics and an ancient steady state of level of stream. They can therefore be used to quantify spatial and/or temporal changes in rates of vertical incision and lateral erosion of the river (Burbank and Anderson, 2012; Malatesta et al., 2017). Fluvial terraces are considered as a near-flat surface flanking river, but their types vary depending on their genesis or according to their transversal organization:

- ***strath or stepped terraces*** present a succession of layers cut into the bedrock where the oldest terrace level occupies the highest topographic position (Bull, 1991; Pazzaglia, 2013). When incision phases are not long or strong enough, the substratum is not reached (Figure 1.11-a)
- ***nested terraces*** are developed in the materials of one or more older fluvial layers. Younger terraces embedded in older ones (Burbank et al., 1996) are the result of a first stage of channel filling and then a second stage of incision and deposition, few, or long time after the first stage (Figure 1.11-b).

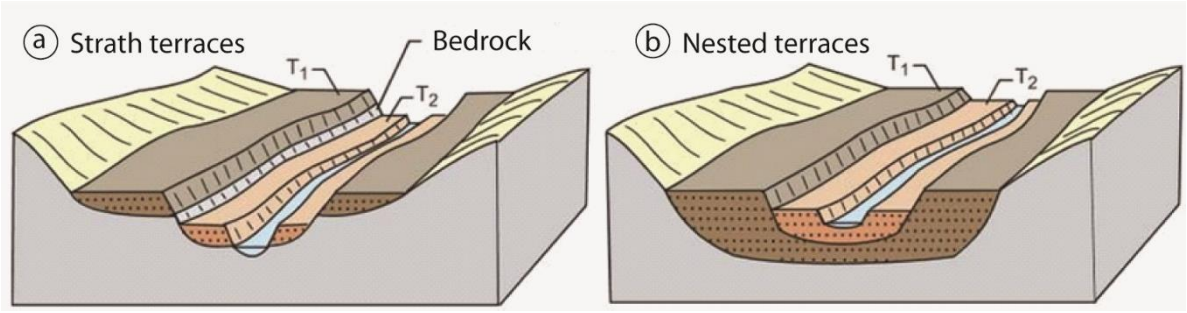

Figure 1.11. (a) Strath terraces. (b) Nested terraces (Peycru et al., 2019).

- ***Paired and unpaired terraces*** (Figure 1.12), terraces are paired when the same elevation on opposite sides of a stream. They occur when it downcuts evenly both sides and terraces on one side of the river correspond in height with those on the other side. Unpaired terraces, occur when a stream encounters materials on one side that resist erosion, leaving a single terrace with no corresponding terrace on the resistant side (Pazzaglia, 2013).

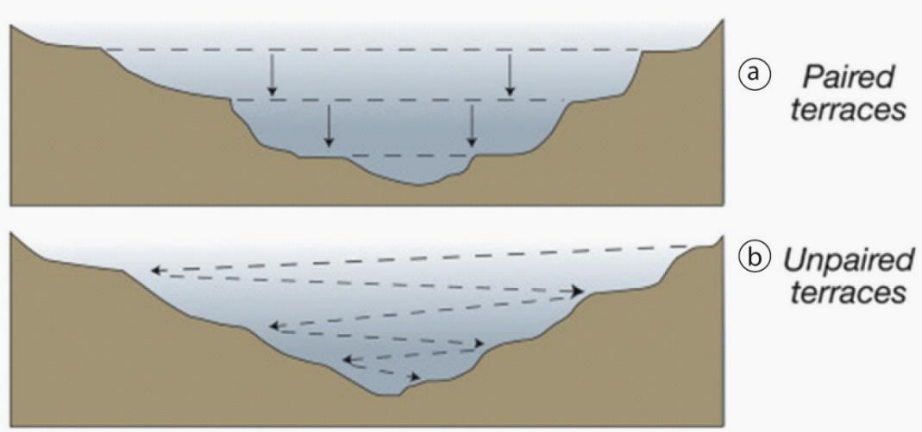

Figure 1.12. (a) Paired Terraces. (b) Unpaired terraces (Burbank and Anderson, 2012).

1.5 Climatic control during the Cenozoic era with focus on the Quaternary system

Climates plays a significant role as an external factor of fluvial dynamics. Extensive research has been conducted on the adaptation of rivers to the overall climate during the Cenozoic era (Mol et al., 2000; Vandenberghe et al., 2001; Pillans and Naish, 2004).

Global climatic variations over the past 65 Ma have mainly been reconstructed using oxygen isotope ratios preserved shells of marine organisms (e.g. foraminifera and coccoliths) and in glacial ice for the most recent periods (Zachos et al., 2008; Campisano, 2012; Pillans and Gibbard, 2012).

1.5.1 Climate variations during the Cenozoic era and the Quaternary system

The Cenozoic era was characterized by i) a warm period from the Paleocene to the lower Eocene and ii) a long-term cooling period from the lower Eocene to the present, interrupted by rapid and strong warming events (Zachos et al., 2008). The three most important global and short warming periods are the Paleocene–Eocene Thermal Maximum (c.a. 55 Ma, PETM), the Middle Eocene Climatic Optimum (c.a. 40 Ma, MECO), and the Middle Miocene Climatic Optimum (c.a. 14 Ma, MMCO). They are related to perturbation of the carbon cycle (Miller et al., 1987; Zachos et al., 2008; Huyghe, 2010; Briais, 2015). Conversely, some rapid events enhanced the cooling trend, such as i) the Oi-1 event at the Eocene–Oligocene boundary (c.a. 34 Ma) which coincided with the formation of the first permanent ice sheet on Antarctica (Tasman and Drake passage opening) and ii) the Plio-Pleistocene cooling, corresponding to the first permanent Northern Hemisphere ice sheets attributed to the closure of Central America detroit (Figure 1.13, Zachos et al., 2008).

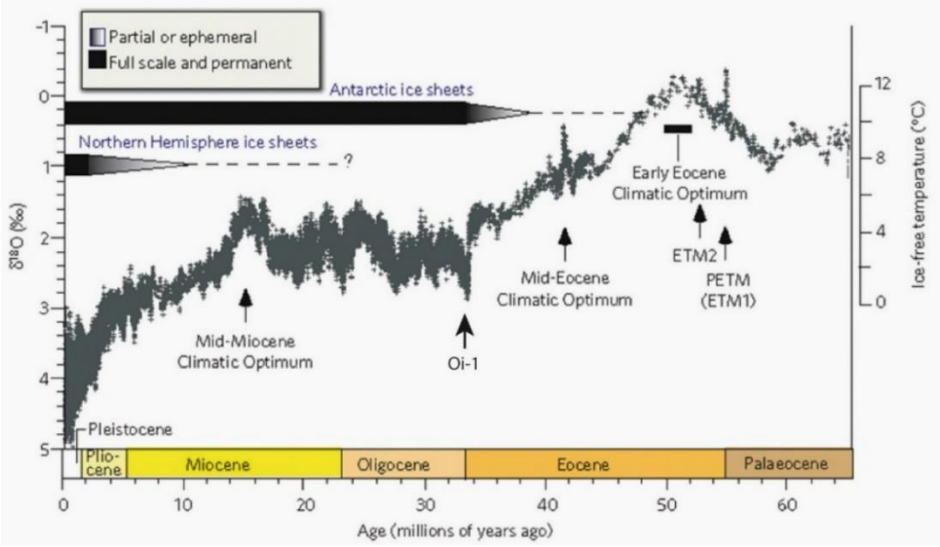

Figure 1.13. Evolution of the global climate over the past 65 Ma. The climate curve is a stacked deep-sea benthic foraminiferal oxygen-isotope curve based on records from deep sea drilling project and ocean drilling project sites. PETM: Paleocene-Eocene Thermal Maximum (also known as Eocene Thermal Maximum 1, ETM1); ETM2: Eocene Thermal Maximum 2 (also known as ELMO) (Zachos, 2008).

The Plio-Pleistocene limit (2.595 Ma, Gauss-Matuyama paleomagnetic transition) represents a main climate transition with the establishment of glacial-interglacial cycles typical of the Quaternary. This short era characterized extremely by rapid and cyclical climatic variations and

has been divided into two epochs: the Pleistocene between 2.595 Ma to 11.7 ka B.P and the Holocene since about 11.7 ka B.P and the present day (Zachos et al., 2008; Campisano, 2012; Pillans and Gibbard, 2012). Over the Pleistocene, two climatic cyclicities have been identified: the Milankovitch cycles on long timescales and the Bond cycles (Heinrich and Dansgaard-Oeschger events) operating on short timescales.

Milankovitch cycles are explained by astronomical variations and depend on the Earth's orbit which changes regularly over time. Changes in the Earth's orbit alter the pattern of solar radiation received by the Earth. There are three different parameters, acting on different timescales in which the Earth's orbit varies:

1) ***Eccentricity*** variations of the Earth's orbit around the sun, which is either circular or elliptical, characterized by two main periods over which this change occurs, one takes around 100 ka, and another takes around 400 ka. The eccentricity implies different seasonal variations between the Earth's hemispheric poles (Figure 1.14-a).
2) ***Obliquity*** variations of the Earth's rotation axis with the ecliptic plane formed an angle about 23.5 degrees which changes over time, varying between 22.1 and 24.5 degrees. It takes about 41 ka to change from one extreme to another (Figure 1.14-b).
3) ***Precession*** of the equinoxes variations which has a periodicity of about 20 ka. The gravitational attraction by the sun and the moon causes the Earth to oscillate on its axis. This axis describes a circle in space and indirectly determines a seasonal variation according to the proximity to the sun (Figure 1.14-c).

Combining the effects of the eccentricity, obliquity and precession parameters acting on four timescales (400 ka, 100 ka, 41 ka and 20 ka) provides the record of the oscillations in the intensity of solar radiation received by the Earth that control climate on a geological timescale (Figure 1.14, Maslin and Ridgwell, 2005). It is the preponderance of one orbital parameter over the others that varies the cycle period, but all parameters are always exercised simultaneously, since the beginning of Earth history.

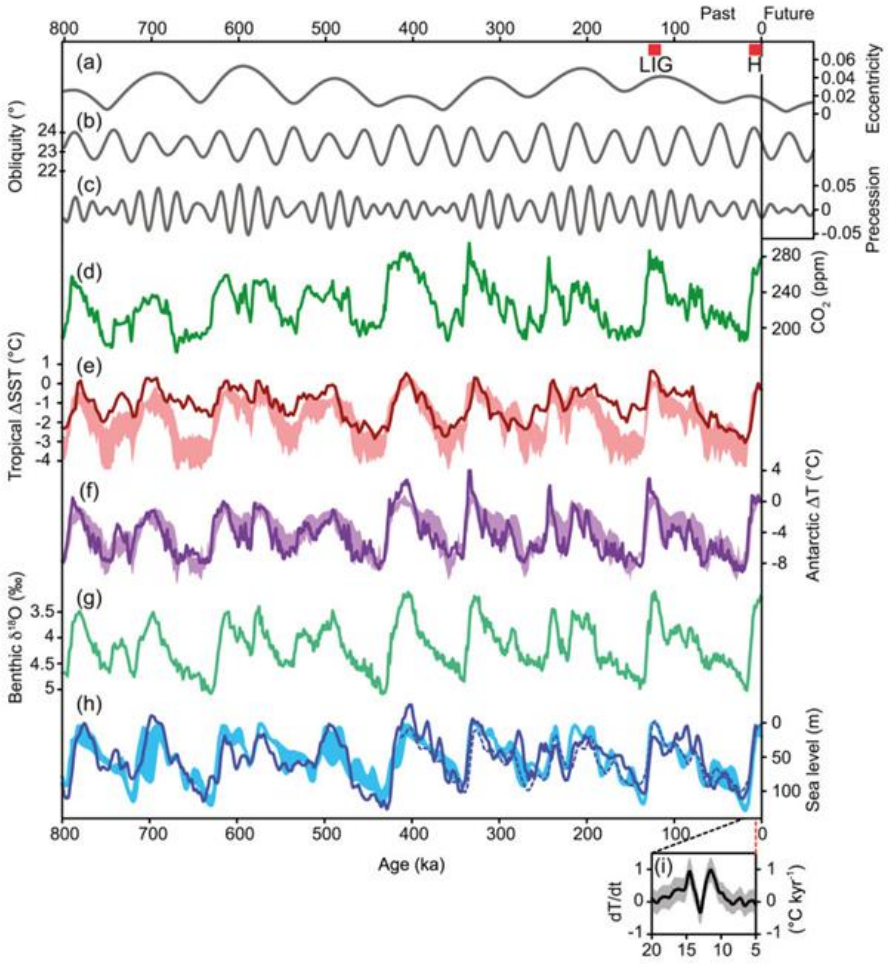

Figure 1.14. Orbital parameters governing the Milankovitch cycles over the past 800 ka. (a) Eccentricity. (b) Obliquity. (c) Precessional parameter (Berger and Loutre, 1991). (d) Atmospheric concentration of CO2 from Antarctic ice cores. (e) Tropical sea surface temperature stack. (f) Antarctic temperature stack based on up to seven different ice cores. (g) Stack of benthic δ18O, a proxy for global ice volume and deep-ocean temperature. (h) Reconstructed global sea level. Lines represent orbital forcing and proxy records, shaded areas represent the range of simulations with climate models. (i) Rate of changes of global mean temperature during Termination I. LIG: Last InterGlacial, H: Holocene Climatic optimum (Masson-Delmotte et al., 2013).

During the Quaternary, the distribution of continental mases since 2.6 Ma, which influence oceanic and atmospheric circulations (drake passage and Tasmania opened around 34 Ma; thermal isolation of Antartica by the circum-Antartic; Isthmus of Panama closed around 3 Ma; separation of Atlantic and Pacific waters) (Pillans and Gibbard, 2012). The distribution of the land surface shows a significant imbalance between the northern and southern hemispheres. The presence of large land masses in the north, which are sensitive to climate variations, easily frozen and therefore where albedo variations can be both large and rapid, means that what

happens in the north will condition the global climate. This particular disposition of the continents will favor a chronic instability of the climate and the establishment of an alternation of hot and cold periods that will affect the entire planet, recording these Milankovitch cycles in the form of glacial/interglacial cycles.

1.5.1.1 Variation in the duration of IG/G cycles in the Quaternary

During the Quaternary, three periods with different glacial (G) and interglacial (IG) phase durations could be highlighted. The ***Plio-Pleistocene transition***, corresponding to the evolution of glacial-interglacial cycles passing from a cyclicity of ~ 20 ka to ~ 40 ka. During ***Middle Pleistocene Revolution (MPR)***, between 1.2 Ma and 0.7 Ma, representing a transition between warm and cold periods and when glacial-interglacial cycles evolved from a cyclicity of ~ 40 ka to ~ 100 ka. ***Post-800 ka***, glacial-interglacial cycles occurred with a frequency of 100 ka and tis change may be attributed to a decreasing in the pCO_2 (Clark et al., 2006; Maslin et al., 2009; Yan et al., 2022) or a long glaciation period followed by a short deglaciation (Ridgwell et al., 1999). However, the absence of frequencies corresponding to the earth's precession of the rotation axis at 19 and 23 ka is still not clear (Yan et al.,2022).

1.5.1.2 Abrupt events

The long period climate modulations previously described are further influenced by i) brief expressions of the most extreme glacial conditions called Heinrich events or by ii) rapid warming phases known as Dansgaard-Oeschger oscillations. Heinrich events occurred on average every 7200 year within the time interval between 70 and 10.5 ka. Between Heinrich events, Dansgaard-Oeschger oscillations induce abrupt warmings followed by gradual cooling that occurred every 1479 ± 532 year. These warming phases are known as Dansgaard-Oeschger oscillations and seem to persist ointo the Holocene interglacial period (called Bon evets)(Figure 1.15, Dansgaard et al., 1993; Bond et al., 1999; Schulz, 2002; Maslin et al., 2009; Mogensen, 2009; Petersen et al., 2012).

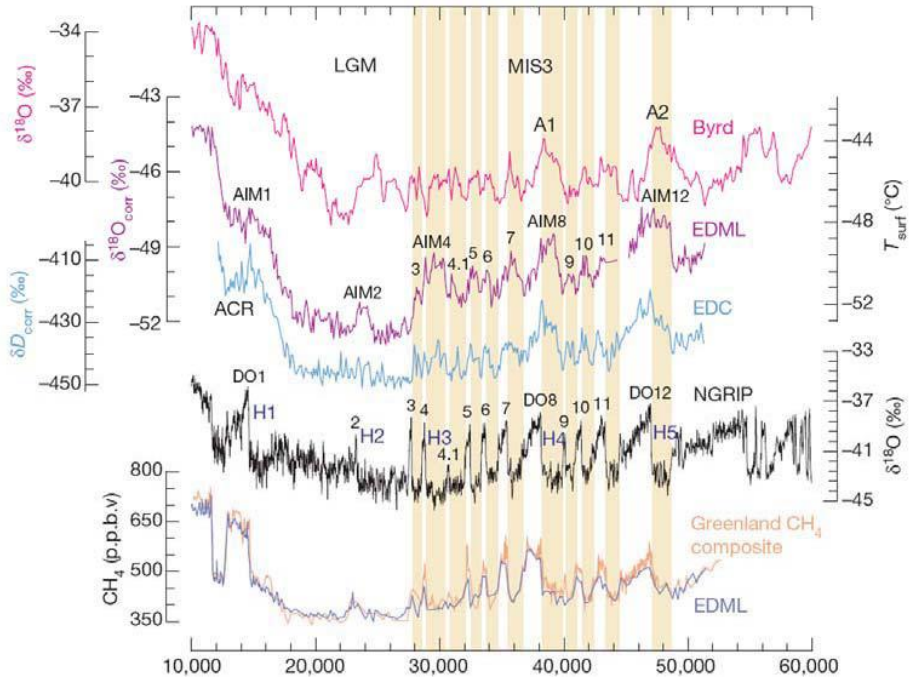

Figure 1.15. Correlation of climate variability recorded during the last glacial period ice ages in the Antarctic (EDML, EDC and Byrd) and Greenland (NGRIP) ice cores (EPICA, 2006). Greenland ice cores (NGRIP) (EPICA, 2006). The Dansgaard-Oeschger (D/O) interstadials are numbered from 1 to 12 on the NGRIP isotope curve. The (cold) stages are interspersed between the interstages. Heinrich events (H1 to H5) precede the most marked interstadials. The yellow bands highlight the simultaneity of the D/O stages in Greenland with significant warming in Antarctica (Toucanne, 2008).

1.5.2 Records of climate changes and paleogeography during the Middle and Late Pleistocene northwest Europe

The Middle and Late Pleistocene were periods characterized by important climate variations accompanied by significant variations in global sea level and can be characterized using Marine Isotopic Stages (MIS) that describe climate variations from oxygen isotopes data (Ehlers, 1990; Toucane et al., 2009). Within the Middle Pleistocene two major glaciations occurred, during MIS 12 and MIS 10-6, named respectively the Elsterian and the Saalian glaciations in Northwestern Europe (Figure 1.16). In this area, the most well-known glaciation during Late Pleistocene is during the MIS 4-2 and called the Weichselian glaciation (Figure 1.16, Kukla et al., 2002; Elhers and Gibbard, 2004; Lauer and Weiss 2018).

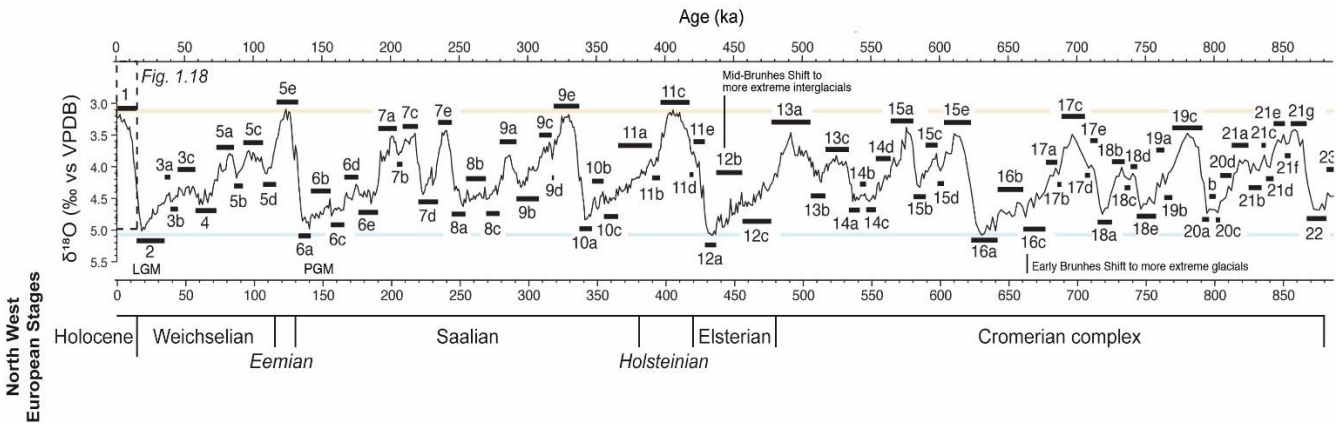

Figure 1.16. Marine Isotopic Stage (MIS) over the last 800 ka. LMG: Last Glacial Maximum; PGM: Penultimate Glacial Maximum. Yellow line representing the minimum and blue line the maximum values in $\delta^{18}O$ (Railsback et al., 2015).

An overview of these glaciations, which strongly modified the flow dynamics of central European rivers (Gibbard, 1995; Busschers et al., 2008) is presented below:

- The ***Elsterian glaciation*** is the most important of all Pleistocene glaciations and occurred between 460 ka and 420 ka. During this period, the British-Irish Ice Sheet (BIIS) and the Fennoscandinavian Ice Sheet (FIS) extended as far south as the southern part of England and also covered portions of the Netherlands, Germany, and Poland (Figure 1.17, Lericolais, 1997; Böse et al, 2012). Numerous studies have shown that the North Sea fluvial systems merged in the English Channel with those of the Somme, Seine, Solent and numerous smaller French and British rivers to form the 'Fleuve Manche' paleoriver. It is considered to be one of the largest systems that drained the European continent and flowed into the Atlantic Ocean (Lericolais et al., 2003; Ehlers et al., 2004; Toucane, et al., 2009). In France, glaciers extended over a large part of the Alps, the Pyrenees, the Massif Central and the Vosges (Antoine et al, 2000; Lautridou et al., 1999). The Elsterian glaciation is often correlated with the MIS 12 (Bowen, 1999; Gibbard and Cohen, 2008).
- The ***Saalian glaciation*** is the second most important after the Elsterian glaciation. It occurs between 238 ka and 128 ka, between the Holsteinian and the Emian interglacials (Figure 1.17, Busschers et al., 2008). This glaciation is conventionally divided into a primary advance phase corresponding to the Older Saalian glaciation in Germany (Ehlers, 1990; Ehlers et al., 2004) or Drenthe glaciation in the Netherlands correlated with the MIS 10-8 (Figure 1.17, Zagwijin, 1973). It ois followed by a second more smaller ice advance corresponding to the Younger Saalian or Warthe glaciation, corelated with the MIS 6 (Figure

1.17). In Europe, during the older Saalian glaciation (Drenthe advance) the Fennoscandian Ice Sheet (FIS) reached its maximum extend in the central Netherlands, Germany, Great Britain, and the Russian Plain. The extension of the FIS forced the Rhine River to flow towards the English Channel (Figure 1.17, Lericolais, 1997; Elhers and Gibbard, 2004). In contrast, the younger Saalian glaciation (Warthe advance) was less extensive but thais may have been offset by ice expansion in Russia and Siberia (Figure 1.17, Hughes and Gibbard, 2018). The Saalian glaciation is often correlated with the Marine Isotopic Stage MIS 10, 8 and 6 and has to be noted that the Drenthe and Warthe glaciations/advances represent two advances of an ice sheet without ice free periods in between (Gibbard and Cohen, 2008).

- The ***Weichselian glaciation*** is the last known glaciation in Europe, occuring after the Eemian interglacial between 116 ka and 12 ka and is correlated with the MIS 4 and 2 (Figure 1.17, Hughes and Gibbard, 2018). The ice sheet covering the northern Europe was divided into two parts, one over the British Isles and the other over the Scandinavia. Bradwell et al., 2008, suggest that the British and the Scandinavian ice sheets became isolated and that the coldest phase occurred around 25 ka. In northwestern Europe the loes redord is synchronous with this period (Lautridou et al., 1999; Antoine et al., 2007). During this glaciation, the English Channel continued to drain the Rhine, Thames, Somme, and Seine rivers as a result of the global sea level fall (Lasberg, 2014; Gibbard and Cohen, 2015). From 20 ka, the entire ensemble of European glaciers experienced a significant retreat, marking the beginning of the deglaciation phase (Eyles and McCabe, 1989). This glaciation ended with a late-glacial warming that marks the beginning of the Holocene period (Figure 1.17).

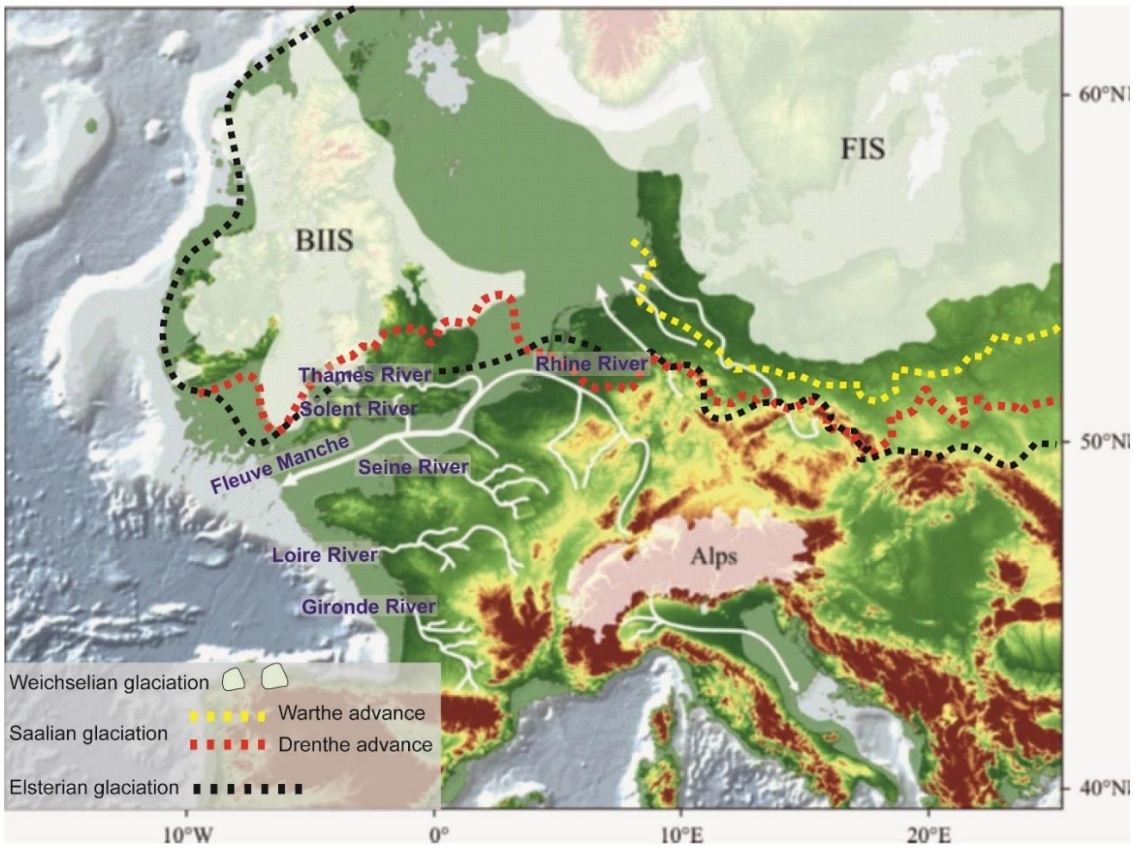

Figure 1.17. Map of NW Europe showing the glacial limits of the British-Irish Ice Sheet (BIIS), Fennoscandian Ice Sheet (FIS) and the Alps Glaciers for: the Late Weichselian (MIS 2 - white shaded area), the Saalian (Drenthe advance=dotted red line; Warthe advance = dotted yellow line)(Ehlers and Gibbard, 2004), and the Elsterian glaciation dotted black line. The white arrows identify the main European rivers (modified after Elhers et al., 2004 in Antoine et al., 2009).

Several interglacial periods are identified between the glacial periods herebefore described. The most representative and well identified ones are the Holstenian and the Eemian interglacials which probably represent the most similar climates to the present-day and Holocene warm interglacial climate (Penaud et al., 2008).

- The ***Holsteinian interglacial*** (MIS 11, from 423 ka to 362 ka), is considered as the most prolonged and warmer known interglacial and was considered as the better analogue for MIS 1 by some authors (Figure 1.16, Zazo, 1999; Penaud et al., 2008; Koutsodendris et al., 2010).
- The ***Eemian interglacial*** (MIS 5e, from 130 ka to 115 ka), represent a warm and humid stage, allowing the expansion of forest vegetation than today (Ehlers et al., 2007; Penaud et al., 2008). Global sea level reached elevations of +3 to +6 m than the present (Figure 1.16, Penaud et al., 2008).

1.5.3 Records of climate changes during the Lateglacial and the Holocene period

The Lateglacial period (from 13 ka to 10 ka) marks the transition between the cold Weichselian and the warmer Holocene (Hoek, 1997). During the Lateglacial and Early Holocene at least two episodes of climatic cooling have occurred since the major climatic melioration of 13000 B.P. These cooling events are characteristics of the Middle and Younger Dryas (MIS 1). The most pronounced climatic cooling is recorded in the Younger Dryas starting at ca. 11000 B.P (Figure 1.18 and Table 1.1, Van Geel et al., 1988; Hoek, 1997).

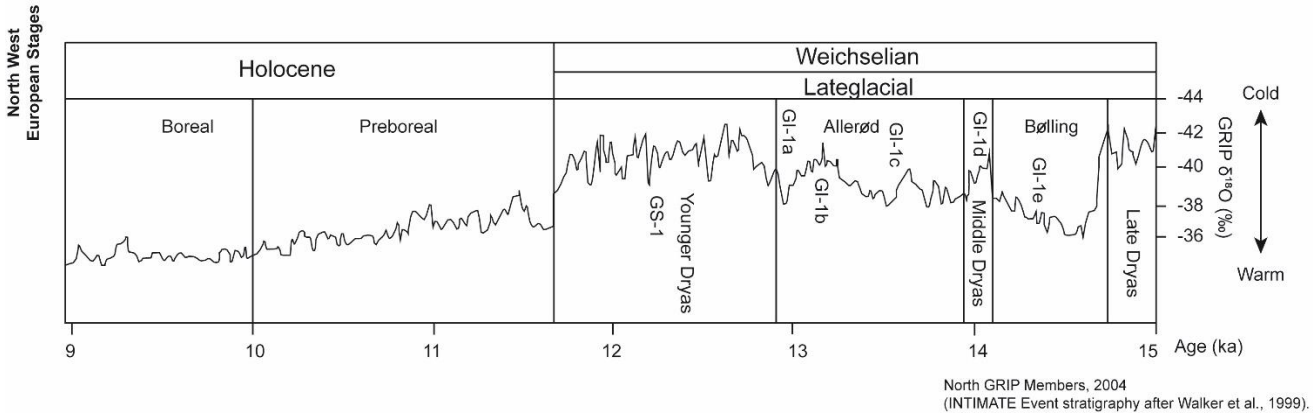

Figure 1.18. Lateglacial and Holocene climatic periods (modified after Limondin-Lozouet, 2011).

During the Holocene (10 000 B.P to the present), many extensive paleoclimatic studies have testified the considerable climate fluctuations in the Holocene. Dergachev et al., 2007, have identified four periods of significative climate change during the time periods (Table 1.1):

- The ***Boreal period***, is considered to be the strongest Holocene cooling episode, known as the '8200-yr cold event' (Alley et al., 1997). This event was characterized by a cold and wet climate in Europe, with extreme weather events such as floods, landslides, and avalanches. This abrupt change may be due a change in the thermohaline circulation (Dergachev et al., 2007).
- After a period of climate improvement, during the ***Atlantic period***, there is evidence for a moisture conditions climate around 5600 and 5300 cal. B.P during the ***Late Atlantic period***. The climate became wetter, as evidenced by variations in seasonal hydrological regimes on the Constance Lake (Switzerland, Germany and Austria) and Jura mountains lakes. Their similarities can serve as a crucial factor when considering the possible impact of climate change on environments (Magny et al., 2006).

- The ***Subatlantic period***, is characterized by a marked climate change between 2800 and 2500 cal. B.P. During this time the climate in northwestern Europe became wetter and colder (Dergachev et al., 2007).
- During the ***younger Subatlantic period***, between 1300 and 1860 A.D., changes in the Holocene climate may have affected human populations during the cold events, as during the Little Ice Age (Le Roy Ladurie, 1967). During the Little Ice Age, the extensive areas around the Europe and the North Atlantic experienced unusually cold and wet conditions, as well as many extreme weather events similar to the '8200-yr cold event', including floods, landslides, and avalanches (Le Roy Ladurie 1967; Grove 2002). Three phases of maximum degradation have been identified: from 1300 to 1380, from 1560 to 1600 and from 1815 to 1860 A.D. and are associated with advances of the glaciers. The Atlantic ice cap expanded, summers became significantly colder, precipitation increased, and mountain glaciers advanced (Le Roy Ladurie, 1967).

Table 1.1. Lateglacial and Holocene climatic periods (modified after Argant and Phillippe., 2011).

Biostratigraphy zones		Calibrated ages beginning cal. B.P	Calibrated ages end cal. B.P
Holocene	Subatlantic	2835	0
	Subboreal	5450	2835
	Late Atlantic	6850	5450
	Early Atlantic	8835	6850
	Boreal	10085	8835
	Preboreal	11490	10085
Lateglacial	Younger Dryas	12710	11490
	Allerød	13600	12710
	Middle Dryas	13900	13600
	Bølling	15075	13900
	Late Dryas	18270	15075

1.5.4 Hydrological dynamic and terrace formation within a glacial-interglacial cycle

Climatic variations are one of the main drivers of the fluvial terrace formation and are often associated to glacial-interglacial cycles during the Quaternary. The terrace formation in response to climatic variations has therefor been proposed (Bourdier 1969; Bridgland, 2000, 2006; Antoine et al., 2000, 2007; Bridgland and Westaway, 2008). There, fluvial incisions are associated with the glacial-interglacial transitions. Terraces often partially record channel

deposition, vertical/lateral erosion over millennia (Finnegan et al., 2014). The model of terrace formation in response to climatic forcing could be divided in five phases (Figure 1.19, Bourdier 1969; Despriée et al., 2017):

- ***Phase 1***: At the beginning of the cooling period, rivers incise their substrate. This incision is generated by an increase in the river discharge (i.e., increased runoff from the permanent permafrost and the limited root penetration of vegetation) and the low amount of sediments produced by erosion.
- ***Phase 2***: During the cooling period, the rivers transport and deposit large amount of sediments that contribute to the construction and the aggradation of the valley bottom. The main difference between the beginning and the end of the cooling phase correspond to highly effective cryoclastic processes that fragment rock mass, releasing large volumes of sediments at the end of the cooling phase.
- ***Phase 3***: At the end of the cooling period, precipitation gradually decreased during the glacial period, which stopped the incision of the river. On the sides of the valley, periglacial phenomena combined with the presence of permanently frozen ground at depth (permafrost) led to the addition of sediment to the bottom of the new valley. Deposits are initially coarse (slope deposits and alluvium), then increasingly fine (sand and gravel, then aeolian silts) as the cold intensify.
- ***Phase 4***: At the glacial-interglacial transition, there is an increase in precipitation, disappearance of the permafrost and stabilization of sediments by soil formation and vegetation development. This implies a reduction in amount of sediments contributing to the rivers, resulting in an incision characterized by a short duration.
- ***Phase 5***: During the interglacial period, the erosion is not sufficient for the river to maintain its equilibrium profile. The river channel changes to a meandering style that contributes to the reworking of the cold phase deposits by lateral migration.

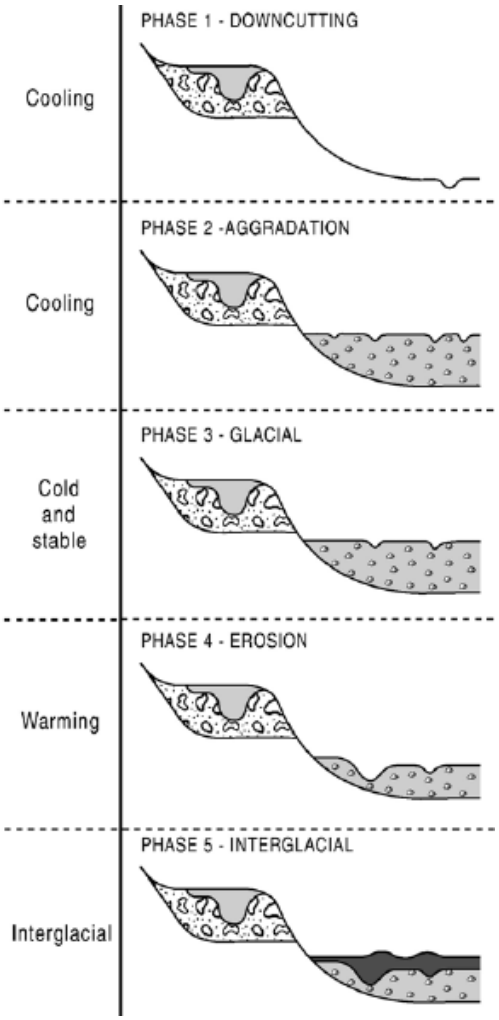

Figure 1.19. Model for terrace formation in response to climatic forcing (from Bridgland and Westaway, 2008).

The repetition of these different phases, and therefore the increasing lowering of the rivers due to incision, throughout the Quaternary period, leads to the creation of a system of strath terraces, with the oldest terraces being the highest with regards to the present-day river bed. In cases where the incision is not deep enough and/or the uplift is not significant enough, the terraces are no longer stepped but nested. The recurrence of this model explains the main formation of the fluvial system in north-western Europe like the Solent and Thames systems in England (Bridgland, 2000; Vanderberghe, 2008), the Meuse, the Creuse, the Somme system in France (Antoine et al., 2000, 2007; Despriée et al, 2011).

1.5.5 Hydrological dynamic during the Lateglacial and Holocene periods

Several studies have focused on the river system and valley bottom environments evolution in northwest Europe (i.e., the Seine catchment) during the Weichselian, Lateglacial and Holocene periods. Climatic evolution and associated change in vegetation, bank stability, sediment load and discharge are responsible for the rapid changes in river patterns (Vandenberghe, 1993; Pastre et al., 2002). These river systems and valley bottom environments evolution are summarized as follows (Figure 1.20, Table 1.1):

- The ***end of the Pleistocene*** is marked by an arid period associated with aeolian sedimentation and braided river development. At the beginning of the ***Bølling*** period, strong incisions of periglacial deposits occur accompanied by a transition from braided to meandering systems. These observations reflect the adaptation of fluvial dynamics to changes related to climate warming, especially the decrease in sediment supply due to landscape stabilization by vegetation development. Throughout the Bølling, loamy-peat deposits accumulate in the channels. The production and preservation of organic matter was favored by warm and more wet climatic conditions (Vandenberghe et al., 1994; Pastre et al., 2002). At the end of Bølling, during the cold episode of the Middle Dryas, an increase in detrital sediments induced the formation of a thin layer cover upon peat deposits.
- During the ***Allerød*** period, the sedimentary dynamic remains very similar to those of the Bølling. The deposits are partly eroded and then covered with limestone silts attributed to Late Dryas. This episode corresponds to a climatic deterioration reflecting the transition from the Allrød to the Early Holocene.
- The ***Holocene*** begins with the ***Preboreal*** period, in which the valley bottom is incised by a meandering single-channel system (Vandenberghe et al., 1994). This incision corresponds to a decrease in sediment deposition due to vegetation development (Pastre et al., 2014). Preboreal deposits are characterized by an increase in the organic fraction associated with a decrease in the detrital fraction, leading to channels infilling and the transition from a meandering to a single-channels course during the Boreal.
- The ***transition from the Boreal to the Atlantic*** is characterized by a re-incision of the riverbeds, which can lead to a partial or total hiatus of the Boreal or the Ancient Atlantic (Pastre et al., 2002).
- The beginning of the ***Subboreal*** shows an increase in fluvial activity and typical elements of a significant environmental change. The second half of the Subboreal is characterized by a

significant increase in detrital sedimentation, explained by an increase in precipitation (Magny, 1992; 2004). The beginning of the ***Subatlantic*** is characterized by a climatic deterioration, with high sedimentation rate in the valley bottom (Pastre et al., 2014).

The Holocene is clearly marked by fine sedimentation deposited by meandering systems, a context that contrasts with the Pleistocene where rivers adopt a braided style and transport gravels.

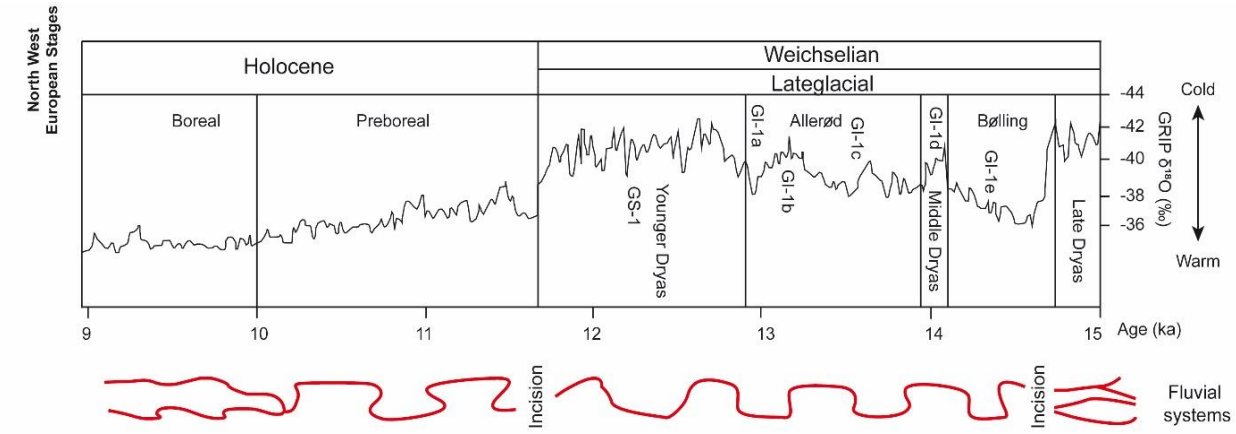

Figure 1.20. Main Lateglacial hydrological dynamics changes in valley bottom (modified after Pastre et al., 2002 and Limondin-Lozouet, 2011). Red line indicates the fluvial system.

1.6 Focus on the studied area: the Paris Basin

In Western Europe, glaciations such as the Elsterian, Saalian and Weichselian have strongly modified the flow dynamics of Central European rivers during glacial stages MIS 12, MIS 10, MIS 8, MIS 6, and MIS 4-2. These glaciations influence the formation of the alluvial terrace and has further implications, especially for in paleoclimate reconstructions. This section summarizes the literature on the Seine catchment and its relationship with the glacial-interglacial cycles.

1.6.1 Geological setting of the Paris Basin

The Paris Basin is one of the most studied basins in the world and is considered as a typical intra-cratonic sedimentary basin. It forms an oblong basin of about 650 km from east to west and 500 km from north to south which records sedimentary deposits since Lower Triassic times (Mégnien et al., 1980; Guillocheau et al., 2000; Briais et al., 2016). It is bounded by the

Ardennes, Morvan, Vosges, Massif Central and Armorican massifs mainly made up with cadomian to variscan basements. Major faults, such as the Seine-Sennely, Metz and Bray-Vittel fault, divide the basement into large structural blocks. These faults have affected the Paris Basin during different tectonic phases since the Permian and delimit the area of maximum sedimentation in the Paris Basin (André, 2003). During Mesozoic times, the basin was affected by subsidence, which stopped during the Paleogene, except in the Sologne area. During the Neogene, low-amplitude uplift was caused by the far-field Alpine compression (Guillocheau et al., 2000; Briais, 2015). Since the Plio-Quaternary period, landscapes have been shaped by repeated climatically induced cycles of global sea level, soil (un)freezing and river discharge changes (Antoine et al., 2000; Bridgland and Westaway, 2008).

River erosion led to the formation of a system of structural platform limited by cuestas corresponding to transitions between the main formations of the basin (Figure 1.21). Four main cuestas were formed identifying as Beauce, Brie, Soissonnais and Parisis. Finally, during the Middle and Late Pleistocene, in which the river network incised in response to a sea level fall and climate changes associated with glacial-interglacial cycles (Pomerol and Feugueur 1974).

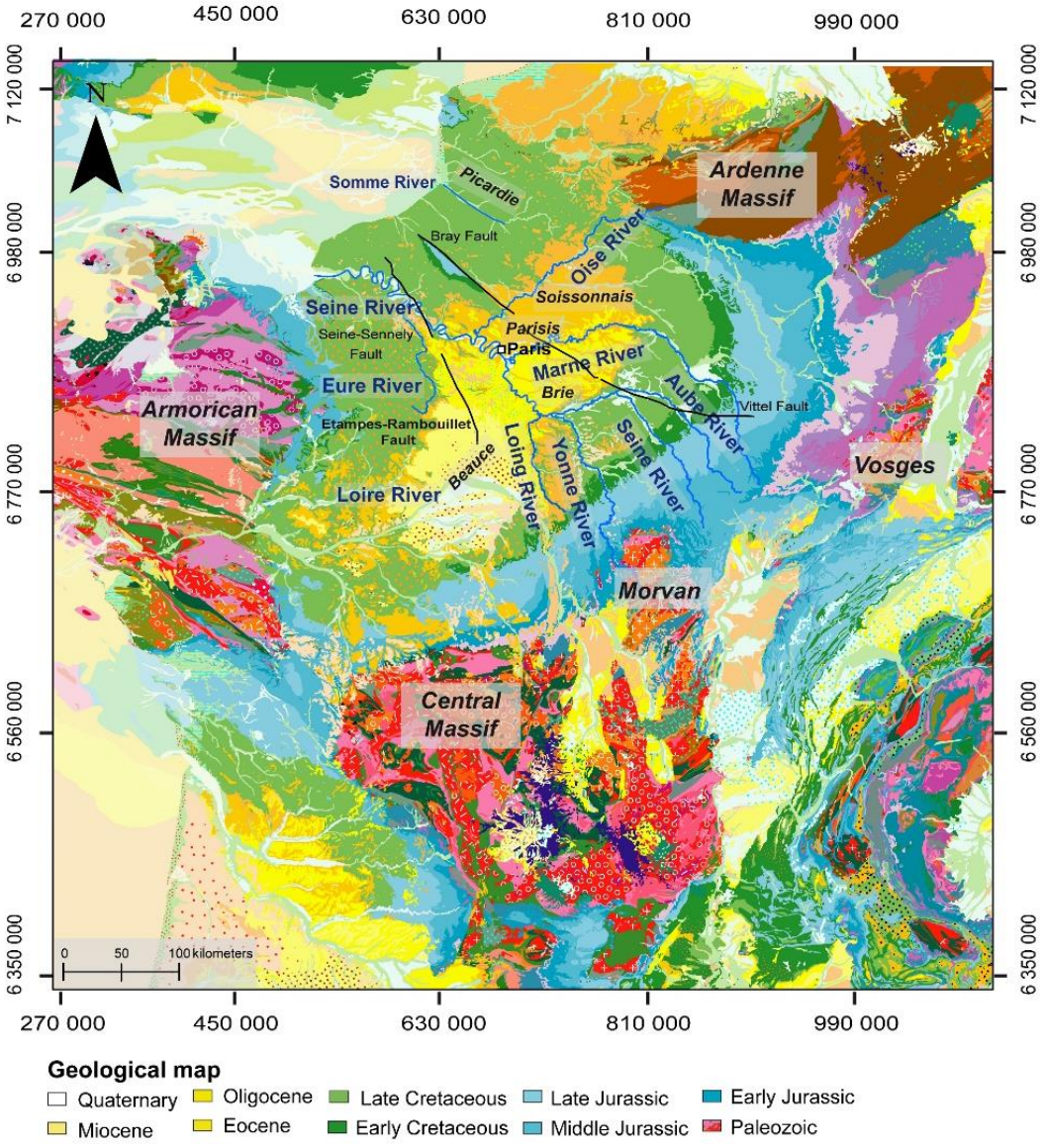

Figure 1.21. Geological map centered on Paris basin, modified from the 1: 1 000 000 geological map of France (BRGM).

This PhD thesis is focused on the Seine catchment and its evolution during the Late Quaternary period, more precisely on the erosion geometry and alluvial infill at the bottom of the Seine River and its major tributaries such as the Oise, Marne, Aube, Yonne, Loing, and Eure rivers (Figure 1.22), in relation to the terrace system. The Seine catchment drains the north-eastern part of the Paris Basin into the English Channel, with a catchment area of ~76 000 km^2. The bedrock is mainly Mesozoic (chalk, marls, limestone, sand) in the Upper Seine, Cenozoic (sand, clay, and limestone) in the Middle Seine and Mesozoic (Upper Cretaceous chalk) in the Lower Seine (Guillocheau et al., 2000; Mortimore, 2008; Nehme et al., 2020). Complex networks of

palaeovalleys highlight that the present-day Somme, Seine, and numerous smaller French rivers merged into the English Channel during the cold stages to form the 'Fleuve Manche' (English Channel) palaeoriver (Larsonneur et al., 1982; Lericolais, 1997; Toucane et al., 2009). Despite its importance,few studies have focused on the Seine catchment and its landscape evolution during the Middle and Late Pleistocene.

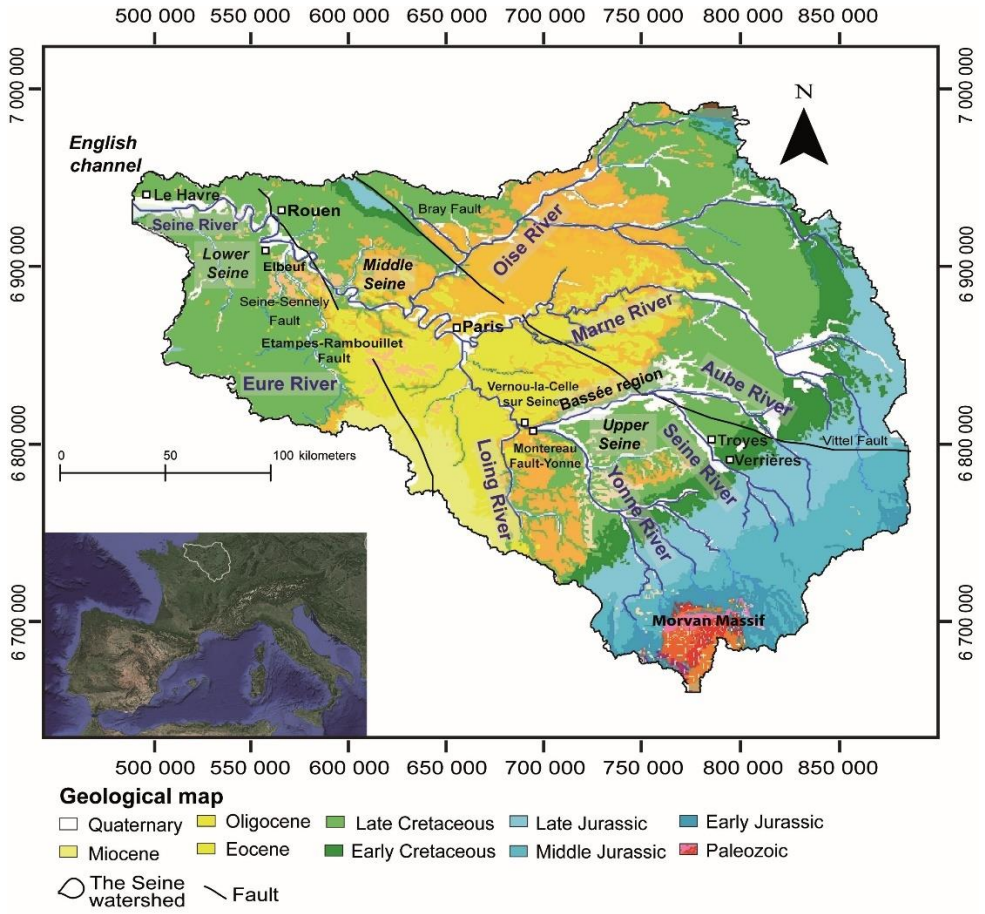

Figure 1.22. Geological map of the Seine catchment, modified from the 1: 1 000 000 geological map of France (BRGM).

1.6.2 Main characteristics of terraces system along the Paris basin example of Somme, Yonne, Aube and Marne valleys

Some detailed fluvial records in the Somme, Yonne, Aube and Marne valleys have been studied and compared with those from the Seine valley. Most of the sequences range from the Pleistocene to the Holocene. These sedimentary archives are related to fluvial activity and climate variations. One of the main differences between these rivers is their geomorphology. The Somme, the Yonne, the Aube and the Marne are straighter than the Seine River, which is

characterized by very large meanders. These rivers differ in terms of erodibility, number of terraces preserved against to tectonic uplift or climate changes (Chaussé, 2003; Antoine et al., 2007; Voinchet et al., 2015). In order to compare the elevation of the different terraces described in the literature, it is necessary to define the relative elevation above the maximum incision of the river (Relative Heigh; RH) or in some cases above the valley bottom of the Seine River (RH') (see Chapter 2 for further explanations). On this basis, a brief description of terrace systems is presented bellow for each valley.

1.6.2.1 The Somme valley

The Somme valley is located in the northern part of the Seine catchment (Figure 1.21). This valley is characterized by a well-developed terrace system in response to climatic variation over the last 1 Ma. This terrace system developed on a homogeneous Upper Cretaceous chalk bedrock (Antoine et al., 2007). Ten alluvial formations have been identified and dated , mainly using the ESR on fluvial quartz, U/Th, TL, and ^{14}C, showing that the terrace chronology follow the glacial-interglacial cycles, and suggesting that the incision started at 1 Ma at an average rate of 0.055-0.060 m/ka (Figure 1.23)(Bourdier, 1969; Lefebvre, 1994; Antoine et al., 1994; 2000; 2007).

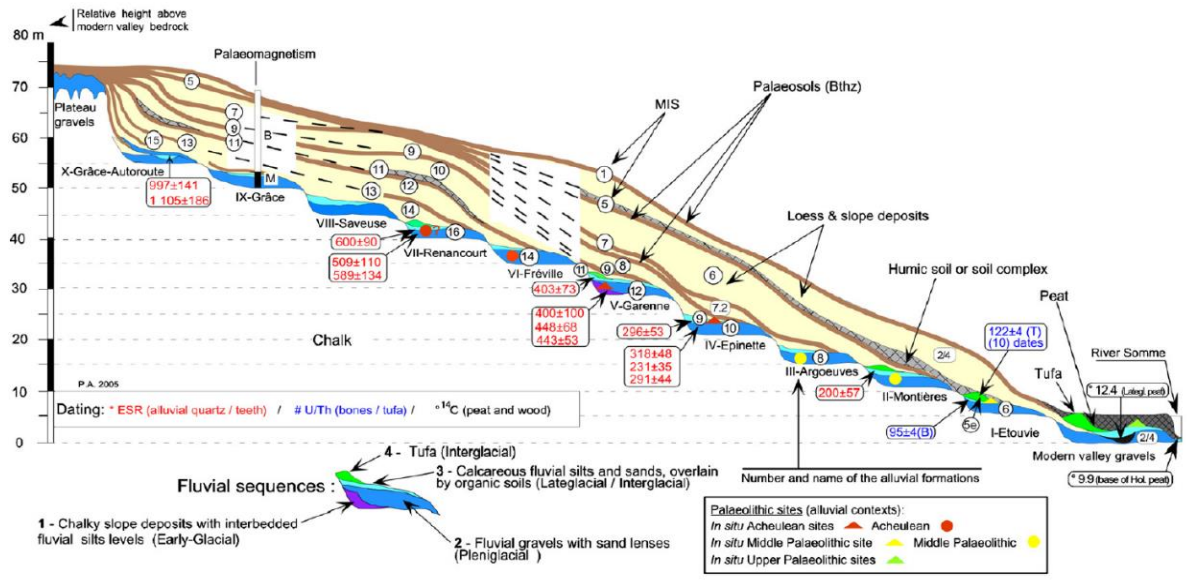

Figure 1.23. Synthetic cross-section through the middle Somme terrace system (Antoine et al., 2007).

1.6.2.2 The Yonne valley

The Yonne River is a left tributary of the Seine River, which flows from the Massif Central through the south-eastern part of the Paris Basin. The lower Yonne River, between Joigny and Montereau, incised the Upper Cretaceous chalk bedrock (Chaussé et al., 2004). The Yonne valley is characterized by twelve well-developed terrace system, dated by ESR on fluvial quartz and U/Th, showing that at each incision, the bedrock is covered by one alluvial formation indicating a glacial-interglacial succession (Figure 1.24)(Chaussé, 2003; Voinchet et al., 2004; Antoine et al., 2007).

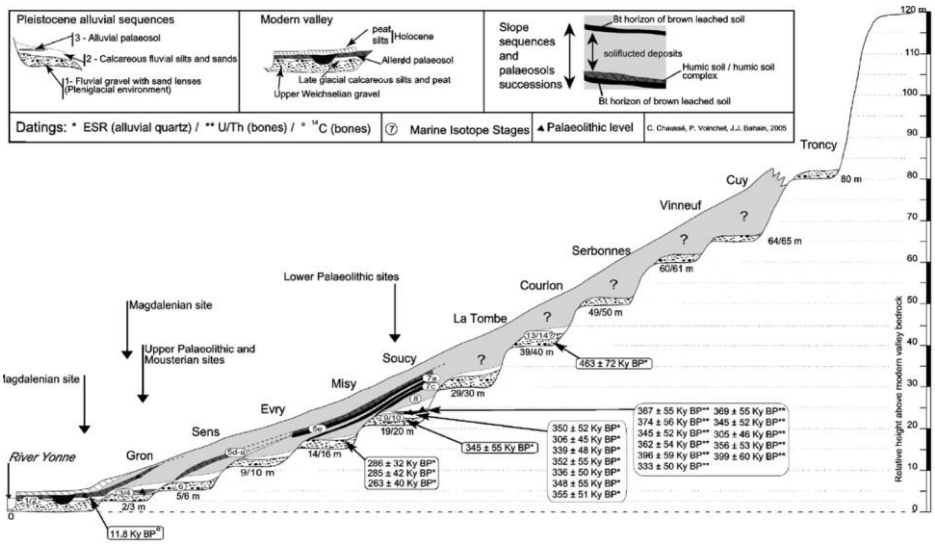

Figure 1.24. Synthetic cross-section through the lower Yonne terrace system (Antoine et al., 2007).

1.6.2.3 The Aube valley

The Aube River is a right tributary of the Seine River, which flows through the limestones and marls bedrock from the Jurassic and chalk bedrock from Upper Cretaceous. This valley is characterized by seven fluvial terraces, fewer that in the Somme and Yonne systems, due to significant erosion in chalky areas and no preservation of ancient terraces (Voinchet et al., 2015). These sequences have been dated by ESR on fluvial quartz, indicating that the terrace evolution follows the general model proposed for the Somme and Yonne rivers, in which each terrace is associated with a glacial-interglacial cycle (Figure 1.25)(Voinchet et al., 2015).

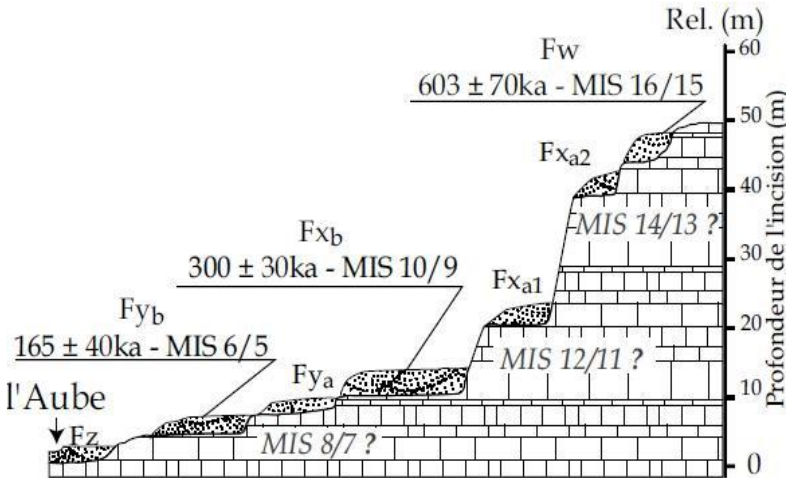

Figure 1.25. Synthetic profile of the Aube terrace system (Voinchet et al., 2015).

1.6.2.4 The Marne valley

The Marne River is a right bank tributary of the Seine River that flows through Cretaceous to Paleogene bedrock, formed mainly of limestone, sand, clay, marl, and chalk. The valley is characterized by a limited number of terraces. Only three alluvial terraces have been identified, at Maisons-Alfort (+ 9 m RH), Changis-sur-Marne (+ 6m RH) and Noisy-le-Grand (+3 m RH) (Figure 1.26). At Maisons-Alfort, near of the confluence with the Seine River, the alluvial terrace located at + 9 m RH has been dated, by U-Th on bones, between 162 and 206 ka corresponding to the end of the Middle Pleistocene (MIS 7- MIS 6) (Durbet et al., 1997; Blaser et al., 2021). At Changis-sur-Marne, the alluvial terrace located at + 6 m RH is characterized by predominantly sand and gravel sediments interdigitated with tuffs and fine sands. This terrace has been dated, by U-Th on travertine tuffs, ESR/U-Th on bones and OSL on fluvial quartz, ranging from 189 to 85 ka, corresponding to the Upper Saalian (MIS 6) and the early (MIS 5c) (Blaser et al., 2021). At Noisy-le-Grand, the + 3 m RH alluvial terrace has been dated by OSL at 50 ka (Vartanian, 2019). This terrace may correlate with the Gron terrasse in the Yonne valley (Chaussé, 2003).

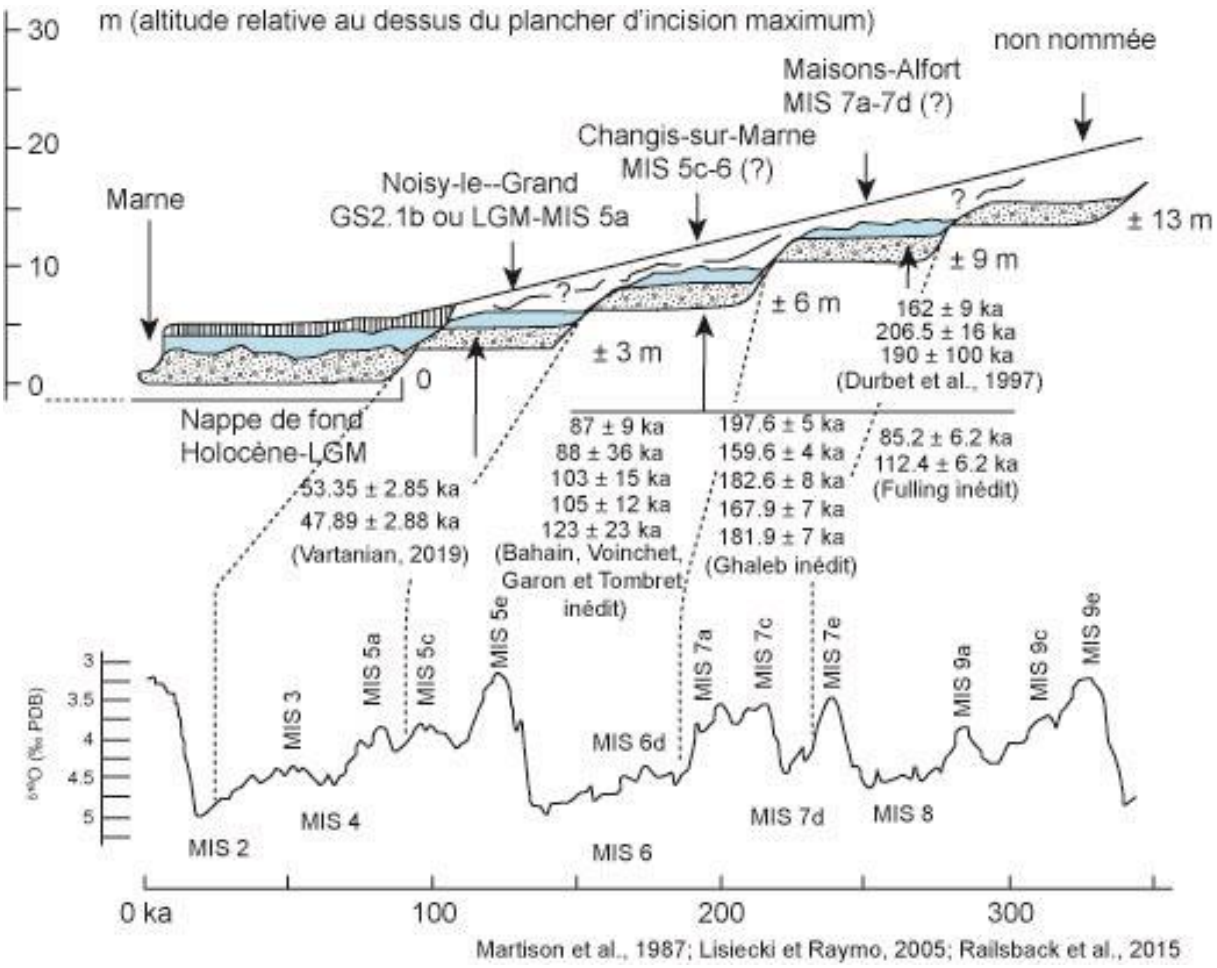

Figure 1.26. Alluvial terrace system in the Marne valley and synthesis of geochronological ages in these terraces (Blaser et al., 2021).

1.6.3 Main characteristics of the Seine terraces system from the lower Pleistocene to the Holocene

Along the Seine catchment, terraces system have been divided into three sections, taking into account the geomorphological considerations and the style of the Pleistocene fluvial record (Lefebvre et al., 1994; Antoine et al., 2007). The upper Seine valley from Troyes to Paris, the middle Seine valley from Paris to Elbeuf, and the lower Seine valley from Elbeuf to Le Havre (Figure 1.22).

1.6.4 The upper Seine valley (from Troyes to Paris).

The upper part of the Seine valley is comprise between Troyes and Paris, where three sites have been identified, including the Verrières site, the Bassée area, the Vernou-la-Celle-sur-Seine site, the Pincevent site and the Maisons-Alfort site (Figure 1.27). From its headwater to the confluence with the Marne River, the Seine River cuts into the Jurassic limestones, the lower Cretaceous sand, marl and clays, the upper Cretaceous chalk and the Cenozoic limestones. The slope of the longitudinal profile of the upper part of the Sein valley has been determined at 0,7 ‰ (Lautridou et al., 1999).

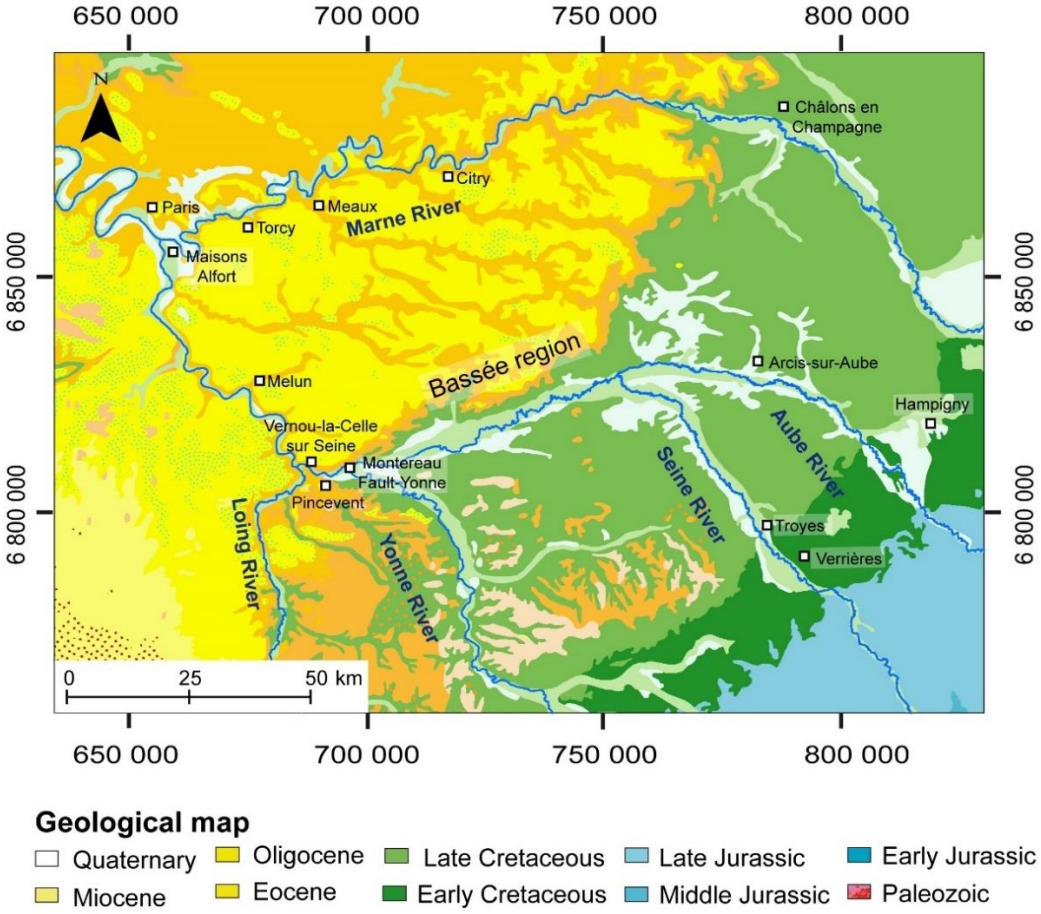

Figure 1.27. The upper part of the Seine valley, from Troyes to Paris and the Geological map at 1: 50000 scale.

1.6.4.1 Verrières site

Upstream of Troyes, at the Verrières site, a Weichselian alluvial plain covers the entire width of the present-day valley, where bedrock lithology consists of Lower Cretaceous marl (Figure 1.28, Krier, 1990 in Limondin-Lozouet and Rousseau, 1991). Archeological studies in the area,

based on malacological analyses, have shown several climatic phases during the Holocene period (Limondin-Lozouet and Rousseau, 1991).

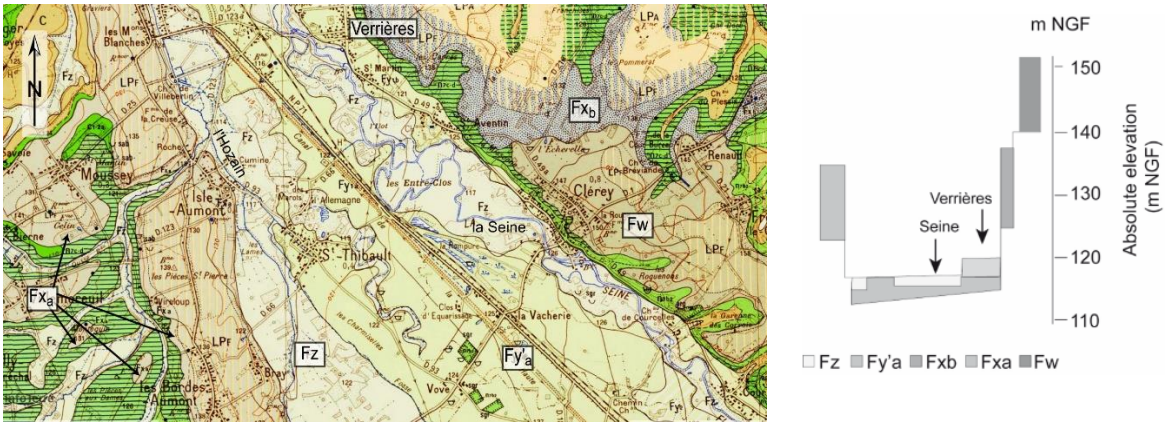

Figure 1.28. Map and stratigraphic diagram of the alluvial plain (modified after Krier, 1990 in Limondin-Lozouet and Rousseau, 1991.

1.6.4.2 Bassée area

The Bassée area is located between the confluences with the Aube river and the Yonne river, upon a bedrock formed by the Upper Cretaceous chalk (Figure 1.27). The terrace system is characterized by two units that has been observed for many years by Mégnien et al. (1965) and more recently by Antoine et al. (2007) and Deleplancque et al. (2018).

The first unit consists of four upper terraces located above the alluvial plain (terraces T_{IV} to T_I), while the second unit is composed of modern alluvial deposits forming two stepped terraces (T_1 and T_2 terraces) (Figure 1.29). These terraces build up the alluvial fill of the present alluvial plain and the nested fluvial sequence of T_{3a} and T_{3b} that reworked and dissected the T_1 or T_2 alluvial deposits (Deleplancque, 2016; Deleplancque et al., 2018). These terraces were correlated with those of the Yonne River (Voinchet et al., 2004; Antoine et al., 2007):

- T_{IV} (+49-54 m RH) would correspond to the Serbonne formation attributed to MIS 13.
- T_{III} (+18-24 m RH) would correspond to the La Tombe formation attributed to MIS 11.
- T_{II} (+14-16 m RH) would correspond to the Soucy formation attributed to MIS 10.
- T_I (+10-12 m RH) is considered equivalent to the Misy formation or Evry formation attributed to MIS 8 and MIS 7.
- T_1 (+3-4 m RH) are correlated with the Sens formation (+5 m relative RH) attributed to MIS 6 (assigned by stratigraphic correlation).

- T_2 (+0 m relative RH) is correlates with the Gron formation (+3 m relative RH) assigned to MIS 4-2.

Along the Bassée alluvial plain, Deleplancque et al., (2018) identified a knickpoint considering as marks as a regional transition in the hydrological processes (Figure 1.29). At Marolles-sur-Seine, sediments have been dated by ESR on fluvial quartz. Two sites were identified, the first one at Marolles Collerette alluvial deposits (+12 m RH, T_{II} terrace) are attributed at 361 ka, and the second at Marolles Moteux (+10-12 m RH, T_I terrace) deposits have been dated at 268 ka. The ages of alluvial deposits are stratigraphically consistent with that of the + 20 m alluvial deposits of La-Celle-sur-Seine (Figure 1.29, Deleplancque et al., 2018).

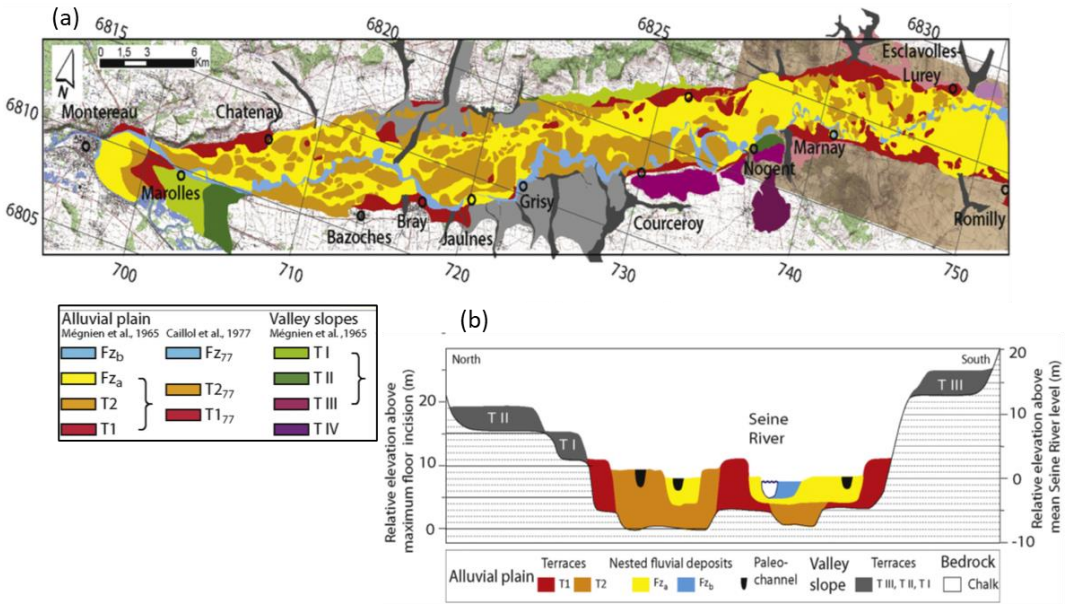

Figure 1.29. Upper Seine valley in the Montereau region, (a) Geopmorphological map and (b) the cross-section of the Bassée alluvial plain (Deleplancque et al., 2018).

1.6.4.3 Confluence Seine-Yonne

At the Monterau-Fault-Yonne site ,at the confluence with the Yonne River, the terraces are well developed (Figure 1.27). Downstream of Monterau-Fault-Yonne, at Pincevent, a lower terrace characterized by clay, silt and sand principalley has been dated using the ^{14}C, and is atributed as a part of the Lateglacial Allerod (10,35 BC), and the Holocene between the Older Atlantic (7,8 BC) and Subboreal periods (3,5 B.P) (Figure 1.30, Roblin-Jouve, 1984; Bodu et al., 2006).

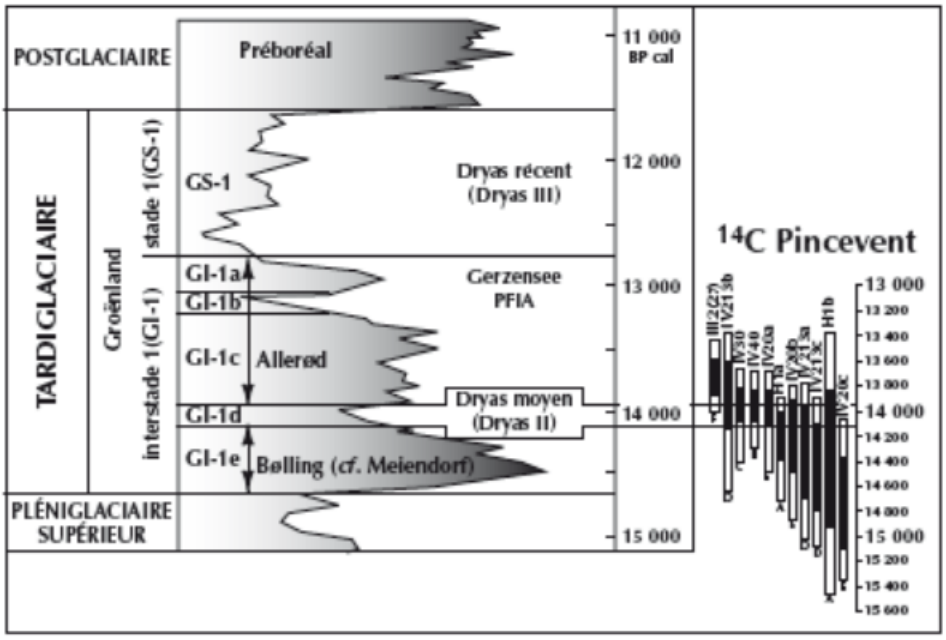

Figure 1.30. Chronological situation of Pincevent during the Lateglacial period (Bodu et al., 2006).

At Vernou-La-Celle-sur-Seine site, calcareous tuffa covered the alluvial deposits at +20 m RH). The age of tuffa depositd were determined by ESR/U-Th on a mammal tooth at 425 ka, corresponding to the early part of an interglacial MIS 11 (Figure 1.31, Limondin-Lozouet et al., 2006).

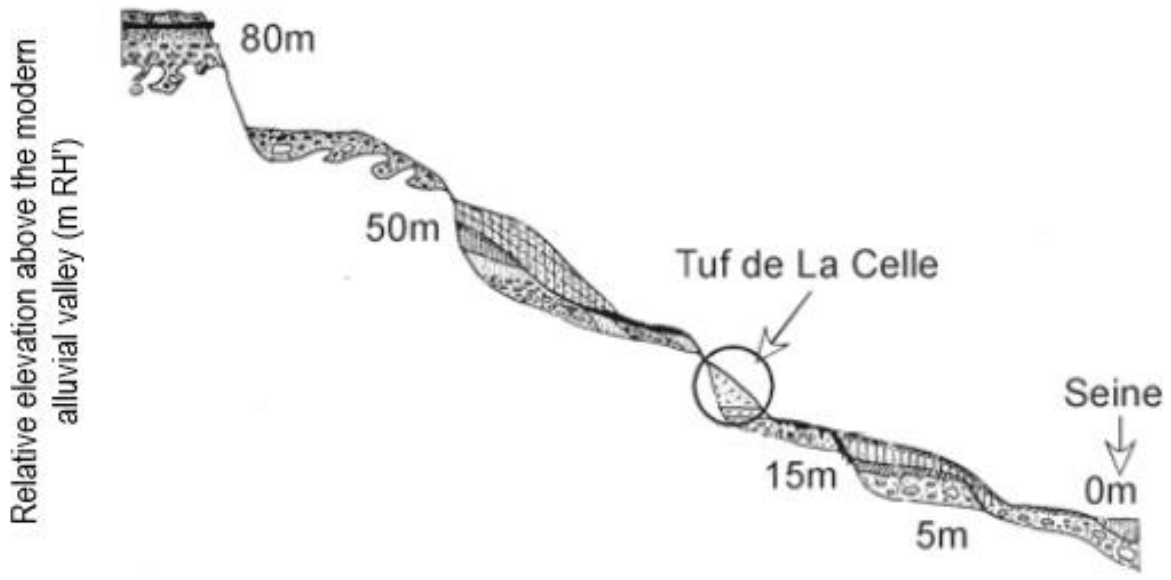

Figure 1.31. Position of La Celle tufa within the Seine River terrace system (Limondin-Lozouet et al., 2006).

1.6.4.4 Confluence Seine-Marne

At Maisons-Alfort, on the left bank of the Marne River, near the confluence with the Seine River, a lower terrace located between 27 and 33 m NGF (+ 9 m RH) overlies the limestone bedrock of the Cenozoic era (Figure 1.27). This terrace is formed by a fluvial sequence characterized by an interdigitation of sand, silt, and clay (Figure 1.32). Three bone samples have been dated, using U/Th dating method, ranging from 162 ka, and 190 ka to 206 ka, corresponding to the end of the Middle Pleistocene (Saalian period) between the MIS 7 and MIS 6 (Rodriguez, 1994; Durbet et al. 1997; Lautridou et al., 1999).

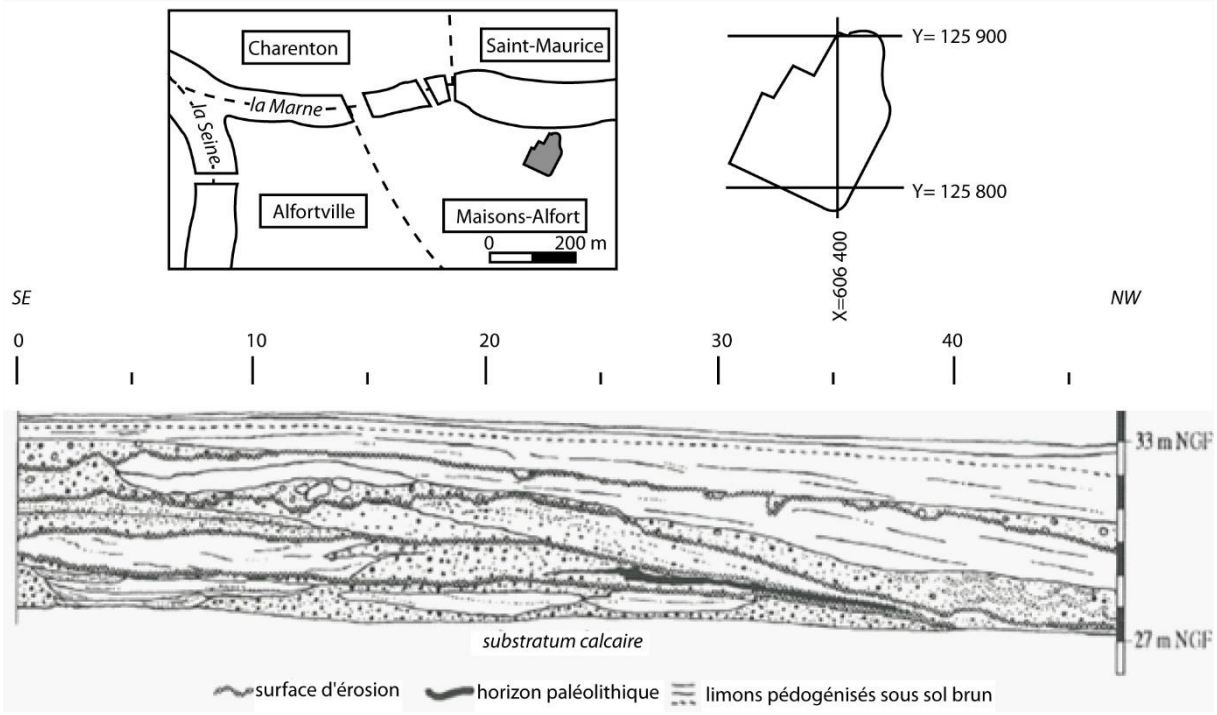

Figure 1.32. Schematic alluvial sequence of Maisons-Alfort near of the confluence with the Seine River (Dubert et al., 1997).

1.6.5 Middle Seine valley in the Region Mantaise (from Poissy to Val-de-Reuil)

The Middle Seine valley is located between Poissy, near of the confluence with the Oise River, and Val-de-Reuil meander (Figure 1.33). After Paris, the Seine river changes into a meandering style which continues in the Lower Seine section. This meandering part can be explained by the reduction in slope (0,2‰) perhaps in relation with the Cenozoic limestone and sand bedrock. The Middle Seine valley is characterised by a smaller meanders than downstream Lower Seine.

The deposits are well preserved, 16 alluvial steps were described, distributed in different terrace levels grouped as lower terraces (12-25 m relative RH), middle terraces (25-40 m relative RH) and upper terraces (> 40 m relative RH) (Lecolle, 1989). Each step presents a succession of lithofacies in relation with glacial-interglacial cycles corresponding to the last 600 ka, from the Elsterian to the lower and middle Weichselian. The upper Weichselian is missing because of an important vertical erosion (Figure 1.34, Lecolle, 1980; Lefebvre et al., 1994).

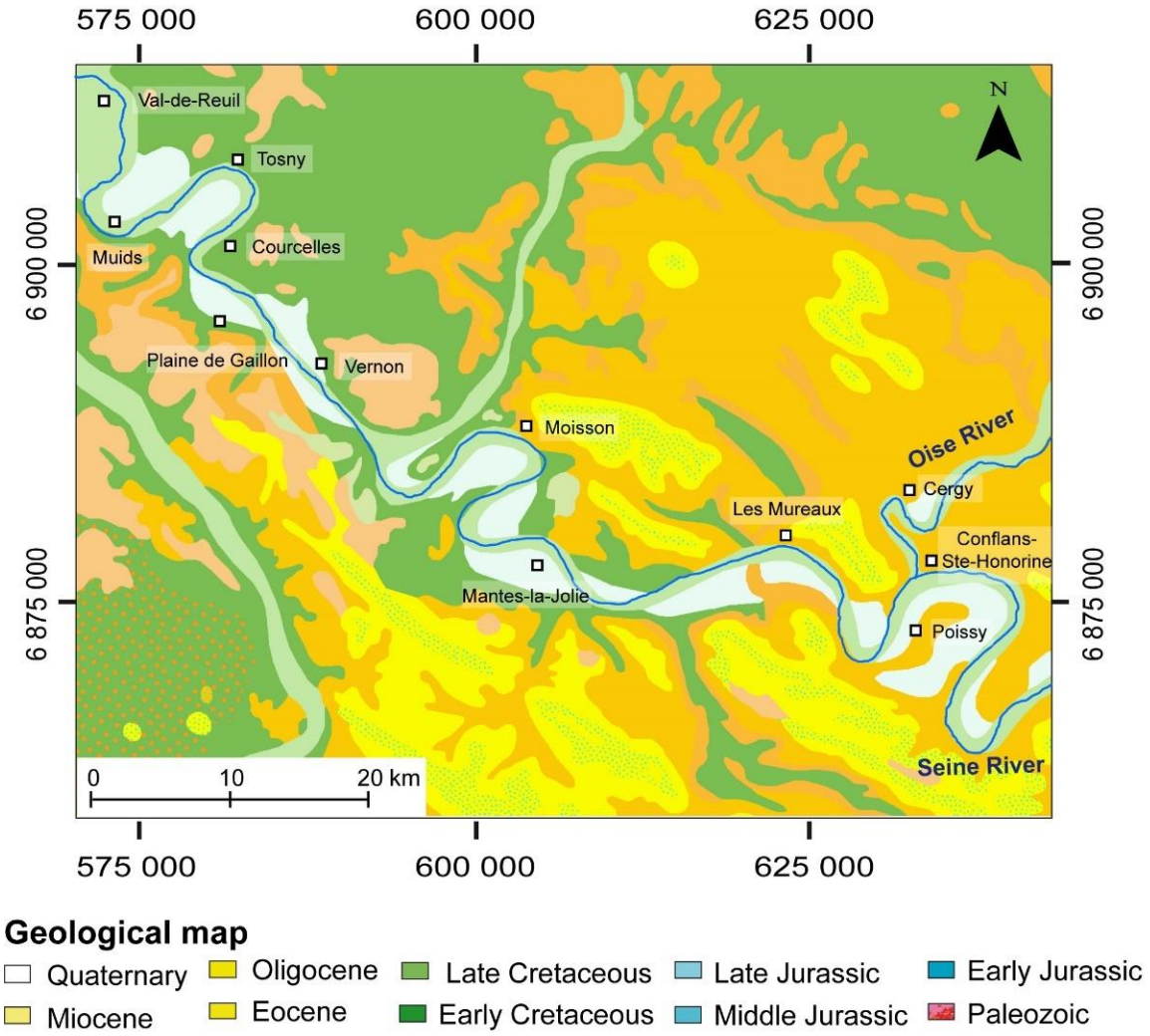

Figure 1.33. The middle part of the Seine valley, from Poissy to Val-de-Reuil and the Geological map at 1: 50000 scale.

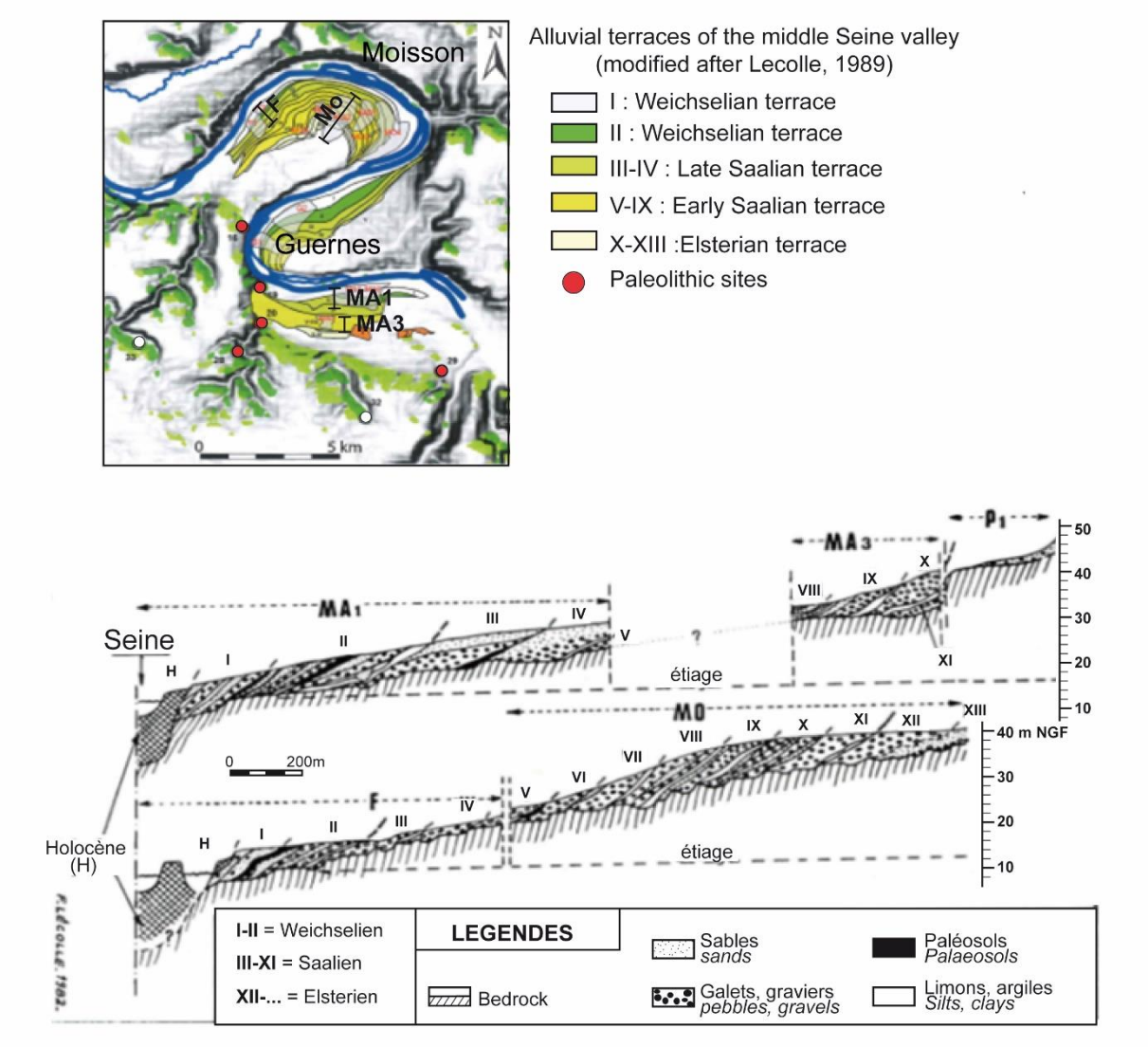

Figure 1.34. Alluvial terraces of the middle part of the Seine valley (modified after Lecolle, 1989).

1.6.6 Lower Seine valley (between Elbeuf and Le Havre)

The lower Seine valley is located between the Elbeuf meander and Le Havre. In this part, the Seine river incised into the Upper Cretaceous chalk bedrock (Jamet, 2014; Mortimore, 2018; Ballesteros et al., 2020) and is characterised by seven major meanders bearing the names of local towns: Elbeuf, Tourville-la-Rivière, Rouen, Duclair, Jumièges, Codebec-en-Caux, Tancarville and Marais Vernier towards the Seine estuary at Le Havre (Figure 1.35, Jamet, 2014). In this area, the slope of the longitudinal profile has been determined at 0,3 ‰, and some interesting outcrops were found (Lautridou et al., 1999).

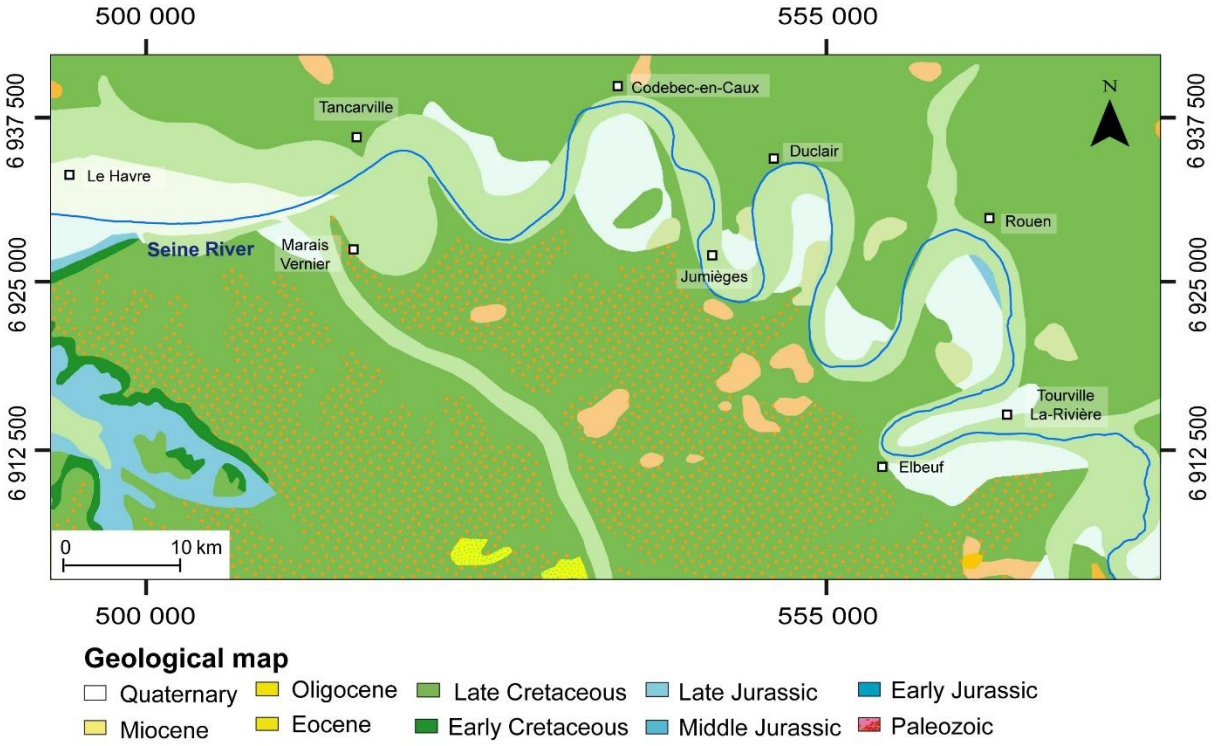

Figure 1.35. The lower part of the Seine valley, from Elbeuf to Le Havre and the Geological map at 1: 50000 scale.

The stratigraphic correlations between terraces are still complex (Lautridou et al., 1984) with several authors identifying 7 generations (Lefebvre et al., 1994, and Antoine et al., 2007) while others recognized 8 generations (Lautridou et al., 1999, and Jamet, 2014). The morphology of the terrace system is very different from that of the middle Seine valley described by Lecolle (1984).

In this area, the fluvial deposits begin with the very high fluvial terrace T8 at +120 m RH. This terrace contains La Londe Formation augite, from the French Massif Central, dated to about 1 Ma, which roughly date this terrace from MIS 26 to 104 (0,98 – 2,6 Ma) (Tourenq and Pomerol, 1995; Westaway, 2004). Terraces T7 (Madrillet, +90-95 m RH), T6 (Damps/ Forêt de Bord, +80 m RH) and T5 (Rond de France, +70m RH), have been correlated with MIS 22, corresponding to 1,03-0,86 Ma (Westaway, 2004). These terraces probably span most of the MIS 23-32 (Lautridou et al., 1999; Nehme et al., 2020).

Near Rouen, at Saint-Pierre-lès-Elbeuf, the T4 terrace formed by the Elbeuf lies at +30-32 m RH, and it is covered by four interglacial paleosols separated by a sandy loess sequence, dated by OSL at 164 to 475 ka (Cliquet at al., 2009). This sequence includes a calcareous tufa dated to 400 ka and contains a characteristic mollusc fauna that is a good biostratigraphic marker for

MIS 11(Antoine et al., 2007; Jamet, 2014; Nehme et al., 2020). The T3 terrace which occurs between +22-25 m RH (Oissel formation), has not been dated. The T2 terrace is characterized by the Tourville formation, which has been extensively studied. This terrace occurs between +17 and +18 m RH and consists ofthree periglacial alluvial deposits separated by two interglacial estuarine silt deposits. These interglacial deposits have been dated to 200 ka by ESR (Stremme, 1985; Bahain et al., 2019) and to 300 ka by OSL (Balescu et al, 1997). The upper part of this terrace contained an exceptional Saalian mammal fauna (Lautridou et al., 1999). Thus, this formation is comprised between the MIS 9 and MIS 6 (Porcher, 1981; Lautridou, 1985; Lautridou et al., 1999; Cordy et al., 2003; Antoine et al., 2007, 2010, Jamet, 2014). Below the Tourville terrace there are two gravel terraces known as T1, represented by Rouen 2 (+5 m RH) and T0, which corresponding to Rouen 1 (0 m RH). Theses terraces are part of the current Fz valley bottom and are covered by the Holocene deposits (Figure 1.36).

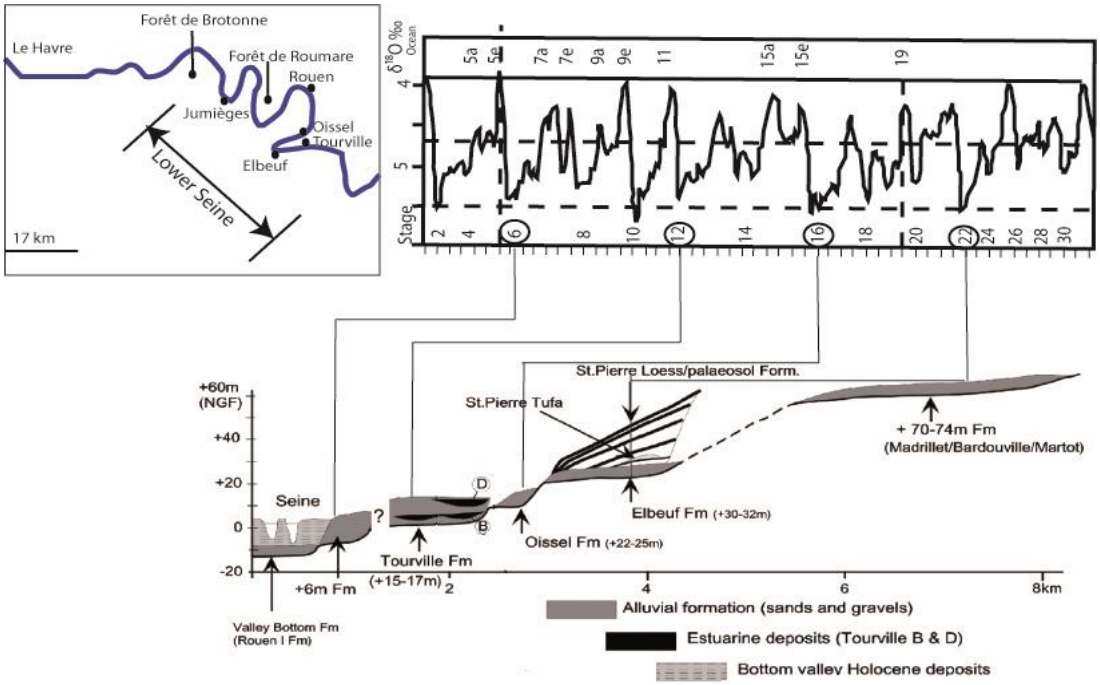

Figure 1.36. The lower Seine valley between Le Havre and Elbeuf, Antoine et al., 2007.

Downstream, in the macrotidal estuary of the Seine, Frouin et al., (2010) shows the paleoenvironmental evolution of the Holocene in relation to sea level rise over the last 6000 years, identifying four main phases: 1) retrogradational shifting of the shoreline from 6000 cal. BC; 2) maximum flooding between 6000-5000 cal. BC; 3) aggrading sequence between 5000-1100 cal. BC and 4) progradational shifting of shoreline from 1100 cal. BC (Figure 1.37).

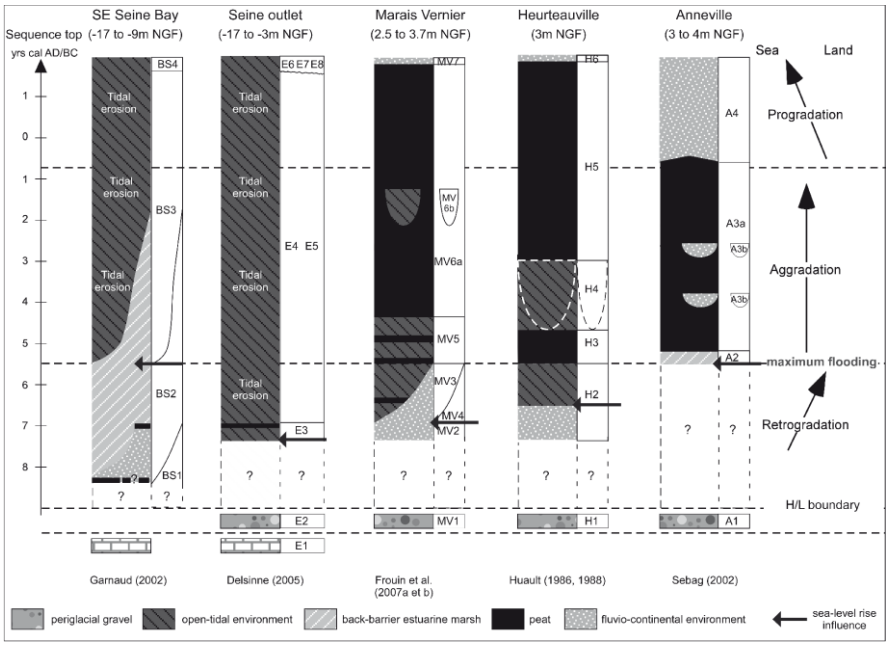

Figure 1.37. Holocene evolution of the lower Seine valley (Frouin et al., 2010).

1.6.7 Lateglacial dynamic within the valley bottom in the Seine catchment

The valley bottoms of the Seine catchment provide a general overview of the valley evolution related to climatic changes from the Weichselian Lateglacial to the Holocene. Some valleys such as the Oise, Marne and Seine, have a sedimentary archive of the valley bottom that documents the major changes during the Lateglacial and the Holocene periods (Pastre et al., 2014). It is important to note that during the Lateglacial and the Holocene periods, Bond events have occurred. However, at the scale of this thesis these events are difficult to observed because we do not have the resolution required to analyse the detailed stratigraphy observation Pleistocene within the Lateglacial or Holocene data.

1.7 Conclusion

The complexity of the alluvial terraces often makes it necessary to divide the analyzed river system into smaller geographical regions with uniform characteristics. Within the Seine River catchment, the evolution of the Upper Seine, Middle Seine, Lower Seine, Somme, Yonne, Aube rivers, could have been influenced by tectonic, climatic variations and sea-level variations during the last 1 Ma, as well as Oise, Marne and Eure rivers in which few data are available. Within the Somme, Yonne, and Aube valleys, the evolution of alluvial terrace as well as the incision process are controlled by climatic variations. In the Seine valley, climate is the

principal control in the upper and the middle part of the valley, and sea-level change do not influence the fluvial system dynamic. In contrast the lower part of the valley is more influenced by sea-level changes, especially during the coldest periods.

From upstream to downstream the Seine river changes is longitudinal slope through 0,7‰ for upper Seine, 0,2 ‰ for middle Seine and 0,3 ‰ for lower Seine. Around les Andelys (40 km upstream of Rouen) a convex knickpoint was inferred from the change in slope of the longitudinal profile, it corresponds to the limit between the eustatic and climatic driven erosive processes (Figure 1.38, Lautridou et al., 1984; Lautridou et al., 1999; Deleplancque et al., 2018).

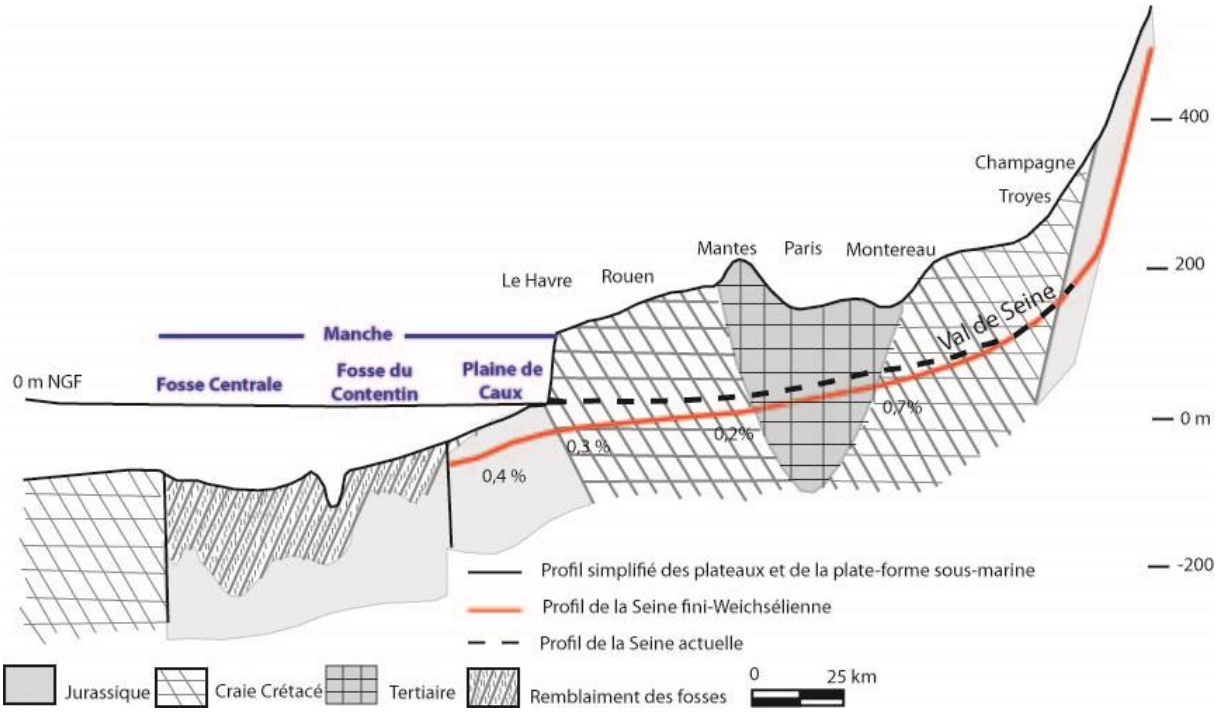

Figure 1.38. Variations of longitudinal profile along the Seine River (Lautridou et al., 1999).

Chapter 2: Field description of the sediments sampled for ESR/OSL chronology

Ce chapitre présente les observations de terrain et la description des dépôts alluviaux qui ont été échantillonnés le long du bassin-versant de la Seine afin de les dater en utilisant la datation par les méthodes ESR et OSL. Les sédiments ont été échantillonnés pour mieux contraindre la chronologie de l'installation des vallées. Ces échantillons ont été prélevés directement dans le fond des vallées ainsi que dans des terrasses se trouvant en bordure du fond de vallée.

Chapter 2

2 Field description of the sediments sampled for ESR/OSL chronology

This chapter introduces the field description of alluvial deposits that were sampled within the Seine catchment for ESR/OSL geochronology. The sites were sampled according to three objectives: dating the valley bottom infill sediments ((i) directly or (ii) indirectly) and (iii) constraining the timing of the establishment of valley geometry, particularly along valleys where constraints are limited. Ultimately the goal was to better understand the incision and aggradation geometries observed in the sedimentary units within the frame of the Late Quaternary climatic evolution. Samples were directly taken from the valley bottoms for objective (i) while other samples were taken in strath terraces to target objective (ii) and (iii). Strath terraces located at the edge of the valley bottom allowed attempting indirect dating of the valley bottom infill (i.e., objective (ii)).

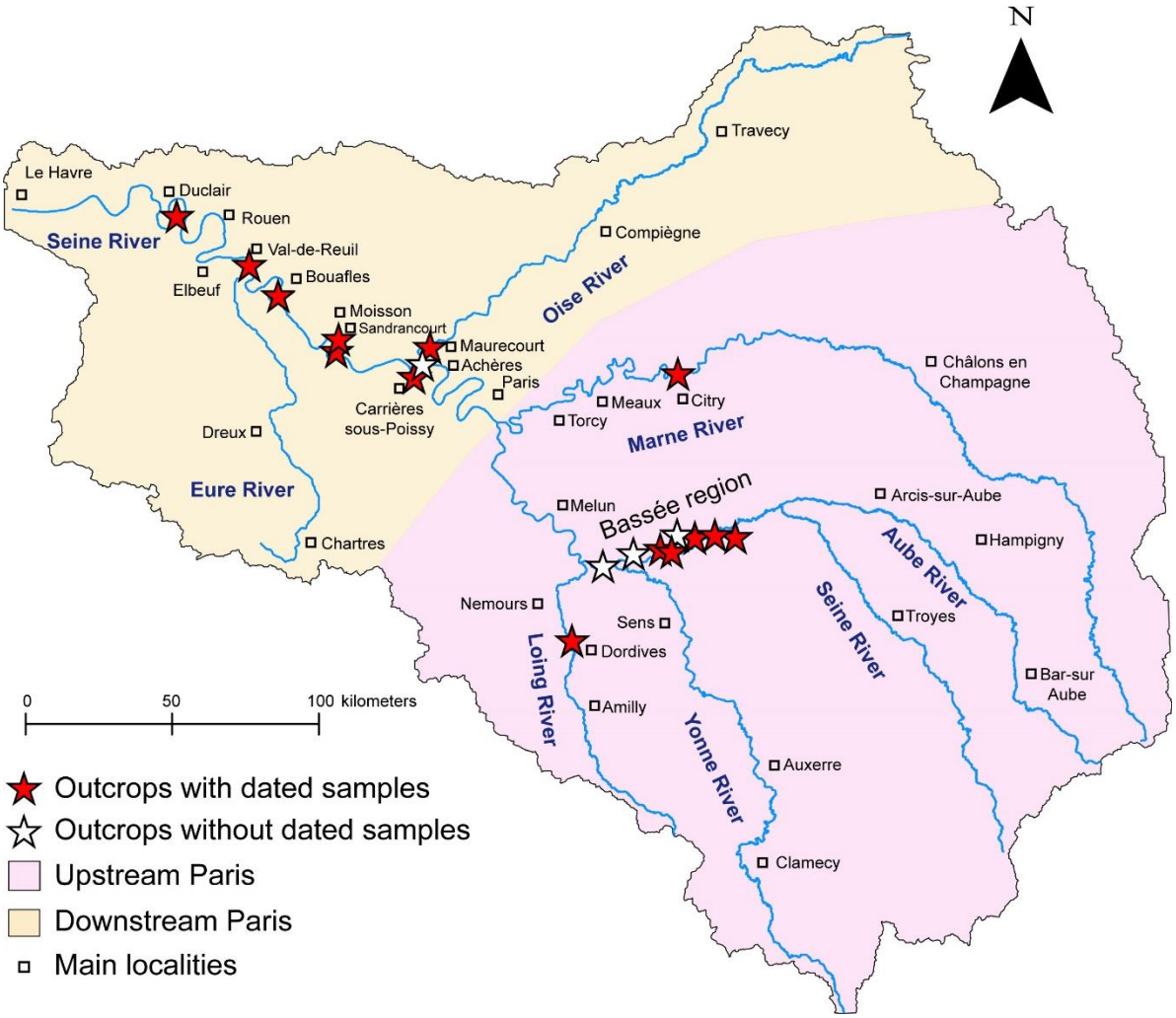

Figure 2.1. Location of field descriptions and sampling outcrps sites for dating along the Seine catchment. Red stars represent outcrops with dated samples using the ESR/OSL dating methods. White stars represent outcrops without dated samples.

The sampling sites were divided into two main sectors within along the Seine catchment (Figure 2.1). The first one is located upstream of Paris. In this area the upstream Seine, the Marne, Aube, Yonne and Loing valleys are included. The second sector is located downstream of Paris. It includes the downstream Seine, Oise and Eure valleys. Sampling sites were identified based on bibliographic sources, 1:50000 France geological maps, and existing boreholes data, which were completed by field surveys. A special attention was given to active quarries where fresh outcrops can be accessed relatively easily.

A precise description was made for each outcrop, including (1) location, (2) RGF Lambert 1993 X, Y coordinates, (3) terrace identification from the 1:50000 France geological maps, (4) elevation of the alluvium-bedrock interface (m NGF), (5) sedimentological descriptions (i.e., alluvial thickness, grain size and sedimentary structures that allow to classify into a lithofacies following the nomenclature of Miall (2006)) (Appendix A table 2.1) and (6) information related to dating (sample number, precise location on the outcrops, and specific observations) (Appendix A table 2.2). When the bedrock could not be observed in outcrops (covered or underwater), the elevation of its top was determined using data from nearby boreholes and/or from observations given by the peoples working in the quarries.

Different studies based on morphological geometry of the terraces define their elevation using a classical term relative height elevation (RH term) to position the strath terrace (Lefebvre et al., 1974; Antoine et al., 2007; Cliquet et al., 2009). The RH is commonly used to understand the local topography variations (i.e., variation in river incision) and also to compare the different nearby terraces. In this chapter we introduce a new term RH' which take into account the elevation above the valley bottom. In this context, RH' provides an opportunity to evaluate local topography variation (i.e., without variation in river incision) in relation to strath terrace. Thus, the RH or RH' could be used either to define the base of the terrace or to position the sample.

To compare the distinct terraces observed in the field with those described in the literature, it was necessary to define these two relative elevations. Firstly, the relative elevation above the maximum incision of the river (RH), was defined classically as the difference between the absolute elevation of the sample (Z sample) and the absolute elevation of the bedrock at the maximal incision (Z max bedrock) along a transect transverse to the river course (Figure 2.2, Cordier et al., 2009). Secondly, the relative elevation above the valley bottom (RH'), was defined as the difference between the absolute elevation of the sample (Z sample) and the absolute elevation of the valley bottom (Z valley bottom) along the same transect (Figure 2.2).

These relative elevations RH or RH' represent a first discrimination to place samples and correlates alluvial terraces, because fluvial dynamic (i.e., migration of river, erosion and sediment deposition) could generate significant difference in elevations of a given fluvial terrace or sample.

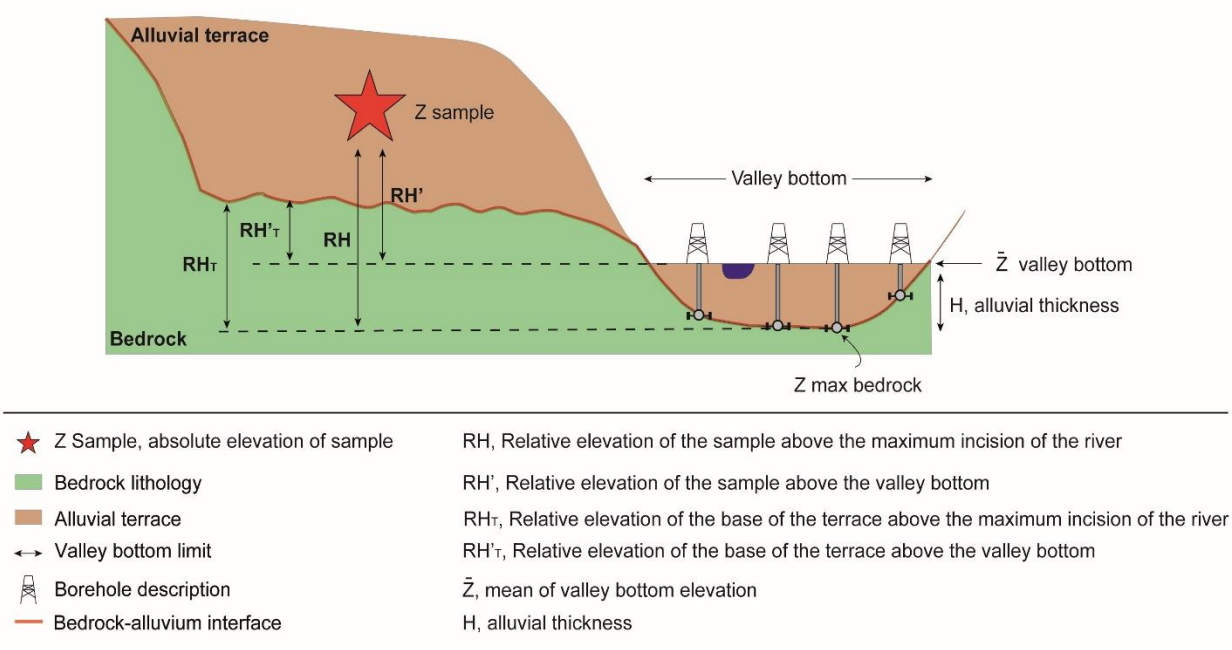

Figure 2.2. Schematic representation of determination of relative elevation with respect to both the maximum incision of the river and the mean river level.

2.1 Upstream Paris

Field work in this area mostly focused on the Bassée area. It was completed by two other samples: in the Loing and the Marne valleys (Figure 2.1).

2.1.1 Samples in the Bassée area

A total of eight sites were described and sampled in the Bassée area. Four sites concerned alluvial sediments from terraces and four sites concerned the valley bottom (Figure 2.3). Two samples were dated from terraces: A3D-006 (T_{IV} terrace; Fontaine Macôn site) and A3D-024 (T_{III} terrace; Courceroy site), while three samples were dated from the current valley bottom: A3D-020 (T_2 terrace; Port Montain site), A3D-021 (T_2 terrace; Bazoche site) and A3D-002 (T_{3a} terrace; Vimpelles site). The others three sites located at Marolles-sur-Seine in the terrace T_I

(A3D-009), Chalmaison in the terrace T_{II} (A3D-008) and Varennes-sur-Seine in the valley bottom (A3D-022) were only described in this work (these samples have not been dated because of the time consuming and also due to the budget available for dating).

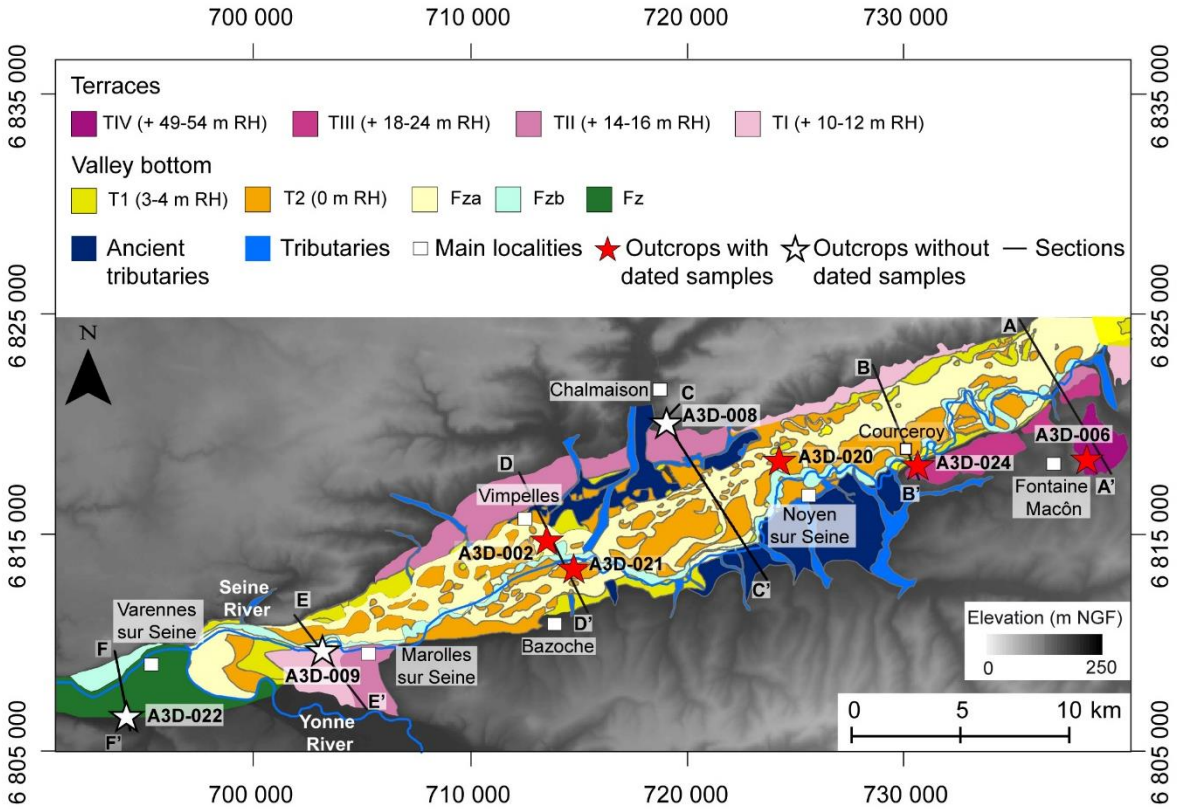

Figure 2.3. Homogenized geomorphological map within the Bassée alluvial plain (modified after Mégnien, 1965; Deleplancque et al., 2018), with location of the eight sites described and sampled for dating. Red stars represent outcrops with dated samples using the ESR/OSL dating methods. White stars represent outcrops without dated samples. Black lines represent topographic sections.

Within the Bassée area, six topographic profiles transverse to the main river direction were built and located in the geological map. These profiles were generated using the SwathProfiler Add-In, implemented in ArcGIS 10.6 (Pérez-Peña et al., 2017) (see locations on Figure 2.3). Each profile shows the sample positions with respect to the swath profiles, the alluvial terraces and the current valley bottom. Four of the samples are situated within the T_{IV}, T_{III} and T_I terraces (Figure 2.4-sections A-A', B-B' and E-E') and four samples are located in current valley bottom (Figure 2.4-sections D-D' and F-F').

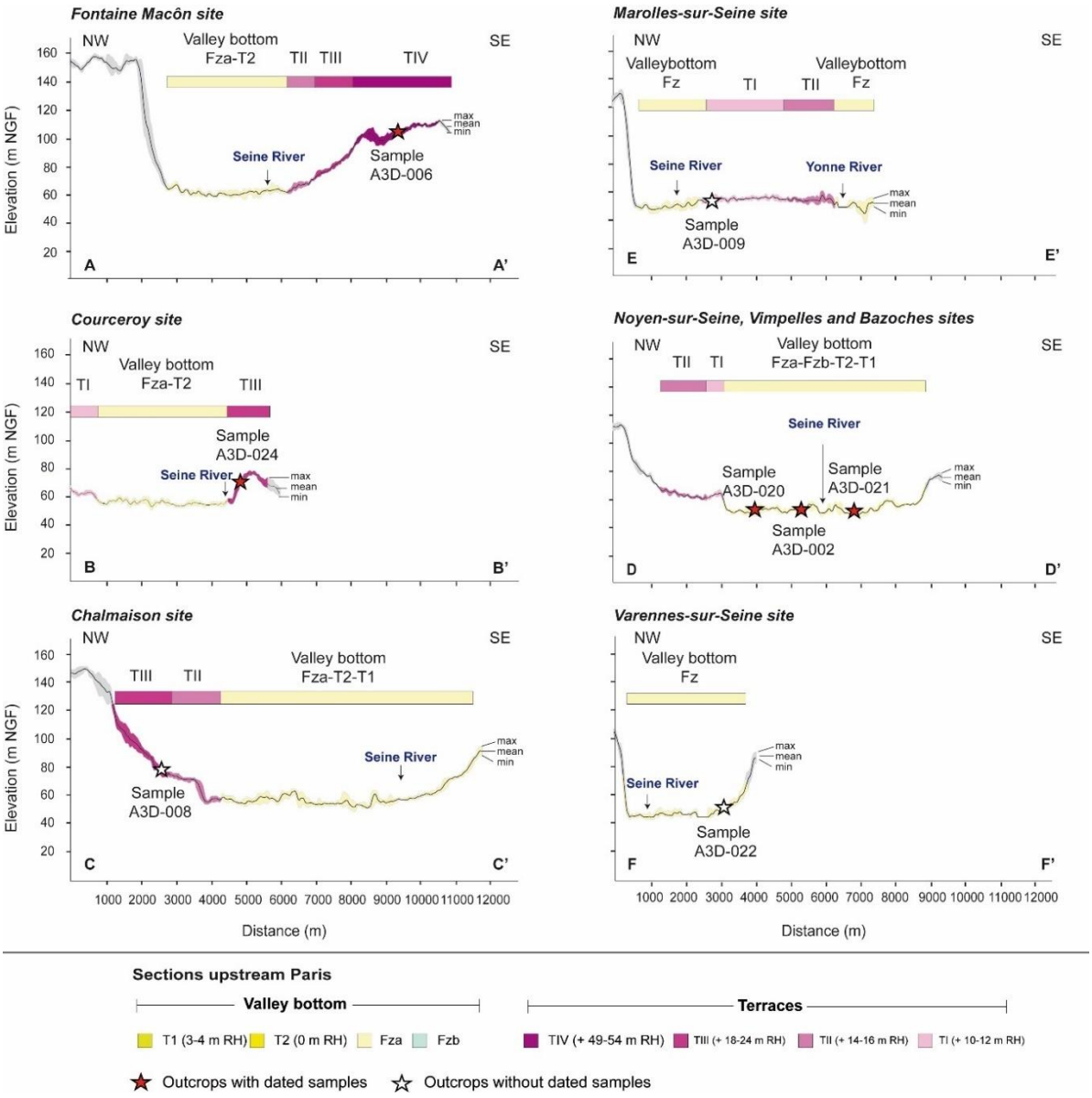

Figure 2.4. Sample location on topographic swath profiles. These profiles detailed statistical information in elevation based on maximum, minimum, and mean topography along the Bassée area, which is represented by black and gray lines.

2.1.1.1 Samples from strath terraces

2.1.1.1.1 T_{IV} terrace : Fontaine Macôn (A3D-006)

The terrace T_{IV} (+49 to +54 m RH, Mégnien, 1965; Deleplancque et al., 2018) has been identified at Fontaine Macôn, in the upper part of the Bassée area, to the south of Nogent-sur-Seine, on the left bank of the Seine River (Figure 2.3). Because of the poor preservation of the T_{IV} terrace, we did not clearly observe any outcrop, thus description and sampling of this terrace

was made using a hand auger. The bedrock was not visible at this location, but its lithology and depth were determined using the BSS boreholes information near of the sample site. As a result, the absolute elevation of the chalk bedrock from Upper Cretaceous was estimated to be approximately 99 m NGF. The borehole was 0.90 m long and was drilled using the hand auger. The firsts 0.10 m consisted of gravels while a layer characterized by the presence of well-organized fine to medium sands lies between 0.8 m and 0.6 m. The uppermost 0.6 m layer consisted of anthropogenic soil overlaying sands with some levels of gravels (Figure 2.5). Sample A3D-006, composed of fine to medium sand, was collected at 104 m NGF (+52 m RH or +46 m RH'). The fact that the sand and gravel were well-sorted points to a fluvial origin of the sediments. Furthermore, the gravel was rounded and similar to the one quarried in the Bassée valley bottom. Therefore, the origin of the sediment can be confidently interpreted as fluvial.

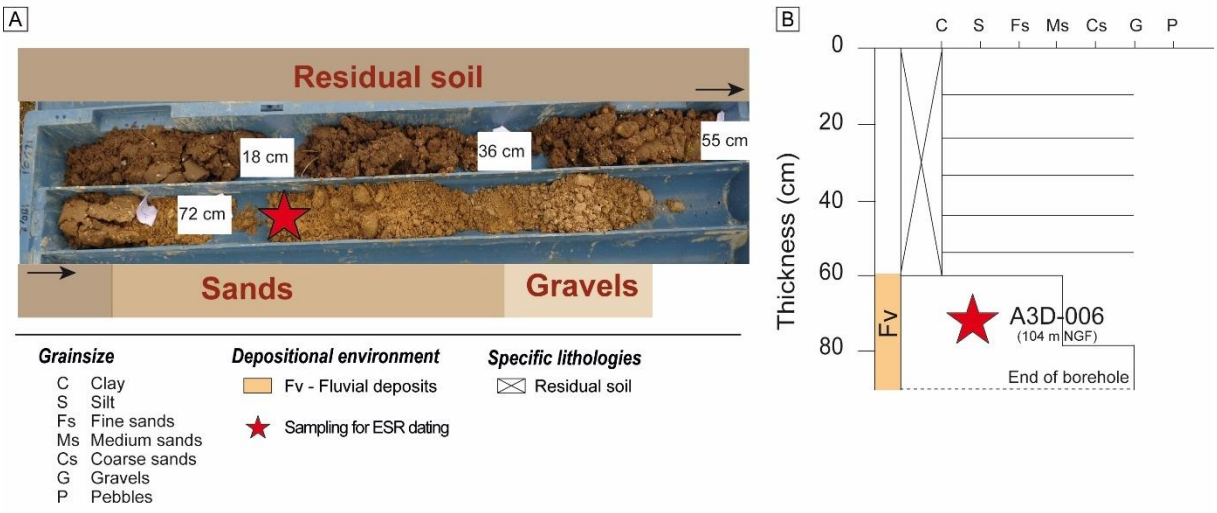

Figure 2.5. The fluvial sequence along the T_{IV} terrace at Fontaine Macôn site. (a) Photography of sampling using a hand auger, red star represents the sample A3D-006. (b) Stratigraphic log with location of the sampling A3D-006 prepared for ESR dating.

2.1.1.1.2 T_{III} terrace: Courceroy (A3D-024) and Chalmaison (A3D-008)

The T_{III} terrace (+18 to +24 m RH, Mégnien, 1965; Deleplancque et al., 2018), was observed in two outcrops at Courceroy and Chalmaison, situated in the upper and middle part of the Bassée area (Figure 2.3). The two sites were separated by only 12 km.

a. The Courceroy site (A3D-024)

The Courceroy site was located south of La Motte-Tilly, on the left bank of the Seine River (Figure 2.3). The visible outcrop was a 2.8 m thick. The bedrock was made of chalk from the Upper Cretaceous up to 68.7 m NGF. The base of the alluvial sequence was characterized by gravels with a planar cross-bedding stratification (Gp facies) containing some flints, that overlied the chalk bedrock. These gravels varied laterally from 0.1 to 0.2 m of thick. Upwards, the sequence went from coarse to fine sands, which were well sorted and laminated (Sh facies) and 0.8 m thick. The sequence then graded to 0.2 m thick of gravels (Gp facies), 0.5 m thick of sands with planar stratification (Sp facies) and 0.25 m thick of gravels (Gp facies). The uppermost part of the sequence consisted of 0.85 m thick of residual soil. Sample A3D-024 was collected from fine sands in the lower part of the sequence at 69.2 m NGF (+22 m RH or +14 m RH') for ESR dating (Figure 2.6).

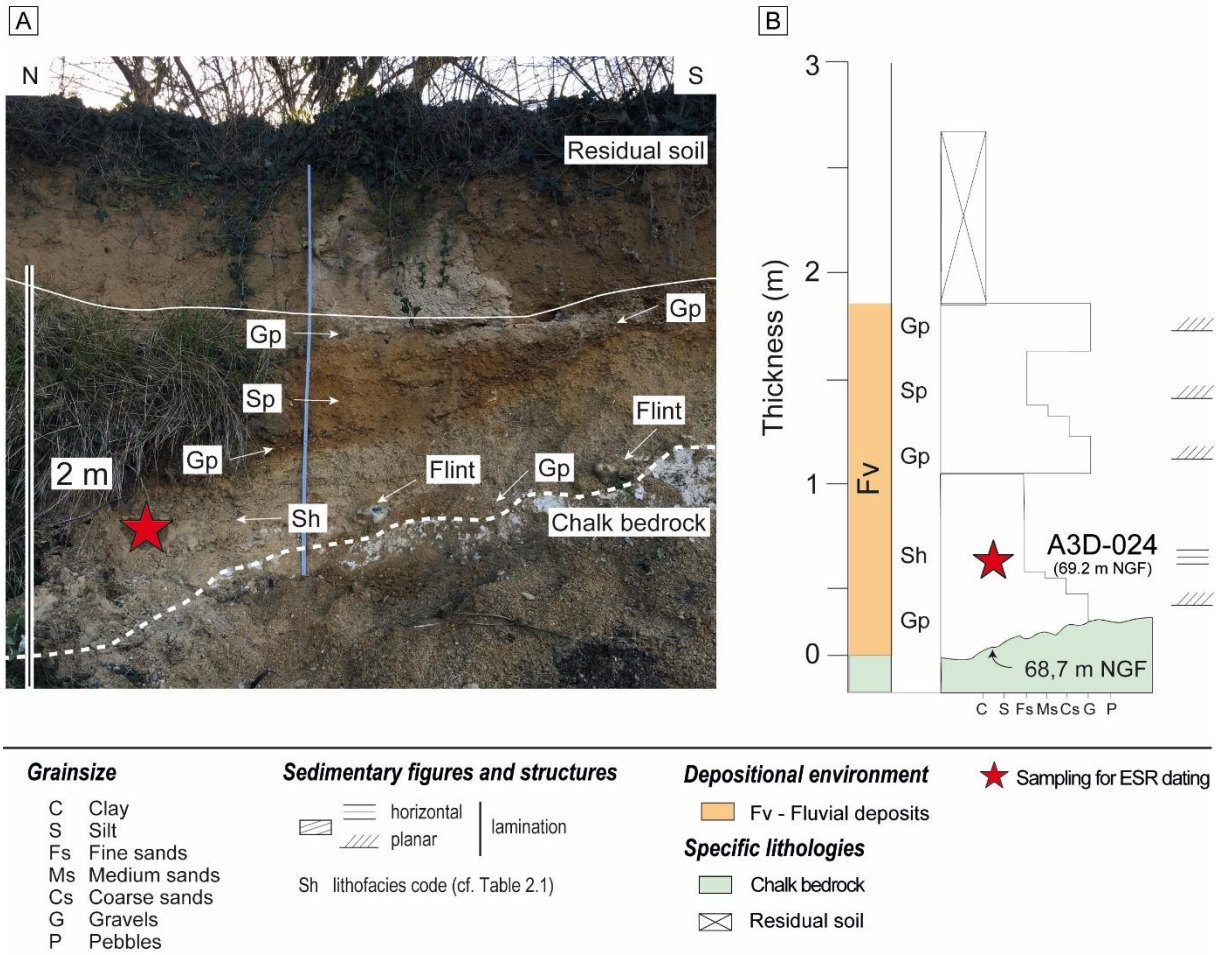

Figure 2.6. The fluvial sequence along the T_{III} terrace at Courceroy site. (a) Photography illustrating the main facies observed at the outcrop, red star represents the sample A3D-024 prepared for ESR dating. (b) Stratigraphic log showing sedimentology and stratigraphic surfaces with sample location.

b. The Chalmaison site (A3D-008)

The Chalmaison site was located in the middle part of the Bassée area, on the right bank of the Seine River (Figure 2.3). In this site, the outcrop was visible along a railway cut with a high slope. Accessibility to the site was limited, making it impossible to uncover and clean the outcrop to closely observe sedimentary structures and layers. The bottom of the outcrop was formed by the chalk bedrock from Upper Cretaceous, its absolute elevation was determined using the BSS boreholes near of the site estimated at 72 m NGF. The outcrop had a thickness of c.a. 6 m. Then, 4 m thick sands overlapped the chalk bedrock. Finally, the upper part of the outcrop consisted of residual soil of c.a. 2 m thickness. Sample A3D-008 was collected from sandy deposits at 75 m NGF (+20 m RH or +20 m RH') (Figure 2.7).

Figure 2.7. Photography of the outcrop located along the T_{III} terrace at Chalmaison site. White star represent the sample A3D-008 only described in this work.

2.1.1.1.3 T_I terrace : Marolles-sur-Seine (A3D-009)

The T_I terrace (+ 10 to +12 m RH) was observed in the southern part of the Bassée area, specifically at Marolles-sur-Seine on the left bank of the Seine River and upstream of the confluence with the Yonne River (Figure 2.3). Due to its proximity to the motorway and limited

accessibility to the outcrop, sedimentary structures and layers were difficult to observe (Figure 2.8). The bedrock constituted of chalk from the Upper Cretaceous, which was not visible. Its absolute elevation was determined using BSS boreholes at 47 m NGF. The outcrop consisted of a 1-m-deep hole. From the base to the top, the sequence was characterized 0.60 m of medium to fine sands with a horizontally lamination (Sh facies) in which some levels of gravels were observed, covered by 0.4 m of anthropogenic soil. Sample A3D-009 was taken from fine sands at 55 m NGF (+14 m RH o +7 m RH'). This sample was prepared for ESR dating, unfortunately, it was not dated successfully because the sample did not contain enough quartz.

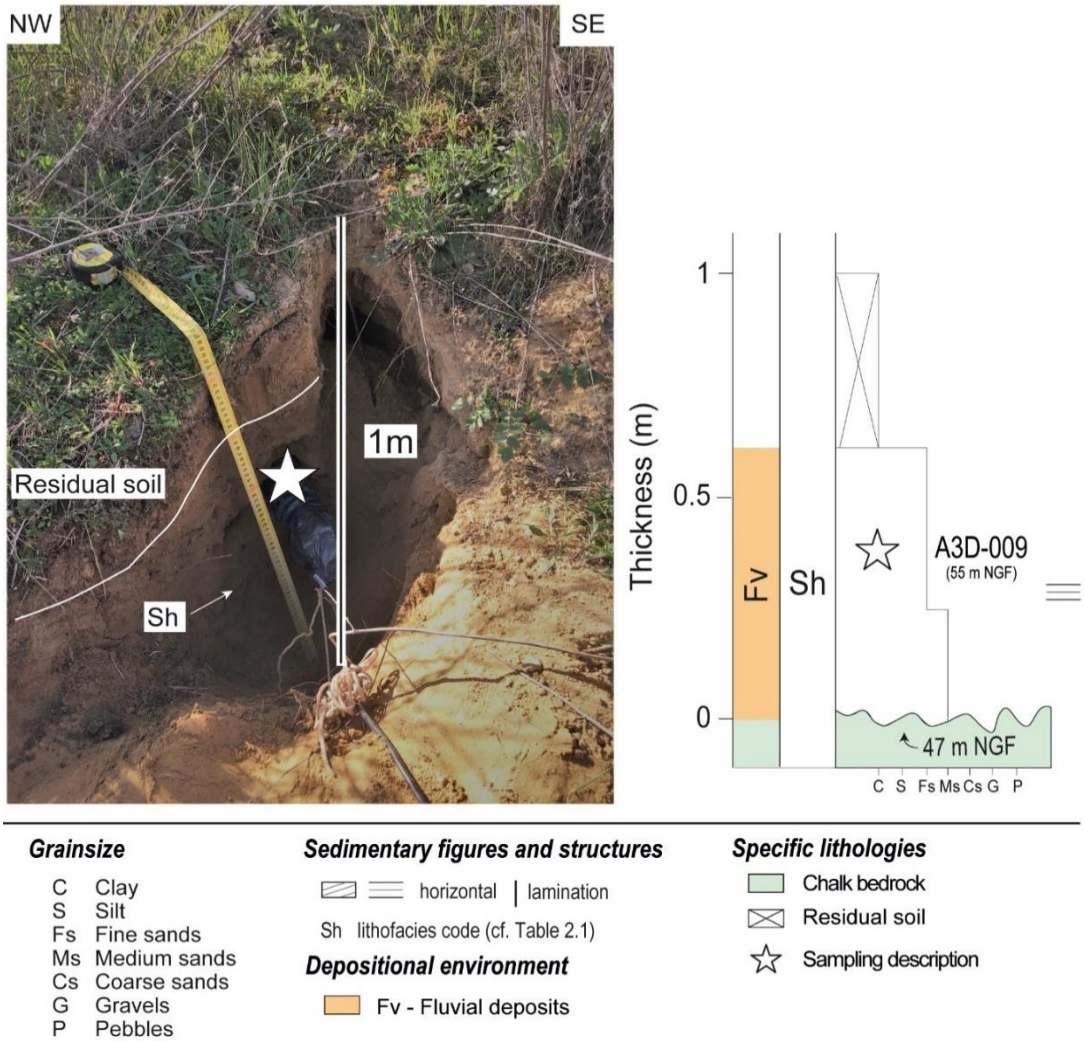

Figure 2.8. The fluvial sequence along the T_I terrace at Marolles-sur-Seine site. (a) Photography illustrating the main facies observed at the outcrop, white star represents the sample A3D-009 only described in this work. (b) Stratigraphic log showing sedimentology and stratigraphic surfaces with sample location.

2.1.1.2 Samples from the valley bottom

2.1.1.2.1 T_2 terrace: Noyen-sur-Seine (A3D-020) and Bazoche-lès-Bray (A3D-021)

The T_2 terrace (top of terrace defined at +0 m RH) was observed in the middle part of the Bassée area, at Noyen-sur-Seine and Bazoche on the left bank of the Seine River (Figure 2.3). Access to sampling was facilitated by active quarries. The sites were separated by about 10.6 km.

a. The A2C Granulat quarry at Noyen-sur-Seine (Port-Montain, A3D-020)

The Port Montain quarry was located north-west of Noyen-sur-Seine site (Figure 2.3). In this site, the bedrock was not observed directly on the outcrop because it was under water. It was made up with chalk from Upper Cretaceous and its absolute elevation, that reached of about 50 m NGF, was determined using the BSS boreholes near of the site. The visible outcrop had a thickness of c.a. 1 m. At the scale of the outcrop, the sequence was characterized by 0.1 m thick of gravels with planar cross-bedding stratification (Gp facies). These gravels were overlain by 0.2 m thick of medium to fine sands (Sp facies). Then, a layer of 0.05 m thick of gravels overlied the sands. Layers formed of silt to fine sands represented 0.1 m thick and showed some mud clasts observed in the silt layer. The sequence graded upwards into a 0.55 m thick, from medium sands to gravels with a planar cross-bedding stratification (Gp facies). Sample A3D-020 was taken from fine sands in the lower part of the sequence at 56 m NGF (+8 m RH or +1 m RH') for OSL dating (Figure 2.9).

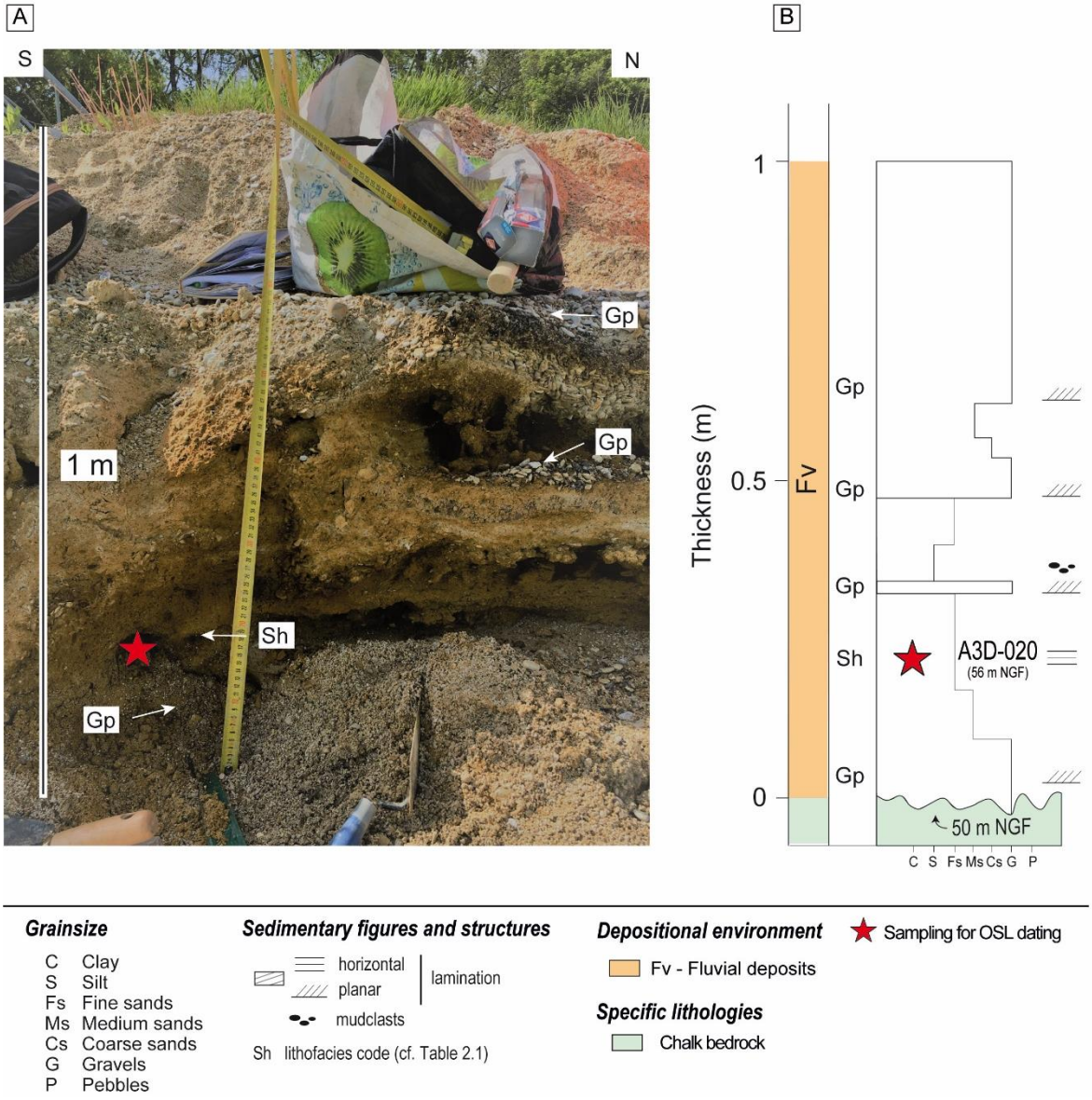

Figure 2.9. The fluvial sequence along the T_2 terrace at Noyen-sur-Seine site. (a) Photography illustrating the main facies observed at the outcrop, red star represents the sample A3D-020 prepared for OSL dating. (b) Stratigraphic log showing sedimentology and stratigraphic surfaces with sample location.

b. The GSM quarry at Bazoches-lès-Bray (A3D-021)

The Bazoche site was situated within the GSM quarry (Figure 2.3). The bottom of the sequence lied on the chalk bedrock from Upper Cretaceous that reaches 46 m NGF, which is not directly observed because it was inaccessible at the outcrop scale. Its absolute elevation was determined using the BSS boreholes near of the site. The outcrop exhibited a sediment thickness of 2 m (Figure 2.10). The lower part of the sequence was composed of 0.25 m thick of fine sands with

planar lamination (Sh facies). Upwards, the 0.5 m thick deposits constituted of gravels clast-supported with planar cross-bedding stratification (Gp facies) grading from coarse to medium sands (Sp facies). Then, 0.6 m thick of massive silt with some fine sands (Fm facies) overlied the sands deposits. The top of this sequence was composed of c.a. 0.8 m thick of head deposits (Gmm facies). Sample A3D-021 was taken for OSL dating from finest sands at 50 m NGF (+6 m RH or +0 m RH').

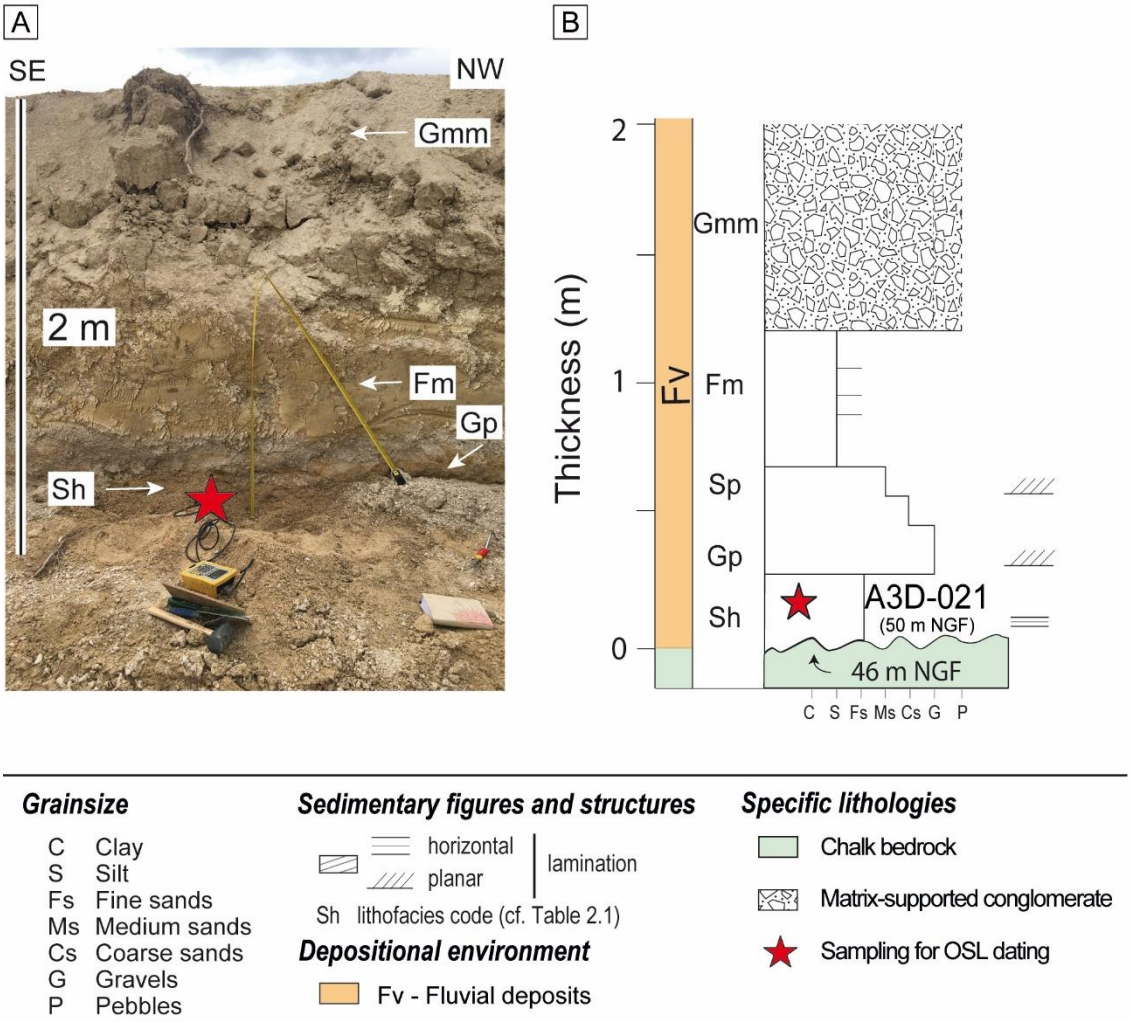

Figure 2.10. The fluvial sequence along the T_2 terrace at Bazoches site. (a) Photography illustrating the main facies observed at the outcrop, red star represents the sample A3D-021 prepared for OSL dating. (b) Stratigraphic log showing sedimentology and stratigraphic surfaces with sample location.

2.1.1.2.2 Fz_a terrace: Lafarge abandoned quarry at Vimpelles (A3D-002)

The Fz_a terrace was observed in the middle part of the Bassée area at Vimpelles site, on the right bank of the Seine River (Figure 2.3). The bottom of the sequence was characterized by the chalk bedrock from Upper Cretaceous which reaches 47 m NGF. In this site the bedrock was not observed directly on the outcrop because it was under water. Its absolute elevation was determined using the BSS boreholes near of the site. The visible outcrop is situated within the Lafarge granulats quarry. The section had a thickness of 2 m (Figure 2.11). At the scale of the outcrop, the sequence began with a 1 m thick alternation of fine to medium sands, in which were observed 0.6 m thick fine sands with horizontally lamination (Sh facies) and cross-lamination (Sr facies), and 0.4 m thick of medium sands with horizontal lamination (Sh). Then the sequence was followed by 0.5 m thick of silt with some fine sands (Fl facies) that overlaid the sand deposits. The uppermost part of the sequence was characterized by a 0.4 m thick residual soil. Sample A3D-002 was collected in the lower part of the section from the fine sands at 51 m NGF (+6 m RH or +0 m RH') for OSL dating.

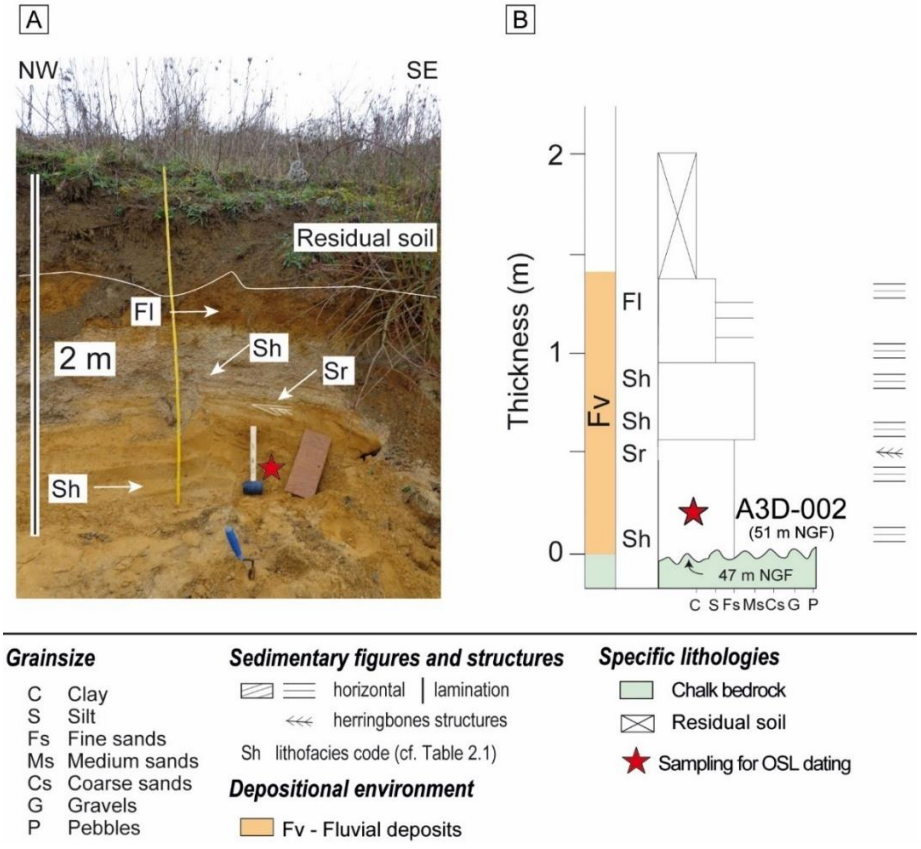

Figure 2.11. The fluvial sequence along the T_{3a} terrace at Vimpelles site. (a) Photography illustrating the main facies observed at the outcrop, red star represents the sample A3D-002 prepared for OSL dating. (b) Stratigraphic log showing sedimentology and stratigraphic surfaces with sample location.

2.1.1.2.3 Fz terrace : Varenne-sur-Seine GSM quarry (A3D-022)

The Fz terrace (the base of the terrace was determined at +5 m RH) was observed near the confluence between the Seine and Yonne rivers at Varenne-sur-Seine site, along the left bank of the Seine River (Figure 2.3). Access to sampling was facilitated by the active quarrying by GSM. The bottom of the section was characterized by the chalk bedrock from Upper Cretaceous, which reaches 46 m NGF. The bedrock was not observed directly on the section because it was under water. Its absolute elevation was determined using the BSS boreholes near the site. The section had a 2.2 m thickness (Figure 2.12). The sedimentary sequence was composed of 0.30 m thick of fine sands with planar stratification (Sp facies). It was overlain by 0.25 m of gravels with planar cross-bedding stratification (Gp facies) that sharply eroded the sands. Then, the sequence graded to well-organized alternations of medium sands to gravels representing 0.65 m thick, 0.25 m thick sands with planar stratification (Sp facies), 0.05 m thick of gravels (Gp facies), 0.1 m thick of medium sands (Sp facies), 0.05 m thick of gravels (Gp facies) and 0.20 m thick of medium sands (Sp facies). The section ended with c.a. 1 m thick of head deposits (Gmm facies). Sample A3D-022 was collected in the lower part of the section from the fine sands at 48.8 m NGF (+ 7 m RH or 0.8 m RH'). This sample was prepared for ESR dating, unfortunately, it was not dated successfully because the sample do not have enough quartz.

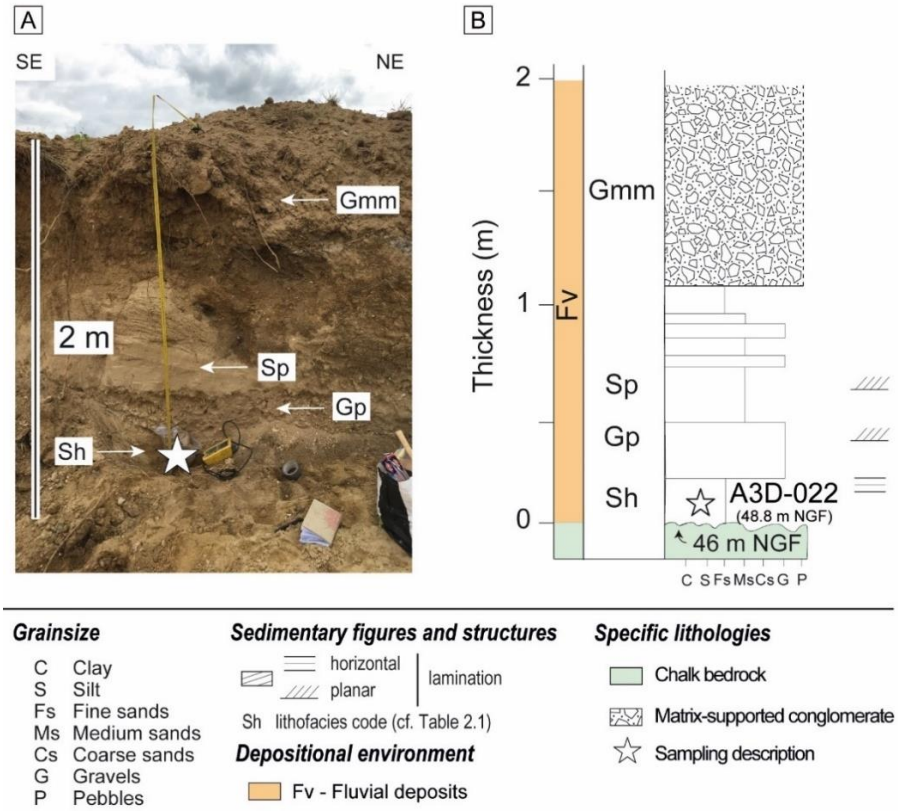

Figure 2.12. The fluvial sequence along the Fz terrace at Varenne-sur-Seine site. (a) Photography illustrating the main facies observed at the outcrop, white star represents the sample A3D-022. (b) Stratigraphic log showing sedimentology and stratigraphic surfaces with sample location.

2.1.2 Samples in the Marne and Loing valley bottoms

Two sites located in the valley bottom of the Marne and Loing valleys were described. (Figure 2.13). In the Marne and Loing valleys, two topographic profiles were projected along the current valley bottom (Figure 2.13). At Citry site in the Marne valley the profile has a length of about 2.5 km and SW-NE orientation (Figure 2.13-section G-G'). In contrast, at Dordives site in the Loing valley the profile has a length of c.a. 5 km and W-E orientation (Figure 2.13-section H-H').

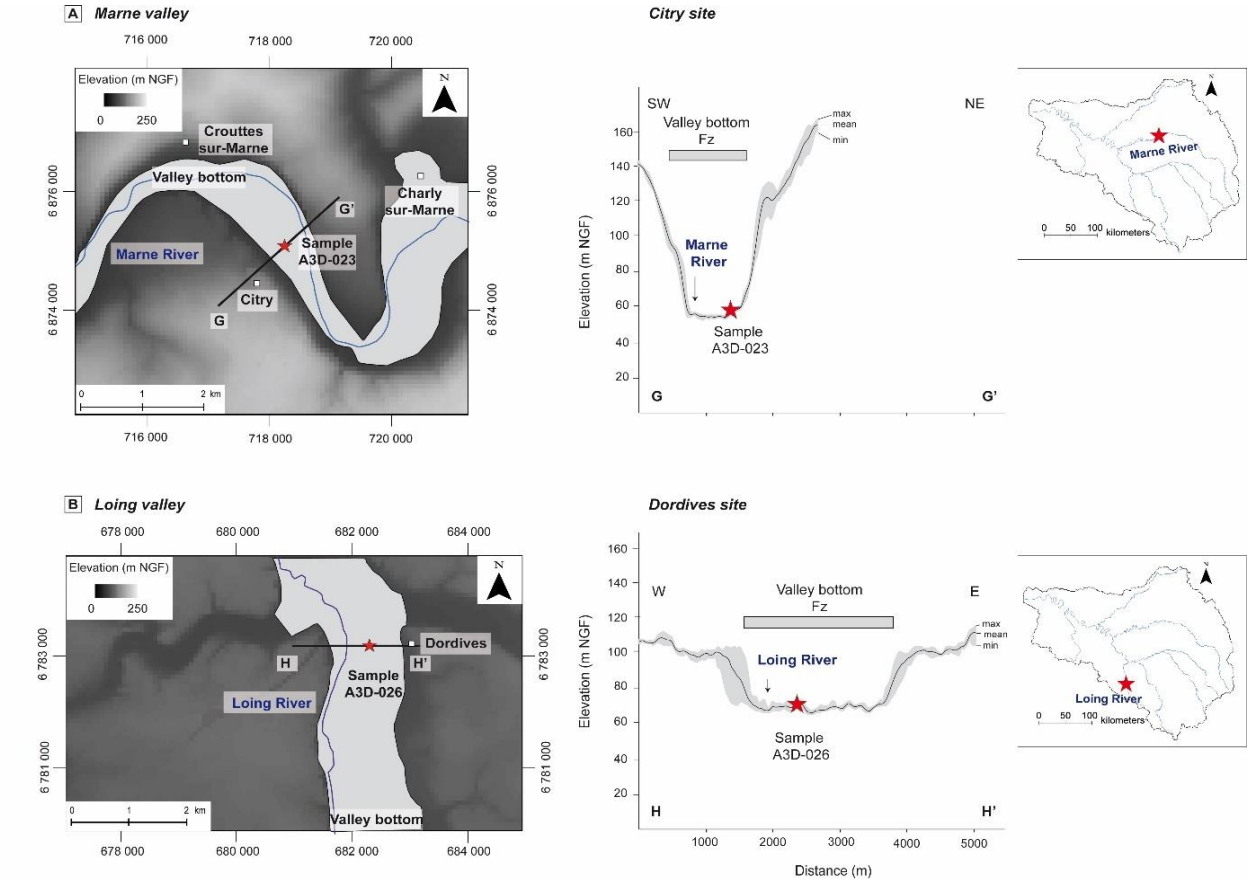

Figure 2.13. Sample locations on topographic swath profiles. (A) Location of Citry site within the Marne valley and section G-G' with the sample location. (B) Location of Dordives site within the Loing valley and section H-H' showing the sample location. The current valley bottom is represented by Fz terrace.

2.1.2.1.1 Fz terrace in the Marne valley: Citry (A3D-023)

In the eastern part of the Seine catchment, more specifically at Citry site, located on the left bank of the Marne River, which is a tributary of the Seine River, the Fz terrace was observed (Figure 2.13). Access to the sampling was facilitated through the active GSM "Luzancy" quarry. The bottom of the outcrop was characterized by Cenozoic limestone bedrock, which reached 46 m NGF. The bedrock was not observed directly on the outcrop because it was under water. Its absolute elevation was determined using the BSS boreholes near of the site. Due to the ongoing quarry operations, it was difficult to observe a representative outcrop and to clearly distinguish sedimentary structures and layers. The observable outcrop had a ca. 2 m thickness (Figure 2.14). The outcrop from its base to top consists of 0.5 m thick of fine sands (Sh facies), 0.5 m thick of gravels (Gp facies), 0.8 m thick of medium to coarse sands (Sm facies) and the

uppermost part of the outcrop is forming by 0.4 m thick of head deposits (Gmm facies). Sample A3D-023 was collected in the lower part of the outcrop from fine sands at 49 m NGF (+19.2 m RH or +13.2 m RH') for OSL dating.

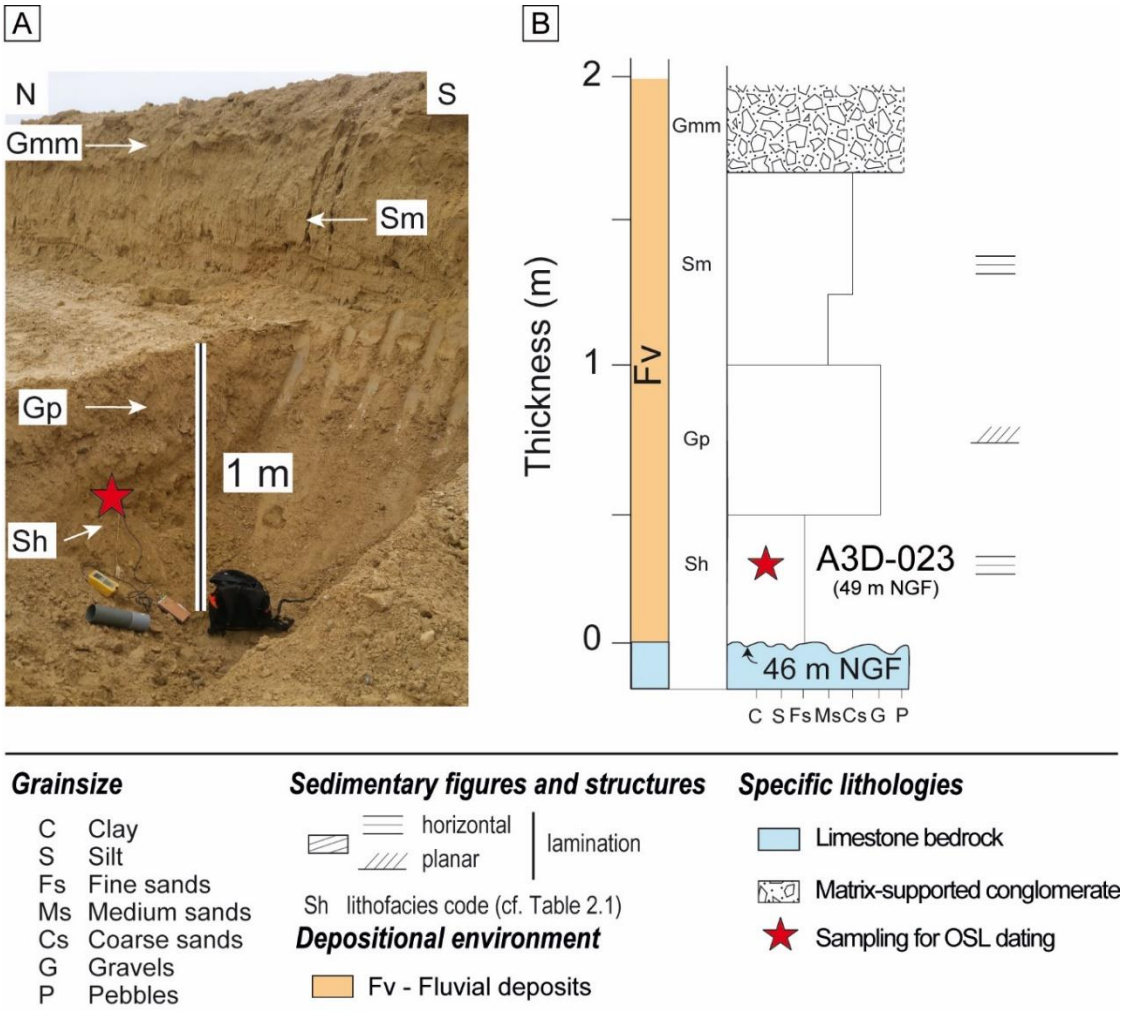

Figure 2.14. The fluvial sequence along the Fz terrace at Citry site. (a) Photography illustrating the main facies observed at the outcrop, white star represents the sample A3D-023 for OSL dating. (b) Stratigraphic log showing sedimentology and stratigraphic surfaces with sample location.

2.1.2.1.2 Fz terrace in the Loing valley: Dordives (A3D-026)

In the western part of the Seine catchment, more specifically at Dordives site, located on the right bank of the Loing River, which is a tributary of the Seine River, the Fz terrace was observed (Figure 2.13). Access to the sampling in quarry was facilitated by Lafarge granulats. The chalk bedrock from Upper Cretaceous was not observed directly because it was under water. Its elevation (62 m NGF) was determined using BSS boreholes near the site. Due to the

ongoing quarry operations, it was difficult to observe a representative outcrop, sedimentary structures and layers. The sediment was thus sampled directly under water on the pit using an excavator operated by a driver of Lafarge granulats. The elevation of the fine sands collected (A3D-026) was estimated to be 63.8 m NGF (+1.8 m RH or -5.2 m RH') (Figure 2.15).

Figure 2.15. Photography of sampling located along the current alluvial plain Fz at Dordives site. Red star represent the sample A3D-026 for OSL dating.

2.2 Downstream Paris

Field work in this area has been focused on the Seine valley between Paris and Le Havre, and in the Oise valley at Maurecourt near the confluence with the Seine River (Figure 2.16).

2.2.1 Samples along the Seine valley from Paris to Le Havre

A total of fourteen sites were described along the Seine valley from Paris to Le Havre. Eleven sites considered alluvial sediments from strath terraces and three sites from the current valley bottom (Figure 2.16 and Figure 2.3). In order to compare the different terrace levels in this area, a homogenization of the geological maps was proposed. For this, the geological map at 1:50000 scale, the recent research of Genuite et al., (2021) and the observations of this work were

considered. Terraces were grouped according to their absolute elevation (NGF), except for the valley bottom where the boundary limits were defined for terraces that are partly 10 m above and partly 10 m below the river elevation.

In total, 11 samples from strath terraces have been all dated in Bouafles (Fyb terrace), Moisson (Fyc terrace), Carrières-sous-Poissy (Fyd terrace), Sandrancourt (Fyd terrace), and Manoir Bresil (Fyd-Fyc terraces). Only two samples from the current valley bottom were dated at Saint-Martin-la-Garenne (Fz terrace) and Val-de-Reuil (Fz terrace). Another sample which is a part of the valley bottom is located at Achères (A3D-012) was only described in this work because the sample did not have enough quartz for dating methods.

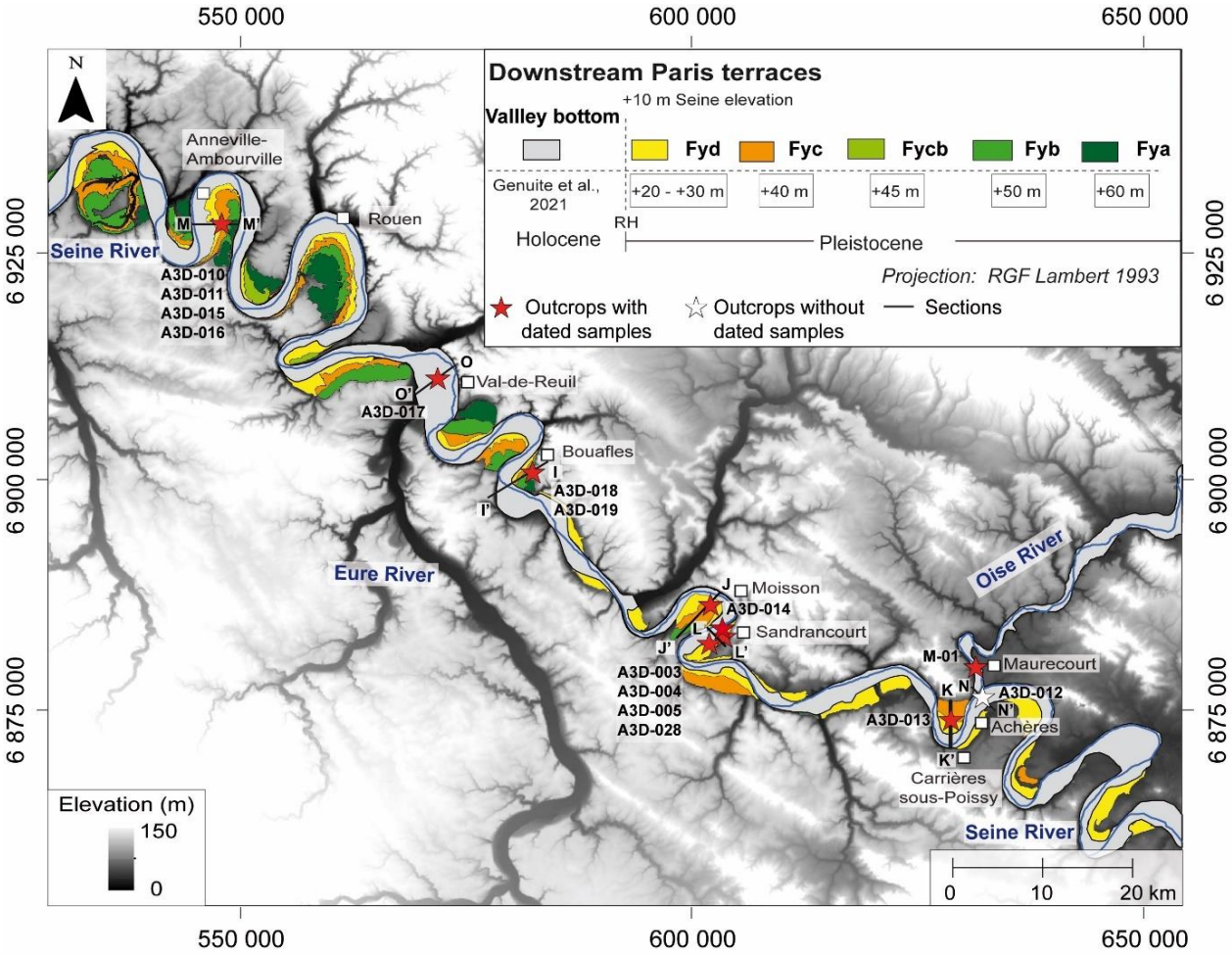

Figure 2.16. Homogenized geomorphological map from Paris to Le Havre (modified after Genuite et al., 2021), with location of the fourteen sites described and sampled for dating. Red stars represent outcrops with dated samples and white stars represents outcrops without dated samples. Black lines indicate topographic sections.

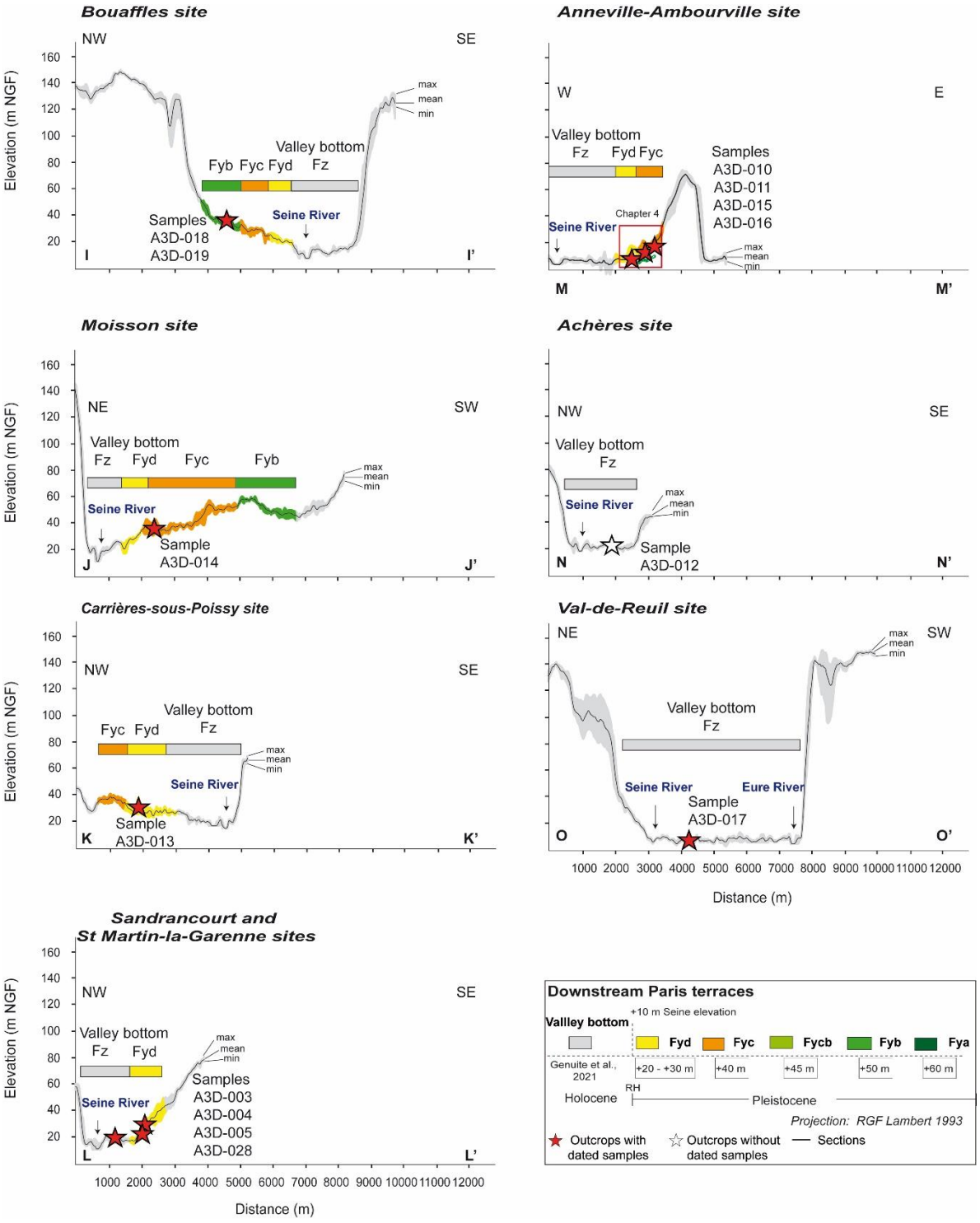

Figure 2.17. SWATH cross-sections showing the location of the samples taken downstream of Paris. See Figure 2.16 for location.

2.2.1.1 Samples from strath terraces

2.2.1.1.1 Fyb terrace: Bouafles CEMEX quarry (A3D-018 and A3D-019)

The Fyb terrace observed at Bouafles site is located on the right bank of the Seine River (Figure 2.16). Access to the quarry was facilitated by CEMEX. The visible outcrop had a c.a. 7.5 m thickness (Figure 2.18). The chalk bedrock from Upper Cretaceous was visible at the bottom of the section at 29 m NGF. Then, the sequence was mainly composed of 1 m thick of gravels with planar stratification (Gp facies), 1.2 m thick of coarse to fine sands (Sm facies), 0.4 m thick of gravels (Gp facies), 1.3 m thick of coarse to fine sands with cross-bedding stratification (Sr facies), 0.3 m thick of gravels (Gp facies), 0.8 m thick of medium sands with horizontally stratification (Sh facies). The sequence then graded to a 0.8 m thick of alternations between gravels and medium sands (Gp facies). The uppermost part of the sequence consisted of c.a. 1 m thick of head deposits (Gmm facies). Samples A3D-018 and A3D-019 were taken at 31 m NGF (+25 m RH o +18 m RH') and 31.5 m NGF (+27.6 m RH o +20.6 m RH') for ESR dating.

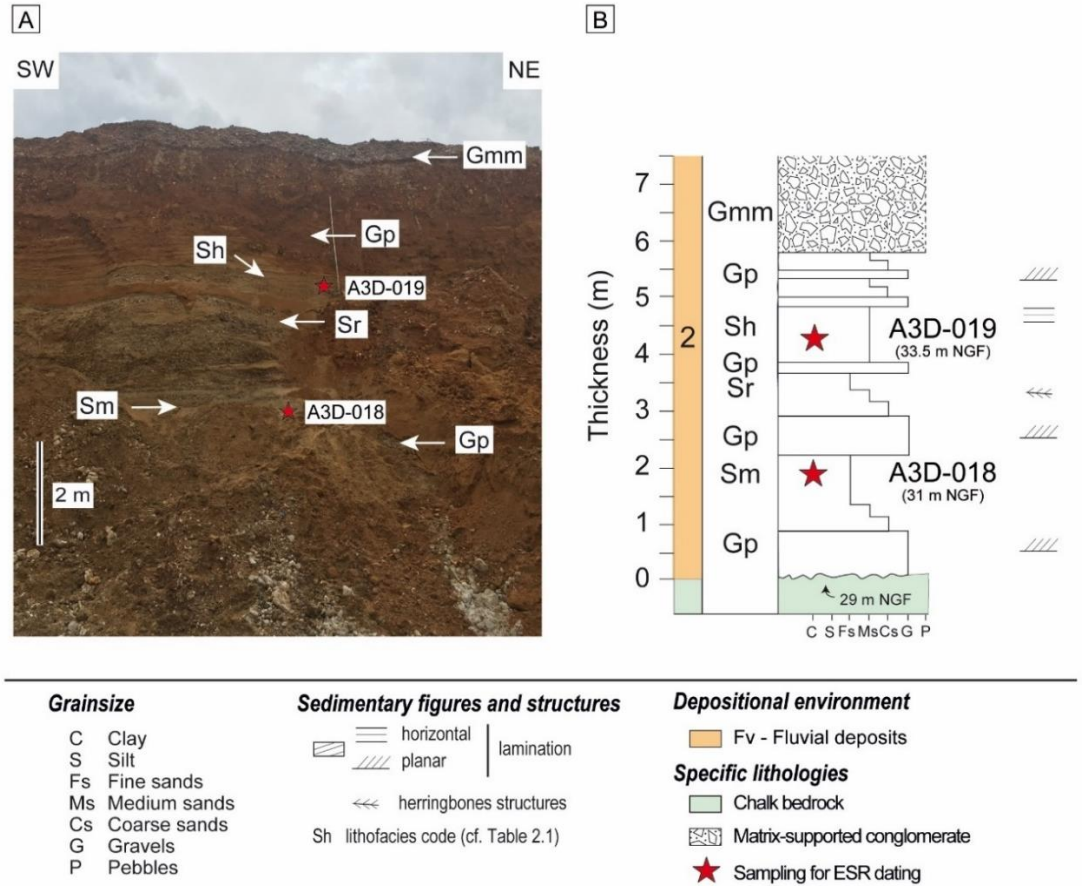

Figure 2.18. The fluvial sequence along the Fyb terrace at Bouafles site. (a) Photography illustrating the main facies observed at the outcrop, red star represents samples A3D-018 and A3D-019 for ESR dating. (b) Stratigraphic log showing sedimentology and stratigraphic surfaces with samples location.

2.2.1.1.2 Fyc terrace: Moisson abandoned quarry (A3D-014)

The Fyc terrace was observed at Moisson site on the left bank of the Seine River (Figure 2.16). The terrace was described by Lécolle (1989) but is now abandoned. Due to limited accessibility to a representative outcrop, sedimentary structures and layers were difficult to observe (Figure 2.19). The bedrock, consisting of the chalk from Upper Cretaceous, was not visible in this site. Its absolute elevation was determined using the BSS boreholes at 27 m NGF. The outcrop was a hole of c.a. 1 m deep, sediments were composed of sandy loam principally. Sample A3D-014 was taken from fine sands at 30 m NGF (+19.5 m RH o +12.5 m RH').

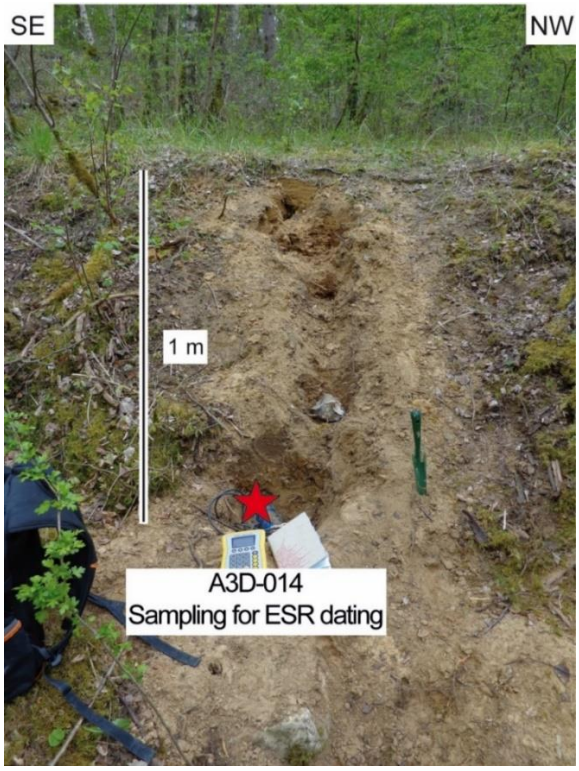

Figure 2.19. Photography of sample located in the Fyc terrace at Moisson site. Red star represents the sample A3D-014 for ESR dating.

2.2.1.1.3 Fyd terrace : Carrières-sous-Poissy (A3D-013)

Access to the sampling was facilitated by GSM. The Carrières-sous-Poissy site is located on the right bank of the Seine River. The outcrop had a 3.8 m thickness (Figure 2.20). The bottom of the sequence lies upon the chalk bedrock from Upper Cretaceous which reached 23 m NGF. Then, the sequence was characterized by 1.4 m thick of gravels to medium sands (Gp and Sm facies), 0.8 m thick of medium sands with horizontal stratification (Sm facies), 0.8 m thick of

gravels (Gp facies) and then 0.8 m thick of by head deposits (Gmm facies). Sample identified as A3D-013 was taken from medium sand at 25 m NGF (+15 m RH or +7.3 m RH'). This sample was prepared for OSL dating.

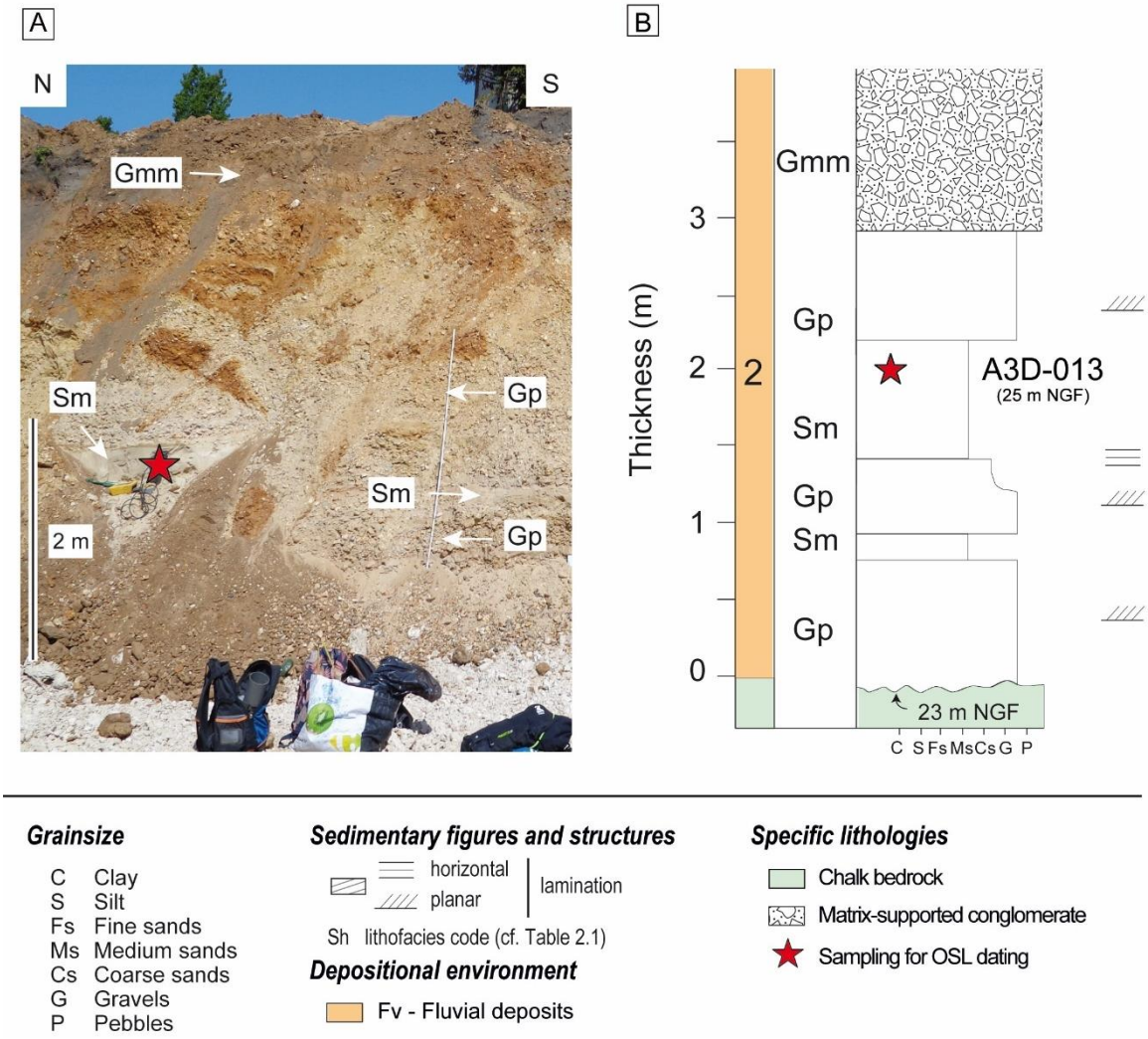

Figure 2.20. The fluvial sequence along the Fyd terrace at Carrières-sous-Poissy site. (a) Photography illustrating the main facies observed at the outcrop, red star represents sample A3D-013 for OSL dating. (b) Stratigraphic log showing sedimentology and stratigraphic surfaces with samples location.

2.2.1.1.4 Fyd terrace: Sandrancourt (A3D-003-004-005)

The Sandrancourt site is situated on the right bank of the Seine River. Access to the sampling was facilitated by Lafarge granulats. Two outcrops were studied in this quarry, they are 1.8 km apart. The first outcrop had a thickness of about 6 m (Figure 2.21). The chalk bedrock from Upper Cretaceous was visible at 16 m NGF. The section was characterized by 1 m thick of gravels with planar stratification (Gp facies), 1.5 m thick from coarse to fine sands (Sm facies),

1 m thick from gravels to coarse sands in which gravels are predominant (Gp facies), 1.5 m thick from coarse to fine sands with planar stratification (Sm facies). The top of the section was covered by c.a. 1 m of head deposits (Gmm facies). Samples A3D-003 and A3D-004 were taken from finest sands at 18 m NGF (+11 m RH or +2 m RH') and 20 m NGF (+13 m RH or +4 m RH') for both ESR and OSL dating.

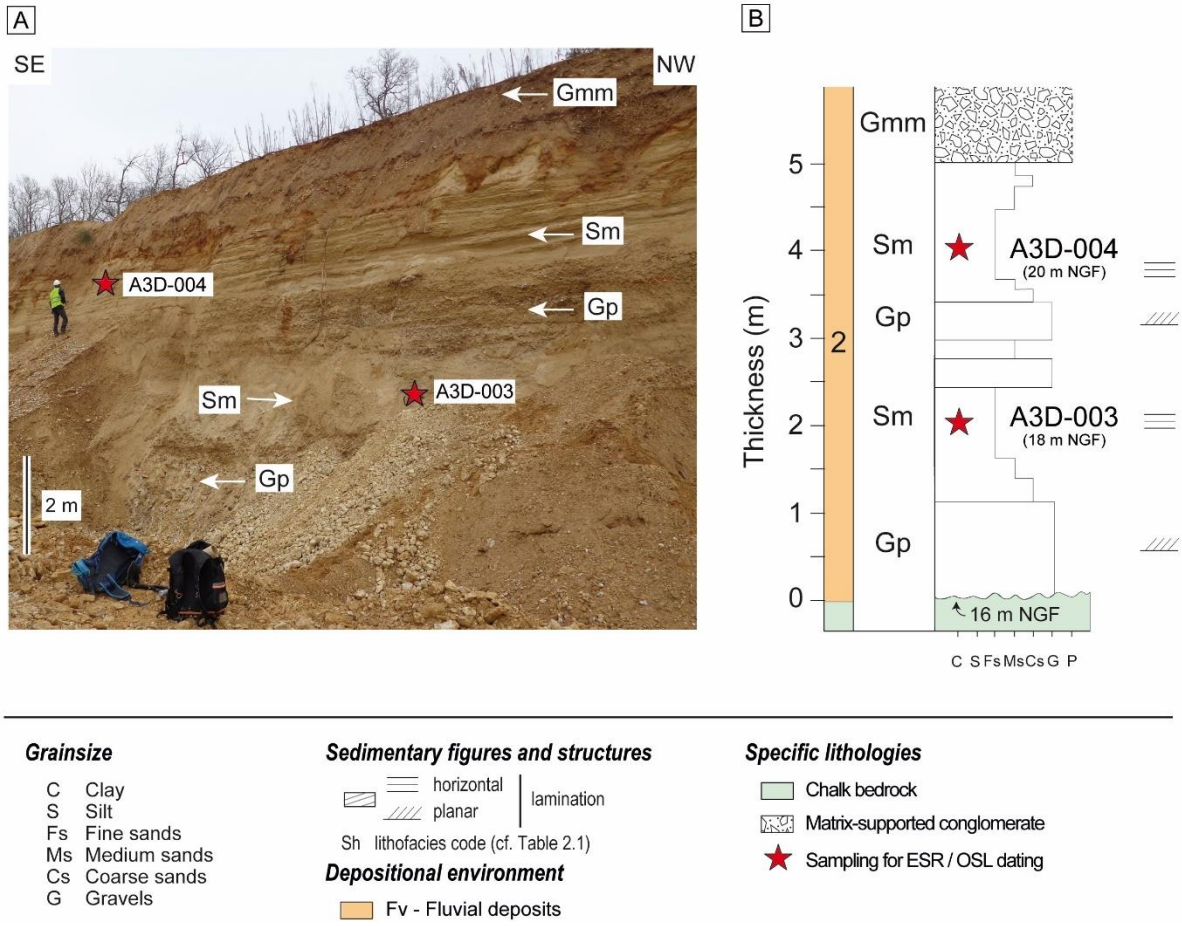

Figure 2.21. The fluvial sequence along the Fyd terrace at Sandrancourt site. (a) Photography illustrating the main facies observed at the outcrop, red star represents samples A3D-003 and A3D-004 for ESR and OSL dating. (b) Stratigraphic log showing sedimentology and stratigraphic surfaces with samples location.

The second outcrop was c.a. 10 m thick (Figure 2.22). The chalk bedrock was visible at 13 m NGF. The sequence was then characterized by 0.5 m thick of gravels (Gp facies), 2 m thick of coarse to fine sands (Sm facies). Then, the sequence graded through 2 m thick of gravels to coarse sands (Gp, Sm facies), 3.5 m thick of medium sands (Sm facies), 0.5 m thick of gravels (Gp facies) and 0.5 m thick of coarse to medium sands (Sm facies). The uppermost part of the

outcrop was covered by c.a. 1.5 m thick of head deposits (Gmm facies). Sample A3D-005 was taken from the fine sands in the lower part of the outcrop at 15 m NGF (+9 m RH or +1 m RH') for both ESR and OSL dating.

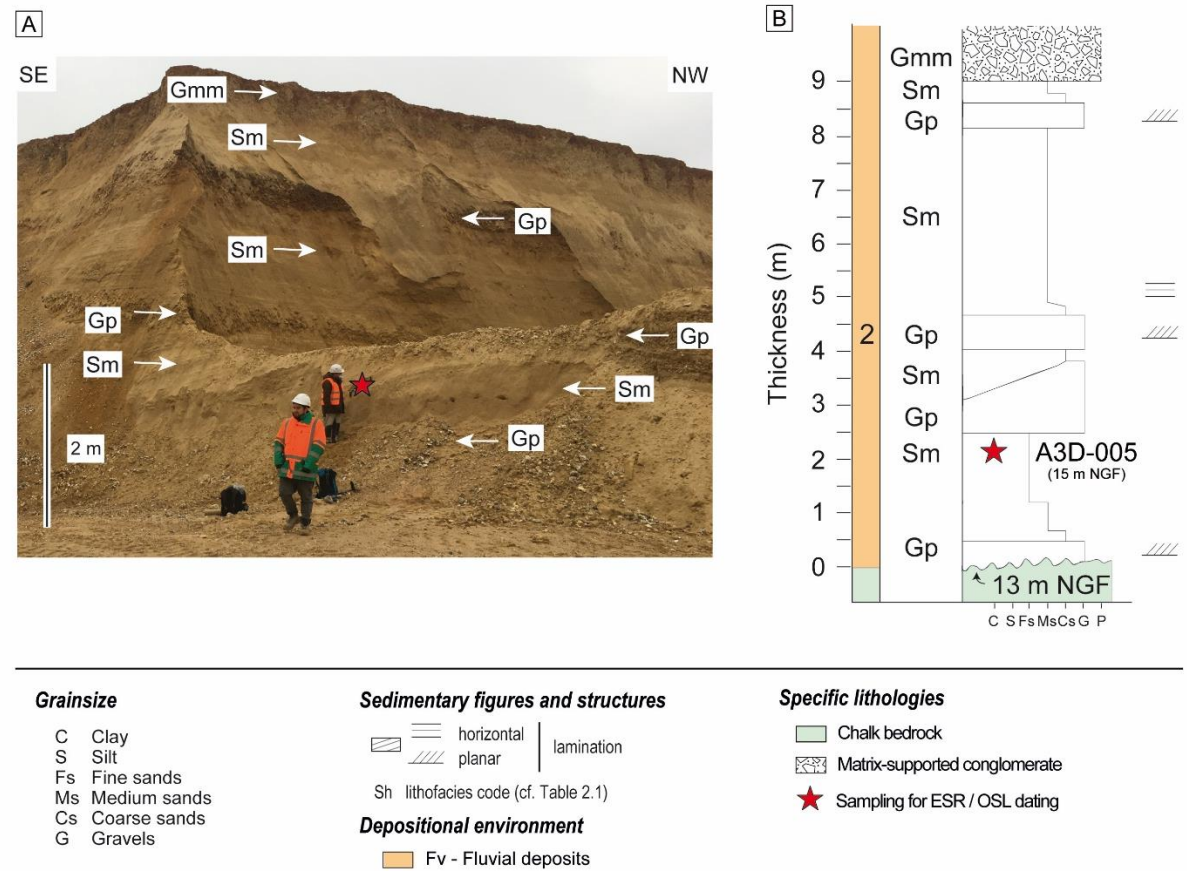

Figure 2.22. The fluvial sequence along the Fyd terrace at Sandrancourt site. (a) Photography illustrating the main facies observed at the outcrop, red star represents sample A3D-005 for ESR and OSL dating. (b) Stratigraphic log showing sedimentology and stratigraphic surfaces with samples location.

2.2.1.1.5 Fyd and Fyc terraces: Manoir Bresil site (A3D-010; 011; 015 and A3D-016)

Field work and sampling in this area was focused on the Anneville-Ambourville site, in a quarry called Manoir Brésil (Figure 2.16). This site was the object of a manuscript focusing on the description and dating of the terraces above the valley bottom (see Chapter 4 for details).

2.2.1.2 Samples from the valley bottoms

2.2.1.2.1 Fz terrace: Achères (A3D-012)

The Fz terrace was observed after the confluence with the Oise River at Achères site, located on the left bank of the Seine River (Figure 2.16). Access to the sampling was facilitated through the active GSM quarry. The outcrop has thickness of c.a. 3.5 m (Figure 2.23). The bottom of the outcrop was characterized by clay bedrock from Cenozoic which reached 13 m NGF. The bedrock elevation was determined using BSS boreholes near the site. The outcrop was composed of 0. 7 m thick of gravels with a planar cross-bedding stratification (Gp facies), 1 m thick of intercalation from coarse to fine sands with trough cross stratification (St facies) and massive sands (Sm facies). Then the sequence was followed by 0.3 m thick of gravels (Gp facies), 0.7 m thick of intercalation from coarse to medium sands (Sm facies). The uppermost part of the outcrop was composed of 0.8 m thick of head deposits (Gmm facies). Sample identified as A3D-012 was taken from finest sand at 22 m NGF (+8 m RH or +1 m RH'). This sample was prepared for ESR/OSL dating, unfortunately, it was not dated successfully because the sample do not have enough quartz.

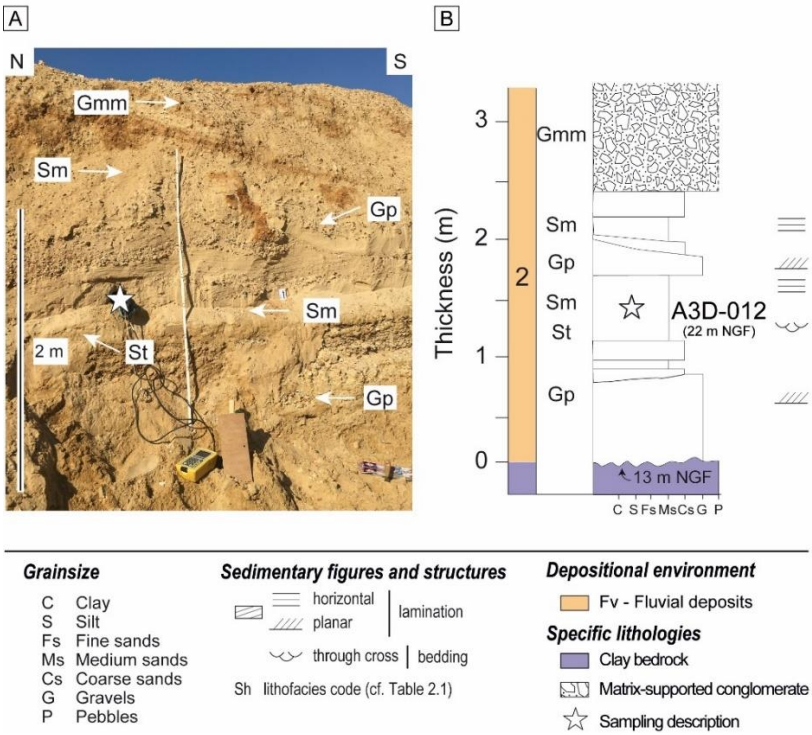

Figure 2.23. The fluvial sequence along the Fz terrace at Achères site. (a) Photography illustrating the main facies observed at the outcrop, white star represents sample A3D-012 for sampling description. (b) Stratigraphic log showing sedimentology and stratigraphic surfaces with sample location.

2.2.1.2.2 Fz terrace: Saint-Martin-la-Garenne (A3D-028),

The Fz terrace was observed at Saint-Martin-la-Garenne at 1.5 km of Sandrancourt (Figure 2.16). Access to the quarry was facilitated by Lafarge granulats. This site was a part of an archeological excavation carried out by the *INRAP* team. The outcrop had thickness of about 1.9 m (Figure 2.24). The bottom of the section was characterized by the chalk bedrock from Upper Cretaceous, which reached 8 m NGF. The bedrock elevation was determined using the BSS boreholes near the site. The sequence was characterized principally by 0.25 m thick of fine sands with horizontally stratification (Sh facies), 0.2 m thick of gravels (Gp facies) and 1.45 m thick of fine sands with some gravel layers (Sm facies), these sands are darker towards the top of the section. Sample A3D-028 was taken from fine sands in the lower part of the sequence at 16.8 m NGF (+10.8 m RH or +2.8 m RH') for OSL dating.

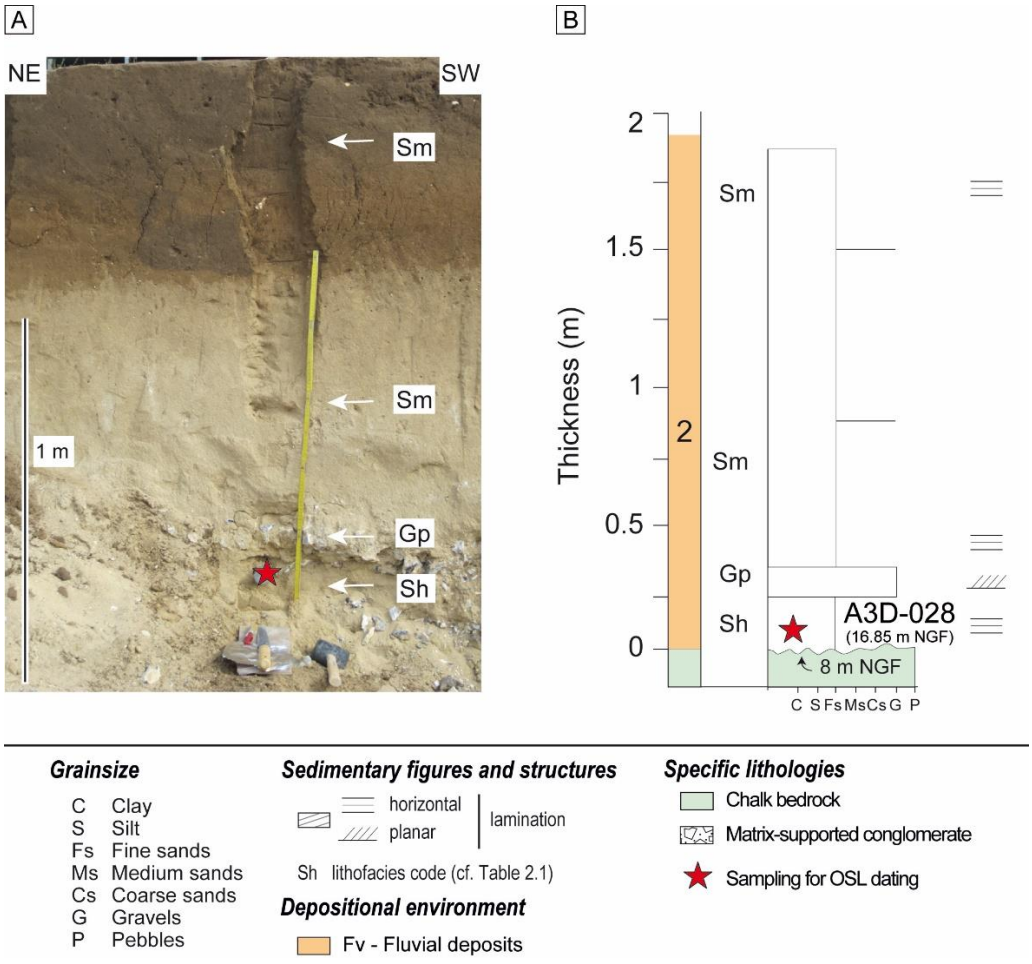

Figure 2.24. The fluvial sequence along the Fz terrace at Saint Martin-la-Garenne site. (a) Photography illustrating the main facies observed at the outcrop, red star represents sample A3D-028 for OSL dating (modified after Coussot et al., in prep). (b) Stratigraphic log showing sedimentology and stratigraphic surfaces with sample location.

2.2.1.2.3 Fz terrace: Val-de-Reuil (A3D-017)

The Fz terrace was observed at Val-de-Reuil (Figure 2.16). Access to the quarry was facilitated by CEMEX. The outcrop had a ca. 1.7 m thickness (Figure 2.25). The bottom of the outcrop was formed by the chalk bedrock from Upper Cretaceous which it was under water. Its absolute elevation was determined using the BSS boreholes (2 m NGF). The sequence was mainly composed of 0.7 m thick of fine sands (Sm facies), 0.3 m thick from gravels to medium sands (Gp facies). The uppermost part was characterized by 0.7 m thick of head deposits (Gmm facies). A sample identified as A3D-017 was taken from the fine sands at 7.6 m NGF (+7 m RH or +0 m RH') for ESR dating.

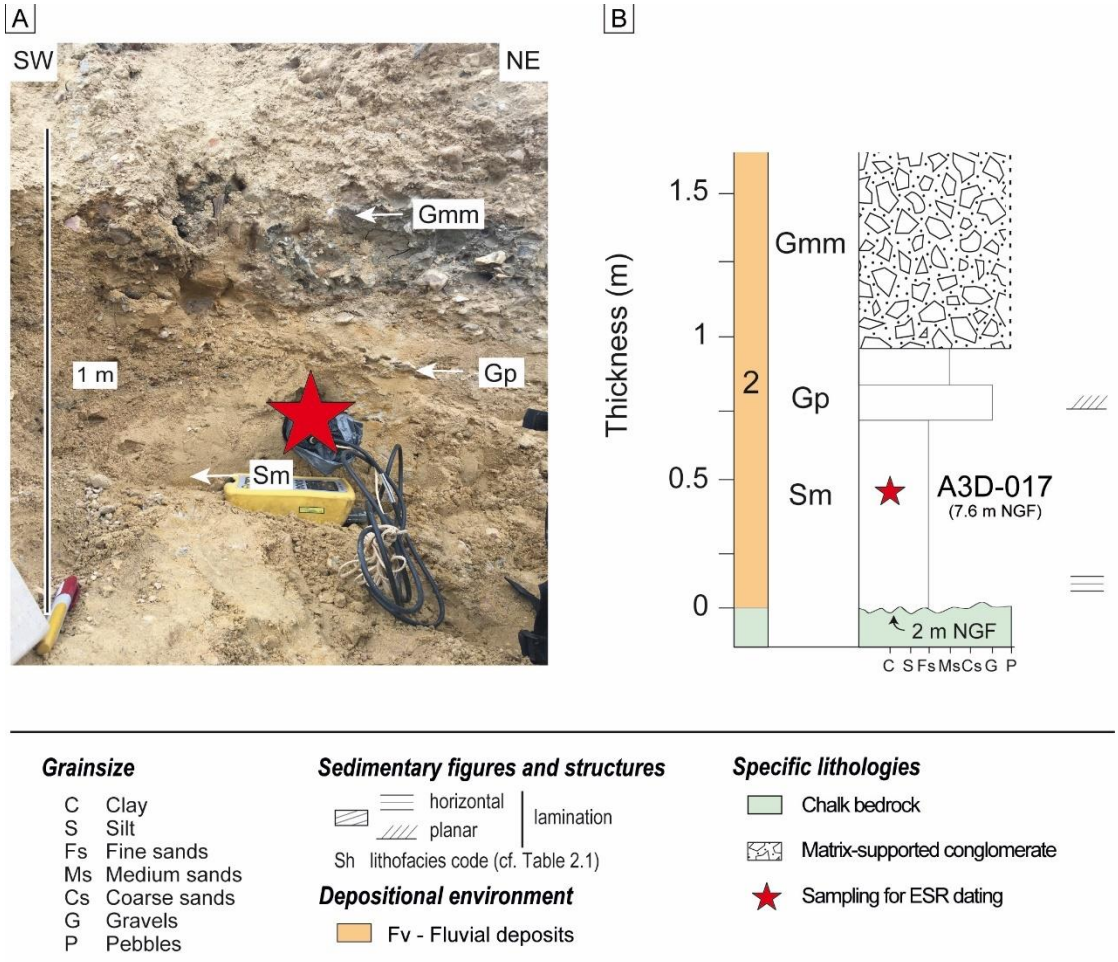

Figure 2.25. The fluvial sequence along the Fz terrace at Val-de-Reuil site. (a) Photography illustrating the main facies observed at the outcrop, red star represents sample A3D-017 for ESR dating. (b) Stratigraphic log showing sedimentology and stratigraphic surfaces with sample location (a) Photography of sampling.

2.2.2 Sample from the Oise valley bottom

2.2.2.1.1 Fz terrace in the Oise valley: Maurecourt (M-01)

The Fz terrace was observed at Maurecourt, located in the right bank of the Oise River (Figure 2.26). Sampling at Maurecourt was made in 2014 by Christine Chaussée during an archeological excavation carried out by the *INRAP* team (French national Institute for Preventive Archaeologic Research, Blaser et al., 2015). The bottom of the section was characterized by the sand bedrock from Cenozoic at 18 m NGF. The bedrock elevation was determined using the BSS boreholes near of the site. The section had thickness of c.a. 6 m. The section was mainly composed of 5.6 m thick of sandy loam with planar lamination (Fl facies). The uppermost part of the section was formed by 0.4 m thick of residual soil. Sample M-01 was collected from the fine sand layer at 20.7 m NGF (+12.7 m RH or 0 m RH') for OSL dating (Figure 2.27). It was kindly given by Fredéric Blaser and Christine Chaussée.

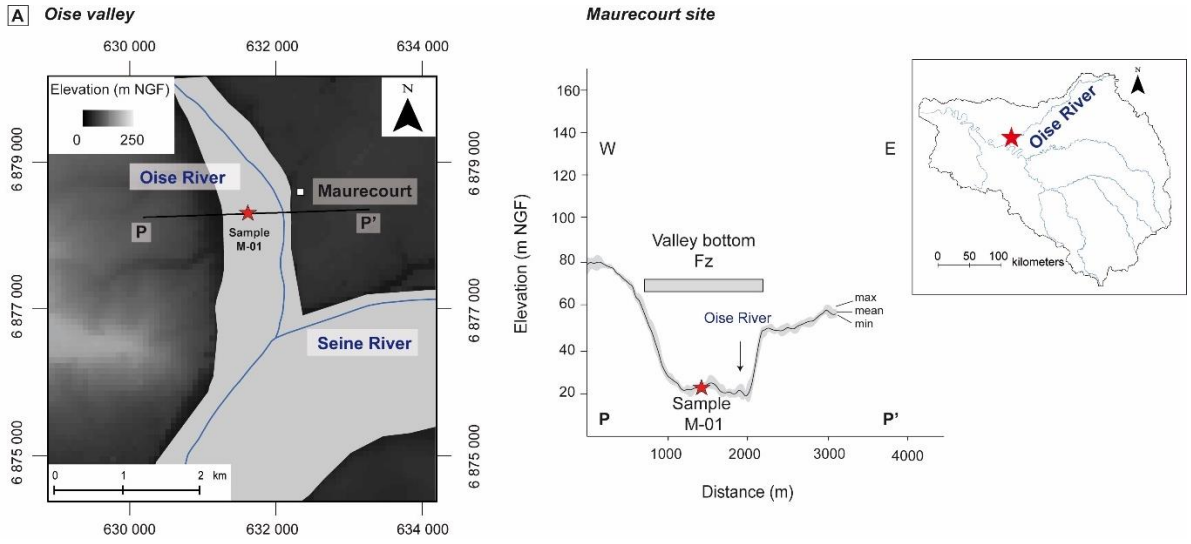

Figure 2.26. Location of Maurecourt site within the Oise valley and section P-P' showing the sample location in the current valley bottom.

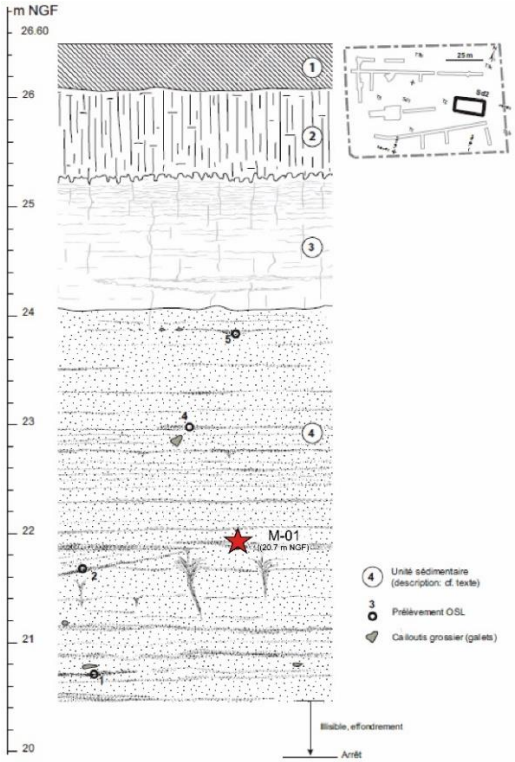

Figure 2.27. Stratigraphic log of sample M-01 located in the current alluvial plain at Maurecourt in the Oise valley (Blaser et al., 2015). Red star represents the position of sample for OSL dating.

2.3 Synthesis

The main sedimentary facies observed are principally of fluvial origin, except downstream Paris at Manoir Brésil where tidal and tidally influenced deposits were found, showing the influence of relative sea level change (see Chapter 4). Nowadays, the tidal influence limit is marked by the Poses dam, near of the confluence with the Eure River (Antoine et al., 2007;2020; Jamet, 2014; Bahain, 2019).

At least, 24 samples were collected only 21 samples have been dated the other three samples was collected but not dated because the amount of quartz presented in the sample was not sufficient. Seven samples located upstream Paris have been dated in which 2 samples were dated by ESR and 5 samples were dated by OSL. Fourteen samples located downstream Paris have been dated in which 4 samples were dated by ESR, 3 samples by OSL and 7 samples coupling both ESR/OSL methods (Table 2.1). The longitudinal profile of the Seine River shows the position of all samples of this study (Figure 2.28). Some of samples are located above de Seine River representing the alluvial terraces, and others located in the current alluvial plain. Sample ages will help to constrain the timing of development of terraces and to reconstruct the

initial chronology framework and to know the incision rate of the Seine valley and its main tributaries.

When it was possible the bedrock elevation was measured directly on the field: upstream Paris only one site at Courceroy in the Bassée area and downstream Paris at Bouafles, Manoir Brésil, Sandrancourt and carriers-sous-Poissy. On the contrary, as the bedrock is frequently unobservable at outcrop level (covered or underwater), the elevation of its top is determined using data from BSS nearby of terrace: upstream Paris at Fontaine Mâcon, Marolles-sur-Seine, Noyen-sur-Seine,Bazoches, Vimpelles, Varenne-sur-Seine in the Bassée area, at Dordives in the Loing valley and at Citry in the Marne valley. Downstream Paris at Moisson, Achères, Saint-Martin-la-Garenne, Val-de-Reuil and Maurecourt site in the Oise valley.

Table 2.1. Summary table of 21 samples collected for ESR/OSL dating method, indicating the terrace, absolute elevation, and relative elevations above the maximum incision of the river RH or above the alluvial plain RH'.

Upstream Paris							
Location	**Terrace**		**Sample**	**Elevation (mNGF)**	**RH (m)**	**RH' (m)**	**Dating method**
Fontaine Mâcon	**T_{IV}**		**A3D-006** Fluvial deposit	104,2	52	46	**ESR**
Courceroy	**T_{III}**		**A3D-024** Fluvial deposit	69,2	22	14	**ESR**
Noyen-sur-Seine	**Valley bottom**	**T_2**	**A3D-020** Fluvial deposit	56	8	1	**OSL**
Bazoches		**T_2**	**A3D-021** Fluvial deposit	51	6	0	**OSL**
Vimpelles		**T_{3a}**	**A3D-002** Fluvial deposit	51.2	6.2	0.2	**OSL**
Citry **		**Fz**	**A3D-023** Fluvial deposit	69.2	19	13	**OSL**
Dordives **		**Fz**	**A3D-026** Fluvial deposit	63.8	1.8	-5.2	**OSL**
Downstream Paris							
Bouafles	**Fyb**		**A3D-018** Fluvial deposit	31	25	18	**ESR**
			A3D-019 Fluvial deposit	33.5	28	21	**ESR**
Moisson	**Fyc**		**A3D-014** Fluvial deposit	30	19	12	**ESR**
Carrières-sous-Poissy	**Fyd**		**A3D-013** Fluvial deposit	25	15	7	**OSL**
Sandrancourt	**Fyd**		**A3D-003** Fluvial deposit	18	11	2	**ESR/OSL**
			A3D-004 Fluvial deposit	20	13	4	**ESR/OSL**
			A3D-005 Fluvial deposit	15	9	1	**ESR/OSL**
Manoir Brésil *	**Fyd**		**A3D-010** Fluvial deposit	2.75	14	3	**ESR/OSL**
	Fyd		**A3D-011** Tidal deposit	5	17	6	**ESR/OSL**
	Fyc		**A3D-015** Tidal deposit	7.5	19	8	**ESR/OSL**
	Fyd		**A3D-016** Periglacial deposit	12.5	24	13	**ESR/OSL**
St-Martin-la-Garenne	**Valley bottom**	**Fz**	**A3D-028** Fluvial deposit	16.85	11	3	**OSL**
Val-de-Reuil		**Fz**	**A3D-017** Fluvial deposit	7.6	7	0	**ESR**
Maurecourt **		**Fz**	**M-01** Fluvial deposit	20.7	13	-0.3	**OSL**

* See chapter 4 for more details
**Tributaries of the Seine River

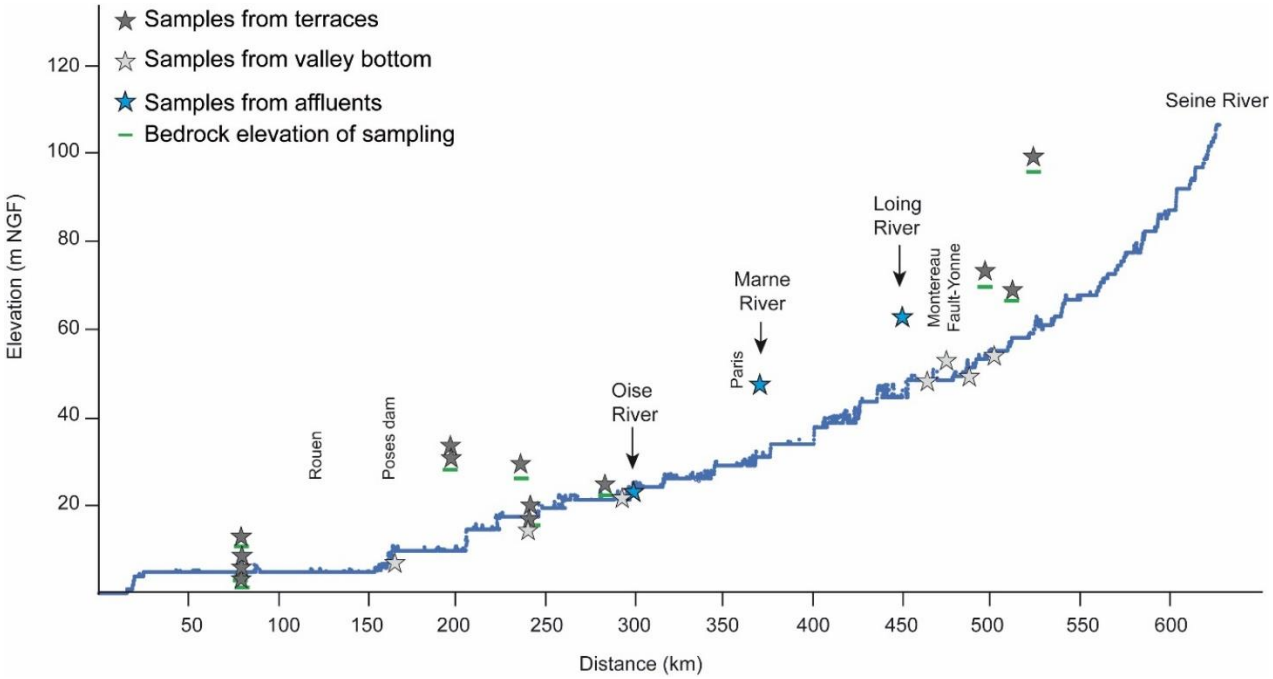

Figure 2.28. Seine River profile and sample locations. Stars represent samples upstream-downstream Paris and within terraces or as a part of the current valley bottom, as well as samples from the main affluents such as Loing, Marne and Oise rivers.

Chapter 3: ESR/OSL chronostratigraphy

Ce chapitre se concentre sur les méthodes de datation par Résonance Electronique de Spin (ESR) et par Luminescence Stimulée Optiquement (OSL), principalement appliquées aux sédiments fluviaux. Il est divisé en deux parties : la première partie présente les principes généraux des deux méthodes. La seconde partie montre les résultats obtenus pour les sédiments échantillonnés le long de la Seine et de ses affluents, fournissant un cadre chronologique pour les basses terrasses alluviales quaternaires et le remplissage du fond de vallée dans le bassin versant de la Seine.

Chapter 3

3 ESR/OSL chronostratigraphy

This chapter focuses on the Electron Spin Resonance (ESR) and the Optically Stimulated Luminescence (OSL) dating methods, mostly applied to fluvial sediments. It is divided into two parts: the first part introduces the general principles of two methods. The second part shows the results obtained for all data sampled along the Seine River and its tributaries, providing a chronological framework for Quaternary alluvial terraces and valley bottom infill within the Seine catchment.

3.1 ESR-OSL dating methods

3.1.1 Electron Spin Resonance (ESR) dating of sedimentary quartz: General principles

The Electron Spin Resonance (ESR) is a paleodosimetric dating method based on the evaluation of the exposure of some materials such as sediments to natural radioactivity (Grün and Stringer, 1991; Voinchet, 2002; Bahain et al., 2002; Duval, 2016). This method can be applied to materials whose crystalline lattice contains impurities or defects capable to trap the effects of radioactivity. In nature, many minerals, or organic materials such as quartz, feldspar, calcite, and enamel have this capacity, due to the presence of the paramagnetic centres in their structure able of trapping electrons set in motion by alpha (α), beta (β) or gamma (γ) radiation (ionisation).

In fluvial geology, the focus is on the quartz because (i) it is a mineral found in many geological contexts and it is particularly abundant in fluvial sediments, (ii) the quartz in sediments is a suitable mineral for ESR dating because it is constantly exposed to radiation from the radioelements in the sample and its surrounding environment. These radioelements are mainly the isotopes of uranium (U) and thorium (Th) families and potassium (K). The natural radioactive decay of these radioelements produces the emission of alpha (α), beta (β), gamma (γ) rays which, together with cosmic rays, allow the creation of unpaired electrons that can be trapped in defects in the quartz crystal lattice (Yokoyama et al., 1985; Falguères et al., 1986; Ikeya, 1993; Toyoda and Ikeya, 1994; Voinchet, 2002).

In the quartz grains, these defects correspond to paramagnetic centres resulting from the substitution of a silica atom by an aluminium or titanium atom (Figure 3.1).

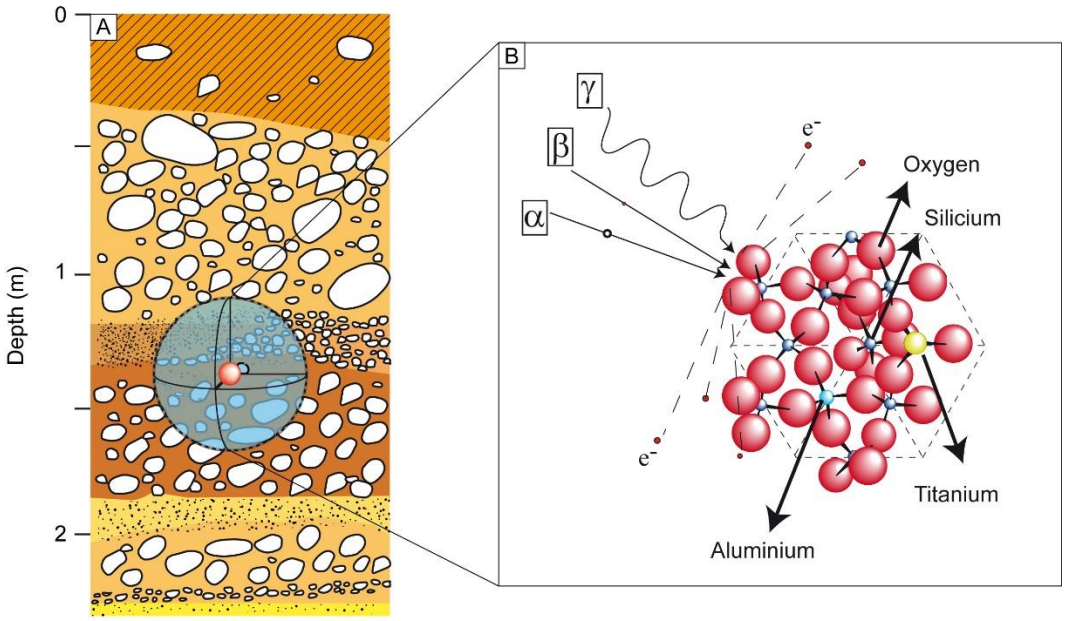

Figure 3.1. Origin of the external dose of quartz. (a) Dateable samples buried in sediments are subjected to ionizing radiation of various origins. (b) Main paramagnetic centres present in the quartz crystal lattice (Voinchet, 2002).

The amount of electrons captured by the grains depends on the quantity of paramagnetic center available of the grain and on the amount of radiation emitted from the environment and from datable material itself. The radiation is received by sample with different efficiency depending on the nature of the minerals and the sediment water content (more water in sediment means more attenuation of the radiation). This received dose calculated for one year is called the "annual dose" (Da). In practice, this dose is determined using both gamma spectrometry in the laboratory (for alpha and beta estimation) and in situ gamma spectrometry (to consider the effect of the environment). The cosmic dose is calculated considering the altitude, latitude and depth of the sample.

In the case of quartz, the most commonly paramagnetic centres observed are related to aluminium (Al-centre, where an electron trapped in substitutional Al replacing Si) and titanium Ti-related impurity defects, in which three sub-centres, Ti-Li, Ti-H and Ti-Na centres (an electron trapped in substitutional Ti replacing Si) (Ikeya, 1989). These paramagnetic centres have the particularity of being detectable and identifiable by ESR spectrometry. The atomic assembly within the crystalline lattice, specific to each of paramagnetic centres leads to obtaining a particular signal. Some centres are radiosensitive, this means that the intensity of the signals increases according to the radiation dose received for each paramagnetic centre. Thus, these paramagnetic centres can be used as geochronometers for dating.

The ESR signals of these centres and the increase of their intensities in response to irradiation is used to determine the radiation dose received by the samples in their natural environment since its deposition. Indeed, the ESR signal intensity is related to the amount of electrons trapped in the paramagnetic centres of the sample since its deposition but also since the last reset to zero of the centres by external energy input such as sunlight, pressure, or heating (Ikeya, 1989). Thus, when sediments are transported by the fluvial system, some electrons trapped in the crystalline lattice of the quartz since their formation are released because of their exposure to sunlight (UV, Tissoux et al., 2007) and the chronometer is reset to zero. This phenomenon is called bleaching. Once the quartz grains have been deposited in an alluvial terrace, protected from the sunlight, the electrons will begin to accumulate again in traps over time. The dose received from that point correspond to the total dose Dt. The total dose cannot be measured directly in laboratory, thus an equivalent dose (De) to the total dose should be determine for the age calculation.

Once the annual dose (Da) and the equivalent dose (De) are known, it is then possible to propose an age of burial of the quartz grains. In case of sedimentary quartz, considering that the Da does not vary over time (*Da(t)=constant= Da*), the ratio of the equivalent dose and the annual dose can be used to give a duration of quartz burial into the sedimentary sequence (i.e., the age of the sedimentary quartz), just after its reset in a fluvial environment during the transport of the sediment (Equation 1, Voinchet et al., 2004, 2015):

$$T = \frac{De}{Da} \qquad \text{Equation 3.1}$$

where *T* is the time that the sample has been exposed to radiation (the ESR age), *De* is the equivalent dose received by the sample, *Da* is the annual dose of natural radiation.

To calculate the age of the deposit it will be necessary to determine the equivalent dose (De) and the annual dose (Da). In such situation, the calculated age determined by ESR in quartz does not correspond to the mineral crystallisation, but to the moment at which they were buried in the alluvial deposits.

3.1.1.1 The multicentre method and interest

The different paramagnetic centres of quartz do not have all the same capacity to easily reset to zero in the presence of sunlight (UV). This is called photosensitivity. The kinetics of bleaching varies from one ESR centre to another centre:

The aluminium (Al) centre is the most used in quartz ESR dating because it is abundant, and it has a good thermal stability over time. It can therefore be used to dates samples up to several million years (Voinchet et al., 2015). In contrast, titanium (Ti) centres are less abundant in samples for dating. Two Ti-centres can be used: the titanium-lithium (Ti-Li) and the titanium-hydrogen (Ti-H) (Toyoda and Ikeya, 1994).
The Al-centre is less light-sensitive to irradiation and reset than Ti-Li-centre, which is itself less light-sensitive than Ti-H-centre. The simultaneous study of these three centres may provide information on the age of transport and deposition but also on the conditions of transport and possible remobilization of sediments (multi-centre approach: Toyoda et al., 2000; Tissoux et al., 2007).
To have a reliable dating of a sediment deposition, at least one of the centres must completely reset, otherwise, the age obtained can be considered as a maximum age. In the history of a quartz grain from source to final deposition in an alluvial formation (Figure 3.2), several phases with different bleaching rates for the three centres can occur:

- In the erosion zones, exposure to light is not sufficient for the Al-centre to be fully bleached but the Ti-centre can be bleached (Figure 3.2-a).
- In the main course of the river bed, the grains strongly exposed to sunlight (UV) allow a maximum bleaching of the three centres (Figure 3.2-b).
- When the three centres have been bleached during transport, once in the fossil terraces, they will have a signal that will increase regularly over time (Figure 3.2-c).
- When transport has been insufficient or in the case of grain remobilisation from an older sediment with a short distance, exposure to light was not sufficient for the Al-centre to be fully bleached but the Ti-centre can be bleached (Figure 3.2-d).
- In old fossil terraces, Ti-H and even Ti-Li may be saturated (Tissoux et al., 2007) and the Ti ages are underestimated, the bleaching cycle of the eroded grains will begin again and can be complete or not (Figure 3.2-e).

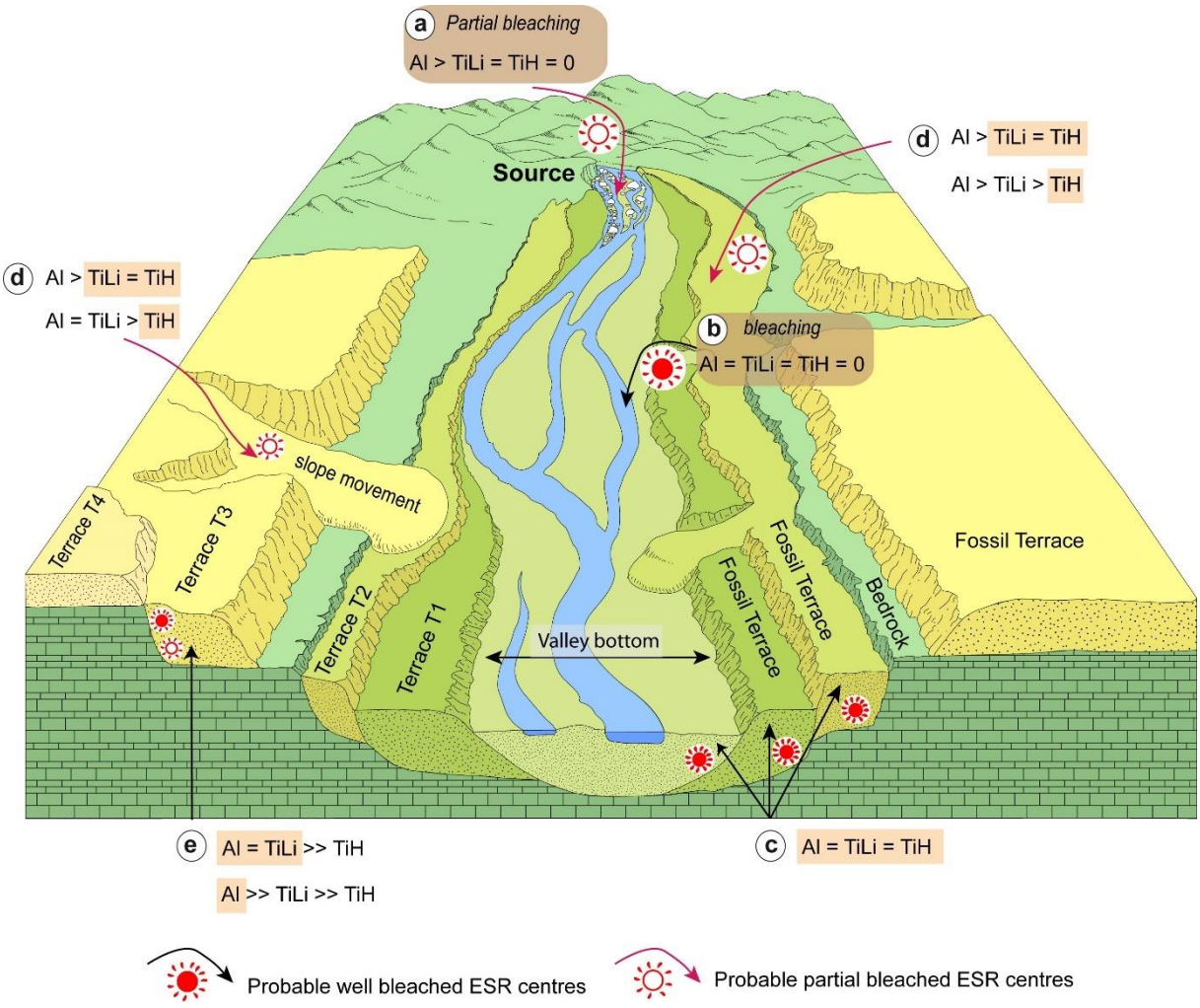

Figure 3.2. Paramagnetic centres intensity expected in a fluvial environment. Orange rectangles represents the preferable centre to give an ESR age. (a) In erosion zone, the Ti-centre can bleach very quickly but Al-centre are not completely bleached. (b) In river bed, all three centres are completely bleached. (c) In the fossil terrace, all three centres have a signal that increase over time. (d) In case of grain remobilisation from an older sediment or when transport has been insufficient, exposure to light was not sufficient for the Al-centre to be fully bleached but the Ti-centre can be bleached. (e) In old fossil terraces, the bleaching cycle of the eroded grains will begin again and can be complete or not.

When studying the sediment deposition of quartz grain, it will be very common to observe different results from these three centres. Three most frequent scenarios are possible when measuring the intensity of Al, Ti-Li and Ti-H centres in sedimentary quartz grain by ESR (Table 3.1).

Table 3.1. Frequent possible scenarios when measuring the intensity of Al, Ti-Li and Ti-H centres in sedimentary quartz grain and choice of the paramagnetic centre(s) chosen for age calculation.

Centre	Process and distance	Age centre
Al = Ti-Li=Ti-H	Long distance transport before deposition: prepositional bleaching is full for the three centres.	Mean of 3
Al>Ti-Li=Ti-H	Reworking of old terraces and/or ± long distance transport: prepositional residual dose for Al centre but Ti-Li and Ti-H fully bleached.	Mean of Ti
Al>Ti-Li>Ti-H Al =Ti-Li>Ti-H	Reworking of old terraces and/or short distance transport: Al and Ti-Li not bleached before deposition; Ti-H was the most/ fully bleached before deposition.	Ti-H
	Reworking of old terraces and ± long distance transport but too old for Ti-H (saturated).	Ti-Li or Mean of Al and Ti-Li

- All three centres provide the same ESR intensity. This means that the post-erosion transport was sufficient for a good reset of all the centres and the average age will be reliable.
- The age obtained by the Al-centre is higher than the age obtained by the two otherwise equal Ti-centres (Al>Ti-Li=Ti-H). This means that there was a short distance transport of sediment from the erosion zone (rocks or old terrace) by a watercourse. This transport was insufficient for a maximum bleaching of the Al-centre. In this case, only the average Ti-centre will be used.
- The age obtained for the Al-centre is higher than the Ti-Li-centre, which is higher than the Ti-H-centre (Al>Ti-Li>Ti-H). This means that there was a very low transport after erosion and/or transport by runoff. In this case, the Ti-H age will be privileged. However, in the case that the equivalent dose obtained by Ti-H is above 300-400 Gy, a saturation of the Ti-H signal can also be expected (Tissoux et al., 2015). This would explain the difference between Ti-Li and Ti-H. In this case the Ti-Li age, or the Ti-Li and Al ages if in agreement, will be favoured.

3.1.1.2 Determination of equivalent dose (De)

The equivalent dose (De) is determined by an additive dose method, where several aliquots of the sample are submitted to increasing gamma-ray doses. The ESR intensity of the different paramagnetic centres is measured for each aliquot by ESR spectrometry. This intensity is proportional to the trapped electrons concentration in the sample (Yokoyama et al., 1985; Voinchet et al., 2004).

The intensity of the different aliquots is used to construct a dose response curve of the intensity as a function of the gamma dose added (Figure 3.3). The extrapolation of this curve to the zero ordinate (corresponding to the bleached state of the sample) allows the equivalent dose received to be determined. Thus, by fitting the aliquots points using an exponential (Yokoyama et al., 1985; Ikeya, 1989) or exponential + linear (Duval, 2008) term function it is possible to calculate the equivalent dose (De), using the Origin software.

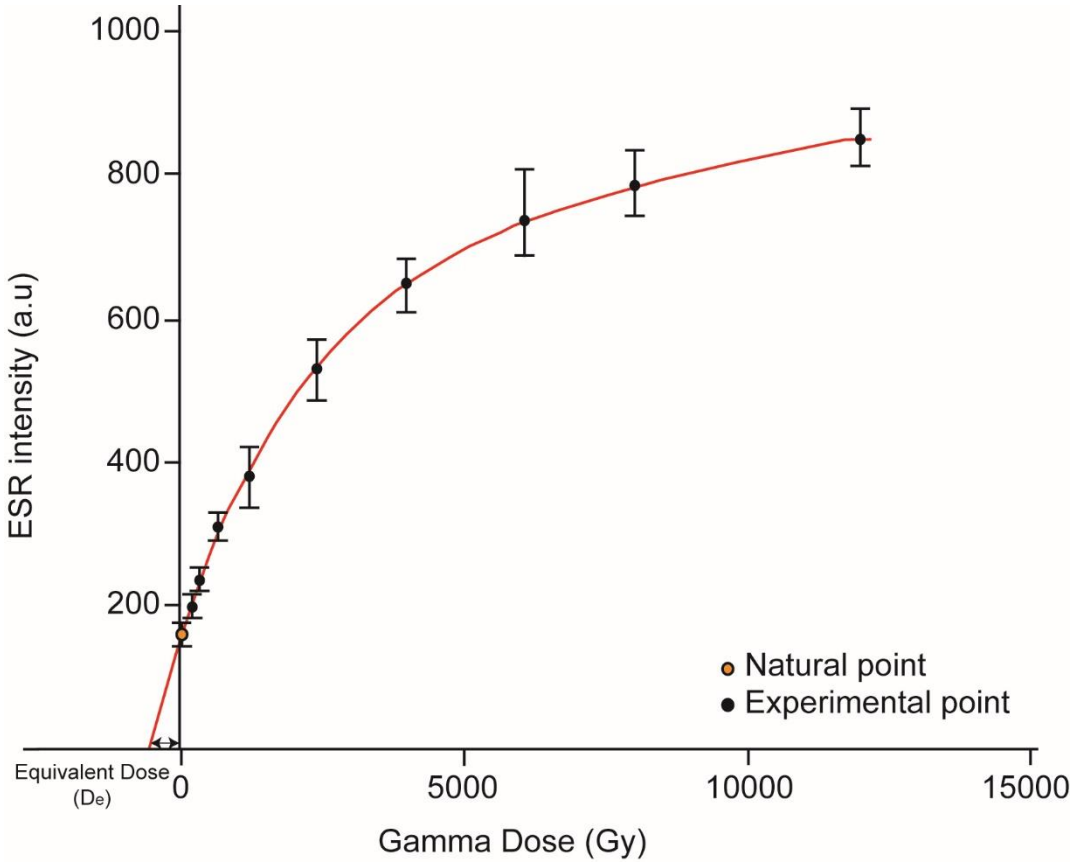

Figure 3.3. Determination of equivalent dose (De) using the additive method in sample A3D-015 using Al-centre.

ESR measurements were performed at the Department of HNHP of the National Museum of Natural History of Paris (MNHN), using a Bruker EMX spectrometer that works at low temperature (90 K) with liquid nitrogen for Al, Ti-Li and Ti-H centres. The following usual conditions were used: a 5-mW microwave power, 1024 points resolution, 20 mT sweep width, 100 kHz modulation frequency, 0.1 mT modulation amplitude, 40 ms conversion time, 20 ms time constant (Tissoux et al., 2015; Voinchet et al., 2020). A global spectrum for these different centres was obtained for each aliquot.

After baseline correction, the signal intensity of Al-centre was measured between the top of the first peak at g=2.018 and the bottom of the 16th peak at g=2.002 of Al hyperfine structure (Toyoda and Falguères, 2003). The ESR intensity of Ti-Li centre was determined by measuring the difference between the peak top at g=1.913 to the baseline (Toyoda et al 2006, Tissoux et al 2007, Duval et al, 2015). The Ti-H centre signal intensity was measured between the peak at g= 1.95 and the baseline (Figure 3.4) (Toyoda et al, 2006, Tissoux et al, 2007, Duval et al, 2015).

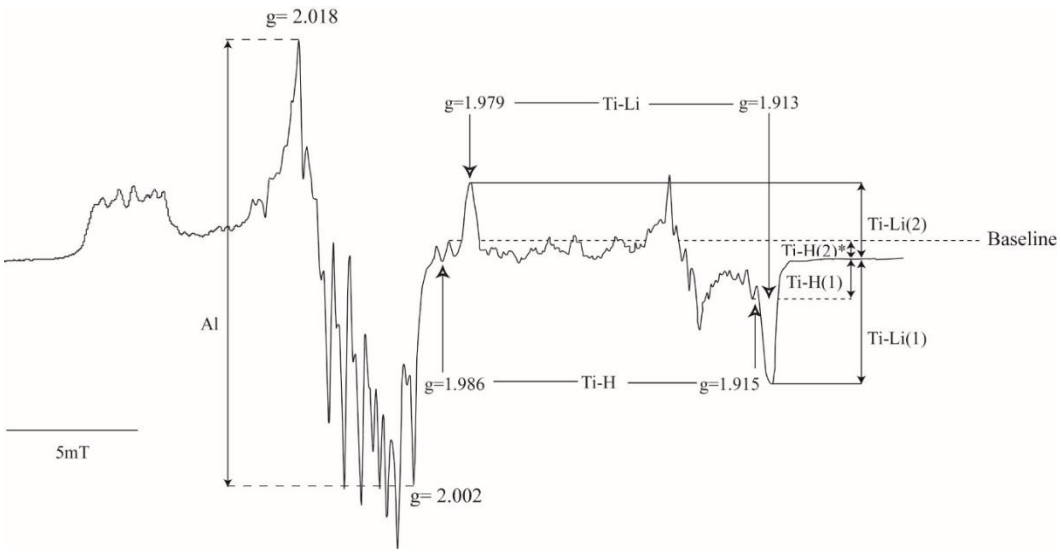

Figure 3.4. Al, Ti-Li, and Ti-H ESR signal in quartz sample and indication of intensities measurements (modified after Toyoda et al., 2000).

a. Particular case of the Al-centre

The Al-centre is not fully bleachable by sunlight. The Al-centre of quartz has two components: one is optically bleachable centres (OBAT), and the other is optically unbleachable deep centres (DAT) (Tissoux et al., 2012, 2015). Only the intensity of the OBAT-centre changes according to the erosion/transport/deposition processes. It is therefore necessary to identify and quantify the fraction of the signal related to the non-bleachable fraction of Al-centre in order to subtract it from the bulk signal. This is done by optical artificial bleaching the sample by measuring the residual intensity related to the DAT and then by systematically subtracting it from the measured intensities for all aliquots.

b. Particular case of the Ti-centre

Contrary to the Al-centre, the Ti-centre can be totally bleached during exposure to sunlight (Toyoda *et al.*, 2000; Tissoux *et al.*, 2007). These centres are also more radiosensitive than aluminium and saturate when highly irradiated. A decrease of the ESR intensity for the higher dose aliquots can often be observed (Figure 3.5). Therefore, the fitting curves obtained from titanium centres will only be done by considering the strictly increasing part of the curve. Depending on the case, a simple exponential or exponential + linear function will be applied.

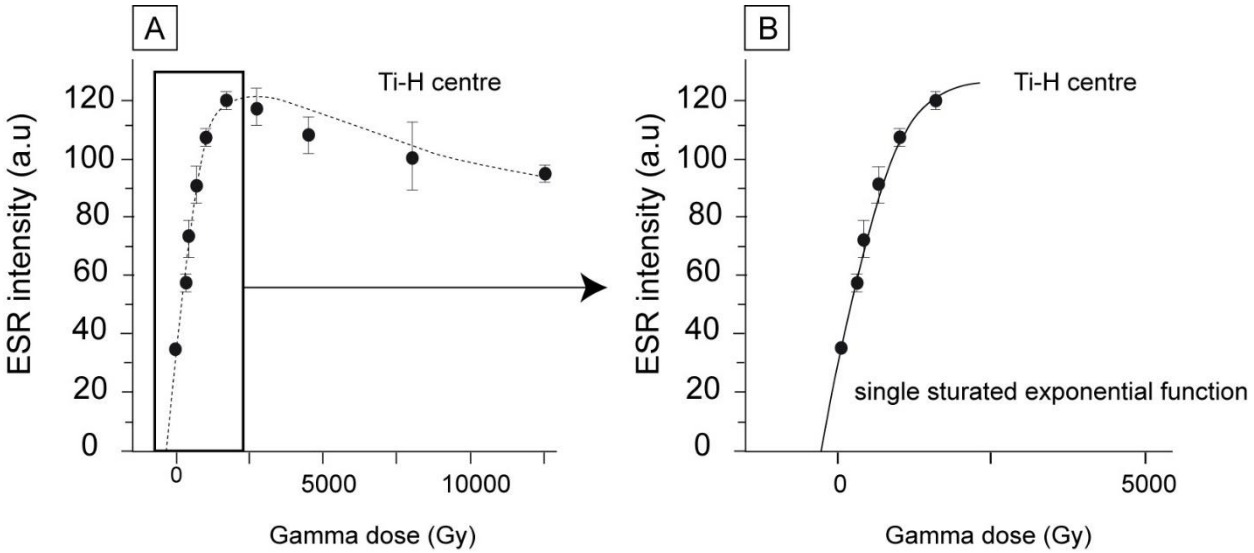

Figure 3.5. Ti-H growth curves for sample A3D-015. (a) Decrease in ESR intensity for higher dose aliquots. (b) Increasing part of the curve for the 6 first aliquots using for fitting Ti-H centre.

For some samples, the weakness of the titanium signal intensity makes it difficult to discern its signal from the background noise. Thus, it is necessary to cumulate several acquisitions spectra in order to increase the signal/noise ratio and to be able to measure an intensity. For these samples, 50 cumulative spectra were made for the natural dose and first doses, 30 cumulative spectra for the second and third doses and 20 cumulative spectra for the fourth and fifth doses. The background noise is variable and tends to disappear when spectra are cumulated, while the ESR signal is always in the same place and therefore increases (Figure 3.6).

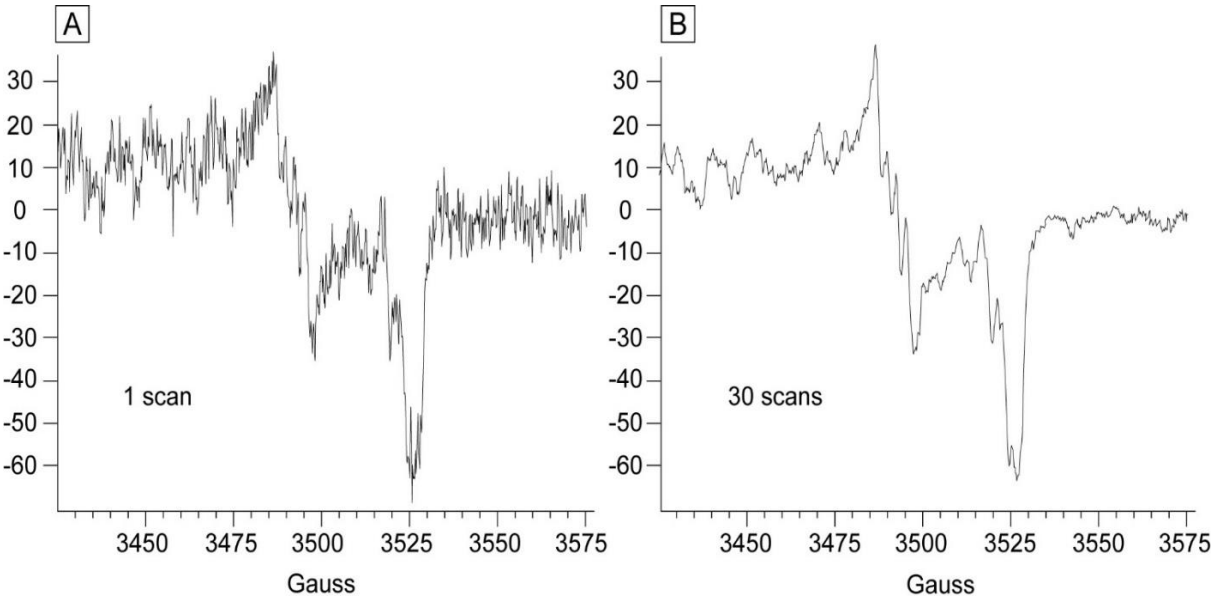

Figure 3.6. Cumulative spectra acquisition focus on the Ti-centre for reduce the impact of background noise for sample A3D-015. (a) Background noise observed when using only 1 scan. (b) Cumulative spectra (30 scans) reducing the background noise.

3.1.1.3 Determination of the annual dose (Da)

The annual dose (D_a) represents the sum of internal and external dose rate contributions received by the sample in one year. For quartz, the internal dose rate was considered as negligible in relation with the low contents of radionuclides in quartz grains (Murray and Roberts 1997; Vandenbergue et al. 2008). It may be expressed as follow:

$$Da = \sum D\alpha + D\beta + D\gamma + Dcosmic \qquad \text{Equation 3.2}$$

where $D\alpha$, $D\beta$, $D\gamma$, $Dcosmic$ are the alpha-particle, beta-particle, gamma-ray, and cosmic dose contributions.

The contribution range of each component may vary (Grün and Stringer, 1991):

- Alpha rays have a short range of ~20-40 μm;
- Beta rays have a range of about ~2 mm;
- Gamma rays have a range of about ~30 cm;
- The cosmic dose rate depends on the geographic latitude, elevation and burial depth of the sample.

$D\alpha$, $D\beta$ are determined from a laboratory measurement using high resolution and low background gamma-spectrometry (Figure 3.7), while $D\gamma$ is measured *in situ* considering the environment of the sample (sphere of 30 cm radius around the sample). The gamma dose is determined using a threshold approach (Falguères and Mercier, 2004). These three radiations will influence the quartz grains differently depending on several parameters: the water content of the sediment and the size of the quartz grains considered. These influences lead to corrections using conversion tables. Due to grain size, alpha and beta attenuations are estimated from the tables of Brennan *et al*. (1991) and Brennan (2003) respectively. The final age calculations were then performed using the dose-rate conversions factors from Guerin *et al*. (2011) and an alpha efficacity factor (k-value) of 0.15 ± 0.1 from Yokoyama *et al*. (1985).

Water content (W%) which decrease the radiation efficiency was estimated using the difference in mass between the natural sample and the dried same sample. The water attenuation was then determined following Grün (1994). The cosmic dose rates were calculated from the equations of Prescott and Hutton (1994).

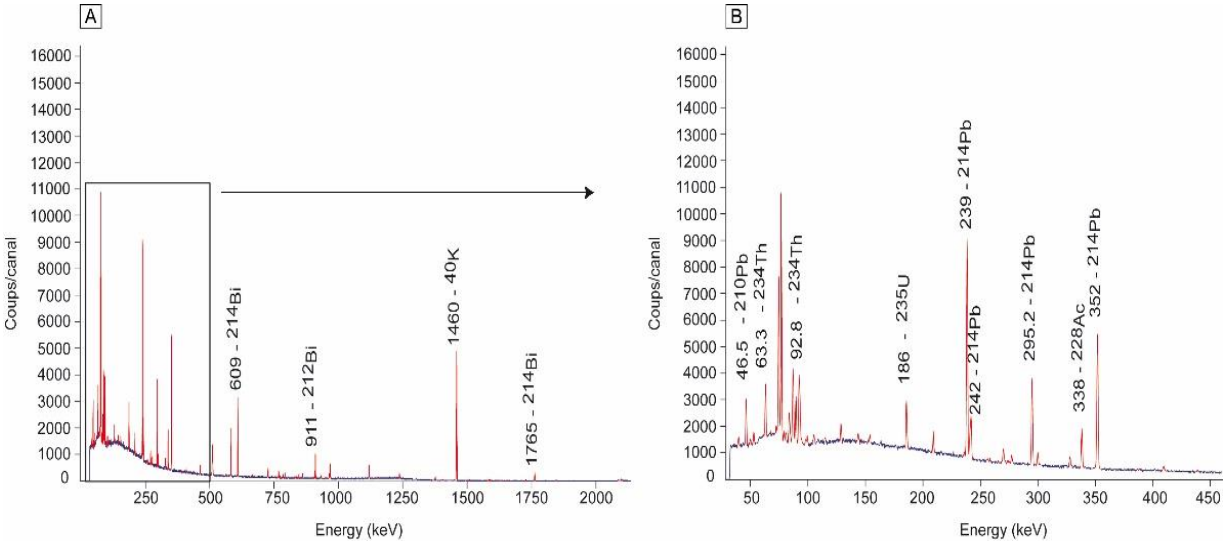

Figure 3.7. Gamma measurements for A3D-015 sample. (A) All gamma measurements. (B) Zoom in U, Th measurements.

a. Sampling

Samples were taken from fresh sections, in sediments non affected by leaching, accumulation (i.e. ferromagnetic elements or clay) or bioturbation to avoid bleaching of the quartz grains after deposition. These sections were described in a detail and sedimentary log shown in Chapter 2.

In addition, *in situ* measurements of the natural radioactivity for each sample were performed directly in the section during a short time (~20 minutes) using a portable gamma spectrometer type Inspector-1000 from Camberra and Digidart from Ortec. All samples were collected in a dark bag in order to avoid parasite bleaching during storage.

b. Experimental procedure

The ESR dating technique need the separation of quartz following the process explained in this section (Figure 3.8).

A part of the sediment is kept as it is to obtain the annual dose (D_a). The sediment is first dried to determine water content and then packed into standard 100g box in order to be measured into a high purity-low background germanium gamma spectrometer.

ESR analyses were made on 100-200 µm quartz grains selected by water sieving. First, chemical attack with hydrochloric acid (HCl) allowed removing carbonates. Second, a hydrofluoric acid at 40% (HF) was used for 90 minutes to eliminate oxides, feldspars as well as the external part of the quartz grains (leaching) that have been subjected to external α-rays. The heavy minerals, magnetic minerals and phyllosilicates were successively extracted from the sample using a dense liquor (density 2,72) and a magnetic separator.

Quartz grains were then submitted to irradiations. The equivalent dose (De) was determined through the additive dose method. For this, the sample was split in 11 aliquots. One aliquot was kept the natural, another aliquot was bleached (for Al DAT determination), and the other nine aliquots were submitted to increase gamma doses of 150, 300, 600, 1200, 2400, 4000, 6000, 8000 and 12000 Gy respectively at the Cenieh laboratory (Spain).

Each aliquot was measured three times at different angles rotation in the ESR spectrometer in order to evaluate samples heterogeneity (angular variation). This procedure was repeated for three days to assess variability of equivalent dose (De).

All ages, using De determined with Origin software and D_a calculated using an excel sheet are then obtained.

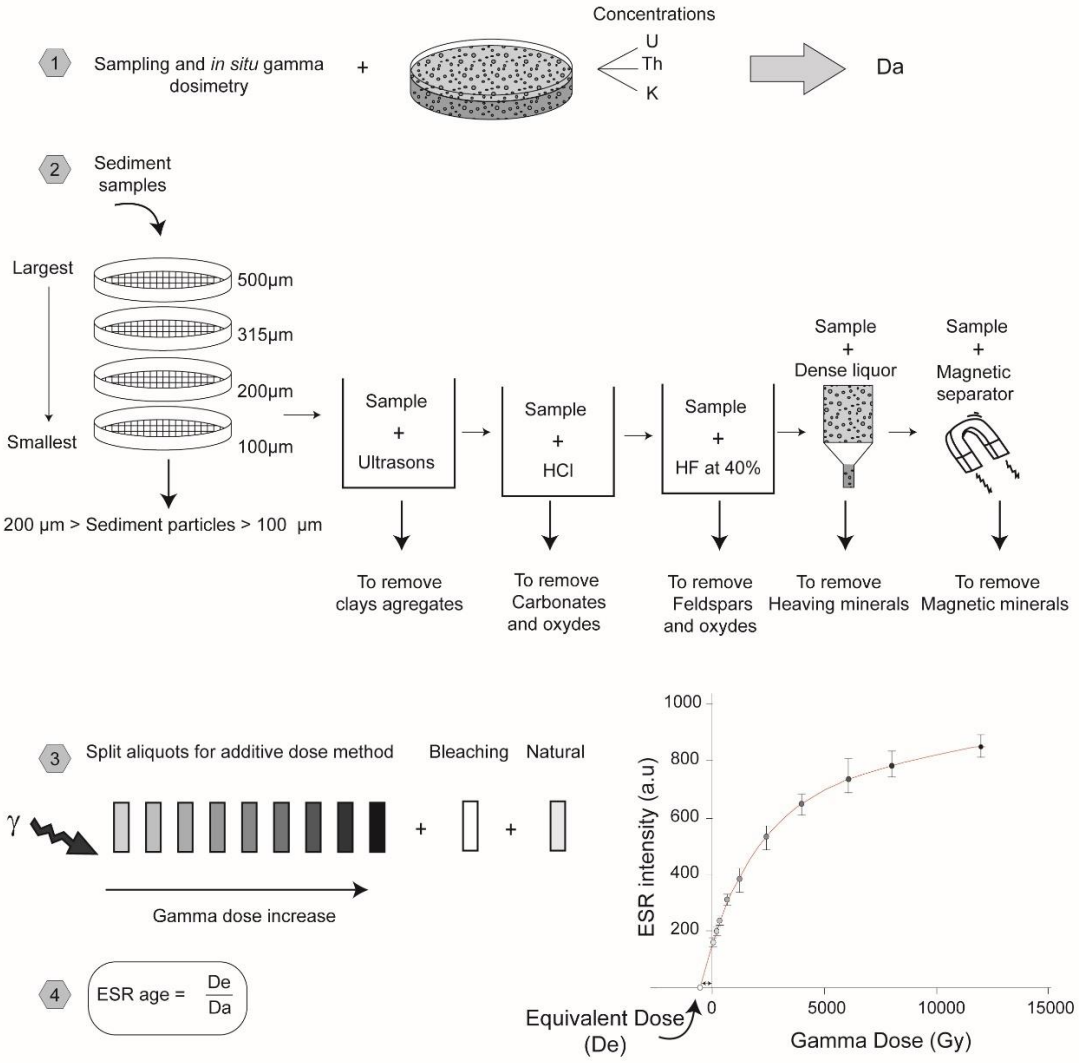

Figure 3.8. Summary of the analytical procedure for samples preparations and measurements.

3.1.2 Optically Stimulated Luminescence (OSL) dating of sedimentary quartz

In this part, the Optically stimulated luminescence will be only shortly introduced. Indeed, unlike the ESR dating method, the OSL analyses were not performed by myself but sent to Re.S.Artes laboratory (analytical reports are available in appendix B).

3.1.2.1 General principles

Optically stimulated luminescence (OSL) dating is a paleodosimetric method that is based on the same principle as ESR dating: the study of natural radioactivity and the ability of crystal (quartz or felspar) to cumulate the effects of this radiation (Huntley et al., 1985).

OSL differs from ESR mostly because their high radiosensitivity of quartz and therefore more rapidly reset to zero (few seconds). This high sensibility limits the problem of partial bleaching encountered in ESR but has the disadvantage of saturating very quickly. The OSL method cannot therefore be used to date events older than a few hundred thousand of years.

One of the most used methods in OSL is the single-aliquot-regenerative-dose (SAR) procedure (Murray and Wintle, 2000, 2003). It is the method used in this study. This protocol involves several cycles of heating, optical stimulation, and irradiation. The first step of the protocol is to measure the natural intensity signal, reset to zero and then, irradiate at increasing dose after each bleaching step. A growth curve is constructed considering every measure of intensity signal as a function of dose received. The interpolation of the natural intensity on the growth curve allows determining the equivalent dose (De) (Figure 3.9).

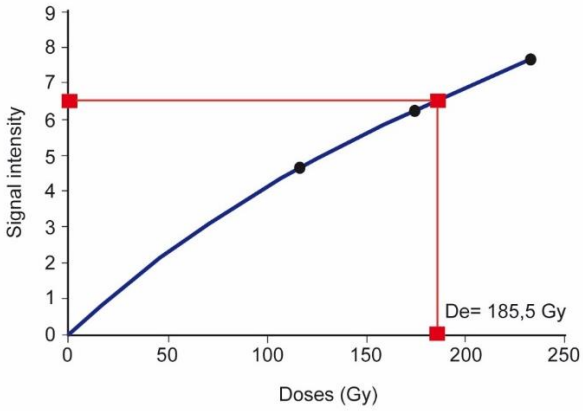

Figure 3.9. Example of natural intensity measurement by OSL for sample A3D-015. The blue curve represents the signal regeneration with known radiation doses. The intersection of the measured intensity value on the y-axis with this curve gives the natural radiation dose on the x-axis (rapport from Re.S.Artes R 244349A-2).

3.1.2.2 Sampling and experimental procedure

Samples for OSL dating were taken strictly at the same time and place as those for ESR dating. Because of the extreme photosensitivity of OSL method, sediment was sampled using a PVC tube and kept away from all-natural light from the time of sampling until the end of the analyses. The in-situ gamma measurements were thus the same for ESR and OSL.

In the Re.S.Artes laboratory, under red light only, the sediment was sieved to select a particle size between 80 and 125µm. The powder thus obtained was chemically treated: 20% HCl to remove carbonates (at the beginning and end of the chemical preparation cycle), H_2O_2 30% to

eliminate organic matter, and HF 40% to eliminate feldspars and thus allow the exclusive selection of quartz.

The radioactivity measurement for annual dose determination was carried out on the raw sediment, dried, and then packaged in an airtight plastic box to allow measurement by low background gamma spectrometry after waiting a month to ensure that the radon returned to equilibrium.

3.1.2.3 Single-aliquot-regenerative-dose (SAR) protocol

All experiments were performed on the same aliquot. To minimize the risk of choosing an aliquot that is not representative of the whole sample, several sub-samples were processed in parallel to obtain a statistically usable result. To do this, the different sub-samples were placed on disc, and measured at the same time by the instrument. A total of 12 or 15 discs were studied, respectively, allowing the same number of measurements of the equivalent dose (De).

When bleaching and regeneration cycles are done, the sensitivity of the sample may sometimes change, which means that with the same dose of irradiation the intensity will not be the same. To be able to do a dating, it is necessary to have no change in sensibility, otherwise it must be corrected. The changes in sensitivity classically observed on quartz are checked and corrected by calibration measurements obtained after irradiation with a test dose (Murray and Wintle, 2000).

The measurements were carried out in dark conditions using nitrogen with a Lexsyg SMART instrument from Freiberg and delivering a beta dose of 0.116 Gy/s. It was equipped with infrared (870 ± 40 nm) and blue (470 ± 40 nm) LED, after having illuminated the crystal on the discs with the infrared diodes. The use of infrared illumination heating to 240 °C (hotbleach) eliminated the possible contribution from the luminescence signal emanating from the residual feldspars. Thus, the equivalent dose (De) was determined for each sample. The annual dose (Da) was determined using the same approach for ESR. Finally, the age OSL can be determined using the equation 3.1.

Chapter 3

3.2 Results and interpretations of ESR and OSL dating within the Seine catchment

One of the crucial points of this thesis is to provide a better understanding of the chronology of valley formation and of the age of valley bottom infill within the Seine catchment. The following section presents the main results obtained using the Electron Spin Resonance (ESR) and Optically Stimulated Luminescence (OSL) dating methods on quartz samples. Figure 3.10 shows the location of the samples. Interpretations in terms of the history of the valley and geomorphological evolution are presented in the discussion section.

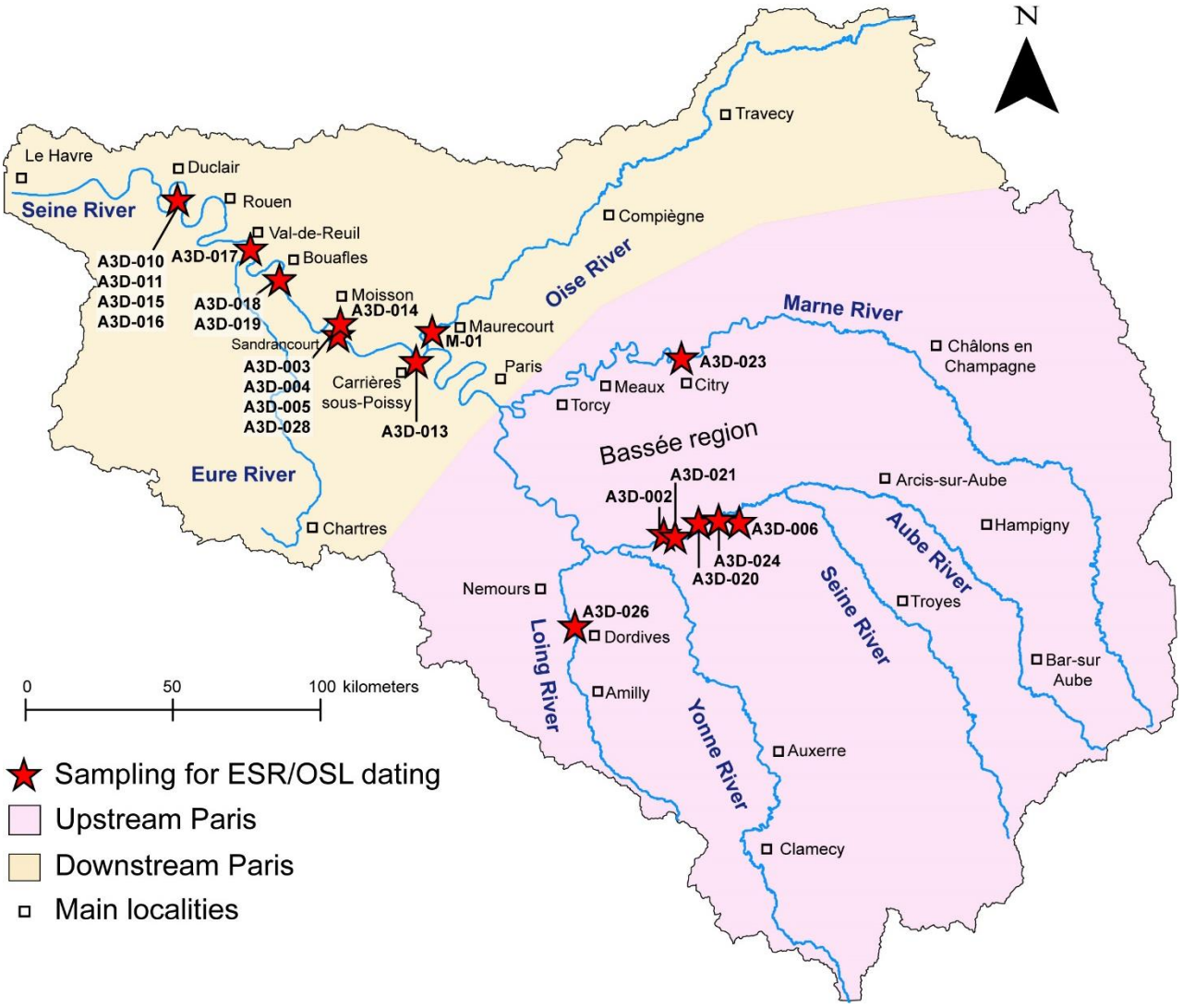

Figure 3.10. Location of sampling for ESR/OSL dating along the Seine catchment. Red stars represent samples location.

3.2.1 Validation criteria for ESR ages

A systematic sorting of experimental results was performed before the construction of the intensity vs irradiation growth curves. A particular emphasis was given on the preservation of data points with lower irradiation doses, with a special focus on allowing the curve to pass through the "natural" point. Consequently, the growth curves are constructed using the most reliable points (represented by black points in figure Figure 3.11) (see all details in appendix C). This analysis allowed giving a validation criterion for measurements, offering insights into the quality of the ESR growth curve fitting and determined the equivalent doses (De) for the constructed doses curves. Four main cases were identified and attributed a notation as follows:

1 When all data points were utilized for age calculation, a (+++) notation was applied (Figure 3.11-a).
2 When a minimum five to nine data points were employed for age calculation, a (++) notation was used (Figure 3.11-b).
3 When a data point with lower intensity was removed, or when four data points only were used for age calculation, a (+) notation was assigned (Figure 3.11-c).
4 When data points did not allow obtaining a good fit a (-) notation was used (Figure 3.11-d).

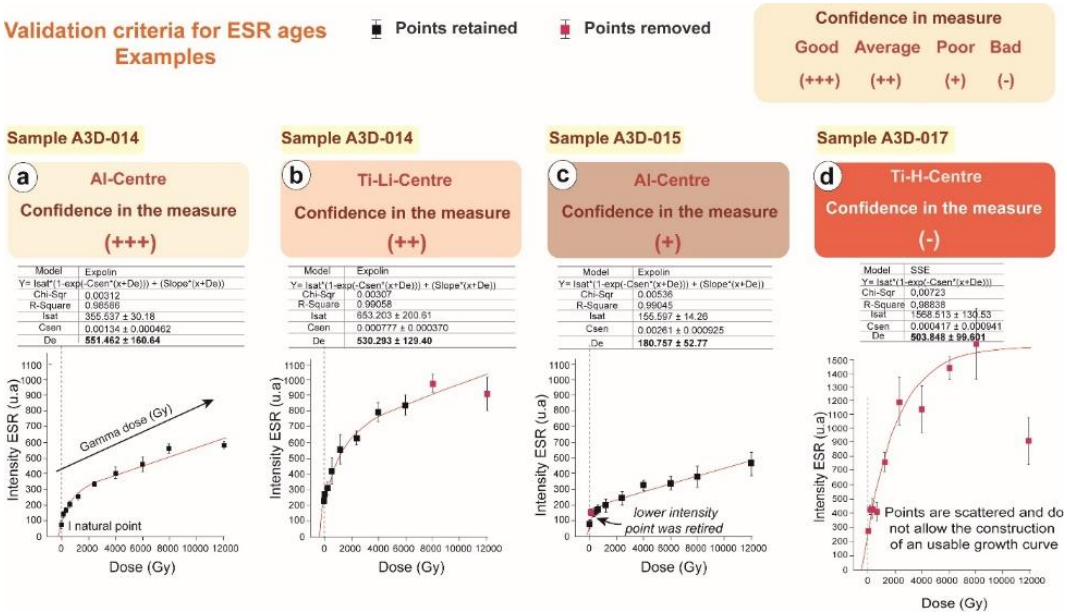

Figure 3.11. Validation criteria for ESR ages using the growth curve fitting. (a) All data points were utilized for age calculation. (b) When a minimum of six data points were employed for age calculation. (c) When a data point with lower intensity was removed, or when at least four data points were used for age calculation. (d) When data points are not used for measurement because of a bad fitting.

3.2.2 ESR and OSL ages within the Seine catchment

3.2.2.1 ESR and OSL ages upstream of Paris

The obtained results for ESR and OSL ages upstream of Paris are displayed in Table 3.2, ages are in bold. Ages with low confidence in the measure (- notation) are indicated in red in Table 3.2. They are from the Bassée alluvial plain (i.e., Seine River between Nogent-sur-Seine and Montereau), the Marne and Loing tributaries of the Seine River. Dose rate determination, and other analytical results such as individual activities of radionuclides U, Th and daughters, K are shown in appendix D.

Table 3.2. ESR and OSL dating results obtained upstream of Paris. Relative elevation above the maximum incision of the river is represented by RH and above the current alluvial plain by RH'. *Da*, *De*, dating method and final ages are given for each sample. The age in red does not meet enough validation criteria to be considered.

Upstream Paris											
Location	**Terrace**		**Sample**	**Elevation (m NGF)**	**Depth (m)**	**RH (m)**	**RH' (m)**	**Da (µGy/a)**	**De (Gy)**	**ESR/OSL**	**Age (ka)**
Fontaine Mâcon	**T_{IV}**		**A3D-006 Fluvial deposit**	104.2	0.8	52	46	529 ± 16	400 ± 52	Al	**756 ± 100**
									422 ± 20	TiLi	**798 ± 42**
									420 ± 49	TiH	**794 ± 94**
Courceroy	**T_{III}**		**A3D-024 Fluvial deposit**	69.2	2.5	22	14	420 ± 14	158 ± 10	Al	**376 ± 25**
									283 ± 26	TiLi	**673 ± 63**
									151 ± 34	TiH	**359 ± 81**
Noyen-sur-Seine	**Valley bottom**	**T_2**	**A3D-020 Fluvial deposit**	56	1	8	1	433 ± 19	7.6 ± 0.2	OSL	**18 ± 1.2**
Bazoches		**T_2**	**A3D-021 Fluvial deposit**	51	2	6	0	386 ± 18	6.5 ± 0.12	OSL	**17 ± 1.1**
Vimpelles		**T_{3a}**	**A3D-002 Fluvial deposit**	51.2	1.8	6.2	0.2	374 ± 18	5.5 ± 0.14	OSL	**15 ± 1.1**
Citry**		**Fz**	**A3D-023 Fluvial deposit**	49	5	0	7	1165 ± 38	28.8 ± 0.6	OSL	**25 ± 1.3**
Dordives**		**Fz**	**A3D-026 Fluvial deposit**	63.8	1.2	1.8	-5.2	1670 ± 54	22.6 ± 0.4	OSL	**14 ± 0.7**

**Tributaries of the Seine River

a. Bassée area

Two samples (A3D-006 and A3D-024) collected from fluvial terraces have been dated by ESR dating method. They are on the left bank of the Seine River and are a part of the T_{IV} terrace located at Fontaine Macôn (sample A3D-006) and T_{III} terrace located at Courceroy (sample A3D-024) (Mégnien 1965; Deleplancque 2016).

The annual doses (Da) for those samples are respectively 529 ± 16 and 420 ± 14 µGy/a. Equivalent doses (De) for sample A3D-006 were similar for the Al-centre, TiLi-centre, and TiH-centre, indicating a good bleaching for this sample. However, for sample A3D-024, the equivalent dose (De) for TiLi-centre was considerably higher than that of the Al-centre and TiH-centre, suggesting problem in intensity determination for natural and lowest irradiation (strong back noise) causing of an overestimation of the De value and making difficult to calculate an age for the TiLi-centre (- notation).

The corresponding ESR ages are shown in Table 3.2**.** The ESR ages for sample A3D-006 from terrace T_{IV} were obtained considering all paramagnetic centres (Al-centre, TiLi-centre and TiH-centre), and are 756 ± 100 ka, 798 ± 42 ka, and 794 ± 94 ka, respectively. For sample A3D-024 from T_{III} terrace, ages were obtained considering the Al-centre and TiH-centre and were estimated of 376 ± 25 ka and 359 ± 81 ka, respectively.

In this region, three samples taken from the valley bottom at Noyen-sur-Seine (sample A3D-020), Bazoches (sample A3D-021) and Vimpelles (sample A3D-002) were dated using OSL. Samples A3D-020 and A3D-021 are part of the T_2 terrace, they have a Da of 433 ± 19 µGy/a and 386 ± 18 µGy/a. Equivalent doses (De) for these two samples are similar at 7.6 ± 0.2 and 6.5 ± 0.12 Gy respectively. Thus, the OSL ages are 18 ± 1.2 and 17 ± 1.1 ka (Table 3.2). Sample A3D-002 are a part of the T_{3a} terrace, the Da is 374 ± 18 µGy/a and the De is 5.5 ± 0.14 Gy, the OSL age is 15 ± 1.1 ka (Table 3.2).

b. Marne and Loing tributaries

Two samples from the valley bottom alluvium were taken at Citry on the left bank of the Marne River (sample A3D-023) and at Dordives on the right bank of the Loing River (sample A3D-026). They were dated by OSL. The annual dose (Da) for sample A3D-023 is 1165 ± 38 µGy/a, the equivalent dose (De) is 28.8 ± 0.6 Gy and the OSL age is 25 ± 1.3 ka (Table 3.2). The annual dose (Da) for sample A3D-026 is 1670 ± 54 µGy/a, the equivalent dose (De) is 22.6 ± 0.4 Gy and the OSL age is 14 ± 0.7 ka respectively (Table 3.2).

3.2.2.2 ESR and OSL ages downstream of Paris

The ESR and OSL ages obtained downstream of Paris are displayed in Table 3.3. They were sampled from either strath terraces (at Bouafles, Moisson, Carrières-sous-Poissy, Sandrancourt and Manoir Brésil) or in the valley bottom (at Saint Martin-la-Garenne, Val-de-Reuil and Maurecourt (in the Oise valley)). Eleven samples were dated by ESR and ten samples by OSL.

Table 3.3. ESR and OSL dating results downstream of Paris obtained. Relative elevation above the maximum incision of the river is represent by RH and above the current valley bottom is represent by RH'. *Da*, *De*, dating method and final ages are given for each sample. The age in red does not meet enough validation criteria to be considered.

Downstream Paris										
Location	**Terrace**	**Sample**	**Elevation (m NGF)**	**Depth (m)**	**RH (m)**	**RH' (m)**	**Da (µGy/a)**	**De (Gy)**	**ESR/OSL**	**Age (ka)**
Bouafles	**Fyb**	**A3D-018 Fluvial deposit**	31	6	25	18	749 ± 18	327 ± 42	Al	**437 ± 56**
								622 ± 33	TiLi	***831 ± 45***
								326 ± 16	TiH	**435 ± 22**
	Fyb	**A3D-019 Fluvial deposit**	33.5	3.5	28	21	880 ± 21	406 ± 63	Al	**462 ± 72**
								408 ± 41	TiLi	**464 ± 47**
								376 ± 22	TiH	**427 ± 25**
Moisson	**Fyc**	**A3D-014 Fluvial deposit**	30	1	19	12	1988 ± 38	551 ± 80	Al	**277 ± 40**
								530 ± 65	TiLi	**267 ± 33**
								366 ± 33	TiH	***184 ± 17***
Carrières-sous-Poissy	**Fyd**	**A3D-013 Fluvial deposit**	25	3	15	7	424 ± 23	83 ± 1	OSL	**196 ± 13.2**
Sandrancourt	**Fyd**	**A3D-003 Fluvial deposit**	18	5	11	2	734 ± 21	332 ± 20	Al	***453 ± 28***
								363 ± 25	TiLi	***495 ± 35***
								98 ± 2	TiH	***134 ± 3***
								197 ± 3.2	OSL	**269 ± 6**
	Fyd	**A3D-004 Fluvial deposit**	20	3	13	4	810 ± 21	216 ± 14	Al	***267 ± 18***
								279 ± 9	TiLi	***344 ± 12***
								155 ± 26	TiH	**191 ± 32**
								165 ± 3.7	OSL	**204 ± 5**
	Fyd	**A3D-005 Fluvial deposit**	15	21	9	1	683 ± 16	468 ± 27	Al	***686 ± 40***
								392 ± 11	TiLi	***574 ± 17***
								242 ± 11	TiH	***354 ± 16***
								150 ± 2.5	OSL	**220 ± 4**
Manoir Brésil **(more details in chapter 4)**	**Fyd**	**A3D-011 Tidal deposit**	5	3	17	6	666 ± 13	172 ± 46	Al	**258 ± 69**
								517 ± 193	TiLi	***776 ± 290***
								182 ± 29	TiH	**273 ± 44**
								161 ± 3.4	OSL	**242 ± 7**
	Fyc	**A3D-015 Tidal deposit**	7.5	3.5	19	8	845 ± 9	181 ± 26	Al	**214 ± 31**
								168 ± 16	TiLi	**199 ± 19**
								173 ± 11	TiH	**205 ± 13**
								162 ± 3	OSL	**192 ± 5**
	Fyd	**A3D-010 Fluvial deposit**	2.75	2.75	14	3	1047 ± 15	341 ± 27	Al	***326 ± 26***
								378 ± 26	TiLi	***361 ± 25***
								196 ± 14	TiH	**187 ± 14**
								192 ± 3	OSL	**184 ± 4**
	Fyd	**A3D-016 Periglacial deposit**	12.5	2	24	13	1752 ± 25	135 ± 12	Al	***77 ± 7***
								78 ± 5	TiLi	***45 ± 3***
								51 ± 16	TiH	**29 ± 9**
								40 ± 1	OSL	**23 ± 1**

Samples ages continued

Downstream Paris											
Location	**Terrace**		**Sample**	**Elevation (m NGF)**	**Depth (m)**	**RH (m)**	**RH' (m)**	**Da (µGy/a)**	**De (Gy)**	**ESR/OSL**	**Age (ka)**
St-Martin-la-Garenne	**Valley bottom**	**Fz**	**A3D-028 Fluvial deposit**	16.85	1.9	11	3	896 ± 26	15.9 ± 0.3	OSL	**18 ± 0.89**
Val-de-Reuil		**Fz**	**A3D-017 Fluvial deposit**	7.6	1.4	7	0	838 ± 20	128 ± 8	Al	**153 ± 10**
									158 ± 10	TiLi	**189 ± 12**
									-	TiH	***Not calculated***
Maurecourt**		**Fz**	**M-01 Fluvial deposit**	20.7	5.8	13	0	1125 ± 49	18.6 ± 0.5	OSL	**17 ± 1.2**

**Tributaries of the Seine River

a. Bouafles site

Two samples (A3D-018 and A3D-019) characterized by fluvial sediments were collected from the same outcrop as part of the Fyb terrace on the right bank of the Seine River. These samples were dated using ESR. Sample A3D-018 being approximately located 2.5 m below sample A3D-019. The annual doses (Da) for those samples were similar comprising between 749 ± 18 and 880 ± 21 µGy/a.

Equivalent doses (De) for sample A3D-018 were similar for Al-centre and TiH-centre, in contrast, TiLi-centre were much higher than those obtained by Al-centre and TiH-centre, suggesting an incomplete bleaching of TiLi-centre at the time of deposition and therefore an overestimation of this equivalent dose (De), making difficult to calculate an age for TiLi-centre (- notation). However, for sample A3D-019, equivalent doses (De) are in agreement for all paramagnetic centres (Al, TiLi and TiH-centres), indicating a good bleaching. Thus, ESR ages for sample A3D-018 were obtained considering the Al-center and TiH-centre and are 437 ± 56 and 435 ± 22 ka, respectively (Table 3.3).

Three sets of ESR ages for sample A3D-019 were obtained considering all paramagnetic centres (Al, TiLi and TiH-centres) and are of 462 ± 72, 464 ± 47 and 427 ± 25 ka respectively (Table 3.3).

b. Moisson site

Sample A3D-014 characterized by fluvial sediments from the Fyc terrace on the left bank of the Seine River were dated using ESR. The annual dose (Da) for this sample is 1988 ± 38 µGy/a, this high value may reflect the mineralogical variability of fine sediments mixing with clay and silts richer in radioelements. Equivalent doses (De) calculated using Al-centre and TiLi-centre

are in agreement. On the contrary, De obtained from TiH-centre is clearly lower than Al-centre and TiLi-centre. Therefore, De for TiH-centre register a value > 300 Gy supposing a saturation in TiH-centre (- notation). Thus, ESR ages for sample A3D-014 were determined using the Al-centre and TiLi-centre and are comprising between 277 ± 40 and 267 ± 33 respectively (Table 3.3).

c. Carrières-sous-Poissy site

Sample A3D-013 characterized by fluvial deposits from Fyd terrace on the right bank of the Seine River were dated using OSL. The annual dose (Da) was estimated at 424 ± 23 µGy/a and the equivalent dose (De) was determined at 82.9 ± 1 Gy. The OSL age is 196 ± 13.2 ka (Table 3.3).

d. Sandrancourt site

Three fluvial samples (A3D-003, A3D-004 and A3D-005) from Fyd terrace on the right bank of the Seine River were dated combining ESR and OSL methods.

Samples A3D-003 and A3D-004 were collected from the same outcrop, the first one being approximately 2 m below the second. Annual doses (Da) for those samples ranges from 734 ± 21 to 810 ± 21 µGy/a. Equivalents doses (De) calculated from Al-centre, TiLi-centre, TiH-centre and from OSL were compared, according to the multi-centre approach (MC).

For sample A3D-003, equivalent doses (De) calculated for TiH-centre consistently produces de lowest De value (<100 Gy) because this centre achieves full resetting much faster than the other centres (Tissoux et al., 2007). While the Al-centre and TiLi-centre provides the highest De values which suggests an incomplete bleaching of these two centres (- notation). The equivalent dose (De) for OSL seems to be consistent with TiH-centre. Nevertheless, the corresponding age for sample A3D-003 were calculated using the OSL because the age is in agreement with the sample A3D-004 and is determined at 269 ± 6 (Table 3.3).

For sample A3D-004, equivalent doses (De) are systematically in agreement for Al-centre, TiH-centre and OSL. In contrast, TiLi-centre were much higher than the other centres, suggesting an incomplete bleaching (- notation) at the time of deposition and therefore an overestimation of this equivalent dose (De). Thus, the ages obtained for this sample considering the Al-centre, TiH-centre and OSL are 267 ± 18, 191 ± 32 and 204 ± 5 ka respectively (Table 3.3).

In the same terrace, sample A3D-005 was taken about 1.8 km north of the other two samples. The annual dose (Da) is estimated at 683 ± 16 µGy/a. Equivalent doses (De) for the three ESR

centres are overestimates because of poor goodness-of-fit (- notation, see appendix C.2-e). Thus, the OSL age is privileged for this sample, given 220 ± 4 ka (Table 3.3).

e. Manoir Bresil site

Four samples characterized by tidal, fluvial, and periglacial facies were observed in the Fyc and Fyd terraces on the left bank of the Seine River (see more details in Chapter 4). These terraces were dated using ESR and OSL methods. Tidal deposits are represented by samples A3D-011 (Fyd terrace) and A3D-015 (Fyc terrace), fluvial deposits by sample A3D-010 (Fyd terrace) and periglacial deposits by sample A3D-016 (Fyd terrace).

The annual doses (Da) for the tidal samples A3D-011 and A3D-015, range from 611 ± 10 to 885 ± 9 µGy/a. Fluvial sample A3D-010, has an annual dose (Da) of 1041 ± 11 µGy/a. Periglacial sample A3D-016 has an annual dose (Da) of 1751 ± 15 µGy/a and is higher than the others. This may reflect mineralogical variability within the fine sediments (e.g., clay and silts richer in radioelements). Equivalent doses (De) calculated using TiH-centre and OSL are systematically in agreement, suggesting a complete pre-depositional reset of these centres.

For sample A3D-011 (tidal facies), equivalent doses (De) for the Al-centre, TiH-centre and OSL are systematically in agreement. In contrast, De for the TiLi-centre were much higher than the other centres, suggesting an incomplete bleaching (- notation), therefore an overestimation of these equivalent doses (De). Equivalent doses (De) for sample A3D-015 (tidal facies) were similar for all paramagnetic centres (Al, TiLi and TiH) and OSL, indicating a good bleaching. For samples A3D-010 (fluvial facies) and A3D-016 (periglacial deposit), equivalent doses (De) obtained for Al-centre and TiLi-centre were much higher than those obtained by the TiH-centre and OSL, suggesting a partial bleaching of these centers (- notation) and therefore an overestimation of their equivalent doses (De). They were not considered for the age calculation.

In sample A3D-011 (tidal facies), ages were obtained considering the Al-centre, TiH-centre and OSL: 258 ± 69 ka, 273 ± 44 ka and 242 ± 7 ka respectively. In sample A3D-015 (tidal facies), ages were determined using all paramagnetic centres: Al-centre, TiLi-centre, TiH-centre and OSL: 214 ± 31 ka, l99 ± 19 ka, 205 ± 13 ka and 192 ± 5 ka respectively. In sample A3D-010 (fluvial facies), ages were determined using the TiH-centre and OSL, returning 187 ± 14 ka and 184 ± 4 ka respectively. Finally, periglacial sample A3D-016 ages determined using TiH-centre and OSL range from 29 ± 9 ka to 23 ± 1 ka (Table 3.3).

f. Saint Martin-la-Garenne site

Sample A3D-028 was taken from valley bottom alluvium (Fz) on the left bank of the Seine River and dated using OSL. The annual dose (Da) was estimated at 896 ± 26 µGy/a and the equivalent dose (De) was determined at 15.9 ± 0.3 Gy. The OSL age is 18 ± 0.89 ka (Table 3.3).

g. Val-de-Reuil site

Sample A3D-017 was taken from the valley bottom alluvium (Fz) on the left bank of the Seine River and dated using ESR. The annual dose (Da) was estimated at 838 ± 20 µGy/a. Dose response curve for TiH-centre did not allow calculating the equivalent dose (De) with a sufficient accuracy and no TiH-age was determined (see appendix C.3-i). On the contrary De calculated from Al-centre and TiLi-centre seems to be in agreement. Thus, the ESR ages were obtained considering the Al-centre and TiLi-centre and are 153 ± 10 and 189 ± 12 ka respectively (Table 3.3).

h. Maurecourt site

Sample M-01 was taken from the valley bottom alluvium (Fz) located at Maurecourt on the left bank of the Oise River and dated by OSL. The annual dose (Da) was estimated at 1125 ± 49 µGy/a and the equivalent dose (De) was determined at 18.6 ± 0.5 Gy. The OSL age is 17 ± 1.2 ka (Table 3.3).

3.2.3 Synthesis

Table 3.4 summarizes the selected ages which will used for each site. Figure 3.12, shows the chronostratigraphic scale of the Seine catchment, coupling the obtained ages calculated for each sample according to the two approaches (ESR and OSL methods) in relation with the overall chronostratigraphic framework of the Quaternary period. This allows assigning to sample a Marine Isotopic Stage (MIS) corresponding to the glacial/interglacial cycles. Finally, the obtained ages are compared with neighboring data.

3.2.3.1 Age determination and comparation with the literature

Table 3.4. ESR and OSL dating results upstream and downstream of. Relative elevation above the maximum incision of the river is represent by RH and above the current valley bottom is represent by RH'. Ages are in bold.

Location	Terrace		Sample	Elevation (m NGF)	Depth (m)	RH (m)	RH' (m)	ESR/OSL	Age (ka)	Mean of age (ka)
Upstream Paris										
Fontaine Mâcon	**T_{IV}**		**A3D-006 Fluvial deposit**	104,2	0.8	52	46	Al	**756 ± 100**	**792±35 (2σ)**
								TiLi	**798 ± 42**	
								TiH	**794 ± 94**	
Courceroy	**T_{III}**		**A3D-024 Fluvial deposit**	69,2	2.5	22	14	Al	**376 ± 25**	**375±23 (2σ)**
								TiH	**359 ± 81**	
Noyen-sur-Seine	**Valley bottom**	**T_2**	**A3D-020 Fluvial deposit**	56	1	8	1	OSL	**18 ± 1.2**	-
Bazoches		**T_2**	**A3D-021 Fluvial deposit**	51	2	6	0	OSL	**17 ± 1.1**	-
Vimpelles		**T_{3a}**	**A3D-002 Fluvial deposit**	51.2	1.8	6.2	0.2	OSL	**15 ± 1.1**	-
Citry**		**Fz**	**A3D-023 Fluvial deposit**	49	5	0	7	OSL	**25 ± 1.3**	-
Dordives**		**Fz**	**A3D-026 Fluvial deposit**	63.8	1.2	1.8	-5.2	OSL	**14 ± 0.7**	-
Downstream Paris										
Bouafles	**Fyb**		**A3D-018 Fluvial deposit**	31	6	25	18	Al	**437 ± 56**	**436 ± 63 (2σ)**
								TiH	**435 ± 22**	
			A3D-019 Fluvial deposit	33.5	3.5	28	21	Al	**462 ± 72**	
								TiLi	**464 ± 47**	
								TiH	**427 ± 25**	
Moisson	**Fyc**		**A3D-014 Fluvial deposit**	30	1	19	12	Al	**277 ± 40**	**271±25 (1σ)**
								TiLi	**267 ± 33**	
Carrières-sous-Poissy	**Fyd**		**A3D-013 Fluvial deposit**	25	3	15	7	OSL	**196 ± 13.2**	-
Sandrancourt	**Fyd**		**A3D-003 Fluvial deposit**	18	5	11	2	OSL	**269 ± 6**	-
			A3D-004 Fluvial deposit	20	3	13	4	Al	***267 ± 18***	
								TiH	**191 ± 32**	
								OSL	**204 ± 5**	
			A3D-005 Fluvial deposit	15	21	9	1	OSL	**220 ± 4**	
Manoir Brésil (more details in chapter 4)	**Fyd**		**A3D-011 Tidal deposit**	5	3	17	6	Al	**258 ± 69**	**269 ± 37 (2σ)**
								TiH	**273 ± 44**	
								OSL	**242 ± 7**	
	Fyc		**A3D-015 Tidal deposit**	7.5	3.5	19	8	Al	**214 ± 31**	**204 ± 10 (2σ)**
								TiLi	**199 ± 19**	
								TiH	**205 ± 13**	
								OSL	**192 ± 5**	
	Fyd		**A3D-010 Fluvial deposit**	2.75	2.75	14	3	TiH	**187 ± 14**	**184 ± 4 (2σ)**
								OSL	**184 ± 4**	
	Fyd		**A3D-016 Periglacial deposit**	12.5	2	24	13	TiH	**29 ± 9**	**23 ± 8 (2σ)**
								OSL	**23 ± 1**	
St-Martin-la-Garenne	**Valley bottom**	**Fz**	**A3D-028 Fluvial deposit**	16.85	1.9	11	3	OSL	**18 ± 0.89**	-
Val-de-Reuil		**Fz**	**A3D-017 Fluvial deposit**	7.6	1.4	7	0	Al	**153 ± 10**	**164 ± 10 (2σ)**
								TiLi	**189 ± 12**	
Maurecourt**		**Fz**	**M-01 Fluvial deposit**	20.7	5.8	13	0	OSL	**17± 1.2**	-

**Tributaries of the Seine River

a. Upstream Paris

As explained in section 3.2.2.1, only two samples from strath terraces were dated by ESR upstream of Paris. Additionally, five samples from the current valley bottom were dated using OSL: three of them in the Bassée area and the other two along the Marne and Loing rivers (Figure 3.12).

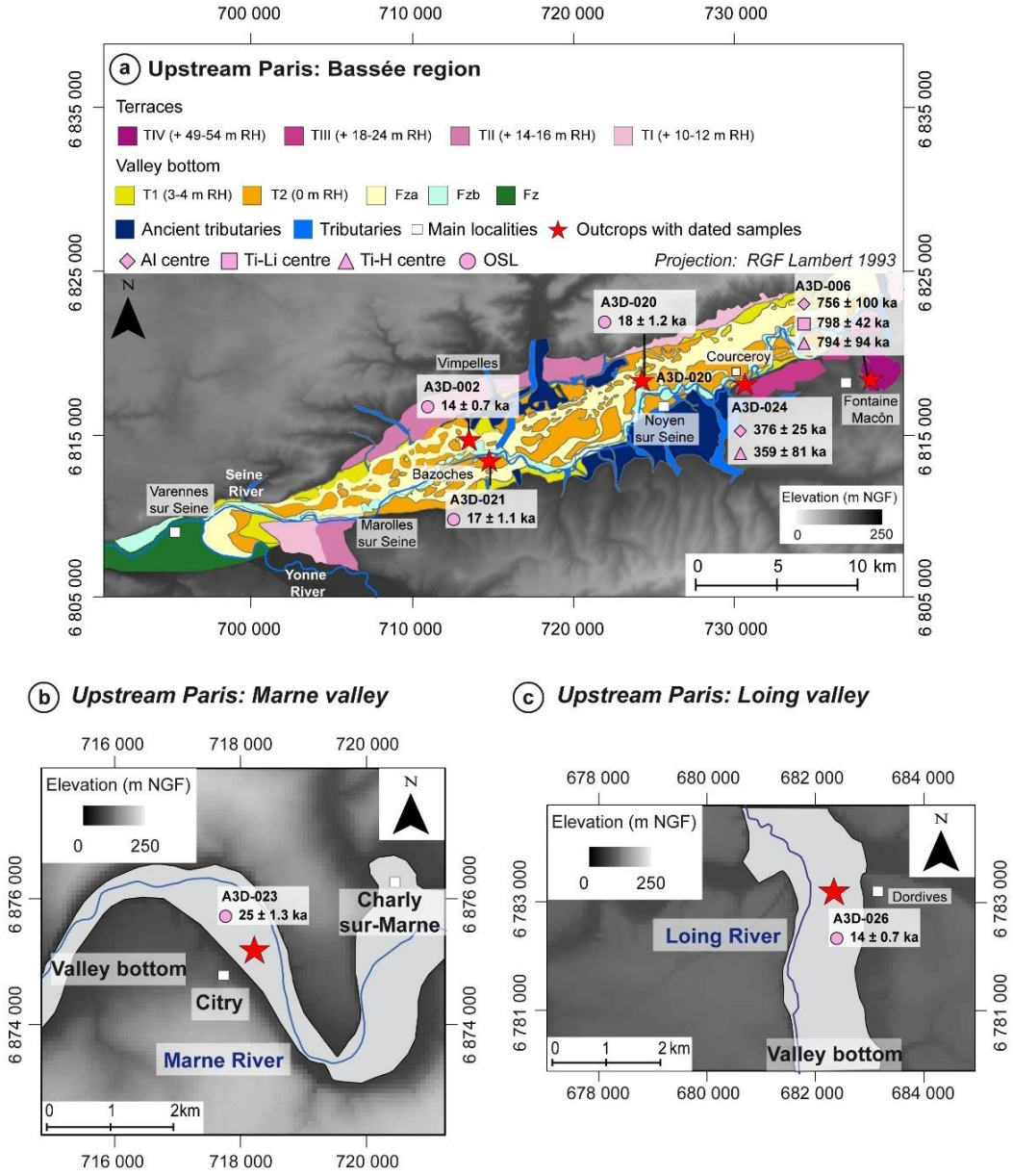

Figure 3.12. Sample location upstream Paris and the corresponding ages. (a) Along the Bassée area. (b) In the Marne valley and (c) In the Loing valley.

In the Bassée area, sample A3D-006 from terrace T_{IV} (+52 m RH) was dated using the ESR Al-centre, ESR TiLi-centre and ESR TiH-centre yielding ages of 756 ± 100, 798 ± 42 and 794 ± 94 ka, respectively. The mean age is thus 792 ± 35 ka (Table 3.4). As a result, it can be deduced that this terrace formed between marine oxygen isotope stage (MIS) 20 and 18 (Figure).
The terrace T_{IV} in the Bassée area represents the oldest terrace dated in this area and it could be correlated with the Serbonne terrace (+50/60 m RH, Chaussé et al., 2004) in the Yonne valley which has not been directly dated, or with the Fw terrace (+45 m RH) in the Aube valley dated by ESR at c.a., 600 ka (MIS 16/15, Voinchet et al., 2015) representing the oldest terrace in the Aube valley (Figure 3.13).

Ages of sample A3D-024 from terrace T_{III} (+22 m RH) were obtained using the ESR Al-centre at 376 ± 25 ka and ESR TiH-centre at 359 ± 81 ka, resulting in a mean age of 375 ± 23 ka (Table 3.4). This suggests the formation of this terrace at the end of MIS 11 and the beginning of MIS 10 (Figure). Consequently, the fluvial deposits of this terrace could be correlated with (i) the sequence observed at La Celle-sur-Seine, where the sequence is characterized by fluvial sediments at +25 m RH and the bedrock at +20 m RH, in which the tufa deposits founding on the top of the sequence have been dated at 425 ± 46 ka coeval to MIS 11 (Limondin-Lozouet et al., 2006). (ii) With the corresponding Soucy formation (+20 m RH) in the Yonne valley, that has been dated at 356 ± 14 ka (Voinchet et al., 2004) attributed to MIS 10 (Antoine et al., 2007) and (iii) with the terrace Fxb (+10/+13 m RH) in the Aube valley, that has been dated at 300 ± 30 ka coeval with the MIS 10/9 (Figure 3.13, Voinchet et al., 2015).

In the same region, three samples from the current valley bottom were dated by OSL, in which samples A3D-020 and A3D-021 from T_2 terrace have been dated between 18 ± 1.2 ka and 17 ± 1.1 ka, and sample A3D-002 from T_{3a} dated at 15 ± 1.1 ka (Table 3.4). Suggesting a deposition during the MIS 2 (Figure). Those ages are coherent with the Fy terrace located at Marcilly-sur-Seine, where sediments from the valley bottom have been dated by OSL at 16.6 ± 0.9 ka (Bertrand et al., 2018). Or in the Yonne valley with the Etigny formation, which overlie the deepest incision valley bottom, where the lowest coarse sediments are attributed to the Weichselian Pleniglacial (MIS 2, Chaussée et al., 2004).
It is important to note that the T_1 terrace (+3-4 m RH) in the Bassée area was not sampled and this terrace could be correlated with the Gron formation in the Yonne valley (+3 m RH) dated at 158 ± 24, 175 ± 26, 278 ± 42 ka (Voinchet et al., 2004), attributed to MIS 4-2 (Chaussée et

al., 2004) or with the Sens formation (+5 m RH) in the Yonne valley attributed to MIS 6 (Figure 3.13, Chaussée et al., 2004).

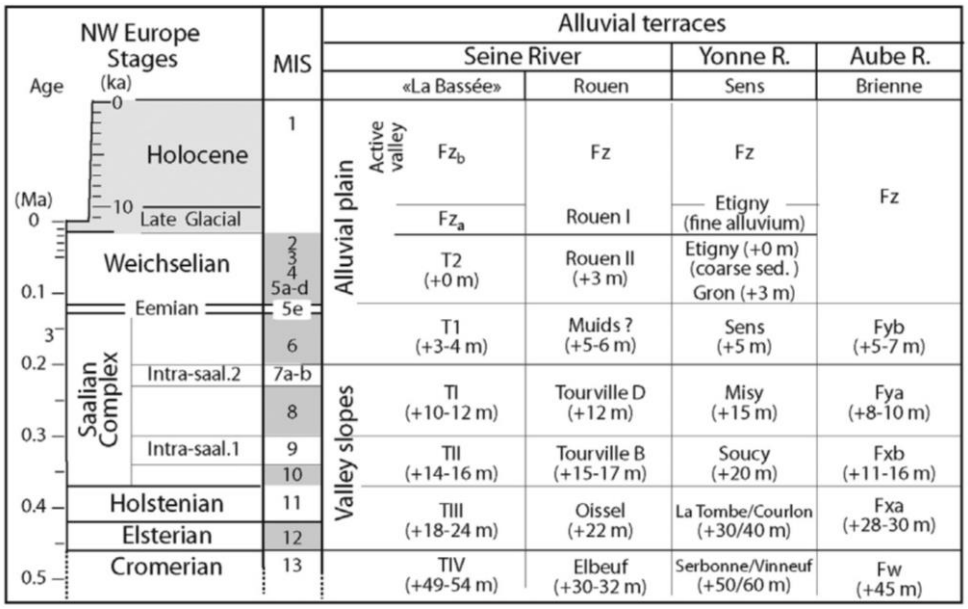

Figure 3.13. Chronostratigraphic scheme of the alluvial terraces along the Seine catchment and its tributaries (Chaussée et al., 2004; Antoine et al., 2007; Voinchet et al., 2015; Deleplancque et al., 2018; Marine Isotope Stages (MIS) from Lisiecki and Raymo, 2005).

Finally, samples from the valley bottom of Marne (A3D-023) and Loing (A3D-026) valleys were dated by OSL, the corresponding ages are 25 ± 1.3 and 14 ± 0.7 ka (Table 3.4). Suggesting that sediments were deposited during the MIS 2 (Figure 3.15). The data from the Loing are consistent with the results in the Bassée area.

In the Marne valley, at Maisons-Alfort (+9 m RH), near of the confluence with the Seine River, at Changis-sur-Marne (+6 m RH) and at Noisy-le-grand (+3 m RH), the fluvial deposits are located within the current valley bottom determined in this work. These deposits were dated by U-Th on bones at Maisons-Alfort, at 206 and 162 ka (comprising between the MIS 7/6) (Durbet et al., 1997; Blaser et al., 2021). Using U-Th on travertine tuffs, ESR/U-Th on bones and OSL on fluvial quartz at Changis-sur-Marne, at 189 to 85 ka (coeval with MIS 6 and early MIS 5c) (Blaser et al., 2021), and using the OSL on quartz at Noisy-le-Grand, at 50 ka (coeval with the MIS 3) (Vartanian, 2019).

At Neuilly-sur-Marne and Citry the alluvial sequence was dated using the ^{14}C showing a good reconstruction of the general evolution since the Weichselian (MIS 2, this work) and the Holocene (Le Jeune et al., 2012; Granai, 2014).

The variability in age of the different deposits withing the Marne valley suggest that the valley bottom is comprise between the MIS 6 and the Holocene, raising the question about the valley bottom age.

b. Downstream Paris

Downstream of Paris, as previously mentioned in section 3.2.2.2, eleven samples were dated using ESR and ten samples using OSL. It is worth nothing that only seven of these samples were dated combining ESR and OSL methods. Eleven samples are a part of the fluvial terraces, and three samples are a part of the current valley bottom (Figure 3.14). Results from Manoir-Brésil, which mostly fall into MIS7-6, will be discussed in chapter 4.

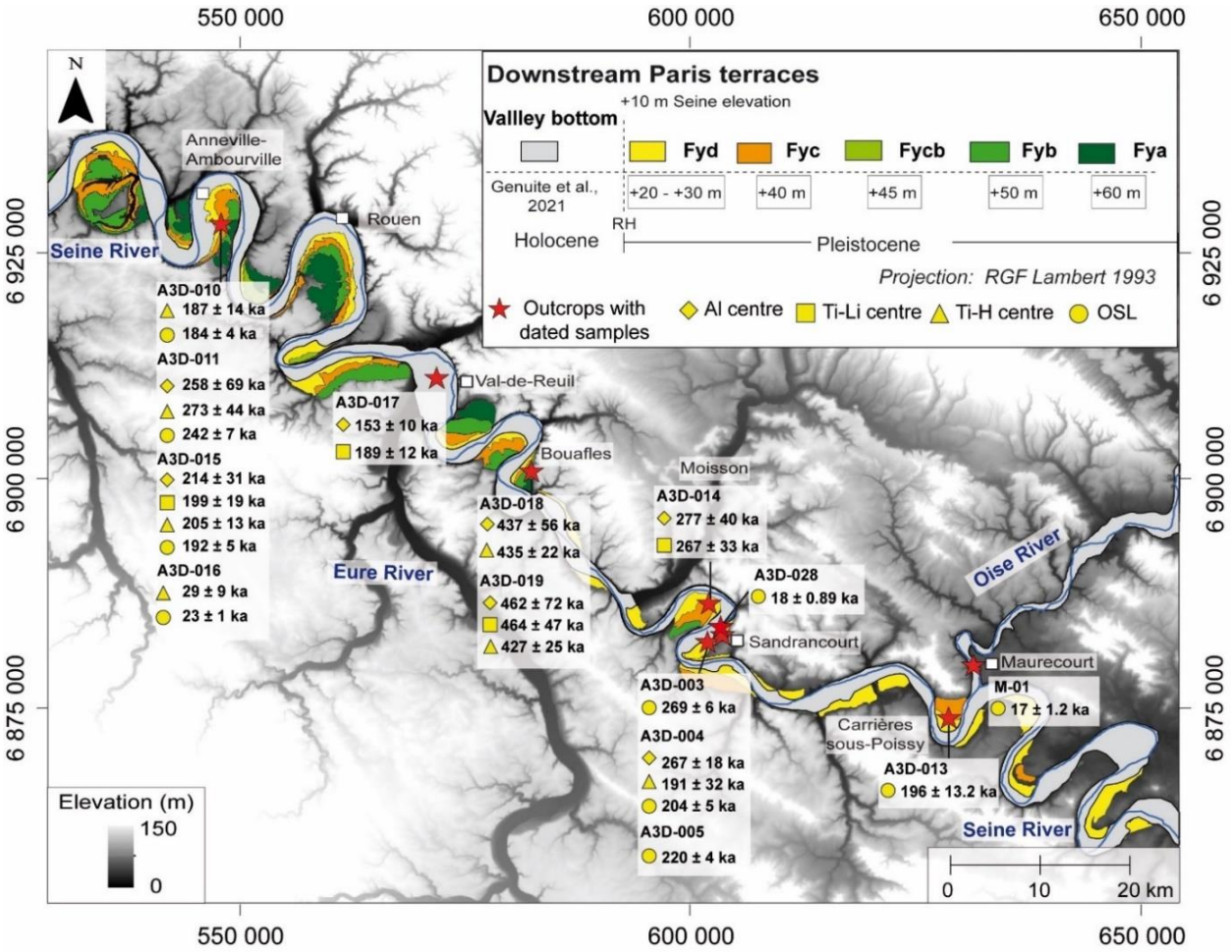

Figure 3.14. Sample locations downstream Paris and the corresponding ages.

Near of Val-de-Reuil, the Poses dam marks the transition between the fluvial dynamic and the influence of the estuary dynamic (Frouin et al., 2010). Between the Poses dam and Paris no direct chronological data was made. Lecolle, (1989), use the Amino Acid Racemisation (AAR) to establish the geochronology of this area. Determining 16 successive units stepped up to +45 m RH and attributed to the last 600 ka by climatic chronostratigraphic correlation (Lécolle, 1989; Antoine et al., 2007).
Thus, to establish the correlation between the different terraces observed in this work and the corresponding bibliography, we use the neighbouring terraces observed at Rouen (Lautridou et al., 1999; Antoine et al., 2007, 2010; Jamet et al., 2014, Nehme et al., 2020; Genuite et al., 2021).

At Boufles site, two samples A3D-018 and A3D-019 from the Fyb terrace (+25 m RH) was dated using the ESR. The obtained ages for sample A3D-018 are Al-centre at 437 ± 56 ka and TiH-centre at 435 ± 22 ka. The deduced ages for sample A3D-019 are Al-centre at 462 ± 72 ka, TiLi-centre at 464 ± 47 ka and TiH-centre at 427 ± 25 ka (Table 3.4). These results are in agreement given a mean of ESR age at 436 ± 63 ka, indicating that sediments of this terrace were deposited during the MIS 12 (Figure 3.15). Thus, the terrace Fyb could be correlated with the Oissel formation (+22 m RH, Figure 3.13) which has not been dated but correlated with the Garenne sequence (+27 m RH) in the Somme valley and dated by ESR on quartz at 430 ±73 ka (Antoine et al., 2007).

At Moisson site, one sample A3D-014 from the Fyc terrace (+19 m RH) was dated using the ESR. Ages results are based on Al-centre at 277 ± 40 ka and TiLi-centre at 267 ± 33 ka, with a mean of 271 ± 25 ka (Table 3.4). Suggesting a sediment deposition during the MIS 8 (Figure). This terrace could be correlate with the gravel terrace sequence exposed in the Tourville formation (+17-18 m RH), attributed to MIS 8 (Jamet, 2014; Bahain et al., 2019) (Figure 3.13), or with the Argoeuves formation (+15 m RH), attributed to MIS 8 using the malacology analysis (Antoine et al., 2000).

At Carrières-sous-Poissy site, one sample A3D-013 from Fyd terrace (+15 m RH) was dated using OSL at 196 ± 13.2 ka (Table 3.4). Suggesting a sediment deposition during the MIS 7 (Figure 3.15).

At Sandrancourt site, three samples A3D-003, A3D-004 and A3D-005 from the Fyd terrace (+9, +11 and +13 m RH) were dated coupling ESR and OSL methods.

Samples A3D-003 and A3D-004 were collected from the same section. For sample A3D-003, the corresponding age were calculated using the OSL at 269 ± 6 ka. For sample A3D-004, the obtained ages are Al-centre at 267 ± 18 ka, the TiH-centre at 191 ± 32 ka and the OSL at 204 ± 5 ka. In the same terrace, sample A3D-005 separate c.a. 1.8 km from the other two samples has an OSL age at 220 ± 4 ka. Considering these three samples for the Fyd terrace, the TiH-centre yields the youngest results, whereas the OSL provides the oldest age with a mean in age of c.a. 212 ± 57 ka (Table 3.4). Suggesting that sediments were deposited between the MIS 8 and MIS 7 principally (Figure).

Thus, the Fyd terrace could be correlate with the Tourville formation (+12 m RH), coeval with the MIS 8 and MIS 7 (Jamet, 2014; Bahain et al., 2019) (Figure 3.13), or with the Montières formation (+12 m RH) in the Somme valley dated at 200 ka and attributed to MIS 7 (Antoine et al., 2000, 2007).

In the current valley bottom, at Saint Martin-la-Garenne site, sample A3D-028 was dated using the OSL given an age of 18 ± 0.89 ka (Table 3.4), suggesting that sediments were deposited during the MIS 2 (Figure 3.15). At Maurecourt site in the Oise valley, sample M-01 was dated using the OSL given an age of 17 ± 1.2 ka (Table 3.4), suggesting that sediments were deposited during the MIS 2 (Figure 3.15). At Val-de-Reuil site, one sample A3D-017 from valley bottom alluvium was dated using ESR. The obtained ages are Al-centre at 153 ± 10 ka and TiLi-centre at 189 ± 12, with a mean of 164 ± 10 ka (Table 3.4), suggesting that sediments were deposited during the MIS 6 (Figure). Surprisingly, the ages for this sample in the current valley bottom seem to be relatively higher when compared to other samples from the valley bottom, suggesting a stacked terraces within the valley bottom. It is important to note that near of this site there is the confluence with the Eure River, but also where the estuary influence begins.

Different studies focus on the valley bottom within the Seine catchment have demonstrated the evolution of the valley bottom from the Weichselian Upper Pleniglacial to the Holocene (i.e., in the Seine valley: Rueil-Malmaison, Héliport Farman, Alizay, Porte-Joie, Rouen, Marais Vernier; in the Eure valley: Louviers; in the Oise valley: Boran-sur-Oise, Isle-Adam, Croix-Saint-Ouen, Choisy-au-Bac, Verberie, Bruyères, Houdancourt). The dating methods was principally the malacological data, the ^{14}C, TL, OSL, ESR-U-Th principally. Reflecting the regional pattern of fluvial dynamic in response to climate changes (Pastre et al., 2000, 2002;

Larue, 2000; Locht et al., 2003; Frouin et al., 2010; Granai, 2014, Chaussée et al., 2017; Blaser et al., 2021).

At lower elevation in the Seine valley, two gravel terraces were documented (Jamet, 2014): T1 or “Rouen 2” (5 m RH) and T0 or “Rouen 1” (0 m RH). These terraces were no date yet because those levels are under the Holocene deposits, they are attributed to MIS 4 and MIS 2 (Lefebvre et al., 1994; Lautridou et al., 1999).

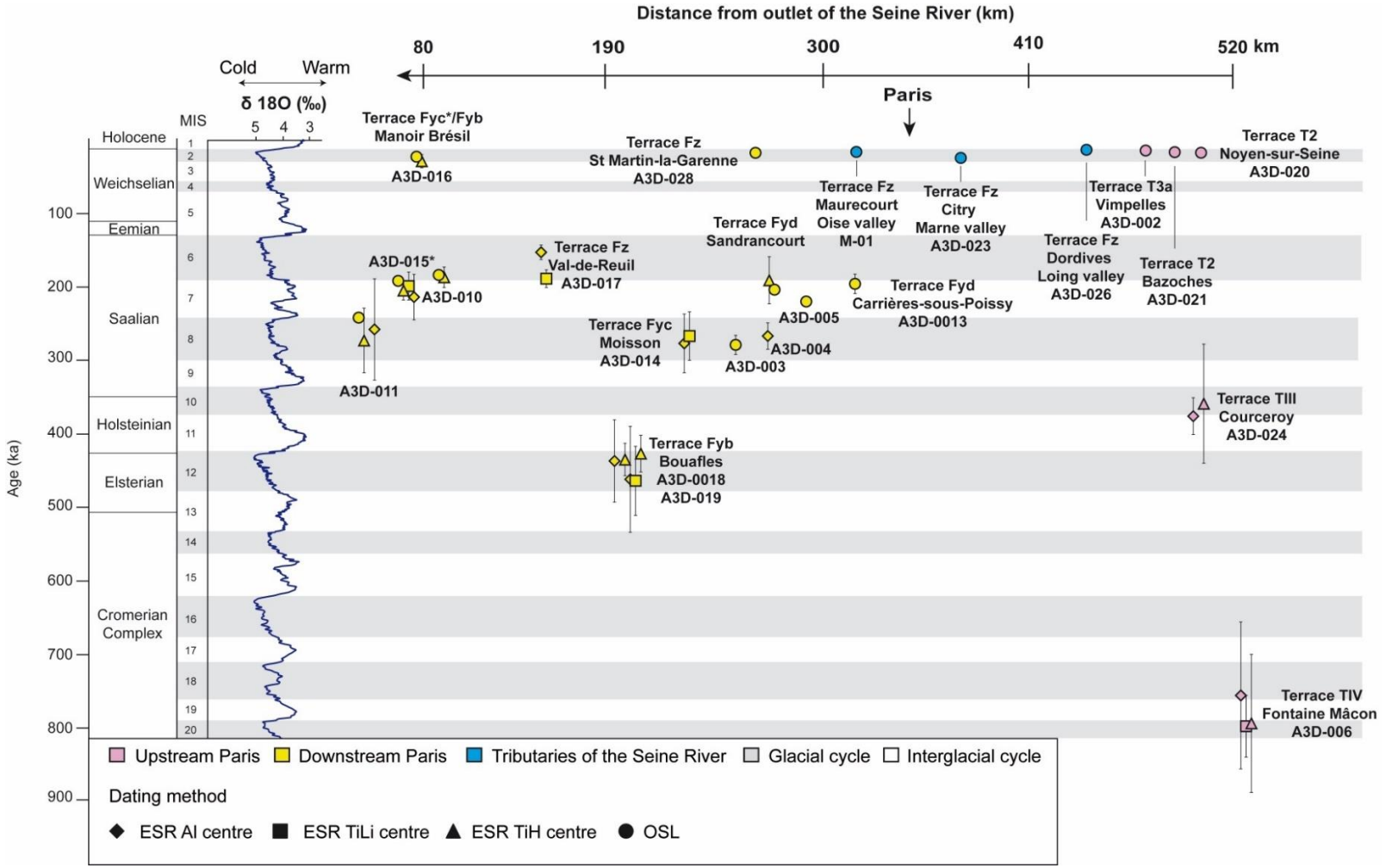

Figure 3.15. Final ESR and OSL results calculated according to different approaches or signals. Samples from upstream Paris are presented in rose colour, samples from downstream Paris in yellow colour and finally samples from tributaries are presented in blue colour. Ages are correlated with the Marine Isotopic Stages (MIS) derived from LR04 benthic $\delta^{18}O$ curve (Lisiecki and Raymo, 2005).

3.2.3.2 Comparison with known erosion rates

The distribution of samples is shown considering the elevation above the maximum incision (Figure 3.16) or above the valley bottom (Figure **3.17** 3.17) in the Seine catchment. Considering the 38 ages obtained from ESR Al-centre, ESR TiLi-centre, ESR TiH-centre and OSL allowed having preliminary, large-scale conclusions.

First, dated samples from the valley bottom correspond in general to the MIS 2 with the noticeable exception of Val-de-Reuil (sample A3D-017) from MIS 6. Thus, these data lead suppose that the bedrock of the valley bottom was incised during the MIS 6 period of relative sea-level fall and the MIS 2 in which the sea-level reaches – 110-130 m (Toucane et al., 2009). Therefore, the mechanism to constrain the age of the valley bottom are in relation with the sea level variation. It is known that during the MIS 6 there was a decrease in sediment coupled with an increase in incision, although this was less pronounced than the subsequent incision during the MIS 2 when sediments were transported into the English Channel (Lefebvre et al., 1994). Concurrently, a regressive erosion is generated during the MIS 2 near of Les Andelys (Lautridou et al., 1984, 1999).

In the Loir valley, the valley bottom is stacking, and it is comprised between the MIS 6 to the Holocene (Despriée et al., 2003; Tissoux et al., 2011).

Second, there is an increase in ages with their relative elevations (RH or RH', figures 3.16 and 3.17): oldest age sample have the highest elevation, and the younger age sample have the lowest elevation. Considering the curve of the absolute incision rates of the Seine valley evolution that was determined between 50 to 60 m since 1 Ma by Antoine et al., (2010), the new data of the Seine catchment show a good accordance with this curve. The progressive incision processes follow the uplift, which often leads to the reorganization of fluvial systems (Genuite et al., 2021). Pedoja et al., (2018) reported apparent uplift rates of 0.04 ± 0.01mm a^{-1} since MIS 5e (~122 ± 6 ka) from marine terraces on the Cotentin Peninsula northwest of the Seine valley.

Some differences are observed when we consider the relative elevations RH or RH'. When the RH is considered (Figure 3.16), samples are positioned according to the maximum incision of the river. However, some areas within the Seine catchment reflect more incision influence than others (i.e., downstream Paris). Therefore, this position is interesting for doing the comparation with the neighboring terraces (references use these elevation) but could influence this relative elevation. On the contrary, when the RH' is considered (Figure 3.17), samples are positioning

according to the valley bottom elevation. Thus, using the RH' may reflect less variability in elevation within the Seine catchment. We note that downstream Paris, all samples are tighter. It is important to note, that in three sites (Carrières-sous-Poissy, Sandrancourt and Manoir Brésil), samples dated as a part of the MIS 7 bordering the current valley bottom, thus, they could help to constrain their age.

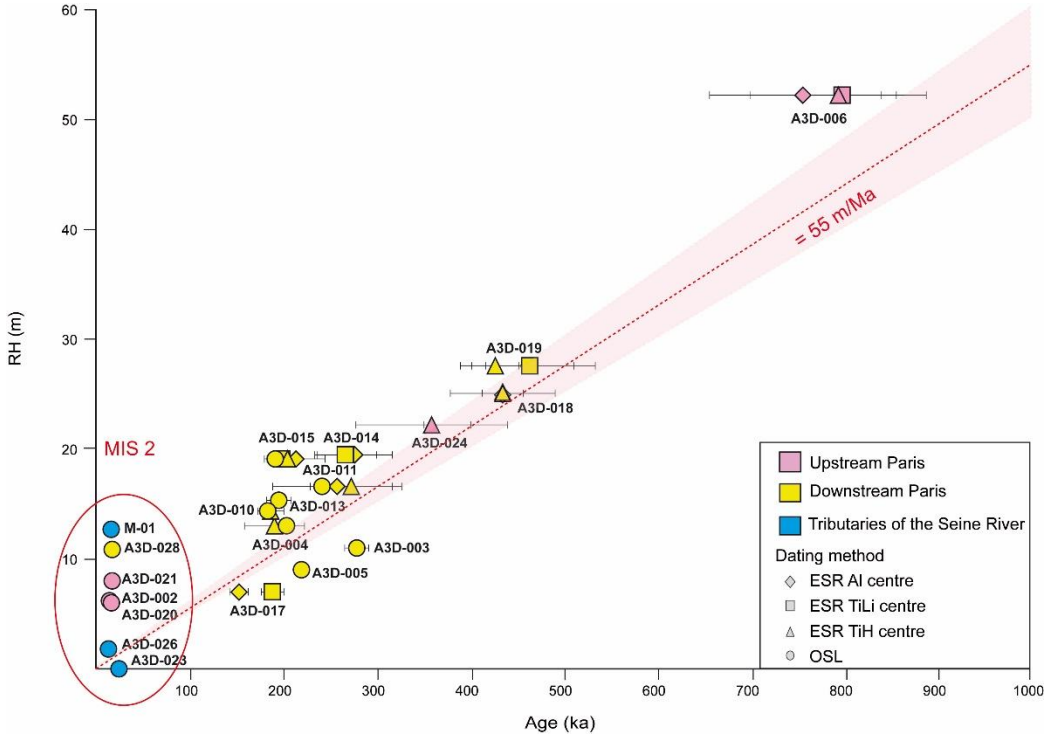

Figure 3.16. Synthesis of ESR and OSL ages obtained as a function of relative elevation above the maximum incision of the Seine catchment. Samples from upstream Paris are presented in pink colour, samples from downstream Paris in yellow colour and finally samples from tributaries are presented in blue colour. Red line represents the absolute value of uplift in the Seine valley modified after Antoine et al., 2010.

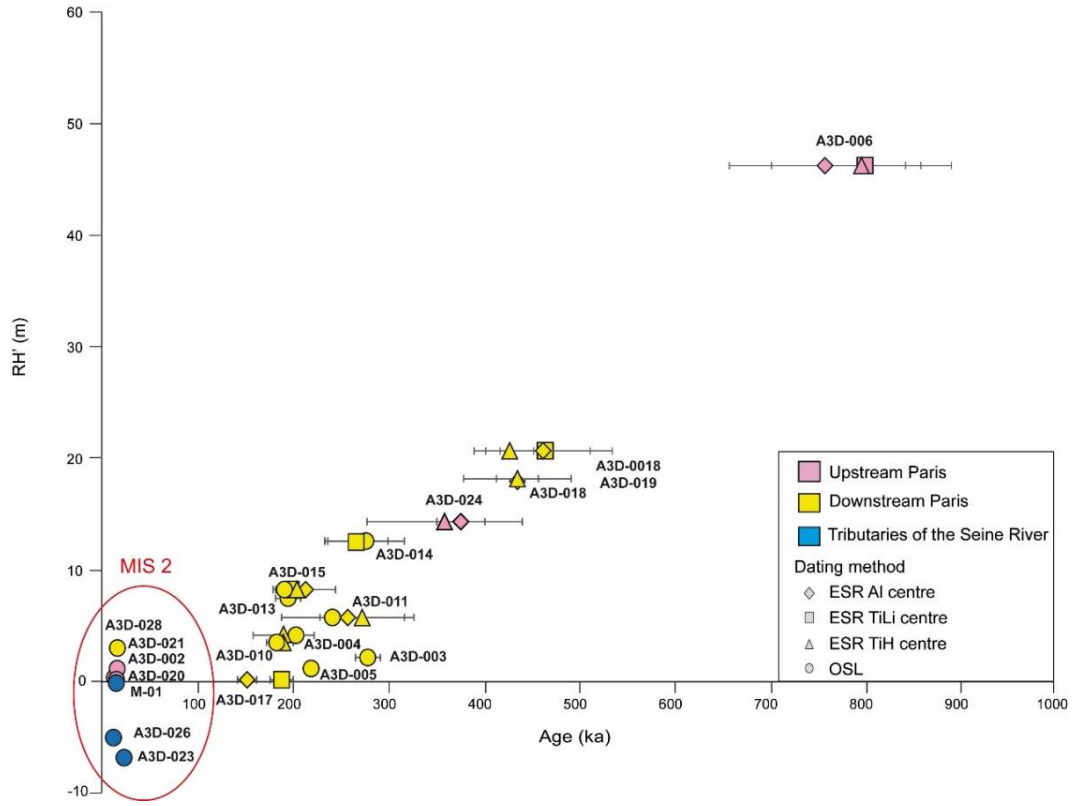

Figure 3.17. Synthesis of ESR and OSL ages obtained as a function of relative elevation above the valley bottom of the Seine catchment. Samples from upstream Paris are presented in pink colour, samples from downstream Paris in yellow colour and finally samples from tributaries are presented in blue colour. Red line represents the absolute value of uplift in the Seine valley modified after Antoine et al., 2010.

3.3 Conclusion

Dating of the samples described in chapter 2 were introduced in this chapter. ESR or OSL dating were performed independently, using the specific methodology and instrumentation for each technique (see more details in section 3.1). A total of twenty-one samples were analysed, in which only seven samples were dated coupling both ESR and OSL methods, six using only the ESR method and eight using the OSL method. The results of ESR/OSL dating provide for the first time the chronology of fluvial evolution of the Seine catchment for the Middle and Lower Pleistocene. Ages of terraces and valley bottom were tentatively correlated with glacial/interglacial cycles (Figure 3.15).

Upstream of Paris in the Bassée area, two samples dated from terraces located at Fontaine Mâcon and Courceroy (terraces T_{IV} and T_{III}), provide for the first time the chronological data of these samples attributed to MIS 18-20 and MIS 10-11, respectively.

The large difference in age of these two samples suggest that there may have another terrace not observed between +25-45 m RH and potentially placing between the MIS 16 to MIS 12. Nevertheless, correlations with the neighboring terraces in other valleys suggest that the TIV terrace could be correlate with the with the Serbonne terrace in the Yonne valley and possibly correlated with the Fw terrace in the Aube valley. In contrast, the TIII terrace may correlated with the Soucy formation in the Yonne valley or with Fxb terrace in the Aube valley.

Samples located in the valley bottom from the Basséee area, Marne and Loing valleys returned ages from MIS 2. In the Bassée area only the T_2 and T_{3a} deposits were dated, it would be interesting to date in the future the sediments from the T_1, to know if this terrace could be correlated with the Gron (coeval with MIS 4-2) or Sens (coeval with MIS 6) formation in the Yonne valley.

Downstream of Paris, samples dated from terraces located at Bouafles, Moisson, Carrières-sous-Poissy, Sandrancourt and Manoir Brésil (terraces Fyb, Fyc and Fyd), are placed as a part of MIS 12, 8, 7 and 6, following the glacial-interglacial cycles. The Fyb terrace, located at Boaufles may correlated with the Oissel formation or with the Garenne sequence in the Somme valley. The Fyc terrace, located at Moisson could be correlated with the Tourville formation or with the Argoeuves formation in the Somme valley. The Fyd terrace, located at Carrières-sous-Poissy and Sandrancourt could correlate with the Tourville formation or with the Montières formation in the Somme valley.

Finally, samples from the current valley bottom, located at Maurecourt, Saint-Martin-la-Garenne and Val-de-Reuil, are dated placing these deposits as a part of the MIS 2 and the MIS 6, these, may reflect the influence of the sea-level during the last two glaciation. The terraces dated as MIS 7-6 that bordering the valley bottom could help to constraint its age.

Chapter 4: Incision and rock uplift along the Lower Seine River since Marine Isotope Stage 8: insights from the Manoir Brésil terrace system

Ce chapitre correspond à un article accepté au Journal of Quaternary Science (JQS) et qui se focalise sur l'incision fluviale au cours du MIS 8 dans la basse vallée de la Seine.

Chourio-Camacho, D., Grimaud J-L., Tissoux H., Bessin, P., Voinchet, P., Vartanian, E., Noble, M., and Bertran, P. Accepted. Incision and rock uplift along the Lower Seine River since Marine Isotope Stage 8: insights from the Manoir Brésil terrace system. JQS.

Chapter 4

4 Incision and rock uplift along the Lower Seine River since Marine Isotope Stage 8: insight from the Manoir Brésil terrace system

This chapter corresponds to a manuscript summited to Journal of Quaternary Science (JQS) with a specific focus on fluvial incision during MIS 8 in the Lower Seine valley.

4.1 Abstract

The study of alluvial terraces helps in reconstructing the past geometries of rivers and makes it possible to assess the rate and pattern of fluvial incision and bedrock uplift. The fluctuations of river base levels are particularly variable and complex during the Late Quaternary in the lower course of rivers due to the interplay of responses to sea level fluctuations, tectonics and glacio-isostasy. In this paper, the geometry and chronology of Manoir Brésil, an outcrop of alluvial terraces of the Lower Seine River, northern France, are investigated through a multidisciplinary study. Fluvial incision during MIS 8 in the Lower Seine in relation to sea level drop is recorded by an erosional surface cut into the chalk bedrock. This surface is covered by MIS 7 tidal deposits and then by younger, mostly periglacial colluvium (head). Manoir Brésil is therefore considered as a chronological equivalent of the nearby, well-studied Tourville-la-Rivière outcrop. The deposits are affected by post-MIS 7 cryoturbation processes. Based on the local elevation of MIS 7 tidal deposits and erosional surfaces at Manoir Brésil, a minimum bedrock uplift rate of 25-40 m/Ma and an erosion rate of 125 m/Ma during glacial periods can be proposed. A regional correlation of the MIS 8 erosional surface is increasingly deformed by uplift towards the North, making it difficult to correlate the fluvial deposits along the Seine without precise chronological control. We interpret this regional tilt as the result of isostasy rebound after glaciations, consistently with the distribution of the elevations of MIS 5e and MIS 7 marine deposits along the English Channel.

KEYWORDS : MIS 7, Lower Seine, alluvial terraces, tidal deposits, periglacial deposits, incision rate, Late Quaternary uplift.

Chapter 4

4.2 Introduction

Late Quaternary Earth surface evolution is influenced by high-frequency oscillations between glacial and interglacial climates combined with the deformation of the lithosphere (Lisiecki and Raymo 2005; Wickert *et al.* 2019). The complex coupling between these processes sets the pace of sedimentary fluxes delivered by rivers to sedimentary basins. Climate changes promote ice sheet advance and retreat, which in turn induce (un)loading on the lithosphere. During glacial periods, the land covered by ice subsides while a peripheral flexural bulge is uplifted (Mitrovica *et al*. 1994; Sella *et al*. 2007; Wickert *et al*. 2018). Ice retreat during interglacial stages is followed by the isostatic rebound of the lithosphere (Bradley *et al*. 2009). In addition, ice sheet formation results in the decrease of the eustatic sea level, which dropped down to -130 m NGF ("Nivellement Général de la France", French official altimetric system) in NW Europe during the Last Glacial Maximum (Lambeck *et al*. 2014). As a result, river incision, which forms canyons on the continental shelf, propagates upstream (Mellet *et al*. 2013; Benabdellouahed *et al*. 2013; Paquet *at al.*, 2023). Another consequence of glacial periods is the increased duration of seasonal soil freezing, leading to changes in vegetation and to the limitation of infiltration on hillslopes (Van Vliet-Lanoë 1998; Mol *et al*. 2000; Ehlers and Gibbard 2004). These modifications affect in turn the delivery of water and sediment to rivers, affecting river incision capacity (Blum *et al.* 2013). At the onset of glacial periods, river discharge increases and favour the incision and abandonment of previous alluvium as terraces. In full glacial conditions, hillslopes deliver more sediment to the river, nourishing alluvial bottoms where braided rivers can aggrade (Westaway *et al.* 2006; Antoine *et al*. 2007; Bridgland and Westaway 2008; Bridgland and Schreve 2009). With the return of interglacial conditions and the elevation of sea level, canyons are submerged and partly buried with marine/coastal deposits.

Climatic alternation thus leads to the development of fluvial terraces (Blum and Törnqvist, 2000; Törnqvist *et al.* 2000; Briant *et al.* 2012). The study of these terraces helps reconstructing the geometries and rates of river incision as well as characterizing the rates and pattern of bedrock uplift (e.g., Pazzaglia and Brandon 2001; Grimaud *et al.* 2014). Recent work, however, has shown the influence of autogenic processes in regulating incision dynamics (Grimaud et al. 2016; Limaye and Lamb 2016; Scheingross *et al.* 2020), complexifying the analysis of the records of rock / surface uplift and erosion.

Regional syntheses of the distribution of contemporaneous fluvial and marine deposits allowed deciphering the spatial distribution of deformation as for MIS 5e in Northwestern Europe (see Cohen *et al.* 2022 and references therein). In comparison, the penultimate interglacial period

(MIS 7; 240-170 ka) is less constrained. However, MIS 7 remnants are found at higher elevation than MIS 5 (i.e., they are not buried below valley bottom and coastal sediments as it is sometimes the case for MIS 5), offering a potentially better opportunity to attempt topographic correlations. After the beginning of interglacial MIS 7 (MIS 7e), a transitioning into glacial conditions (MIS 7d) generated a decrease in global sea-level of approximately 60 m. It was then followed by a rapid deglaciation event (MIS 7d to MIS 7c) (Choudhury *et al.* 2020). Such event had the potential to leave a record in alluvial terraces.

Along the Somme River, in Northern France, the record of alluvial terraces, slope deposits and loess-paleosoil sequences is well-documented and consistent with climatic (allogenic) forcing on landscape evolution and river incision for since before 1 Ma (Antoine 1994, 1997, 2019; Antoine *et al.* 2000, 2007, 2010). In contrast, the neighbouring Seine River is less documented, although some sites have been analysed in detail (e.g. Tourville-la-Rivière; Jamet (2014), Bahain *et al.* (2019)). The difficulty of restituting the Seine River evolution compared to the Somme River owes to a larger system and to the complexity of the terraces record along different segments of its longitudinal profile (Lécolle 1989; Lautridou *et al.* 1999; Antoine *et al.* 2000, 2007, 2010; Chaussée *et al*. 2021). It is also simply a consequence of a lack of field descriptions. Regional syntheses on the incision dynamics of the Seine River drainage basin have only recently resumed (e.g., Chaussé *et al.* 2021; Génuite *et al.* 2021). Overall, there is still a crucial need to investigate (and correlate) alluvial terraces along the Seine River, requiring detailed stratigraphic and geochronological studies.

In this study, we focus on the terrace above the Lower Seine valley bottom in the Anneville-Ambourville meander bend, in a quarry called Manoir Brésil with exceptional outcropping conditions. We combine measurements of the top of bedrock elevation using a differential GPS, sediment facies description and ESR/OSL dating to better constrain the timing and geometry of the development of a typical terrace of the Lower Seine River. These data are then compared to those provided by other regional sites. The results allow constraining vertical movements since MIS 8. A first estimation of bedrock uplift rate is made and its potential relation to glacio-isostatic flexure is discussed.

4.3 Geomorphic settings

The Seine valley is located within the Paris basin, an intracratonic sedimentary basin (Pomerol 1978; Mégnien 1980) bounded by the Ardennes, Morvan, Vosges, Massif Central and Armorican crystalline massifs. During Mesozoic times, the basin was affected by slow subsidence, which stopped during the Paleogene and the Pyrenean orogeny. In the Neogene, low amplitude uplift was caused by the far-field Alpine compression (Briais, 2015; Bourgeois *et al*. 2007). Since the Plio-Quaternary, the landscape has been shaped by repeated climatically induced cycles of global sea level changes, periglacial and karst processes and river discharge fluctuations (Pomerol and Feugueur 1974; Gibbard 1988; Antoine *et al.* 2007, 2010; Bridgland and Westaway 2008).

The Seine River drains the northeastern part of the Paris basin into the English Channel. The lower part of the Seine valley, i.e., the Lower Seine, is located between Les Andelys and Le Havre (Figure 4.1). In this part, the Seine valley exhibits a meandering pattern (Lefèbvre 1988) incised into the Cretaceous chalk bedrock (Jamet 2014; Mortimore 2018; Ballesteros *et al.* 2020). Alluvial terraces can be found in this area, with elevations ranging from 0 to 80 m NGF, with their number varying between 7 or 8 depending on the authors (Lefèbvre *et al.* 1994; Lautridou *et al.* 1999; Antoine *et al.* 2007; Jamet 2014). While some authors use the absolute (m NGF) elevation to correlate terraces (Lefèbvre *et al.* 1986; Le Joncour 1995; Lautridou *et al.* 2003), others argue that the relative height (RH) above the maximum incision level of the Seine River is the best value to consider (Chaput 1924; Cholley and Firmin 1945; Chancerel 1986; Antoine *et al.* 2007; Bahain *et al.* 2019; Génuite *et al.* 2021). In this study, we use both methods and discuss their relevance.

The Manoir Brésil terrace is located along the left bank of the Anneville-Ambourville meander, approximately 30 km downstream of Rouen and 80 km upstream of Le Havre (Figure 4.1 and Figure 4.2-a). It is exposed in a gravel quarry whose elevation ranges from 3 to 30 m NGF. According to the 1:50,000 BRGM geological map (Janjou, 2004; Quesnel *et al.* 2008), the quarry is located within the Fy_c and Fy_d alluvial formations. The relative elevation of these terraces is +20-28 m RH and + 17-21 m RH for Fy_c and Fy_d, respectively. We used borehole data in the valley bottom (Figure 4.2) for a measurement of the elevation of the maximum incision (at -16 m NGF) near Manoir Brésil. The terraces may be tentatively correlated with the neighbouring T3 terrace (Oissel formation) found at +22-25 m RH and the T2 terrace (Tourville-la-Rivière formation) found at +17-18 m RH (Antoine *et al.* 2007; Jamet 2014). The Tourville-la-Rivière formation was extensively studied and includes three periglacial alluvial

units separated by two interglacial estuarine units (Porcher 1981; Lautridou 1985; Lautridou *et al.* 1999; Cordy *et al.* 2003; Antoine *et al.* 2007, 2010; Jamet 2014; Bahain *et al.* 2019). At lower elevation, two gravel terrace deposits were documented (Jamet 2014) in Tourville: T1 or "Rouen 2" (5 m RH) and T0 or "Rouen 1" (0 m RH). Theses terraces are covered by Fz Holocene deposits in Marais Vernier, Heurteauville and Anneville-Ambourville (Sebag 2002; Delsinne 2005; Frouin *et al.* 2010).

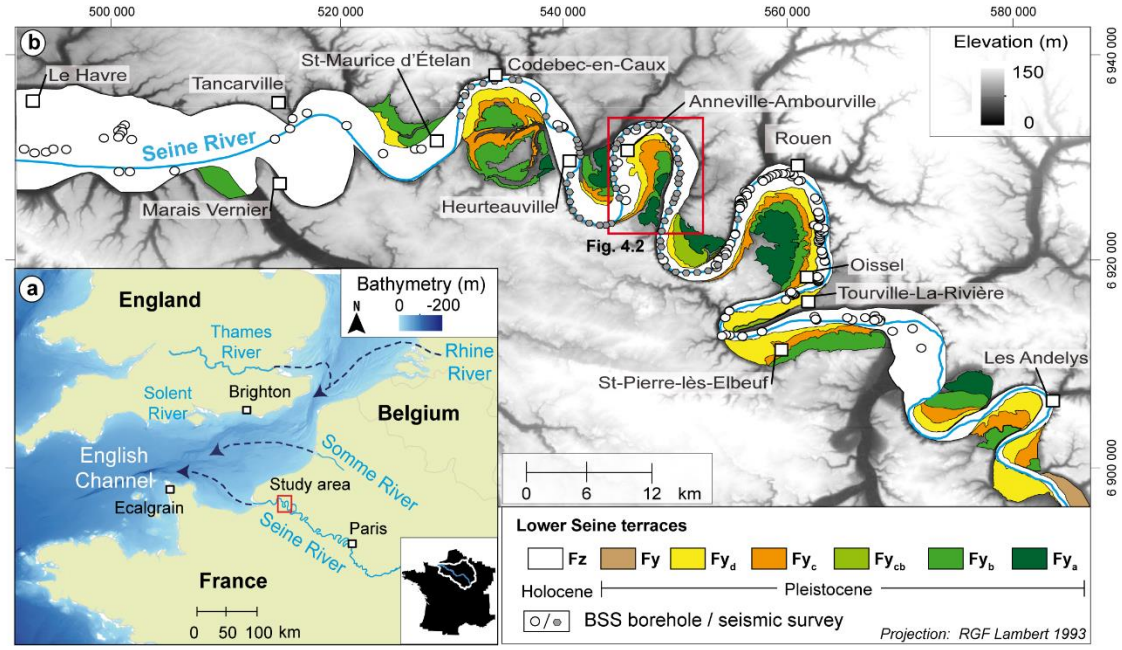

Figure 4.1. (a) Location of the study area. The dashed blue arrows correspond to the paleo-"fleuve Manche" during Quaternary lowstands when the English channel was dry. (b) Detail of the geomorphology of the Lower Seine area, terraces are from the harmonized BRGM geological map (scale 1:50 000).

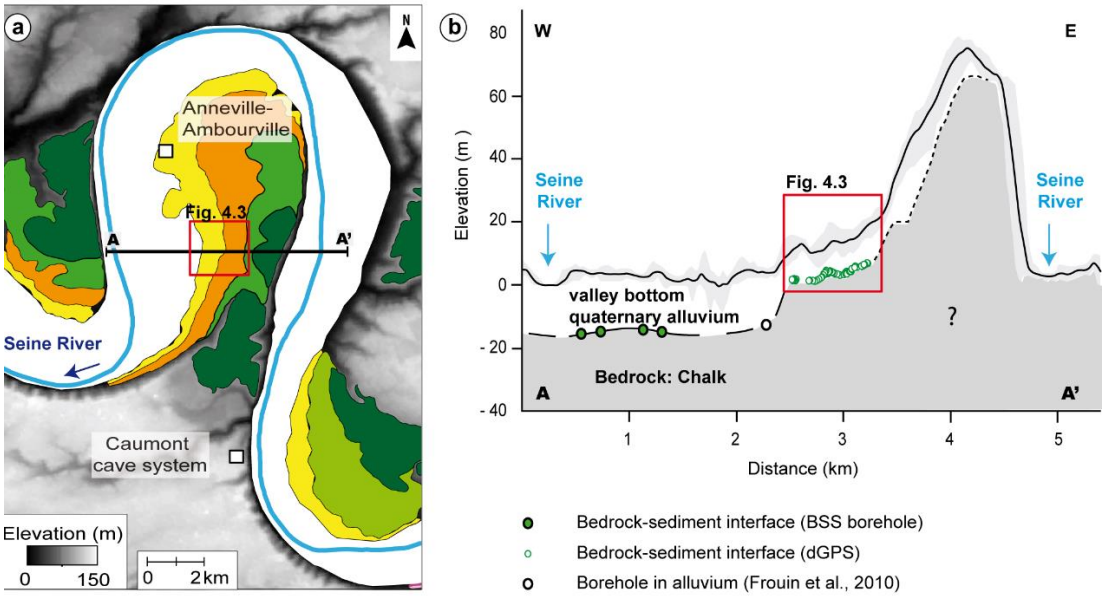

Figure 4.2. (a) Detail of the Anneville-Ambourville meander. For the legend of the terraces, see Figure 4.1. (b) Topographic SWATH section of the meander together with the interpretation of the limits of Quaternary deposits from borehole data. The red square represents the location of the Manoir Brésil quarry.

4.4 Methods

4.4.1 Field observations and data collection

4.4.1.1 Top of bedrock elevation

Quarry

Topographic profiles were acquired using a Leica differential-GPS, with measurements taken approximately every 10 m horizontally, and an acquisition time of 90 s. The resulting vertical precision was approximately ± 0.035 m. This resulted in the construction of 13 elevation profiles (Figure 4.2-b and Figure 4.3). Eight of these profiles directly measured the chalk bedrock elevation below the alluvial deposits, while the remaining five profiles corresponded to mining benches (Figure 4.3). These benches profiles were used to facilitate the interpolations between the studied sections.

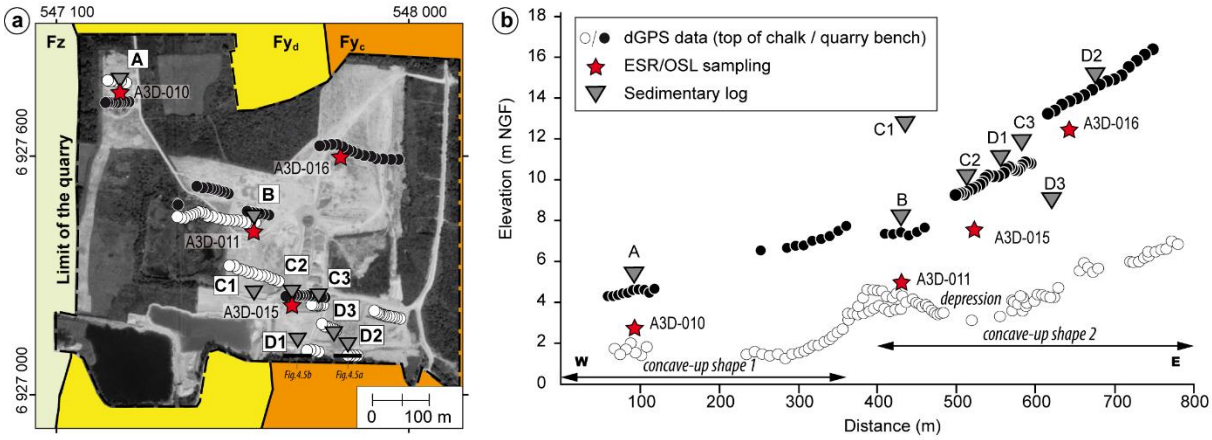

Figure 4.3. Locations of dGPS acquisition, sedimentary logs and sampling for ESR/OSL dating in the Manoir Brésil quarry using map (a) and cross-section (b) views.

Valley Bottom

Additional information on the geometry of the bedrock-alluvium interface in the valley bottom using, was gathered from 60 borehole descriptions available in the "Banque du Sous-Sol" (https://infoterre.brgm.fr/page/banque-sol-bss, locations on Figure 4.1). One borehole from the literature (Frouin *et al.* 2010) was also included **(**Figure 4.2-b).

Furthermore, in 2012, the "Grand Port Maritime de Rouen" conducted a seismic survey between Rouen and Saint-Maurice-d'Etelan (Figure 4.1), involving both refraction and reflection techniques. Across the entire 60-kilometer-long seismic profile, the interface separating the bedrock and alluvium layers stands out distinctly as a prominent reflector (strong density contrast). In this study, the interface depth was picked at one-kilometre intervals (Figure 4.1). Depth uncertainty is estimated to be less than 1 m.

4.4.2 Observations and descriptions of sedimentary deposits

A field description of the different sedimentary deposits was conducted at the study site, taking advantage of the extensive outcrops made available due to the rapidly evolving Manoir Brésil quarry. Two field campaigns were undertaken in 2020 and 2021. Between these campaigns, outcrops were buried, while new ones became accessible. Sedimentary facies were observed and described in the field along eight outcrops (Figure 4.4 and Figure 4.5) according to lithofacies and sedimentary structures following the nomenclature of Miall (2006) (Table 4.1). According to their spatial organization, these facies were grouped into architectural elements

(following Miall, 2006) and facies associations, which were then interpreted into distinctive depositional environments (Table 4.1). In order (i) to define the thickness of the depositional units, (ii) to establish correlations between different units and (iii) to identify the main unconformities, 8 sedimentary logs distributed over the Manoir Brésil quarry were constructed and named from A to D3 (Figure *4.6*). Finally, post-deposition deformation features were also observed and described (Figure 4.7). Four samples (Figure *4.6* and Figure *4.7*) were dated combining both ESR and OSL dating methods.

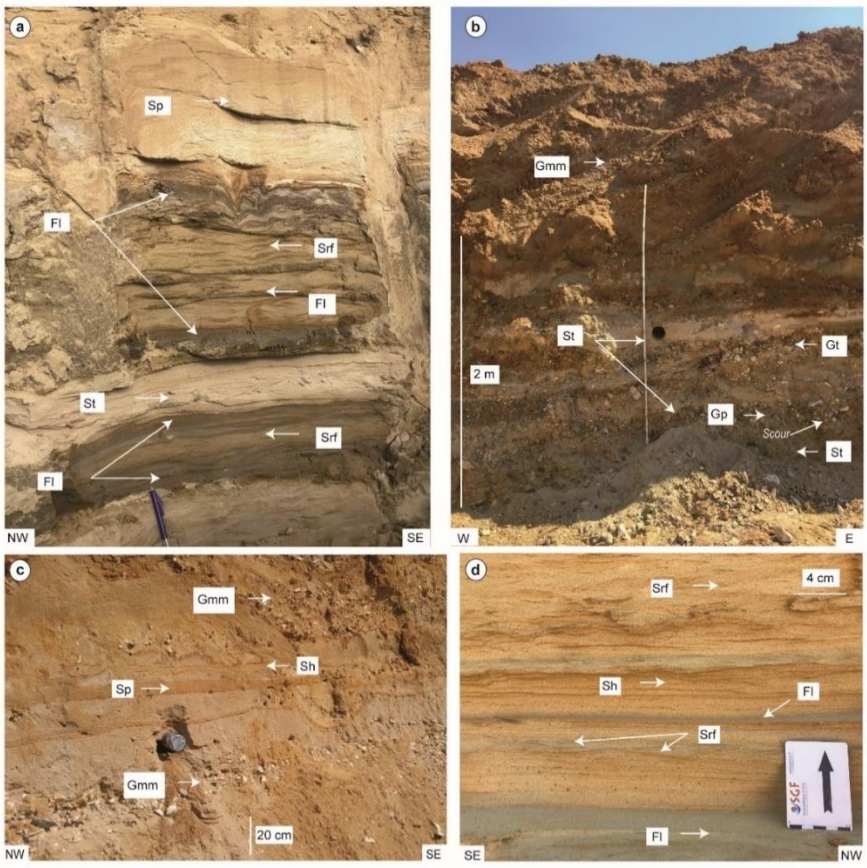

Figure 4.4. Photographs of the main lithofacies observed in Manoir Brésil. See description in Table 4.1.

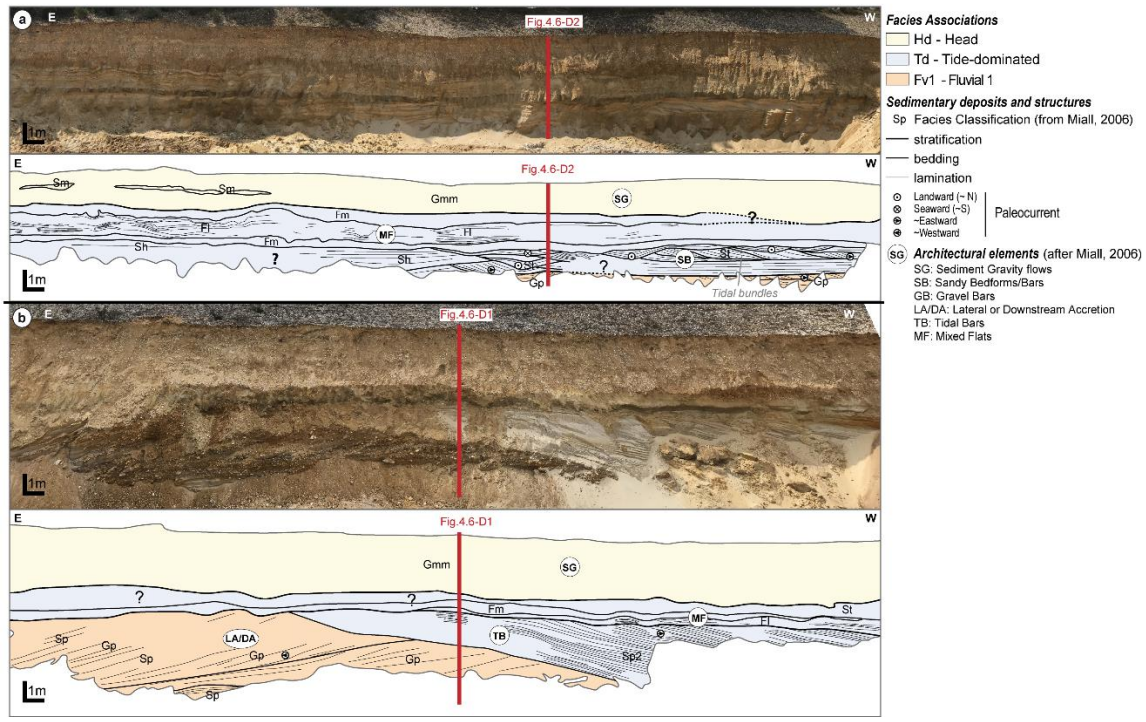

Figure 4.5. E-W panoramas of the quarry showing the geometrical distribution between the different architectural elements observed in the upper part of the quarry.

4.4.3 ESR/OSL geochronology

4.4.3.1 Sediment sampling

Four samples for both ESR and OSL dating were taken strictly at the same time and place. These samples of fine to medium sand (A3D-010, A3D-011, A3D-015 and A3D-016) were collected at elevations of 17.35 m RH (2.75 m NGF), 19.7 m RH (5 m NGF), 22.2 m RH (7.5 m NGF) and 27.2 m RH (12.50 m NGF), respectively (locations shown in Figure 4.3, Figure *4.6*, Figure *4.7*-a and Figure *4.10*). To ensure the accuracy of dating methods, the sediment samples were collected from fresh sections, avoiding sediment affected by leaching, accumulation (i.e., ferromanganic elements or clay) or bioturbation to prevent samples from having quartz grains bleached after deposition. Because of the extreme photosensitivity of OSL centres, sediments were sampled using a dark PVC tube and kept away from light from the time of sampling until the end of the analyses. In addition, *in situ* measurements of the natural radioactivity for each sample was collected with a 20-minute acquisition time using a portable gamma spectrometer type Inspector-1000 from Canberra or Digidart from Ortec. All samples were kept in dark bags to prevent potential bleaching during storage.

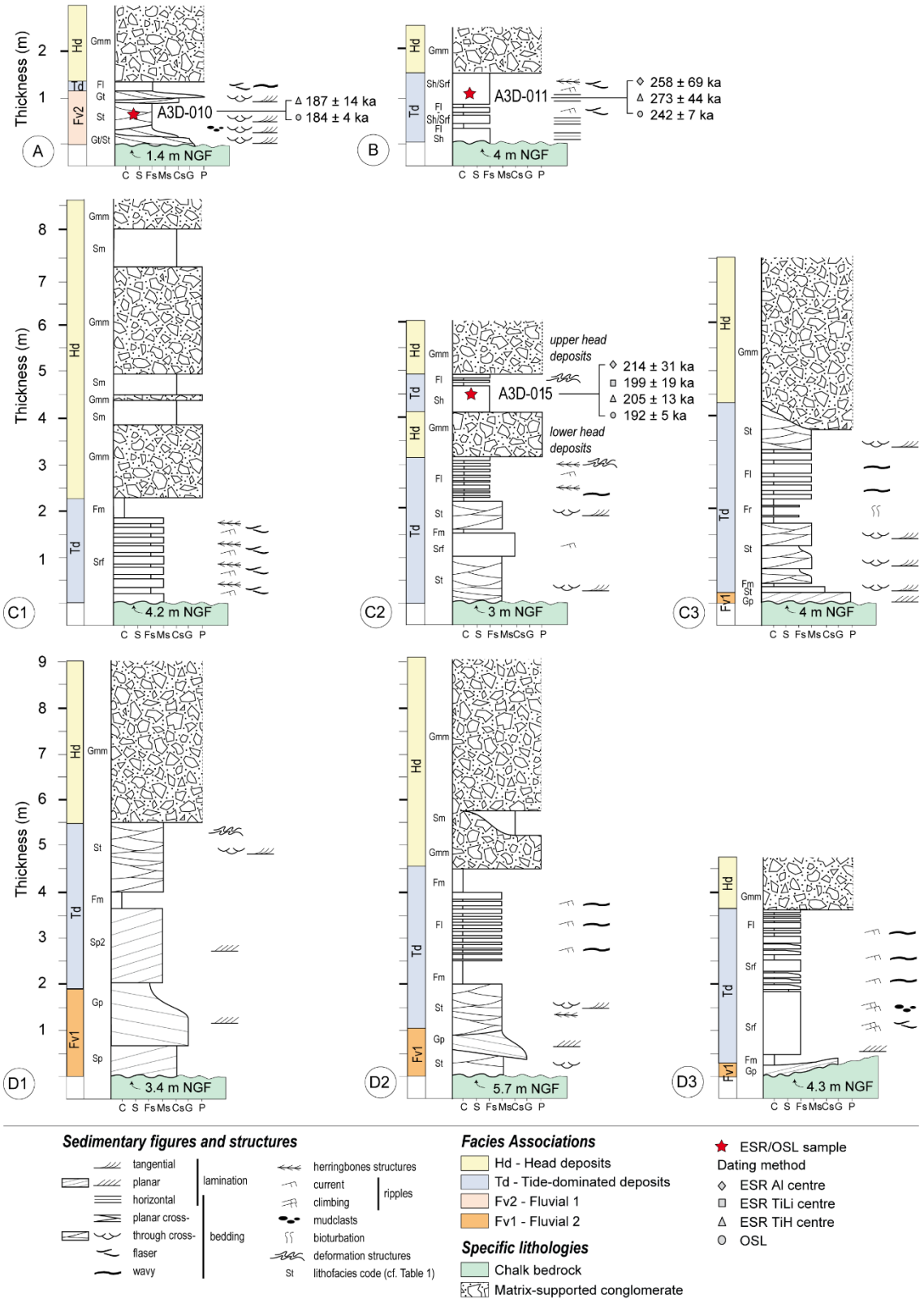

Figure 4.6. Stratigraphy from eight sedimentary logs made in the Manoir Brésil quarry (see figure 3 for locations). Grain size: C (clay), S (silt), Fs (fine sands), Ms (medium sands), Cs (Coarse sands), G (Gravel), P (Pebble). ESR/OSL samples are represented by red stars.

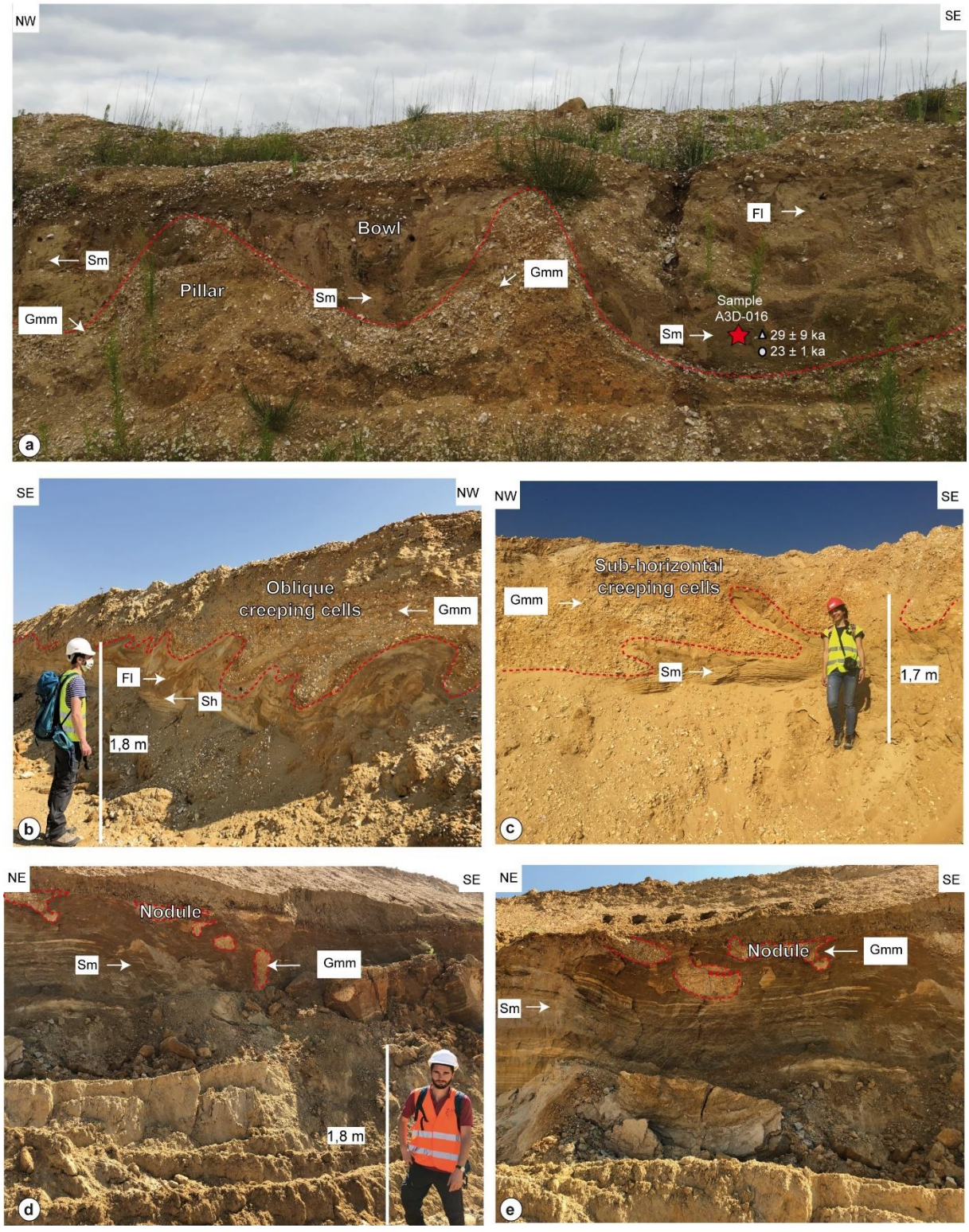

Figure 4.7. Main types of involutions observed in Manoir Brésil: bowl-shaped involutions filled with fine sand separated at regular intervals by pillars of gravel facies (a), oblique to sub-horizontal creeping cells (b and c) and pseudo-nodules of gravel into tidal sand deposits (d and e).

4.4.4 ESR/OSL methodologies

The chronological framework of the Manoir Brésil site was established by combining ESR and OSL dating methods on bleached quartz grains from the alluvial sediments (Figure 4.10). ESR samples preparation and measurements were done according to the protocol used in the National Museum of Natural History laboratory (MNHN, Paris, France) (Voinchet *et al.* 2004). Equivalent doses (*De*) were determined using the multiple aliquot additive (MAA) dose method. The annual doses (*Da*) of radionuclide activities were calculated by combing (i) gamma-ray spectrometry measured in the laboratory on the sample, (ii) *in situ* measurement of the external dose (Dγ) and (iii) an estimation of the cosmic dose emitted from the environment based on the location of the sample. The multi-centre approach (Toyoda *et al.* 2000; Tissoux *et al.* 2007; Duval and Guilarte, 2015) was used. The different paramagnetic centres of quartz do not have all the same capacity to easily reset to zero in the presence of sunlight (UV). This is called photosensitivity. The kinetics of bleaching varies from one ESR centre to another: The Al-centre is less light-sensitive to irradiation and reset than Ti-Li-centre, which is itself less light-sensitive than Ti-H. Therefore, to obtain a reliable dating of a sediment deposition, at least one of the centres must completely reset, otherwise, the age obtained can be considered as a maximum age. The simultaneous study of these three centres (multicentre method) may then provide information on the age of transport and deposition but also on the conditions of transport and potential remobilisation of sediments.

OSL samples were prepared and measured at Re.S.Artes laboratory (Bordeaux, France). All OSL measurements were done using a regular OSL reader (LexsygSmart reader) equipped with infrared (850 ± 30 nm) and blue (458 ± 30 nm) LEDs for stimulation. A Single-aliquot-regenerative-dose protocol (SAR; Murray and Wintle, 2000; Wang and Wintle, 2012) was applied for equivalent doses (De) determination. All aliquot measurements were conducted on stainless steel discs. To minimize the risk of choosing an aliquot that is not representative of the whole sample, several (12 to 15) sub-samples were processed in parallel to obtain a statistically usable result of the equivalent dose (De). The annual dose (Da) was determined using the same approach for ESR. ESR and OSL age errors were given at 1σ. The ESR and OSL curves show a signal that is not saturated (Figure *4.8* and data available in appendix E).

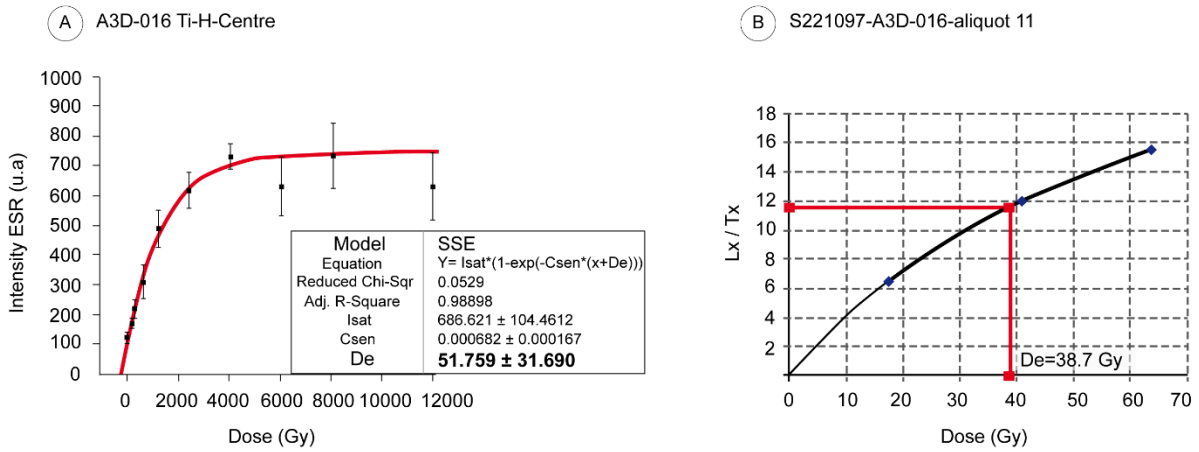

Figure 4.8. Doses curves rates. (a) ESR and (b) OSL dating methods.

4.5 Results and interpretations

4.5.1 Topography of the chalk bedrock top

Two E-W topographic profiles (i.e., transverse to the modern Seine River flow) were constructed, (i) at the scale of the meander bend (Figure 4.2-b) and (ii) at the scale of the quarry (Figure 4.3). The former indicates that the Seine River valley bottom is filled with about 20 m of late Quaternary alluvium (between ca. -15 and 5 m NGF) over a 2-3 km width across the Anneville-Ambourville meander bend (Figure 4.2). In comparison, the latter profile shows that Quaternary deposits are 5-10 m thick in the quarry and found at elevations between 2 and 16 m NGF (Figure 4.3-b).

In details, the interface between the Quaternary sediments and the chalk bedrock is not horizontal in the quarry. Instead, it exhibits two concave-up staircases suggesting distinct incision stages (Figure 4.3). One is visible at 1-2 m NGF (+12-13m RH) and is overlain by a 5 m thick sediment layer in the western part of the quarry (concave-up shape 1 on Figure 4.3). The other, in the eastern part of the quarry, is found at higher elevation (4-6 m NGF; +15-17m RH) and is overlain by a thicker sediment layer (8-10 m; concave-up shape 2 on Figure 4.3). This latter upper erosional level shows a slight depression, where the elevation reaches 3 m NGF, which is approximately 250 m wide and centered at ca. 525 m along the profile (Figure 4.3).

4.5.2 Facies associations and depositional environments

In the Manoir Brésil quarry, fourteen lithofacies were determined and were grouped into four facies associations (FA; Table 4.1).

Table 4.1. Facies classification from Miall, 2006.

Facies code	Lithofacies	Sedimentary structures	Architectural elements: genetic interpretation	Facies Association	Depositional environment
Gmm	Matrix supported, massive medium to coarse cobble sandy to clayey matrix	Not observed	**Sediment Gravity flows (SG):** plastic debris flow (high-strength, viscous) sediment gravity-flow deposits	Hd "Head"	Periglacial
Sm	Massive fine to coarse sand				
Gp	Clast supported pebble to granule coarse sand matrix	Solitary or grouped planar crossbedding in lenses of metric width	**Gravel Bars and bedforms (GB):** transverse bedforms	Fv1 "Fluvial 1"	Gravel wandering fluvial
Sp	Medium to coarse sand		**Sandy Bedforms (SB):** transverse and lingoid bedforms		
Gt	Clast supported pebble to granule coarse sand matrix	Solitary or grouped through crossbedding normal grading, scours	**GB:** minor channels fills transverse bedforms	Fv2 "Fluvial 2"	Shallow gravel-bed braided fluvial
Gp		Solitary or grouped planar crossbedding in lenses of metric width			
St	Fine to medium sand	Solitary or grouped through crossbedding	**SB:** transverse and lingoid bedforms		
Sp	Medium to coarse sand	Solitary or grouped plannar crossbedding			
St	Fine to coarse sand	Grouped through cross-beddings with paleocurrent orientation reversals (landward and seaward) and tidal bundles	**SB:** 3D dunes within alternating (tidal) currents	Td "Tide-dominated"	Median to outer estuary
Sp2	Fine to medium sand (well sorted)	Grouped planar cross-bedding within wedges of plurimetric width	**Tidal Bars (TB)**: longitudinal bedforms		
Srf	Fine to medium sand	Ripples, climbing ripples, herringbones, flaser bedding	**Sand Flat (SF):** alternating currents of varying strength planar-bed flow		
Sh	Very fine to medium sand	Horizontal lamination			
Fl	Clays, silts and fine sand	Ripples, wavy and/or flaser bedding, sometimes herringbones cross-beddings	**Mixed Flat (MF):** alternating currents of varying strength decantation, low strength flow		Inner estuary
Fm	Clay and silt	Not observed			
Fr		Vertical burrows			

4.5.2.1 Fv1 association: gravel wandering fluvial environment

Description

This facies association is up to 4 m thick and located in the eastern part of the quarry. Its base has a subhorizontal to concave upward erosive contact with the chalk bedrock (Figure 4.6-d1, d2, d3). The thicker facies consists of poorly sorted clast-supported granules to pebbles (diameter: 2 to 8 cm) within a coarse sand matrix (Gp). The crossbedding is planar and occurs as 10 m wide for 4 m thick convex up lenses, bounded by erosional (reactivation) surfaces (Figure 4.5-b). Clasts are composed of subrounded to rounded flint (Figure 4.6-d1). Lenses of ca. 1.5 m thick well-sorted medium to coarse sand with planar crossbedding (Sp) (Figure 4.6-d1, Figure 4.5) and sometimes trough crossbedding (St) are observed. These lenses are intercalated within or overlying the Gp facies (Figure 4.6-d2). Laterally, sandy facies are often progressively predominant (Figure 4.5-b). Unfortunately, no material for ESR or OSL dating (i.e., 10 cm thick layer of sorted fine-medium sand) was found within this unit.

Interpretation

This coarse grained association is interpreted as formed by high energy fluvial flow within a channel (Miall, 2006). The lenticular geometry of the planar crossbedded gravel bodies together with the sand intercalations (Sp, St ; Figure 4.5-b) is indicative of the Downstream (DA) and/or Lateral Accretion (LA) of gravel and sand within bars (e.g., Gravel Bars (GB); Miall, 2006) while reactivation surfaces reflect slight variations in bars migration direction and/or sediment supply within the channel (Allen, 1983). This association of facies and architectural elements is very consistent with a gravel wandering fluvial style (Miall, 2006).

4.5.2.2 Fv2 association: shallow gravel-bed fluvial environment

Description

This facies association was observed along a 2 m thick and 10 m wide outcrop, in the lowermost part of the quarry, to the west (Figure 4.6-a). The contact with the chalk bedrock is erosive. The deposits are composed of 3 m wide and 25 cm thick lenses of trough cross-bedded, poorly sorted granule to pebble (diameter: 2 to 8 cm) deposits within a coarse sand matrix (Gt). Planar cross-beds are sometimes observed (Gp, Figure 4.4-b). Clasts are subrounded to rounded and composed of flint, chalk and occasionally mud. Scours often affect the bases of beds (Figure

4.4-b). Upward fining is often observed and lenses of trough cross-stratified fine to medium sand (St) are intercalated within the gravel beds (Figure 4.4-b and Figure 4.6-a). In the top of the outcrop, the facies St is found alternating with pluri-centimetric units of clay, silt and fine sand showing wavy and flaser bedding (Fl).

Interpretation

The erosive basal surface in the chalk bedrock indicates channel incision. The 20 cm thick gravel bodies with trough and planar cross-bedding indicate numerous Gravel Bars (GB) associated with shallow water channels while the thin lenses of sand indicate Sandy Bedforms (SB) probably deposited during channel disconnection (at low stage) (Miall, 2006; Figure 4.4-b). The widespread lateral occurrence of GB and SB suggests a shifting network of low-sinuosity channel threads across the major river bed (Miall, 2006). This association of facies and architectural elements corresponds to shallow gravel-bed braided rivers (Miall, 2006) while mud clasts could reflect bank erosion and/or tidal influence (Li *et al*. 2017). This tidal influence would be compatible with the alternation between St and Fl facies (see next section). Nevertheless, these clasts support a local origin, i.e., short transport distance. However, due to the limited extension of the outcrop, it is difficult to interpret the depositional environment as either purely fluvial or estuarine. Indeed, without accurately defining the geometrical relationships between St / Fl and Gb / Gp facies, one cannot conclude whether these facies are contemporaneous or distant in time.

4.5.2.3 Td association: Tide-dominated environment

Description

This facies association is usually 1.5 to 4 m thick and up to 200 m wide. It is deposited either directly above the eroded chalk bedrock or above fluvial deposits (mainly Fv1 and locally on Fv2). The facies association consists mostly of heterolytic sediment showing an alternation of cm to mm-thick fine sand and clay layers (Figure 4.6-a, b, c1, c2, c3, d1, d2 and d3; Figure 4.5; Figure 4.4-a and 4.4-d). Seven facies are identified in this association. The coarser one (St) is characterized by trough crossbedding, some herringbone trough crossbedding and tidal bundles (Figure 4.6-c2, c3, d2 and Figure 4.5-a). The second facies (Srf) consists of fine to medium sand with herringbone ripple bedding and flaser bedding (Figure 4.6-b, c1, c2, d3). The third

facies (Sh) consists of horizontally bedded very fine to medium sand (Figure 4.6-b and Figure 4.5-a). The fourth sandy facies (Sp2) consist of wedges of decametric width and plurimetric thickness of well-sorted fine to medium sand with planar crossbedding (Figure 4.6-d and Figure 4.5-b). This latter sandy facies alternates with laminated to massive (0.005 to 0.5 m thick) clayey facies (Fl and Fm) where vertical bioturbation features are often observed (Fr; Figure 4.6 and Figure 4.5). These fine facies form locally lenses within Srf facies units and often show wavy bedding (Figure 4.6-d3).

Interpretation

The alternation between sand and clay, typical of this association, corresponds to changes in hydrodynamics conditions. Together with the abundant herringbones structures that indicate bidirectional flow, these deposits are typical of a tide-dominated deposits (Miall 2006; Van den Berg *et al.* 2007, Souza *et al*. 2023). Wavy and horizontal sand bedding with clay intercalations originates during alternating intervals of fast-moving flow and slack water (Martin 2000). The ripples formed during strong flow of the dominating current, while the clay layers correspond to the periods of slack water where the flow velocity decreases and allows the deposition of suspended particles (Mellere and Steel 1995; Martin 2000). Mud drapes and flaser bedding reflect the high-suspended mud concentration. We interpreted the association of facies Ft, Fm and Fr as deposited under hydrodynamic conditions providing sufficient protection against wave action, in a Mixed Flat deposition located within an inner estuary environment (MF) (Jamet 2014; Morales 2022). Sandy deposits with ripples and herringbone structures likely correspond to Sand Flat deposition (SF) (Morales 2022) in median to outer estuary environments while decametric-wide sand wedges are interpreted as Tidal Bars (TB).

4.5.2.4 Hd association: Head deposits, periglacial environment

Description

Located in the uppermost parts of the outcrops, this facies association is 1 to 7 m thick and several hundreds of meters wide. It either overlies or truncates facies Fv1, Fv2 and Td (Figure 4.5). It is mainly characterized by massive, matrix-supported, poorly-sorted medium to coarse cobble flint clasts (diameter: 1 to 8 cm) with a sandy to clayey matrix (Gmm; Figure 4.4-b-c, Figure 4.5 and Figure 4.6). Locally, massive fine to coarse sand (Sm) forms lenses of 0.5 to 1

m thick and 1 to 2 m width intercalated within the cobble facies Gmm (Figure 4.5-a and Figure 4.6-c1, d2).

Interpretation

This facies association is interpreted as being formed dominantly by debris flows (Van Steijn et al., 1995). Clasts and matrix derived from frost shattering of the Upper Cretaceous chalk and from the erosion of the weathering mantle (Clay-with-Flints Formation) that outcrop upslope (Laignel, 1997; Quesnel, 1997). This facies association overlies unconformably the other facies associations everywhere. Deformation features related to periglacial processes are widespread (cf. 4.3). This facies association is interpreted as periglacial slope deposits, usually called "heads" in Northern France where they are widespread (Mercier, 2008; Jamet, 2014).

4.5.2.5 Post-depositional deformation

The sediment units along the Manoir Brésil quarry were affected by post-depositional deformation features symptomatic of periglacial involutions. Three types were identified (Figure 4.7). The first type was mostly observed to the east of the quarry in the upper level, i.e., overlying the upper head deposits. It consists of large bowl-shaped involutions filled with fine sand separated at regular intervals by gravel pillars (Figure 4.7-a). The heigh of the bowls is about 2 m, with a width ranging from 1 m to ca. 1.5 m. The fine sand filling an involution (A3D-016) was sampled for ESR-OSL dating (Figure 4.7-a). The second type of involutions consisted of cells that were deformed by downslope soil creep. They affect head deposits and the upper parts of tide-dominated deposits (Figure 4.7-b and 4.7-c).

The size of these involutions is variable and follow the slope towards the current Seine River (Figure 4.7-b and 4.7-c). The last type are pseudo-nodules.

These pseudo-nodules are irregular and are made up of gravel material (Gmm) sinking in tide-dominated sand deposits (Figure 4.7-d and 4.7-e).

4.5.3 Distribution of the Facies associations in Manoir Brésil

The distribution of facies associations over the whole outcrop was synthetized (Figure 4.10). Overall, about 50% of the deposits are composed of colluvial (head) deposits (Figure 4.4, Figure 4.5 and Figure 4.10). Of the remaining deposits, more than half is composed of tide-dominated deposits.

Shallow gravel braided fluvial deposits (Fv2) are only observed along the lower, western part of the quarry (Figure 4.6-a; Figure 4.10), where sample A3D-010 was taken. Additionally, wandering fluvial deposits (Fv1) are found in the upper, eastern part of the quarry (Figure 4.6-d1, d2, d3). At least two Fv1 units could be identified: one in the middle of the topographic depression and another along the easternmost edge of the quarry (Figure 4.10).

The eastern part of the quarry is covered by tide-dominated deposits (Td), which progressively overlap the Fv1 units. Tide-dominated deposits are characterized by rapid lateral variations between the St, Srf, Sh, Sp2, Fl, Fm and Fr facies (Figure 4.6-b, c1, c2, c3, d1, d2 and d3). They are overlain by head deposits (Hd). Several periods of head deposit activity are suggested by the sedimentary succession. First, lenses of either coarse or fine-medium sand layers are identified within the head deposits in several sedimentary logs in the eastern part of the quarry (Figure 4.6-c1, c2 and d2). Second, interdigitations of head deposits and tide-dominated deposits (10 cm-thick Sh / 5 cm-thick Fl alternations) are locally observed (7.2 to 7.8 m NGF in Figure 4.4-c and Figure 4.6-c2). Sample A3D-015 was taken in a sand level of these tide-dominated deposits (Figure 4.6-c2). In the western part of the quarry, the head deposits (Hd) have an erosional lower boundary and overlain both the fluvial (Fv2) or tide-dominated deposits (Td).

4.5.4 ESR and OSL ages

The results of ESR and OSL dating are displayed in Table 4.2 and *Figure 4.9*. They are discussed chronologically from the oldest to youngest. Tide-dominated facies (Td) are represented by samples A3D-011 and A3D-015, shallow gravel-bed river deposits (Fv2) by sample A3D-010 and periglacial deposit (Hd) by sample A3D-016. Samples ages were determined as the ratio of equivalent dose *De* which is expressed in Gy to the annual dose *Da*, expressed in µGy/a (Table 4.2).

Da was determined for all samples tacking into account the contents of radioactive elements such as U, Th and daughters and K. This measured were the same for ESR and OSL dating. *Da* is 666 ± 13, 845 ± 9 and 1047 ± 15 µGy/a for samples A3D-011, A3D-015 and A3D-010, respectively. Sample A3D-016 (facies Hd) has a higher *Da* (1752 ± 25 µGy/a), which may reflect mineralogical variability of fine sediments mixing with clay and silts richer in radioelements (Table 4.2).

Equivalents doses (*De*) calculated from ESR Al, Ti-Li, Ti-H and from OSL were compared, according to the multi-centre approach. The *De* calculated using Ti-H center and by OSL are

systematically in agreement. We thus consider these data as reliable and indicating a good pre-depositional reset of these Ti-H and OSL centres. Surprisingly, for A3D-011(tide-dominated facies) the low bleachable Al-centre

provided *De* in agreement with those of the Ti-H-centre and OSL, which is not the case for the apparently overestimated Ti-Li equivalent dose. On the contrary, for A3D-015 (tide-dominated facies) the three ESR centres are in agreement and could be correlated with OSL results. It is thus clear that the sediments were remobilized and exposed to light long enough for these low-sensitivity centres to be fully reset before sediment burial. Finally, the *De* obtained for samples A3D-010 and A3D-016 using the Al and Ti-Li ESR centres, which were higher than those obtained by the Ti-H ESR centers and OSL, were not considered for the age calculation. This indicates a partial bleaching of these centers (Al and Ti-Li centres) and therefore an overestimation of these *De*.

In tide-dominated deposits, A3D-011 ages obtained using the Al and Ti-H centres and OSL are respectively of 258 ± 69 ka, 273 ± 44 ka and 242 ± 7 ka suggesting a deposition during MIS 7e. A3D-015 ages were obtained using Al, Ti-Li and Ti-H ESR centres and OSL and were respectively 214 ± 31 ka, 199 ± 19 ka, 205 ± 13 ka and 192 ± 5 ka, which corresponds to MIS 7a. The ages of the gravel-bed river sample A3D-010 were determined using Ti-H centre and OSL and gave respectively 187 ± 14 ka and 184 ± 4 ka, which corresponds to MIS 6e. Finally, the ages of sample A3D-016 determined using Ti-H centre and OSL range from 29 ± 9 ka to 23 ± 1 ka, which point to a MIS 2 age for the periglacial deformation. The age model used in this study places the tide-dominated deposits (Td) within the MIS 7 (interglacial) and the shallow gravel-bed braided fluvial deposits in the early MIS 6 (glacial). An important hiatus separates these deposits from the sampled cryoturbation phase (MIS 2) (Figure 4.9).

Table 4.2. Synthesis of OSL / ESR data

Sample	Depositional environment	Depth (m)	Annual dose D_a (µGy/a)	ESR/OSL	Equivalent dose De (Gy)	Age (ka)
A3D-010	Gravel wandering fluvial	2,75	1047 ± 15	Al	341 ± 27	326 ± 26
A3D-010				Ti-Li	378 ± 26	361 ± 25
A3D-010				Ti-H	196 ± 14	**187 ± 14**
A3D-010				OSL	192,2 ± 3	**184 ± 4**
A3D-011	Estuarine	3	666 ± 13	Al	172 ± 46	**258 ± 69**
A3D-011				Ti-Li	517 ± 193	776 ± 290
A3D-011				Ti-H	182 ± 29	**273 ± 44**
A3D-011				OSL	161,1 ± 3,4	**242 ± 7**
A3D-015	Estuarine	3,5	845 ± 9	Al	181 ± 26	**214 ± 31**
A3D-015				Ti-Li	168 ± 16	**199 ± 19**
A3D-015				Ti-H	173 ± 11	**205 ± 13**
A3D-015				OSL	161,9 ± 3	**192 ± 5**
A3D-016	Periglacial	2	1752 ± 25	Al	135 ± 121	77 ± 7
A3D-016				Ti-Li	78 ± 5	45 ± 3
A3D-016				Ti-H	51 ± 16	**29 ± 9**
A3D-016				OSL	40,4 ± 0,9	**23 ± 1**
12% of water content						

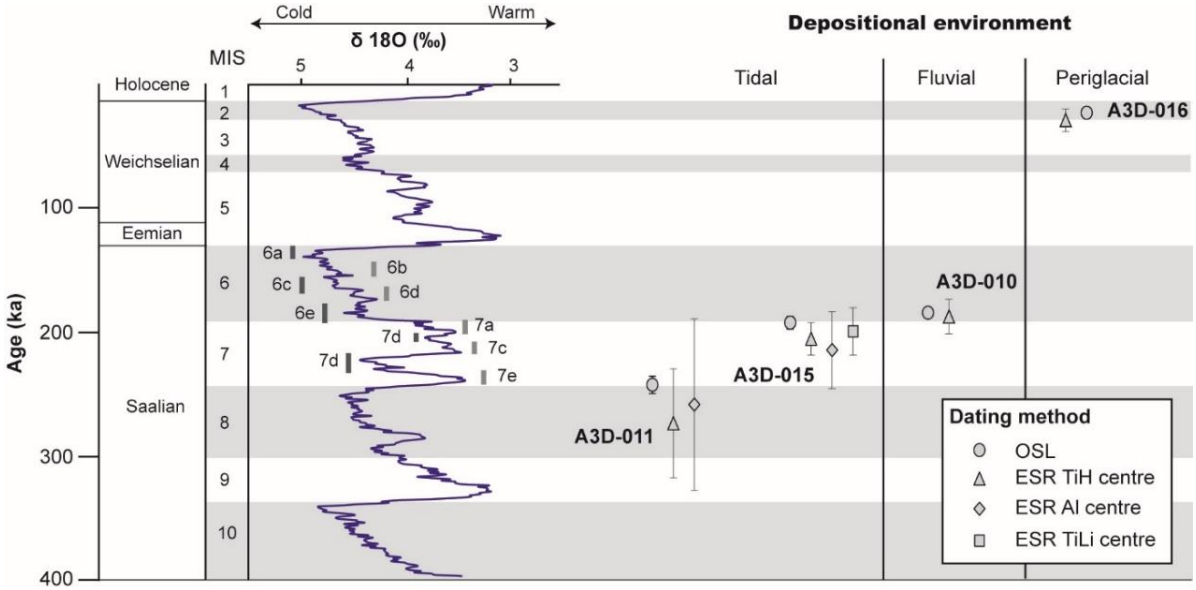

Figure 4.9. Geochronology of the Manoir Brésil quarry deposits. Stacked $\delta^{18}O$ records of benthic foraminifera is from Lisiecki and Raymo (2005).

4.6 Discussion

The analysis of geomorphological, sedimentological, and geochronological data from the Manoir Brésil quarry provides new insights on rates of river incision and bedrock uplift along the Lower Seine River valley since MIS 8.

4.6.1 A genetic model for Manoir Brésil

The synthesis of the sedimentary interpretations together with the topographic and geochronological data allowed building a geometric model of architectural elements separated by three main unconformities (Figure 4.10). The oldest dated deposits correspond to the lower tide-dominated deposits (Td) that lie upon the undated gravel wandering fluvial deposits (Fv1). ESR-OSL dating provided ages of 258 ± 69 ka, 273 ± 44 ka and 242 ± 7 ka (i.e., MIS 7e) for these tide-dominated deposits. It is however not clear whether the underlying gravel wandering fluvial deposits belong to MIS 7e and correspond to wandering channels in a tide-dominated environment, or if they correspond to remnants of fluvial deposits from MIS 8 that were later buried under the tide-dominated deposits (as proposed in Tourville-la-Rivière; Lautridou, 1985; Jamet, 2014). The contact between the underlying chalk bedrock and the fluvial/tide-dominated sediments may nevertheless be interpreted as the MIS 8 erosional surface (Figure 4.10).

ESR-OSL dating of a thin tide-dominated sequence interdigitated within two head deposits of ca. 2 m-thick (lower level) and 5-m tick (upper level) head deposits (Figure 4.4-c and Figure 4.6-c2) returned 214 ± 31 ka, 199 ± 19 ka, 205 ± 13 ka and 192 ± 5 ka, which corresponds to MIS 7a-c. The lower head deposit (i.e., intercalated between MIS 7e and MIS 7a tide-dominated units; Figure 4.6-c2) may be interpreted as reflecting MIS 7d or 7b, which are substages of climatic cooling during the interglacial MIS 7. To the east, the lateral continuity of the MIS 7d-b head deposits (Figure 4.6-c2) may have the form of an erosional surface within the tide-dominated deposits (Figure 4.10). The remaining upper head deposits that cover indistinctively the fluvial, tide-dominated and lower head deposits may be interpreted as MIS 6 or younger (up to MIS 2; Figure 4.10).

The fluvial deposits found in the lower level of the Manoir Brésil quarry (Fv2) yielded ESR-OSL ages of 187 ± 14 ka and 184 ± 4 ka, which correspond to MIS 6e. Thus, they were deposited at the onset of a sea level drop early at the beginning of a glacial period. This stage was followed by a phase of relative climatic melioration (MIS 6d) and then sea level dropped again, which likely enhanced river incision (MIS 6c to 6a). Consequently, the associated late

MIS 6 fluvial deposits could exist in the valley bottom below the Holocene deposits as suggested in the Lower Seine (Porcher, 1981; Gacquerel, 1984; Lautridou et al. 1999).

To summarize, deposition of fluvial sediments probably began after an incision stage during MIS 8. During MIS 7e, sea level rise was associated with the deposition of tide-dominated deposits (Td). Deteriorating climatic conditions during MIS 7d or 7b are inferred from the presence of head deposits (Hd) intercalated between two tide-dominated deposits. The overlying tide-dominated deposits (Td) were deposited during MIS 7a. A new phase of incision occurred at the beginning of MIS 6. It is suggested by the fact that the corresponding erosional surface is sealed during MIS 6e by wandering / braided deposits that are locally overlain by tide-dominated deposits. Currently, it is not clear whether these tide-dominated deposits belong to early MIS 6 (i.e., before the major MIS 6 river incision) or to the Eemian (MIS 5e), i.e., when the sea level rose again sufficiently to inundate the lower part of the quarry area (Figure 4.10). In any case, the Seine River incised during MIS 6c to 6a and disconnected the MIS 6e deposits of the Manoir Brésil terrace from the valley bottom.

In the quarry, the two observed topographic steps can thus be divided into two strath terraces. The upper strath (+15-17m RH) corresponds to the MIS 8 incision phase, and we interpret the depression within this strath as the erosional base of a paleo-Seine River channel. The lower strath (+12-13m RH) is interpreted as an early MIS 6 incision. Similar stepped geometries with erosional channel bases were observed by Lécolle (1989) along the Middle Seine between Paris and Les Andelys. Thus, as suggested by geological map and earlier work, Manoir Brésil, may thus be considered as a terrace system and not a single terrasse. However, (i) the lower strath may doubtfully be considered at the maximum incision of MIS 6 -which occurred near 140 ka- and (ii) the mapping of the limit between Fy_c and Fy_d terraces from the geological maps does not match the identified limits in this study (i.e., comparing Figure 4.3-a and Figure 4.3-b). Indeed, the limit between Fy_c and Fy_d is based on the topography of the top of the terrace deposits, which we showed to be strongly influenced by periglacial involutions and colluvial activity, while we used the top of the bedrock. The upper strath at Manoir Brésil is therefore consistent with the T2 terrace (Tourville-la-Rivière formation) found at +17-18 m RH (Antoine et al. 2007; Jamet 2014). Finally, the tidal-fluvial chronology in Manoir Brésil is consistent with the temporal framework of fluvial and karst deposits studied in the nearby in the Caumont cave system (Ballesteros et al. 2023) located a 7 km upstream (Figure 4.2). The tide-dominated sequence (MIS 7a) at Manoir Brésil is coeval to speleothem and slackwater deposits within the caves, while fluvial deposition and karst incision occurred in Caumont caves during MIS 6.

This MIS 6 incision event is also considered as a major event in the English Channel (Mellet et al. 2013).

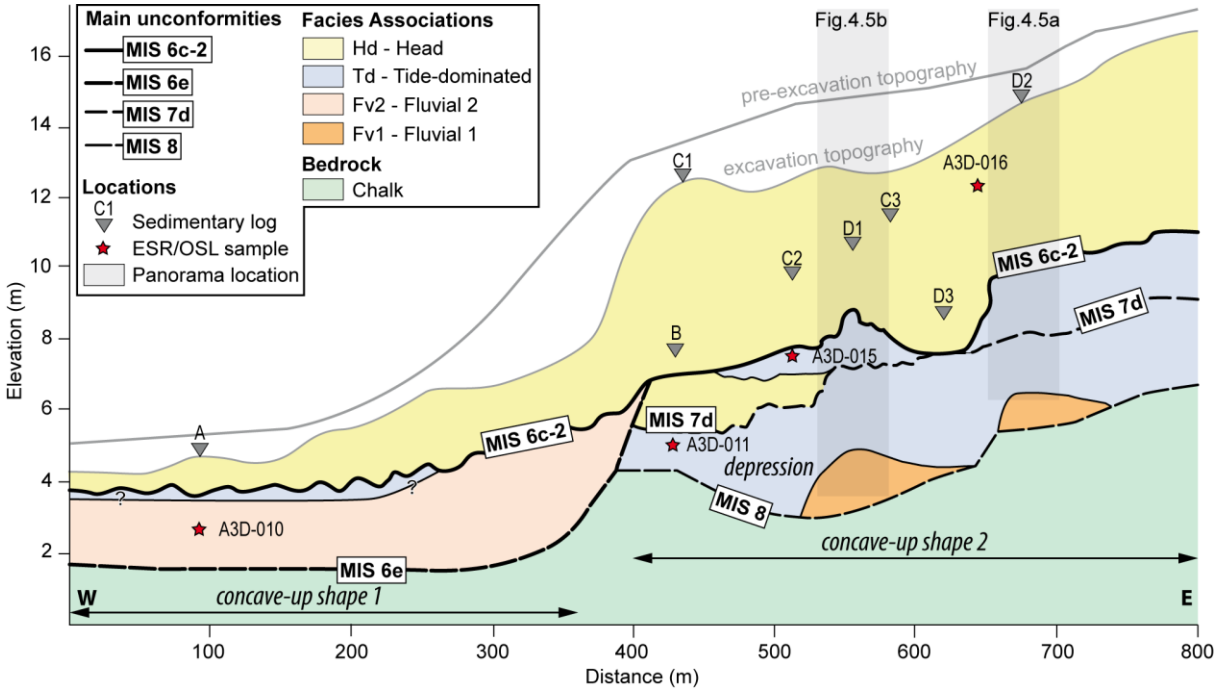

Figure 4.10. Geometric model of Manoir Brésil, illustrating the relationships between the major erosion/deposition events, particularly the major unconformities. See discussion for details.

4.6.2 Record of the MIS 7

Results from the Manoir Brésil terrace analysis have thus allowed identifying a new sequence from the MIS 7 period, which can be correlated with other sites of the Paris basin. Contemporaneous MIS 7 interglacial sediments are found along the Thames River (Figure 4.1-a) and the Solent River, in England and are preserved at several localities, allowing reconstituting the paleogeography of the English Channel during MIS 7 (Bates *et al.* 2003). They can be separated into fluvial deposit (in the upper River Thames, near Cerney Wick (Lewis *et al.* 2006; Hogue *et al.* 2023), at Latten, Wiltshire, close to the Churn-Thames confluence (Lewis *et al.* 2006), at Stanton Harcourt, Ilford, Aveley (Bridgland 1994; Lewis *et al.* 2004) and marine (e.g., tidal, estuary, beach) deposits (in Pennington Marshes (Allen *et al.* 1996), Stanswood Bay, (Briant *et al.* 2006), Norton Farm and Westhampnett (Bates *et al.* 2003). In the Lower Seine River valley, the most investigated estuarine deposits are those of Tourville-la-Rivière near Rouen, 60 km upstream of Manoir Brésil. There, the chalk bedrock at 0 m NGF

is overlain by 2 sequences of interglacial estuarine deposits (MIS 9 and MIS 7) with an intercalation of wandering fluvial deposits from the MIS 8 (Stremme 1985; Balescu *et al.* 1997; Bahain *et al.* 2019; Figure 10). The elevations of the two interglacial deposits are respectively 3-5 m NGF (MIS 9) and 10-13 m NGF (MIS 7) (Lautridou 1982; Bates *et al.* 2003; Cordy *et al.* 2003; Lautridou *et al.* 2003; Jamet 2014)(Figure 4.11). In the Lower Seine valley, at Tancarville near Le Havre, the chalk bedrock at 4 m NGF is overlain by periglacial and fluvial gravels, head deposits and sands (Lautridou 1982; Lefèbvre *et al.* 1994; Bates *et al.* 2003; Cordy *et al.* 2003)(Figure 4.11). The microfauna and malacofauna found in sands suggest an estuarine origin from the MIS 7 (Cordy *et al.* 2003), although no geochronological data are available.

The sequence of Manoir Brésil is therefore very consistent with that of Tancarville and Tourville-la-Rivière. A novelty in Manoir Brésil is the identification of head deposits within an otherwise tide-dominated sequence (Figure 4.10). The ESR dating of bounding tide-dominated deposits suggests these head deposits correspond to either MIS 7d or 7b. The 7d event is favoured here, as it is among the fastest glaciation event known during the Pleistocene when the sea level is thought to have dropped down to -60 m, providing the most favourable conditions for such head deposition (Pillans *et al.* 1998; Zazo 1999; Desprat *et al.* 2007; Choudhury *et al.* 2020). This sea level drop would have participated to river incision and above all destabilization of the interfluve, leading to head deposition in Manoir Brésil during the MIS 7d glacial substage. Ultimately, the OSL/ESR results provide a good resolution for interglacial climatic dynamics, complementing studies based on tufa and paleosols (e.g., Antoine *et al.* 2000, 2007; Coutard *et al.* 2018).

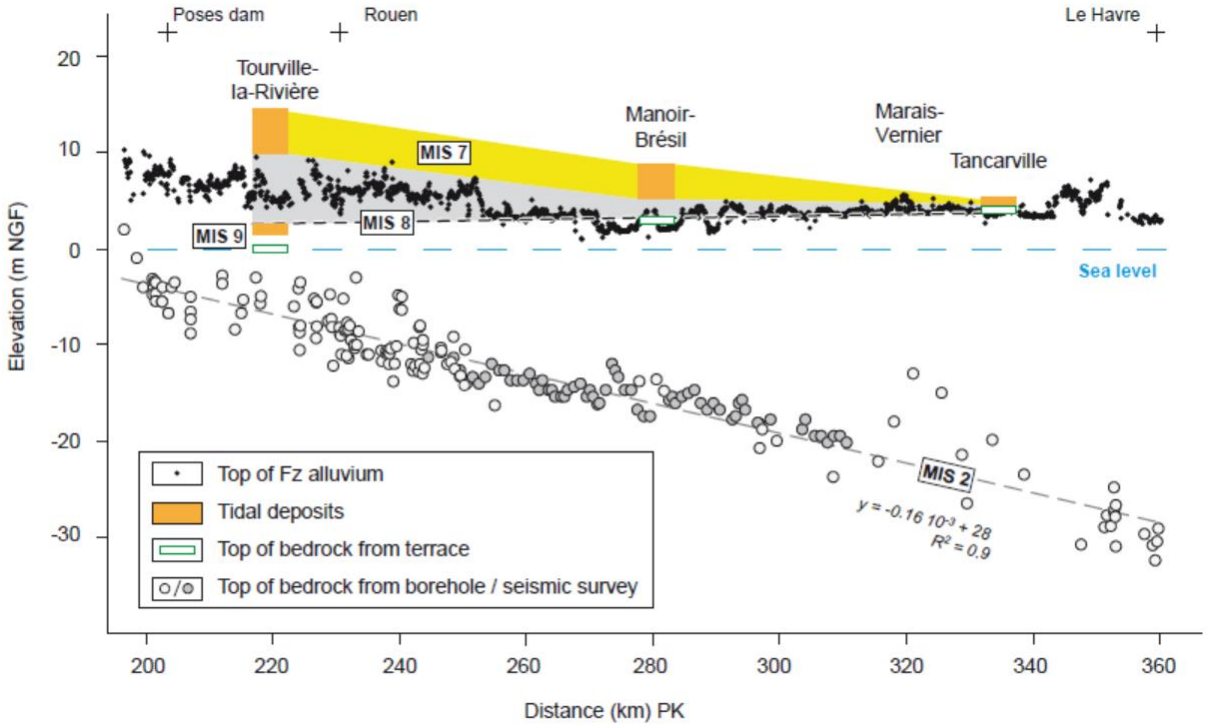

Figure 4.11. Profile along the Lower Seine comparing the record of Manoir Brésil with that of Tourville-la-Rivière and Tancarville. The interface between the valley bottom alluvium and the bedrock -thought to result from the last glacial maximum incision- is based on a compilation of borehole and seismic data.

4.6.3 Vertical bedrock movements along the Lower Seine River

Bedrock uplift and denudation rates (sensus England and Molnar 1990) since MIS 7 can be estimated in Manoir Brésil. MIS 7 tide-dominated deposits are found at elevations up to 5-8 m NGF in the site (Figure 4.10). Based on reconstructions, which estimate that the global sea level did not rise more than 0 m NGF during MIS 7 (Waelbroek *et al*. 2002; Bintanja *et al*. 2005; Spratt *et al*. 2016; Choudhury *et al.* 2020), a first estimation of bedrock uplift since 200 ka can be estimated. Assuming tidal deposition at sea level, which is a maximum, returns a minimum uplift rate of 25-40 m/Ma since MIS 7 (i.e., 2.5-4 cm/ka). It is close to the incision rates of 50-60 m/Ma inferred from the geomorphic record of the Paris basin (Middle Somme and Yonne River) (see Antoine *et al*. 2007 and references therein). Such rates are high for non-orogenic settings. For instance, they are an order of magnitude higher than the cratonic background estimated in West Africa (5-10 m/Ma; Grimaud *et al*. 2018). This difference is likely explained by higher bedrock uplift, which could be related to far field alpine compression (Guillocheau *et al.* 2000; Bourgeois *et al*. 2007) and/or glacial-eustatic flexure (Bradley *et al.* 2009). In

comparison, the elevation difference between the maximum incision associated with the MIS 8 erosional surface in Manoir Brésil and the valley bottom (i.e., assuming that it corresponds to the Last Glacial Maximum (MIS 2)) is ca. 25 m (Figure 4.2), providing an erosion rate estimated at 125 m/Ma. The comparison between this erosion rate and the bedrock uplift rates, shows that the erosion during glacial periods was at least twice greater than known rates of bedrock uplift. Ultimately, these results suggests (i) that modest bedrock uplift rates in non-orogenic area can be a limiting factor for erosion despite favourable eustatic and climatic conditions during glacial periods and/or (ii) that high rates of incision do not propagate too far upstream in non-orogenic drainages.

The Tourville, Tancarville and Manoir Brésil, terraces can be used to discuss rock uplift patterns along the Lower Seine River since MIS 8 (Figure 4.11). The MIS 8 erosional surface is found at 3-4 m NGF at Tourville upstream, 4-5 m NGF at Manoir Brésil and at ca. 5 m in Tancarville downstream. Joining these elevations together suggests a null to inverse slope (i.e., tilted towards the land) for the longitudinal profile of the MIS 8 maximum incision. In comparison, the slope of the MIS 2 valley bottom is 0.16 ‰ towards the sea, as suggested by a rough interpolation between the borehole and seismic data (Figure 4.11). The striking difference between the geometry of MIS 8 and MIS 2 longitudinal profiles suggests post- MIS 8 deformation. The surface of the top of MIS 7 deposits between Tourville, Manoir Brésil and Tancarville has a similar slope to the top of the modern alluvium (Fz on BRGM geological maps (Janjou, 2004; Quesnel *et al*. 2008)). Therefore, we interpret these geometries as the deformation of the MIS 8 profile (before the end of MIS 7) driven by the isostatic adjustments related to glacial (un)loading of the British-Irish ice cap (Bradley *et al.* 2009; Kuchar *et al.* 2012).

The pattern -although subtle- would suggest uplift occurring to the North, which is also suggested using MIS 5e deposit elevations (Cohen *et al.* 2022). Along the coast of Normandy a MIS 7 shore platform is found at ca. 5 m NGF at Ecalgrain while the Brighton raised beach is at about 8-12m NGF (Lautridou 1985; Pellerin *et al.* 1987; Cliquet *et al.* 2009; Bates *et al.* 2010; Pedoja *et al.* 2018). In the future, further mapping of MIS 7 and MIS 8 remnants would be another promising way to characterize Late Quaternary regional deformation in NW Europe.

In addition to this general pattern, the valley bottom topography shows local variations in elevation, which is in the order of 5 m and can reach up to 12 m (Figure 4.11). The maximum variation is observed in the Marais Vernier, near Tancarville, where an oxbow geometry related

to a channel cut-off has been described (Lefebvre *et al.* 1974; Sebag 2002; Frouin *et al.* 2010). These geometries highlight the complexity of correlating terraces based on elevation, even more so if we assume a slope for the alluvium deposited during glacial isotopic stages similar to that of the maximum incision observed at the bottom of the valley. This further supports the use of geochronology to validate correlations between terraces.

4.6.4 Slope dynamics and periglacial deformation

The important thickness of head deposits covering the other deposits likely reflect conditions favourable to the formation of a great amount of debris through the gelifraction of the chalk, a sparse vegetation and the impermeabilization of soils. These slope deposits and the underlying fluvial and tide-dominated sediments have been strongly deformed by periglacial involutions over a thickness of ca. 2 m. The distribution of the main types of involutions are variable. The bowl-shaped involutions affecting sand and gravel are located in the upslope part of the quarry and are similarly to those described at Le Crotoy in the Somme valley (Bertran *et al.* 2017). These involutions are probably linked with the soil stripes visible near the Manoir Brésil quarry (database published in Andrieux *et al.* 2016; Bertran *et al.* 2016, 2017). Large soil stripes are features widely reported in current periglacial environments (e.g., French, 2007). They developed in a layer subjected to freezing and thawing cycles over permafrost (the active layer) due to differential frost heave and/or periglacial load casting. The sand filling the bowls was dated to 29 ± 9 ka and 23 ± 1 ka by Ti-H-centre and OSL, indicating that the involution developed most probably during MIS 2 and likely correspond to a recent permafrost phase, in a context of climatic melioration.

In contrast, the involutions affecting the MIS 7 tide-dominated deposits are located in the lower part of the quarry with a gentle slope towards the Seine River. These involutions are smaller and stretched along the slope. Their formation may have involved periglacial load casting and/or liquefaction and fluidisation processes in connection with excess of pore-water pressure generated during freezing of the sand layer above permafrost (Bertran *et al.* 2018). The age of deformation is poorly constrained at this place. The involutions are younger than MIS 7 and probably developed synchronously with the bowl-shaped involutions visible upslope. Thus, they would correspond to MIS 6 or more likely MIS 2.

4.7 Conclusion

A multidisciplinary approach combining geomorphology, sedimentology, geophysical data and geochronology (ESR and OSL) made it possible to better characterize the geometry and age of Manoir Brésil, a terrace system recording Late Quaternary surface dynamics in the Lower Seine River. Fluvial incision probably during MIS 8 was recorded by an erosional surface cut into the chalk bedrock. It is covered by MIS 7 tide-dominated deposits and head deposits with some interdigitation between both deposits. Manoir Brésil can be considered as a temporal equivalent to the well-studied, upstream site of Tourville-la-Rivière. The deposits are affected by post-MIS 7 involutions typical of cryoturbation processes. The uppermost deformed sediments were dated to 23-28 ka, which suggests that a major phase of cryoturbation occurred during MIS 2, although some of the involution may date back to MIS 6. Based on the local elevation of tide-dominated deposits and erosional surfaces, a bedrock uplift of 25-40 m /Ma and an erosion rate of 125 m/Ma during glacial periods can be proposed. Uplift of the MIS 8 erosional surface increases towards the North, which makes it difficult to correlate terrace deposits without precise chronological data. Such regional tilt -likely due to glacio-isostatic flexure- is consistent with the elevation data of MIS 5e and MIS 7 marine deposits around the English Channel.

Chapter 5: Valley bottom alluvium of the Seine catchment: database construction

Ce chapitre est focalisé sur la construction d'une base de données des sondages présents dans les fonds des vallées du Bassin versant de la Seine, à l'interface entre le substrat lithologique et les alluvions. Cette base de données sera utilisée par la suite pour appliquer la méthode du krigeage directionnel dans le chapitre 7.

Chapter 5

5 Valley bottom alluvium of the Seine catchment: database construction

This chapter provides a detailed description of the database that was developed to reconstruct the large-scale geometries of the valley bottom and alluvial infill along the main valleys of the Seine River catchment. The database was compiled on a GIS software, ArcGIS 10.6 (© ESRI). The acquire database will be used in the following chapters 6 and 7 for the geomorphic analyses and directional kriging, respectively.

5.1 Construction of the limits of the valley bottom

To delimit the boundaries of the valley bottom, the French 1:50 000 scale geological maps digitized and harmonized for each department and 75-m resolution of DEM were used. The youngest terraces along the valleys were merged to constitute a unique polygon of the valley bottom. Because of harmonization issues between the different maps available, we had to be careful when selecting the terraces. Terraces with elevations more than 10 m above the river were excluded from the valley bottom polygon. In the Seine, Marne, Yonne, Loing and Eure valleys, we combined the Fz and Fy terraces only, while in the Oise valley, some Fx terraces have an elevation comprises between 8 and 10 m, so there were also included. Finally, the valley bottom polygon for the Seine catchment was manually refined on ArcGIS, for terraces that are partly 10 m above and partly 10 m below the river elevation (Figure 5.1-a-b).

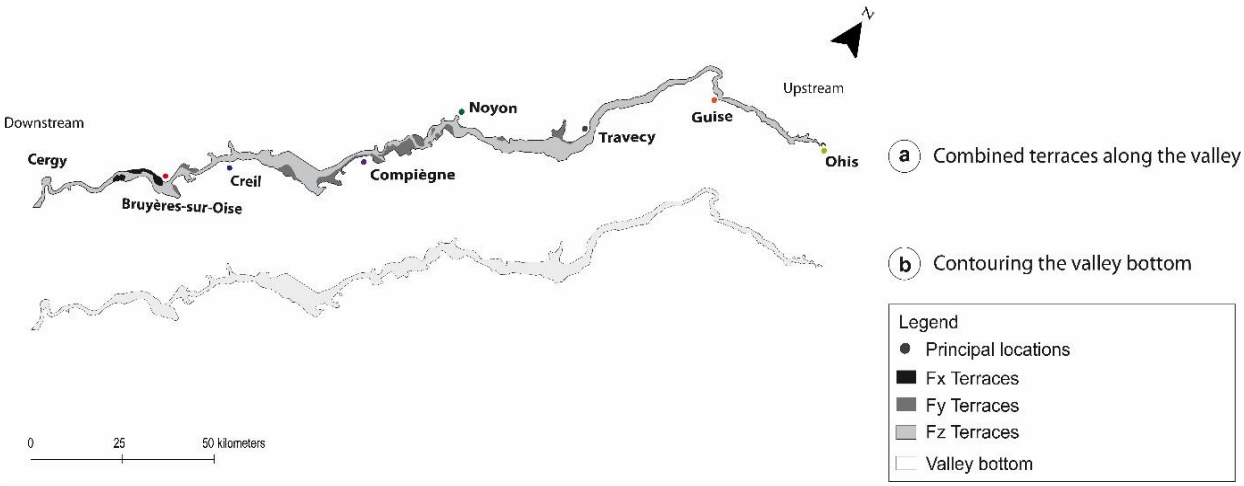

Figure 5.1. Valley bottom delimitation, example of Oise valley.

Chapter 5

5.2 Borehole database construction

5.2.1 Boreholes from the Banque du Sous-Sols of BRGM

A database consisting of thousands of boreholes that intersect the alluvium mapped on the French 1:50 000 scale geological maps was created, using data from the "Banque du Sous-Sols" of BRGM (BSS). The BSS contains information on the geological substrate covering the whole territory of France (

Figure 5.**2.**). Most of the data come from boreholes drilling, core samples, wells and springs and are disponible in a database archiving open access via Infoterre (https://infoterre.brgm.fr/). A total of 4 692 boreholes intersecting the alluvium were identified using the BSS.

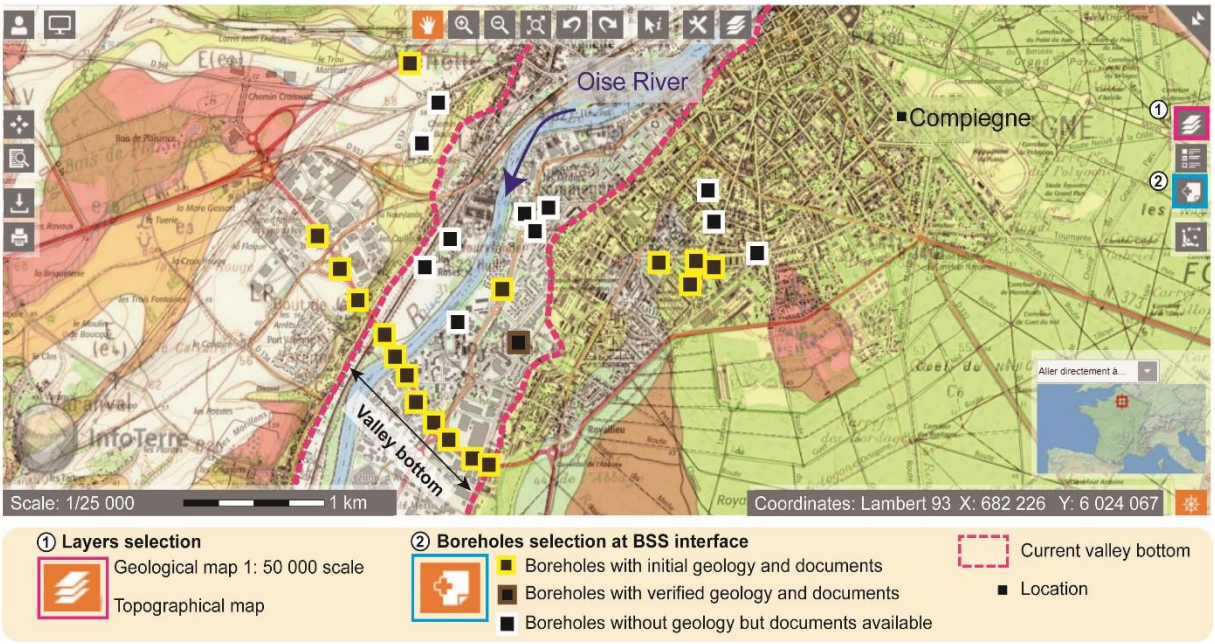

Figure 5.2. The Infoterre display interface from the "Banque du Sous-Sols" of BRGM with an example of the Oise valley, where some boreholes are located either outside or inside of the valley bottom. Specifically, only the boreholes in the valley bottom were used. Modified after https://infoterre.brgm.fr/.

In a first step, identification of all georeferenced boreholes located inside the harmonized polygon delimitating the valley bottom (see section 5.1) and according to the geological map at 1:50 000 scale were selected. Because of the variability in the borehole's descriptions, their content was manually checked for consistency. An illustrative example of a borehole record is shown in Figure 5.3, in which are represent the total alluvial thickness, each alluvial lithology description, the geological stage and the bedrock-alluvium interface. Boreholes without information and data showing inconsistencies were not considered for the final database.

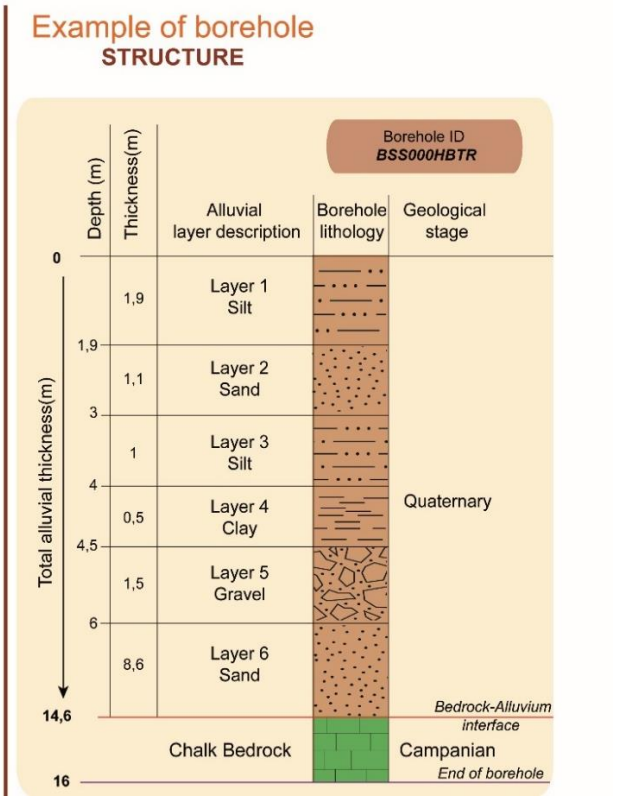

Figure 5.3. Example of alluvial description borehole from BSS, where the total alluvial thickness, depth of each alluvial layer as well as their lithology and the bedrock lithology were obtained for each borehole. The current borehole characterization was applied along the Seine catchment. Modified after https://infoterre.brgm.fr/.

The database is structured using different attributes. For identification, borehole ID (considering the new identifier code BSS000-ID), elevation, x and y coordinates determined using the RGF Lambert 1993 projection, and valley location were used (Figure 5.3 and Figure 5.4-a).

Boreholes data characterization is divided into (i) a description of the alluvium (total alluvial thickness, alluvial layers description, depth and thickness of each individual alluvial layer), (ii) maximum elevation at the bedrock-alluvium interface, and finally (iii) bedrock characteristics (lithology, geological formation and age) (Figure 5.4-b).

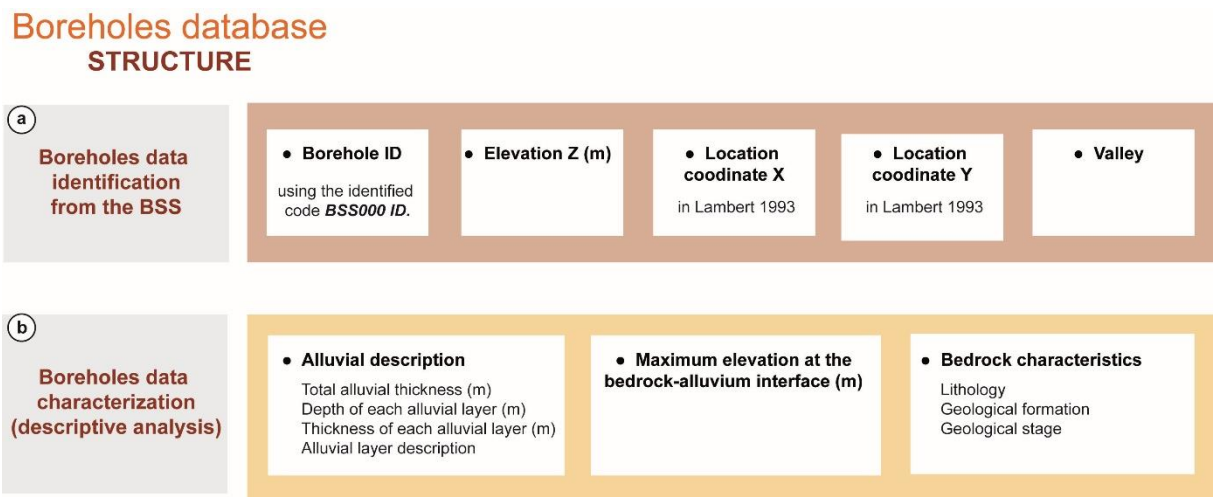

Figure 5.4. Boreholes database structure is based on two main aspects: (a) boreholes identification (borehole ID, elevation coordinates and valley name) and (b) boreholes characterization (alluvial description, maximum elevation at the bedrock alluvium interface and bedrock characteristics).

Alluvial thickness is defined as the difference between the borehole top elevation and the bedrock interface elevation within the borehole. This information is used to determine the minimum (min) and maximum (max) known elevations of the alluvium-bedrock interface. Four distinct cases have been identified: 1) an alluvial interface of known depth where alluvium are in contact with the bedrock; 2) an alluvial interface located within a part of the borehole where information is missing, 3) an alluvial interface located below the borehole end elevation and 4) an alluvial interface within a part of the borehole where information is missing, upon a first non-alluvial formation identified depth (Figure 5.5). Most of the time (92 %), the minimum and maximum elevations of the alluvium-bedrock substrate are similar. They can be used to apply the kriging method (see Chapter 7).

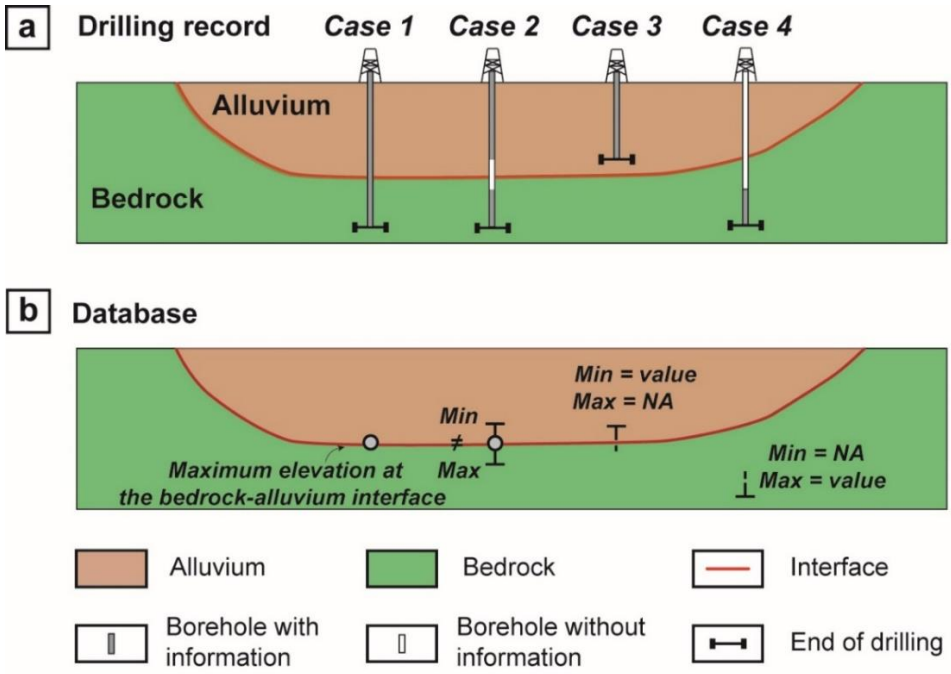

Figure 5.5. Database construction from boreholes. (a) The four cases identified. (b) The interpretation of the database recorded.

5.2.2 Geophysical database

Additional information on the geometry of the bedrock-alluvium interface in the valley bottom was achieved by utilizing very high-resolution seismic data along the Lower Seine River. These data were obtained from the geophysical surveys on nautical sites of the Grand Port Maritime de Rouen project acquired in 2012 between Rouen and Saint-Maurice-d'Etelan, downstream of Paris. Across the entire 71 kilometers-long seismic profiles, the transect was divided into 18 sections, where 7 sub-parallel profiles with a spacing of 25 m were acquired at each seismic section (Figure 5.6).

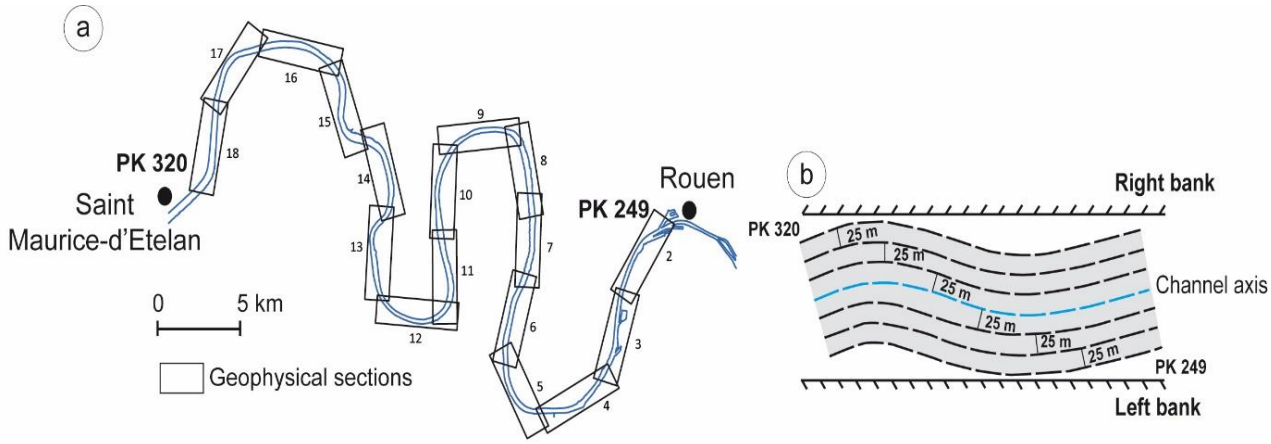

Figure 5.6. (a) Location of study area. The black box shows the geophysical sections between the PK 249 and 320. (b) Schematic methodology with 7 sub-parallel profiles spacing 25 m at each seismic section.

For each seismic profiles, deep reflectors were identified as the relative elevation at the bedrock-alluvium interface. To construct the database of the bedrock elevation, this interface was picked every kilometer from the reflection sections containing time-depth information.

In sections, the vertical scale is represented in two-way travel time in milliseconds. On surface, the vertical referencing altimetry is related to 4.38 m above the zero IGN. Therefore, the relative elevation at bedrock interface for each kilometric point can be determined applying the equation 5.1:

$$relatif\ elevation\ (m) = 4{,}38m - \frac{v}{2} * t \qquad \text{Equation 5.1}$$

where ***v*** is the velocity value of sediments and water with a mean about 1500 m/s and ***t*** is the propagation time.

Generally, two horizons could be characterized along the seismic profiles. The first represents unconsolidated water saturated sediments and the second formed by consolidated sediments represents the bedrock. Their interface provides the relative elevation of the bedrock interface and allow estimating the alluvial infilling in the Lower part of the Seine valley (Figure 5.7). A total of 63 points were added to the database, as explained before these points were selected each kilometer along the seismic profile. Where borehole from the BSS is available, the bedrock interface elevation interpreted from seismic data demonstrates a good agreement with lithological information obtained (see more details in chapter 4).

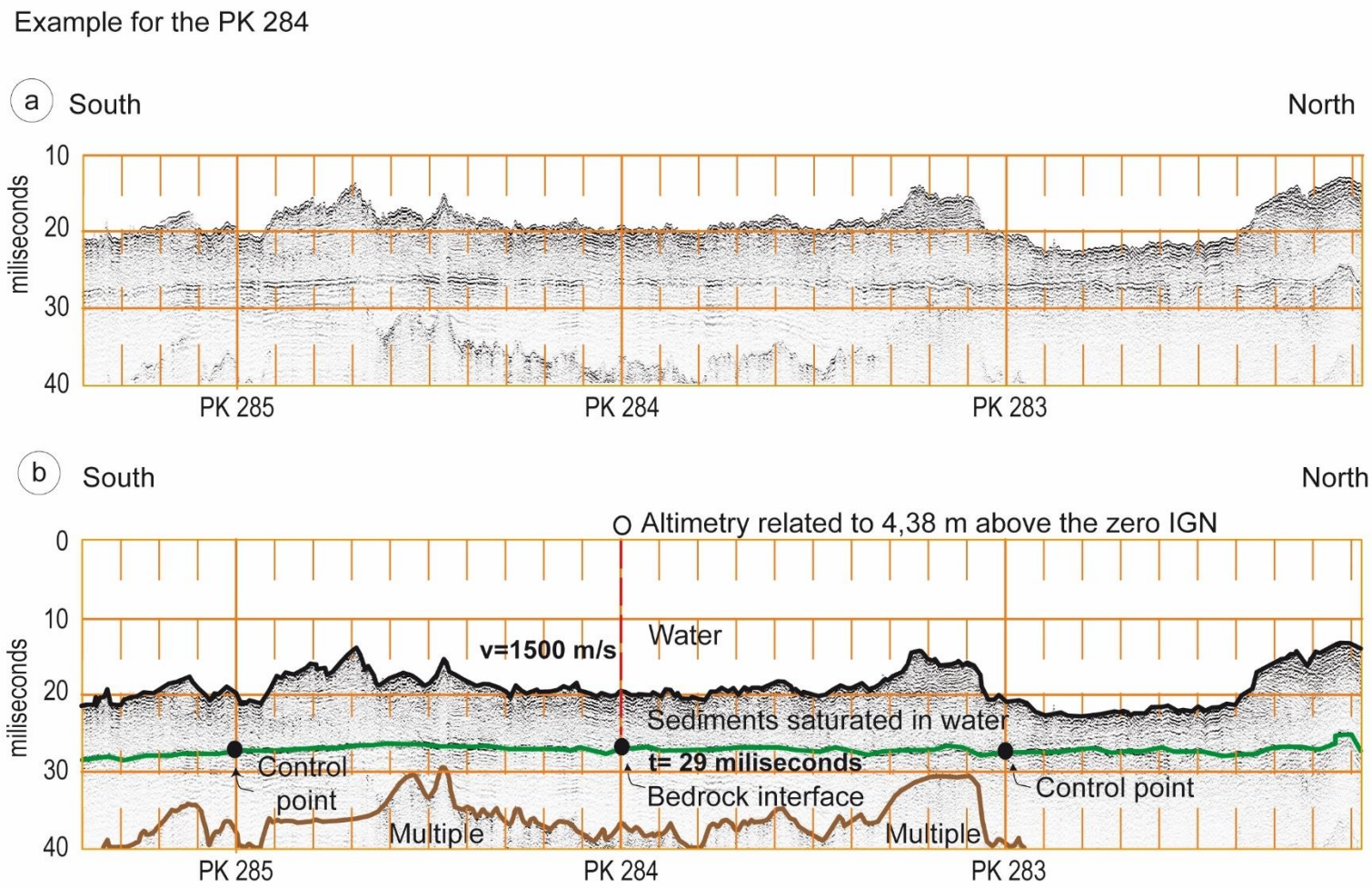

Figure 5.7. Example of the seismic profile analyzed. (a) Original seismic profile. (b) Interpreted seismic profile. Solid green line represents the continuity of reflectors at the bedrock interface, black line represents the river floor and brown line shows the seismic multiple.

5.2.3 Data from bibliography

The database was completed with data from the literature. These data were georeferenced in ArcMap 10.6 to better characterize the boreholes points. Upstream of Paris, at Troyes, the notice of the geological map (1:50 000 scale; Pomerol and Monciardini, 1992) shows the map of alluvium isopach. There, alluvial thickness varies between about 3 and 10 m. A total of 31 boreholes were collected based on the information from the isopach map, these boreholes are not referenced in the BSS (Figure 5.8). Downstream of Paris, between Trouville-la-Haule and Le Havre, Lefebvre et al., (1974) combined boreholes data and seismic profiles to determine the bedrock morphology and the characteristics of alluvial infill in the Seine estuary. A total of 31 boreholes were identified and subsequently added to the final database (Figure 5.9). In summary, the database contains 4 817 boreholes distributed over the Seine catchment, representing 1,7 boreholes/km^2 (Figure 5.10).

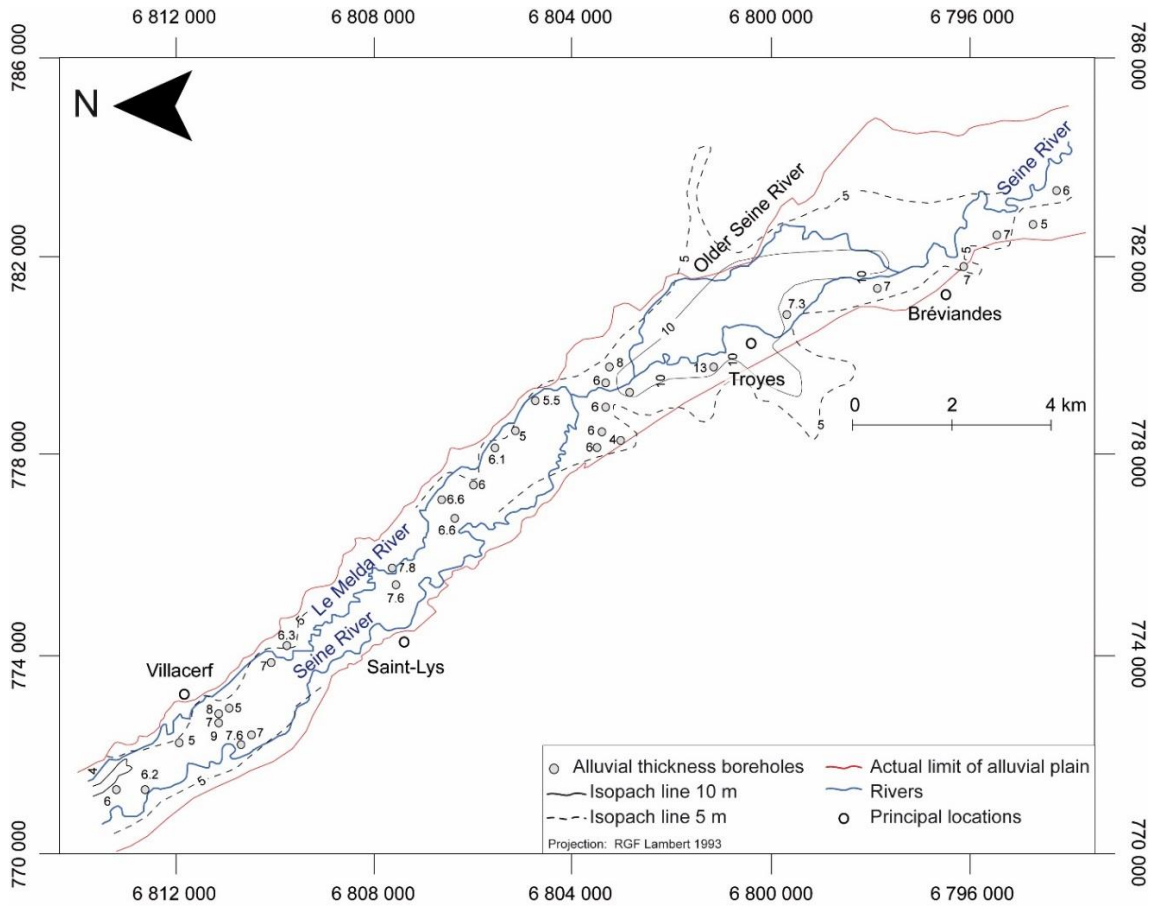

Figure 5.8. Isopach map of the alluvium near of Troyes, upstream Paris (modified after Pomerol and Monciardini, 1992).

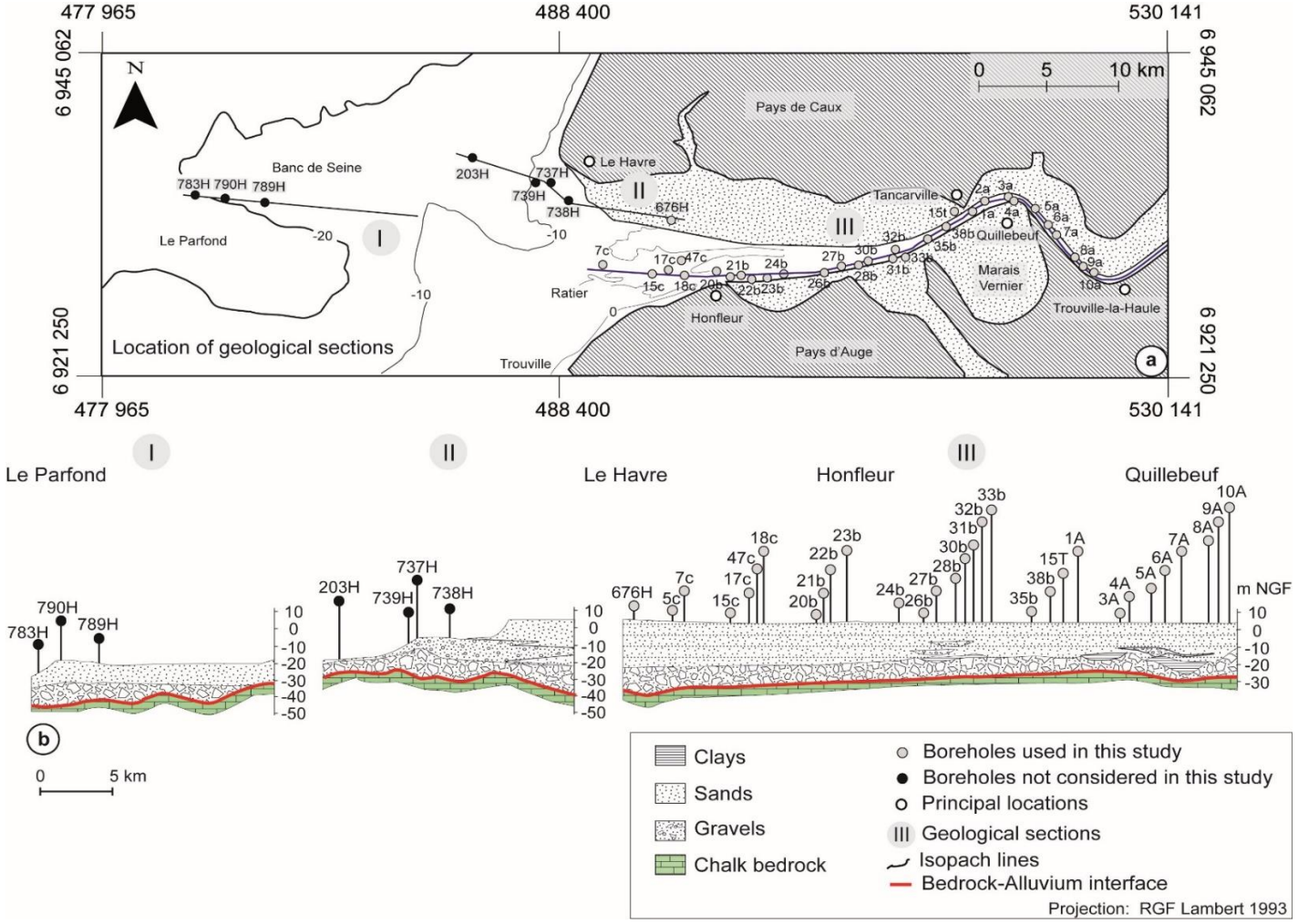

Figure 5.9. Database obtained downstream Paris. (a) Localization of boreholes. (b) Geological sections showing the main characteristics of the alluvial infilling, modified after Lefebvre et al., 1974.

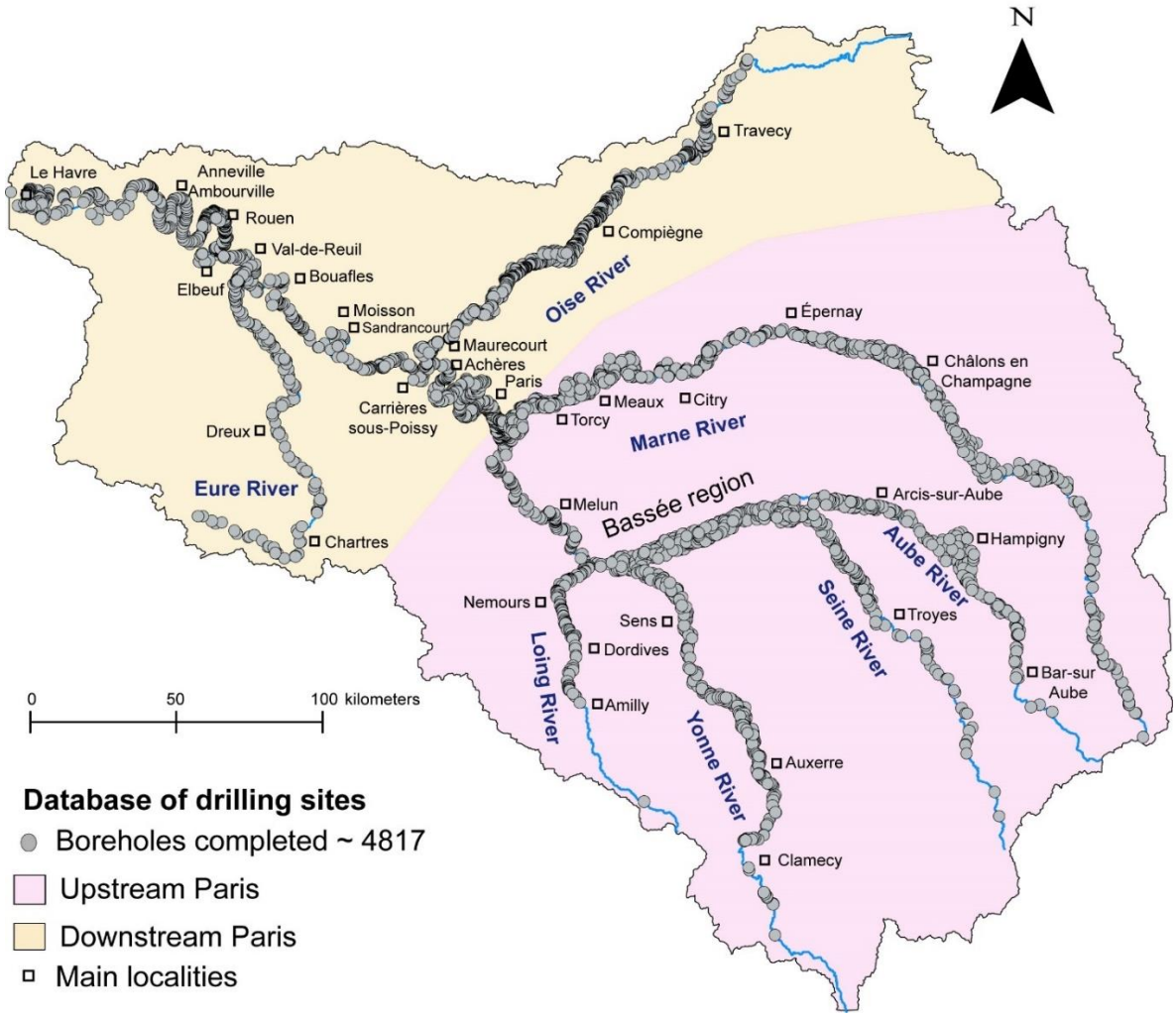

Figure 5.10. Total database along the Seine catchment. Grey circles will be used for the geometric analysis and kriging method in Chapters 6 and 7.

5.3 Analysis

5.3.1 Bedrock lithology

Based on the alluvial description in the database, the distribution of bedrock lithology was mapped at the bottom of the major valleys of the Seine catchment. It was grouped into five main lithologies: limestone, clay, marl, sand, and chalk bedrock from different geological ages (Figure 5.11).

In the Upper part of the Seine catchment, the Marne (until the Épernay location), the Aube, the Seine (until the confluence with Loing River), the Yonne and the Loing rivers have a bedrock from different geological ages characterized principally by:

- Upper Jurassic limestones (from Tithonian, Kimmeridgian, and Oxfordian) and marls (from Kimmeridgian).
- Lower Cretaceous clays (from Albian, Aptian, Barremian), marls and sands (from Albian).
- Upper Cretaceous chalk (from Campanian, Santonian, Coniacian, Turonian, and Cenomanian).

Between the confluence with the Loing River until the confluence with the Oise River, the Seine, the Oise and the Marne (downstream Épernay location) have a bedrock characterized by:

- Upper Cretaceous chalk (from Campanian, Santonian, Coniacian, Turonian, and Cenomanian).
- Paleocene sands, clays and marls (from Thanetian).
- From Eocene: Marls, limestones, sands (from Bartonian, Lutetian), sands and clays (from Ypresian).
- From Oligocene: Clays (from Rupelian).

After the confluence with the Oise River until Le Havre location, the Seine and the Eure rivers have a bedrock characterized principally by:

- Lower Cretaceous clays and sands (from Albian and Aptian).
- Upper Cretaceous chalk (from Campanian, Santonian, Coniacian, Turonian, and Cenomanian) and clay (from Cenomanian).

The geological setting of the dominant bedrock lithology along the Seine catchment is therefore well suited (i) to determine how variable lithology potentially influence long rivers and valley centerline profiles (ii) to know the principal geometric relation between valley width and drainage area and (iii) to identify the more easily erodible lithologies compared to more resistant lithologies (more details in chapter 6).

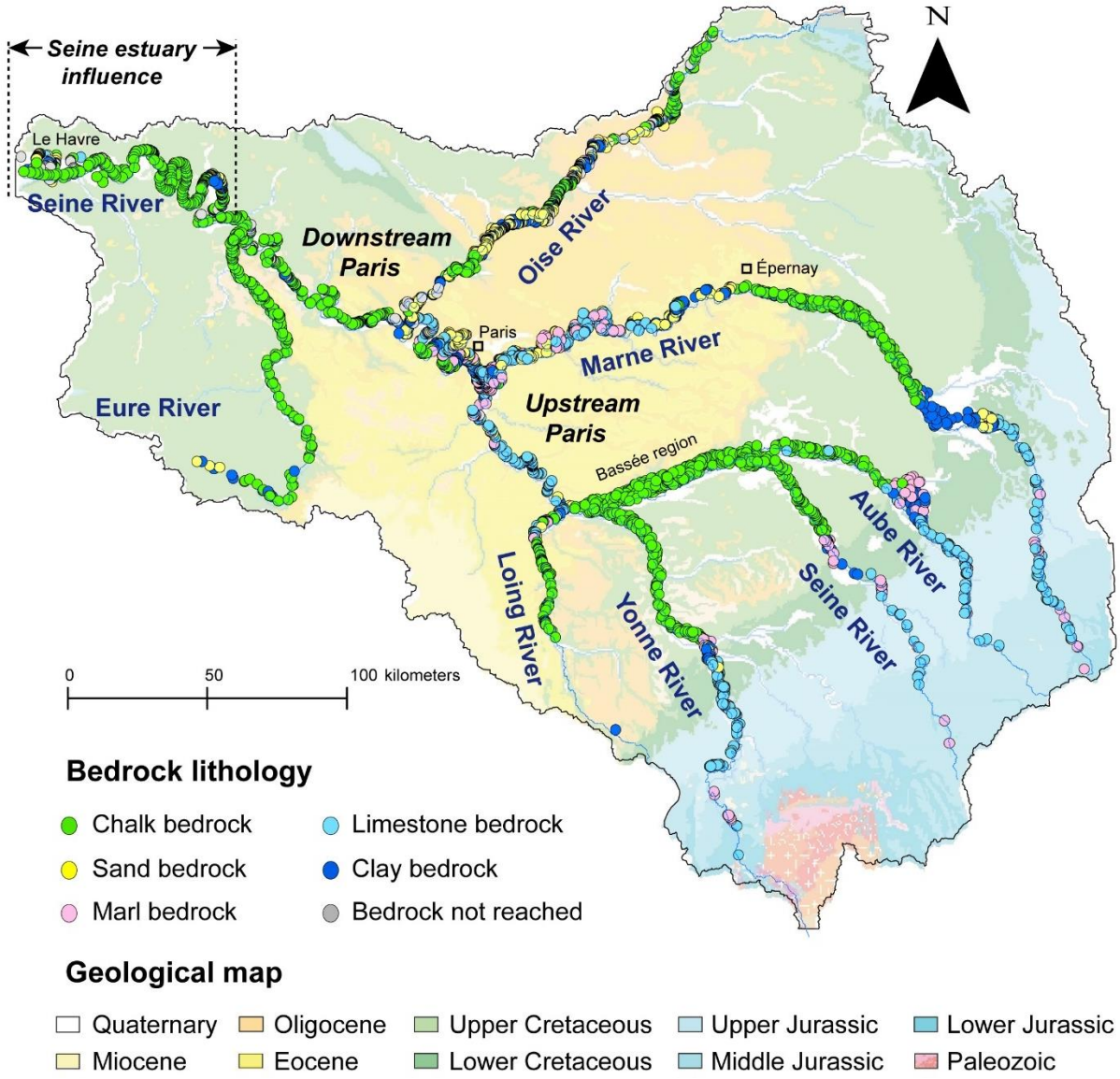

Figure 5.11. Bedrock distribution along the Seine catchment considering the geological map.

5.3.2 Bedrock-alluvium interface elevation

Bedrock elevation is variable within the Seine catchment. In general, bedrock elevation decreases from ESE (382 m NGF max) to WNW (-55 m NGF min) ("Nivellement Général de la France", French official altimetric system, Figure 5.12).

The upper part of the Seine catchment that includes first kilometers of the Oise, the Marne, the Yonne, the Loing and the Eure rivers and the Seine River until the confluence with the Aube River as well as the entire Aube River, shows bedrock elevation values ranging between 382 and 75 m NGF.

Then, the downstream part of the Oise, the Marne, the Yonne, the Loing, and the Eure rivers as well as the Seine between Bassée region until the confluence with the Oise River, as bedrock elevation ranging between 75 and 17 m NGF. Finally, the bedrock elevation dips to the lower part of the Seine catchment after the confluence with the Oise River, ranging values between 17 and -55 m NGF.

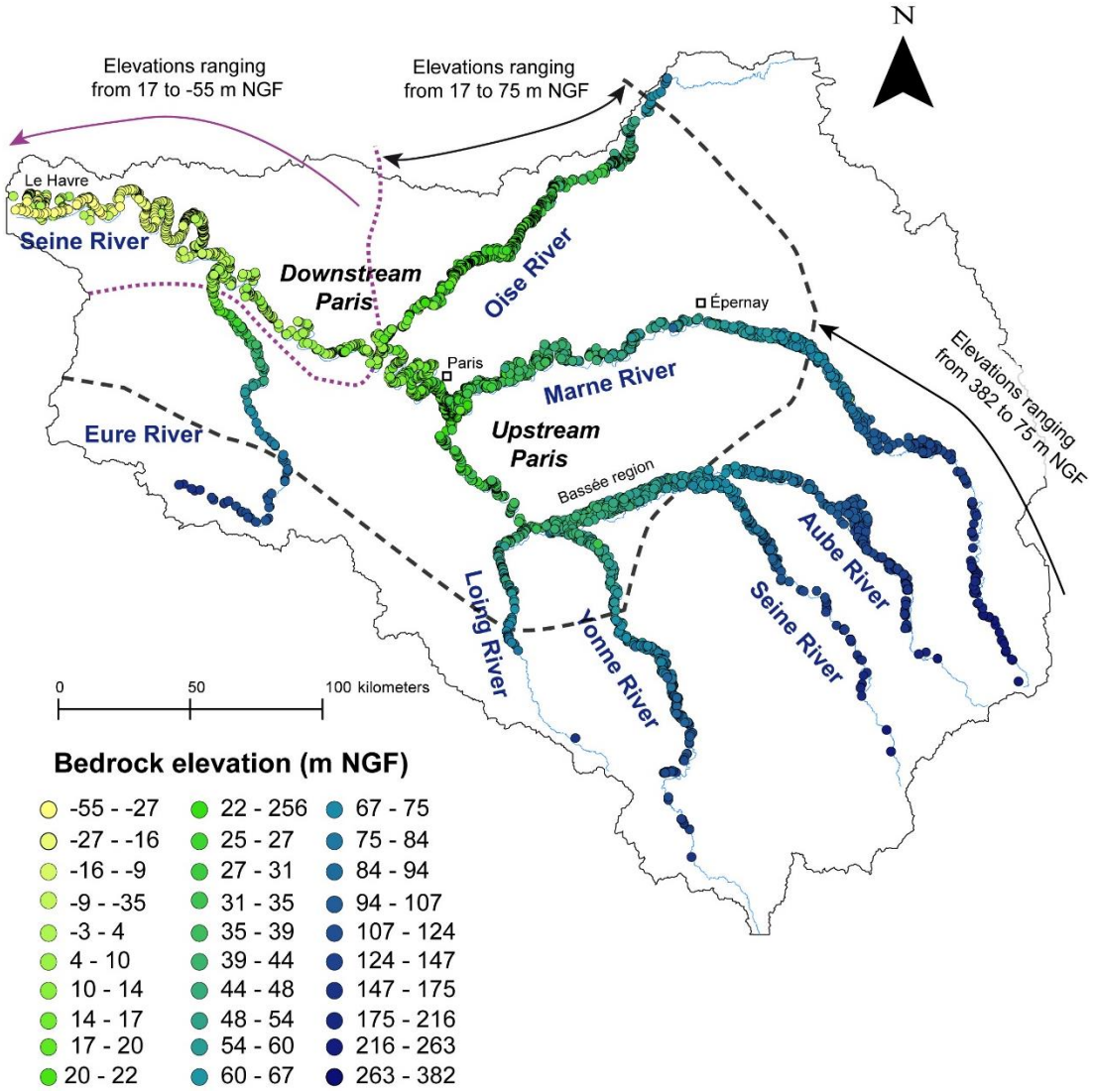

Figure 5.12. Bedrock elevation distribution along the Seine catchment. Lines and narrows indicate the approximately limits of bedrock elevation changes.

This bedrock-alluvium interface elevation is used (i) to determine the relative elevation (RH) of samples considering the maximal incision of the river (see chapter 2) and (ii) to characterize this bedrock-alluvium interface using the directional kriging in order to know the principal mechanism causing the variability in bedrock elevation (see chapter 7).

5.3.3 Distribution of alluvium thickness

The alluvial infilling varies in thickness and composition. The mean of alluvial thickness is 8 m as determined through the analysis of 4 817 boreholes.

According to the alluvial description, the spatial distribution of their thickness varies from upstream to downstream. For most tributaries such as Oise, Marne, Aube, Yonne, Loing and Eure valleys, as well as the upper part of the Seine valley (until the confluence with the Marne River), the alluvial thickness varies from 0.3 to 10 m. In contrast, downstream Paris (after the confluence with the Marne River), the alluvial thickness of the Seine valley increases considerably and is well remarkably in the Seine estuary with values ranging from 11 to 52 m (Figure 5.13).

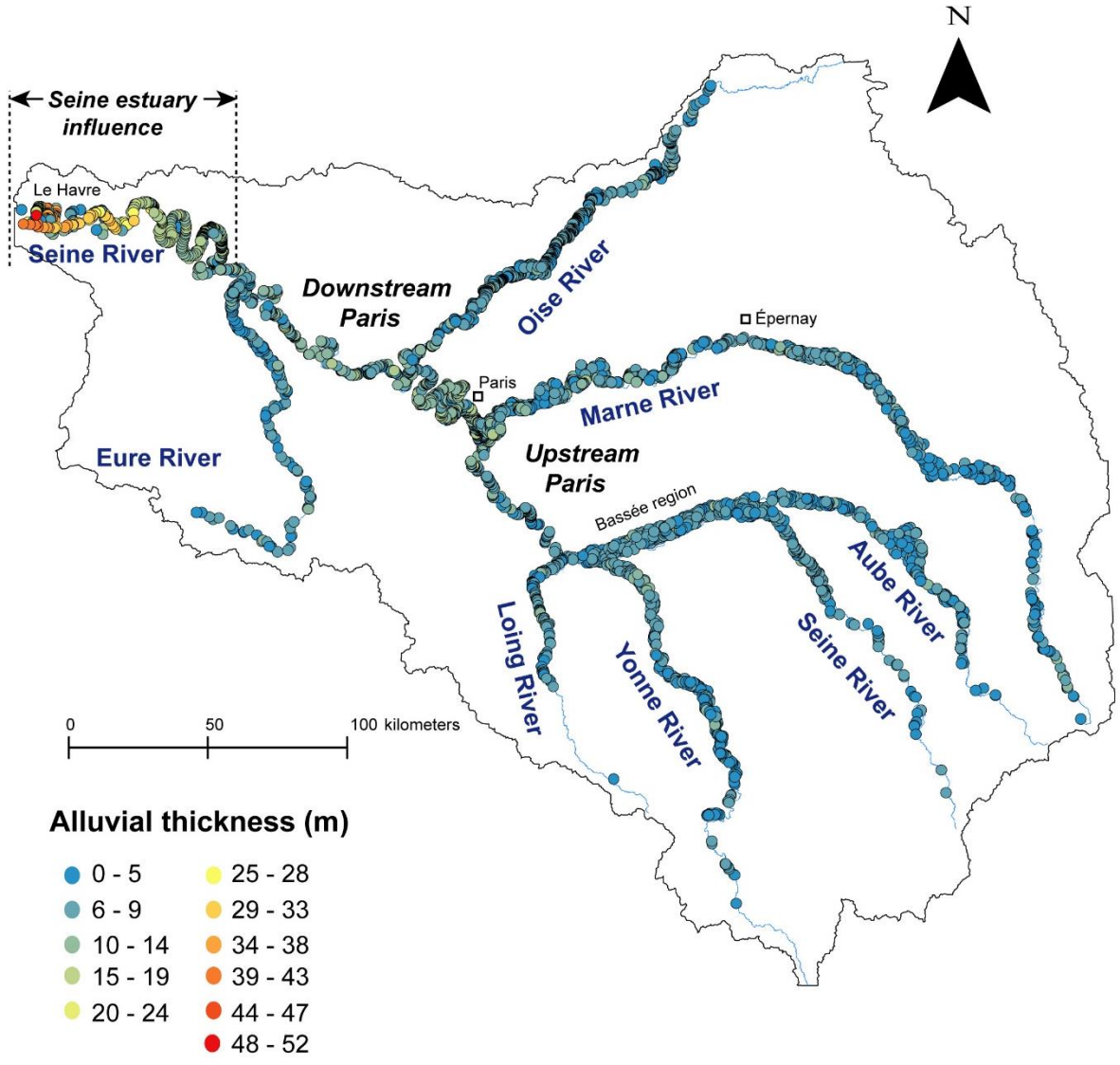

Figure 5.13. Alluvial thickness distribution along the Seine catchment.

Histograms are used to compare the distribution of the alluvial thickness among various groups of bedrock lithologies. These graphs help to compare the alluvial thickness over the different bedrock lithologies. When considering chalk bedrock (Figure 5.14-a), the average thickness is approximately 8.1 m over 2084 boreholes. In sand bedrock (Figure 5.14-b), the average thickness is 8.3 m over 682 boreholes. In limestone bedrock (Figure 5.14-c), average is 7.4 m over 819 boreholes. In clay bedrock (Figure 5.14-d) the average is 8.4 over 471 boreholes. In marl bedrock (Figure 5.14-e), average thickness is 8.1 m over 386 boreholes, and considering all database (Figure 5.14-f), , the average thickness is 8 m over 4817 boreholes.

These histograms exhibit an asymmetric distribution. The distribution is characterized by a positively skewed, indicating a skewness between higher to lower thickness values. The asymmetry in the distribution suggest that the alluvium thickness is not evenly distributed across the catchment. Certain areas may experience higher rates of sediment deposition, resulting in thicker alluvial accumulation, while other areas may be subject to greater erosion, leading to thinner alluvial deposits.

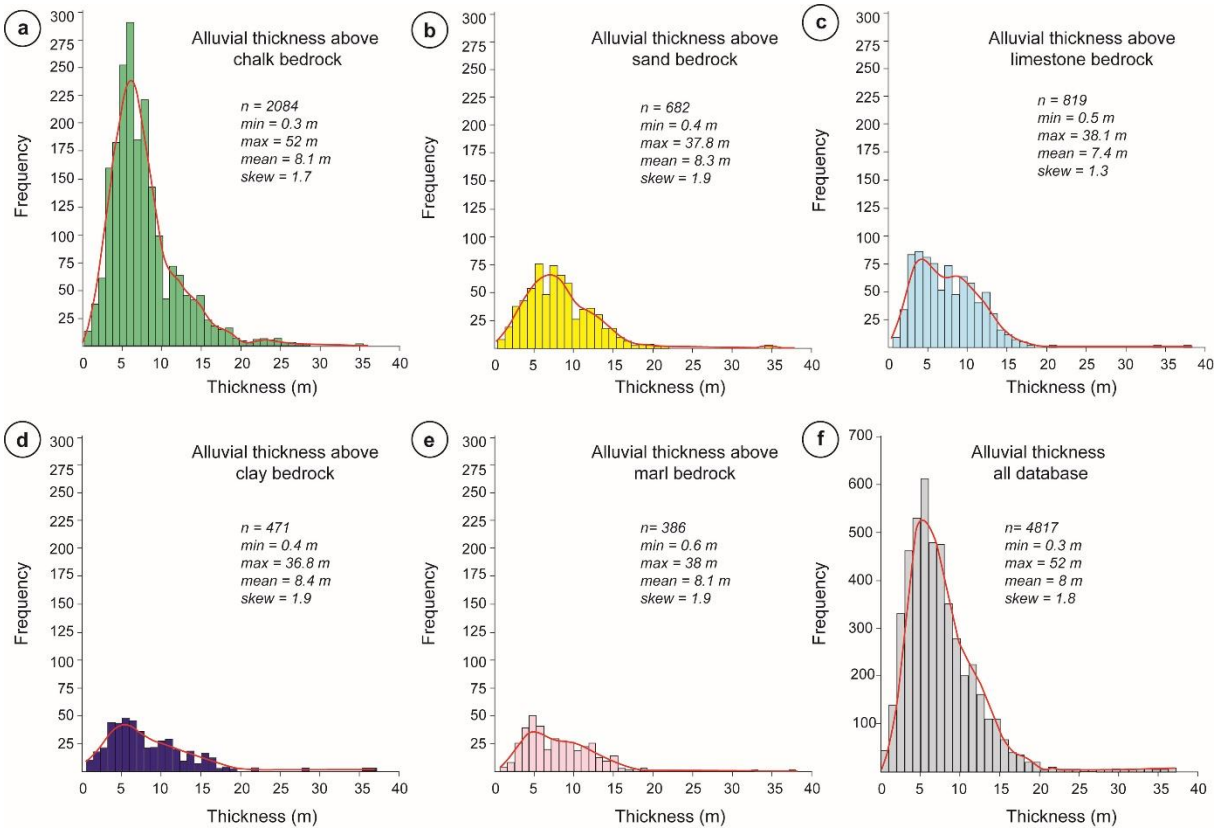

Figure 5.14. Histograms of Alluvial thickness above the chalk, the sand, the limestone, the clay, the marl bedrock along the Seine catchment.

The Figure 5.15 shows the alluvial thickness distribution of each borehole along the Seine catchment, considering the bedrock lithology. The Seine valley (Figure 5.15-a) shows an increase in alluvial thickness from upstream to downstream. This increase is also marked at the confluence with affluents. Boreholes located within the chalk, sand and clay bedrocks seem to have the highest alluvial thickness. In contrast, boreholes located within marls and limestones bedrocks seem to have the lowest alluvial thickness. Similarly, the Oise and the Marne valleys reflects this trend in alluvial thickness increase. Near of the confluence with the Seine River, boreholes located within the chalk, clay and sand bedrocks in the Oise valley (Figure 5.15-b) and boreholes located within marls, limestones, and sand bedrocks in the Marne valley (Figure 5.15-c) seem to have the highest alluvial thickness. In contrast, in the Aube, Yonne, Loing and Eure valleys (Figure 5.15-d-e-f-g), there is an increase in alluvial thickness from upstream to downstream but is less marked due to of number of boreholes. Nevertheless, near of the confluence with the Seine River, boreholes located within the chalk bedrock (for Aube, Yonne and Eure valleys) and within the limestone bedrock (for Loing valley) seem to have the highest alluvial thickness.

The relationship between the alluvial thickness and bedrock lithology remains important to determine the geometric relations as well as the influence of alluvial thickness in the whole Seine catchment (see chapters 6 and 7).

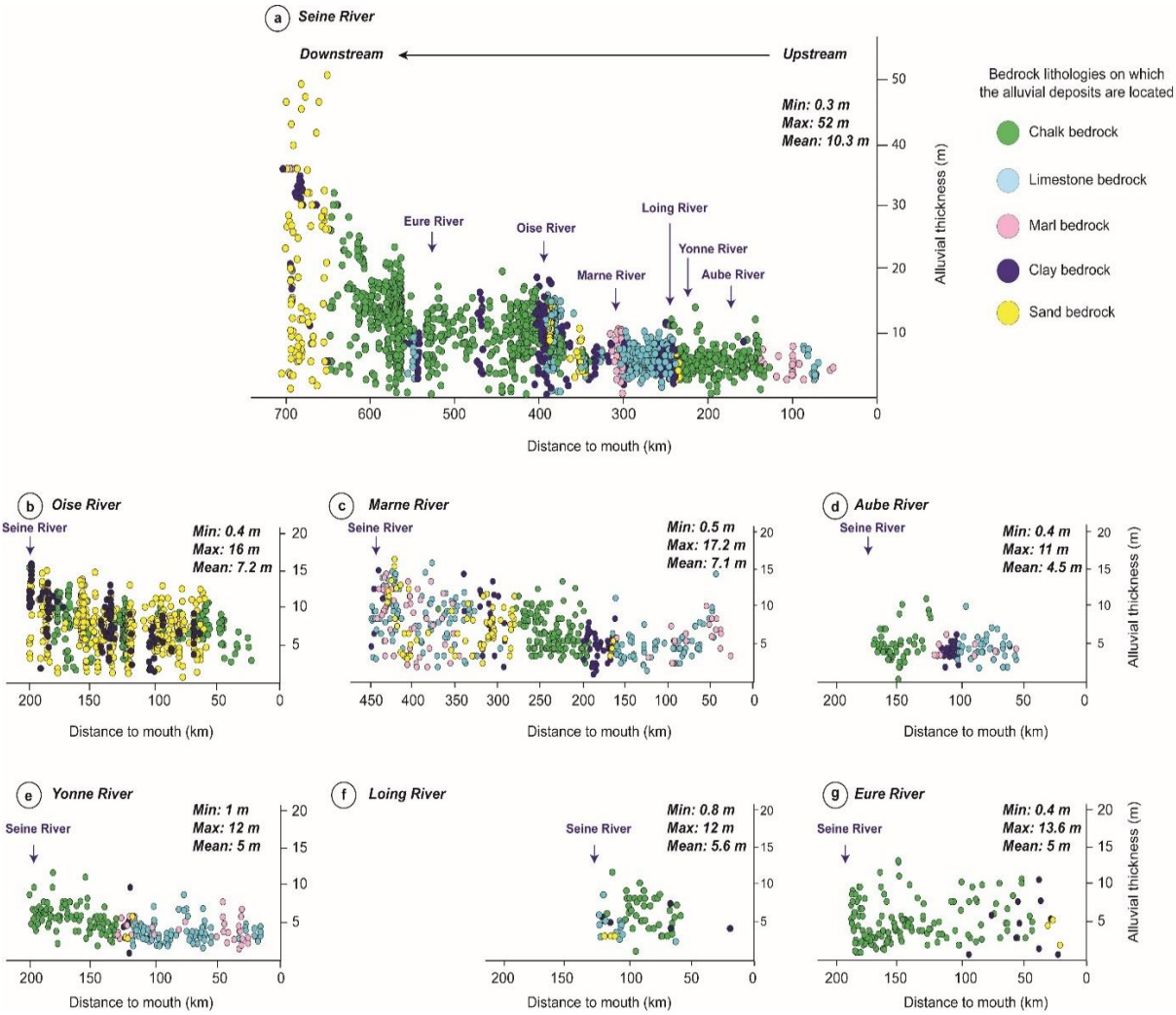

Figure 5.15. Alluvial thickness distribution along the Seine catchment. Colors represent the bedrock on which the alluvial deposits are located.

5.3.4 Composition of the alluvial infill

Significant variability exists in the occurrence, thickness, and lithology of the alluvial infill along the Seine catchment. The main alluvial lithologies within the 4 817 boreholes is characterized principally by sands (44%), gravels (12%), clays (12%) and silts (10%). These alluvium lithologies represents 78% in terms of thickness. The other 22% of alluvial thickness is represented by boreholes that do not contain alluvial description and by surface formations such as backfill and topsoil (Figure 5.16).

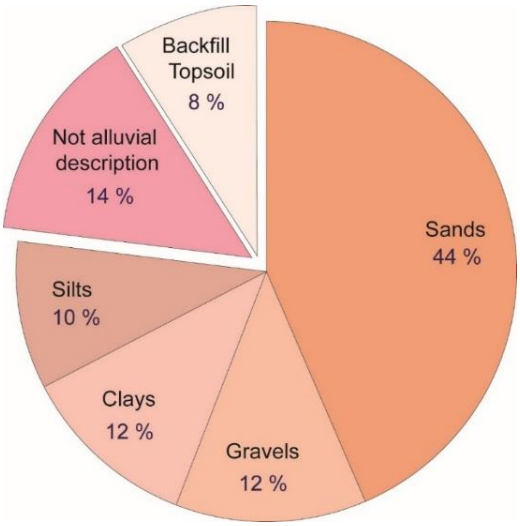

Figure 5.16. Dominant lithologies within the alluvium in the whole Seine catchment.

The alluvial infill along the Seine catchment is conditioned by each valley. Notably, the Seine valley represents the valley which have the greatest number of boreholes, totally 1854. The occurrence of alluvial lithologies within these boreholes are characterized by sands (54 %), gravels (17 %), clay (13 %), silt (16 %) (Figure 5.17-a).

The Oise valley is characterized by a total of 1015 boreholes, where the dominant lithology within the alluvium is characterized as follows: sands (39 %), gravels (24 %) clay (19 %), silt (18 %) (Figure 5.17-b).

The Marne valley has 1100 boreholes, in which the dominant lithology within the alluvium is characterized by: sands (65 %), gravels (10 %), clay (14 %), silt (11 %) (Figure 5.17-c).

The Aube valley has 343 boreholes, in which the dominant lithologies are characterized by: sands (59 %), gravels (19 %), clay (15 %), silt (7 %) (Figure 5.17-d).

The Yonne valley is characterized by a total of 206 boreholes, where the dominant lithologies are characterized by: sands (52 %), gravels (27 %), clay (18 %), silt (3 %) (Figure 5.17-e).

The Loing valley has 100 boreholes, in which the dominant lithologies are characterized by: sands (71 %), gravels (18 %), clay (9 %), silt (2 %) (Figure 5.17-f).

Finally, the Eure valley has 200 boreholes, in which the dominant lithologies are characterized by: sands (65 %), gravels (15 %), clay (16 %), silt (4 %) (Figure 5.17-g).

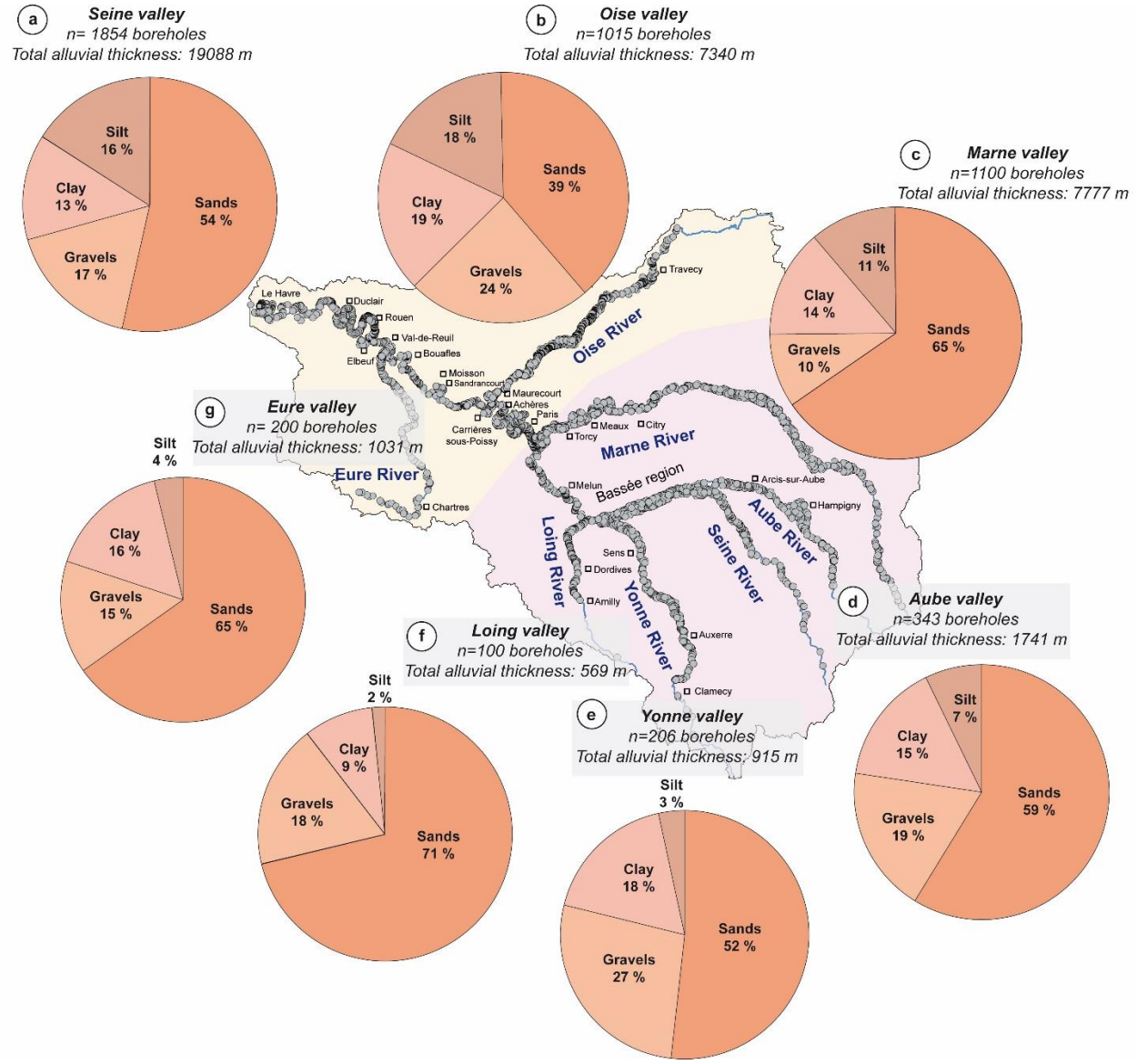

Figure 5.17. Dominant lithologies within the alluvium in the Seine catchment.

5.4 Conclusion

A method for geomorphological delimitation of valley bottom features from geological data were established. This method selects the valley bottom and terraces using a threshold of elevation (in this case lower than 10 m), which are determinate from the 1:50 000 scale geological map combining with the 75-m resolution of DEM. Furthermore, some terraces were harmonized in the final valley bottom polygon.

A database composed of 4817 boreholes representing 1,7 boreholes/km^2 was constructed from the BSS and completed by data from seismic acquisitions and the literature. These data describe

the geometry, the main lithologies of the alluvial infill and the underlying bedrock. Several findings arise:

- Bedrock lithologies can be grouped into five main lithologies with chalk, sand, limestone, clay, and marl.
- For most tributaries (Oise, Marne, Aube, Yonne, Loing, Eure and Upper Paris), alluvium thickness is comprised between 0.3 to 10 m. In contrast, in downstream Paris alluvium thickness is between 11 and 52 m.
- The most dominant alluvium lithologies within the Seine catchment is represented by sands from 26 to 66% of the alluvial infilling depending on the river. Then, lithologies such as gravels, clays and silts. These lithologies are more or less representative for each valley.
- In general, the integrated use of data from the geophysical acquisition and from bibliography demonstrates a good agreement with the available data from the BSS at the bedrock-alluvium interface.
- This robust database has numerous applications, (i) it can allow to determine the relative elevation considering the maximal incision of the river along the catchment, (ii) contribute to the analysis of geomorphic variations within the catchment, (iii) allow to determine the directional kriging considering the alluvial thickness as well as the bedrock-alluvium interface and (iv) to quantify the sediment volume storage along the valley bottom of the Seine catchment, based on an empirical volume-area of valley infill.

Chapter 6:
Geomorphic analysis of the fluvial corridor topography in the Seine catchment

Ce chapitre présente une étude géomorphologique du Bassin versant de la Seine réalisée à partir des données topographiques, du réseau de drainage et des données géologiques. Les principaux paramètres morphométriques tels que la longueur de la rivière, largeur du fond de vallée, délimitation des sous-bassins versant et la surface ont été déterminés pour étudier l'évolution de la largeur du fond de vallée par rapport à l'aire drainé en tenant en compte du substrat lithologique le long du cours d'eau.

Chapter 6

6 Geomorphic analysis of the fluvial corridor topography in the Seine catchment

In this chapter, a geomorphic analysis of the Seine River catchment is performed from topography, river network and geological data. The whole Seine catchment is formed by different sub-catchments corresponding to the main Seine River tributaries (Oise, Marne, Aube, Yonne, Loing and Eure rivers).

Several morphometric parameters of this catchment provide a means of easily comparing the drainage networks across the different sub-catchments. The principal morphometric parameters such as river length, sub-catchment delimitation, and surface were extracted. Also, the evolution on valley width with drainage area was investigated according to the main bedrock lithologies.

A general methodology is presented in the following section. This methodology was applied to the entire Seine catchment, it is exemplified here in the Oise valley, one of the major tributaries of the Seine River.

6.1 General methodology

6.1.1 Data used

The data used in this study are principally:

- The Digital Elevation Model (DEM) with 75-m resolution, from the BD ALTI® (v.2, downloaded on October 2020) provided by the Institut National de l'Information Géographique et Forestière (IGN).
- The database available in the CARtographie THématique des AGences de l'eau et du ministère chargé de l'environnement (BD Carthage), which describes, codifies, and standardizes streams, catchment areas, lakes and other hydrographic surface for the French hydrographic network. This database was used to extract the stream network along the Seine catchment and its majors affluents such as Oise River, Marne River, Aube River, Yonne River, Loing River and Eure River.
- The database introduced in chapter 5. This database enables the identification of valley bottom polygon, the extraction of the valley centerline to determine both the longitudinal valley (centerline) and river profiles. It thus provided valuable insights into variations in valley width with bedrock lithologies and drainage area.

6.1.2 DEM analysis for catchment delimitation and longitudinal profiles extraction

6.1.2.1 Delimitation of Seine catchment and its major tributaries

To delimitate the Seine catchment and its major tributaries with the 75-m resolution DEM, the ArcHydrotools package was used. The procedure involved a sequence of 8 steps (Figure 6.1). After DEM input on ArcGIS 10.6© (Figure 6.1-1), a correction of the DEM is performed to remove its depressions by raising elevations of theses sinks to match the one of adjacent cell to ensure a continuous stream network, and an exorheic network for the whole study area (Prodanovic et al., 2009; Figure 6.1-2). Then, the corrected ("filled") DEM is used as input data to compute the river flow direction, i.e., the direction in which a given cell will flow (Figure 6.1-3). This flow direction data is the input to the compute the flow accumulation at each cell location of the area, i.e., the number of pixels drained by a given pixel following the flow direction of each pixel of the study area (Figure 6.1-4). To extract the river network, a threshold value is applied to the flow accumulation data, defining the number of pixels to be considered as part of a river (Figure 6.1-5). In this study, a threshold value of 37 pixels was iteratively defined, by searching the best fit between the "true" BD Carthage River network and the computed flow accumulation (Figure 6.1-5). Then, the stream order module of each trunk of the Seine River network was performed (Figure 6.1-6). Downstream the Seine River, and downstream each tributary of interest, i.e., Oise, Marne, Aube, Yonne, Loing and Eure rivers, an outlet point was defined (Figure 6.1-7). Outlet points were used to initiate the computation of the Seine catchment outline and of each sub-catchment outline corresponding to a tributary of interest (Figure 6.1-8).

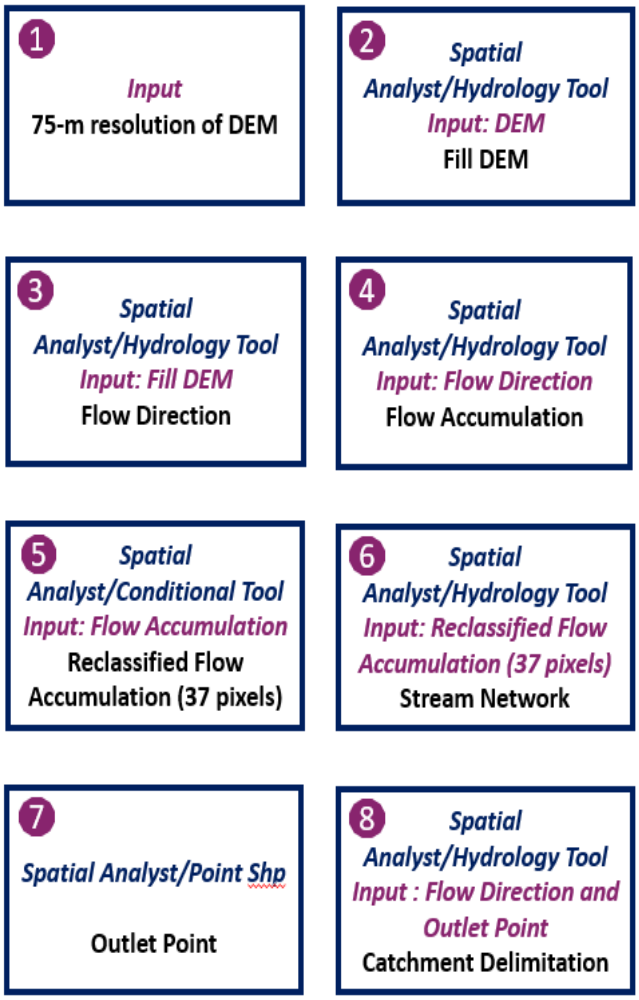

Figure 6.1. General workflow for delimiting the Seine catchment (Blue: ArcGIS 10.6 tool used; Pink: input data; Black: output data).

6.1.2.2 Longitudinal river and valley centerline profiles

Longitudinal profiles as well as valley centerline profiles were produced as they provide a set of diagnostics for examining fluvial response to external forcing such as climate, tectonic or base level change or the influence of internal processes such as lithology. The centerline of the Seine catchment was extracted using the defined valley polygon obtained from 1:50000 scale geological map (see chapter 5). For this, we determine the median along the valley polygon to obtain the centerline using ArcGIS 10.6. In previous section 6.1.2-a, the stream network obtained from the DEM were used only to search the best fit with the BD Carthage. In the following sections we work with the BD Carthage and the valley centerline principally.

The longitudinal profiles as well as the valley centerline profiles were determined doing an interpolation with the 75-m resolution of DEM respectively (i) along the BD Carthage River

path and (ii) along the valley centerline. These profiles have been used to characterize the regional scale topography for the seven major rivers in the Seine catchment and to determine the valley width, the elevation and the drainage at each kilometric point. The Figure 6.2 illustrate an example of the Oise valley bottom and the respective profiles showing the plot of elevation against the distance.

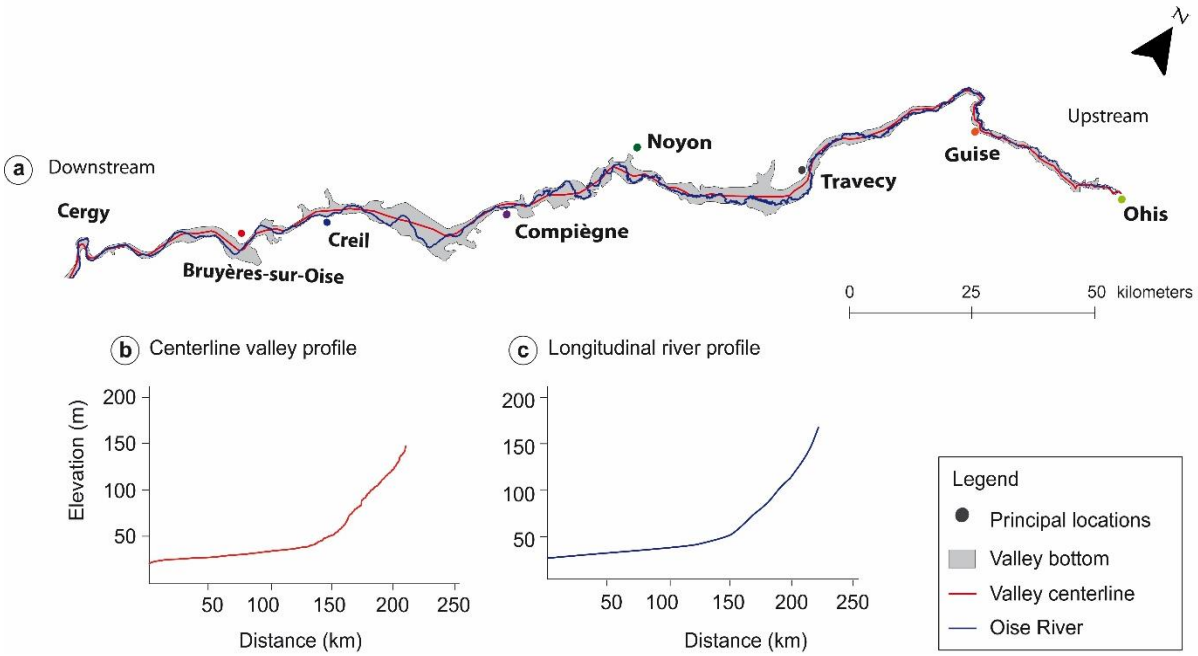

Figure 6.2. Example of the Oise valley bottom and the valley and longitudinal profiles. (a) The valley centerline as well as the Oise River over the valley bottom polygon. Profiles shows the elevation against the distance along (b) the valley centerline profile and (c) the longitudinal profile of the Oise River.

6.1.2.3 River normalized profiles

In order to compare rivers of different lengths and of different elevation ranges, here along the Seine catchment River, normalized profiles were extracted using the automatic algorithm compiled in the *Nprofiler* ArcGIS add-in (Pérez-Peña et al., 2017). For each river of interest, this profile is constructed by normalizing elevations by the maximum elevation, and normalizing distance by the total length of the river (Figure 6.3). Using these profiles, three main parameters are defined: (i) the concavity factor (Cf) defined as the percent area on the plot between the river profile and the straight line connecting the source and outlet of the river. (ii) The maximal concavity (Cmax) defined as the maximal difference between normalized profile elevation and straight-line elevation for a given distance along the whole profile. (iii) Distance

maximal (Lmax) defined as the distance where maximal concavity is found. Theoretically, values of concavity factor (Cf) vary between -100% (convex-up profiles) to 100% (concave-up profiles), through 0% (straight profiles). Values of maximal concavity (Cmax) in convex-up profiles are strongly negative and far from the source. Lower values of Cmax without precise location characterized rectilinear profiles and maximal positive values of Cmax close to the source for concave-up profiles. Generally, graded rivers have a characteristic concave-up profile, with a high concavity factor (Cf) and maximal concavity (Cmax) close to the source (lower Lmax) (Figure 6.3, Demoulin, 1998; Ruszkiczay-Rüdiger et al., 2009; Pérez-Peña et al., 2017).

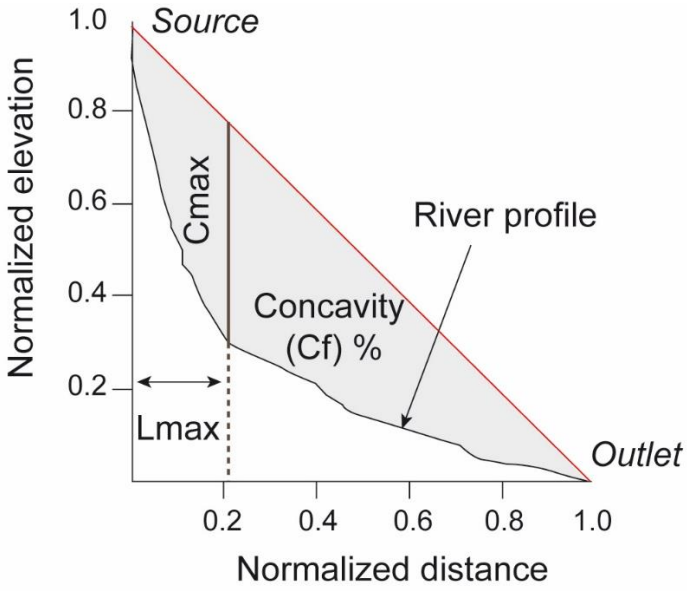

Figure 6.3. The normalized profile and its associated parameters, the Concavity factor (Cf), the Maximal concavity (Cmax) and the distance to the source Lmax where maximal concavity is found (modified after Pérez-Peña et al., 2017).

6.1.2.4 Drainage area along valley centerline profiles

The drainage area along the valley centerline profiles were determined using the Hydrological toolset in ArcGIS10.6. The flow accumulation raster (75-m resolution) and the valley centerline previously computed were extracted for the Seine catchment and the rivers of interest (see section 6.2.1). For each catchment, the drainage area was measured and extracted at sampling points located every kilometer along the valley centerline of interest. For each sampling point, flow accumulation raster value (corresponding to the number of cells drained by the sampling point) was extracted and converted to square kilometers.

6.1.3 Valley width measurement and lithology extraction

6.1.3.1 Valley width measurement

The valley bottom polygons determined previously for the Seine River and its tributary of interest were used together with the centerline to extract the valley bottom width at 1 km intervals across the Seine catchment (Figure 6.4-a). First, centerlines were split up every kilometer to define the 1 km sampling points (Figure 6.4-b). Then, vectors orthogonal to the centerline were calculated for each sampling point using a gradient method on Python to construct cross-sections across the valley (Figure 6.4-c). These sections were exported into ArcGIS 10.6 and intersected with the contour of the valley bottom polygon (Figure 6.4-d) to measure valley width between intersection points (Figure 6.4-e).

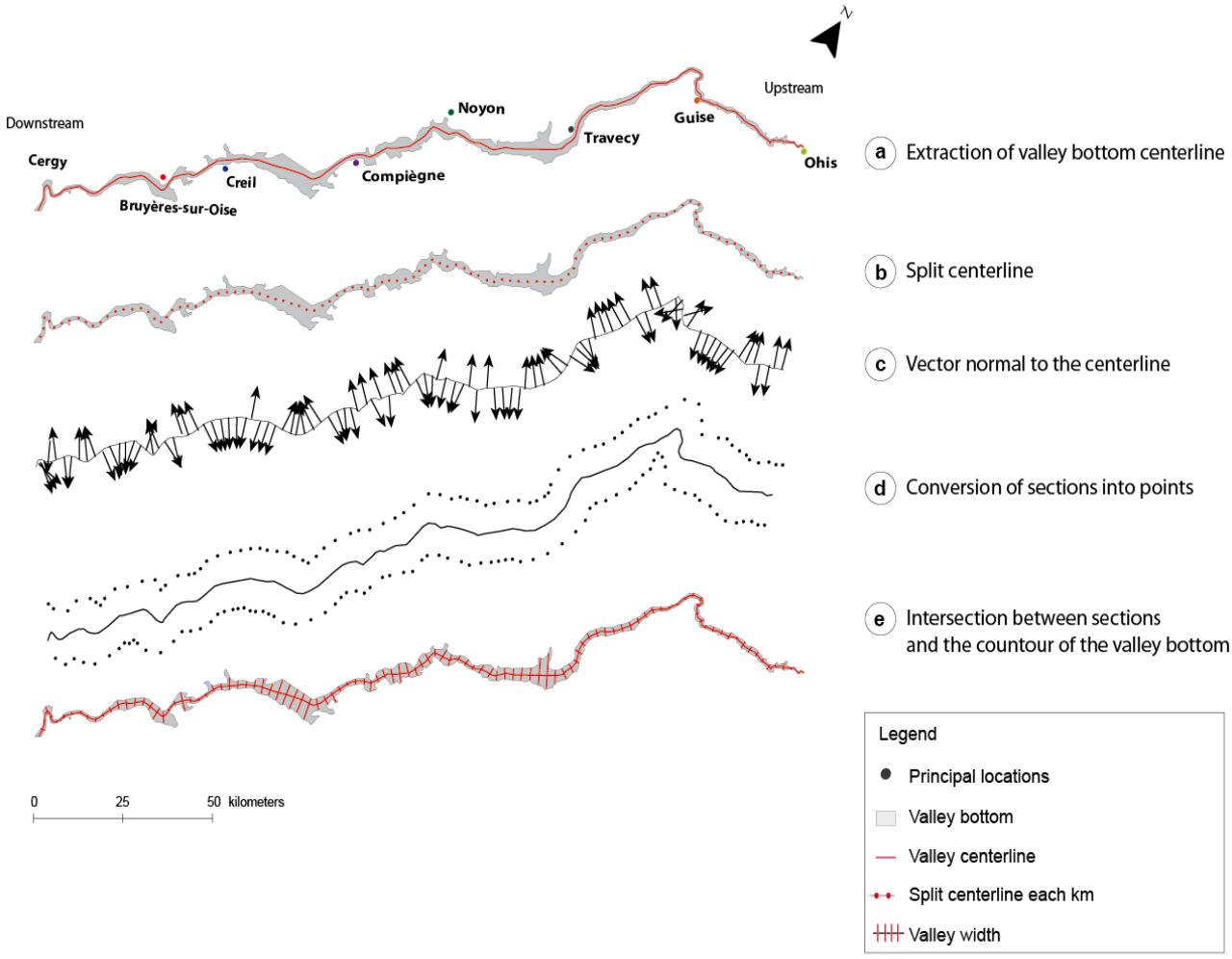

Figure 6.4. General workflow to measure valley width. Example of the Oise valley. This methodology was applied along the Seine catchment.

6.1.3.2 Bedrock lithology along the valleys

Using the boreholes database (see Chapter 5), the valley bottom has been divided manually in ArcGIS 10.6 into different lithologies of the bedrock. This division allowed a better understanding of the effect of lithological bedrock and drainage area on valley width (Figure 6.5).

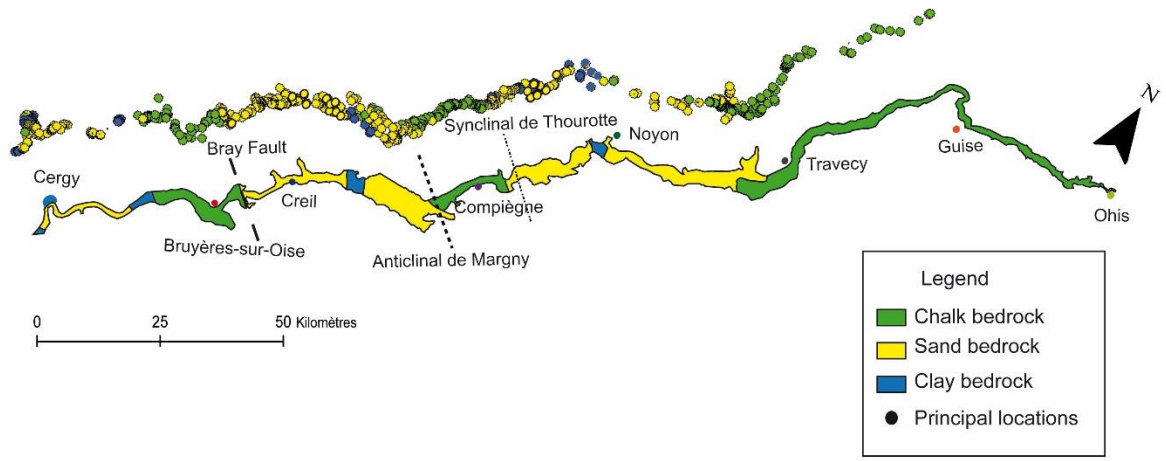

Figure 6.5. Bedrock valley development of the alluvial plain of the Oise River.

6.2 Results

6.2.1 Seine catchment and its major tributaries

The Seine catchment covers an area of 76 350 km^2, in which the Seine River constitutes the principal river with a total length of 774 km (Figure 6.6-a) and where several main sub-catchments contribute to the overall drainage of the catchment. One of the most significant sub-catchment area is represent by the Oise with approximately 16 948 km^2 and a river length of 341 km (Figure 6.6-b). The Marne sub-catchment area is 12 410 km^2 and represent the longest tributary of the Seine catchment with 514 km (Figure 6.6-c). The Yonne sub-catchment area is 10 815 km^2, with a total river length of 292 km (Figure 6.6-f). The Eure sub-catchment is 5 934 km^2, with a total river length of 229 km (Figure 6.6-h). The Aube sub-catchment is 4 649 km^2, with a total river length of 249 km (Figure 6.6-d). The Loing sub-catchment is 4 150 km^2, with a total river length of 143 km (Figure 6.6-g).

In order to compare the Seine River with other tributaries, it was necessary to determine the upstream Seine River sub-catchment, before its first confluence with the Aube River. In this case the sub-catchment is 4 042 km^2, with a river length of 221km (Figure 6.6-e).

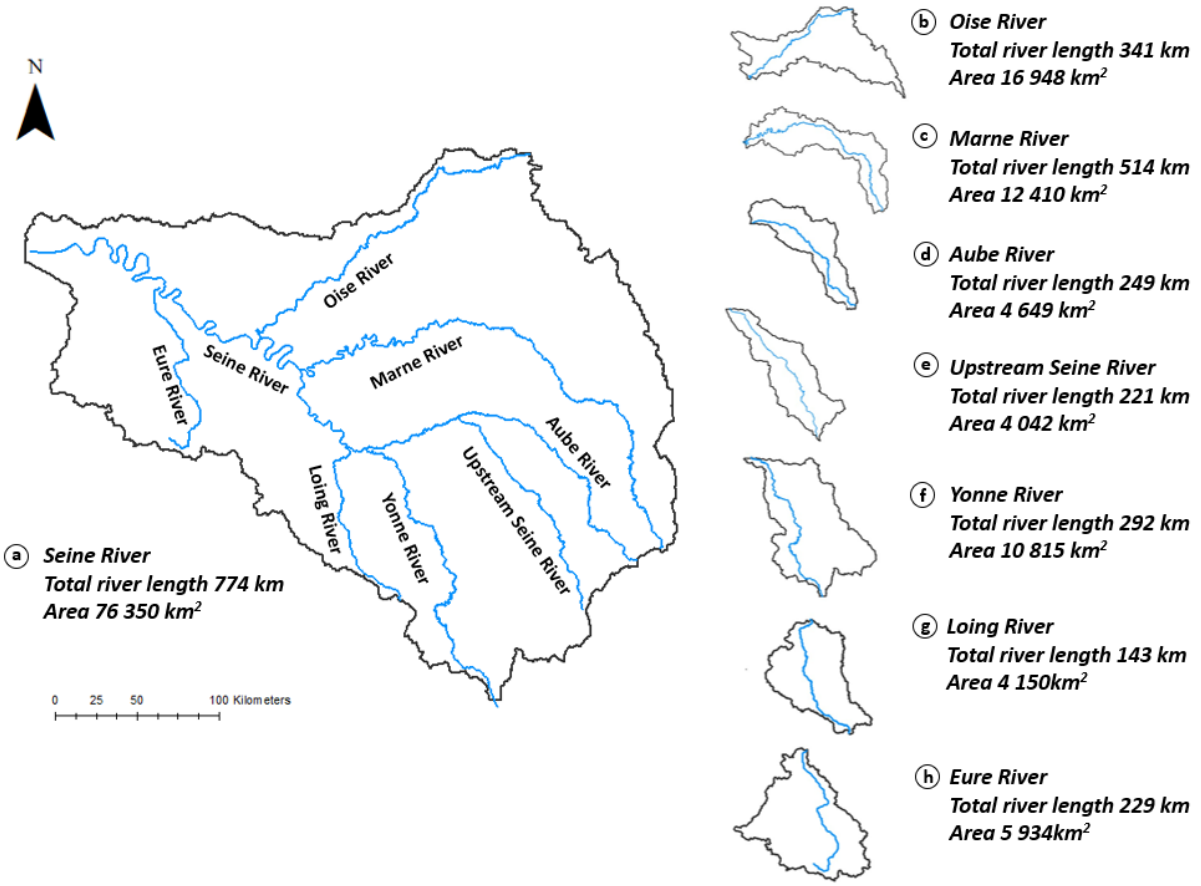

Figure 6.6. The Seine River catchment, sub-catchment and main tributaries area and length.

6.2.2 Long river profiles of the Seine and its major tributaries

Longitudinal river profiles show the elevation of the river against its length. As described before, each river of the Seine catchment has a variable length, reflecting this variation on the profile shape. Differences in profiles from one river to another are found. Principally, the Eure River presents a sublinear shape whereas the Seine River and its other major tributaries exhibit a characteristics concave-upward profile (Figure 6.7). Elevations are variable, ranging between 0 m and 530 m. Deviations in the shape of longitudinal river profiles may reflect signals of climatic or tectonic influence. Also, some breaks in the slope are observed and led suppose a location of knickpoints that may occur at changes in bedrock lithologies. In the upper part of the Yonne River a prominent break in the longitudinal profile is observed and it is linked to a transition in bedrock lithologies and the influence of the presence of the Pannecière dam, located near of the Corancy at ~50 m from the break. Finally, some artifacts errors generate perturbations on longitudinal profiles. I.e., downstream of Seine River, from km 450 to its outlet, some steps perturbations are observed and may be due to DEM processing.

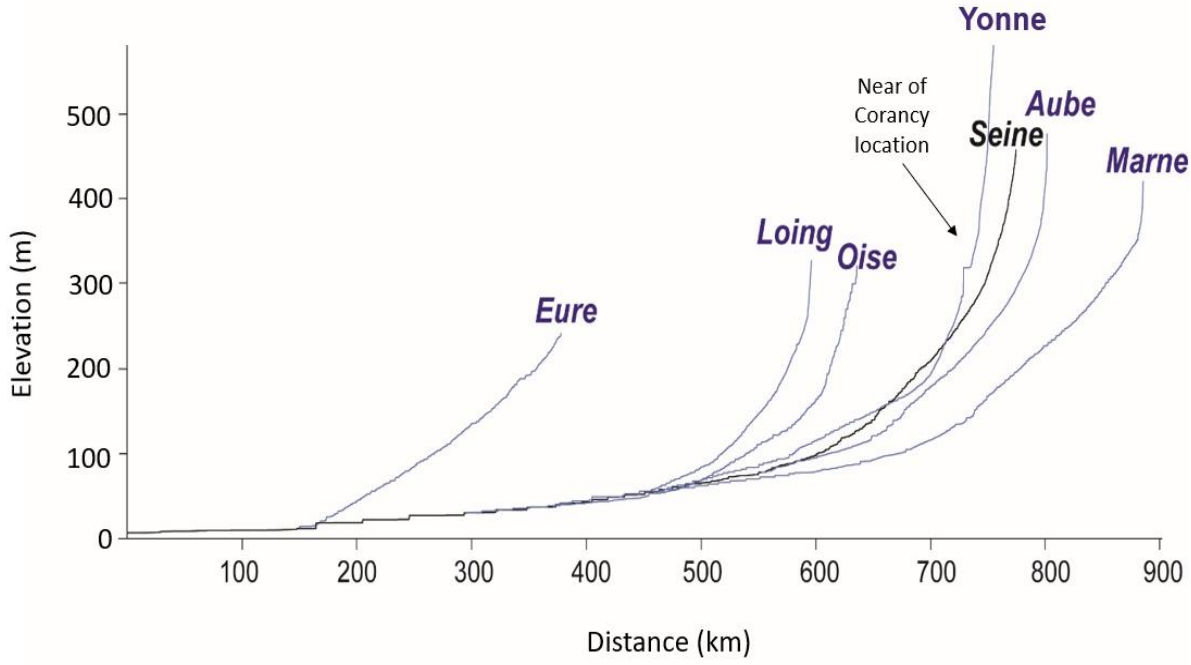

Figure 6.7. Longitudinal river profile of the Seine River and its major tributaries from BD Carthage interpolate with the 75-m resolution DEM (see section 6.1.2-b).

6.2.3 Normalized profiles

Normalized longitudinal profiles and their concavity factor (Cf) were extracted for all the main rivers draining the Seine catchment. The general concavities values for the seven selected rivers are all positive, the analysis of longitudinal profiles for the Seine, Oise, Marne, Aube, Yonne and Loing rivers is defined as concave whereas the Eure River provided a sub-rectilinear profile (Table 6.1 and Figure 6.8). The values of concavity factor (Cf) vary between 7.45 % (Eure River) and 68.21 % (Seine River). The maximal concavity values (Cmax) are between 0.06 (Eure River) and 0.56 (Seine River) while its distance from the source (Lmax) always ranges between 0.17 (Oise River) and 0.36 (Marne River) and is always located in the upper half of the longitudinal profiles. In the Seine catchment, the longest rivers, such as the Seine River, tend to display the highest concavity values. To compare the Seine River with other ones, it was divided into two parts (i) upstream Seine until the Aube confluence and (ii) downstream Seine after the Aube confluence (Table 6.1).

Table 6.1. Normalized longitudinal profiles parameters along the Seine catchment.

Stream	Stream lenght (km)	Concavity factor C_f (%)	Maximal concavity Cmax	Distance from the source Lmax
Seine	774	68.21	0.56	0.23
Upstream Seine	221	43.98	0.32	0.26
Downstream Seine	553	28.11	0.24	0.33
Oise	341	53.71	0.49	0.17
Marne	514	51.43	0.42	0.36
Aube	249	49.39	0.35	0.22
Yonne	292	62.88	0.53	0.18
Loing	143	46.95	0.35	0.27
Eure	229	7.45	0.06	0.28

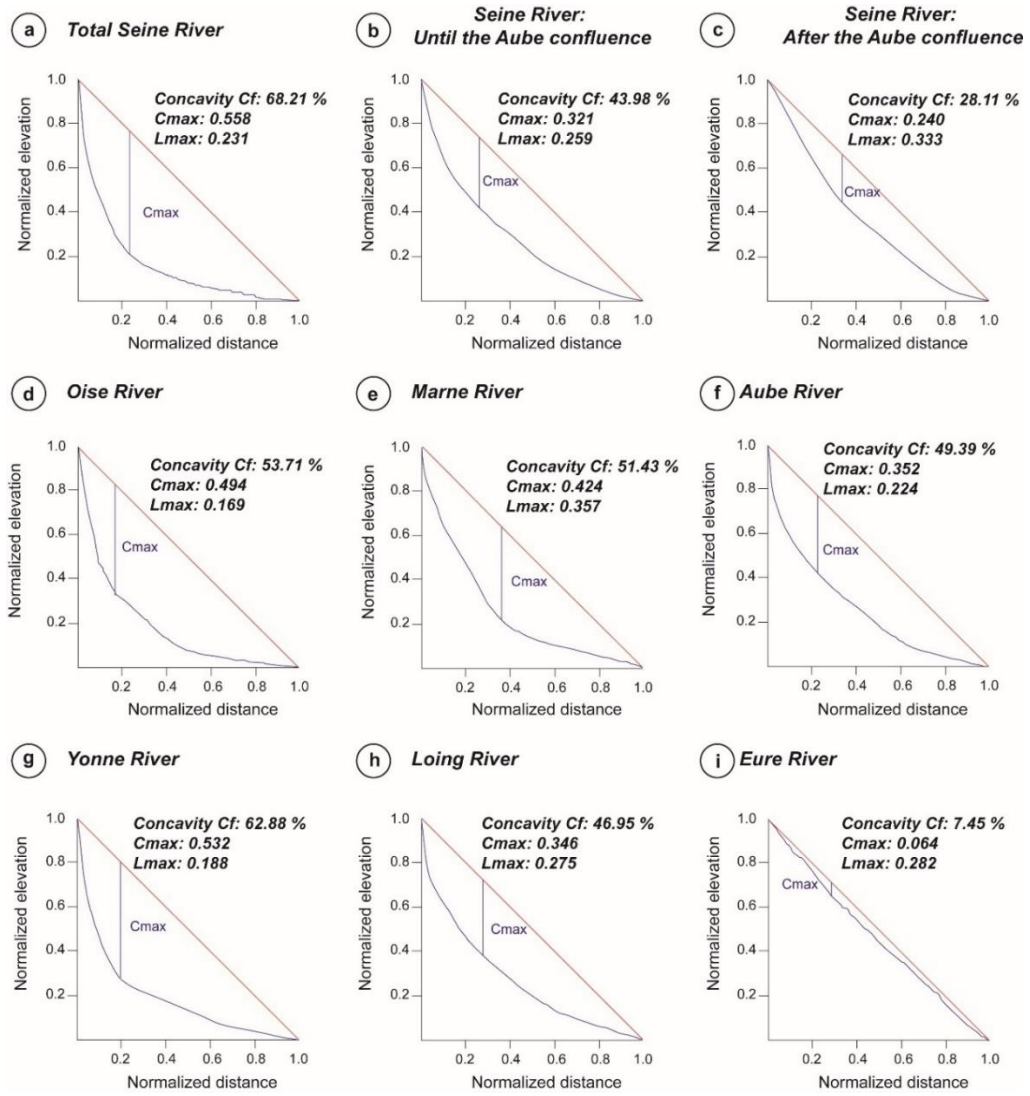

Figure 6.8. Normalized longitudinal profiles of the Seine catchment. The Concavity factor (Cf), the maximal concavity (Cmax) and its distance from the source (Lmax) refer to the state of the valley equilibrium.

To compare the river longitudinal profiles and to identify similar patterns between them, Lmax was plotted i) against Cmax and ii) against Cf. Three cluster were discriminated in the drainage system data on the Lmax against Cmax scatter plot (Figure 6.9). Cluster S1 includes the Seine, Oise and Yonne rivers with concavity (Cf) values ranging from 68.88 and 53.71 %, Cmax values ranging from 0.56 and 0.49 and are closer to the source with values of Lmax comprises between 0.17 and 0.23. Cluster S2 includes the Upstream Seine (until the Aube confluence), Marne, Aube and Loing rivers with Cf values ranging from 51.43 and 46.95 %, Cmax values ranging from 0.42 and 0.35 respectively. Their Lmax are positioned in the middle part section of the longitudinal profiles, with Lmax values between 0.22 and 0.36. Finally, cluster S3 is opposed to S1 and S2. It includes the Eure River with Cf value of 7.45 %, Cmax value of 0.06 and Lmax value of 0.3.

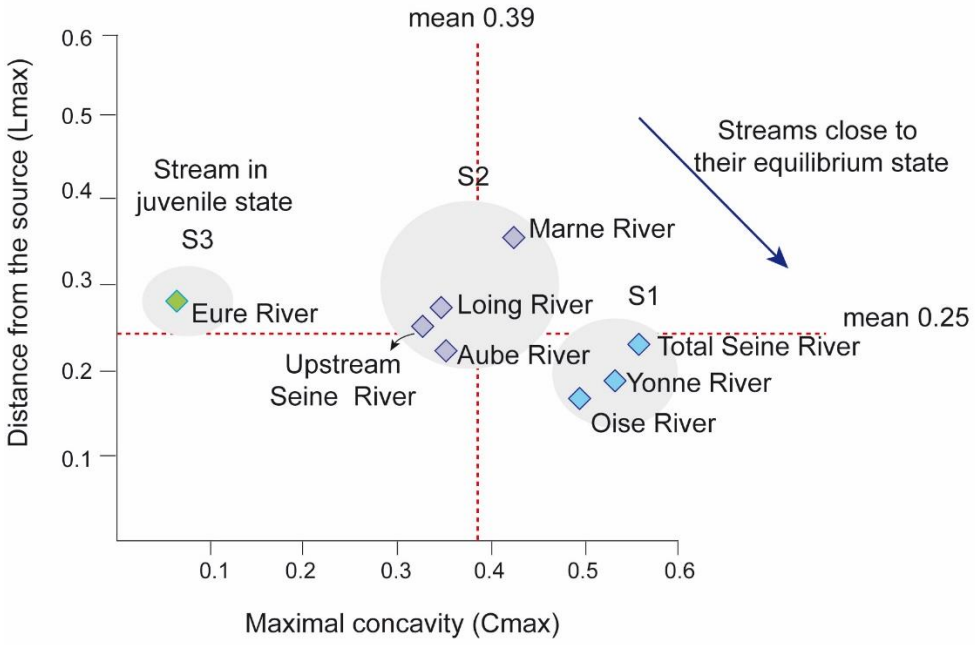

Figure 6.9. Scatter plot of maximal concavity (Cmax) and distance from the source (Lmax) values. River profiles statistical parameters are clustered into three groups S1, S2 and S3.

In contrast, on the Lmax versus Cf plot, no clear clusters are identified except for the Eure River, located apart from the other rivers. Indeed, other rivers have a Lmax situated close to the valley-head such as the total Seine River, Yonne, Oise, Marne, Aube and Loing rivers are close to their equilibrium state while the Eure River is close to the outlet, pointing to a juvenile state (Figure 6.10).

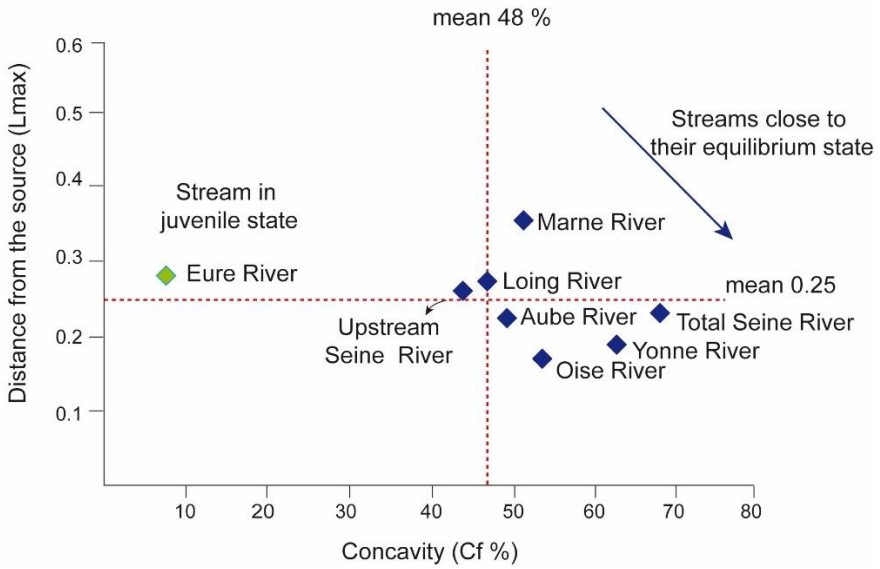

Figure 6.10. Scatter plot of distance from the source (Lmax) values and concavity factor (Cf %) in the Seine catchment.

6.2.4 Longitudinal valley centerline of the Seine River and major tributaries with regards to bedrock lithology

To assess the bedrock lithology influence on the river longitudinal profiles, lithologic changes were plotted along the valley centerline profiles (Figure 6.11). In general, the valley centerline profiles show abrupt slope at the transition between lithologies. The higher slopes mainly occur at the transition between Upper Jurassic limestones and marls and the Cretaceous chalk with values ranging from 1.27‰ to 2‰ (Figure 6.11-a-c-d-e). In the Oise valley at the transition between the Cretaceous chalk and the Cenozoic sand, slopes of 1.41‰ and 0.31‰ are observed (Figure 6.11-b). In the Loing valley at the transition between the Cretaceous clay and the Cretaceous chalk from slopes of 3.84‰ to 1.39‰ (Figure 6.11-f). In the Eure valley at the transition between the Cretaceous chalk and the Cretaceous clay slopes are of 1.18‰ and 0.72‰ (Figure 6.11-g). While lower slopes tend to occur downstream of valley profiles at the transition between Cretaceous chalk and Cenozoic sands, clays, marls and limestones, with values ranging from 0.11 to 4‰ (Guillocheau et al. 2000b) (Figure 6.11-from-a-to-g).

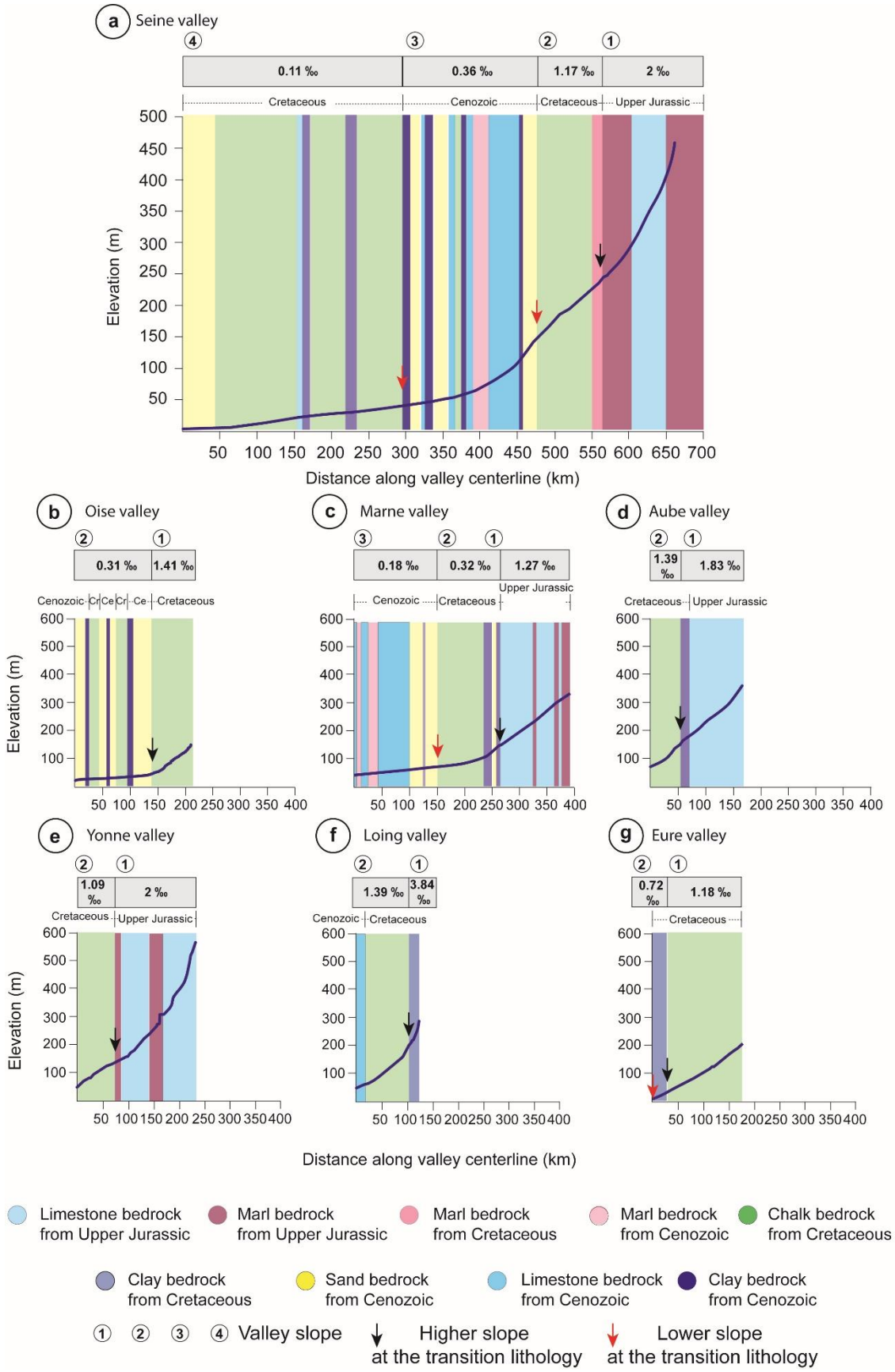

Figure 6.11. Longitudinal centerline profiles along the Seine River and its main tributaries and main along profiles bedrock lithologies identified. Cr and Ce refers to Cretaceous and Cenozoic bedrock.

6.2.5 Valley width of the Seine and major tributary valleys with regards to bedrock lithologies

To further assess the influence of bedrock lithology, the valley widths were plotted considering the valleys distance from upstream to downstream. These data show different variations in valley width considering the bedrock lithologies (Figure 6.12). Valleys are narrower in areas where they cut into Upper Jurassic limestones and marls bedrock (Figure 6.12-a-c-d-e) or at the confluence with the Oise and Loing River (Figure 6.12-b-f). In contrast, the widest valleys are observed at the confluence between the Seine valley with the Oise, Marne, Aube, Yonne and Eure rivers (Figure 6.12-a) or when rivers cuts chalk bedrock from Cretaceous (Figure 6.12-from-a-to-e) and sand, clay, marl bedrock from Cenozoic (Figure 6.12-a-b-c-d-e-g).

As explained before, valley width is variable:

- When valleys cut the Upper Jurassic limestone and marls bedrock valleys are narrower. Widths range from 38 to 1600 m in the Seine valley (the first 104 km, Figure 6.12-a), from 22 to 1500 m in the Marne valley (the first 134 km, Figure 6.12-c), from 47 to 1834 m in the Aube valley (the first 96 km, Figure 6.12-d), and from 27 to 3340 m in the Yonne valley (the first 161 km, Figure 6.12-e).
- Widest valleys tend to occur when valleys cut into the Cretaceous chalk and clay bedrock. In chalk bedrock, widths in the Seine valley (Figure 6.12-a) varies from 1300 to 11200 m between km 104 and km 235 and from 527 to 10200 m between km 404 to the Seine outlet. In the Oise valley (Figure 6.12-b), widths vary from 123 to 2621 m the first 80 km, from 767 to 4700 m between km 122 and km 138, from 590 to 4118 m between km 171 and km 186. In the Marne valley (Figure 6.12-c), widths vary from 624 to3737 m between km 269 and km 253. In the Aube valley (Figure 6.12-d), widths vary from 1085 to 3572 m between km 119 until the confluence with the Seine River. In the Yonne valley (Figure 6.12-e), widths vary from 673 to 6045 m between km 161 until the confluence with the Seine River. In the Loing valley (Figure 6.12-f), widths vary from 11 to 1870 m in the first 104 km. In the Eure valley (Figure 6.12-g), widths vary from 78 to 2214 m in the first 146 km. In clay bedrock, widths vary in the Marne valley (Figure 6.12-c) from 2340 to 8010 m between km 134 and km 269. In the Aube valley (Figure 6.12-d) from 2005 to 6985 m between km 96 and km 119. In the Eure valley (Figure 6.12-g) widths vary from 999 to 3717 m between km 146 until the confluence with the Seine River.
- Valley widths are more variable when valleys cut into limestone, sand, marl and clay bedrock from Cenozoic. In the Seine valley (Figure 6.12-a), width vary from 241 to 5743 m

between km 235 and 404 km. In the Oise valley (Figure 6.12-b) width vary from 1060 to 7684 m between km 80 and 122 km, from 664 to 4700 between km 138 and km 171 and from 530 to 1800 m between km 186 until the confluence with the Seine River. In the Marne valley (Figure 6.12-c), width vary from 256 to 3116 m between km 253 until the confluence with the Seine River. In the Loing valley (Figure 6.12-f), width vary from 622 to 2010 m between km 104 until the confluence with the Seine River.

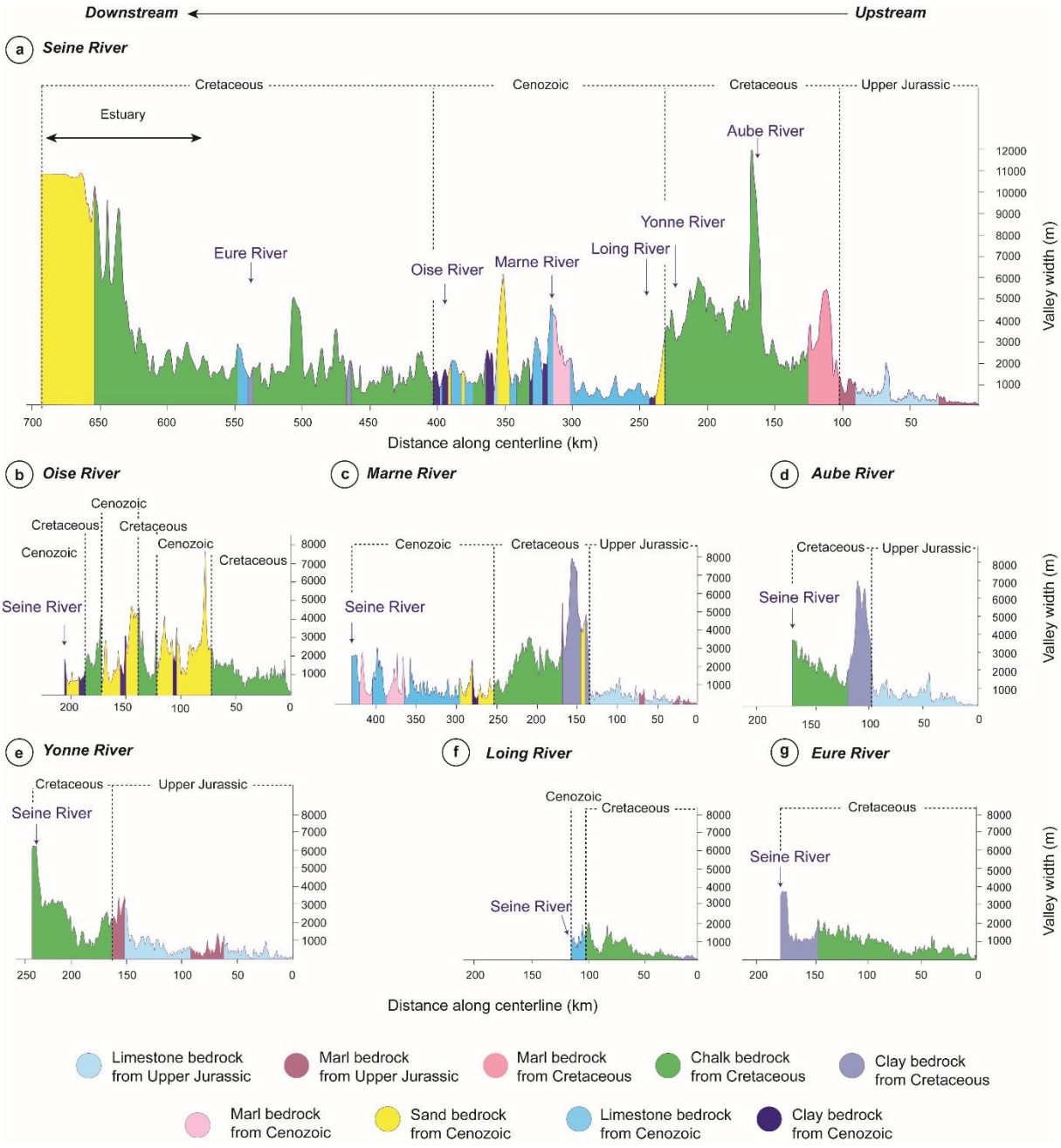

Figure 6.12. Valley width as a function of distance for the Seine catchment. Colors indicates the bedrock lithology crossed by each river. Distance is measured in kilometers from upstream to downstream; valley width is measured in meters.

6.2.6 Valley width versus drainage area

As described before, valley widths in the Seine catchment are highly variable when valleys cut into different bedrock lithologies. It is well known that bedrock lithologies influence in valley width but also river discharge can exert control on valley width. In order to know the impact of these parameters, here we analyse the valley width and drainage area along the catchment considering the main bedrock lithologies. Previous research established a power-law relationship considering these parameters (Snyder et al., 2003; Brodcard and Van der Beek, 2006; May et al., 2013; Schanz and Montgomery, 2016; Langston and Temme, 2019; Clubb et al., 2022). This power-law is given by the equation 6.1.

$$Wv = KvA^{c} \qquad \text{Equation 6.1}$$

where Wv is the valley bottom width, Kv is a coefficient that describes lithological control on widening, A is the drainage area (a proxy for river discharge), and c is an exponent that describes how quickly valley width increases with increasing in drainage area.

To apply the power-low relation along the Seine catchment, we plot the valley width against its drainage area considering the main bedrock lithologies. Five main lithologies were selected: limestone and marl from Upper Jurassic and Cenozoic, chalk from Cretaceous, and finally sand and clay from Cenozoic. In these lithologies valley widths varies substantially.

In the literature, due to the strong dispersion of data points, the correlation coefficient R^2 is usually low. We have thus constrained values of c and Kv parameters for different bedrock lithologies using only $R^2 > 0.1$. When applying the power-law fit for the different lithologies, we found values for c exponent and Kv as: 0.156 and 288.51 in chalk bedrock (Figure 6.13-a), 0.240 and 65.16 in limestones (Figure 6.13-b), 0.399 and 20.09 for marls (Figure 6.13-c), 0.128 and 438.02 for clays (Figure 6.13-d), and 0.017 and 1272.1 for sands (Figure 6.13-e). We found that there was generally a good confidence in measure between width and drainage area for limestone and marls, the goodness of fit is $R^2=0.15$ respectively. In contrast, chalk, clays and sands showed a poor-goodness of fit varies between $R^2=0.087$, $R^2=0.0004$ and $R^2=0.014$ respectively.

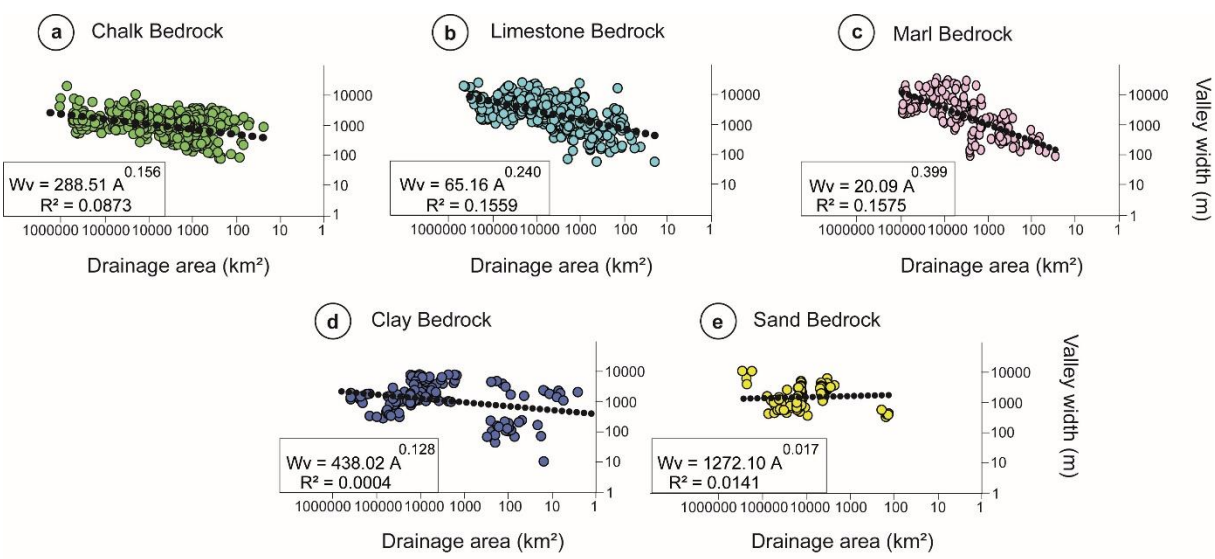

Figure 6.13. Valley width as a function of drainage area for the main bedrock lithologies and associated Valley width/Drainage area power laws calculated.

In order to determine more accurately the influence of bedrock lithologies in *c* exponent, the five main lithologies were subdivided according to their geological depositional ages (Figure 6.14). In chalk bedrock, a remarkable trend is observed. When considering the chalk bedrock from Santonian the *c* exponent is 0.263 (Figure 6.14-a). These data have a confidence in measure with R^2=0.12, similarly to those obtained in previous research (Brodcard and Van der Beek, 2006; Langston and Temme, 2019; Clubb et al., 2022). Also, lower values of *Kv* were determined at 44.58 and 64.06 respectively. In contrast, data from Coniacian and Campanian chalk bedrock have a *c* exponent between -0.017 and 0.069 respectively, with a poor-goodness of fit between R^2=0.006 and R^2=0.081 and higher values in *Kv* between 1828 and 936 (Figure 6.14-b-c).

In limestones from Upper Jurassic, the *c* exponent is 0.36, with a confidence in measure of R^2=0.21 and *Kv* value of 24.64 (Figure 6.14-d). Conversely, a negative relation in valley width and drainage area was found in limestones from Cenozoic with a *c* exponent of -0.05, with a poor-goodness of fit R^2=0.0057 and highest *Kv* value of 1468 (Figure 6.14-e). Marls from Upper Jurassic have a *c* exponent of 0.55 with a confidence in measure of R^2=0.13 and lower *Kv* value of 6.58 (Figure 6.14-f). In contrast, marls from Cretaceous and from Cenozoic have a negative relation in *c* exponent of -0.32 and -0.09 respectively with a R^2=0.49 and R^2=0.062, and highest *Kv* values between 38975 and 2705 respectively (Figure 6.14-g-h).

Finally clays from Cretaceous and Cenozoic have a *c* exponent of 0.40 and -0.04, with a poor-goodness of fit R^2=0.063 and R^2=0.11, with higher *Kv* values comprises between 3828 and 1993 (Figure 6.14-i-j).

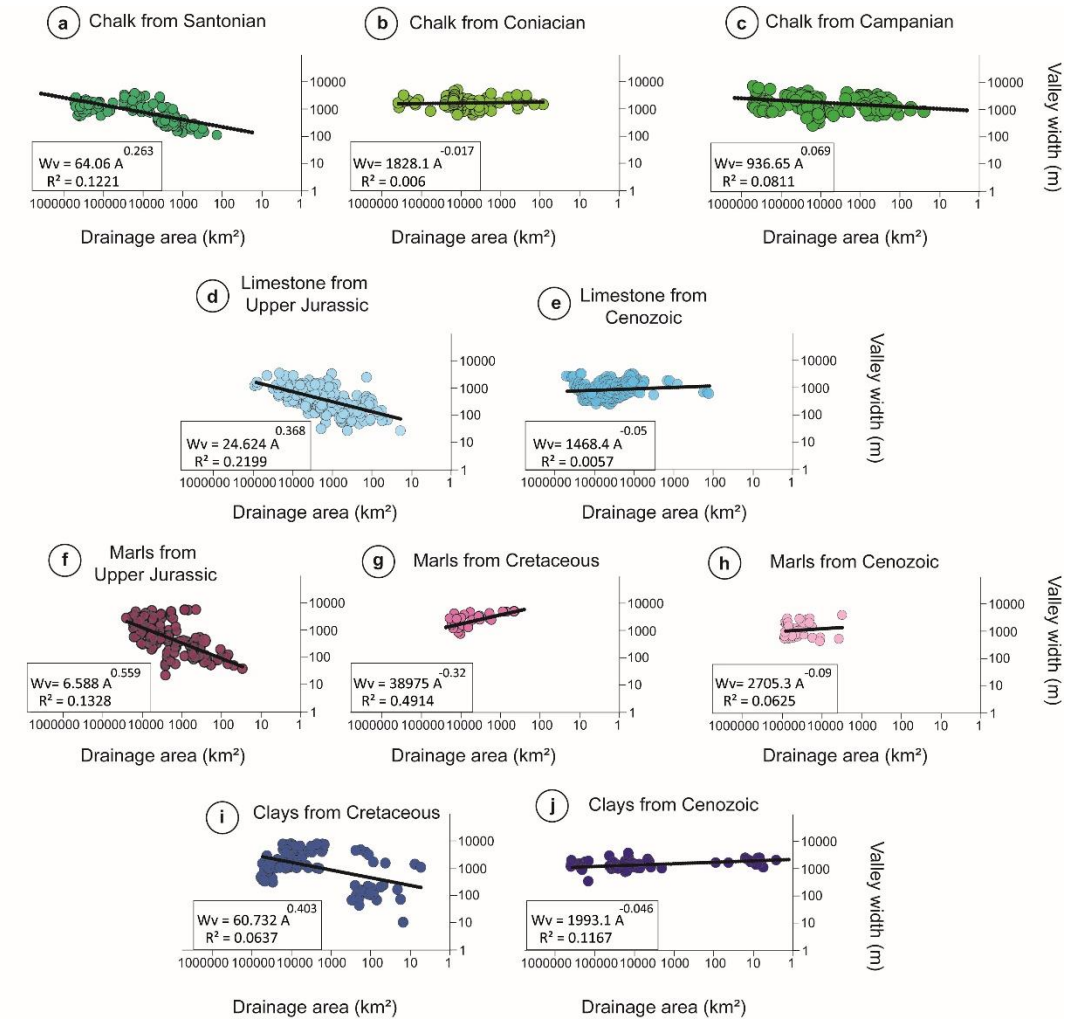

Figure 6.14. Details in valley width as a function of drainage area considering different geological intervals for the same lithology.

To summarize, the Table 6.2 shows the values calculated considering the different bedrock lithologies, the retained values are showed in bold. In this work we retained these values because they show a coherence with data disponible in previous studies (Brodcard and Van der Beek, 2006; Schanz and Montgomery, 2016; Langston and Temme, 2019; Clubb et al., 2022).

Table 6.2. Values of *Kv*, c exponent and R^2 for the main bedrock lithologies. The retained values are showed in bold and have a $R^2 > 0.1$.

Geological stage			Bedrock lithology	*Kv*	*c* exponent value	R^2
Cenozoic			Clay	1993.1	-0.046	0.1167
			Sand	1272.1	0.018	0.0141
			Limestone	1468.4	-0.05	0.0057
			Marl	2705.3	-0.09	0.0625
Cretaceous	Maastrichtian		Chalk	174.28	0.15	0.082
	Senonian	Campanian		936.65	0.069	0.0811
		Santonian		***64.09***	***0.26***	***0.1221***
		Coniacian		1828.1	-0.017	0.006
	Turonian			4793.4	-0.12	0.3826
	Cenomanian			112356	-0.42	0.3743
	Cretaceous marls		Marl	38975	-0.32	0.4914
	Cretaceous clays		Clay	60.73	0.40	0.0637
Upper Jurassic			Limestone	***24.62***	***0.36***	***0.2199***
			Marl	***7***	***0.55***	***0.1328***

6.2.7 Valley width and relation to river longitudinal profile elevation

In order to know the influence of elevation in valley width, we plot the valley width as a function of the longitudinal profile elevation (Figure 6.15). In the Seine catchment, the maximum elevation is about 572 m, with a mean of 125 m and a minimum of -4 m. At elevations comprises between 572 and 236 m, valleys tend to be narrower (valleys width between 11 and 1988 m) and are in general more stepper (see Figure 6.11 and Figure 6.15). Then, at elevations between 236 and -4 m, valleys are wider (valleys width between 45 and 10283 m) and slope decrease. These increase in valley width at these lower elevations reflect the increase in drainage area going downstream in the catchment (see Figure 6.11 and Figure 6.15).

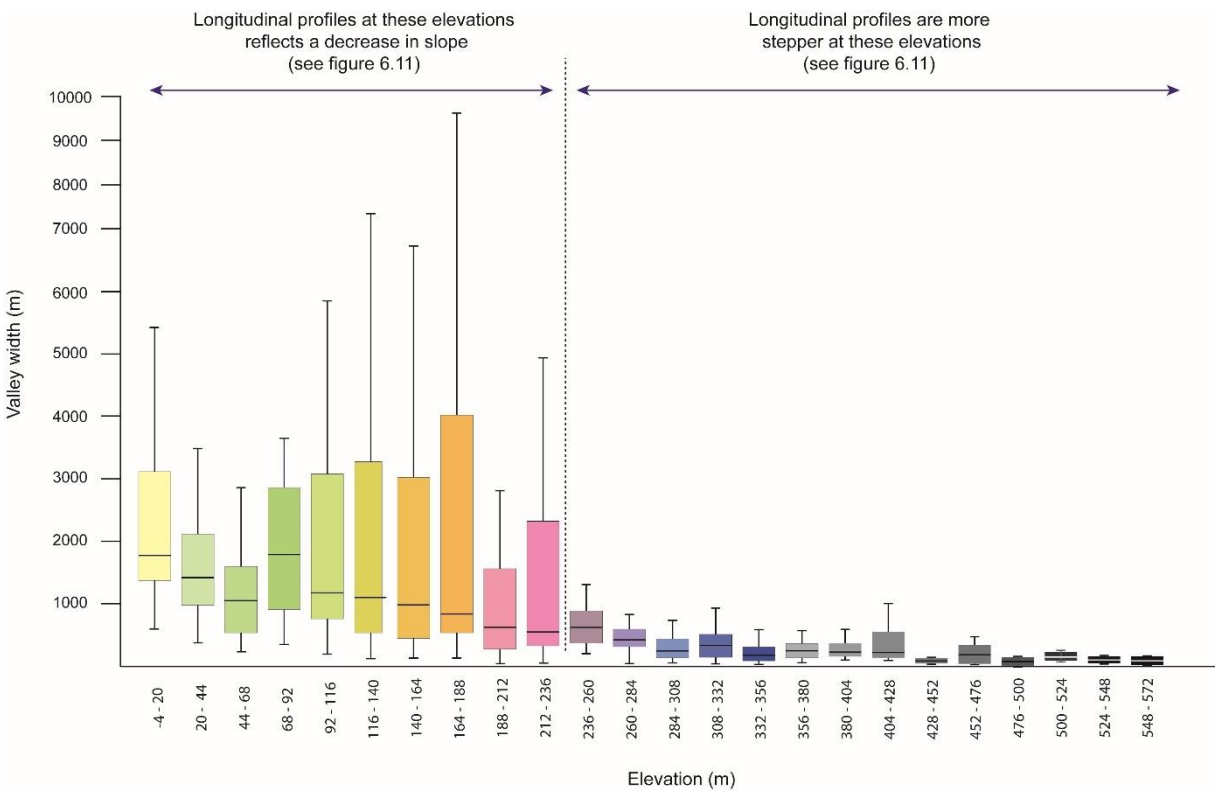

Figure 6.15. Box plots of valley width considering the elevation along the Seine catchment. The central black line indicates the median. The bottom and the top of the box indicate the 25th and the 75th quartiles. Box color indicate the gamma in elevation.

6.3 Discussion

6.3.1 Longitudinal profiles

The results obtained in longitudinal profiles show that the main rivers of the Seine catchment (Seine, Oise, Marne, Aube, Yonne and Loing rivers) present a concave-up shape in profiles, except for the Eure River, which has a sub-rectilinear shape profile.

Considering results in maximal concavity (Cmax, Figure 6.9), three main clusters were identified. The first group S1 formed by the total Seine, Oise and Yonne rivers displays well graded profiles (characterized by high values in Cmax and relative low values in Lmax). The second group formed by Upstream Seine, Marne, Aube and Loing rivers, with still graded profile, though slightly less concave profiles (characterized by intermediates values in Cmax and in Lmax). This could suggest that these profiles are moving towards to their equilibrium state. Finally, the third group S3 is formed by the Eure River (characterized by lower value in Cmax and intermediate value in Lmax), suggesting that this river is in the juvenile stage. In contrast, doing the same analysis but considering the concavity factor (Cf, Figure 6.10) for the

Seine, Oise, Marne, Aube, Yonne and Loing rivers, is more difficult to identify different clusters. The concavity analysis could suggest that these rivers are close to their equilibrium, except for the Eure River which would still be in the juvenile state. The Seine catchment is characterized by a lower tectonic influence. One of the mechanisms that could influence the shape of profiles is the bedrock uplift, which could be slightly more important to the South-East of the Seine catchment in relation to far alpine compression (Guillocheau et al., 2000). It remains however complex to have a definite answer because of the influence of bedrock lithology changes in the slope of valley long profiles (Figure 6.11).

6.3.2 Influence of bedrock lithology

Changes in slope at the main bedrock lithological transitions were observed along valley centerline profiles suggesting a strong impact of bedrock lithology. Also, bedrock lithology along the Seine catchment influences the width of the valley bottom. Valleys tend to be wider in chalk, clay or sand lithologies or at the junctions between tributaries. It is exemplified upstream of the chalk cuesta (Figure 6.16), where valleys widen above clay bedrock (i.e., Gault Formation). In contrast, narrowest valleys generally occur along the limestone lithologies (e.g., downstream of Fontainebleau; Figure 6.16).

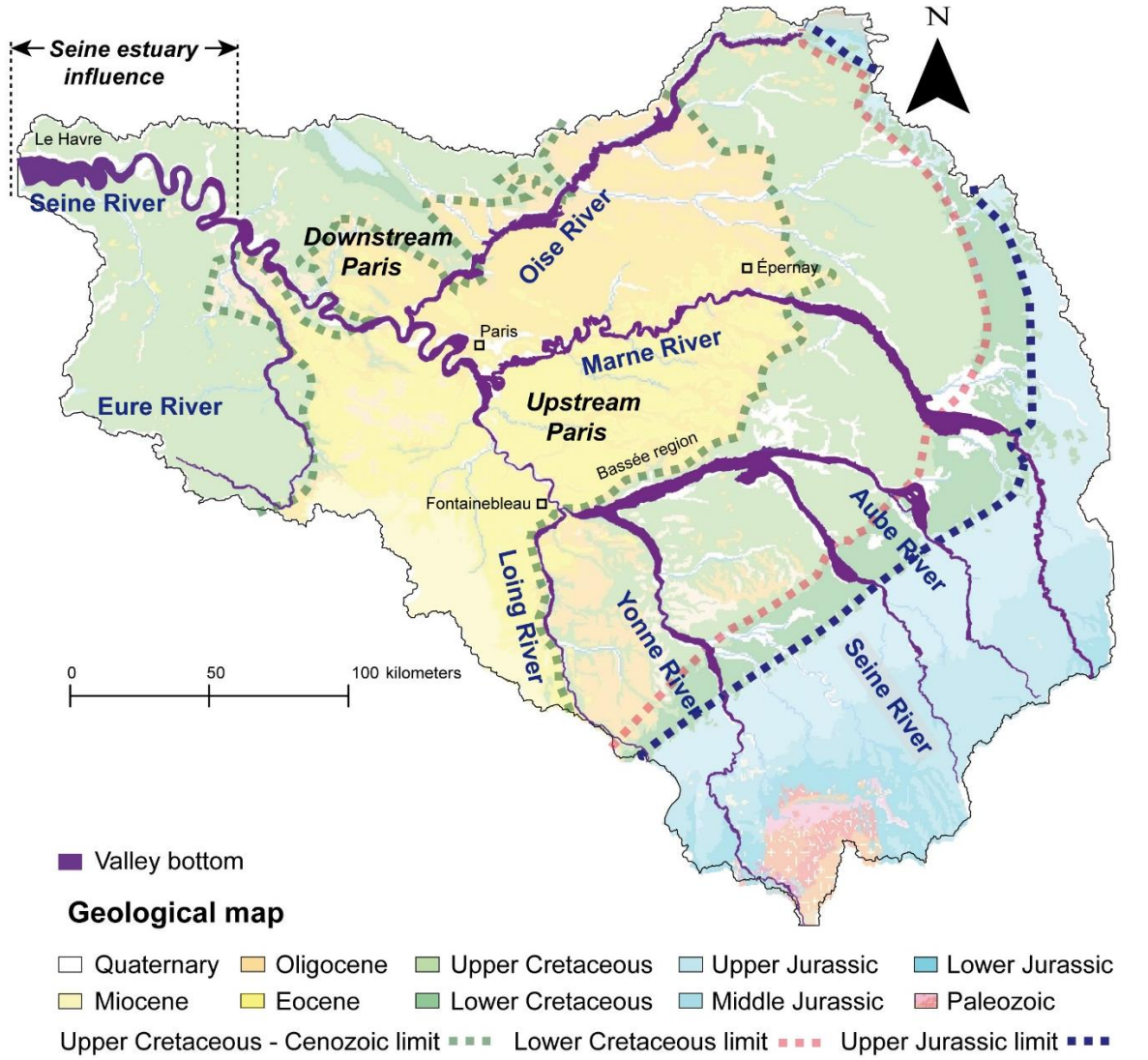

Figure 6.16. Valley bottom polygon within the Seine catchment.

Overall, the valley width increases with drainage area (i.e., a proxy for discharge) along the Seine valley and its tributaries. One of the two parameters in the power-law function is represented by the *c* exponent, which describes how quickly valleys width increase with drainage area (Brocard and Van Der Beek, 2006; Langston et al., 2019). Previous studies have found different *c* exponent values considering bedrock lithology. Brocard and Van Der Beek (2006) and Langston et al., (2019), report small *c* exponents for resistant lithologies and strong *c* exponents with less resistant lithologies. The trends of valley width increase with drainage area is presented here within the Seine catchment, providing an interesting comparison with existing data that mostly originate from orogenic settings. Different *c* values were thus calculated for the main lithologies such as chalk, limestone and marls.

When considering all database acquired in this work for marl bedrock lithology, the value of the *c* exponent is 0.39. This value is similar to those obtained for the marl lithology from the Upper Jurassic along the Roanne River, near at the confluence with the Drome River (South of France). With a *c* exponent value of 0.42, they were classified as a soft lithology (Brocard and Van Der Beek, 2006; Langston et al., 2019). In detail, when considering only the data for marls from the Upper Jurassic, we found a *c* value of 0.55. Finally, and in agreement with the observed wide valley upstream of the chalk cuesta, clay from the Lower Cretaceous returned a *c* exponent value of about 0.4, although with a low R^2 (0.06).

Limestone from Upper Jurassic in Roanne River is classified as hard lithology by Brocard and Van Der Beek (2006), with a *c* exponent value of 0.18. In contrast, Langston et al. (2019), classified the dark marly limestone in the same unit as intermediate lithology with a *c* exponent value of 0.26. In the Seine, when considering all limestone lithologies the *c* exponent value is 0.24 while it is ca. 0.16 for the whole chalk lithology, although with a low correlation coefficient (0.09). These lithologies could thus be considered as intermediate and hard, respectively. When taken separately, limestones from the Upper Jurassic yield *c* value of 0.37 in the Paris Basin, which would correspond to a soft lithology. This can be explained by the differences in sedimentary facies. The Tithonian of the Alps is composed of reef to slumped platform deposits, well-known for their thickness of several hundreds of meters and strength that makes it easily identifiable in the landscapes. In the Paris basin, the Tithonian is much thinner and less resistant. Additionally, this suggests that it is the Cenozoic limestones that may be considered as a hard lithology, as exemplified downstream of Fontainebleau. Unfortunately, no clear *c* exponent value was found for this lithology. Finaly, the Santonian chalk bedrock may thus be considered as an intermediate lithology (*c* exponent value of 0.26). The variability observed in the chalk bedrock can be explained by its original lithologic variability of by secondary diagenesis processes (Lasseur, 2007; AGBP, 2014).

Unfortunately, we did not find a clear relation in *c* exponent value for marl and clay from the Cenozoic and chalk from the Coniacian and Campanian (Figure 6.14-b-c). The poor constraint on these *c* exponent value is due to the limited distribution of data, particularly the lack of data for high values of drainage area.

Previous studies showed that wider valleys tend to occur in less resistant lithologies and narrow valleys in more resistant lithology (Lave and Avouac, 2001; Montgomery, 2004; Spotila et al., 2015). In the Seine catchment, valleys are overall narrower in Cenozoic limestone and wider in Cretaceous clay. Interestingly, the *c* exponents from this study are consistent with those from the literature, in particular those from the French Alps (Brocard and Van Der Beek, 2006;

Langston et al., 2019) (Figure 6.13). Because these similar results are found in very different tectonic settings, it suggests that valley widening may be independent from uplift rate. Such assertion seems in contradiction with recent findings by Clubb et al. (2022). One may note however that the mechanism they invoke for valley widening is aggradation above a V-shape valley. Such configuration does not apply to the Paris basin, where valleys are not V-shaped and where valley bottom aggradation is overall limited, as will be shown in the next section. Only in the Bassée region or in the estuary -where valley are exceptionally wide (Figure 6.12 a)- could sediment deposition have an additional impact on valley width.

6.4 Conclusion

A novel method for the delimitation of valleys bottoms were determined along the Seine catchment. This approach coupling with the database acquired in chapter 5, provides a new opportunity to explore how the geomorphic parameters such as valley width, drainage area, and bedrock lithology influence on the valley bottom geometry in the Seine catchment characterized by a low tectonic influence. The relationships in valley width and drainage area are different for the main bedrock lithologies. This study allowed to determine the properties in different lithologies using the power-law. As expected, valley widths along the Seine catchment tend to increase with increasing in discharge, but also, when increasing in bedrock erodibility or in sediment supply. However, the data presented in this chapter reflect the effect of bedrock heterogeneity throughout the study area.

Chapter 7: Alluvial infill within the valley bottom of the Seine catchment using the kriging method

Ce chapitre présente la méthode du krigeage basée sur les équations différentielles partielles stochastiques (SPDE), avec un intérêt particulier pour le remplissage alluvial dans le fond de vallée. Ce chapitre est divisé en deux parties, la première partie (section 7.1) correspond à un manuscrit soumis à *Mathematical Geology*, dans lequel la méthode du krigeage a été testée le long de la vallée de l'Oise. La deuxième partie (section 7.2) montre les résultats du krigeage appliqués à l'échelle du bassin-versant de la Seine, dans l'objectif de (i) déterminer à grande échelle l'épaisseur des alluvions, (ii) quantifier le volume de sédiment stocké dans le fond de vallée et (iii) déterminer l'altitude du substratum rocheux de la Seine sous les alluvions.

Chapter 7

7 Alluvial infill withing the valley bottom of the Seine catchment using the kriging method

This chapter introduces the kriging method based on Stochastic Partial Differential Equations (SPDE), with a specific focus on alluvial infill in the valley bottom. The first section (7.1) corresponds to a manuscript to be summited to *Matematical geology*, in which the kriging method was tested along the Oise valley. The second section (7.2) shows the results of the kriging method applied at the scale of the Seine catchment, with the aim of (i) estimating the large scale-geometry of alluvium thickness, (ii) quantifying the volume stored at the valley bottom and (iii) to determine the bedrock elevation of the Seine catchment below the alluvium.

7.1 Development of the method and test on the Oise valley

Kriging alluvial thicknesses in valley bottoms using nonstationary geometric anisotropies

Jean-Louis Grimaud[1*], Nicolas Desassis[1], Diana Chourio-Camacho[1], Didier Renard[1], Mike Pereira[1], Fabien Ors[1], Hélène Tissoux[2,3], Paul Bessin[4], Mark Noble[1]

[1] PSL University/ MINES Paris/ Centre de Géosciences, 35 rue St Honoré, 77305 Fontainebleau Cedex, France

[2] BRGM, 3 Avenue Claude Guillemin, BP 36009, 45060 Orléans, France

[3] Histoire Naturelle de l'Homme Préhistorique (HNHP), UMR 7194, Département « Homme et Environnement », Muséum National d'Histoire Naturelle, 1 rue René Panhard, 75013, Paris, France

[4] Laboratoire de Planétologie et Géosciences, UMR 6112, CNRS, Le Mans Université, Avenue Olivier Messiaen, 72085 Le Mans, CEDEX 9, France

7.1.1 Abstract

Modeling the geometry and volumes of alluvial infill at the bottom of river valleys is important for a better understanding of river dynamics and alluvial infill, which buffers sedimentary signal transmission from source to sink. This study introduces a method for estimating alluvial thickness geometries in the valley bottom using random fields with nonstationary geometric anisotropies based on Stochastic Partial Differential Equations (SPDE). These anisotropies are

constructed using the contours of the alluvial plain. The method is compared to the usual kriging approach, and the choices of parameters are explored in agreement with knowledge about the physics of alluvial rivers. Finally, the geological significance of the observed geometries is discussed.

It is found that the SPDE method has fewer uncertainties than the usual kriging approach and produces more realistic patterns. Evidence of braided patterns, riffle-pool geometry related to meandering, and scouring at confluences is observed at the scale of the valley width. Finally, it is estimated that about 1.4 ± 0.4 km^3 of alluvium is currently stored in the studied Oise valley bottom. Although the method was applied to an alluvial example, it could easily be adapted to other geological contexts where an anisotropy field can be estimated such as faulted and folded structures, supergene mineralization or environmental context to track pollutants dissemination in rivers.

7.1.2 Introduction

Reconstructing the geometry and volumes of alluvial infill at the bottom of river valleys is crucial for a comprehensive understanding of river dynamics and alluvial infill during the Late Quaternary (e.g., Pastre et al., 2000; Antoine et al., 2007; Bridgeland and Westaway, 2008). Additionally, assessing the volume of alluvium stored in alluvial plains is essential, as it reflects the landscape's capacity to temporarily store alluvium in the transfer zone, thereby buffering sedimentary signal transmission from source to sink (Castelltort and van den Driessche, 2003; Blothe and Korup, 2013). Recent studies have demonstrated that the geometry and incision dynamics of fluvial corridors are influenced not only by external forcings but also by bedrock lithology and total valley height (e.g., Grimaud et al., 2014; Langstone et al., 2019; Tofelde et al., 2022). A wide variety of tools are now available for measuring the planform geometry of valleys and terraces using digital elevation models (e.g., Clubb et al., 2017, 2022). In addition, a complementary approach involves reconstructing the full 3D geometry of alluvium (Blothe and Korup, 2013). This geometry can be estimated based on borehole data that reports alluvium thickness in valley bottoms, employing geostatistical methods such as kriging (e.g., Deleplancque et al., 2018)

Kriging techniques are widely employed in geosciences to ensure the spatial continuity of properties from referenced observations (Matheron, 1962, 1963; Chilès and Desassis, 2018). These techniques interpolate the value of a variable at a given location by employing a weighted

sum of observations of the variables at known locations. The weights consider the spatial structure of the data and the relative positions of the observations. Kriging has been successfully used to reconstruct alluvial bottom geometry from borehole data within the Seine River catchment, North France (Labarthe, 2016; Deleplancque et al., 2018). A current limitation of traditional kriging is the need to tune correlation ranges for a fixed regional direction and with fixed ranges. While suitable for nearly straight valleys (Deleplancque et al., 2018), this approach becomes problematic in sinuous valleys where the direction constantly changes, particularly in the case of elongated and narrow valleys. Consequently, the restituted alluvial thickness may exhibit an unrealistic corrugated geometry (Labarthe, 2016). This phenomenon is well-known; the use of regional variograms along a linear axis of anisotropy can lead to linear features (Seifert and Jensen, 2000). Instead, there is a desire for the kriging pattern to align with the average paleo direction of the flow that carved the valley.

In this study, we introduce a kriging method to restore alluvial bottom geometries, building on recent progress in modeling Gaussian random fields with nonstationary geometric anisotropies using stochastic partial differential equations (SPDE) (Lindgren et al., 2011; Fuglstad et al., 2015; Pereira et al., 2022). The method is tested along the Oise valley, a sinuous valley with frequent variations in bedrock lithology, located in the North of France. The resulting (i) bottom valley alluvium thickness and (ii) bedrock elevation maps are presented, along with their uncertainties, and discussed in relation to the Late Quaternary river dynamics of the study area.

7.1.3 Study area

The study area encompasses the Oise valley, situated in the northern region of France within the Paris Basin (Figure 7.1). Originating south of Chimay in Belgium, the Oise River is a 341 km long tributary of the Seine River. Our investigation concentrates on a approximately 180 km-long segment of the Oise River valley, spanning from its confluence with the Noirrieu River near Vadencourt to its junction with the Seine River in Conflans-Saint-Honorine. The Paris Basin, characterized as an intracratonic basin, underwent gradual subsidence during the Jurassic and Cretaceous periods (Guillocheau et al., 2000; Briais et al., 2018). The Late Cretaceous period was characterized by the extensive deposition of hundreds of meters of chalk in the Paris Basin (Lasseur, 2007; Figure 1). During the Paleogene, subsidence stopped, and rock uplift was limited (Guillocheau et al., 2000). It is interpreted as the result of Pyrenean compression phase, which is recorded in the form of several NW-SE folds in the study area (i.e., Vigny, Bray and

Margny anticlines, Artois bulge; Figure 7.1) (Wyns, 1980). Several Paleogene episodes of marine transgression and regression resulted in the deposition of alternating layers of conglomerates, sand and clays as well as limestones of either continental or marine origin within the Paris Basin (Pomerol, 1989; Huyghe et al., 2015). Such alternations are observed in the Oise valley above the Cretaceous chalk (Figure 7.1).

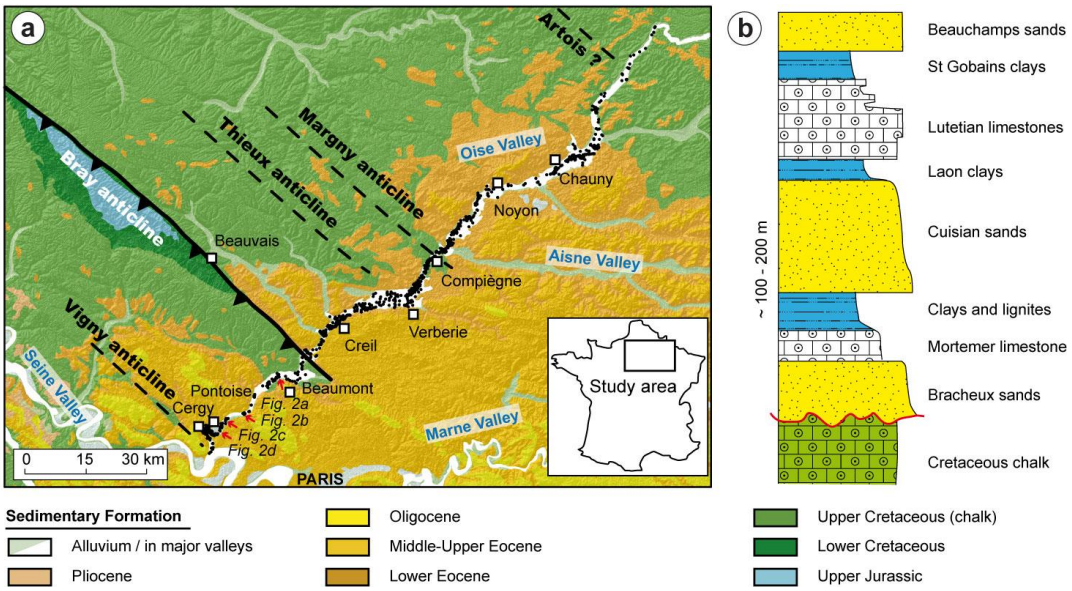

Figure 7.1. a) Geological settings of the study area from the 1/1000,000 geological map of France (Chantraine et al., 2003). The locations of boreholes (n=1010) are shown with black dots. b) Simplified sedimentary log of the Oise valley bedrock lithologies (after Maton et al., 2014).

Quaternary incision dynamics is largely influenced by climatic variations and moderate uplift in the study area (Larue, 2000; Cojan et al., 2005; Antoine et al, 2007). A long-term incision rate of 50-60 m/Ma is inferred from chronology of valley slope terraces, with fluvial erosion majorly occurring at the transition from interglacial to glacial periods (Antoine et al., 2007). In the Oise Valley, existing radiocarbon and Optically Stimulated Luminescence (OSL) dating is sparse, with the oldest known alluvium dating back to 32,750 years BP (Valladas, 1981, 1994; Audouze et al., 1981; Pastre et al., 1997, 2000, 2002; Larue, 2000; Granai, 2014; Blaser et al., 2017; Granai and Limondin-Lozouet, 2018) (Table 7.1). Consequently, it is likely that the geometries of the valley bottom and alluvium infill are largely inherited from the incision during the last glacial period and subsequent aggradation during the Tardiglacial and Holocene periods (Pastre et al., 1997, 2000; Krier, 2004; see Figure 7.2). Recent OSL dating of fluvial sands in

Maurecourt, located in the lower part of the Oise Valley, returned an age corresponding to Marine Isotope Stage 2 (MIS 2) (Blaser et al., 2015; Chourio Camacho, Chapter 3 in this volume), suggesting that Holocene deposits may be less widespread than originally thought by Krier (2004).

Table 7.1. Synthesis of existing ages in the Oise alluvial plain.

Location	Dating methods	Dated material	Age (ka)	Error (ka)	References
Boran-sur-Oise	radiocarbon	Wood stack	3.88	0.07	Krier, 2004
l'Isle-Adam	OSL	Fine sand	10.28	0.80	Blaser et al., 2017
			32.75	2.90	
Croix-Saint-Ouen	radiocarbon	Organic sediment	12.40	0.12	Pastre et al., 2000
Choisy-au-Bac	radiocarbon	Organic sediment	5.12	0.04	Granai and Limondin-Lozouet, 2018; Granai, 2014
Verberie	radiocarbon	Organic sediment	12.50	0.01	Pastre et al., 1997 (Audouze et al., 1981; Valladas, 1981, 1994)
	thermoluminescence	Silty sand	13.00	1	
Béthisy-Saint-Martin	radiocarbon	Organic sediment	11.14	0.10	
Bruyères	radiocarbon	Organic sediment	4.25	0.28	Larue, 2000
			10.28	0.11	
Les Epinières Houdancourt	radiocarbon	Plant remains	12.54	0.11	Pastre et al., 2002, 2004, 2005, 2006
		Wood	12.06	0.11	
		Wood	11.62	0.09	
		Plant remains	11.26	0.09	
		Peat	10.90	0.14	

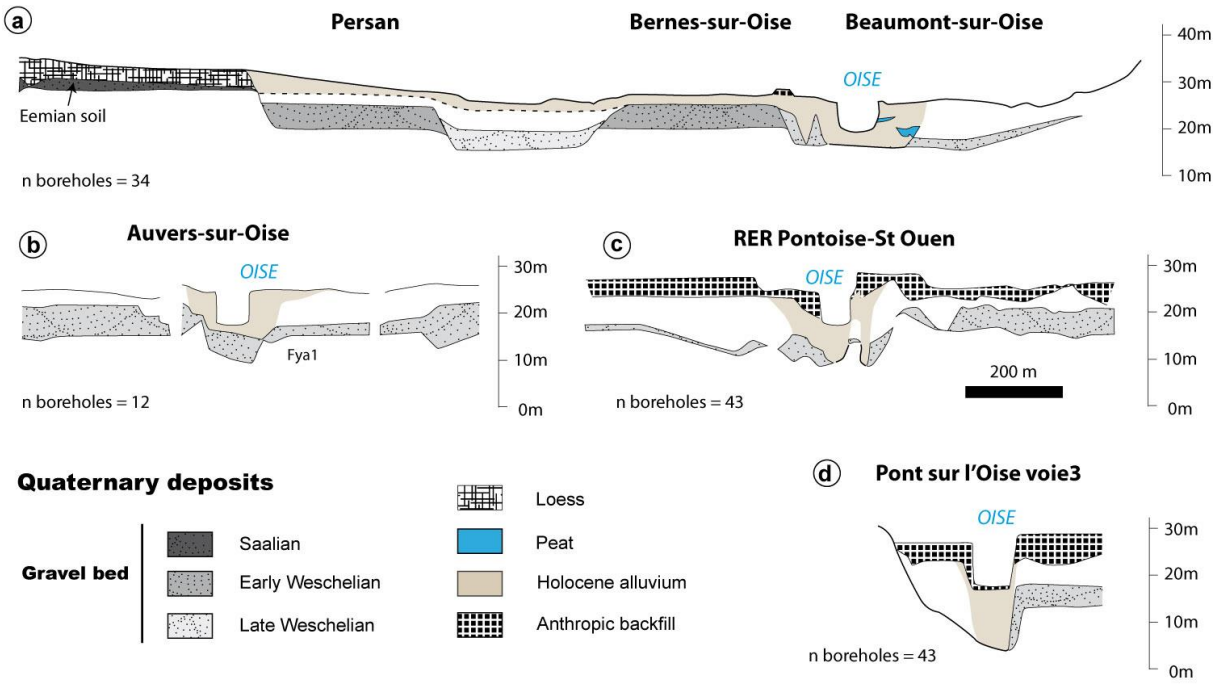

Figure 7.2. Cross-sections in the alluvium of the lower part of the Oise valley (after Krier, 2004). See Figure 1 for location. Based on existing and recent (Blaser et al., 2015; Chourio Camacho, this thesis Chapter 3) dating of alluvial sediments (Table 7.1), the extension of Holocene sediment has been largely reduced compared to the initial interpretation by Krier (2004).

7.1.4 Methods

Kriging models were programmed with Python scripts that called the gstLearn library (Renard et al., 2016). The Jupyter Notebook files used in the study and the data are available on a Github repository (see Supporting Information).

7.1.4.1 Datasets

Kriging was performed using two kinds of data (Figure 7.3): (i) a polygon representing the limits of the alluvial plain and (ii) a set of 1010 points containing information about either the bedrock-alluvium interface elevation, the top of borehole elevation (Figure 7.3-a) or the alluvium thickness (Figure 7.3-b).

The limits of the alluvial plains were computed from harmonized 1/50,000 scale geological maps of the French geological survey. The youngest alluvial deposits (i.e., *Fx*, *Fy* and *Fz* terraces) were merged to constitute one polygon of the valley bottom using the ArcGIS

software. Additionally, it was defined that terraces more than 10 m above the river could not be included into the valley bottom polygon. Finally, an inconsistency was corrected to the South of the Thieux anticline, near Verberie (Figure 7.1) where the Oise valley is about 5 km wide. There, sands from the Ypresian (i.e., Bracheux sands) were mistakenly reported on the geological map (Compiègne and Senlis; http://infoterre.brgm.fr/) instead of valley bottom alluvium as showed by Pastre et al. (2000) and confirmed by our field observations and analyses of the boreholes.

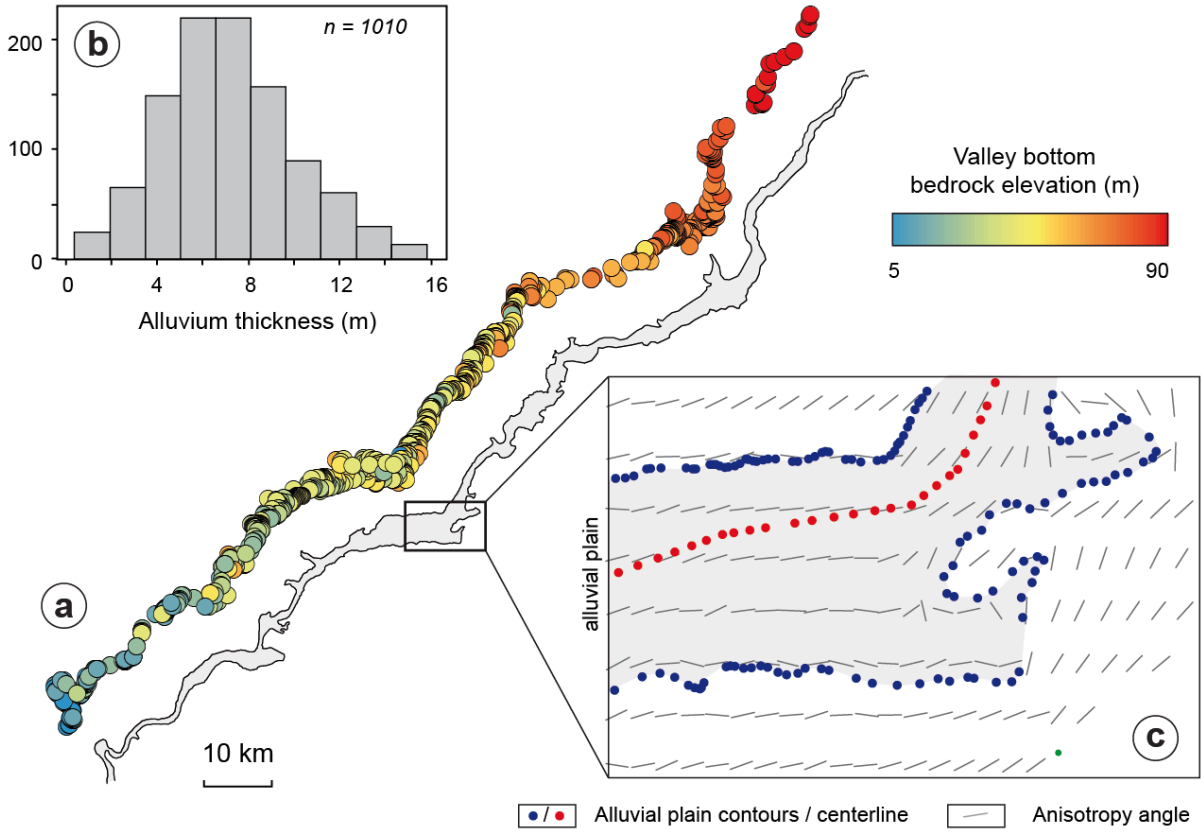

Figure 7.3. Datasets used to perform the directional kriging. (a) Data points, colored by elevation of the bedrock-alluvium interface, and polygon of the limits of the alluvial plain (see text for details). (b) Histogram of alluvium thickness. (c) Zoom in the Verberie area showing the construction of the anisotropy field based on the contours of the alluvial plain. Note that a 1000 m resolution is used for visualization while it is 50 m in the simulations.

Borehole data were extracted from the BSS (Base du Sol et Sous-sol) database available on the French Geological Survey (BRGM) website (http://infoterre.brgm.fr/). Each borehole was manually analyzed to ensure consistency between data. Inconsistent data, accounting for approximately 20% of the analyzed boreholes, were discarded. For kriging the alluvium thickness, we also incorporated the coordinates of the limits of the alluvial plain as zero-thickness values (i.e., except in the case of confluences where alluvial thickness is different from zero), thereby increasing the number of data points to 2319.

7.1.4.1.1 Construction of the vector field

To perform the nonstationary kriging, an anisotropy field was generated based on the limits of the alluvial plain. This polygon was first used to build a centerline of the alluvial plain (using the ArcGIS® software) and was then divided into two polylines (i.e., northern and southern edges of the plain). Two lines of supplementary control points bordering the outside of the plain to the North and to the South (with a 45° N direction) were also added. Thus, five polylines were constructed. The tangential vectors at each vertex of these 5 polylines were generated using the NumPy gradient method and then converted into angles using the Numpy® arctan2 function. Finally, these angles were interpolated linearly into a structured map using the SciPy method for interpolating unstructured data to grid (Figure 7.3).

7.1.4.1.2 Kriging estimations

Two types of kriging estimations are considered. The first is the “classical” kriging approach, in which a model with a slight regional anisotropy is applied. The second is the “SPDE” kriging which accounts for local geometric anisotropies using the SPDE approach presented by Pereira et al (2022). First, variograms on 1010 data of alluvium thickness were computed using a 45° direction (i.e., following the mean orientation of the valley) and a secondary, orthogonal direction of 135° (Figure 7.4). The zero values corresponding to the limits of the alluvial plain were not used to calculate the variogram. The model estimated from the variogram was used for the classical kriging (Figure 7.4) and to set the ranges. In the SPDE case, inferring ranges directly from data is not easy, especially for anisotropic estimations. Two ranges were therefore tested: using either 8000 m and 800 m or 2000 m and 200 m for the first and second ranges, respectively. These ranges were voluntarily chosen wide, they will be further justified in the discussion section. In the low ranges case (2000 m, 200 m), the SPDE kriging was performed

without (Figure 7.5-b) and with (Figure 7.5-c) the zeros values at the limits of the alluvial plain. Finally, uncertainties on alluvial thickness were estimated based on the calculation of the standard deviation of 100 simulations.

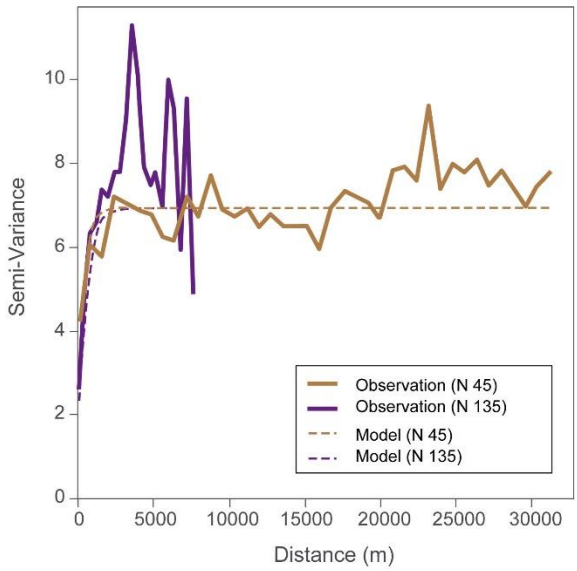

Figure 7.4. Experimental variogram of alluvial thicknesses (1010 data points) estimated according to the direction of the valley (N45) and to a direction orthogonal to the valley (N135).

The models of the bedrock-alluvium interface elevation were created by subtracting the kriging estimation of alluvial thickness to the estimation of the top of the alluvial plain. The latter was obtained from a 500 m resolution DEM (i.e., STRM2 degraded). Values of the DEM were extracted using the Raster to Point routine in ArcGIS. A SPDE kriging (ranges [2000 m, 200 m]) was performed on the 2470 evenly spaced points extracted from the DEM. The Topographic Analysis Toolbox (TAK; Forte and Whipple, 2019) - based on the TopoToolbox Matlab library (Schwanghart et Kuhn, 2010; Schwanghart et Scherler, 2014) - was used to extract the thalweg of the Oise Valley (Figure 7.6). Three SWATH profiles were computed from the top of the alluvial plain, low ranges SPDE (2000 m, 200 m) and large ranges SPDE (8000 m, 800 m) bedrock-alluvium interface simulations. Only the minimum elevations were kept for the thalwegs (Figure 7.6).

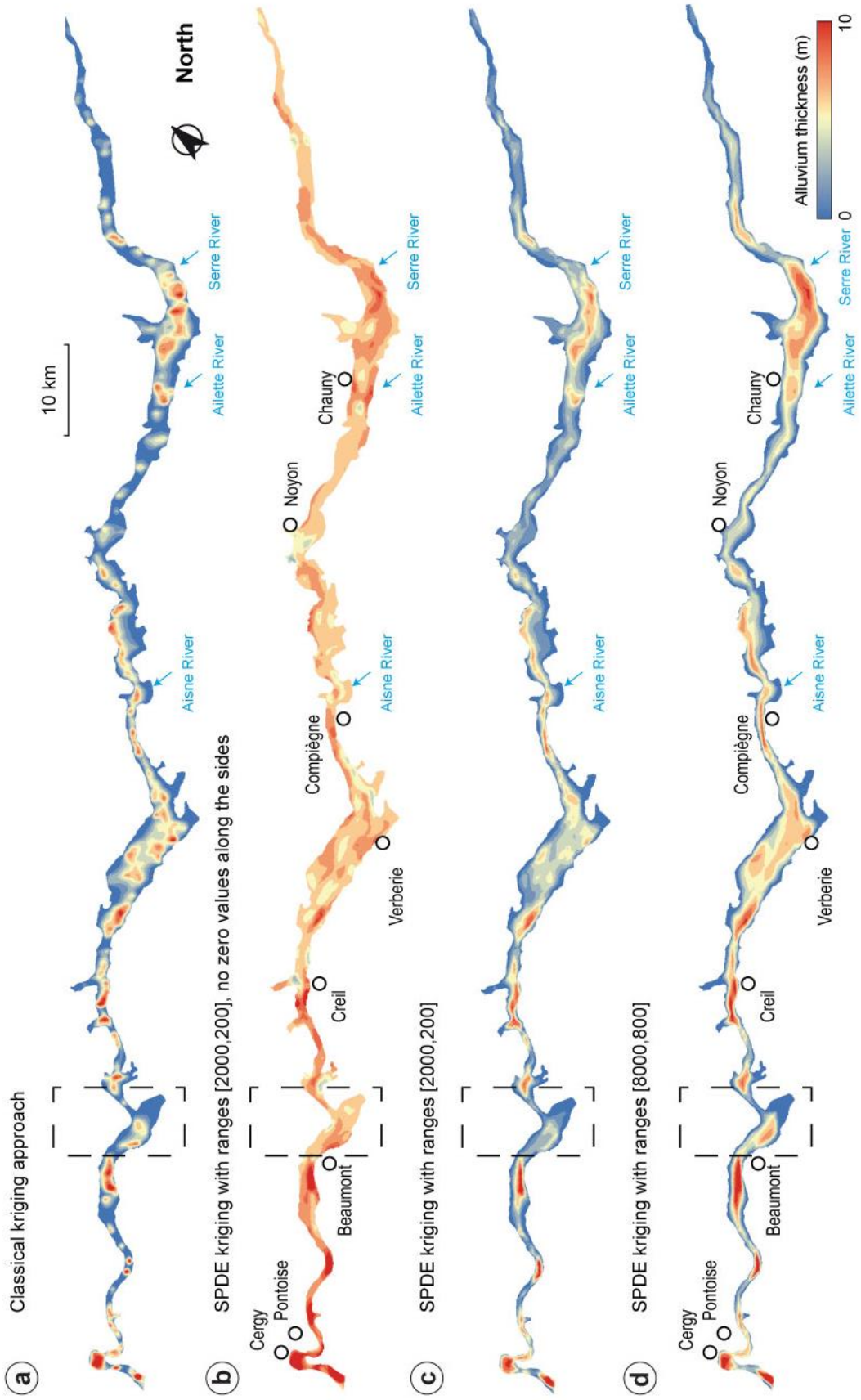

Figure 7.5. Results of the different estimations simulations. See method section for details. Blue arrows indicate major confluences. The dashed-line rectangle shows the Bray anticline.

7.1.5 Results and interpretations

7.1.5.1 Variograms

For alluvial thickness, the experimental variograms along the 45° and 135° directions are shown in (Figure 7.4). In both cases, a nugget effect is useful. The estimated ranges are approximately 1000 and 1500 m along the 45° and 135° direction, respectively. The sill is around 7. The direction that follows the valley (i.e., 45°) has enough data to calculate a variogram while it is not satisfactory using the 135° direction, due to the limitation with the data. Hence, by default, the isotropic model -or simply keeping a slight regional anisotropy (Figure 7.5) - seems to be the most suitable.

7.1.5.2 Comparison between estimations

The map of alluvium thickness generated with the classical kriging shows rounded contours and an overall patchy geometry (Figure 7.5-a). A slight anisotropy is observed along the 135°, consistently with the calculated ranges (1000 and 1500 m, respectively along the 45° and 135° directions). In cases where the valley is narrow (< 2000 m wide), a corrugate pattern is visible, as exemplified by the areas from Chauny to Noyon and from Beaumont-sur-Oise to Pontoise (Figures 7.1 and 7.5-a). In cases where the density of data is low, the patchiness is increased. Overall, the pattern - although consistent with the data distribution - lacks continuity and produces geometries that are not expected for a river system flowing into a valley and carving into the bedrock. The associated uncertainties are greater than that of SPDE simulations (minimum of 1.02 m, average of 1.9 m and maximum of 3.02 m).

The SPDE kriging maps exhibit more continuity along the valley direction compared to the classical kriging model. The uncertainties estimated for the SPDE kriging maps are quite similar: minimum of 1.02 m, average of 1.68 m, and maximum of 2.56 m for the small ranges (2000, 200); minimum of 1.09 m, average of 1.62 m, and maximum of 2.55 m for the large ranges (8000, 800) (see Supporting Information). The map with the shorter ranges (2000 m, 200 m) allows a better fitting of small-scale variations in the data. The shorter ranges map that does not consider the zero values at the edges of the alluvial plain strictly follows the anisotropy field (Figure 7.5-b). In the short ranges SPDE map that includes alluvial thicknesses set to zero at the edges of the alluvial plain (Figure 7.5-c), the estimation has values approaching zero when no other constrain that the sides exist. It is therefore a side effect due to the lack of borehole data, which diminish alluvial thicknesses in the short ranges SPDE estimation when

considering these zero values. In contrast, the estimation without zero values along the edges overestimates alluvial thickness (i.e., comparison between Figures 7.5-b and 7.5-c). This yields a difference in the estimated total volume of alluvium. It is 1.17 km^3 in the case with additional zero constraints and 2.27 km^3 in the cases with only 1010 borehole data points. In comparison the model with the largest ranges (8000 m, 800 m; Figure 7.5-d) has an overall smoother geometry. This model fits the larger scale trends and does a better job in limiting the side effect due to the impact of the zero constraints placed along the edges of the alluvial plain on the estimation. However, it misses some of the detailed changes of the bed topography. It yields an estimated volume of 1.4 km^3 of alluvium stored in the alluvial plain.

7.1.5.3 Details of SPDE maps geometries

As shown above, the pattern of alluvial thickness of the classical kriging is rather uniform and patchy. In the SPDE case, distinct types of geometry are observed. One endmember is visible in wide alluvial plains, particularly near Verberie (Figure 7.5-b, 7.5-c and 7.5-d). There, alluvial thickness varies across the width of the valley. In the short ranges cases (Figures 7.5-b and 7.5-c), it mimics a braided pattern. The width and length of the associated bars are in the order of 750-1500 m and 1000-3000 m respectively. Similar patterns are observed near Beaumont-sur-Oise and upstream of Chauny (Figure 7.5-b and 7.5-c). The other endmember is the alternation of topographic highs and lows along narrow, sinuous valley sections that has a riffle and pool geometry (Wolman and Leopold, 1957). This pattern is dominant downstream of Beaumont-sur-Oise, particularly in the Cergy-Pontoise area (Figure 7.5). There, the spacing between pools (i.e., topographic lows or thickness highs) is 3000-7000 m. Similar patterns are observed near Compiègne and Creil (Figure 7.5-b and 7.5-c). Finally, an increase of alluvial thickness is observed downstream of confluences (Figure 7.5) in all simulations.

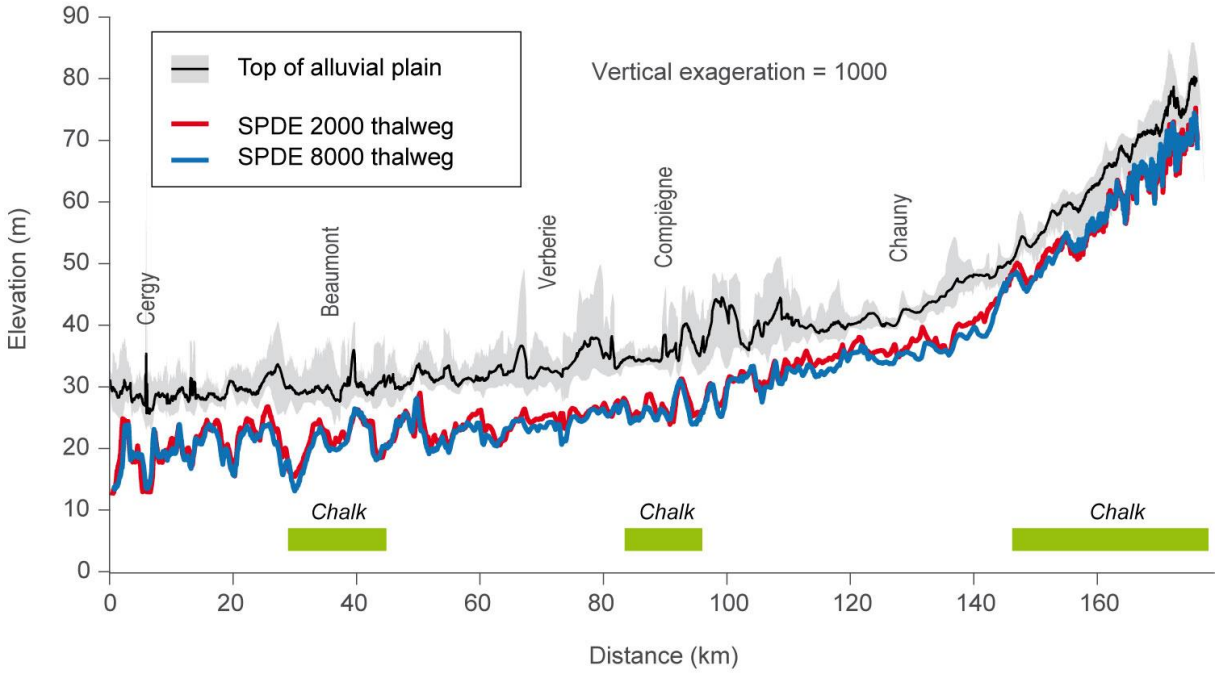

Figure 7.6. Elevation (SWATH) profiles along the centerline of the Oise valley showing the top of the alluvial plain and the valley thalwegs at the bedrock-alluvium interface computed with the TAK (Forte and Whipple, 2019). Green rectangles correspond to areas with chalk bedrock lithology.

The Oise Valley thalwegs (refer to Figure 7.6) exhibit contrasted geometries, consistent with the observations made on the maps. Firstly, it should be noted that the short- and long-range thalwegs are not very different, with the latter having an overall slightly higher elevation. In both cases, different segments of the valley can be observed. The upstream section of the Oise Valley (i.e., > 150 km) has a steeper slope and smaller alluvial thickness compared to the downstream section (i.e., 0-150 km) (Figure 7.6). This corresponds to the transition to chalk bedrock but also to the confluence with the Serre River. Finally, the two identified styles (braided and meandering) can be distinguished from the thalweg. Riffle-pool geometry is visible with ups and downs (up to 10 m in elevation) of the thalweg, mostly from Cergy to Beaumont-sur-Oise but also near Compiègne. In comparison, braided-like patterns correspond to sections with shorter amplitude oscillations of the thalweg elevation (less than 5 m), visible in the Verberie and Chauny areas.

7.1.6 Discussion

7.1.6.1 Relevance of the SPDE kriging to model valley bottom alluvial thickness

In this study, SPDE kriging using nonstationary geometric anisotropies demonstrates its relevance for simulating alluvial thicknesses geometries in the case of the sinuous Oise valley. Indeed, in addition to having reduced uncertainties compared to estimation performed with a regional, nearly isotropic model, the SPDE realizations have a wealth of detailed and realistic geometries ((Figure 7.5). For instance, one can observe braided-like patterns along wide valleys, and riffle-pool geometries along narrow and sinuous valley bottoms, consistently with the existing theory (Parker, 1976). Finally, alluvial thickness increases immediately after large confluences, likely reflecting scouring, as observed in the field (Best and Ashworth, 1997) and experimentally (Grimaud et al., 2017). Together, these observations point towards the specifics of flow and sediment transport carving the bedrock at the valley floor. In a sense, using nonstationary geometric anisotropies is further recognition that the direction of the valley (i.e., 45° on average) is the most suited to restoring the valley bottom geometry, similar to previous studies that used kriging for alluvial thickness reconstruction in the Paris Basin (e.g., Labarthe, 2016; Deleplancque et al., 2018).

Figure 7.5 shows that the chosen ranges for SPDE kriging have an impact on the resulting alluvial thickness geometries. Differences are observed in the patterns (refer to Figure 5c and 5d) and in the resulting volumes (i.e., a 17% difference), although uncertainties are comparable. In this study, the applied ranges purposely varied significantly to test these impacts. However, the ratio between long and short ranges is 10 in both cases (i.e., [2000, 200] and [8000, 800]). This can be physically justified based on (i) existing compilations of geometric parameters in natural river systems and experiments and (ii) geological observations from the Oise valley (Figures 7.1 and 7.2). In meandering river systems, recent compilations indicate for instance that ratio of the meander wavelength to the bankfull width of river cross-section is c.a. 11 (Lemay et al., 2020). For braided rivers, the average aspect ratio of bars (length divided by width) is about 5 (Kelly, 2006), although some dispersion is observed, with values from 2 to 10 (Limaye et al., 2018). Finally, the confluence-bifurcation spacing is 4-5 times the width of channels for braided systems (Hundey and Ashmore, 2009).

In the Beaumont-sur-Oise area, the high density of boreholes has allowed for the construction of very detailed cross-sections of the alluvial bottom, particularly the geometry of the bedrock-interface (Krier, 2004). Locally, very densely spaced boreholes (along cross-sections realized

in the frame of subway tunnels) indicate rapid fluctuations of the elevation of the erosional bedrock-alluvium interface. There, the width and spacing of channelized erosion features than can be individualized is in the order of 100-200 m (Figure 7.2), justifying a 200 m as the minimum range orthogonal to the valley direction. Finally, the meander amplitude is 8000 m between Beaumont-sur-Oise and Pontoise, while the lengths of meander bends are roughly 4000 m in the area. This supports the use of 8000 m for the longest range. Hence, the short ranges (2000 m, 200 m) look more adapted to smaller scale details - such as the erosive bases of channels - while the large ranges (8000 m, 800 m) are adapted to larger scales features, particularly the meandering pattern observed along the downstream section of the Oise River valley. In the former, it should be noted that despite ranges with an aspect ratio of 10, the resulting aspect ratio of "braids" is significantly less (3-5) and fits well with observations in natural systems (Kelly, 2006).

In the future, and although assessing the relevance of the chosen ranges with a physic-based approach remains recommended, it would be interesting to develop new techniques for estimating the ranges directly from the data. A complementary approach that estimates the ranges directly from the data using the nonstationary geometric anisotropies, i.e., and not a regional orientation, could for instance be tested.

7.1.6.2 Geological implications

The geometries of alluvial deposits observed in the Oise valley bottom likely reflect paleo-hydraulic conditions from Glacial to Tardi-glacial times, the Late Holocene representing only limited modifications of the alluvial plains' morphologies in the Seine River catchment (Pastre et al., 1997; 2000; Antoine, 1997). This is supported by the dating of the deeper overlying sands, which belong to MIS2 period in the downstream Oise valley in Maurecourt (Figure 7.3). The braided patterns observed in the SPDE kriging are consistent with the interpretation that fluvial systems of Western Europe, and in particular the Seine River system, were dominated then by braided-like systems (Brigdeland and Westaway, 2000; Antoine et al., 2007). These morphologies observed at the alluvium-bedrock interface would correspond to erosion inherited from glacial periods. A novelty is the observed riffle-pool geometry at the scale of the valley along narrow valley sections. Such geometry is well known for rivers (Richards, 1976) but not so much at the scale of valleys. It is exemplified by the geometry of the valley thalweg, which displays ups and downs that are saliant in the downstream part of the Oise valley near Cergy

and Pontoise (Figure 7.6). This supports a link between valley aspect ratio and valley bedrock patterns (i.e., braided vs meandering), as shown for rivers (Parker, 1976). Ultimately, it points out that braided patterns may not be systematically associated with the glacial deposits, an assertion that must be verified with the facies analysis of alluvial deposits, in the valley bottom or alluvial terraces.

At the scale of the valley, the change in slope and alluvial thickness upstream of Chauny (Figure 7.6) confirms the coincidence of bedrock lithology change and alluvial/bedrock slope change (Grimaud et al., 2014). This transition also corresponds to the confluence with the Serre River, and there could be an equally important effect of increasing discharge after the confluence on the observed changes (i.e., Crosby et al., 2007). Krier (2004) speculated that the talweg in the downstream Oise valley would be "over"-incised and would mark regressive incision attributed to condition before the Tardiglacial. In the Cergy-Pontoise, the thalweg profile - perhaps limited by the amount of available borehole data - indicates that erosion did not erase the riffle-pool geometry. Unfortunately, the riffle-pool geometry makes it difficult to accurately identify knickpoints that would be related to regressive erosion in response to base level drop during glacial periods, as suggested by Deleplancque et al. (2018) along the Bassée alluvial plain (Figure 7.6). Alluvial thickness rarely exceeds 10 m upstream of Compiègne and the few areas with increased thickness are related to confluences (i.e., Serre and Ailette Rivers). One may thus tentatively suggest that a transition exists there, but it remains speculative. Narrowing and shallowing of the valley bottom was shown upstream of Beaumon-sur-Oise by Larue (2000) who suggested that this could be the result of Late Quaternary uplift of the Bray anticline. The SPDE kriging simulations show geometry that is consistent with this pattern. However, it also shows other ups and downs of the bedrock elevation elsewhere, which are related to meandering pattern. Although enhanced when compared to other areas, the increased elevation of the bedrock when crossing the Bray anticline may not be related to active uplift but simply to the local change of bedrock lithology to chalk.

Finally, the estimations allow calculating the volume of alluvium in the Oise valley. The largest volume difference is observed when calculating without or with consideration of zero values along the sides of the alluvial plain (i.e., respectively 1.17 and 2.3 km^3 for ranges [2000 m, 200 m]). Simulations with zeros on the sides are more realistic and thus seem to be the most adapted. They should be considered as estimates of the total volume because of the side effect described in section 7.1.5.2, which may locally decrease the estimation of alluvial thickness. Considering the uncertainties on thickness, volume estimations yield a 30% error. It is thus reasonable to

estimate that a c.a. 1.4 ± 0. 4 km^3 volume of alluvium is currently stored in the studied Oise valley bottom. Knowing this volume is of importance to estimate the temporary storage in transfer zones from a source-to-sink point of view (Castelltort and van den Driessch, 2003; Blothe and Korup, 2013), but also to constructing, gravel-mining and hydrology companies, who manage and supervise valley bottom landscapes.

7.1.7 Conclusion

In this study, a new SPDE method for kriging alluvial thickness geometries in valley bottom using nonstationary geometric anisotropies is introduced. These anisotropies are built using the contours of the alluvial plain. The method is compared to the classical kriging approach and the choices of parameters are explored in agreement with knowledge on the physics of alluvial rivers. The geological significance of observed geometries is then discussed. We find that the SPDE method shows less uncertainties than classical kriging and produces more realistic patterns. Evidence for braided patterns, riffle-pool geometry related to meandering and scouring at confluences are observed at the scale of the valley width. Finally, it is estimated that about 1.4 ± 0. 4 km^3 of alluvium is currently stored in the studied Oise valley bottom. Although the method was applied to an alluvial example, it could well be adapted to other geological contexts where an anisotropy field can be estimated such as faulted and folded structures, supergene mineralization or environmental management to track pollutants dissemination in rivers.

7.2 Results of the kriging method at the scale of the Seine catchment

7.2.1 Construction of the total alluvial thickness in the bottoms of valleys in the Seine catchment

The alluvial infill of the geometry of the Seine catchment was determined using 4817 boreholes from the Banque du Sous-Sol (BSS) that intersect the alluvium at the bottom of the valleys (see details in chapter 5). Similarly to section 7.1, SPDE kriging was applied. The shapefile of the valley bottom built in chapter 5 and analyzed in chapter 6 (Figure 6.16) was used and the associated vertices were used as further constraints for alluvium thickness (i.e., they were set to zero). Two sets of ranges were tested (using either 2000 and 200 m (Figure 7.7) or 8000 and 800 m (Figure 7.8). The bedrock elevation was built by subtracting alluvial thicknesses

estimation maps to an estimation of the top of the alluvial plain built using a kriging of 500 m spaced data points form a digital elevation model.

Alluvium thickness distributions estimated from the kriging show contrasted geometries along the valley bottom. Overall, thickness of alluvial fills increases downstream. The estimated thickness of the alluvial deposits varies from 0 to approximately 30 m (i.e., in the estuarine area). Similar variabilities of the patterns are observed for the two tested ranges (using either 2000 and 200 m (Figure 7.7) or 8000 and 800 m (Figure 7.8)).

Some general observations are made along the Seine catchment considering the total alluvium thickness (Figure 7.7). One should note that this thickness includes backfill, which may be locally important (Figure 7.9) and will be corrected latter (Figure 7.10).

7.2.1.1 Upstream Paris

When the Marne, Aube, Seine and Yonne valleys cut limestones and marls bedrock from the Jurassic (until the Jurassic Cuesta):

- In this area (i.e., in the Marne valley between Balesmes-sur-Marne and Ancerville location, in the Aube valley between Auberive and Bar-sur-Aube locations, in the Seine valley between Chanceux and Bar-sur-Seine locations and in the Yonne valley between Fâchin and Vincelles locations (Figure 7.7)), the alluvial thickness of valleys is relatively thin < 2 m and is also characterized by lower discharges and narrowest valleys. There, not much data is available the first kilometres.

When the Marne, Aube, Seine and Yonne valleys cuts clays and marls bedrock from Cretaceous (between the Jurassic Cuesta until the Lower Intracretaceous Cuesta):

- In this area valleys tend to former widening alluvial cones in which alluvial thickness varies from 2 to 4 m. This area is characterized by an increase in valley width (between 1 and 3 km of wide) and increase in discharge, that reflects the effect of soft lithologies. As shown in chapter 6, marls and clay bedrock represents the more easily lithologies, thus, when increase discharge lateral erosion and valley widening tend also to increase (Figure 7.7).

When the Marne, Aube, Seine, Yonne and Loing valleys cuts chalk bedrock from Cretaceous (between the Lower Intracretaceous Cuesta until the Upper Cretaceous-Cenozoic Cuesta):

- In this area alluvial thickness of valleys tend to increase from upstream to downstream and is comprise between 3 and 8 m (Figure 7.7).
- Near of Troyes in the Seine valley an increase in alluvial thickness between 5 and 6 m was observed (Figure 7.7).
- A change in alluvial thickness is observed in the Bassée area, near of Courceroy location. It may reflect the influence of the knickpoint that was observed by Deleplancque et al., (2018). A similar pattern is observed in the Yonne valley near of Sens, where alluvial thickness increases from approximately 3 m of thick upstream of Yonne valley to 6–7 m of thick until the confluence with the Seine River. Also, in the Loing valley, near of Montigny-sur-Loing, where alluvial thickness increases from 4 m upstream of Loing valley to 6 – 8 m of thick util the confluence with the Seine River (Figure 7.7).
- In the Aube and Marne valleys, alluvial thickness tends to increase downstream of these valleys until the Cenozoic Cuesta. In this part valleys reflects an increase in thickness between 3 and 6 m (Figure 7.7).

When the Marne, and Seine valleys cuts into the limestones, clays, sands and marls bedrock from Cenozoic:

- In this area, the Seine and Marne valleys tend to become more meandering with valleys narrower (Figure 7.7).
- In the Seine valley (between the confluence with the Loing River until Paris), alluvial thickness increase and is comprise between 6 and 14 m approximately. In the surrounding area of Paris alluvial thickness increases (~14 m of thick) reflecting the anthropogenic influence (Figure 7.7).
- In the Marne valley, at Etampes-sur-Marne alluvial thickness reaches ~7 m of thick, then, a decrease in thickness is observed (comprise between 2-3 m of thick) until Maux location. After that, the alluvial thickness tent to increase between Torcy until the confluence with the Seine River (varying between 4 and 10 m of thick) (Figure 7.7).

7.2.1.2 Downstream Paris

In this area the Oise, the Seine and Eure valleys cut into limestones, clays, sands, marls and chalk bedrock from Cenozoic and Cretaceous:

- The Oise valley shows an increase in alluvial thickness going downstream, varying between 3 and 10 m (Figure 7.7) (see section 7.1).
- Downstream Paris, the Seine valley shows a well-developed meandering system, with a pool and riffle geometry. The Poses dam indicates the limit where the estuarine influence of the system begins. Near the Poses dam a remarkable increase in alluvial thickness (i.e., above 10 m) is observed (Figure 7.7).
- In the estuarine area alluvial thickness reaches the highest values comprises between 20 and 50 m (Figure 7.7).
- In the Eure valley, alluvial thickness tends to increase near of Garenne-sur-Eure until the confluence with the Seine River (Figure 7.7).

It is important to note that the Eure, Loing, Yonne and Aube valleys are characterized by a morphology less meandering than the Seine, Oise and Marne valleys.

In areas where meandering is well marked, the mechanism of pools and riffles explains rapids variations in alluvium thickness (i.e., at Rouen in the Seine valley, at Cergy in the Oise valley and at Bonneuil-sur-Marne in the Marne valley).

Chapter 7

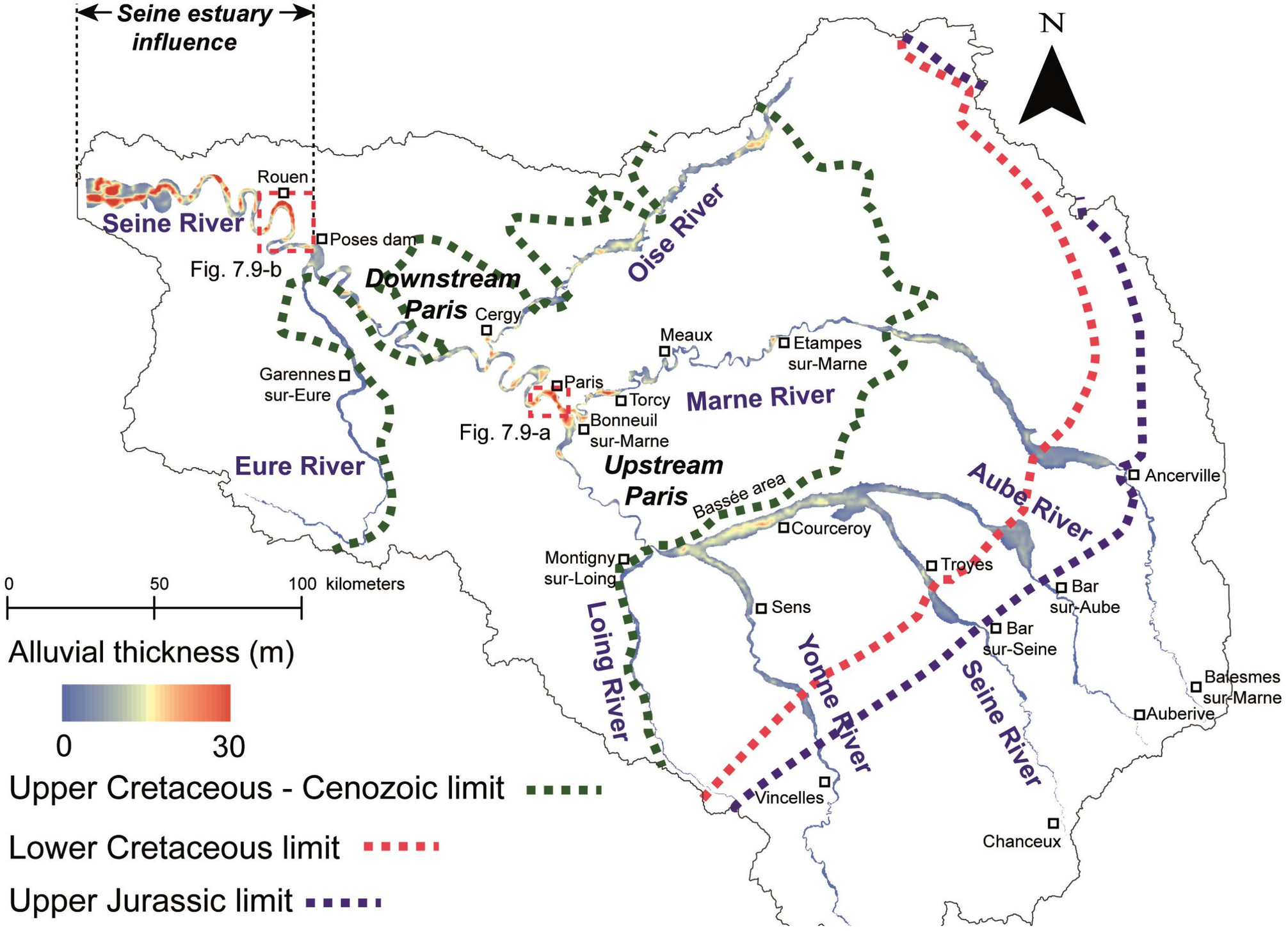

Figure 7.7. Results of the SPDE kriging model along the Seine catchment applied in alluvium thickness, using both (a) range 2000 and 200 m. Dashed lines indicate the geological limits within the catchment.

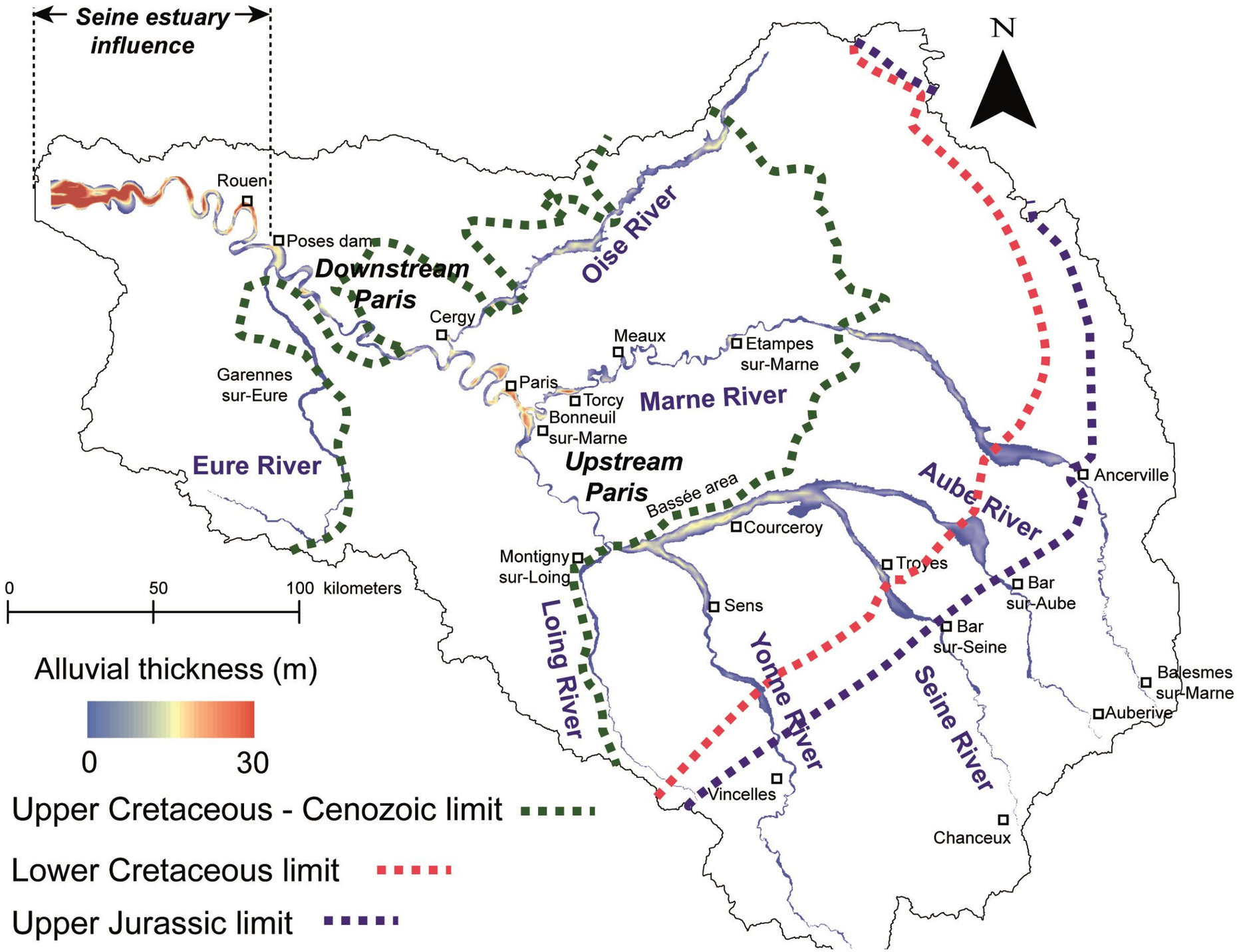

Figure 7.8. Results of the SPDE kriging model along the Seine catchment applied in alluvium thickness, using range of 8000 and 800 m. Dashed lines indicate the geological limits within the catchment.

7.2.2 Influence of anthropogenic backfill deposits

As previously mentioned, the analysis of the boreholes database using the BSS (see chapter 5) has facilitated the identification of the backfill for some boreholes along the Seine catchment. These anthropogenic backfill deposits are associated with human active

ity, resulting in modification of the sedimentary environments. These deposits tend to overlie the alluvial sediments increasing their real thickness. A thickness raster map of the anthropogenic backfill was calculated using the SPDE kriging (using the low ranges case 2000 and 200 m). The resulting raster estimates the thickness of the anthropogenic backfill within the Seine catchment, where the most important variation in thickness influenced by backfills are in the surrounding areas of Paris as well as near of Rouen. The map of anthropogenic backfill thickness estimates values generally are comprise between 1 and 5.5 m at Paris (Figure 7.9-a), and between 1 and 4 m at Rouen (Figure 7.9-b). This anthropic backfill could induce some irregularities in the kriging model (i.e., influencing the total alluvial thickness). Thus, to reduce the impact of backfill in the alluvium thickness model, the subtraction of the total alluvial thickness to the backfill were performed using the SPDE kriging (low ranges case 2000 and 200 m). This map reflects the alluvial thickness without backfill (Figure 7.10).

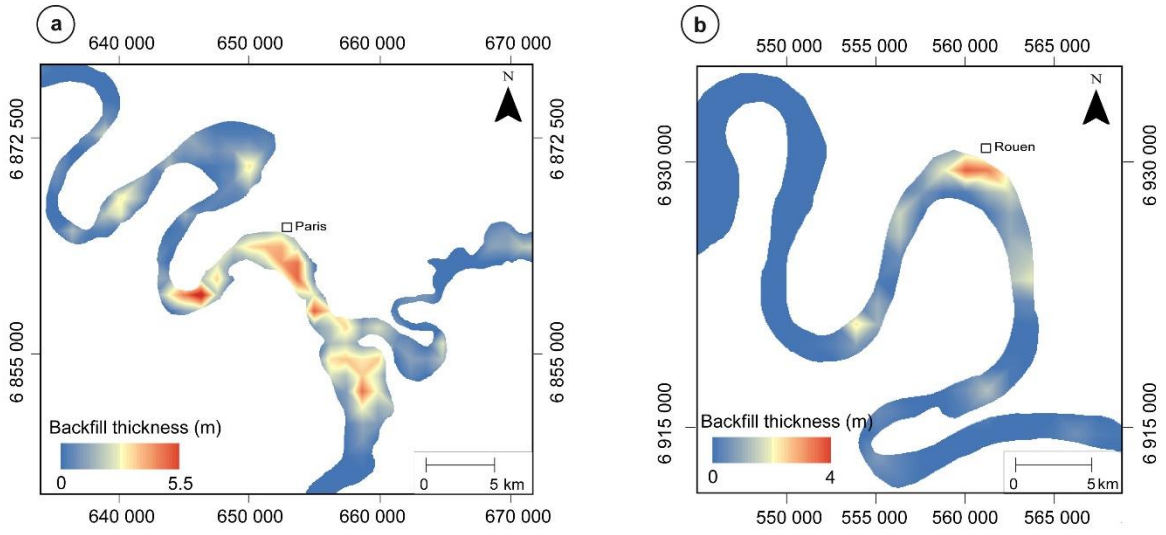

Figure 7.9. Influence of backfill thickness, (a) at Paris and (b) at Rouen. Range (8000,800 m).

Chapter 7

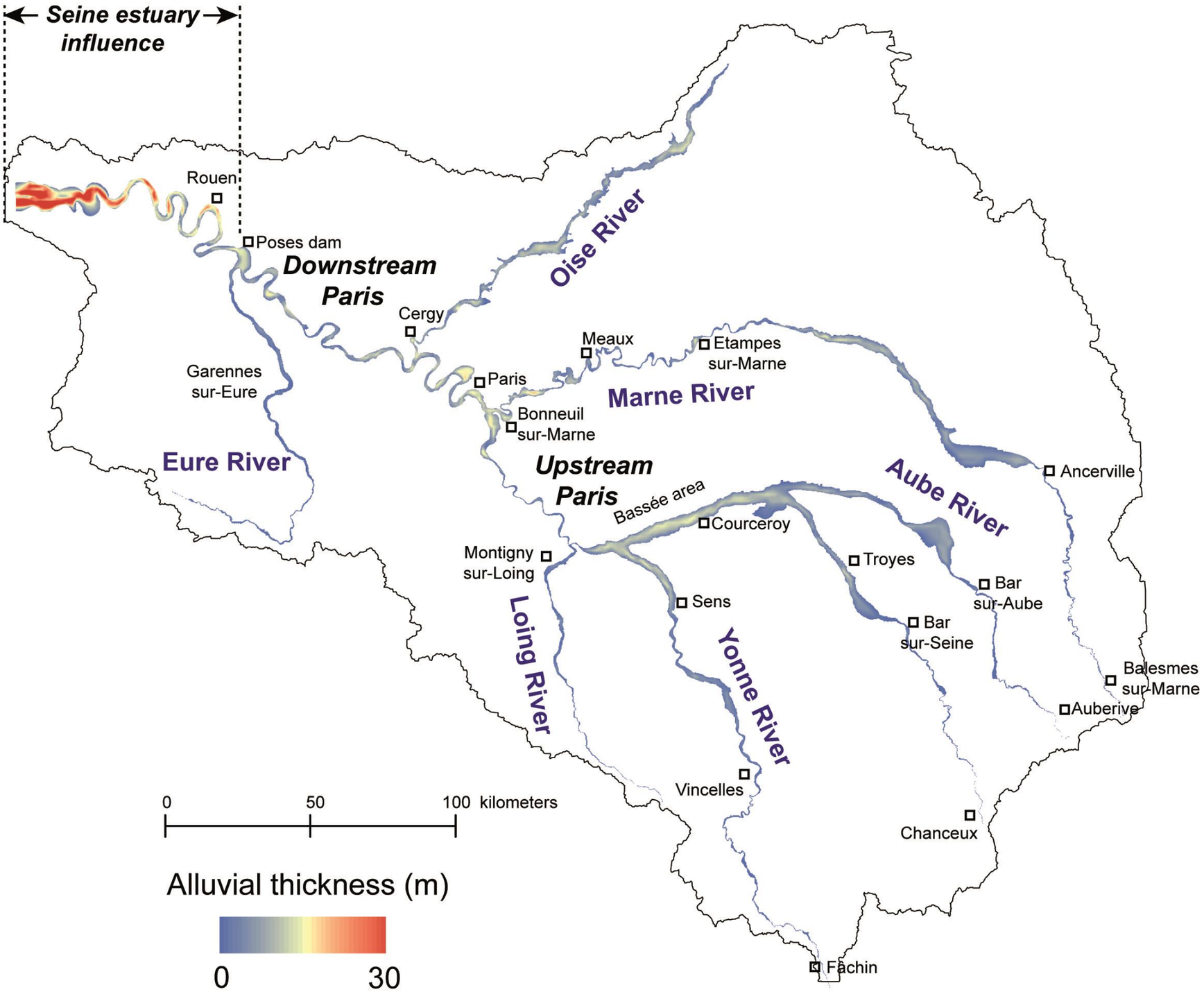

Figure 7.10. Alluvial thickness within the Seine catchment without backfill. 8000 and 800 m.

7.2.3 Volume and sediment supply

The SPDE kriging within the Seine catchment considering the long range (8000 and 800 m) allows determining the volume of sediment stored along the valley bottom. As in section 7.1.6.2, the volume is calculated using the simulations with zeros on the sides because they are more realistic and more adapted for the geometry of the valley bottom. Volume estimations including the backfill is ca. 10.13 km^3. When removing the backfill (0.91 km^3), the volume estimate is 9.22 km^3. In Paris, Fernandez (2014), was determined the volume of backfill at 0.295 km^3, this volume would thus 32% of the total of the backfill of the catchment. This confirms that the importance of backfilling in Paris related to other cities.

Quantifying sediment storage is important to better understand the transfer zone within the sediment routing system (Castelltort and van den Driessch, 2003). The volume of alluvial bottoms may be involved in the substantial lag times that could potentially buffer signals of climatic disturbances (Métivier and Gaudemer, 1999; Jerolmack and Paola, 2010).

If we consider the total volume determined at 10.13 km^3 and the incision rates of the Paris basin at 55 m/Ma (Antoine et al., 2007; 2010) applied over the entire Seine catchment, the valley bottoms stock about 1.2% of the eroded material. This estimate is based on a MIS 6 age for the valley bottom. It is therefore a minimum for several reasons: (1) 55m/Ma is estimated based on river incision rate and somewhat corresponds to a maximum erosion rate, (2) the alluvial volume may be underestimated in the upstream valleys due to limited data points (see discussion in section 7.1.6) (3), there is reworking of the alluvial volume through time, as is exemplified by the MIS6 age of the valley bottom that would imply several episodes of accumulation and degradation of the sediment stock, and (4) the calculation does not take into account smaller scale valleys, tributaries to the ones studied here, and that stock alluvium. Nevertheless, a rapid estimation of volume within the smaller valleys (Ormain, Serain, Armaçon, Vanne, Ouanne, Yerres, Essone, Yvette, Orge, Grand Morin, Petit Morin, Ourc, Servais, Serre, Aisne, Orrouy, Breche, Therain, Nonette, Presles, Esches, Sausseron, Real, Epte, Cambon, Robec, Andelle, Clerette, Austreberthe, La Voise, La Vesgre, Blaise, Ilton and Risle tributaries) was calculated hypnotizing that alluvial thickness has a mean of about 5 m ± 3, thus, the volume estimate is c.a. 6.52 km^3.

Castelltort and Van Den Driessche (2003) reported the sediment flux within the Seine catchment at 4.9 x 10^{-3} km^3/a, considering the suspended and solute load (Meybeck and Helmer, 1989). Assuming that a minimum 16.65 km^3 is stored in the valley bottom, it would take c.a.

3.4 ka to evacuate the stock (i.e., considering no input from the slope or resolution of reworked sediments). Again, this time scale is a minimum, because we consider only the main tributaries and some small tributaries of the Seine catchment. Interestingly, this time is similarly to those obtained in the Himalaya valley bottom, where the residence time is determined as 3 ka (Blöthe and Korup, 2013).

7.2.4 Bedrock-alluvial interface

The boreholes database is relatively well distributed along the valley bottom, except in the upper part of the Seine catchment where database is less dense (i.e., when valley cuts into the limestones and marls from the Jurassic). Although it may be complicated by the uneven elevation of the bedrock-alluvium interface due to the riffle-pool geometry, the map of the bedrock elevation allows identifying several knickpoints. The position of these knickpoints can sometimes also be inferred from the alluvial thickness map. Several knickpoints are suggested (Figure 7.11) in order of confidence:

- Downstream Paris, near the Poses dam
- In the Bassée area near Courceroy
- In the Yonne valley near Sens
- In the Loing valley near Montigny-sur-Loing
- In the Eure valley near Garenne-sur-Eure
- In the Marne valley near Torcy

The valley longitudinal profiles further highlight these knickpoints. In the Bassée area the knickpoints have a smooth slope in comparation whit the knickpoints observed in the Yonne, Marne, Eure and Poses dam where slope higher. These profiles are also characterized by the presence of pool and riffles mechanism due to of meandering system.

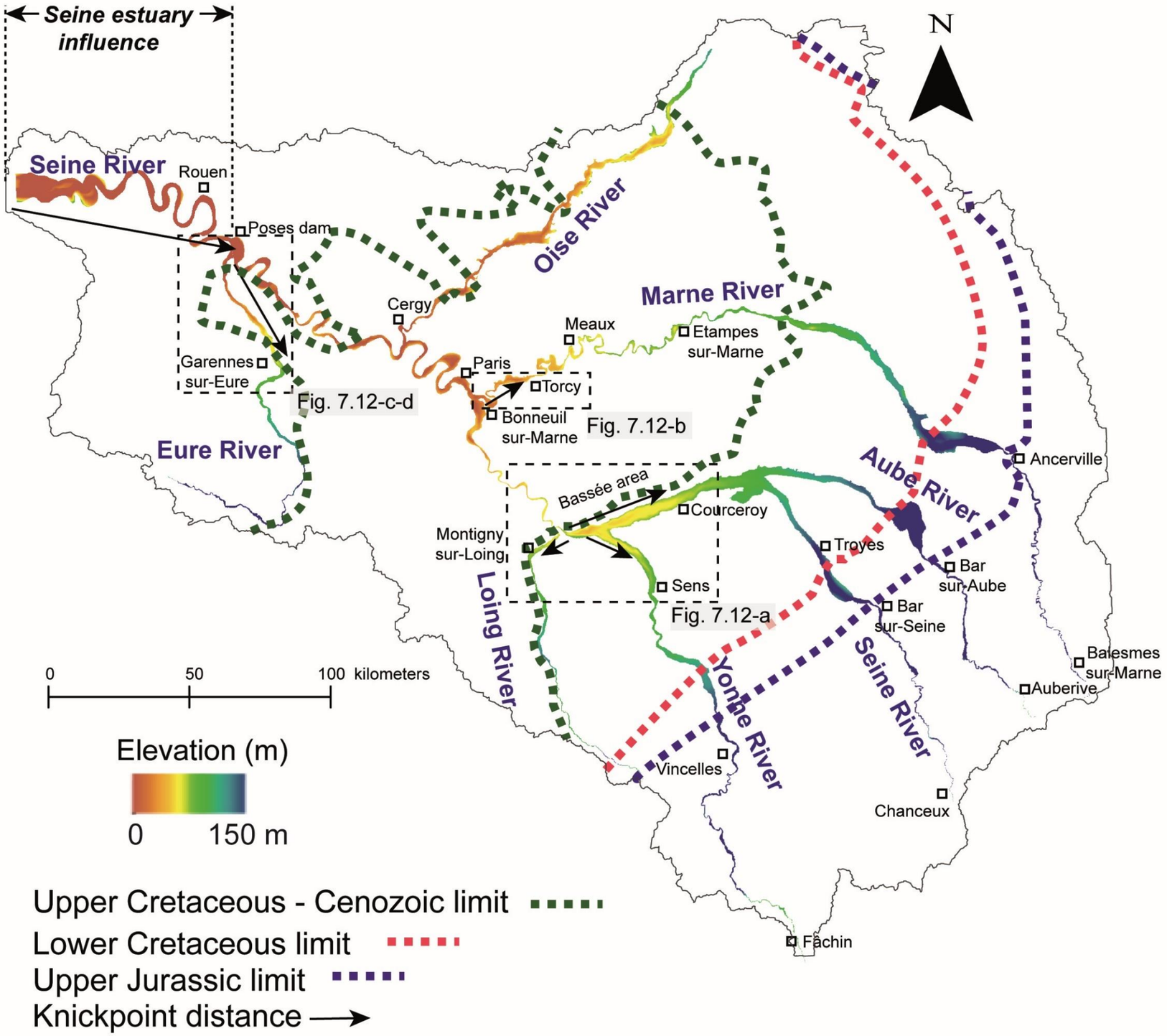

Figure 7.11. Bedrock interface within the Seine catchment. Dashed lines indicate the geological limits within the catchment. The dashed line rectangles zoom the areas of interest.

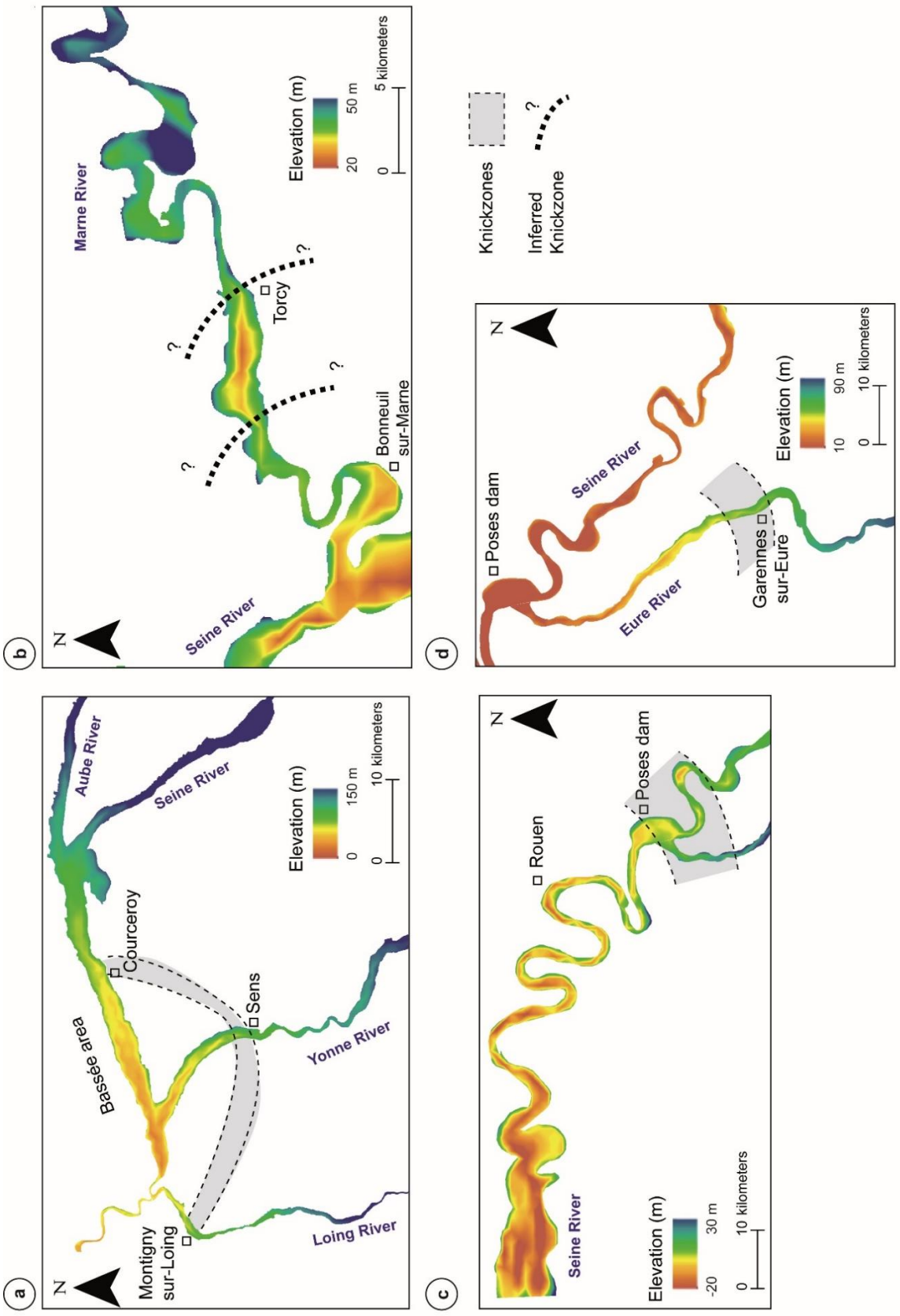

Figure 7.12. Knickpoints localization. (a) In the Bassée area at Courceroy, Yonne and Loing valleys. (b) In the Marne valley. (c) Downstream Paris at Poses Dam and (d) in the Eure valley.

Chapter 7

7.3 Conclusion

The restitution of the valley bottom geometry at the bedrock-alluvium interface using the kriging method highlighted the following. The alluvium infill within the catchment tend to increase from upstream to downstream. Where the most remarkably increase is observed in the estuarine area, after the Poses dam. Evidence for braided patterns, riffle-pool geometry related to meandering and scouring at confluences are observed at the scale of the valley width. The volume of alluvium currently stored within the valley bottom along the Seine catchment is c.a., 16.65 km^3 implying a “residence” timescale of c.a. 3.4 ka. Pool and riffle are salient features of estimation maps of alluvium thicknesses and valley bedrock longitudinal profiles. As a result, the identification of knickpoints is more difficult in valley such as the Oise and Marne. Nevertheless, several knickpoints may be observed above the chalk bedrock in the Bassée area, Yonne, Loing, Poses dam and in the Eure valleys.

Synthesis

8 Synthesis

The work provided in this PhD thesis brings new constraints on the Late Quaternary surface evolution within the Seine catchment. A large fraction of the thesis is dedicated to dating of alluvial and tidal terraces, which record long-term incision dynamics during the Quaternary period. These new data allow also discussing the age of alluvial bottoms settlement. This work was possible thanks to the access given in sand and gravel quarries, ensuring the quality of the visited outcrops. Another novelty of the work is the constitution of a large set of about 5000 data that record alluvial thickness in valley bottom together with their elevation, composition, and bedrock lithologies. This dataset is used through a novel SPDE method of kriging to estimate the geometry of the alluvial bottom in the main valleys of the Seine catchment and discussing the controlling factors.

8.1 Incision rates and valley formation since the Middle Pleistocene

The few strath terrace deposits dated in this work provide additional constraints on the ages of the valley formation and on incision rates since the Middle Pleistocene within the Seine catchment, complementing scarse data from the literature. Overall, the incision rates estimated from these terrasses are in good agreement with the long-term incision rates known in the Paris Basin. This long-term incision rate was deduced using a linear interpolation between the elevation of terraces above the maximum incision of the river and their respective age, yielding an average rate of 50-60 m/Ma considering fluvial terraces since the end of MIS 19 (Antoine et al., 2007, 2010). Hence, at the large scale, the data indicate a rather stable configuration of the valleys since the Middle Pleistocene. In details, the variations of incision rates -although modest- give additional information on vertical movement in the Paris basin during the Late Quaternary.

8.1.1 Upstream of Paris

In the Bassée area, two strath terraces were dated along the valley slopes. The sampled deposits were fluvial. The highest dated terrace corresponds to the T_{IV} terrace located at Fontaine Mâcon (+52 m RH). This terrace contains sediments deposited during the MIS 20-18 and represents the oldest sediments dated in this work (ages comprised between 756 and 798 ka). The associated long-term (i.e., calculated until the present) incision rate based on the relative

elevation RH would be 65-69 m/Ma. At Courceroy, the T_{III} terrace (+22 m RH) was dated as a part of the MIS 10 (359 and 376 ka), yielding a long-term incision rate of about 58-61 m/Ma. This terrace can be compared with the alluvial deposits found at +20 m RH at La Celle-sur-Seine and covered by calcareous tufa that belongs to MIS 11 (Limondin-Lozouet et al., 2006). Considering the two previously terraces an incision rate comprised between 71 and 75 m/Ma during the 750-360 ka interval.

In the Aube valley, a comparable terrace in terms of elevation was found near Brienne-le-Château (+50 and +55 m RH) and dated by ESR on quartz between 614 and 592 ka (MIS 16-15; Voinchet et al., 2015). This yields a long-term incision rate comprised between 81 m/Ma and 93 m/Ma. The terrace located at Juvanzé (+10 m RH, 333 ka) and at Pel-et-Der (+12 m RH, 269 ka) corresponds to long-term incision rates comprised between 30 m/Ma and 45 m/Ma respectively, i.e., lower than the 50-60 m/Ma (Antoine et al., 2010). When calculated between these two terraces, the incision rate is very high and comprised between 142 and 154 m/Ma.

Similarly, the Courlon Formation (Chaussé, 2003) in the Yonne valley (+40 m RH, 463 ka) returned an incision rate of about 86 m/Ma. Sediments from the Misy (+15 m RH) and Evry (+10 m RH) formations, were dated by ESR on quartz and yield long-term incision rates comprised between 52 and 57 m/Ma and between 39 and 34 m/Ma, respectively. Hence, these lower terraces returned lower incision rates compared to the upper ones. Considering the terraces +40 and +15 m RH, the estimate incision rate is 125 m/Ma.

The incision rates deduced from these terraces are subject to caution when taken individually because they may be biased or incomplete (see Figure 8.1). When considered together however, the dating of these terraces highlights incision rates (comprised between 70 and 150 m/Ma) higher than the average of the Paris Basin in the upstream part of the Seine River catchment for elevated terraces (i.e., above 40 m RH).

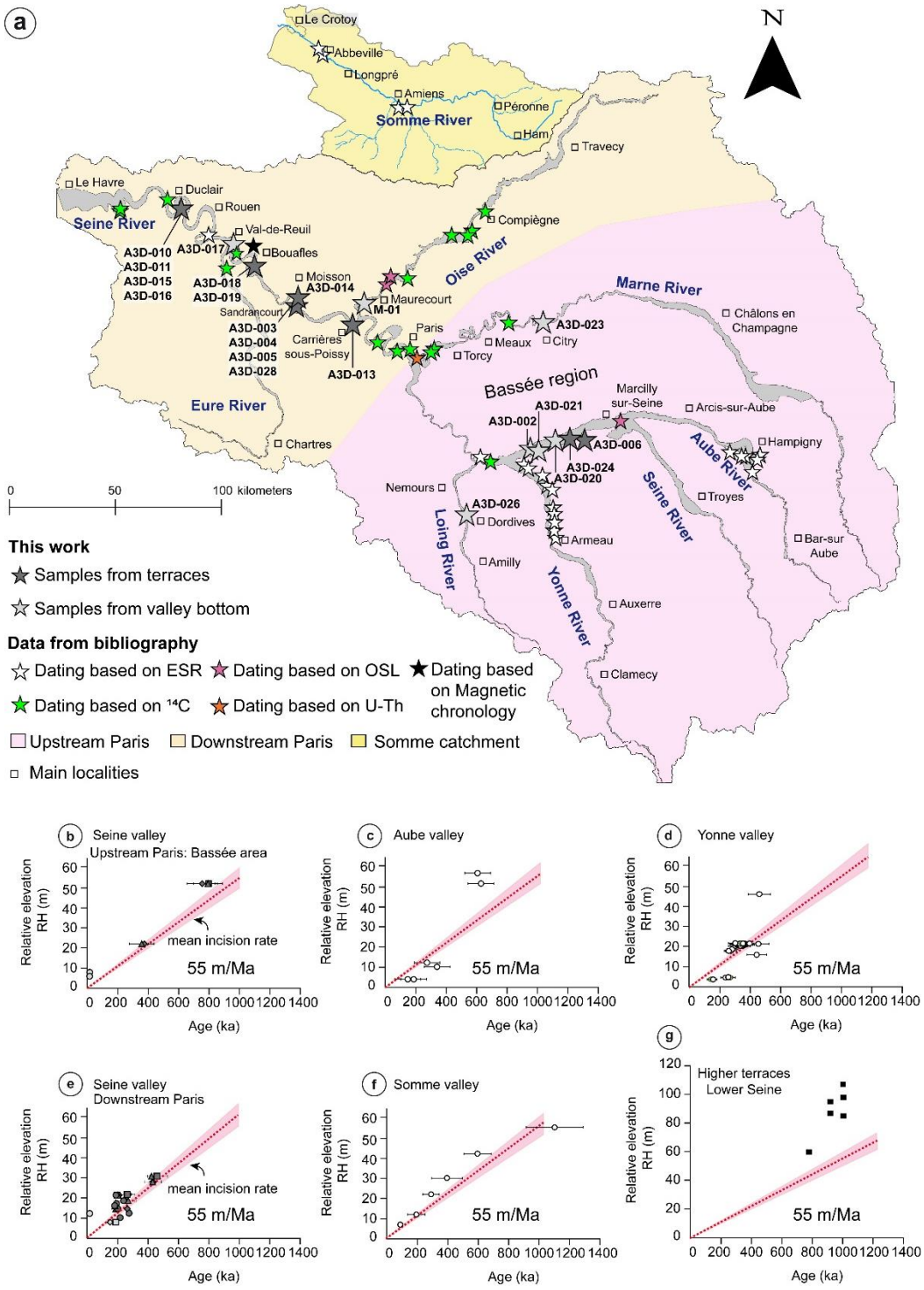

Figure 8.1. (a) Location of the Seine and Somme catchments and previous work focusing on the chronology of fluvial deposits. (b) This work samples dated upstream of Paris. (c) Data available in the Aube valley (Voinchet et al., 2015). (d) Data available in the Yonne valley (Chaussé et al., 2003; Chaussé, 2004). (e) This work samples dated downstream of Paris. (f) Data available in the Somme valley (Antoine et al., 2007; 2010). (g) Data available from higher terraces in the Lower Seine valley (Nehme et al., 2020). Red line indicates the mean of incision rates of the Seine catchment at 55 m/Ma (Antoine et al., 2007; 2010).

8.1.2 Downstream of Paris

Between Paris and Bouafles the chronological attribution of fluvial deposits remained poorly constrained. In this area (so-called Middle Seine), 16 alluvial units stepped up to +45 m RH, corresponding to the last 600 ka were determined based on Amino Acid Recemisation (AAR) (Lécolle, 1989; Antoine et al., 2007). In contrast, between Bouafles and Le Havre (so-called Lower Seine), only 7 or 8 alluvial terraces -depending on the authors- were described (Lefèbvre *et al.*, 1994; Lautridou *et al.*, 1999; Antoine *et al.*, 2007; Jamet, 2014; Nehme *et al.*, 2020). Early work (Lefebvre et al., 1994) determined incision rates of about 50 m/Ma for the lower Seine and 65 m/Ma for the Middle Seine.

At Bouafles, the Fyb terrace (+25 m RH) was dated as a part of the MIS 12 (~436 ka), representing an incision rate of 57 m/Ma. At Moisson, the Fyc terrace (+19 m RH) was dated as a part of the MIS 8 (~271 ka), with an incision rate of c.a., 70 m/Ma. At Carrières-sous-Poissy and Sandrancourt, the Fyd terrace (comprise between +9 and +15 m RH), was dated and are a part of the MIS 8 and MIS 7 (comprise between 196 ka and 269 ka), yielding incision rates between 77 m/Ma and 40 m/Ma. Overall, ages from the terraces are very, dispersed (Figure 8.1).

At Manoir Brésil, located in the Anneville-Ambourville meander (downstream Rouen and upstream of Le Havre), sediments from terraces Fyc (+20-28 m RH) and Fyd (+17-21 m RH), characterized by fluvial and tidal sediments were dated as a part of the MIS 7 and MIS 6. Comprise between 273 and 192 ka for tidal deposits and between187 ka and 184 ka for fluvial deposits. In this area, a minimum bedrock uplift of 25 m/Ma was determined using the marine deposits since 200 ka. In the Contentin (Normandie), Pedoja et al., (2018), based on OSL dating determined the apparent Pleistocene uplift rate for the Upper Pleistocene (MIS 5) at 40 m/Ma. For instance, these values are higher than in a cratonic context estimated in West Africa between 5 and 10 m/Ma (Grimaud *et al*., 2018). This difference could be explained by the alpine compression (Guillocheau *et al.*, 2000) and/or glacial-eustatic flexure (Bradley *et al.*, 2009).

8.1.3 Synthesis

The regional significance of the high incision rates for the most elevated terraces upstream of Paris is still unknown. Several hypotheses can be tentatively proposed. On the one hand, the higher incision rates could be related to the lithospheric buckling in response to far field compression by the alpine orogeny (Guillocheau et al., 2000). This proposition is consistent with their spatial distribution, i.e., higher rates of erosion found going toward the Alps would indicate higher rates of rock uplift towards the Southeast. On the other hand, and it may not be incompatible with the first hypothesis, the higher incision rates could reflect a change in the incision rates during the Middle Pleistocene, i.e., incision would have been slower sometimes after 600-400 ka than in the Early Pleistocene. Tissoux et al. (2011) reported a similar evolution along the Loire River (Loire Basin). A somewhat comparable evolution, i.e., reduction of fluvial efficiency throughout the Quaternary, was suggested by Genuite et al. (2021) along the course of the Lower Seine River. These authors further hypothesized that it could be climate-driven. Nehme et al. (2020) also documented the decrease of incision rates during the Quaternary in this area and suggested that this phase was triggered by the incision of the English Channel River (Gibbard and Cohen, 2015). However, data from the Somme River (Figure 8.1) somewhat record a different evolution, with the incision rates monotonically increasing from the oldest to the youngest terraces. Further dating seems therefore required to carefully test the different hypotheses and assess the regional patterns of incision.

8.2 Valley bottom age

8.2.1 Ages determined directly in the valley bottom

As explained in chapter 3, many samples from the valley bottom were dated as a part of the MIS 2. These includes (i) samples of affluents of the Seine River such as Oise, Marne and Loing valleys, (ii) samples from the Bassée area at Bazoches, Vimpelles and Noyen-sur-Seine, and (iii) at Saint-Martin-la-Garenne, lower Seine. These samples dated as MIS 2 were thus deposited during the Last Glacial Maximum (LGM). During this period, the LGM records ice volume maxima and sea level minima (-120 m from c.a. 29-18 ka) during the last 100 ka glacial cycles (Waelbroeck et al., 2002).

Many dating based on radiocarbon, OSL and thermoluminescence similarly returned ages from the Weschelian or the Holocene:

- In the Oise valley, the oldest ages being 32.75 ka BP at Isle-Adam (Blaser et al., 2017), corresponding to the Middle Weichselian (MIS 3) ongoing to the Holocene (MIS 1) (Pastre et al., 1997, 2000, 2002; Larue, 2000; Krier, 2004; Granai, 2014; Blaser et al., 2017; Granai and Limondin-Lozouet, 2018).
- Many sediments in the Marne valley were dated as a part of the MIS 5 and the Holocene MIS 1 (Le Jeune et al., 2012; Granai, 2014; Blaser et al., 2021).
- In the Eure valley, the available data show ages comprising between 5.53 and 1.85 ka BP, corresponding to the Holocene (Atlantic, Subboreal, Subatlantic periods) (Granai, 2014).
- In the Seine valley, the available data show the evolution of the valley bottom withing the Holocene (MIS 1). Samples located in the surrounding area of Paris comprises ages between 5.745 and 2.835 ka BP, corresponding to the MIS 1 (Atlantic and Subboreal periods). Going downstream, at Rueil-Malmaison ages are comprises between 7.01 and 0.47 ka BP, corresponding to the MIS 1 (Boreal and Subatlantic periods). Upstream of Poses dam, at Porte-Joie, the available data are comprised between 2.98 and 1.18 ka BP corresponding to the MIS 1 (Subboreal). Downstream of Poses dam, at Alizay the available data are comprise between 3.81 and 2.14 ka BP, corresponding to the MIS 1 (Subboreal period). In the Seine estuary, at Anneville-Ambourville meander, at Heurteauville and at Marais Vernier, the available data show the Holocene evolution of this area comprise between the Boreal and Subatlantic periods (Sebag, 2002; Frouin, 2007; Frouin et al., 2010).

It seems thus likely that the geometries of valley bottom and alluvium infill are largely inherited from the last glacial period incision and subsequent aggradation during the Tardiglacial and Holocene periods (Pastre et al., 1997, 2000; Krier, 2004). However, at Val-de-Reuil near the Poses dam, a sample from valley bottom was dated from MIS 6 using ESR. Additionally, in the Marne valley, the oldest ages based on U-Th in bones were 206 ka and 190 at Maisons-Alfort (MIS 7 and MIS 6) (Durbet et al., 1997; Blaser et al., 2021). Although these ages are subject to uncertainties, they reveal ages potentially older than MIS 2.

8.2.2 Indirect ages of valley bottom using terraces near of valley bottom

In order to constrain the valley bottom age, we use the previous ages obtained in terraces at the edge of valley bottom. The most representative site to constrain the age of valley bottom is Sandrancourt. In this area, four samples were dated, in which, three of the samples are a part of the Fyd terraces (samples A3D-003, A3D-004 and A3D-005) and are situated about 500 m of

distance to valley bottom limit, and sample A3D-028 located in the current valley bottom. Samples located in the Fyd terrace, have an age attributable from MIS 8 to MIS 7, supposing that the aggradation of the Fyd terrace could well represent MIS 7, indeed, the subsequent incision may occur during the MIS 6. A similar pattern was observed at Manoir Brésil site in which sediments near of the valley bottom related to the MIS 7, this lead to suppose that a part of the valley bottom belongs to MIS 6.

In the Bassée area, Deleplancque et al., 2018 correlated the terrace T_1 that bordering the valley bottom as a part of the MIS 7-6, considering the observations in terraces from the Yonne valley from Chaussé et al., (2004) and also the terrace Fyb in the Aube valley dated as a part of the MIS 6-5 at +4 m RH (Voinchet et al., 2015).

As a conclusion, we can propose that along the valley bottom of the Seine catchment, at least two Marine Isotopic Stage are recorded: MIS 6 and MIS 2. It is known that at the end of the Weichselian glaciation (MIS 2) erosion was less powerful than at the end of the MIS 6 (Toucane, 2008). Therefore, it is possible that the deposits in valley bottoms from MIS 6 to MIS 2 were not entirely removed during the Weichselian glaciation MIS 2, preserving deposits from the MIS 6 in the valley bottom. Also, and it is a limitation o this study, the valley bottom was delimited including all deposits located less than 10 m above the river. This delimitation could influence which deposits are included or not in the valley bottom and then on this one's age. This limit could be modified in the future to test its impact.

8.3 Valley bottom geometry

8.3.1 Alluvium thickness geometries

Using the BSS and bibliography data, the database that as defined in chapter 5, the geometry of the valley bottom geometry at the bedrock-alluvium interface along the Seine catchment was estimated. This data was interpolated using the directional kriging defined in chapter 7. Valley bottom along the Seine catchment is variable in valley width providing the space for sediment accumulation or alluvial infill. Although dating largely returned ages from MIS 2 or younger, the previous ages determined in the valley bottom suggest that the alluvial infill could occur since as old as 180 ka (MIS 6). These alluvial sediments overlie the main bedrock lithologies (identified in chapter 6) dominated by chalk, limestone, marl, clay and sand. These lithologies was classified according to their erodibility, founding that chalk and limestones are medium

lithologies. In contrast, marls and clays are soft lithologies. Due to limited outcropping, no relation was found for sand lithologies and erodibility.

Within the Seine catchment, the alluvial thickness is variable with a mean of about 8 m, increasing from upstream to downstream. When the increase in discharge occurs, these can trigger the formation of a new incision that could be reflect in the valley bottom affecting their valley width and its depth. In meandering areas (Lower Seine, Oise and Marne), the mechanisms of pool and riffle is well observed. The most remarkable increases in alluvium thickness were observed (i) in the estuarine area, between Poses dam and Le Havre, where the alluvium infill reaches 30 m of thick, (ii) at the confluence between the Oise and Marne with the Seine River and (iii) in the Bassée area.

8.3.2 Assessment of the volumes of alluvium stored in the transfer zone

The volume of sediment supply along the valley bottom of the Seine catchment was calculated using the SPDE kriging for ranges [8000 m, 800 m]. This volume was determined of c.a. 10.13 km^3 and represents a minimum value in the Seine catchment. If we consider a mean of incision rates at 55 m/Ma over the whole Seine catchment, the stored volume will correspond to c.a. 1.2% of the total denudated volume. Further taking into account the main tributaries of the Seine catchment, considering some smaller tributaries, an additional surface of 1304 km^2 can be added to the valley bottom. If we hypothesize that in these tributaries (Ormain, Serain, Armaçon, Vanne, Ouanne, Yerres, Essone, Yvette, Orge, Grand Morin, Petit Morin, Ourc, Servais, Serre, Aisne, Orrouy, Breche, Therain, Nonette, Presles, Esches, Sausseron, Real, Epte, Cambon, Robec, Andelle, Clerette, Austreberthe, La Voise, La Vesgre, Blaise, Ilton and Risle tributaries) alluvial thickness is in between 2 and 8 m, an average of 5 m can be considered. This yields an additional volume of 6.52 km^3. The total volume estimate is then c.a. 16.65 km^3. Considering this volume, and the sediment flux that was calculated Castelltort and Van Den Driessche (2003) within the Seine catchment at 4.9 x 10^{-3} km^3/a, we estimate the residence time of valley infill determined to evacuate this volume at 3.4 ka. This time is similarly to those obtained in the Himalaya valley bottom, where the residence time is determined at 3 ka (Blöthe and Korup, 2013), in a geological context completely different to the Seine catchment.

8.3.3 Geometry of the bedrock-alluvium interface: identification of regressive knickpoints?

The longitudinal profile of the Seine River that includes the part in the English Channel shows a significant break in their slope of the bedrock at the Contentin troughs between -80 and -100 m (Lautridou et al., 1999; Paquet et al., 2023). Supposing that knickpoints were initiated at the Seine catchment outlet in response to climate, eustatic and/or tectonic forcing, they migrated upstream. When reaching confluences, the change in trunk channel elevation acted like a base level change for the tributary causing the propagation of the knickpoint within the tributary (Wolpert and Forte, 2021). Finally, their location in the drainage system could impact their migration rates (Crosby et al., 2007). For example, drainage area is significantly less along the Eure, Yonne and Loing valleys compared to the Bassée area, Marne, or downstream Paris at Poses dam. Knickpoints may thus retreat faster in the latter than in the former (Loget et al., 2009).

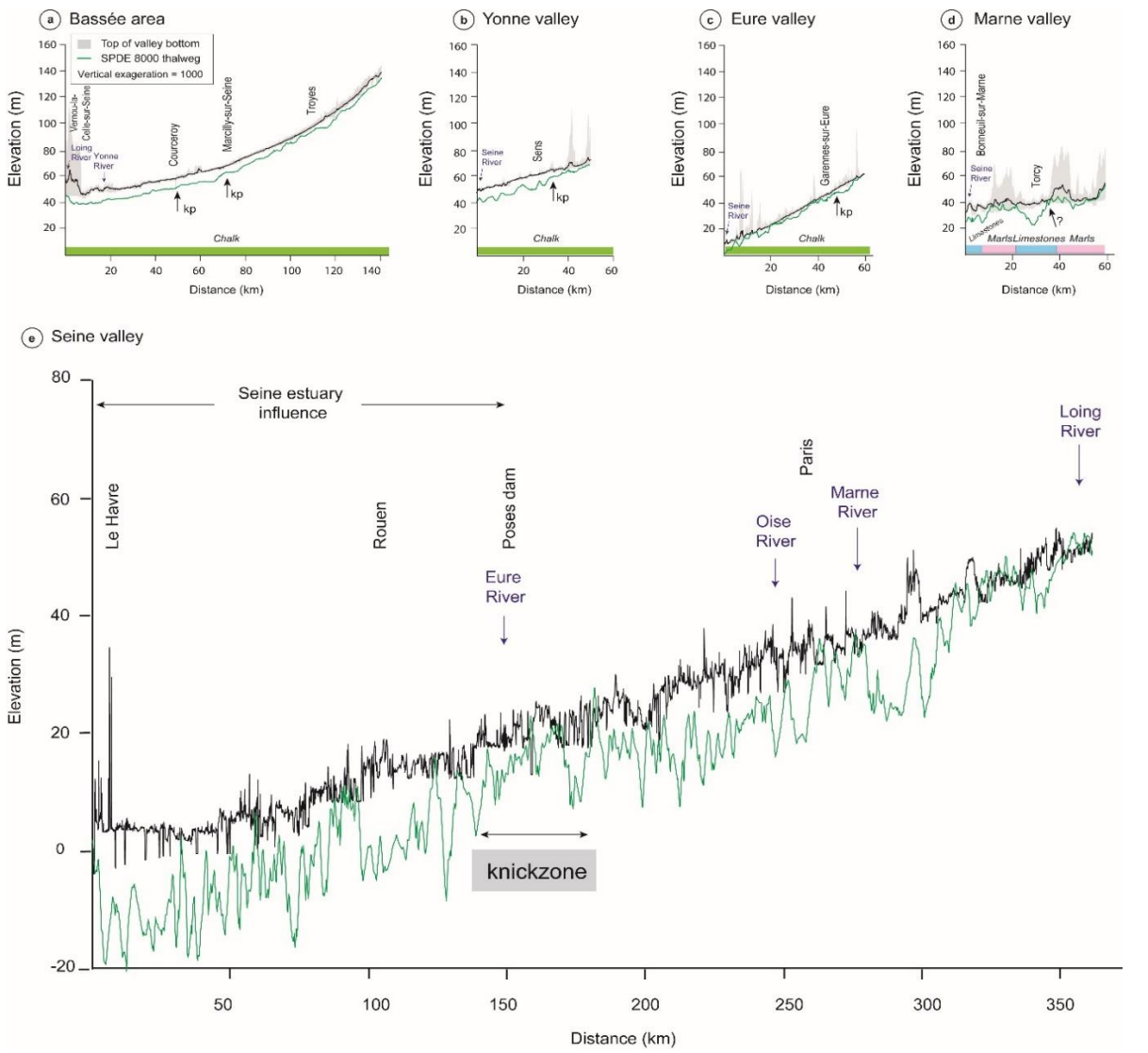

Figure 8.2. Elevation (SWATH) profiles along the centerline of (a) the Bassée area; (b) Yonne valley; (c) Eure valley, (d) Marne valley and (e) In the Seine valley after the confluence with the Loing River. green line represents the valley thalwegs at the bedrock-alluvium interface. Green rectangles correspond to areas with chalk bedrock lithology. Pink rectangles correspond to areas with marl bedrock lithology. Blue rectangles correspond to areas with limestone bedrock lithology.

Many knickpoints are observed above chalk bedrock, in the Bassée area, Yonne, Loing, Eure valley and near the Poses dam (Figure 8.2-a-b-c). In contrast, a possible knickpoint at the lithological transition between marls and limestones may be inferred in the Marne valley (Figure 8.2-d). Interestingly, our study reveals two knickpoints in tributaries that are compatibles with the one described by Deleplancque et al. (2018) in the Bassée: one along the Loing valley and another one in the Yonne valley (Figure 8.2-b). Together, these three knickpoints strongly support regressive erosion from a common origin. Deleplancque, (2016)

hypothesized knickpoint migration from the Contentin throughs until the Bassée area during a duration of either 23.5 or 10.1 ka (i.e., further hypothesizing that they occurred during limited periods of MIS 2 or MIS 6) and found migration rates between 25 and 47 m/y, which is high in the literature (Loget et al., 2009). Furthermore, recent experimental work highlights that knickpoints may arise autogenically (Scheingross et al., 2020): they do not necessarily originate from sea level fall. A test for the hypothesis that the knickpoints found upstream of Fontainebleau originate from the Cotentin would be to find their equivalent downstream of Paris, as a proof of a "wave" propagating and splitting throughout the entire catchment. As mentioned before, it is complicated along the Marne and Oise valleys due to the riffle and pool geometry. The Eure knickpoint may however be a potential equivalent that could validate this hypothesis.

At Poses dam, the large knickpoint observed raises several questions. Its location at the limit of the tidal influence could support that it is not only due to regressive erosion but also to changes in the hydraulics of the Seine River system. Another question is the origin of this knickpoint in a regressive erosion paradigm if the ones in the Bassée also originated from the base level fall. It could be either originate from two events, i.e., the Poses one would be younger (Weichselian) while the upstream ones would be older (Saalian) as advocated by Deleplancque (2016). Alternatively, it could originate from the same continuous base level fall, which would have resulted in the formation of several knickpoints (Cantelli and Muto, 2014; Grimaud et al., 2016). Assuming pure regressive erosion for this knickpoint and using an approach like that of Deleplancque (2016), a migration rate between 6.4 and 14.9 m/y is estimated, which is more consistent with those reported by Loget et al., (2009).

Conclusions

Conclusions

Conclusions

This PhD focused on the Late Quaternary incision dynamics and alluvial infill in valley bottoms within the Seine catchment to reconstruct their large-scale geometry at the bedrock-alluvium interface and to better constrain the timing of their evolution. The challenge of the limited availability of the data in the field was partly overcome by the access given to outcrops in active quarries and by the analysis of boreholes (mainly from the BSS).

In the field, the sedimentary facies observed were principally fluvial, except downstream Paris at Manoir Brésil where tidal deposits were found. Dating of samples allowed precising the chronology of fluvial evolution of the Seine catchment during the Middle and Lower Pleistocene. While ESR-OSL dating of sediments in valley bottoms or along the edges indicates ages predominantly associated with the last major glacial period, a body of evidence, both direct and indirect, suggests an origin of at least part of the current valley bottoms as early as isotopic stage 6. Ages obtained from alluvial terraces complement existing literature on incision rates, particularly in the Bassée area and downstream of Rouen, where detailed studies elucidate the interactions between incision and substrate uplift.

A new term was introduced to give the relative elevation of the sample RH' (elevation above the valley bottom) in comparation with the RH (classical relative elevation), we consider that downstream Paris (i.e., in the Lower Seine valley) is more appropriate to use RH' due to incision variations. Overall, a lack of harmonization between alluvial terraces on geological maps upstream and downstream Paris was observed. Some suggestions that would need to be further completed were made.

An original method (SPDE kriging) was used to estimate alluvium thickness geometries in the valley bottoms. It allowed estimating the volume stored in alluvial plains and -combined with dating of alluvial bottoms- to estimate residence timescale of sediments that is comparable with that of the Himalaya. The main bedrock lithologies (chalk, limestone, marl, sand and clay) of the valley bottom were identified from boreholes. A GIS analysis demonstrate the influence of discharge, lithology, and fluvial style on the geometry of valley bottom alluvium. Finally, some observed knickpoints could potentially highlight regressive erosion during the last two glacial periods.

References

References

Allen, J.R.L. 1983. Studies in fluviatile sedimentation: bars, bar-complexes and sandstone sheets (low-sinuosity braided streams) in the Brownstones (L. Devonian. Welsh Borders. Sedimentary Geology, 33, 237–293.

Allen, J. R. L. 1965. Late Quaternary Niger delta, and adjacent areas: sedimentary environments and lithofacies. AAPG Bulletin, 49(5), 547-600.

Allen, L.G., Gibbard, P.L., Pettit, M.E., Preece, R.C. and Robinson, J.E. 1996. Late pleistocene interglacial deposits at pennington marshes, Lymington, Hampshire, southern England. Proceedings of the Geologists' Association, 107, 39–50.

Allen, P.A. 2008. From landscapes into geological history. Nature, 451, 274–276, https://doi.org/10.1038/nature06586.

Allen, P.A. 2017. Sediment Routing Systems: The Fate of Sediment from Source to Sink.

Alley RB, Mayewski PA, Sowers T, Stuiver M, Taylor KC, Clark PU. 1997. Holocene climatic instability: a prominent, widespread event 8200 yr ago. Geology 25(6):483–6.

André, G., 2003. Caractérisation des déformations méso-cénozoïques et des circulations de fluides dans l'Est du Bassin de Paris (Doctoral dissertation, Université Henri Poincaré-Nancy 1).

Andrieux, E., Bertran, P. and Saito, K. 2016. Spatial analysis of the French Pleistocene permafrost by a GIS database. Permafrost and periglacial processes, 27, 17–30.

Antoine, P. 1994. The Somme Valley terrace system (Northern France); a model of river response to quaternary climatic variations since 800 000 BP. Terra-Nova, 6, 453–464.

Antoine, P. 1997. Modifications des systèmes fluviatiles à la transition Pléniglaciaire–Tardiglaciaire et à l'Holocène : l'exemple du bassin de la Somme (Nord de la France. Géographie Physique et Quaternaire, 51, 93–106.

Antoine, P. 2019. Le quaternaire de la vallée de la Somme (terrasses fluviatiles, loess et paléosols): une contribution à l'inventaire national du patrimoine géologique. Quaternaire. Revue de l'Association française pour l'étude du Quaternaire, 30, 257–270.

Antoine, P., Lautridou, J.P. and Laurent, M. 2000. Long-termfluvial archives in NWFrance: response of the Seine and Somme rivers to tectonic movements, climatic variations and sea-level changes. Geomorphology, 32, 183–207, https://doi.org/10.1016/S0169-555X.

Antoine, P., Lozouet, N.L., Chaussé, C., Lautridou, J.-P., Pastre, J.-F., Auguste, P., Bahain, J.-J., Falguères, C., Galehb, B., 2007. Pleistocene fluvial terraces from northern France (Seine, Yonne, Somme): synthesis, and new results from interglacial deposits. Quat. Sci. Rev. 26, 2701–2723.

Antoine, P., Auguste, P., Bahain, J.J., Chausse, C., Falgueres, C., Ghaleb, B. and Voinchet, P. 2010. Chronostratigraphy and palaeoenvironments of Acheulean occupations in

Northern France (Somme, Seine and Yonne valleys. Quaternary International, 223, 456–461.

Antoine, P., Rousseau, D. D., Fuchs, M., Hatté, C., Gauthier, C., Marković, S. B., and Rossignol, J. 2009. High-resolution record of the last climatic cycle in the southern Carpathian Basin (Surduk, Vojvodina, Serbia). Quaternary International, 198(1-2), 19-36.

Argant, J., and Philippe, M. 2011. L'analyse pollinique des coprolithes: un outil pour la reconstruction du paléoenvironnement. Quaternaire. Hors-série.

Armitage, J. J., Duller, R. A., Whittaker, A. C., & Allen, P. A. (2011). Transformation of tectonic and climatic signals from source to sedimentary archive. Nature Geoscience, 4(4), 231-235.

Audouze, F., Cahen, D., Keeley, L.H., Schmider, B., 1981. Le site magdalénien du Buisson Campin à Verberie (Oise). Gall. Préhistoire 24, 99–143.

Bahain, J.J., Duval, M., et al. 2019. ESR and ESR/U-series chronology of the Middle Pleistocene site of Tourville-la-Rivière (Normandy, France) - A multi-laboratory approach. Quaternary International, 556, 66–78.

Bahain, J. J., Laurent, M., Falguères, C., Voinchet, P., Farkh, S., and Tissoux, H., 2002. Datation par résonnance paramagnétique électronique (RPE) des formations fluviatiles pléistocènes et des gisements archéologiques ou paléontologiques associés. Quaternaire, 13(2), 91-103.

Balescu, S., Lamothe, M. and Lautridou, J.P. 1997. Luminescence evidence for two Middle Pleistocene interglacial events at Tourville, northwestern France. Boreas, 26, 61–72.

Ballesteros, D., Farrant, A., Nehme, C., Woods, M., Todisco, D. and Mouralis, D. 2020. Stratigraphical influence on chalk cave development in Upper Normandy, France: implications for chalk hydrogeology. International Journal of Speleology, 49, 2.

Bates, M.R., Keen, D.H. and Lautridou, J.P. 2003. Pleistocene marine and periglacial deposits of the English Channel. Journal of Quaternary Science: Published for the Quaternary Research Association, 18, 319–337.

Bates, M.R., Briant, R.M., Rhodes, E.J., Schwenninger, J.L. and Whittaker, J.E. 2010. A new chronological framework for Middle and Upper Pleistocene landscape evolution in the Sussex/Hampshire Coastal Corridor, UK. Proceedings of the Geologists' Association, 121, 369–392.

Berg, J.H., Boersma, J.R. and Gelder, A.V. 2007. Diagnostic sedimentary structures of the fluvial-tidal transition zone–Evidence from deposits of the Rhine and Meuse. Netherlands Journal of Geosciences/Geologie en Mijnbouw, 86.

Bertran, P., Liard, M., Sitzia, L. and Tissoux, H. 2016. A map of Pleistocene deposits in Western Europe, with special emphasis on France. Journal of Quaternary Science, 31, 844–856.

References

Bertran, P., Andrieux, E., Antoine, P., Deschodt, L., Font, M. and Sicilia, D. 2017. Pleistocene involutions and patterned ground in France: examples and analysis using a GIS database. Permafrost and periglacial processes, 28, 710–725.

Bertran, P., Andrieux, E., Bateman, M., Font, M., Manchuel, K. and Sicilia, D. 2018. Features caused by ground ice growth and decay in Late Pleistocene fluvial deposits, Paris Basin, France. Geomorphology, 310, 84–101.

Bertran, P., Stadelmaier, K.H. and Ludwig, P. 2022. Last Glacial Maximum active layer thickness in Western Europe, and the issue of 'tundra gleys' in loess sequences. Journal of Quaternary Science, 37, 1222–1228.

Best, J.L., Ashworth, P.J., 1997. Scour in large braided rivers and the recognition of sequence stratigraphic boundaries. Nature 387, 275–277.

Bintanja, R., Roderik, S. W., and van de Wal, O. J. 2005. Modeled atmospheric temperatures and global sea levels over the past million years, Nature, 437, 125–128, doi:10.1038/nature03975.

Bishop, P., Hoey, T. B., Jansen, J. D., and Artza, I. L. 2005. Knickpoint recession rate and catchment area: the case of uplifted rivers in Eastern Scotland. Earth Surface Processes and Landforms: The Journal of the British Geomorphological Research Group, 30(6), 767-778.

Blaser, F., Chaussée, C., Raymond, P., Blaser, R., 2015. Maurecourt «78 Sentier des Carreaux » (Diagnostic INRAP No. D108832).

Blaser, R., Chaussé, C., Roncin, O., Rochart, X., Bayle, G., Lefèvre, A., Raymond, P., Roque, C., 2017. L'Isle-Adam Intersection des avenues Paul Thoureau & Chemin Vert (Diagnostic INRAP No. D101013).

Blaser, F., Djema, H., Locht, J. L., and Chaussé, C. 2021. De l'Île-de-France à l'Europe du Nord-Ouest. Les peuplements humains avant le Dernier Maximum Glaciaire. Revue archéologique de Picardie. Numéro spécial, 36.

Blondeau, P., Cavelier, C., Pfeffer, D., Jovet, P., Pomerol, C., 1967. Senlis, carte géologique de la France 1/50000.

Blöthe, J. H., and Korup, O. 2013. Millennial lag times in the Himalayan sediment routing system. Earth and Planetary Science Letters, 382, 38-46.

Blum, M., Martin, J., Milliken, K. and Garvin, M. 2013. Paleovalley systems: insights from Quaternary analogs and experiments. Earth Sci. Rev, 116, 128–169, https://doi.org/10.1016/j.earscirev.2012.09.003.

Blum, M.D. and Törnqvist, T.E. 2000. Fluvial responses to climate and sea-level change: a review and look forward. Sedimentology, 47, 2–48.

Bodu, P., Julien, M., Valentin, B., Debout, G., Averbouh, A., Bemilli, C., ... & Enloe, J. G. 2006. Un dernier hiver à Pincevent : les Magdaléniens du niveau IV0 (Pincevent, La grande Paroisse, Seine-et-Marne). Gallia préhistoire, 48, 1-180.

Bond, G. C., Showers, W., Elliot, M., Evans, M., Lotti, R., Hajdas, I., and Johnson, S., 1999. The North Atlantic's 1-2 kyr climate rhythm: relation to Heinrich events,

Dansgaard/Oeschger cycles and the Little Ice Age. Geophysical Monograph-American Geophysical Union, 112, 35-58.

Bonnet, S., and Crave, A. 2003. Landscape response to climate change: Insights from experimental modeling and implications for tectonic versus climatic uplift of topography. Geology, 31(2), 123-126.

Böse, M., Lüthgens, C., Lee, J. R., and Rose, J. 2012. Quaternary glaciations of northern Europe. Quaternary Science Reviews, 44, 1-25.

Bourdier, F. 1969. Excursion dans le bassin de Paris de l'Association Internationale pour l'Etude du Quaternaire du 18 au 28 aout t 1969 : Etude comparé des dépôts quaternaires des bassins de la Seine et de la Somme. Bulletin d'information des Géologues du Bassin de Paris, 21, 169–220.

Bowen, D. Q., 1999. Only four major 100-ka glaciations during the Brunhes Chron? Intertional Journal of Earth Sciences 88, 276-284.

Bradley, S.L., Milne, G.A., Teferle, F.N., Bingley, R.M. and Orliac, E.J. 2009. Glacial isostatic adjustment of the British Isles: new constraints from GPS measurements of crustal motion. Geophysical Journal International, 178, 14–22.

Bradwell, T., Stoker, M. S., Golledge, N. R., Wilson, C. K., Merritt, J. W., Long, D., Everest, J. D., Hestvik, O. B., Stevenson, A. G., Hubbard, A. L., Finlayson, A. G., Mathers, H. E. 2008. The northern sector of the last British Ice Sheet: Maximum extent and demise. Earth-Science Reviews 88, 207-226.

Brennan, B., Lyons, R., Phillips, S., 1991. Attenuation of alpha particle track dose for spherical grains. Nucl. Tracks Radiat. Meas. 18, 249–253.

Brennan, B.J., 2003. Beta doses to spherical grains. Radiat. Meas. 37, 299–303.

Briais, J. 2015. Le Cénozoïque du bassin de Paris : un enregistrement sédimentaire haute résolution des déformations lithosphériques en régime de faible subsidence 451.

Briais, J., Guillocheau, F., Lasseur, E., Robin, C., Châteauneuf, J. J., and Serrano, O. 2016. Response of a low-subsiding intracratonic basin to long wavelength deformations: the Palaeocene–early Eocene period in the Paris Basin. Solid Earth, 7(1), 205-228.

Briant, R.M., Bates, M.R., Schwenninger, J.L. and Wenban-Smith, F. 2006. An optically stimulated luminescence dated Middle to Late Pleistocene fluvial sequence from the western Solent Basin, southern England. Journal of Quaternary Science: Published for the Quaternary Research Association, 21, 507–523.

Briant, R.M., Bates, M.R., Marshall, G.D., Schwenninger, J.L. and Wenban-Smith, F.F. 2012. Terrace reconstruction and long profile projection: a case study from the Solent River system near Southampton, England. Proceedings of the Geologists' Association, 123, 438–449.

Bridge, J.S., Jalfin, G.A. and Georgieff, S.M. 2000. Geometry, lithofacies, and spatial distribution of Cretaceous fluvial sandstone bodies, San Jorge Basin, Argentina: outcrop analog for the hydrocarbon-bearing Chubut Group. Journal of Sedimentary Research, 70, 341–359.

References

Bridgland, D.R. 2000. River terrace systems in north-west Europe: an archive of environmental change, uplift and early human occupation. Quat. Sci. Rev, 19, 1293–1303.

Bridgland, D.R. 2006. The Middle and Upper Pleistocene sequence in the Lower Thames: a record of Milankovitch climatic fluctuation and early human occupation of southern Britain. Proceedings of the Geologists' Association, 117, 281–305.

Bridgland, D. and Westaway, R. 2008. Climatically controlled river terrace staircases: a worldwide Quaternary phenomenon. Geomorphology, 98, 285–315.

Bridgland, D.R. 1994. The Quaternary of the Thames. Geological Conservation Review Series.

Bridgland, D.R. and Schreve, D.C. 2009. Implications of new Quaternary uplift models for correlation between the Middle and Upper Thames terrace sequences, UK. Global and Planetary Change, 68, 346–356.

Brierley, G. J., and Fryirs, K. A. 2013. Geomorphology and river management: applications of the river styles framework. John Wiley & Sons.

Brocard, G. Y., and Van der Beek, P. A. 2006. Influence of incision rate, rock strength, and bedload supply on bedrock river gradients and valley-flat widths: Field-based evidence and calibrations from western Alpine rivers (southeast France).

Bufe, A., Turowski, J. M., Burbank, D. W., Paola, C., Wickert, A. D., and Tofelde, S. 2019. Controls on the lateral channel-migration rate of braided channel systems in coarse non-cohesive sediment. Earth Surface processes and landforms, 44(14), 2823-2836.

Bull, W. B., 1991. Geomorphic Responses to Climatic Change. Oxford: Oxford University Press.

Burbank, D. W., and Anderson, R. S. (2012). Tectonic geomorphology. John Wiley & Sons.

Castelltort, S. and Van Den Driessche, J. 2003. How plausible are high-frequency sediment supply-driven cycles in the stratigraphic record? Sediment. Geol, 157, 3–13, https://doi.org/10.1016/S0037-0738(03)00066-6.

Burbank, D. W., Leland, J., Fielding, E., Anderson, R. S., Brozovic, N., Reid, M. R., and Duncan, C. 1996. Bedrock incision, rock uplift and threshold hillslopes in the northwestern Himalayas. Nature, 379(6565), 505-510.

Busschers, F. S., Van Balen, R. T., Cohen, K. M., Kasse, C., Weerts, H. J., Wallinga, J., & Bunnik, F. P. 2008. Response of the Rhine–Meuse fluvial system to Saalian ice-sheet dynamics. Boreas, 37(3), 377-398.

Campisano, C.J. 2012. Milankovitch Cycles, Paleoclimatic Change, and Hominin Evolution. Nature Education Knowledge, 4.

Castelltort, S., Fillon, C., Lasseur, É., Ortiz, A., Robin, C., Guillocheau, F., Tremblin, M., Bessin, P., Guerit, L., Dekoninck, A., Allanic, C., Gautheron, C., Barbarand, J., Loget, N., Uzel, J., Yans, J., Briais, J., Al-Reda, M., Baby, G., François, T., Roig, J-Y.,and Calassou, S. 2023. The Source-to-Sink Vade-mecum : History, Concepts and Tools| Vade-mecum de l'approche Source-To-Sink: Histoire, Concepts et Outils.

References

Chancerel, A. 1986. Le système de nappes alluviales de la Seine en aval de Rouen. Bulletin du Centre de Géomorphologie, Caen, 31, 73–82.

Chantraine, J., Autran, A., Cavelier, C., 2003. Carte géologique de la France à 1/1 000 000, 6e édition révisée. Orléans BRGM.

Chaput, E. 1924. Les principales phases de l'évolution de la vallée de la Seine. Annales de Géographie, t, 36, 125–135.

Chaussé, C. 2003. Les nappes alluviales de la basse vallée de l'Yonne, approche géométrique et chronostratigraphique et l'apport de l'étude de la Nappe de Soucy à la compréhension des occupations du Paléolithique inférieur de Soucy.

Chaussé, C., Coussot, C., et al. 2021. Données quaternaires franciliennes antérieures au dernier maximum glaciaire: éléments de synthèse issus de deux décennies de recherche en archéologie préventive. Revue archéologique de Picardie. Numéro spécial, 36, 97–126.

Chaussé, C., Voinchet, P., Bahain, J. J., Connet, N., Lhomme, V., and Limondin-Lozouet, N. 2004. Middle and upper Pleistocene evolution of the river Yonne valley (France). First result [Evolution de la vallée de l'Yonne {France} au Pléistocène moyen et supérieur; premiers résultats]. Quaternaire, 15(1), 53-64.

Chilès, J.-P., Desassis, N., 2018. Fifty years of kriging. Handb. Math. Geosci. Fifty Years IAMG 589–612.

Cholley, A. and Firmin, H. 1945. La vallée et les méandres de la Basse-Seine. Bulletin de l'Association de Géographes Français, 22, 70–75.

Choudhury, D., Timmermann, A., Schloesser, F., Heinemann, M. and Pollard, D. 2020. Simulating Marine Isotope Stage 7 with a coupled climate–ice sheet model. Climate of the Past, 16, 2183–2201.

Church, M. 2006. Bed material transport and the morphology of alluvial river channels. Annu. Rev. Earth Planet. Sci., 34, 325-354.

Clark, P. U., Archer, D., Pollard, D., Blum, J. D., Rial, J. A., Brovkin, V., and Roy, M. 2006. The middle Pleistocene transition: characteristics, mechanisms, and implications for long-term changes in atmospheric pCO2. Quaternary Science Reviews, 25(23-24), 3150-3184.

Cliquet, D., Lautridou, J.P., Antoine, P., Lamothe, M., Leroyer, M., Limondin Lozouet, N. and Mercier, N. 2009. La séquence loessique de Saint Pierre lès Elbeuf (Normandie, France) : nouvelles données archéologiques, géochronologiques et paléontologiques. Quaternaire. Revue de l'Association française pour l'étude du Quaternaire, 20, 321–343.

Clubb, F.J., Mudd, S.M., Milodowski, D.T., Valters, D.A., Slater, L.J., Hurst, M.D., Limaye, A.B., 2017. Geomorphometric delineation of floodplains and terraces from objectively defined topographic thresholds. Earth Surf. Dyn. 5, 369–385.

References

Clubb, F. J., Mudd, S. M., Schildgen, T. F., Van Der Beek, P. A., Devrani, R., and Sinclair, H. D. 2023. Himalayan valley-floor widths controlled by tectonically driven exhumation. Nature Geoscience, 16(8), 739-746.

Clubb, F.J., Weir, E.F. and Mudd, S.M. 2022. Continuous measurements of valley floor width in mountainous landscapes. Earth Surface Dynamics, 10, 437–456.

Cohen, K., Cartelle, V., Barnett, R., Busschers, F.S. and Barlow, N. 2022. Last Interglacial sea-level data points from Northwest Europe. Earth System Science Data, 14, 2895–2937.

Cojan, I., Brulhet, J., Corbonnois, J., Devos, A., Gargani, J., Harmand, D., Jaillet, S., Jouve, A., Laurain, M., Lejeune, O., 2007. Morphologic evolution of eastern Paris Basin:«ancient surfaces» and Quaternary incisions. Mém. Société Géologique Fr. 178, 135–155.

Cordier, S., Frechen, M. and Harmand, D. 2009. The pleistocene fluvial deposits of the moselle and middle rhine valleys: new correlations and compared evolutions. Quaternaire. Revue de l'Association française pour l'étude du Quaternaire, 20, 35–47.

Cordy, J.M., Carpentier, G. and Lautridou, J.P. 2003. Les paléo-estuaires du stade isotopique 7 à Tourville-La-rivière et à Tancarville (Seine) : faune de rongeurs et cadre stratigraphique. Quaternaire, 14, 15–23.

Coutard, S., Antoine, P., et al. 2018. La séquence loessique Pléistocène moyen à supérieur d'Etricourt Manancourt (Picardie, France) : un enregistrement pédo sédimentaire de référence pour les derniers 350 ka. Quaternaire. Revue de l'Association française pour l'étude du Quaternaire, 29, 311–346.

Covault, J. A., Craddock, W. H., Romans, B. W., Fildani, A., and Gosai, M. 2013. Spatial and temporal variations in landscape evolution: Historic and longer-term sediment flux through global catchments. The Journal of Geology, 121(1), 000-000.

Crosby, B. T., and Whipple, K. X. 2006. Knickpoint initiation and distribution within fluvial networks: 236 waterfalls in the Waipaoa River, North Island, New Zealand. Geomorphology, 82(1-2), 16-38.

Crosby, B.T., Whipple, K.X., Gasparini, N.M., Wobus, C.W., 2007. Formation of fluvial hanging valleys: Theory and simulation. J. Geophys. Res. Earth Surf. 112.

Dansgaard, W., Johnsen, S. J., Clausen, H. B., Dahl-Jensen, D., Gundestrup, N. S., Hammer, C. U., and Bond, G. 1993. Evidence for general instability of past climate from a 250-kyr ice-core record. nature, 364(6434), 218-220.

Davy, P., and Lague, D. 2009. Fluvial erosion/transport equation of landscape evolution models revisited. Journal of Geophysical Research: Earth Surface, 114(F3).

Deleplancque, B. 2016. Caractérisation des heterogeneities sédimentaires d'une plaine alluviale : Exemple de l'évolution de la Seine supérieure depuis le dernier maximum glaciaire. PhD dissertation.

Deleplancque, B., Cojan, I., Beucher, H., Mehl, C. and Stab, O. 2018. Spatial and temporal patterns of the upper Pleistocene alluvial fill deposits of the upstream Seine River alluvial plain, la Bassée, France. Geomorphology, 318, 148–161, https://doi.org/10.1016/j.geomorph.2018.06.005.

References

Delsinne, N. 2005. Evolution pluri-millénaire à pluri-annuelle du prisme sédimentaire d'embouchure de la Seine. Facteurs de contrôle naturels et d'origine anthropique.

Demoulin, A., 1998.Testing the tectonic significance of some parameters of longitudinal river profiles: the case of the Ardennes (Belgium, NW Europe).Geomorphology 24,189–208. http://dx.doi.org/10.1016/S0169-555X(98)00016-6.

Dergachev, V. A., Raspopov, O. M., Damblon, F., Jungner, H., and Zaitseva, G. I. 2007. Natural climate variability during the Holocene. Radiocarbon, 49(2), 837-854.

Desprat, S., Goñi, M.S., et al. 2007. 25. Climate variability of the last five isotopic interglacials: Direct land-sea-ice correlation from the multiproxy analysis of North-Western Iberian margin deep-sea cores. In: Developments in Quaternary Sciences. 375–386.

Despriée, J., Voinchet, P., Bahain, J. J., Falguères, C., Lorain, J. M., and Duvialard, J. 2003. Les nappes alluviales pléistocènes du Loir dans la région de Vendôme (Loir-et-Cher, France) : contexte morphosédimentaire et chronologie RPE [The pleistocene alluvial formations of the Loir river in the Vendôme region (Loir-et-Cher, France) morphosedimentary context and ESR chronology]. Quaternaire, 14(4), 207-218.

Despriée, J., Voinchet, P., Tissoux, H., Bahain, J.-J., Falguères, C., Courcimault, G., Dépont, J., Moncel, M.-H., Robin, S., Arzarello, M., Sala, R., Marquer, L., Messager, E., Puaud, S., Abdessadok, S., 2011. Lower and Middle Pleistocene human settlements recorded in fluvial deposits of the middle Loire River basin, centre region. France Quaternary Science Reviews 30 (11–12), 1474–1485.

Durbet, G., Rimbault, S., & Huard, P. 1997. Données préliminaires sur la préhistoire holocène à Maisons-Alfort (Val-de-Marne). Bulletin de la Société préhistorique française, 85-92.

Duval, M. 2016. Electron spin resonance (ESR) in archaeological contexts. Springer Dordrecht.

Duval, M. 2008. Evaluation du potentiel de la méthode de datation par Résonance de Spin Electronique (ESR) appliquée aux gisements du Pléistocène inférieur: étude des gisements d'Orce (bassin de Guadix-Baza, Espagne) et contribution à la connaissance des premiers peuplements de l'Europe (Doctoral dissertation, Paris, Muséum national d'histoire naturelle).

Duval, M. and Guilarte, V. 2015. ESR dosimetry of optically bleached quartz grains extracted from Plio-Quaternary sediment: evaluating some key aspects of the ESR signals associated to the Ti-centers. Radiation Measurements, 78, 28–41.

Duval, M., Sancho, C., Calle, M., Guilarte, V., and Peña-Monné, J. L..2015. On the interest of using the multiple center approach in ESR dating of optically bleached quartz grains: Some examples from the Early Pleistocene terraces of the Alcanadre River (Ebro basin, Spain). Quaternary Geochronology, 29, 58-69.

Ehlers, J. 1990. Reconstructing the dynamics of the north-west European Pleistocene ice sheets. Quaternary Science Reviews, 9(1), 71-83.

References

Ehlers, J., Astakhov, V., Gibbard, P. L., Mangerud, J., & Svendsen, J. I. 2007. Glaciations| Late pleistocene glaciations in Europe. In Encyclopedia of quaternary science (pp. 1085-1095).

Ehlers, J. and Gibbard, P.L. 2004. Quaternary Glaciations-Extent and Chronology.

England, P. and Molnar, P. 1990. Surface uplift, uplift of rocks, and exhumation of rocks. Geology, 18, 1173–1177.

Eyles, N., McCabe, A., 1989. The Late Devensian (<22,000 BP) Irish Sea Basin: The sedimentary record of a collapsed ice sheet margin. Quaternary Science Reviews 8, 307-351.

Falguères C., Yokoyama Y., and Quaegebeur J.P. 1986. Datations par la méthode de résonance de spin électronique (ESR) de sédiments quaternaires. Cahiers du Quaternaire, 16, 39-52.

Fernandez M., 2014, Approche topographique historique du sous-sol parisien (1800-2000). La ville épaisse : genèse et évolutions morphologiques, thèse de doctorat : histoire des techniques, sous la direction d'André Guillerme, Conservatoire national des Arts et Métiers.

Finnegan, N. J., Roe, G., Montgomery, D. R., and Hallet, B. 2005. Controls on the channel width of rivers: Implications for modeling fluvial incision of bedrock. Geology, 33(3), 229-232.

Forte, A.M., Whipple, K.X., 2019. The topographic analysis kit (TAK) for TopoToolbox. Earth Surf. Dyn. 7, 87–95.

Friend, P. F., and Sinha, R. 1993. Braiding and meandering parameters. Geological Society, London, Special Publications, 75(1), 105-111.

Frouin, M. 2007. Enregistrement sédimentaire des facteurs de contrôle (globaux, régionaux et locaux) sur l'évolution holocène des géosystèmes du Marais Vernier et de la Basse Vallée de Seine dans le cadre de l'Europe du NW.

Frouin, M., Sebag, D., Durand, A. and Laignel, B. 2010. Palaeoenvironmental evolution of the Seine River estuary during the Holocene. Évolution paléoenvironnementale de l'estuaire de Seine au cours de l'Holocène. Quaternaire. Revue de l'Association française pour l'étude du Quaternaire, 21, 71–83.

Fryirs, K., and Brierley, G. J. 2010. Antecedent controls on river character and behaviour in partly confined valley settings: Upper Hunter catchment, NSW, Australia. Geomorphology, 117(1-2), 106-120.

Fryirs, K. A., Wheaton, J. M., and Brierley, G. J. 2015. An approach for measuring confinement and assessing the influence of valley setting on river forms and processes. Earth Surface Processes and Landforms, 41(5), 701-710.

Fuglstad, G.-A., Lindgren, F., Simpson, D., Rue, H., 2015. Exploring a new class of non-stationary spatial Gaussian random fields with varying local anisotropy. Stat. Sin. 115–133.

References

Gaquerel, C. 1984. Les formations alluviales saaliennes de Tourville et Cléon (Seine-Maritime): sédimentologie et interprétation dans le cadre quaternaire de la Basse-Seine (Doctoral dissertation, Ph. D. Thesis, Université de Rouen).

Gardner, T. W. 1983. Experimental study of knickpoint and longitudinal profile evolution in cohesive, homogeneous material, Geol. Soc. Am. Bull., 94(5), 664-672.

Genuite, K., Todisco, D., Nehme, C., Ballesteros, D. and Mouralis, D. 2021. Morphological evolution of the middle and lower Seine valley (Normandy, France) during the Quaternary: morphometric analysis of the paleo-meanders. Quaternaire. Revue de l'Association française pour l'étude du Quaternaire, 32, 203–220.

Gibbard, P. L. 1995. The formation of the Strait of Dover. Geological Society, London, Special Publications, 96(1), 15-26.

Gibbard, P.L. 1988. The history of the great northwest European rivers during the past three million years. Philosophical Transactions of the Royal Society of London. B, Biological Sciences, 318, 559–602.

Gibbard, P. L., and Cohen, K. M., 2015. Quaternary evolution of the North Sea and the English Channel. Proceedings of the Open University Geological Society, 1, 63-74.

Gibbard, P., and Cohen, K. M. 2008. Global chronostratigraphical correlation table for the last 2.7 million years. Episodes Journal of International Geoscience, 31(2), 243-247.

Gilbert, J. T., Macfarlane, W. W., and Wheaton, J. M. 2016. The Valley Bottom Extraction Tool (V-BET): A GIS tool for delineating valley bottoms across entire drainage networks. Computers & Geosciences, 97, 1-14.

Granai, S. 2014. L'anthropisation des milieux du Néolithique à l'âge du Fer dans le bassin de la Seine enregistrée par les malacofaunes continentales (Doctoral dissertation, Paris 1).

Granai, S., Limondin-Lozouet, N., 2018. The Holocene expansion of grassland in northern Europe reconstructed from molluscan assemblages. Boreas 47, 768–779.

Grimaud, J.L., Chardon, D. and Beauvais, A. 2014. Very long-term incision dynamics of big rivers. Earth and Planetary Science Letters, 405, 74–84.

Grimaud, J.L., Paola, C. and Ellis, C. 2017. Competition between uplift and transverse sedimentation in an experimental delta. Journal of Geophysical Research: Earth Surface, 122, 1339–1354.

Grimaud, J. L., Paola, C., and Voller, V. 2016. Experimental migration of knickpoints: influence of style of base-level fall and bed lithology. Earth Surface Dynamics, 4(1), 11-23.

Grimaud, J.L., Rouby, D., Chardon, D. and Beauvais, A. 2018. Cenozoic sediment budget of West Africa and the Niger delta. Basin Research, 30, 169–186.

Grove J.M. 2002. Climatic change in northern Europe over the last two thousand years and its possible influence on human activity. In: Wefer G, Berger W, Behre K-E, Jansen E, editors. Climate Development and History of the North Atlantic Realm. Berlin: Springer- Verlag. p 313–26.

References

Grün, R., 1994. A cautionary note: use of the "water content" and "depth for cosmic ray dose rate" in AGE and DATA. Ancient TL 12, 50–51.

Grün R. and Stringer C.B., 1991. Electron spin resonance dating and the evolution of modern humans. Archaeometry, 33, 153-199.

Guérin, G., Mercier, N., and Adamiec, G., 2011. Dose-rate conversion factors: update. Ancient TL, 29(1), 5–8.

Guillocheau, F., Robin, C., et al. 2000. Meso-Cenozoic geodynamic evolution of the Paris Basin: 3D stratigraphic constraints. Geodinamica Acta, 13, 189–245, https://doi.org/10.1080/09853111.2000.11105372.

Hack, J.T., 1957. Studies of longitudinal stream profiles in Virginia and Maryland. U.S. Geological Survey Professional Paper 267-A, Washington, D.C. 43 pp.

Hjulstrøm, F. 1935. Transportation of debris by moving water. In: Trask, P. D. (ed.) Recent Marine Sediments, A Symposium. 5–31.

Hoek, W. Z. 1997. Late glacial and early Holocene climatic events and chronology of vegetation development in the Netherlands. Vegetation History and Archaeobotany, 6, 197-213.

Hogue, J.T., Wilkinson, K.N., et al. 2023. Pleistocene environments, climate, and human activity in Britain during Marine Isotope Stage 7: insights from Oak Tree Fields, Cerney Wick, Gloucestershire. Journal of Quaternary Science.

Hovius, N., 1998. Controls on sediment supply by large rivers. In: Shanley, K.W., McCabe, P.J. (Eds.), Relative Role of Eustasy, Climate and Tectonism in Continental Rocks. Soc. Econ. Paleontol. Mineral. Spec. Publ., vol. 59, pp. 3 –16. Tulsa.

Howard, A. D. 1994. A detachment-limited model of drainage basin evolution. Water resources research, 30(7), 2261-2285.

Huggett, R.,and Shuttleworth, E. 2022. Fundamentals of geomorphology. Taylor & Francis.

Hughes, P., and Gibbard, P. L. 2018. Global glacier dynamics during 100 ka Pleistocene glacial cycles. Quaternary Research, 90(1). https://doi.org/10.1017/qua.2018.37.

Hundey, E., Ashmore, P., 2009. Length scale of braided river morphology. Water Resour. Res. 45 (8).

Huntley, D. J., Godfrey-Smith, D. I., & Thewalt, M. L. 1985. Optical dating of sediments. Nature, 313(5998), 105-107.

Huyghe, D. 2010. Changements climatiques globaux et forçage tectonique au Paléogène: exemples du bassin de Paris et des Pyrénées au Paléogène. (Doctoral dissertation).

Huyghe, D., Lartaud, F., Emmanuel, L., Merle, D., Renard, M., 2015. Palaeogene climate evolution in the Paris Basin from oxygen stable isotope (δ18O) compositions of marine molluscs. J. Geol. Soc. 172, 576–587.

References

Ikeya, M. 1989. Use of Electron Spin Resonance Spectrometry in Microscopy, Dating and Dosimetry A Review. Analytical sciences, 5(1), 5-12.

Ikeya M., 1993. New applications of Electron Spin Resonance Dating, Dosimetry and Microscopy. Eds World Scientific, 500 p.

Jamet, G. 2014. Réponses sédimentaires d'un bassin versant côtier aux variations glaçio-eustatiques et au soulèvement plio-quaternaires : l'exemple du bassin versant côtier de la baie de Seine (Seine, Touques et Dives. (Doctoral dissertation, Université de Caen Basse-Normandie.

Janjou, D. 2004. Descriptif des cartes géologiques à 1/50 000 format 'vecteurs'. In: BRGM/RP-53473-FR. 21, 6.

Jerolmack, D. J., and C. Paola. 2010. Shredding of environmental signals by sediment transport, Geophys. Res. Lett., 37(19), L19401.

Kelly, S., 2006. Scaling and hierarchy in braided rivers and their deposits: examples and implications for reservoir modelling. Blackwell Oxford.

Kirby, E., and Whipple, K. X. 2012. Expression of active tectonics in erosional landscapes. Journal of structural geology, 44, 54-75.

Koutsodendris, A., Müller, U. C., Pross, J., Brauer, A., Kotthoff, U., and Lotter, A. F. 2010. Vegetation dynamics and climate variability during the Holsteinian interglacial based on a pollen record from Dethlingen (northern Germany). Quaternary Science Reviews, 29(23-24), 3298-3307.

Kuchar, J., Milne, G., Hubbard, A., Patton, H., Bradley, S., Shennan, I. and Edwards, R. 2012. Evaluation of a numerical model of the British–Irish ice sheet using relative sea-level data: implications for the interpretation of trimline observations. Journal of Quaternary Science, 27, 597–605.

Kukla, G., Bender, M., De Beaulieu, J., Bond, G., Broecker, W., Cleveringa, P., and Winograd, I., 2002. Last Interglacial Climates. Quaternary Research, 58(1), 2-13. doi:10.1006/qres.2001.2316.

Krier V. 2004. La plaine alluviale de l'Oise : milieu et système fluvial ; stratigraphie des formations alluviales et archéologie, Conseil général du Val d'Oise et INRAP, 2 vol.

Labarthe, B., 2016. Quantification des échanges nappe-rivière au sein de l'hydrosystème Seine par modélisation multi-échelle.

Langston, A. L., and Temme, A. J. 2019. Impacts of lithologically controlled mechanisms on downstream bedrock valley widening. Geophysical Research Letters, 46(21), 12056-12064.

Lasberg, K., Kalm, V., and Kihno, K., 2014. Ice-free interval corresponding to Marine Isotope Stages 4 and 3 at the Last Glacial Maximum position at Kileshino, Valdaj Upland, Russia. Estonian Journal of Earth Sciences, 63(2), 88.

Laignel, B. 1997. Les altérites à silex de l'ouest du Bassin de Paris: caractérisation lithologique, genèse et utilisation potentielle comme granulats (Doctoral dissertation).

References

Lambeck K., Rouby H., Purcell A., Sun Y., Sambridge, M., 2014. Sea level and global ice volumes from the Last Glacial Maximum to the Holocene, Proceedings of the National Academy of Sciences 111, 15296-15303.

Lane, E. W. 1955. Design of stable channels. Transactions of the American society of Civil Engineers, 120(1), 1234-1260.

Larsonneur, C., Auffret, J. P., Smith, A. J., 1982. Carte des paléo-vallées et des bancs de la Manche orientale (1/50 000). BRGM, Brest.

Larue, J. P., 2000. Morphodynamique fluviale et neotectonique dans la vallee de l'Oise (Bassin parisien, France). Bulletin de la Société Géologique de France, 171(5), 577-585.

Lasseur E. 2007. La Craie du Bassin de Paris (Cénomanien-Campanien, Crétacé supérieur). Sédimentologie de faciès, stratigraphie séquentielle et géométrie 3D, Thèse doct. univ. Rennes 1, 409 p.

Lauer, T., and Weiss, M. 2018. Timing of the Saalian-and Elsterian glacial cycles and the implications for Middle–Pleistocene hominin presence in central Europe. Scientific Reports, 8(1), 5111.

Lautridou, J.P. 1982. The quaternary of Normandy-Guide-book of the QRA Normandy meeting and IGCP 24 Normandy meeting. Bulletin du Centre de géomorphologie de Caen Caen, 26, 1–88.

Lautridou, J.P. 1985. Le cycle périglaciaire pléistocène en Europe du Nord-Ouest et plus particulièrement en Normandie. Thèse doct. état, univ. De Caen, 2 vol., 908 p.

Lautridou, J.P., Auffret, J.P., et al. 1999. Le fleuve Seine, le fleuve Manche. Bull. Soc. Géol. Fr, 170, 545–558.

Lautridou, J.P., Auguste, P., Carpentier, G., Cordy, J.M., Lebret, P., Lechevalier, C. and Lefebvre, D. 2003. L'Eemien et le Pléistocène moyen récent fluvio-marin et continental de la vallée de la Seine de Cléon au Havre (Normandie)[marine and continental Eemian and Middle Pleistocene of the Seine of Cléon to the Havre. Quaternaire, 14, 25–30.

Lautridou, J. P., Lefebvre, D., Lécolle, F., Carpentier, G., Descombes, J., Gaquerel, C., and Huault, M. F. 1984. Les terrasses de la Seine dans le méandre d'Elbeuf. Corrélations avec celles de la région de Mantes. Quaternaire, 21(1), 27-32.

Lautridou, J. P., Sommé, J., Heim, J., Puisségur, J. J., & Rousseau, D. D. 1985. La stratigraphie des loess et formations fluviatiles d'Achenheim (Alsace): nouvelles données bioclimatiques et corrélations avec les séquences pléistocènes de la France du Nord-Ouest. Quaternaire, 22(2), 125-132.

Lave, J., Avouac, J.P., 2001. Fluvial incision and tectonic uplift across the Himalayas of central Nepal. J. Geophys. Res. 106, 26,561–26,591.

Le Joncour, K. 1995. Les ballastières de la boucle d'Anneville (Seine-Maritime. Rapport BRGM, R38709.

References

Lécolle, F. 1989. Le cours moyen de la Seine au Pléistocène moyen et supérieur. Géologie et Préhistoire. 1–549.

Lécolle, F. 1984. Les formations alluviales quaternaires de la Seine entre Paris et Rouen. Bulletin du Centre de géomorphologie de Caen Caen, (29), 19-36.

Lécolle, F., 1980. Le Pléistocène moyen et supérieur alluvial de la vallée de la Seine en aval de Mantes (Yvelines) : Paliers d'érosion et nappes alluviales. Méthodologie. Quaternaire, 17(3), 117-128.

Lefèbvre, D. 1988. - Les méandres hypertrophiés de la Basse Seine sont une forme dégradéede méandres surimposés. Bulletin de la Société Géologique de Normandie et des Amis duMuséum du Havre, 75, 43–57.

Lefebvre, D., Huault, M.F., Guyader, J., Giresse, P., Hommeril, P. and Larsonneur, C. 1974. Le prisme alluvial de l'estuaire de la Seine; synthèse sédimentologique, stratigraphique et paléogéographique. Bulletin d'information des géologues du Bassin de Paris, 39, 27–36.

Lefèbvre, D., Carpentier, G. and Evrard, H. 1986. Les terrasses de la Seine de Pont-de-l'Arche a` Elbeuf. Bulletin du Centre de Géomorphologie de Caen, 31, 41–71.

Lefèbvre, D., Antoine, P., Auffret, J.-P., Lautridou, J.-P. and Lecolle, F. 1994. Réponses de la Seine et de la Somme aux événements climatiques, eustatiques et tectoniques du Pléistocène moyen et récent: rythmes et taux d'érosion. Quaternaire, 5, 165–172.

Lemay, M., Grimaud, J.-L., Cojan, I., Rivoirard, J., Ors, F., 2020. Geomorphic variability of submarine channelized systems along continental margins: Comparison with fluvial meandering channels. Mar. Pet. Geol. 115, 104295.

Lericolais, G., 1997. Evolution du Fleuve Manche depuis l'Oligocène: stratigraphie et géomorphologie d'une plate-forme continentale en régime périglaciaire. Thèse de doctorat, Université Bordeaux 1, 265 pp.

Lesueur, P., Lesourd, S., Lefèbvre, D., Garnaud, S. and Brun-Cottan, J.C. 2003. Holocene and modern sediments in the Seine estuary (France): a synthesis. Journal of Quaternary Science: Published for the Quaternary Research Association, 18, 339–349.

Lericolais, G., Auffret, J. P., Bourillet, J. F., 2003. The Quaternary Channel River: seismic stratigraphy of its palaeo-valleys and deeps. Journal of Quaternary Science 18, 245-260.

Leopold, L. B., and Bull, W. B. 1979. Base level, aggradation, and grade. Proceedings of the American Philosophical Society, 123(3), 168-202.

Leopold, L. B., and Wolman, M. G. 1957. River channel patterns: braided, meandering, and straight. US Government Printing Office.

Le Roy Ladurie E. 1967. Histoire du climat depuis l'an mil. Paris: Flammarion. 287 p. In French.

References

Lewis, S., Maddy, D. and Glenday, S. 2004. The Thames valley sediment conveyor: fluvial system development over the last two interglacial-glacial cycles [Le" convoyeur sédimentaire" de la vallée de la Tamise. Quaternaire, 15, 17–28.

Lewis, S.G., Maddy, D., et al. 2006. Pleistocene fluvial sediments, palaeontology and archaeology of the upper River Thames at Latton, Wiltshire. England. Journal of Quaternary Science, 21, 181–205.

Li, S., Li, S., Shan, X., Gong, C. and Yu, X. 2017. Classification, formation, and transport mechanisms of mud clasts. International Geology Review, 59, 1609–1620.

Limaye, A. B. S. 2020. How do braided rivers grow channel belts? Journal of Geophysical Research: Earth Surface, 125, 1–24. https://doi.org/10.1029/2020JF005570.

Limaye, A.B., Grimaud, J., Lai, S.Y., Foreman, B.Z., Komatsu, Y., Paola, C., 2018. Geometry and dynamics of braided channels and bars under experimental density currents. Sedimentology 65, 1947–1972.

Limaye, A.B. and Lamb, M.P. 2016. Numerical model predictions of autogenic fluvial terraces and comparison to climate change expectations. Journal of Geophysical Research: Earth Surface, 121, 512–544.

Limondin-Lozouet, N. 2011. Successions malacologiques à la charnière Glaciaire/Interglaciaire: du modèle tardiglaciaire-Holocène aux transitions du Pleistocène. Quaternaire. Revue de l'Association française pour l'étude du Quaternaire, 22(3), 211-220.

Limondin-Lozouet, N., Antoine, P., et al. 2006. Le tuf calcaire de La Cellesur- Seine (Seine et Marne) : nouvelles données sur un site clé du stade 11 dans le Nord de la France. Quaternaire. Revue de l'Association française pour l'étude du Quaternaire, 17, 5–29, https://doi.org/10.4000/quaternaire.722.

Limondin, N., and Rousseau, D. D. 1991. Holocene climate as reflected by a malacological sequence at Verrières, France. Boreas, 20(3), 207-229.

Lindgren, F., Rue, H., Lindström, J., 2011. An explicit link between Gaussian fields and Gaussian Markov random fields: the stochastic partial differential equation approach. J. R. Stat. Soc. Ser. B Stat. Methodol. 73, 423–498.

Lisiecki, L.E. and Raymo, M.E. 2005. A Pliocene-Pleistocene stack of 57 globally distributed benthic δ18O records. Paleoceanography, 20.

Locht, J. L., Antoine, P., Bahain, J. J., Dwrila, G., Raymond, P., Limondin-Lozouet, N.,and Metsdagh, H. 2003. Le gisement paléolithique moyen et les séquences pléistocènes de Villiers-Adam (Val-d'Oise): chronostratigraphie, environnement et implantations humaines. Gallia Préhistoire–Archéologie de la France préhistorique, 45, 1-111.

Loget, N., and Van Den Driessche, J. 2009. Wave train model for knickpoint migration. Geomorphology, 106(3-4), 376-382.

Malatesta, L.C., Prancevic, J.P. and Avouac, J.P. 2017. Autogenic entrenchment patterns and terraces due to coupling with lateral erosion in incising alluvial channels. Journal of Geophysical Research: Earth Surface, 122, 335–355.

References

Magny M, Leuzinger U, Bortenschlager S, Haas JN. 2006. Tripartite climate reversal in Central Europe 5600–5300 years ago. Quaternary Research 65(1):3–19.

Matheron, G., 1963. Traité de géostatistique appliquée. 2. le krigeage. Editions Technip.

Matheron, G., 1962. Traité de géostatistique appliquée. Editions Technip.

Maton, D., Pannet, P., Sandifort, C., 2014. Inventaire des mouvements de terrain du département de l'Oise et la Somme. (No. BRGM/RP-63956-FR), Rapport BRGM.

Martin, A.J. 2000. Flaser and wavy bedding in ephemeral streams: a modern and an ancient example. Sedimentary Geology, 136, 1–5.

Maslin, M., and Gornitz, V. 2009. Quaternary climate transitions and cycles. Encyclopedia of Palaeoecology and Ancient Environments. Springer, Dordrecht, 841-855.

Masson-Delmotte, V., Schulz, M., Abe-Ouchi, A., Beer, J., Ganopolski, A., González Rouco, J. F., and Timmermann, A. 2013. Information from paleoclimate archives. Climate change, 383464, 2013.

May, C., Roering, J., Eaton, L. S., and Burnett, K. M. 2013. Controls on valley width in mountainous landscapes: The role of landsliding and implications for salmonid habitat. Geology, 41(4), 503-506.

Mégnien, C. 1980. Synthèse géologique du bassin de Paris : Lexique des noms de formation, Bureau Recherches Géologiques et Minières.

Mégnien, Cl., Berton, Y., Dassibat, C., Diffre, Ph., Duermael, G., Jonquet, P., Rampon, G., Stanudin, B., Ramon, S., Beaufond, S., Berger, G., Cardona, A., Marquet, G., Mercier, F., Pinelli, M., Renault, Ph., Turland, M., Marrec, C., Muller, J.-P., Oltra, M., Strat, P., Mazoit, M., Villemaine, H., 1965. Possibilités aquifères des alluvions du val de Seine entre Nogent-s-Seine et Montereau. Ministère de l'industrie, BRGM, Paris (DSGR.65. A76, 1065 pp.).

Mellere, R. and Steel, R. 1995. Facies architecture and sequentially of nearshore and shelf sandbodies, Haystack Mountains Formation. Sedimentology, 42, 551–574.

Mercier, D. 2008. Paraglacial and paraperiglacial landsystems: concepts, temporal scales and spatial distribution. Géomorphologie : relief, processus, environnement, 14, 223–233.

Merritts, D. J., Vincent, K.R, and Wohl, E.E. 1994. Long river profiles, tectonism, and eustasy: A guide to interpreting fluvial terraces, J. Geophys. Res., 99(B7), 14031-14050.

Métivier, F., and Gaudemer, Y. 1999. Stability of output fluxes of large rivers in South and East Asia during the last 2 million years: implications on floodplain processes, Basin Res., 11(4), 293-303.

Meybeck, M., and Helmer, R. 1989. The quality of rivers: from pristine stage to global pollution. Palaeogeography, Palaeoclimatology, Palaeoecology, 75(4), 283-309.

Miall, A. 1996. The Geology of Fluvial Deposits: Sedimentary Facies, Basin Analysis and Petroleum Geology.

References

Miall, A.D. 2006. The Geology of Fluvial Deposits: Sedimentary Facies, Basin Analysis, and Petroleum Geology, 4th ed.

Miller, K.G., Fairbanks, R.G. and Mountain, G.S. 1987. Tertiary oxygen isotope.

Mol, J., Vandenberghe, J. and Kasse, C. 2000. River response to variations of periglacial climate. Geomorphology, 33, 131–148.

Mogensen I.A., 2009. Dansgaard-Oeschger Cycles. In: Gornitz V. (eds) Encyclopedia of Paleoclimatology and Ancient Environments. Encyclopedia of Earth Sciences Series. Springer, Dordrecht. https://doi.org/10.1007/978-1-4020-4411-3_55.

Montgomery, D.R., 2004. Observations on the role of lithology in strath terrace formation and bedrock channel width. Am. J. Sci. 304, 454–476. http://dx.doi.org/10.2475/ajs.304.5.454.

Morales, J.A. 2022. Tide-Dominated Systems II: Tidal Flats and Wetlands. In: Coastal Geology. 289–307.

Mortimore, R.N. 2018. Late Cretaceous tectono-sedimentary events in NW Europe. Proceedings of the Geologists' Association, 129, 392–420.

Murray, A. S., and Roberts, R. G. 1997. Determining the burial time of single grains of quartz using optically stimulated luminescence. Earth and Planetary Science Letters, 152(1-4), 163-180.

Murray, A. and Wintle, A.G. 2000. Quartz OSL: effects of thermal treatment and their relevance to laboratory dating procedures. Radiation Measurements, 32, 387–400.

Murray, A. S., & Wintle, A. G. 2003. The single aliquot regenerative dose protocol: potential for improvements in reliability. Radiation measurements, 37(4-5), 377-381.

Nehme, C., Farrant., A., et al. 2020. Reconstructing Fluvial Incision Rates Based on Palaeo-water Tables in Chalk Karst Networks along the Seine Valley (Normandy, France. Earth Surface Processes and Landforms, 45, (8, 10 1002 4851.

Parker, G. 2015, 1-D Sediment Transport Morphodynamics With Applications to Rivers and Turbidity Currents, Univ. of Illinois. Available at http://hydrolab.illinois.edu/people/parkerg.

Parker, G. 1976. On the cause and characteristic scales of meandering and braiding in rivers. Journal of fluid mechanics, 76(3), 457-480.

Pastre, J.-F., Fontugne, M., Kuzucuoğlu, C., Leroyer, C., Limondin-Lozouet, N., Talon, M., Tisnérat, N., 1997. L'évolution tardi et postglaciaire des lits fluviaux au nord-est de Paris (France). Relations avec les données paléoenvironnementales et l'impact anthropique sur les versants. Géomorphologie Relief Process. Environ. 3, 291–312.

References

Pastre, J. F., Leroyer, C., Limondin-Lozouet, N., Chaussé, C., Fontugne, M., Gebhardt, A., and Krier, V. 2000. Le Tardiglaciaire des fonds de vallée du Bassin parisien France). Quaternaire, 11(2), 107-122.

Pastre, J. F., Limondin-Lozouet, N., Leroyer, C., Ponel, P., and Fontugne, M. 2003. River system evolution and environmental changes during the Lateglacial in the Paris Basin (France). Quaternary Science Reviews, 22(20), 2177-2188.

Pastre, J. F., Leroyer, C., Limondin-Lozouet, N., Antoine, P., Chaussé, C., Gauthier, A., and Wuscher, P. 2014. The Holocene evolution of the Paris basin (France). Contribution of geoecology and geoarcheology of floodplains. French geoarcheology in the 21st century. Paris: CNRS Éditions, 87-103.

Pazzaglia, F. J. 2013. Fluvial Terraces. Treatise of Geomorphology, edited by: Wohl, E., Elsevier, Amsterdam, the Netherlands.

Pazzaglia, F.J. and Brandon, M.T. 2001. A fluvial record of long-term steady-state uplift and erosion across the Cascadia forearc high, western Washington State. American Journal of Science, 301, 385–431.

Pedoja, K., Jara-Muñoz, J., et al. 2018. Neogene-Quaternary slow coastal uplift of Western Europe through the perspective of sequences of strandlines from the Cotentin Peninsula (Normandy, France. Geomorphology, 303, 338–356.

Pellerin, J., Brebion, P., et al. 1987. Données nouvelles sur le gisement marin quaternaire+ 14, 5/+ 15, 7 m NGF du cimetière de Luc-sur-Mer. 32, 99–115.

Penaud, A., Eynaud, F., Turon, J. L., Zaragosi, S., Marret, F., & Bourillet, J. F. (2008). Interglacial variability (MIS 5 and MIS 7) and dinoflagellate cyst assemblages in the Bay of Biscay (North Atlantic). Marine Micropaleontology, 68(1-2), 136-155.

Pereira, M., Desassis, N., Allard, D., 2022. Geostatistics for large datasets on Riemannian manifolds: a matrix-free approach. ArXiv Prepr. ArXiv220812501.

Pérez-Peña, J. V., Al-Awabdeh, M., Azañón, J. M., Galve, J. P., Booth-Rea, G., and Notti, D. 2017. SwathProfiler and NProfiler: Two new ArcGIS Add-ins for the automatic extraction of swath and normalized river profiles. Computers & Geosciences, 104, 135-150.

Petersen, S. V., Schrag, D. P., and Clark, P. U. 2013. A new mechanism for Dansgaard-Oeschger cycles. Paleoceanography, 28(1), 24-30.

Peycru, P., Fogelgesang, J-F., Grandperrin, D., Perrier, C., Augère, B., Darribère, T., Dupin, J. M., and Van Der Rest, C. 2019. Biologie tout-en-un BCPST 1re année. Dunod.

Phillips, J.D., 2003. Toledo Bend Reservoir and geomorphic response in the lower Sabine River. River Research and Applications 19, 137–159.

Phillips, J. D., and Slattery, M. C. 2006. Sediment storage, sea level, and sediment delivery to the ocean by coastal plain rivers. Progress in Physical Geography, 30(4), 513-530.

References

Pillans, B., Chappell, J. and Naish, T.R. 1998. A review of the Milankovitch climatic beat: template for Plio–Pleistocene sea-level changes and sequence stratigraphy. Sedimentary geology, 122, 5–21.

Pillans, B. and Gibbard, P. 2012. The quaternary period. The geologic time scale, 2, 979–1010.

Pillans, B. and Naish, T. 2004. Defining the quaternary. Quaternary Science Reviews, 23, 2271–2282.

Pomerol, C. 1978. Evolution paléogéographique et structurale du Bassin de Paris, du Précambrien à l'actuel, en relation avec les régions avoisinantes.

Pomerol, C., 1989. L'évolution du Bassin Parisien. Assoc. Sédimentologistes Fr.-Dyn. Méthodes Détude Bassins Sédimentaires Ed. Tech. Paris 165–178.

Pomerol, C. and Feugueur, L. 1974. Bassin de Paris –Ile de France – Pays de Bray, Guides géologiques régionaux Masson, E. (ed.). 215.

Pomerol and Monciardini. 1992. Notice explicative, carte géologique France (1/50000), feuille Troyes (298). Orléans: BRGM, 56p.

Porcher, M. 1981. - Etude géologique et géotechnique des alluvions fluviales holocènes de labasse vallée de la Seine à Tourville-la-Rivière et Anneville-sur-Seine. Thèse de docteur-ingénieur. Université Paris, 6, 140.

Prescott, J.R., Hutton, J.T., 1994. Cosmic ray contributions to dose rates for Luminescence and ESR Dating: Large depths and long-term time. Rad. Meas. 23, 497–500.

Prodanović, D., Stanić, M., Milivojević, V., Simić, Z., & Arsić, M. (2009). DEM-based GIS algorithms for automatic creation of hydrological models data. Journal of Serbian Society for Computational Mechanics, 3(1), 64-85.

Quesnel, F. 1997. Cartographie numérique en géologie de surface. Application aux altérites à silex de l'Ouest du Bassin de Paris. (Doctoral dissertation, Université de Rouen.

Railsback, L. B., Gibbard, P. L., Head, M. J., Voarintsoa, N. R. G., and Toucanne, S. 2015. An optimized scheme of lettered marine isotope substages for the last 1.0 million years, and the climatostratigraphic nature of isotope stages and substages. Quaternary Science Reviews, 111, 94-106.

Renard, D., Bez, N., Desassis, N., Beucher, H., Ors, F., Freulon, X., 2016. RGeostats: The Geostatistical R package [v11. 2.3]. MINES ParisTech ARMINES.

Richards, K., 1976. The morphology of riffle-pool sequences. Earth Surf. Process. 1, 71–88.

Ridgwell, A. J., Watson, A. J., and Raymo, M. E. 1999. Is the spectral signature of the 100 kyr glacial cycle consistent with a Milankovitch origin?. Paleoceanography, 14(4), 437-440.

Roblin-Jouve, A. 1984. La très basse nappe alluviale de la Seine dans la région du site archéologique de Pincevent (Montereau, Seine-et-Marne). Quaternaire, 21(1), 45-51.

Rodriguez, P. 1994. Maisons-Alfort : ZAC d'Alfort I: étude géomorphologique. Laboratoire départemental d'archéologie du Val-de-Marne.

References

Romans, B. W., Castelltort, S., Covault, J. A., Fildani, A., and Walsh, J. P. 2016. Environmental signal propagation in sedimentary systems across timescales. Earth-Science Reviews, 153, 7-29.

Ruszkiczay-Rüdiger,Z., Fodor,L., Horváth,E., Telbisz,T. 2009. Discrimination of fluvial, eolian and neotectonics features in a low hilly landscape: a DEM-based on morphotectonic analysis in the Central Pannonian Basin, Hungary. Geomorphology 104,203–217. http://dx.doi.org/10.1016/j.geomorph.2008.08.014.

Savi, S., Tofelde, S., Wickert, A. D., Bufe, A., Schildgen, T. F., & Strecker, M. R. 2020. Interactions between main channels and tributary alluvial fans: channel adjustments and sediment-signal propagation. Earth Surface Dynamics, 8(2), 303-322.

Schanz, S. A. and Montgomery, D. R. 2016. Lithologic controls on valley width and strath terrace formation, Geomorphology, 258, 58–68. https://doi.org/10.1016/J.GEOMORPH.2016.01.015.

Scheingross, J.S., Limaye, A.B., McCoy, S.W. and Whittaker, A.C. 2020. The shaping of erosional landscapes by internal dynamics. Nature Reviews Earth & Environment, 1, 661–676.

Schulz, M. 2002. On the 1470-year pacing of Dansgaard-Oeschger warm events. Paleoceanography, 17, 4–1.

Schumm, S. 1977. The fluvial system. New York, John Wiley &Sons, 338 p.

Schumm, S. 1973. Geomorphic thresholds and complex response of drainage systems. Fluvial geomorphology, 6, 69-85.

Schwanghart, W., Kuhn, N.J., 2010. TopoToolbox: A set of Matlab functions for topographic analysis. Environ. Model. Softw. 25, 770–781.

Schwanghart, W., Scherler, D., 2014. TopoToolbox 2–MATLAB-based software for topographic analysis and modeling in Earth surface sciences. Earth Surf. Dyn. 2, 1–7.

Sebag, D. 2002. Apports de la matière organique pour la reconstitution des paléoenvironnements holocènes de la basse vallée de la Seine : fluctuations des conditions hydrologiques locales et environnements de dépôt.

Seifert, D., Jensen, J., 2000. Object and pixel-based reservoir modeling of a braided fluvial reservoir. Math. Geol. 32, 581–603.

Sklar, L. S., and Dietrich, W. E. 2006. The role of sediment in controlling steady-state bedrock channel slope: Implications of the saltation–abrasion incision model. Geomorphology, 82(1-2), 58-83.

Sklar, L., and Dietrich, W. E. 1998. River longitudinal profiles and bedrock incision models: Stream power and the influence of sediment supply. Geophysical Monograph-American Geophysical Union, 107, 237-260.

Snyder, N. P., Whipple, K. X., Tucker, G. E., and Merritts, D. J. 2003. Channel response to tectonic forcing: field analysis of stream morphology and hydrology in the Mendocino triple junction region, northern California. Geomorphology, 53(1-2), 97-127.

References

Sella, G.F., Stein, S., Dixon, T.H., Craymer, M., James, T.S., Mazzotti, S. and Dokka, R.K. 2007. Observation of glacial isostatic adjustment in "stable". North America with GPS. Geophysical Research Letters, 34.

Spotila, J. A., Moskey, K. A., and Prince, P. S. 2015. Geologic controls on bedrock channel width in large, slowly-eroding catchments: Case study of the New River in eastern North America. Geomorphology, 230, 51-63.

Spratt, R. M. and Lisiecki, L. E. 2016. A Late Pleistocene sea level stack, Clim. Past, 12, 1079–1092, https://doi.org/10.5194/cp-12-1079- 2016, 2016.

Stock, J. D., and Montgomery, D. R. 1999. Geologic constraints on bedrock river incision using the stream power law. Journal of Geophysical Research : Solid Earth, 104(B3), 4983-4993.

Stremme, H. 1985. Altersbestimmung und Paläoböden in der Quartärstratigraphie [Détermination de l'age et paléosols dans la stratigraphie quaternaire. Quaternaire, 22, 159–166.

Tissoux, H., Despriée, J., Voinchet, P., Bahain, J. J., & Falguères, C. 2011. Intérêt de la datation par ESR d'un transect complet pour la compréhension d'un système fluviatile : exemple de la vallée du Loir. Quaternaire. Revue de l'Association française pour l'étude du Quaternaire, 22(4), 345-356.

Tissoux, H., Falguères, C., Voinchet, P., Toyoda, S., Bahain, J.J. and Despriée, J. 2007. Potential use of Ti-center in ESR dating of fluvial sediment. Quaternary Geochronology, 2, 367–372.

Tissoux, H., Voinchet, P., Lacquement, F., and Despriée, J., 2015. ESR as a method for the characterization of alluvial sediments. Radiation Measurements, 81, 2-8.

Tofelde, S., Bernhardt, A., Guerit, L. and Romans, B.W. 2021. Times associated with source-to-sink propagation of environmental signals during landscape transience. Front. Earth Sci, 9, https://doi.org/10.3389/feart.2021.628315.

Tofelde, S., Bufe, A., and Turowski, J. M. 2022. Hillslope sediment supply limits alluvial valley width. AGU Advances, 3(6), e2021AV000641.

Tofelde, S., Savi, S., Wickert, A.D., Bufe, A. and Schildgen, T.F. 2019. Alluvial channel response to environmental perturbations: fill-terrace formation and sediment-signal disruption, Earth Surf. Dynam, 7, 609-631, https://doi.org/10.5194/esurf-7-609-2019.

Tofelde, S., Schildgen, T.F., Savi, S., Pingel, H., Wickert, A.D., Bookhagen, B. and Strecker, M.R. 2017. 100 kyr fluvial cut-and-fill terrace cycles since the Middle Pleistocene in the southern Central Andes, NW Argentina. Earth and Planetary Science Letters, 473, 141–153.

Tomkin, J. H., Brandon, M. T., Pazzaglia, F. J., Barbour, J. R., and Willett, S. D. 2003. Quantitative testing of bedrock incision models for the Clearwater River, NW Washington State. Journal of Geophysical Research: Solid Earth, 108(B6).

References

Toucanne, S. 2008. Reconstruction des transferts sédimentaires en provenance du système glaciaire de Mer d'Irlande et du paléofleuve Manche au cours des derniers cycles climatiques.

Toucanne, S., Zaragosi, S., et al. 2009. Timing of massive 'Fleuve Manche'discharges over the last 350 kyr: insights into the European ice-sheet oscillations and the European drainage network from MIS 10 to 2. Quaternary Science Reviews, 28, 1238–1256.

Tourenq, J., and Pomerol, C. 1995. Mise en évidence, par la présence d'augite du Massif Central, de l'existence d'une pré Loire-pré Seine coulant vers la Manche au Pléistocène. Comptes rendus de l'Académie des sciences. Série 2. Sciences de la terre et des planètes, 320(12), 1163-1169.

Törnqvist, T.E., Wallinga, J., Murray, A.S., Wolf, H., Cleveringa, P. and Gans, W. 2000. Response of the Rhine–Meuse system (west-central Netherlands) to the last Quaternary glacio-eustatic cycles: a first assessment. Global and Planetary Change, 27, 89–111.

Toyoda S., and Ikeya M., 1994. ESR dating of quartz with stable components of impurity centers. Quaternary Geochronology, 13, 625-628.

Toyoda, S., and Falguères C. 2003. The method to represent the ESR signal intensity of the aluminium hole center in quartz for the purpose of dating. Advances in ESR applications, 20, 7-10.

Toyoda, S., Tsukamoto, S., Hameau, S., Usui, H., Suzuki, T. 2006 Dating of Japanese Quaternary tephras by ESR and luminescence methods Quaternary Geochronology, 1, 320–326

Toyoda, S., Voinchet, P., Falguères, C., Dolo, J.M. and Laurent, M. 2000. Bleaching of ESR signal by the sunlight: a laboratory experiment for establishingthe ESR dating of sediments. Applied Radiation and Isotopes, 52, 1357–1362.

Tucker, G. E., and Slingerland, R. 1997. Drainage basin responses to climate change. Water Resources Research, 33(8), 2031-2047.

Turowski, J. M., Hovius, N., Meng-Long, H., Lague, D., and Men-Chiang, C. 2008. Distribution of erosion across bedrock channels. Earth Surface Processes and Landforms: The Journal of the British Geomorphological Research Group, 33(3), 353-363.

Umeuduji, J.E. 2017. An introduction to the science of landforms. Jodigs and Associates. ISBN, 978-34122-6–4.

Valladas, H., 1994. Chronologie des sites du Magdalénien final du Bassin parisien : Le milieu naturel et son exploitation. I: Climats et paysages. Doc. Archéologie Fr. 65–68.

Valladas, H., 1981. Thermoluminescence de grès de foyers préhistoriques : estimation de leur température de chauffe. Archaeometry 23, 221–229.

References

Vandenberghe, J., 1993. Changing fluvial processes under changing periglacial conditions. Zeitschrift fur Geomorphologie, Suppl. Bd 88, 17–28.

Vandenberghe, J. 2001. A typology of Pleistocene cold-based rivers.Quaternary International 79 ,111–121.

Vandenberghe, J. 2008. The fluvial cycle at cold–warm–cold transitions in lowland regions: a refinement of theory. Geomorphology, 98, 275–284.

Vandenberghe, J., Kasse, C., Bohncke, S., and Kozarski, S., 1994. Climate related river activity at the Weichselian-Holocene transition: a comparative study of the Warta and Maas rivers. Terra Nova 6, 476–485.

Van den Berg, J.H., Boersma, J.R. and Gelder, A.V. 2007. Diagnostic sedimentary structures of the fluvial-tidal transition zone–Evidence from deposits of the Rhine and Meuse. Netherlands Journal of Geosciences/Geologie en Mijnbouw, 86.

Van Geel, B., Coope, G. R., and Van Der Hammen, T. 1989. Palaeoecology and stratigraphy of the Lateglacial type section at Usselo (The Netherlands). Review of palaeobotany and palynology, 60(1-2), 25-129.

Van Steijn H., Bertran P., Francou B., Hétu B., Texier J.P., 1995. Review of models for genetical interpretation of stratified slope deposits. Permafrost and Periglacial Processes 6, 125-146

Van Vliet-Lanoë. 1998. Frost and soils: implications for palaeosols, palaeo-climates and stratigraphy. Catena, 34, 157–183.

Voinchet, P. 2002. Datation par résonance paramagnétique électronique (RPE) de quartz blanchis extraits de sédiments fluviatiles pléistocènes: contribution méthodologique et application aux systèmes de la Creuse, du Loir et de l'Yonne (Doctoral dissertation, Paris, Muséum national d'histoire naturelle).

Voinchet, P., Bahain, J.J., et al. 2004. ESR dating of quartz extracted from Quaternary sediments application to fluvial terraces system of northern France. Quaternaire, 15, 135–141.

Voinchet, P., Brulhet, J., Cojan, I., Bahain, J. J., and Falguères, C., 2015. Datation ESR des terrasses alluviales pléistocènes de la vallée de l'Aube : premiers résultats. Quaternaire, 26(3), 185-193.

Voinchet, P., Pereira, A., Nomade, S., Falguères, C., Biddittu, I., Piperno, M., and Bahain, J. J. 2020. ESR dating applied to optically bleached quartz-A comparison with 40Ar/39Ar chronologies on Italian Middle Pleistocene sequences. Quaternary International, 556, 113-123.

Waelbroeck, C., Labeyrie, L., Michel, E., Duplessy J.C., McManus J. 2002. Sea-level and deep water temperature changes derived from benthic foraminifera isotopic records, Quaternary Sci. Rev., 21, 295–305.

Wang, X.L. and Wintle, A.G. 2012. Optically stimulated luminescence production in the single-aliquot regenerative dose protocol. Radiation measurements, 47, 121–129.

References

Wheaton, J. M., Fryirs, K. A., Brierley, G., Bangen, S. G., Bouwes, N., and O'Brien, G. 2015). Geomorphic mapping and taxonomy of fluvial landforms. Geomorphology, 248, 273-295.

Westaway, R. 2004. Pliocene and Quaternary surface uplift evidenced by sediments of the Loire Allier river system (France)[Mise en évidence du soulèvement des surfaces continentales au Quaternaire et au Pliocène d'après les sédiments du système Loire-Allier (France).]. Quaternaire, 15(1), 103-115.

Westaway, R., Bridgland, D. and White, M. 2006. The Quaternary uplift history of central southern England: evidence from the terraces of the Solent River system and nearby raised beaches. Quaternary Science Reviews, 25, 2212–2250.

Wickert, A.D., Anderson, R.S., Mitrovica, J.X., Naylor, S. and Carson, E.C. 2019. The Mississippi River records glacial-isostatic deformation of North America. Science Advances, 5, 2366.

Whipple, K. X. 2001. Fluvial landscape response time: How plausible is steady-state denudation?. American Journal of Science, 301(4-5), 313-325.

Whipple, K. X., and Tucker, G.E. 1999. Dynamics of the stream-power river incision model; implications for height limits of mountain ranges, landscape response timescales, and research needs, J. Geophys. Res., 104(B8), 17.

Wolman, M.G., Leopold, L.B., 1957. River flood plains: some observations on their formation, in: US Government Printing Office Washington, DC. US Government Printing Office Washington, DC, pp. 87–109.

Wyns, R., 1980. Apports de la microtectonique à l'étude de l'anticlinal du pays de Bray: proposition d'un mécanisme de pli en compression avec décrochements associés. Bull. Soc. Géol. France 7, 681–684.

Yan, S., Blankenship, D. D., Greenbaum, J. S., Young, D. A., Li, L., Rutishauser, A., and Sun, B. 2022. A newly discovered subglacial lake in East Antarctica likely hosts a valuable sedimentary record of ice and climate change. Geology, 50(8), 949-953.

Yokoyama Y., Falguères C., and Quaegebeur J.P., 1985. ESR dating of quartz from quaternary sediments: first attempt. Nuclear Tracks and Radiation Measurements, 10 (4-6), 921-928.

Zachos, J. C., Dickens, G. R., and Zeebe, R. E. 2008. An early Cenozoic perspective on greenhouse warming and carbon-cycle dynamics. nature, 451(7176), 279-283.

Zagwijn, W. H., 1973. Pollen-analytical studies of Holsteinian and Saalian Beds in the Northern Netherlands. Mededelingen Rijks Geologische Dienst 24, 139-156.

Zazo, C. 1999. Interglacial sea levels. Quaternary international, 55, 101–113.

Appendix A: Supplementary data chapter 2

Supplementary information about Miall facies classification and sample location.

Appendix

Table A.2.1. Facies classification from Miall, 2006.

Facies code	Lithofacies	Sedimentary structures	Architectural elements: genetic interpretation	Facies Association	Depositional environment
Gmm	Matrix supported, massive medium to coarse cobble sandy to clayey matrix	Not observed	**Sediment Gravity flows (SG):** plastic debris flow (high-strength, viscous) sediment gravity-flow deposits	Hd "Head"	Periglacial
Sm	Massive fine to coarse sand				
Gp	Clast supported pebble to granule coarse sand matrix	Solitary or grouped planar crossbedding in lenses of metric width	**Gravel Bars and bedforms (GB):** transverse bedforms	Fv1 "Fluvial 1"	Gravel wandering fluvial
Sp	Medium to coarse sand		**Sandy Bedforms (SB):** transverse and lingoid bedforms		
Gt	Clast supported pebble to granule coarse sand matrix	Solitary or grouped through crossbedding normal grading, scours	**GB:** minor channels fills transverse bedforms	Fv2 "Fluvial 2"	Shallow gravel-bed braided fluvial
Gp		Solitary or grouped planar crossbedding in lenses of metric width			
St	Fine to medium sand	Solitary or grouped through crossbedding	**SB:** transverse and lingoid bedforms		
Sp	Medium to coarse sand	Solitary or grouped plannar crossbedding			
St	Fine to coarse sand	Grouped through cross-beddings with paleocurrent orientation reversals (landward and seaward) and tidal bundles	**SB:** 3D dunes within alternating (tidal) currents	Td "Tide-dominated"	Median to outer estuary
Sp2	Fine to medium sand (well sorted)	Grouped planar crossbedding within wedges of plurimetric width	**Tidal Bars (TB)**: longitudinal bedforms		
Srf	Fine to medium sand	Ripples, climbing ripples, herringbones, flaser bedding	**Sand Flat (SF):** alternating currents of varying strength planar-bed flow		
Sh	Very fine to medium sand	Horizontal lamination			
Fl	Clays, silts and fine sand	Ripples, wavy and/or flaser bedding, sometimes herringbones cross-beddings	**Mixed Flat (MF):** alternating currents of varying strength decantation, low strength flow		Inner estuary
Fm	Clay and silt	Not observed			
Fr		Vertical burrows			

Appendix

Table A.2.2. Sample location using for dating ESR-OSL.

Sample	Location	Coordinates Lambert 93		Elevations (m NGF)			Sample burial depth (m)	Valley	Terrace on 1:50000 geological map	Quarry
		X	Y	Section	Bedrock	Sample				
A3D-002	Vimpelles	713647	6814295	53,0	47,00	51,20	1,80	Bassée	Fz	Lafarge Granulats
A3D-003	Sandrancourt	601735	6881829	23,0	16,00	18,00	5,00	Middle Seine	Fya	Lafarge Granulats
A3D-004	Sandrancourt	601735	6881822	23,0	16,00	20,00	3,00	Middle Seine	Fya	Lafarge Granulats
A3D-005	Sandrancourt	603402	6882557	36,0	13,00	15,00	21,00	Middle Seine	Fya	Lafarge Granulats
A3D-006	Fontaine Mâcon	738280	6818083	105,0	99,00	104,20	0,80	Bassée	Fy	NA (augered sample)
A3D-007	Vimpelles	713490	6814415	53,0	47,00	51,00	2,00	Bassée	Fz	Lafarge Granulats
A3D-008	Chalmaison	719150	6819965	78,0	72,00	75,50	2,50	Bassée	LP	-
A3D-009	Marolles-sur-Seine	703278	6809276	56,0	47,00	55,20	0,80	Bassée	Fx-y	-
A3D-010	Manoir Brésil	547289	6927742	5,5	1,40	2,75	2,75	Lower Seine	Fyd	CEMEX
A3D-011	Manoir Brésil	547623	6927403	8,0	4,00	5,00	3,00	Lower Seine	Fyd	CEMEX
A3D-012	Achères	632427	6875564	24,0	13,00	22,00	2,00	Middle Seine	Fy	GSM
A3D-013	Carrières Sous-Poissy	628299	6872937	28,0	23,00	25,00	3,00	Middle Seine	Fy	GSM
A3D-014	Moisson	602504	6885902	31,0	27,00	30,00	1,00	Middle Seine	Fyb	-
A3D-015	Manoir Brésil	547721	6927229	11,0	3,00	7,50	3,50	Lower Seine	Fyc	CEMEX
A3D-016	Manoir Brésil	547834	6927593	14,5	-	12,50	2,00	Lower Seine	Fyd	CEMEX
A3D-017	Val-de-Reuil	571975	6911041	9,0	2,00	7,60	1,40	Lower Seine	Fyd	CEMEX
A3D-018	Bouafles	581997	6900724	37,0	29,00	31,00	6,00	Middle Seine	Fyc	CEMEX
A3D-019	Bouafles	581994	6900731	37,0	29,00	33,50	3,50	Middle Seine	Fyc	CEMEX
A3D-020	Noyen-sur-Seine	724043	6818253	57,0	50,00	56,00	1,00	Bassée	Fz	Port Montain
A3D-021	Bazoches	714653	6813318	53,0	46,00	51,00	2,00	Bassée	Fz	GSM Bazoches
A3D-022	Varennes-sur-Seine	694128	6806407	51,0	46,00	48,80	2,20	Bassée	Fy	GSM
A3D-023	Carrière Luzancy	718213	6874033	54,0	46,00	49,00	5,00	Marne	Fy	GSM
A3D-024	Courceroy	730584	6818157	71,7	68,70	69,20	2,50	Bassée	Chalk?	NA
A3D-025	Dordives-Loing	682151	6783098	65,0	62,0	63,8	1,2	Loing	Fz	Lafarge Granulats
A3D-026	Dordives-Loing	682151	6783098	65	62,0	63,8	1,2	Loing	Fz	Lafarge Granulats
A3D-027	Les Bretelles-zone 1	602547	6883415	17,8	< 8	15,8	2,0	Middle Seine	Fz	-
A3D-028	Les Bretelles-zone 6	603054	6883299	18,75	< 8	16,85	1,9	Middle Seine	Fz	-
M-01	Maurecourt	631594	6878270	26,5	18	20,7	5,8	Oise	Fy	-

Appendix B: Supplementary data for chapter 3. Results of OSL from Re.S.Artes laboratory

Available online at:

https://cloud.minesparis.psl.eu/index.php/s/6f80SlBPNzqwP7f?path=%2FAppendix.

Appendix C: Supplementary data for chapter 3. Validation criteria ESR dating

Supplementary information about the Electron Spin Resonance (ESR) dating method applied of optically bleached quartz grains from the upper to downstream Seine catchment, using the multiple centres approach (MC). This dose is determined by the additive method to obtain a dose response curve, that allow to determine the equivalent dose (De) for the age calculation.
In general, two fitting functions employing Origin software were used: the SSE and the Exp+Lin, in order to have a better goodness-of-fit in curves.

Appendix

C.1 Upstream Paris: Sample A3D-006 at Fontaine Mâcon and sample A3D-024 at Courceroy sites

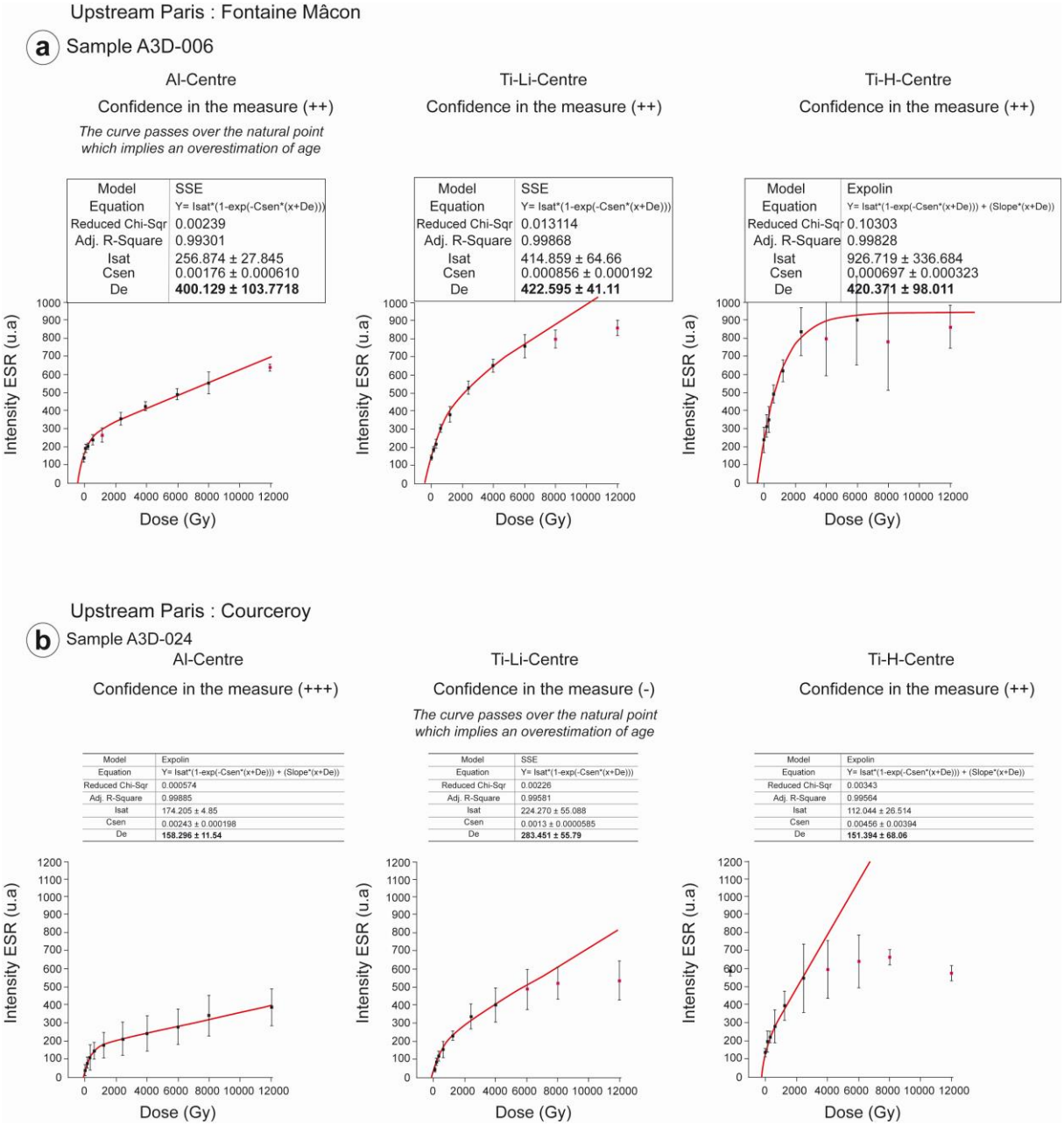

Figure C.1. Dose response curves were derived from the ESR signal of Al-centre, TiLi-centre and TiH-centre for samples located upstream of Paris. Black points represent points used for final fitting, while red points represent data points removed for the fitting curve. Red line indicates the goodness-of-fit-curve found.

C.2 Downstream Paris: Samples A3D-003,004 and A3D-005 at Sandrancourt site

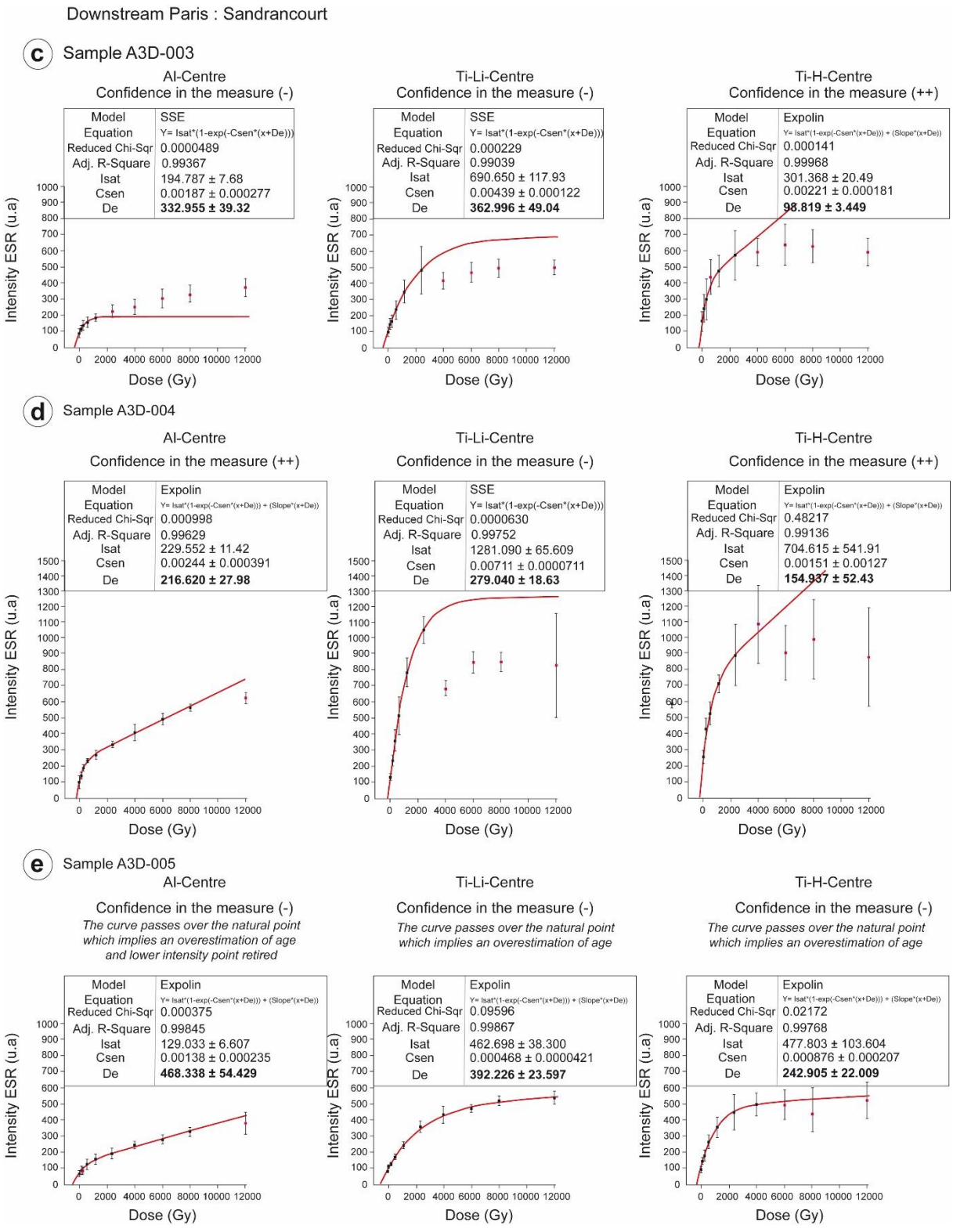

Figure C.2. Dose response curves were derived from the ESR signal of Al-centre, TiLi-centre and TiH-centre for samples located downstream of Paris, at Sandrancourt site, located in the Fyd terrace. Black points represent points used for final fitting, while red points represent data points removed for the fitting curve. Red line indicates the goodness-of-fit-curve found.

C.3 Downstream Paris: Sample A3D-014 at Moisson, samples A3D-018 and A3D-019 at Bouafles and sample A3D-017 at Val-de-Reuil sites

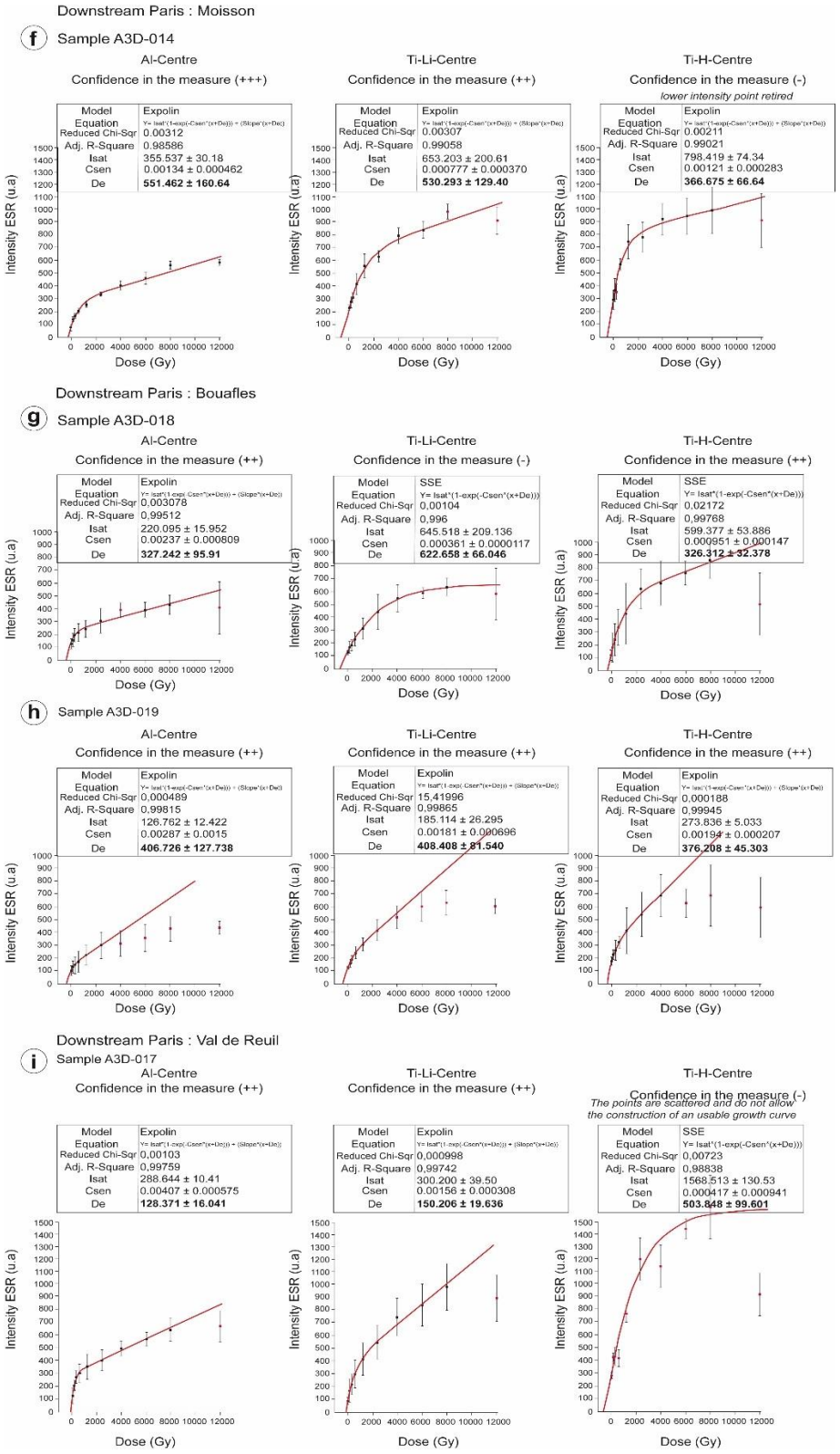

Figure C.3. Dose response curves were derived from the ESR signal of Al-centre, TiLi-centre and TiH-centre for samples located downstream of Paris at Moisson, Bouafles and Val-de-Reuil sites. Black points represent points used for final fitting, while red points represent data points removed for the fitting curve. Red line indicates the goodness-of-fit-curve found.

C.4 Downstream Paris: Manoir Brésil. More details in chapter 4

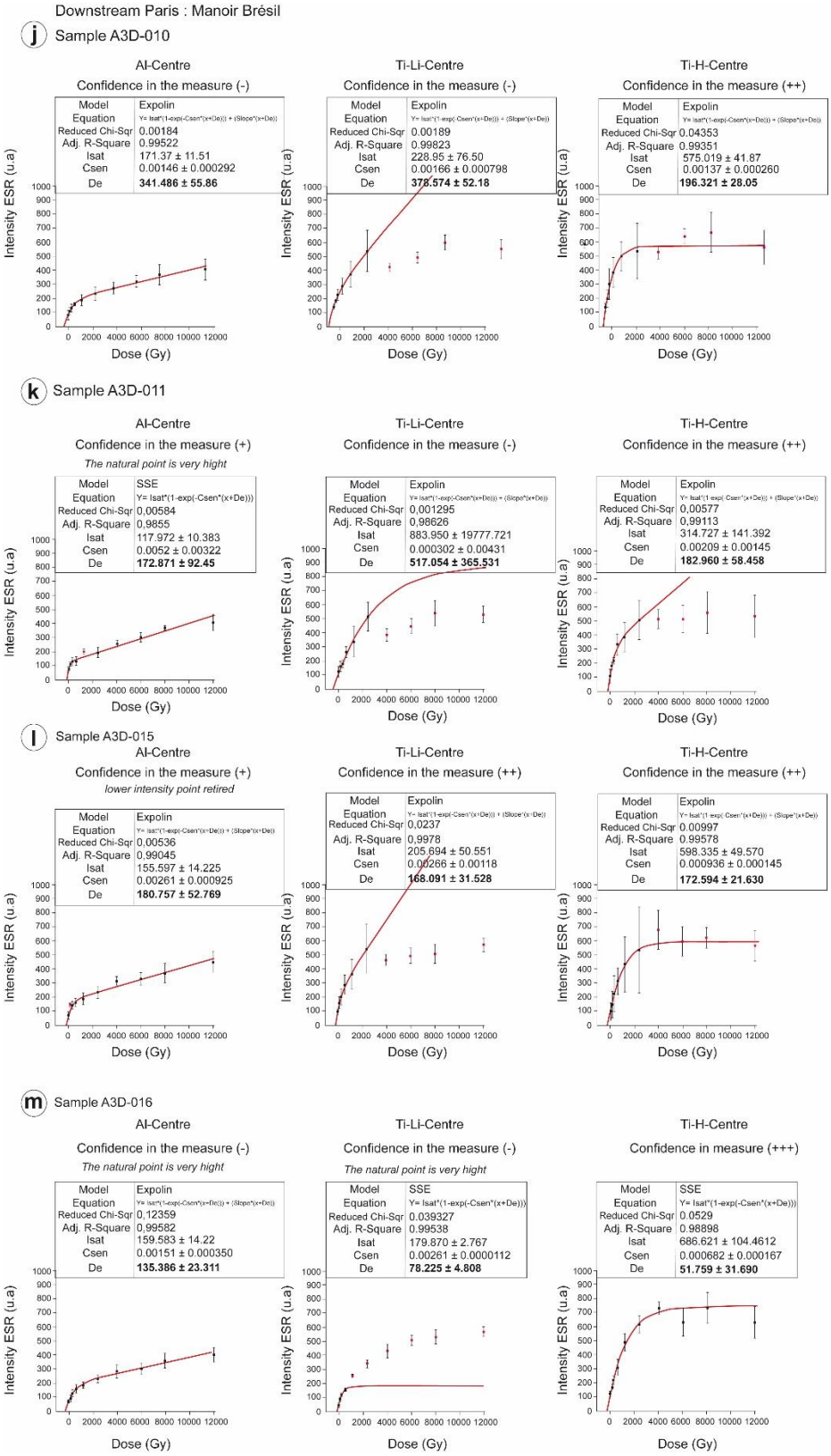

Figure C. 1. Dose response curves derived from the ESR signal of Al-centre, TiLi-centre and TiH-centre for samples located downstream of Paris, at Manoir Brésil site from the Fyc and Fyd terrace. Black points represent points used for final fitting, while red points represent data points removed for the fitting curve. Red line indicates the goodness-of-fit-curve found.

Appendix

C.5 Equations of the fitting functions calibrated in Origin software

Table C.1. Equation of the various fitting functions using in this work.

Function	Equation
SSE	Y=Isat*(1-exp(-Csen*(x+De)))
Exp+Lin	Y=Isat*(1-exp(-Csen*(x+De))) + (Slope*(x+De))

Appendix D: Supplementary data for chapter 3

Supplementary information about the ESR and OSL ages. The contents of radioelements (U, Th and daughters and K) for both ESR and OSL were measured by gamma spectrometry. Water contents (W%) were estimated using the difference in mass between the natural sample and the dried same sample. Water contents considering all samples ranging between 6 and 15 %.

D.1 Results ESR Upstream Paris

Table D.1. ESR results obtained upstream Paris at Fontaine Mâcon and Courceroy sites on quartz extracted from alluvial sediments. Relative elevations (RH) or (RH') are indicated. Cosmic dose, radionuclide contents, in situ gamma dose, annual dose (Da), equivalent doses and the corresponding final age are indicated. Retained ages are in bold, in contrast, red ages are not used.

Fontaine Mâcon				**10 % of water content**						**Terrace T_{IV}**			
Sample:	**RH (m)**	**RH' (m)**	**Depth (m)**	**Cosmic dose (µGy/a)**	**^{238}U (ppm)**	**^{232}Th (ppm)**	**^{40}K (%)**	***in situ* gamma dose D_Y (µGy/a)**	**D_a (µGy/a)**	**ESR**	**De (Gy)**	**Age (ka)**	**Mean age* (ka)**
A3D-006 Fluvial deposit	52	46	0.8	171± 9	0.497±0.042	1.048±0.055	0.097±0.0044	208±11	529±16	Al	400±52	**756±100**	**792±35 (2σ)**
										TiLi	422±20	**798±42**	
										TiH	420±49	**794±94**	
Courceroy				**10 % of water content**						**Terrace T_{III}**			
Sample:	**RH (m)**	**RH' (m)**	**Depth (m)**	**Cosmic dose (µGy/a)**	**^{238}U (ppm)**	**^{232}Th (ppm)**	**^{40}K (%)**	***in situ* gamma dose D_Y (µGy/a)**	**D_a (µGy/a)**	**ESR**	**De (Gy)**	**Age (ka)**	**Mean age* (ka)**
A3D-024 Fluvial deposit	22	14	2.5	130 ± 6	0.391±0.034	0.212±0.15	0.095±0,005	142±5	420±14	Al	158±10	**376±25**	**375±23 (2σ)**
										TiLi	283±26	**673±63**	
										TiH	151±34	**359±81**	

Appendix

D.2 Results OSL Upstream Paris

Table D.2. OSL results obtained upstream Paris at Noyen-sur-Seine, Bazoches, Vimpelles, Citry and Dordives sites on quartz extracted from alluvial sediments. Relative elevations (RH) or (RH') are indicated. Cosmic dose, radionuclide contents, in situ gamma dose, annual dose (Da), equivalent doses and the corresponding final age are indicated. Retained ages are in bold, in contrast, red ages are not used.

Noyen-sur-Seine				**6.8 % of water content**						**Terrace T_2**		
Sample:	**RH (m)**	**RH' (m)**	**Depth (m)**	**Cosmic dose (mGy/a)**	**^{238}U (mGy/a)**	**^{232}Th (mGy/a)**	**^{40}K (mGy/a)**	***in situ* gamma dose D_Y (mGy/a)**	**Annual dose D_a (mGy/a)**	**OSL**	**De (Gy)**	**Age (ka)**
A3D-020 Fluvial deposit	8	1	1	0.186±0.009	0.013±0.005	0.018±0.003	0.036±0.009	0.133±0.005	0.433±0.019	OSL	7.60±0.2	**17.57±1.2**
Bazoches				**8.6 % of water content**						**Terrace T_2**		
Sample:	**RH (m)**	**RH' (m)**	**Depth (m)**	**Cosmic dose (mGy/a)**	**^{238}U (mGy/a)**	**^{232}Th (mGy/a)**	**^{40}K (mGy/a)**	***in situ* gamma dose D_Y (mGy/a)**	**Annual dose D_a (mGy/a)**	**OSL**	**De (Gy)**	**Age (ka)**
A3D-021 Fluvial deposit	6	0	2	0.164±0.008	0.011±0.005	0.017±0.003	0.034±0.009	0.125±0.005	0.386±0.018	OSL	6.48±0.12	**16.80±1.1**
Vimpelles				**8.5 % of water content**						**Terrace T_{3a}**		
Sample:	**RH (m)**	**RH' (m)**	**Depth (m)**	**Cosmic dose (mGy/a)**	**^{238}U (mGy/a)**	**^{232}Th (mGy/a)**	**^{40}K (mGy/a)**	***in situ* gamma dose D_Y (mGy/a)**	**Annual dose D_a (mGy/a)**	**OSL**	**De (Gy)**	**Age (ka)**
A3D-002 Fluvial deposit	6.2	0.2	1.8	0.168±0.008	0.006±0.003	0.015±0.002	0.028±0.009	0.119±0.007	0.374±0.018	OSL	5.48±0.14	**14.63±1.1**
Citry				**6.5 % of water content**						**Terrace Fz**		
Sample:	**RH (m)**	**RH' (m)**	**Depth (m)**	**Cosmic dose (mGy/a)**	**^{238}U (mGy/a)**	**^{232}Th (mGy/a)**	**^{40}K (mGy/a)**	***in situ* gamma dose D_Y (mGy/a)**	**Annual dose D_a (mGy/a)**	**OSL**	**De (Gy)**	**Age (ka)**
A3D-023 Fluvial deposit	0	7	5	0.116±0.006	0.029±0.006	0.088±0.007	0.327±0.025	0.451±0.017	1.165±0.038	OSL	28.8±0.6	**24.7±1.3**
Dordives				**13.1 % of water content**						**Terrace Fz**		
Sample:	**RH (m)**	**RH' (m)**	**Depth (m)**	**Cosmic dose (µGy/a)**	**^{238}U (ppm)**	**^{232}Th (ppm)**	**^{40}K (%)**	***in situ* gamma dose D_Y (µGy/a)**	**D_a (µGy/a)**	**OSL**	**De (Gy)**	**Age (ka)**
A3D-026 Fluvial deposit	1.8	-5.2	1.2	0.181±0.009	0.016±0.005	0.174±0.017	1.149±0.045	1.489±0.0554	1.67±0.054	OSL	22.6±0.4	**13.53±0.7**

Appendix

D.3 Results ESR Downstream Paris

Table D.3. ESR results obtained downstream Paris at Bouafles, Moisson, Sandrancourt and Val-de-Reuil sites on quartz extracted from alluvial sediments. Relative elevations (RH) or (RH') are indicated. Cosmic dose, radionuclide contents, in situ gamma dose, annual dose (Da), equivalent doses and the corresponding final age are indicated. Retained ages are in bold, in contrast, red ages are not used.

Bouafles				**10 % of water content**						**Terrace Fyb**			
Sample:	**RH (m)**	**RH' (m)**	**Depth (m)**	**Cosmic dose (µGy/a)**	**^{238}U (ppm)**	**^{232}Th (ppm)**	**^{40}K (%)**	***in situ* gamma dose D_Y (µGy/a)**	**D_a (µGy/a)**	**ESR**	**De (Gy)**	**Age (ka)**	**Mean age* (ka)**
A3D-018 Fluvial deposit	25	18	6	77±4	0.338±0.041	1.266±0.055	0.5510±0.007	236±13	749±18	Al	327±42	**437±56**	**436±63 (2σ)**
										TiLi	622±33	**831±45**	
										TiH	326±16	**435±22**	
A3D-019 Fluvial deposit	28	21	3.5	111±6	0.278±0.048	1.530±0.068	0.6413±0.009	274±14	880±21	Al	406±63	**462±72**	
										TiLi	408±41	**464±47**	
										TiH	376±22	**427±25**	
Moisson				**15% of water content**						**Terrace Fyc**			
Sample:	**RH (m)**	**RH' (m)**	**Depth (m)**	**Cosmic dose (µGy/a)**	**^{238}U (ppm)**	**^{232}Th (ppm)**	**^{40}K (%)**	***in situ* gamma dose D_Y (µGy/a)**	**D_a (µGy/a)**	**ESR**	**De (Gy)**	**Age (ka)**	**Mean age* (ka)**
A3D-014 Fluvial deposit	19	12	1	166±8	2.964±0.082	10.104±0.133	1.038±0.012	615±30	1988±38	Al	551±80	**277±40**	**271±25 (1σ)**
										TiLi	530±65	**267±33**	
										TiH	366±33	**184±17**	
Sandrancourt				**10 % of water content**						**Terrace Fyd**			
Sample:	**RH (m)**	**RH' (m)**	**Depth (m)**	**Cosmic dose (µGy/a)**	**^{238}U (ppm)**	**^{232}Th (ppm)**	**^{40}K (%)**	***in situ* gamma dose D_Y (µGy/a)**	**D_a (µGy/a)**	**ESR**	**De (Gy)**	**Age (ka)**	**Mean age* (ka)**
A3D-003 Fluvial deposit	11	2	5	89±4	0.452±0.055	0.833±0.072	0.531±0.011	219±10	734±21	Al	332±20	**453±28**	**138±15 (2σ)**
										TiLi	363±25	**495±35**	
										TiH	98±2	**134±3**	
A3D-004 Fluvial deposit	13	4	3	120±10	0.430±0.055	0.891±0.073	0.5896±0.011	227±10	810±21	Al	216±14	**267±18**	
										TiLi	279±9	**344±12**	
										TiH	155±26	**191±32**	
A3D-005 Fluvial deposit	9	1	21	20±1	0.386±0.038	0.9864±0.049	0.572±0.007	214±11	683±16	Al	468±27	**686±40**	
										TiLi	392±11	**574±17**	
										TiH	242±11	**354±16**	
Val-de-Reuil				**10 % of water content**						**Terrace Fz**			
Sample:	**RH (m)**	**RH' (m)**	**Depth (m)**	**Cosmic dose (µGy/a)**	**^{238}U (ppm)**	**^{232}Th (ppm)**	**^{40}K (%)**	***in situ* gamma dose D_Y (µGy/a)**	**D_a (µGy/a)**	**ESR**	**De (Gy)**	**Age (ka)**	**Mean age* (ka)**
A3D-017 Fluvial deposit	7	0	1.4	155±8	0.572±0.049	1.65±0.067	0.533±0.008	221±12	838±20	Al	128±8	**153±10**	**164±10 (1σ)**
										TiLi	158±10	**189±12**	
										TiH	Not calculated		

Appendix

D.4 Results OSL Downstream Paris

Table D.4. OSL results obtained downstream Paris at Carrières-sous-Poissy, Sandrancourt St Martin-la-Garenne and Maurecourt sites on quartz extracted from alluvial sediments. Relative elevations (RH) or (RH') are indicated. Cosmic dose, radionuclide contents, in situ gamma dose, annual dose (Da), equivalent doses and the corresponding final age are indicated. Retained ages are in bold, in contrast, red ages are not used.

Carrières-sous-Poissy				**10 % of water content**						**Terrace Fyd**		
Sample:	**RH (m)**	**RH' (m)**	**Depth (m)**	**Cosmic dose (mGy/a)**	**^{238}U (mGy/a)**	**^{232}Th (mGy/a)**	**^{40}K (mGy/a)**	***in situ* gamma dose D_Y (mGy/a)**	**Annual dose D_a (mGy/a)**	**OSL**	**De (Gy)**	**Age (ka)**
A3D-013 Fluvial deposit	15	7	3	0.145±0.007	0.005±0.002	0.046±0.007	0.148±0.018	0.306±0.024	0.424±0.023	OSL	82.9±1	**195.79**±13.2
Sandrancourt				**10 % of water content**						**Terrace Fyd**		
Sample:	**RH (m)**	**RH' (m)**	**Depth (m)**	**Cosmic dose (mGy/a)**	**^{238}U (mGy/a)**	**^{232}Th (mGy/a)**	**^{40}K (mGy/a)**	***in situ* gamma dose D_Y (mGy/a)**	**Annual dose D_a (mGy/a)**	**OSL**	**De (Gy)**	**Age (ka)**
A3D-003 Fluvial deposit	11	2	5	0.116±0.007	0.008±0.002	0.023±0.002	0.324±0.016	0.219±0.011	0.734±0.021	OSL	197.1±3.2	**269±6**
A3D-004 Fluvial deposit	13	4	3	0.145±0.006	0.011±0.001	0.027±0.003	0.316±0.018	0.227±0.010	0.810±0.021	OSL	164.9±3.7	**204±5**
A3D-005 Fluvial deposit	9	1	21	0.030±0.002	0.010±0.002	0.025±0.003	0.310±0.017	0.214±0.011	0.683±0.016	OSL	150.4±2.5	**220±4**
St-Martin - la - Garenne				**10 % of water content**						**Terrace Fz**		
Sample:	**RH (m)**	**RH' (m)**	**Depth (m)**	**Cosmic dose (mGy/a)**	**^{238}U (mGy/a)**	**^{232}Th (mGy/a)**	**^{40}K (mGy/a)**	***in situ* gamma dose D_Y (mGy/a)**	**Annual dose D_a (mGy/a)**	**OSL**	**De (Gy)**	**Age (ka)**
A3D-028 Fluvial deposit	11	3	1.9	0.165±0.008	0.011±0.003	0.028±0.003	0.373±0.022	0.254±0.005	0.896±0.026	OSL	15.9±0.3	**17.720±0.89**
Maurecourt				**13.8 % of water content**						**Terrace Fz**		
Sample:	**RH (m)**	**RH' (m)**	**Depth (m)**	**Cosmic dose (mGy/a)**	**^{238}U (mGy/a)**	**^{232}Th (mGy/a)**	**^{40}K (mGy/a)**	***in situ* gamma dose D_Y (mGy/a)**	**Annual dose D_a (mGy/a)**	**OSL**	**De (Gy)**	**Age (ka)**
M-01 Fluvial deposit	13	-0.3	5.8	0.106±0.005	0.021±0.006	0.217±0.019	0.573±0.034	1.019±0.049	1.125±0.049	OSL	18.6±0.5	**16.5±1.2**

Appendix

D.5 Results ESR Downstream Paris: Manoir Brésil

Table D.5. ESR results obtained downstream Paris at Manoir Brésil site on quartz extracted from alluvial sediments. Relative elevations (RH) or (RH') are indicated. Cosmic dose, radionuclide contents, in situ gamma dose, annual dose (Da), equivalent doses and the corresponding final age are indicated. Retained ages are in bold, in contrast, red ages are not used.

Manoir Brésil				**12 % of water content**						**Terrace Fyd / Fyc***			
Sample:	**RH (m)**	**RH' (m)**	**Depth (m)**	**Cosmic dose (µGy/a)**	**^{238}U (ppm)**	**^{232}Th (ppm)**	**^{40}K (%)**	***in situ* gamma dose D_Y (µGy/a)**	**D_a (µGy/a)**	**ESR**	**De (Gy)**	**Age (ka)**	**Mean age* (ka)**
A3D-010 Fluvial deposit	14	3	2.75	124.6±6.2	0.374±0.049	1.342±0.067	0.883±0.011	288±12	1047±15	Al	341±27	**326±26**	-
										TiLi	378±26	**361±25**	
										TiH	196±14	**187±14**	
A3D-011 Tidal deposit	17	6	3	119.8±6	0.260±0.049	1.188±0.070	0.428±0.009	219±10	666±13	Al	172±46	**258±69**	**269±37 (2σ)**
										TiLi	517±193	**776±290**	
										TiH	182±29	**273±44**	
A3D-015* Tidal deposit	19	8	3.5	110.8±5.5	0.850±0.055	3.005±0.080	0.452±0.008	272±9	845±9	Al	181±26	**214±31**	**204±10 (2σ)**
										TiLi	168±16	**199±19**	
										TiH	173±11	**205±13**	
A3D-016 Periglacial deposit	24	13	2	140.4±7	2.294±0.096	7.690±0.152	0.721±0.0128	702±21	1752±25	Al	135±12	**77 ± 7**	-
										TiLi	78±5	**45±3**	
										TiH	51±16	**29 ± 9**	

Appendix

D.6 Results OSL Downstream Paris: Manoir Brésil

Table D.6. OSL results obtained downstream Paris at Manoir Brésil site on quartz extracted from alluvial sediments. Relative elevations (RH) or (RH') are indicated. Cosmic dose, radionuclide contents, in situ gamma dose, annual dose (Da), equivalent doses and the corresponding final age are indicated. Retained ages are in bold, in contrast, red ages are not used.

Manoir Brésil				**12 % of water content**						**Terrace Fyd / Fyc***		
Sample:	**RH (m)**	**RH' (m)**	**Depth (m)**	**Cosmic dose (mGy/a)**	**^{238}U (mGy/a)**	**^{232}Th (mGy/a)**	**^{40}K (mGy/a)**	***in situ* gamma dose D_Y (mGy/a)**	**Annual dose D_a (mGy/a)**	**OSL**	**De (Gy)**	**Age (ka)**
A3D-010 Fluvial deposit	14	3	2.75	124.6±6.2	0.374±0.049	1.342±0.067	0.883±0.011	288±12	1.047±0.015	OSL	192.2±3	**184±4**
A3D-011 Tidal deposit	17	6	3	119.8±6	0.260±0.049	1.188±0.070	0.428±0.009	219±10	0.666±0.013	OSL	161.1±3.4	**242±7**
A3D-015* Tidal deposit	19	8	3.5	110.8±5.5	0.850±0.055	3.005±0.080	0.452±0.008	272±9	0.845±0.009	OSL	161.9±3	**192±5**
A3D-016 Periglacial deposit	24	13	2	140.4±7	2.294±0.096	7.690±0.152	0.721±0.0128	702±21	1.752±0.025	OSL	40.4±0.9	**23±1**

Appendix E: Supplementary data for chapter 4

E.1 ESR experimental procedure

ESR measurements were performed by myself at the Department of HNHP of the National Museum of Natural History of Paris (MNHNP). Analyses were made on 100-200 µm quartz grains selected by water sieving. First, chemical attack with hydrochloric acid (HCl) allowed removing carbonates. Second, a hydrofluoric acid at 40% (HF) was used for 90 minutes to eliminate oxides, feldspars as well as the external part of the quartz grains (leaching) that have been subjected to external α-rays. The heavy minerals, magnetic minerals and phyllosilicates were successively extracted from the sample using a dense liquor (density 2,72) and a magnetic separator.

Quartz grains were then submitted to irradiations. The equivalent dose (De) was determined through the additive dose method. For this, the sample was split in 11 aliquots. One aliquot was kept the natural, another aliquot was bleached (for Al DAT determination), and the other nine aliquots were submitted to increase gamma doses of 150, 300, 600, 1200, 2400, 4000, 6000, 8000 and 12000 Gy respectively at the Cenieh laboratory (Spain).

Each aliquot was measured three times at different angles rotation in the ESR spectrometer in order to evaluate samples heterogeneity (angular variation). This procedure was repeated for three days to assess variability of equivalent dose (De).

All ages, using De determined with Origin software and Da calculated using an excel sheet are then obtained.

E.1.1 Equations of the fitting functions calibrated in Origin software

Table E.1.1. Equations of the various fitting functions used in this work.

Function	Equation
SSE	Y=Isat*(1-exp(-Csen*(x+De)))
Expo+Lin	Y=Isat*(1-exp(-Csen*(x+De))) + (Slope*(x+De))

Appendix

E.1.2 ESR dose response curves

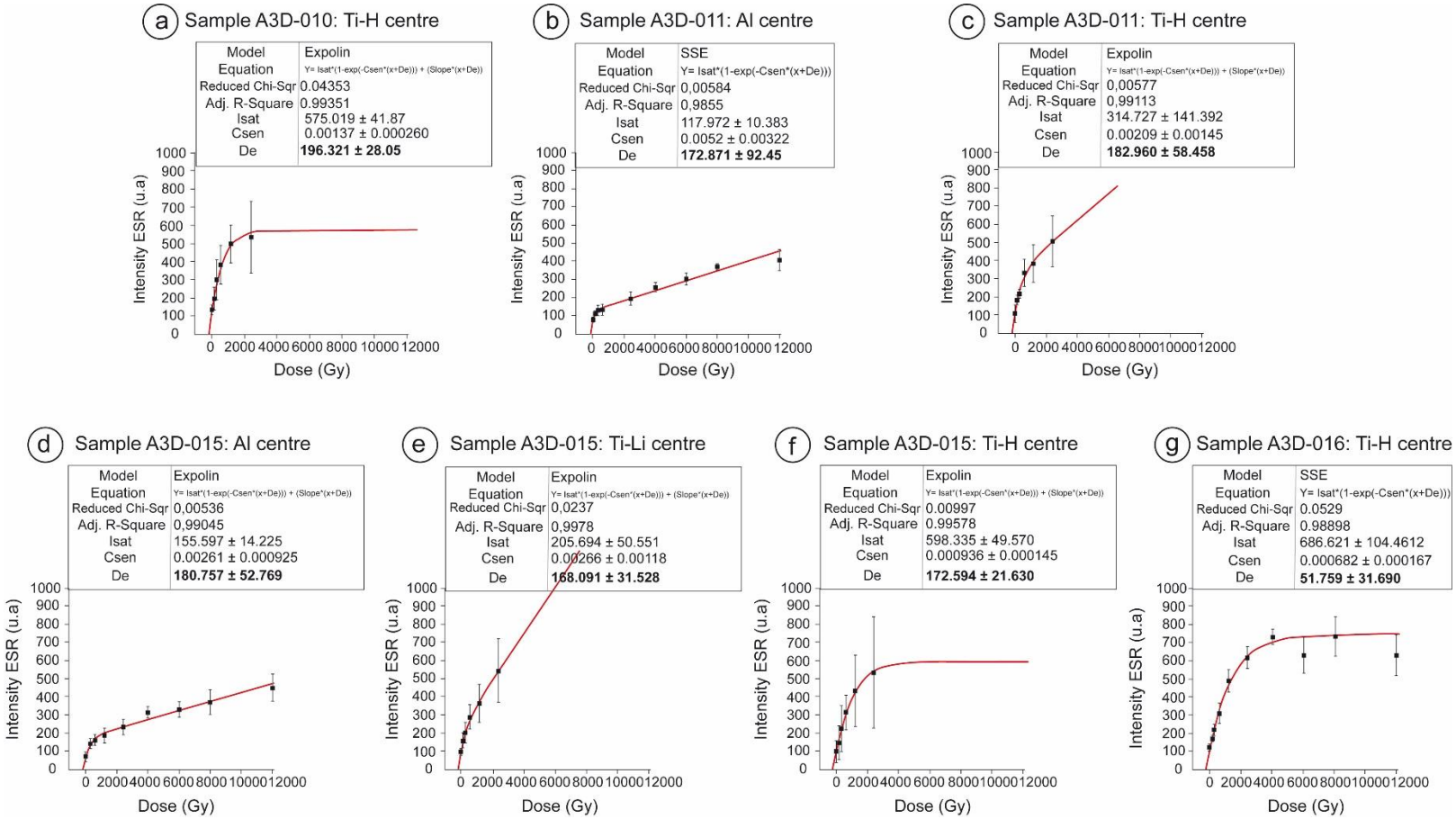

Figure E.1.2. Dose response curves derived from the measurements of the (a) Ti-H centre (sample A3D-010), (b) Al centre (sample A3D-11), (c) Ti-H centre (sample A3D-11), (d) Al centre (sample A3D-015), (e) Ti-Li centre (sample A3D-015), (f) Ti-H centre (sample A3D-015) and (g) Ti-H centre (sample A3D-016). Fitting was performed using the SSE or Expolin functions.

E.2 OSL experimental procedure

OSL analysis were performed at Re.S.Artes laboratory (Bordeaux, France), under red light only. The sediment was sieved to select a particle size between 80 and 125µm. The powder thus obtained was chemically treated: 20% HCl to remove carbonates (at the beginning and end of the chemical preparation cycle), H_2O_2 30% to eliminate organic matter, and HF 40% to eliminate feldspars and thus allow the exclusive selection of quartz.

The radioactivity measurement for annual dose determination was carried out on the raw sediment, dried, and then packaged in an airtight plastic box to allow measurement by low background gamma spectrometry after waiting a month to ensure that the radon returned to equilibrium. After that, the natural intensity signal, reset to zero and then, irradiate at increasing dose after each bleaching step. A growth curve is constructed considering every measure of intensity signal as a function of dose received. The interpolation of the natural intensity on the growth curve allows determining the equivalent dose (De). The annual dose (Da) was determined using the same approach for ESR method.

E.2.1 SAR-generated doses response curves

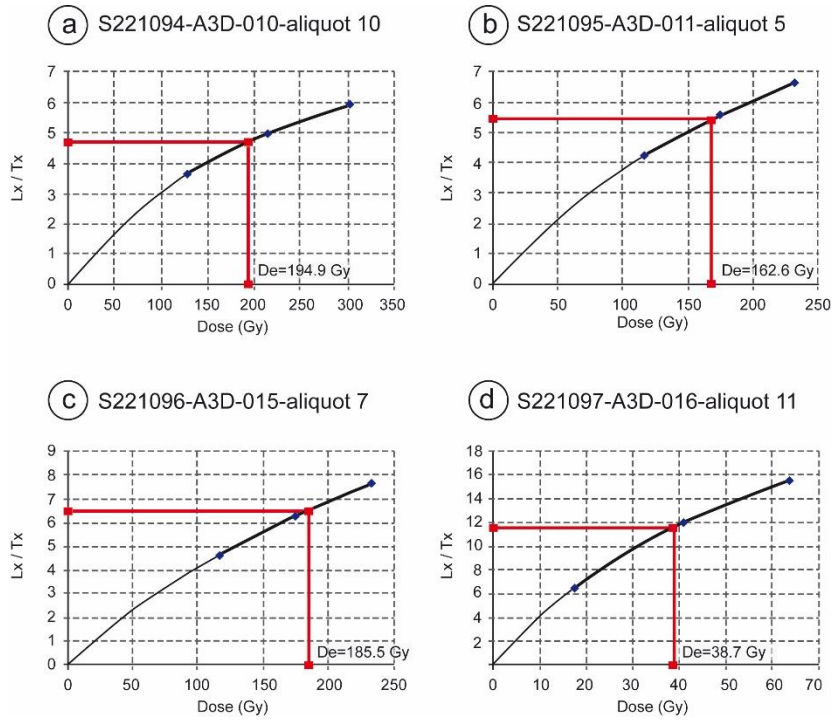

Figure E.2.1. Examples of growth curves using the SAR protocol. Black curve represents the signal regeneration with known radiation doses. The intersection of the measured intensity value on the y-axis with this curve gives the natural radiation dose on the x-axis.

E.2.2 OSL decay curves

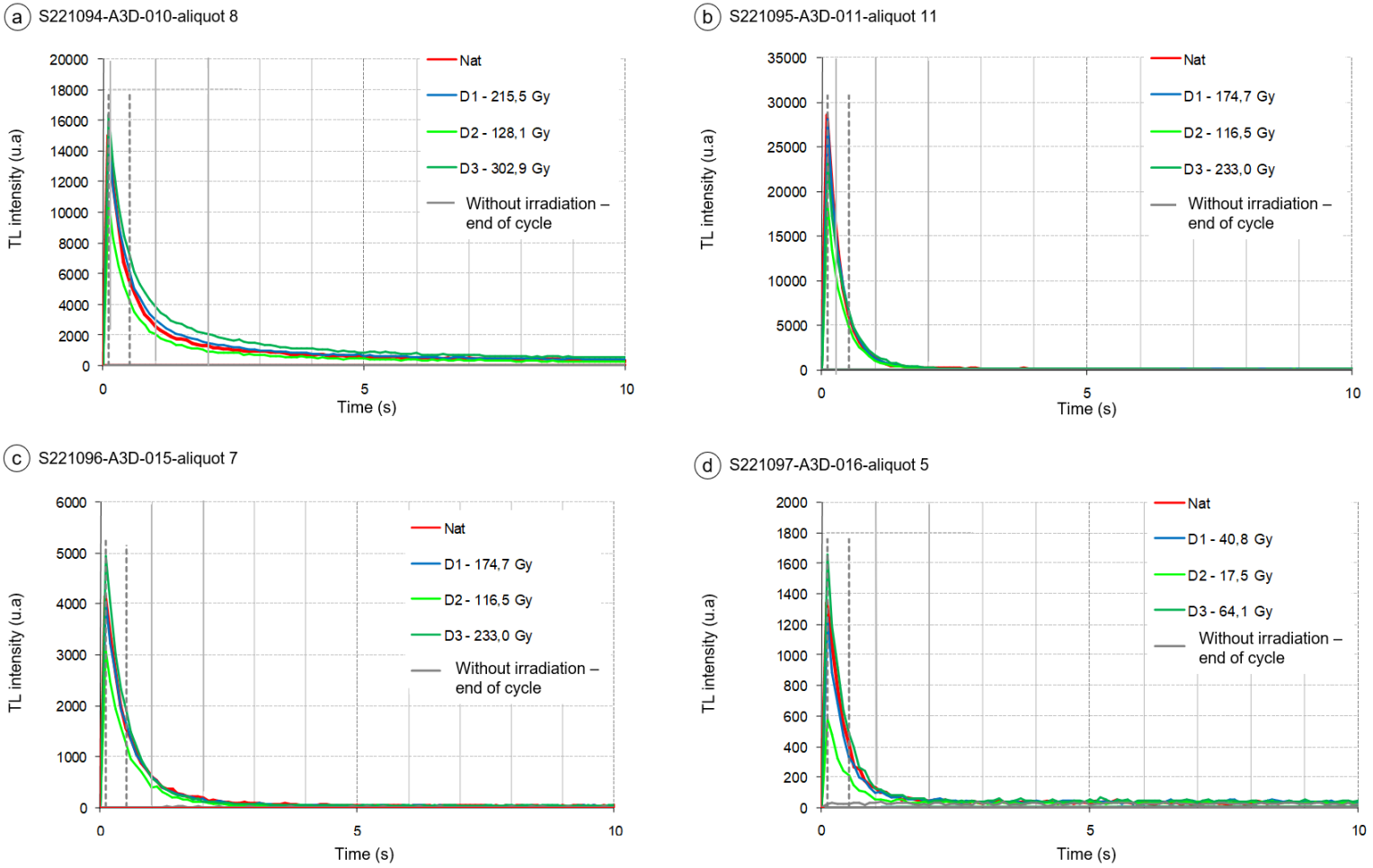

Figure E.2.2. Decay curves obtained with the SAR protocol for the four samples. The OSL signals are strongly dominated by the fast components.

Appendix

E.2.3 OSL measurements distribution

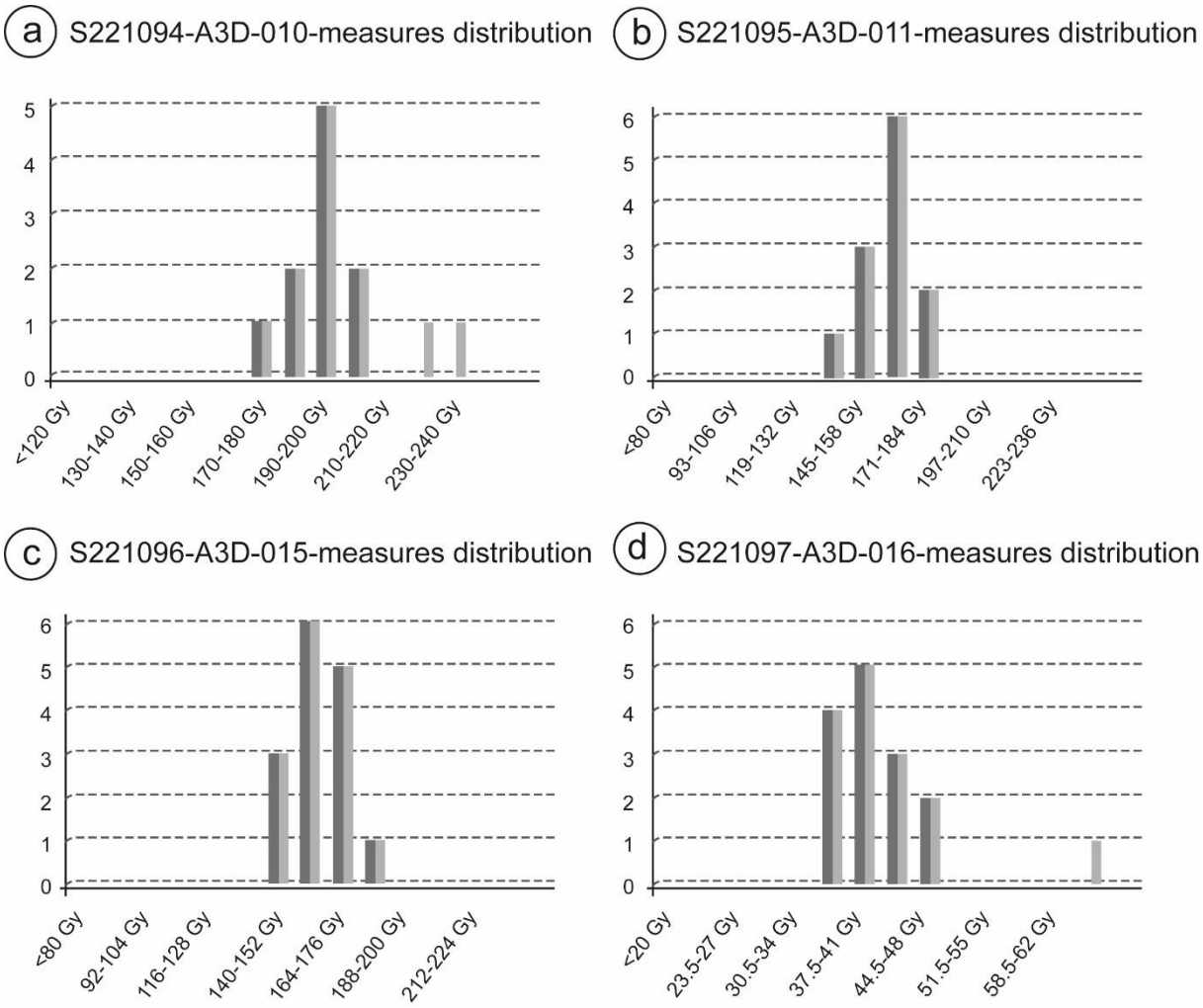

Figure E.2.3. Example of distribution of the equivalent doses values (De) obtained for each sample. They show that sediments were sufficiently exposed to sunlight before they were covered. The distribution of measured values is show in light gray and the distribution of selected equivalent doses retained values is show in dark gray. A Chi-2 test was applied and an arithmetic mean of equivalent dose (De) was used. The given doses were regenerated using the SAR protocol.

Table E.2. OSL Equivalent doses, De.

Samples	Equivalent doses, De (Gy)
A3D-010	**192.2 ± 3**
A3D-011	**161.1 ± 3.4**
A3D-015	**161.9 ± 3**
A3D-016	**40.4 ± 0.9**

Appendix

Table E.3. Physical parameters used for age calculation for Manoir Brésil samples. Radionuclide contents are obtained with Gamma spectrometry. Annual dose (Da) is determined using the following parameters: external alpha and beta contributions using the dose-rate conversion factors of Guérin et al. (2011). A k-value of 0.07 ± 0.01 (Bartz et al., 2019), alpha and beta attenuations from Brennan (2003) and Brennan et al. (1991), water attenuation formulae from Grün (1994) were used in the age calculation. Gamma dose rate was determined by in situ measurements using a portable Na-I probe (Ortec digidart gamma spectrometer). The cosmic dose rate was estimated from the equations of Prescott and Hutton (1994). Water content (%) determined at the time of sampling as the weight of water as a percentage of the dry weight. The initial measurements indicated that the samples were very dry (<5%). To provide a more realistic estimate in water content, a value of 12%, representing the average of measurements taken at equivalent sites in the Seine valley across different studies and seasons was used.

Sample	Depositional environment	Depth (m)	Cosmic dose (µGy/a)	^{238}U (ppm)	^{232}Th (ppm)	^{40}K (%)	*in situ* gamma dose D_γ (µGy/a)	Annual dose D_a (µGy/a)	ESR/OSL	Equivalent dose De (Gy)	Age (ka)
A3D-011	Estuarine	3	119,8 ± 6	0,260 ± 0,049	1,188 ± 0,070	0,428 ± 0,009	219 ± 10	666 ± 13	Al	172 ± 46	**258 ± 69**
A3D-011									TiLi	517 ± 193	776 ± 290
A3D-011									TiH	182 ± 29	**273 ± 44**
A3D-011									OSL	161,1 ± 3,4	**242 ± 7**
A3D-015	Estuarine	3,5	110,8 ± 5,5	0,850 ± 0,055	3,005 ± 0,080	0,452 ± 0,008	272 ± 9	845 ± 9	Al	181 ± 26	**214 ± 31**
A3D-015									TiLi	168 ± 16	**199 ± 19**
A3D-015									TiH	173 ± 11	**205 ± 13**
A3D-015									OSL	161,9 ± 3	**192 ± 5**
A3D-010	Gravel wandering fluvial	2,75	124,6 ± 6,2	0,368 ± 0,048	1,342 ± 0,067	0,883 ± 0,011	288 ± 12	1047 ± 15	Al	341 ± 27	326 ± 26
A3D-010									TiLi	378 ± 26	361 ± 25
A3D-010									TiH	196 ± 14	**187 ± 14**
A3D-010									OSL	192,2 ± 3	**184 ± 4**
A3D-016	Periglacial	2	140,4 ± 7	2,294 ± 0,096	7,690 ± 0,152	0,721 ± 0,0128	702 ± 21	1752 ± 25	Al	135 ± 121	77 ± 7
A3D-016									TiLi	78 ± 5	45 ± 3
A3D-016									TiH	51 ± 16	**29 ± 9**
A3D-016									OSL	40,4 ± 0,9	**23 ± 1**
12% of water content											

Appendix

RÉSUMÉ

Cette thèse est une contribution à la compréhension de l'évolution des vallées et leur fonds alluviaux sur l'exemple du bassin-versant de la Seine qui constitue un exemple typique de zone située à distance (>1000km) de l'influence de déformation tectonique. La géométrie du remplissage alluvial y est héritée de différents épisodes d'incision et d'aggradation au cours du Quaternaire Supérieur. Si les datations par méthodes ESR-OSL sur des sédiments du fond des vallées ou en bordure montrent des âges principalement liés à la dernière grande période glaciaire, un faisceau d'indices -directs ou indirects- tend à montrer une origine d'une partie des fonds de vallée actuels dès le stade isotopique 6. Les âges obtenus sur des terrasses alluviales permettent de compléter les taux d'incision de la littérature, notamment en Bassée et en aval de Rouen, où sont précisé les interactions entre incision et soulèvement du substrat. Une analyse SIG et une estimation par krigeage de l'interface substratum-alluvions montrent l'influence du débit, de la lithologie et du style fluviatile sur la géométrie des fonds alluviaux. Enfin, des possibles knickpoints observés pourraient souligner de l'érosion régressive liée aux deux dernières périodes glaciaires.

MOTS CLÉS

Fond de vallée, krigeage SPDE, ESR, OSL, Quaternaire, Bassin-versant de la Seine, géométrie du remplissage alluvial

ABSTRACT

This thesis contributes to the understanding of valley evolution and alluvial deposits, using the example of the Seine River catchment, which serves as a typical illustration situated far (>1000km) from the influence of tectonic deformation. The geometry of the alluvial infill is inherited from various episodes of incision and aggradation during the Late Quaternary. While ESR-OSL dating of sediments in valley bottoms or along the edges indicates ages predominantly associated with the last major glacial period, a body of evidence, both direct and indirect, suggests an origin of at least part of the current valley bottoms as early as isotopic stage 6. Ages obtained from alluvial terraces complement existing literature on incision rates, particularly in the Bassée area and downstream of Rouen, where detailed studies elucidate the interactions between incision and substrate uplift. A GIS analysis and kriging estimation of the bedrock-alluvium interface demonstrate the influence of discharge, lithology, and fluvial style on the geometry of valley bottom alluvium. Finally, some observed knickpoints could potentially highlight regressive erosion during the last two glacial periods.

KEYWORDS

Valley bottom, SPDE kriging, ESR, OSL, Quaternary, Seine catchment, Alluvial infill geometry